

ANALYTICA CHIMICA ACTA

International journal devoted to all branches of analytical chemistry

EDITORS

A. M. G. MACDONALD (Birmingham, Great Britain)

HARRY L. PARDUE (West Lafayette, IN, U.S.A.)

ALAN TOWNSHEND (Hull, Great Britain)

J. T. CLERC (Bern, Switzerland)

Editorial Advisers

F. C. Adams, Antwerp
H. Bergamin F^o, Piracicaba
G. den Boef, Amsterdam
A. M. Bond, Waurin Ponds
D. Dyrssen, Göteborg
J. W. Frazer, Livermore, CA
S. Gomišček, Ljubljana
S. R. Heller, Bethesda, MD
G. M. Hieftje, Bloomington, IN
J. Hoste, Ghent
A. Huianicki, Warsaw
G. Johansson, Lund
D. C. Johnson, Ames, IA
P. C. Jurs, University Park, PA
D. E. Leyden, Fort Collins, CO
F. E. Lytle, West Lafayette, IN
H. Malissa, Vienna
D. L. Massart, Brussels
A. Mizuike, Nagoya
E. Pungor, Budapest

W. C. Purdy, Montreal
J. P. Riley, Liverpool
J. Růžička, Copenhagen
D. E. Ryan, Halifax, N.S.
S. Sasaki, Toyohashi
J. Savory, Charlottesville, VA
W. D. Shults, Oak Ridge, TN
H. C. Smit, Amsterdam
W. I. Stephen, Birmingham
G. Tölg, Schwäbisch Gmünd, B.R.D.
B. Trémillon, Paris
W. E. van der Linden, Enschede
A. Walsh, Melbourne
H. Weisz, Freiburg i. Br.
P. W. West, Baton Rouge, LA
T. S. West, Aberdeen
J. B. Willis, Melbourne
E. Ziegler, Mülheim
Yu. A. Zolotov, Moscow

ELSEVIER

ANALYTICA CHIMICA ACTA

International journal devoted to all branches of analytical chemistry
Revue internationale consacrée à tous les domaines de la chimie analytique
Internationale Zeitschrift für alle Gebiete der analytischen Chemie

PUBLICATION SCHEDULE FOR 1984

	J	F	M	A	M	J	J	A	S	O	N	D
Analytica Chimica Acta	156	157/1	157/2	158/1 158/2	159	160	161	162	163	164	165	166

Scope. *Analytica Chimica Acta* publishes original papers, short communications, and reviews dealing with every aspect of modern chemical analysis, both fundamental and applied.

Submission of Papers. Manuscripts (three copies) should be submitted as designated below for rapid and efficient handling:

Papers from the Americas to: Professor Harry L. Pardue, Department of Chemistry, Purdue University, West Lafayette IN 47907, U.S.A.

Papers from all other countries to: Dr. A. M. G. Macdonald, Department of Chemistry, The University, P.O. Box 3f Birmingham B15 2TT, England. Papers dealing particularly with computer techniques to: Professor J. T. Cle Universität Bern, Pharmazeutisches Institut, Baltzerstrasse 5, CH-3012 Bern, Switzerland.

Submission of an article is understood to imply that the article is original and unpublished and is not being considered for publication elsewhere. Upon acceptance of an article by the journal, authors will be asked to transfer the copyright of the article to the publisher. This transfer will ensure the widest possible dissemination of information.

Information for Authors. Papers in English, French and German are published. There are no page charges. Manuscripts should conform in layout and style to the papers published in this Volume. Authors should consult Vol. 150/2 for detailed information. Reprints of this information are available from the Editors or from: Elsevier Editor Services Ltd., Mayfield House, 256 Banbury Road, Oxford OX2 7DH (Great Britain).

Reprints. Fifty reprints will be supplied free of charge. Additional reprints (minimum 100) can be ordered. An order form containing price quotations will be sent to the authors together with the proofs of their article.

Advertisements. Advertisement rates are available from the publisher.

Subscriptions. Subscriptions should be sent to: Elsevier Science Publishers B.V., Journals Department, P.O. Box 211, 1000 AE Amsterdam, The Netherlands. Tel: 5803 911, Telex: 18582.

Publication. *Analytica Chimica Acta* appears in 11 volumes in 1984. The subscription for 1984 (Vols. 156–166) Dfl. 2145.00 plus Dfl. 231.00 (p.p.h.) (total approx. U.S. \$950.40). All earlier volumes (Vols. 1–155) except Vols. 1 and 28 are available at Dfl. 215.00 (U.S. \$82.70), plus Dfl. 15.00 (U.S. \$6.00) p.p.h., per volume.

Our p.p.h. (postage, packing and handling) charge includes surface delivery of all issues, except to subscribers in Australia, Brazil, Canada, China, Hong Kong, India, Israel, Japan, Malaysia, New Zealand, Pakistan, Singapore, South Africa, South Korea, Taiwan and the U.S.A. who receive all issues by air delivery (S.A.L. — Surface Air Lifted) at an extra cost. For the rest of the world, airmail and S.A.L. charges are available upon request.

Claims for issues not received should be made within three months of publication of the issues. If not they cannot be honoured free of charge.

For further information, or a free sample copy of this or any other Elsevier Science Publishers journal, readers in the U.S.A. and Canada can contact the following address: Elsevier Science Publishing Co., Inc., Journal Information Center, 52 Vanderbilt Avenue, New York, NY 10017, U.S.A., Tel: (212) 867-9040.

ANALYTICA CHIMICA ACTA
VOL. 159 (1984)

ANALYTICA CHIMICA ACTA

International journal devoted to all branches of analytical chemistry

EDITORS

A. M. G. MACDONALD (Birmingham, Great Britain)

HARRY L. PARDUE (West Lafayette, IN, U.S.A.)

ALAN TOWNSHEND (Hull, Great Britain)

J. T. CLERC (Bern, Switzerland)

Editorial Advisers

F. C. Adams, Antwerp
H. Bergamin F^o, Piracicaba
G. den Boef, Amsterdam
A. M. Bond, Waurin Ponds
D. Dyrssen, Göteborg
J. W. Frazer, Livermore, CA
S. Gomisček, Ljubljana
S. R. Heller, Bethesda, MD
G. M. Hieftje, Bloomington, IN
J. Hoste, Ghent
A. Hulanicki, Warsaw
G. Johansson, Lund
D. C. Johnson, Ames, IA
P. C. Jurs, University Park, PA
D. E. Leyden, Fort Collins, CO
F. E. Lytle, West Lafayette, IN
H. Malissa, Vienna
D. L. Massart, Brussels
A. Mizuike, Nagoya
E. Pungor, Budapest

W. C. Purdy, Montreal
J. P. Riley, Liverpool
J. Růžička, Copenhagen
D. E. Ryan, Halifax, N.S.
S. Sasaki, Toyohashi
J. Savory, Charlottesville, VA
W. D. Shults, Oak Ridge, TN
H. C. Smit, Amsterdam
W. I. Stephen, Birmingham
G. Tölg, Schwäbisch Gmünd, B.R.D.
B. Trémillon, Paris
W. E. van der Linden, Enschede
A. Walsh, Melbourne
H. Weisz, Freiburg i. Br.
P. W. West, Baton Rouge, LA
T. S. West, Aberdeen
J. B. Willis, Melbourne
E. Ziegler, Mülheim
Yu. A. Zolotov, Moscow



ELSEVIER Amsterdam—Oxford—New York—Tokyo

Anal. Chim. Acta, Vol. 159 (1984)

ห้องสมุดกรมวิทยาศาสตร์บริการ
-3. ต.ค. 2527

All rights reserved. No part of this publication may be reproduced, stored in a retrieval system or transmitted in any form or by any means, electronic, mechanical, photocopying, recording or otherwise, without the prior written permission of the publisher, Elsevier Science Publishers B.V., P.O. Box 330, 1000 AH Amsterdam, The Netherlands. Upon acceptance of an article by the journal, the author(s) will be asked to transfer copyright of the article to the publisher. The transfer will ensure the widest possible dissemination of information.

Submission of an article for publication entails the author(s) irrevocable and exclusive authorization of the publisher to collect any sums or considerations for copying or reproduction payable by third parties (as mentioned in article 17 paragraph 2 of the Dutch Copyright Act of 1912 and in the Royal Decree of June 20, 1974 (S. 351) pursuant to article 16b of the Dutch Copyright Act of 1912) and/or to act in or out of Court in connection therewith.

Special regulations for readers in the U.S.A. — This journal has been registered with the Copyright Clearance Center, Inc. Consent is given for copying of articles for personal or internal use, or for the personal use of specific clients. This consent is given on the condition that the copier pays through the Center the per-copy fee for copying beyond that permitted by Sections 107 or 108 of the U.S. Copyright Law. The per-copy fee is stated in the code-line at the bottom of the first page of each article. The appropriate fee, together with a copy of the first page of the article, should be forwarded to the Copyright Clearance Center, Inc., 21 Congress Street, Salem, MA 01970, U.S.A. If no code-line appears, broad consent to copy has not been given and permission to copy must be obtained directly from the author(s). All articles published prior to 1980 may be copied for a per-copy fee of US \$ 2.25, also payable through the Center. This consent does not extend to other kinds of copying, such as for general distribution, resale, advertising and promotion purposes, or for creating new collective works. Special written permission must be obtained from the publisher for such copying.

Review

THEORY AND APPLICATIONS OF ION-SELECTIVE ELECTRODES Part 5^a

JIŘÍ KORYTA

J. Heyrovský Institute of Physical Chemistry and Electrochemistry, Czechoslovak Academy of Sciences, Opletalova 25, CS-110 00 Prague 1 (Czechoslovakia)

(Received 4th October 1983)

SUMMARY

This review of ion-selective electrodes is arranged in the same way as earlier reviews in this series. The whole subject is steadily growing. More attention has been given to automatic methods of analysis with ion-selective electrodes, electrolysis at the interface of two immiscible electrolyte solutions, and to ion-selective field-effect transistors. The number of publications on traditional subjects like fluoride ion-selective electrodes has dropped. About 700 papers published between Spring 1981 and Spring 1983 are mentioned.

CONTENTS

Theory of membrane phenomena at ion-selective electrodes	3
Technology of ion-selective electrodes	7
Construction of ion-selective electrodes	7
Calibration, selectivity and detection limit	9
Response time	9
Measuring procedures	9
Automatic procedures	10
Ion-selective electrodes in non-aqueous media	12
Ion-selective field-effect transistors	12
Electrolysis at the interface of two immiscible electrolyte solutions (ITIES)	12
Miscellaneous	13
Fixed-site ion-selective electrodes	14
Silver halide electrodes and similar systems	14
Silver sulfide ion-selective electrodes	17
Divalent metal chalcogenide electrodes	18
Fluoride ion-selective electrodes	20
Other systems	21
Liquid-membrane ion-selective electrodes	21
Calcium-selective electrodes	21
Nitrate-selective electrodes	24

^aFor Part 4 see ref. 1.

Potassium-selective electrodes	24
Sodium and similar electrodes	25
Other systems based on ionized ion-exchangers	26
Other systems based on neutral ligands	27
Potentiometric biosensors	29
Miscellaneous	29

Since 1978, the rate of publications on ion-selective electrodes has been characterized by a steady growth of about 350–400 publications per year. For the period considered now, the number of publications has been fairly typical with regard to papers on automatic methods of analysis with ion-selective electrodes, on ion-selective field-effect transistors, and on the voltammetric version of ion-selective electrode potentiometry, electrolysis at the interface of two immiscible electrolyte solutions. In contrast, traditional subjects such as the use of the fluoride electrode in environmental analysis have become a matter of routine and the number of publications has decreased.

Part 1 of this series of reviews on Theory and Applications of Ion-selective Electrodes [1] covered the literature to the beginning of 1972. In addition to the general theory of membrane potentials of various types, the theory of the potential of ion-selective electrodes and a survey of applications of non-glass ion-selective electrodes, Part 1 also included the theory of the glass electrode and dealt in some detail with the general properties of ion-carriers. The subject matter of Part 2 [1], which covered about 1200 papers published before mid-1976, was restricted to non-glass membrane systems (with exception of chalcogenide glasses). Part 3 [1] dealt with more than 800 papers published to the end of 1978. Part 4 [1] covered about two and a half years (from the end of 1978 to the beginning of 1981) and was concerned with about 800 papers from this period. The present review covers about two years (from Spring 1981 to Spring 1983) and deals with about 700 papers from this period. The subject is treated in an order similar to that used previously. First, progress in theory is dealt with, then problems of methodology are discussed, and finally new information on the basic properties of various types of electrodes, together with their analytical application, is reviewed.

Between Spring 1981 and Spring 1983 several books as well as numerous reviews were published [1–87]. A monograph on Applications of Ion-selective Microelectrodes [2] was edited by Zeuthen. The Russian version of Cammann's book appeared in 1980 [3] and Cosofret and Thomas wrote the book, Membrane Electrodes in Drug-Substances Analysis [3a]. The monograph on Chemically Sensitive Electronic Devices [4] deals mainly with ion-selective electrodes and similar systems. Koryta and Štulík [6] published the 2nd edition of Ion-selective Electrodes. Perhaps not a favourite field of ion-selective electrode application, organic analysis has become subject of another monograph, now a two-volume work by Ma and Hassan [7]. Morf summarized his excellent work in The Principles of Ion-selective Electrodes and of Membrane Transport [8]. Progress in Enzyme

and Ion-Selective Electrodes was edited by Lübbers, Acker, Buck, Eisenman, Kessler and Simon [9]. Flow-injection Analysis by Růžička and Hansen [10] and Marine Electrochemistry, A Practical Introduction, edited by Whitfield and Jagner, contains important chapters on ion-selective electrodes [11]. Orion Research published their Handbook of Electrode Technology [11a].

Three new volumes of Ion-Selective Electrode Reviews were published [12]. A number of general, mainly analytically orientated, reviews were published [13–30]. The specialized reviews are listed in Table 1.

A bibliography on ion-selective electrodes has been published periodically [88, 89]. A computer data base on ion-selective electrodes has been built [90]; its general construction is outlined in Table 2. A detailed compilation of selectivity coefficients has been published [90a].

THEORY OF MEMBRANE PHENOMENA AT ION-SELECTIVE ELECTRODES

Numerous attempts have been made to elucidate basic phenomena occurring at the membranes of ion-selective electrodes [34, 35, 66, 82, 91–118].

TABLE 1

Specialized reviews on ion-selective electrodes

Subject	Reference	Subject	Reference
Neutral carrier-based electrodes	31, 31a, 79	Tobacco analysis by ion-selective electrodes	59
Biosensors	46, 60, 81, 74, 84	Feed analysis by ion-selective electrodes	61
Surfactant ion-selective electrodes	33, 58	Detection limit	62, 70
Impedance method for ion-selective electrode investigation	32	Linear response characteristics	63
Theory	35, 82	Crown ether-based ion-selective electrodes	64, 78, 87
Ion-selective electrodes in microbial process control	36	Selectivity of ion-selective electrodes	65
Solid membranes of inorganic ion-exchangers	37	Mechanistic studies with radiotracers	66
Reference electrodes and liquid-junction effects	37a	Ion-selective electrodes in clinical chemistry	39, 67, 80, 81
Ion-selective electrodes in marine chemistry	38, 49	In vivo drug monitoring with ion-selective electrodes	69
Ion-selective electrodes in blood analysis	40, 77	Automated analysis with ion-selective electrodes	71
Ion-selective electrodes in water analysis	41, 47, 48	Ion-selective electrodes in pharmaceutical analysis	72
Ion-selective microelectrodes	42, 44, 55, 68, 85	Ion-selective electrodes in industrial analysis	75
Gas-sensitive electrodes	45	Analysis with quaternary ammonium halides	76
Ion-selective electrodes in enzymology	46, 67	Biological applications of ion-selective electrodes	80, 81
Solvent effects	50	Solid-state ion-selective electrodes	86
Ion-selective electrodes in soil analysis	51	Ion-selective electrodes in ion-association study	42a
Electrolysis at the interface of two immiscible electrolyte solutions (ITIES)	52, 53, 54		
ISFET	43, 56		
Response-time problems	57, 83		
Surfactant ion-selective electrodes	58		

TABLE 2

Outline of the ISES data base with COOD as DBMS [90]

 DATABASE ISES: Ion Selective Electrodes and Electrochemical Sensors

TABLE LISES: Literature on Ion Selective Electrodes and Sensors

NO	(I5)UNIQUE: Serial number
CANO	(A15): Chemical Abstracts No; Volume(Issue):No
AUTHOR	(A25): Author(s)
TITLE(4)	(A72): Title
JOURNAL	(A70): Name of journal
CODEN	(A6): CODEN
YEAR	(I4): Year of publication
VOL	(I4): Number of volume
PAGE(RANGE)	(I4): Page(s)
ADDRESS(2)	(A72): Address of author to communicate
KEY(5)	(A72): Keyword phrases
REMARK(2)	(A72): Remark(s); Literature code(LC)
DATNO(RANGE)	(I5): Number(s) of data table; INISES-No
DATE	(I6): Date of last updating

TABLE INISES: Investigations on or with Ion Selective Electrodes and Sensors

NO	(I5)UNIQUE: Serial number
PURPOSE	(A50): Purpose of investigation
ION	(A30): Primary ion(I) or molecule
FORM(2)	(A15): Chemical formula & functional group; Denote I+-n for inorg ion
SAMPLE(2)	(A50): Sample(s) for measurement
METHOD	(A50): Method or technique
ELECT(2)	(A72): Electrode or sensor used; Name of commercial electrode
MEMBRANE(2)	(A72): Membrane compositions; Active material, Solvent, Matrix
TITRANT	(A50): Titrant for titration
RANGE(RANGE)	(J8): Range available after normalization (M)
LINEAR(RANGE)	(J8): Linear response range (M)
PRETREAT(2)	(A72): Chemical pretreatment and membrane conditioning
INTERFER	(A70): Major interfering substances
JION	(A30): Interfering ion(J); Denote J+-z for inorg ion
LOGK	(J8): Logarithmic selectivity coefficient; $\log K(i/j)$
COND(3)	(A72): Exptl. conditions for $K(i/j)$; Method, $C(i) \& C(j)$ and Eq used
NOTE(2)	(A72): Notes; Slope(S), Response speed(RS), Lifetime(LT), Drift(D)
LITNO	(I5): Number of literature table; LISES-No
CLASS	(A8): Classification code of electrode or sensor
COMPILER	(A25): Compiler(s)

Thermodynamics

The potential difference between the electrolyte solution and the region inside a liquid membrane close to the interface (or a potential difference established at an ITIES, the interface between two immiscible electrolyte solutions) is a kind of a distribution potential [103a]. A general theory of the distribution potential with a number of practical examples has been worked out by Hung [98], who later gave a more sophisticated treatment. This theory includes distribution equilibria in which an arbitrary number of free ions, ion-pairs and complexes participate [99].

Bates [92] worked out a thermodynamic theory of ion-selective electrode behavior in the presence of a weak base in the analyte and proposed a method for activity coefficient determinations.

Electric double layer

The basic paper concerning the structure of the double layer at an ITIES was published in 1939 by Verwey and Niessen [118]. They assumed that the

overall potential difference at an ITIES is situated in two diffuse double layers with no compact layer between them (a detailed discussion was given in Part 4). Samec et al. [116] arrived at the same conclusion, when the differential capacity/potential curves measured by the impedance method were close to those calculated on the basis of the Gouy—Chapman theory. However, Kakiuchi and Senda [103] found on the basis of their measurements at higher electrolyte concentrations that a significant potential difference exists at the water/nitrobenzene interface. They assumed that the compact layer is a low permittivity region consisting of two monolayers, one of water and the other of nitrobenzene molecules, aligned perpendicularly to the interface.

The surface-charge density/potential curves obtained by integration of differential capacity/potential curves [112] and by differentiation of interfacial tension/potential curves [102] are identical, which proves the sound basis of electrocapillary phenomena at the ITIES (Fig. 1).

Transport processes

Ion and ligand fluxes in liquid membranes have been discussed in detail in the reviews by Stefanova and Shultz [82] and by Morf [111]. The parameters of the Sandblom—Eisenman—Walker equation have been determined by the mixed-electrolyte method [110]. The chronopotentiometric curves at ITIES have been simulated for cases without and with a base electrolyte by Buck et al. [106—109]. Convolution analysis of potential-sweep voltammetric curves at ITIES has been studied by Samec et al. [117].

Mixed-potential approach to the theory of ion-selective electrode potential

The analogy between an ion-selective electrode and a corroding metallic electrode has been discussed in Part 3, pp. 5; 10—13. The voltammetric

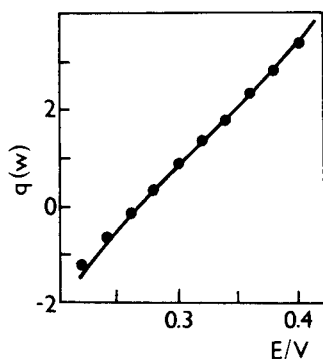


Fig. 1. Comparison of surface charge densities at the aqueous side of the interface obtained from the differentiation of the interfacial tension/potential curve (●) and from the integration of the differential capacity/potential curve (—) for the interface between aqueous 0.1 M LiCl and 0.1 M tetrabutylammonium tetraphenylborate in nitrobenzene. From [102].

approach to the interpretation of ion-selective electrode potentials based on this idea was exploited experimentally by Fujinaga et al. [95]. Their voltammetric curves at water/nitrobenzene interfaces were obtained with current-scan polarography and an electrolyte dropping electrode. On the basis of linear-sweep voltammetry at water/nitrobenzene interfaces, Samec et al. [115] determined the selectivity parameters for two calcium carriers and compared them with those obtained with calcium ion-selective electrodes with *o*-nitrophenyloctyl ether as membrane solvent; they achieved reasonable qualitative agreement. Ilyushenko and Mirkin [100, 101] also used the mixed-potential treatment of ion-selective electrodes. In contrast to systems without amphipathic surfactants, the processes at ITIES in their presence are inhibited, particularly at low temperatures, as shown by voltammetry at an ITIES in the presence of lecithin [104]. This effect may be also expected to appear in the behavior of ion-selective electrodes in the presence of surfactants.

Experimental methods

Faradaic impedance studies of liquid membranes have been reviewed by Buck [34]. Ahmad-Bitar et al. [91] have studied the impedance behavior of poly(vinyl chloride) membrane ion-selective electrodes; they found two components of the impedance, one corresponding to transport in the bulk and the other to the Warburg impedance at an ITIES. Obviously, the study of complete membranes is complicated, because processes at two interfaces and in the bulk of the membrane have to be taken into account; thus, whenever possible, investigations at an ITIES only should be preferred. Even more complicated for theoretical treatment seems to be the bipolar pulse conductometric monitoring used for studies of calcium and fluoride ion-selective electrodes [113, 114]. Impedance measurements have been used in ITIES capacity studies [112, 116].

Doyle et al. [93, 94] have studied penetration of ions into poly(vinyl chloride) matrices of ion-selective electrodes. Thus, in the case of membranes containing metal complexes of a nonylphenoxypoly(ethyleneoxy)-ethanol, the permeation of ^{133}Ba and ^{45}Ca is slow while that of ^{36}Cl is nil, indicating the permselectivity of the membrane. The application of the radiotracer method to ion-selective electrode study has been reviewed by Nikolskii et al. [66].

Electric charge conduction of polymer membranes

Higachi et al. (see Part 1) described an ion-selective membrane electrode containing no imbedded ion-exchanger ions which responded to hydrophobic cations. Using a plastic electrode incorporating a poly(vinyl chloride)-dioctylphthalate membrane, Luch et al. [105] have recently shown that the membrane can transmit the hydrophobic cations because of the presence of combined negative sites (at a concentration of about $50 \mu\text{mol dm}^{-3}$) in the molecules of the plasticizer, dioctylphthalate (cf. Kedem et al. and Perry et al., Part 3, p. 8).

Biosensors

Hameka and Rechnitz [96, 97] have worked out a theory of a biocatalytic membrane electrode, accounting for the diffusion of the measured species from the aqueous solution into the enzyme layer where its diffusion coefficient is changed and where it is transformed to an electroactive product by a chemical reaction obeying Michaelis–Menten kinetics. The transient as well as the steady state were discussed.

TECHNOLOGY OF ION-SELECTIVE ELECTRODES

Relatively, the technology of ion-selective electrodes has been the most investigated subject in the whole field [43, 50, 52–54, 56, 57, 62, 95, 102–104, 106–109, 112, 115–117, 119–265].

Construction of ion-selective electrodes

Many papers have dealt with the construction of ion-selective electrodes [133, 138, 139, 144, 145, 154, 155, 161, 166, 167, 172, 176, 187, 187a, 199, 200, 203–205, 212, 215, 217, 222, 227, 231, 232, 246, 247, 254, 264].

Ion-selective polymer-membrane electrodes with covalently-bound active sites (see Part 4) have been further studied [133, 144, 154, 155, 176, 215, 222]. A scheme of immobilization of organophosphate groups [144] to a triblock copolymer is shown in Fig. 2. The grafting of the organophosphate group to other polymer matrices has also been discussed [176]. A chloride ion-selective electrode based on plasticized polystyrene films with covalently-bound quaternary ammonium groups has been designed [222]. A potas-

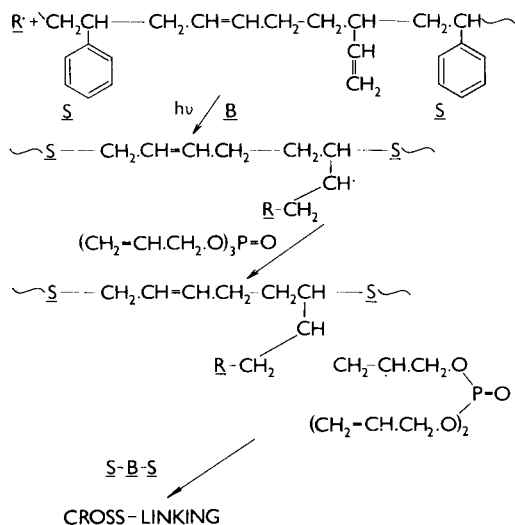


Fig. 2. A scheme of immobilization of phosphate groups in a styrene–butadiene–styrene (S–B–S) triblock copolymer [155].

sium ion-selective electrode based on the ionic polymer Nafion 120, has been suggested [215].

Various liquid-membrane anion-selective electrodes based on an epoxy matrix have been constructed [187, 187a, 246, 247]. Conductive silver-epoxy has been used as a support for heterogeneous-membrane ion-selective electrodes [203–205] (see also [161]). The effect of plasticizer on the selectivity of a potassium ion-selective electrode based on a crown ether in a PVC membrane has been investigated [138].

A substance like octadecanol which solidifies at room temperature can be used with advantage as liquid-membrane solvent [172]. A *p*-toluenesulfonate ion-selective electrode of this type shows good performance in comparison with an electrode based on 1-decanol, though the selectivities towards anions are different.

A sodium electrode based on cation/proton counter-transport has been constructed [167].

Several papers [139, 199, 200, 217] are concerned with various constructions of liquid-membrane ion-selective microelectrodes. The problems of ion-selective electrodes with a metallic internal contact (i.e., without an internal reference electrode) were discussed in Part 4. In the case of liquid-membrane electrodes, such a contact shows a mixed potential dependence on oxygen concentration [232]. Therefore, it is not surprising that the ion-selective electrode potential depends on the condition of the surface of the internal platinum contact [212, 254]. The best solution seems to be to use a second-kind electrode, based, for example, on Ag/AgCl with Harvard cement [232].

In a comparative study of different air-gap electrodes for cyanide, the sensor shown in Fig. 3 was used [161]. In the presence of a small volume of a dicyanoargentate(I) solution, sensors based on silver or silver sulfide electrodes show a “double-Nernstian” response ($2 \times 2.3 RT/F$ slope) whereas those based on silver iodide electrodes show the normal Nernstian behavior.

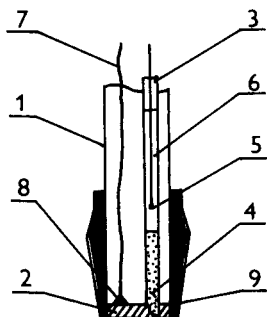


Fig. 3. A cyanide sensor [161]. (1) glass tube; (2) disc pellet of ion-selective material with a hole; (3) narrow glass tube; (4) 1 M KCl solution immobilized with agar-agar; (5) Ag/AgCl reference electrode; (6) 1 M KCl; (7) silver wire; (8) silver epoxy; (9) ground glass joint. The electrolyte layer on the disc is formed by touching it with a sponge saturated with the $\text{Ag}(\text{CN}_2)^-$ -containing solution.

Multipurpose ion-selective catheter electrodes have been constructed [234]. Ion-selective electrolyte slides have been designed for multilayer film analysis [145]. A teflon-graphite ion-selective probe has been equipped with integrated electronics [218]. A housing for liquid ion-selective electrodes has been described [264]. A redox reference electrode has been suggested [227]. A system for trigger voltage impact on an ion-selective electrode has been described [166].

Calibration, selectivity and detection limit

Various aspects have been discussed [62, 126, 151, 180–183, 223, 239, 256, 258]. Dynamic calibration and memory effects of ion-selective electrodes have been described [258]. A procedure for calibration of ion-selective electrodes at elevated temperatures has been suggested [151]. Detection limits of ion-selective electrodes have been discussed [62, 126].

Some papers have been devoted to selectivity problems [180, 223], particularly those of solid-membrane ion-selective electrodes [181, 182]. A method for calculation of the concentration dependence of the selectivity coefficient has been suggested [239]. The effect of surfactants on the response of ion-selective electrodes with poly(vinyl chloride) membranes has been described [183].

Single ion activities at high ionic strengths have been determined and discussed [256].

Response time

A thorough analysis, described in a series of papers [206–209], has been made of the response times of precipitate-based ion-selective electrodes. The general problems of the definition [255] and of interpretation of the response time [57, 250] have been discussed. Rather short response times have been measured for solid-state ion-selective electrodes with integrated electronics [220]. Response time curves for an ammonium ion-selective electrode have been presented [152].

Response times of micro ion-selective field-effect transistors have been studied with a flow-injection system [171]. Obviously, these devices are sufficiently fast for studies of intracellular processes on the time scale of seconds.

Measuring procedures

Measuring procedures have received considerable attention [122, 129, 137, 153, 156, 158, 179, 210, 216, 228, 237, 240, 249, 253, 257, 260–263, 265].

Flow-injection analysis with ISFETs has been described [228]. A flow-injection analyzer with a multiple ion-selective electrode detector has been designed [260]. The limitations of linear response in flow-injection analysis with ion-selective electrodes have been discussed [253].

A method for rapid-flow continuous analysis with ion-selective electrodes has been suggested [122].

Ion-selective electrodes have been used for high-precision on-line measurements [257]. A high-volume flow-through cell has been designed for this purpose [129]. A review has been published [251].

The conditions for double standard addition [210] and multiple standard addition [240] methods for ion-selective electrode potentiometry have been discussed. An improved standard addition method has been suggested [216].

Differential potentiometry for end-point detection in complexometric titrations with ion-selective electrodes [153] and a continuous differential potentiometry with a single ion-selective electrode [262] have been described. The determination of the equivalence point in potentiometric titrations with ion-selective electrodes has been discussed [237].

A Monte-Carlo simulation has helped to elucidate the error propagation in the double known-addition method with ion-selective electrodes [156]. An error equation for a single increment in ion-selective electrode potentiometry has been derived [265].

Various aids have been suggested for measurements with ion-selective electrodes, e.g., a multi-increment nomograph for determination of ion activities [137], an isopotential adjuster [158], an antilog converter [262a, 263] and an antilog amplifier [179] have been suggested.

"Lime potentials" of soils have been measured directly by means of two ion-selective electrodes [261]. A thorough study of the determination of thermodynamic ionization constants of weak bases with ion-selective electrodes has been reported [249].

Automatic procedures

Great attention has been given to automatic measurements with ion-selective electrodes [39, 119, 123–125, 127, 128, 132, 135, 140, 142, 143, 146, 148–150, 157, 160, 162–165, 170, 173, 174, 186, 192, 193, 197, 198, 201, 202, 224, 224a, 225, 233–235, 241, 243–245, 251, 252]. There are four main themes in this work: construction of automatic analyzers for biomedical purposes; the accuracy and reliability of automatic sodium and potassium determinations in blood, serum and urine; ion-selective electrodes as chromatographic detectors; and other automatic systems.

Biomedical automatic analyzers based on ion-selective electrodes. [119, 123, 125, 135, 140, 146, 157, 162, 163, 165, 186, 197, 202, 224, 233, 234]. Electrolyte determinations represent about 20% of clinical routine analysis [197], so that automation of the analytical procedure is of primary importance.

The Nova-1 ion-selective electrode analyzer for sodium and potassium determination has been evaluated [123]; and the Nova-1A-5 analyzer (Nova Biomedical) has been introduced. After the original Astra-8 ion-analyzer, Beckman Corporation introduced the Electrolyte-2 Analyzer [165, 186] and E4A System. The Technicon SMAC system has been adapted

for blood plasma [224]. Before the time span of this review, the commercial electrolyte analyzers in use were the Orion SS-30, Stat-Ion (Technicon), Stat/Lyte C-800 (Technicon), ACA (DuPont), Corning 902 (Corning), Hitachi 705 (Clinicon), IL 502 (Instrumentation Laboratory) and Microlyte (KONEOY) models. An automated system for K^+ , Na^+ , Ca^{2+} and Cl^- determinations in blood and serum has been described [119]. A flow-optimized multipurpose system for ion-selective electrode measurements for blood analysis has been developed [233, 234]. A multichannel electrochemical centrifugal analyzer has been designed [140]. Other analyzers have been discussed [135, 146, 157, 162, 163, 202].

The accuracy and reliability of sodium and potassium determination in blood, serum and urine. [39, 124, 125, 127, 132, 135, 142, 143, 146, 148–150, 157, 160, 162–164, 173, 174, 193, 197, 198, 201, 202, 224a, 225, 235, 241]. First, it should be noted that most clinical chemists term potentiometric determinations in the undiluted samples (blood, plasma, etc.) as “direct” method while potentiometry of diluted samples is termed “indirect”. On the whole, the results of sodium and potassium measurements by automated potentiometry of undiluted samples seem to be higher than those obtained by flame photometry whereas there is little difference between the data of “indirect” potentiometry and flame photometry [124, 149, 160, 197, 198, 224a, 225] (see also Part 4, p. 13). The cause of this discrepancy is that what is measured in direct potentiometry is sodium activity in blood serum whereas the data of flame photometry refer to whole blood [125]. The binding of sodium by serum represents only 1% of its total content [193]. In fact, the activity of sodium and potassium in undiluted samples may be physiologically more significant than the total content of sodium and potassium. For comparative studies, the changing contents of lipids and proteins [201], the activity coefficients, any complex formation with anions like hydrogen carbonate and liquid-junction effects [142, 142a, 143, 148, 150] have to be taken into account; the influence of erythrocytes on liquid-junction potentials has been discussed [127]. The sodium drift observed with Astra-8 Analyzer is due to the wash solution [235]. The ion-selective electrode potential of blood serum controls may be influenced by ethylene glycol present in the standard [241]. A small lithium effect on sodium determinations has been discussed [174]. Finally, the potentiometric analysis of Na^+ and K^+ in blood and serum has been recommended for clinical routine [197, 225].

For Na^+ and K^+ determination in urine, good agreement has been found between potentiometry and flame photometry [132]. The influence of the potassium content on sodium data obtained with the Beckman Electrolyte-2 Analyzer is apparently due to transient phenomena at the sodium-glass electrode surface [173].

A workshop on direct potentiometric measurements in blood was held at the National Bureau of Standards in May 1983; the meeting was cosponsored by the National Measurement Laboratory Center for Analytical Chemistry and the National Committee for Clinical Laboratory Standards. The aim was

to establish a working basis for the standardization of measurement techniques, nomenclature and symbols [39].

Other automatic systems. [170, 192, 252]. A multiple potentiometric system for the continuous determination of chloride, fluoride, nitrate and ammonia in natural waters has been constructed [252]. An automated computer-controlled device for ion determination with ion-selective electrodes has been designed [192]. A microcomputer-based system for potentiometric titrations of fluoride has been built [170].

Chromatographic detectors based on ion-selective electrodes. [128, 243–246]. The electrochemical detectors used in high-performance liquid chromatography have been reviewed [244, 245]. Simultaneous determinations of free sulfide and cyanide [128] and bromide and fluoride [243] by means of ion chromatography with ion-selective electrodes as detectors have been described. An epoxy membrane electrode has been suggested as a detector for ion chromatography [246].

Ion-selective electrodes in non-aqueous media

The effect of organic solvents on ion-selective electrode potential has been studied [50, 136]. The shift of the potential in a mixed solvent has been utilized for determining the content of the organic solvent [188, 189].

A fluoride ion-selective electrode has been used for fluoride activity measurement in low-melting, fused-salt systems [178]. A teflon double-junction reference electrode has been designed for investigations in organic solvents [141].

Ion-selective electrodes have been applied in the determination of ionization constants of weak bases in D_2O [226].

Ion-selective field effect transistors

The development of this field has continued [43, 56, 120, 121, 131, 134, 147, 171, 221, 228, 242, 248]. Besides two general papers [43, 56] and a treatment of the theory [131], ISFETs were described for phenobarbital anion [147], penicillin [134], sodium and ammonium ions [221] and fluoride (for titrations) [120].

An ISFET based on silicon-on-sapphire [121] and an ISFET reference electrode [248] have been constructed.

On-line measurement of potassium ions in blood by an ISFET has been reported [242]. A flow-injection system based on ISFETs has been designed for discrete and continuous assays [228]. Response times of micro-ISFETs has been determined in a flow-injection system [171].

Electrolysis at the interface of two immiscible electrolyte solutions (ITIES)

Several groups concerned with electrolysis at ITIES have reported their results obtained with this voltammetric analogy of ion-selective electrode potentiometry [52–54, 95, 102–104, 104a, 106–109, 112, 115–117, 159, 168, 169a, 177, 184, 185, 190, 191, 193a, 194–196, 213, 214, 219, 229,

230, 238, 259]. Some of these papers are of general character [52–54] or deal with the theory [95, 102, 103, 106–109, 116], but the others are concerned primarily with instrumentation and simple or facilitated ion transfer across ITIES.

Instrumentation

[95, 102, 112, 159, 185, 190, 191, 213, 214, 219, 238]. Designs of four-electrode potentiostats [159, 238], of a galvanostat [219] and of a circuit for ohmic drop compensation [185] have been described for electrolysis at ITIES. A stationary electrolyte drop electrode for accumulation of the species to be measured [213, 214] has been designed; this species is subsequently transferred across the ITIES in an analytical differential-pulse polarography mode. A current-scan polarography [95] (Fig. 4) and a chronoamperometric method [190] at ITIES have been described, as well as various a.c. methods [112, 116]. An electrolyte dropping electrode [95, 191] (cf. Part 4) has been reported. Not only nitrobenzene but also dichloroethane [168, 193a, 229] and dichloromethane [229] have been used as the organic solvent.

Simple ion transfer. [104, 168, 184, 193a, 196, 229, 230]. The transfer of cesium [168, 230], tetrabutyl- and tetramethyl-ammonium [193a], various tetracyclines [196], tris(2,2'-bipyridine)ruthenium and alkylviologen [229] cations, of nitrate, perchlorate and thiocyanate anions [184] and of electrons [230] across the ITIES has been studied. Ion transfer may be inhibited by an adsorbed phospholipid monolayer at the ITIES [104].

Facilitated ion transfer. [115, 169a, 177, 194, 195, 259]. In the presence of hydrophobic ligands (ionophores) in the organic phase, ion transfer can be facilitated. At low ligand concentrations, the current peaks in linear-sweep voltammetry are proportional to this concentration (see Part 4). The ionophores studied include crown polyethers [177], nonactin [177], valinomycin [259] and monensin (Fig. 5) [169a, 195]. The last-mentioned process could be utilized for the determination of monensin in culture extracts of *Streptomyces cinnamonensis* [195]. Determinations of antibiotics by means of voltammetry at ITIES has been reviewed [194].

Transfer of alkaline earth and alkali metals facilitated by neutral carriers (ETH 1001 and a cyclic polyether diamide) has been used to estimate selectivity coefficients of ion-selective electrodes based on these ligands [115].

Miscellaneous aspects of technology

The kinetic, static and stirring errors of liquid junctions to reference electrodes have been discussed [130]. On the basis of a thorough analysis, the reliability of calculations of liquid-junction potentials on the basis of the Henderson equation has been evaluated, at least for practically important cases [175]. The results of this treatment, of the Planck equation and of experiments were compared.

The valinomycin-based membranes show long-term stability, which has been proven by comparison of freshly prepared membranes with those prepared 2–10 years ago [169].

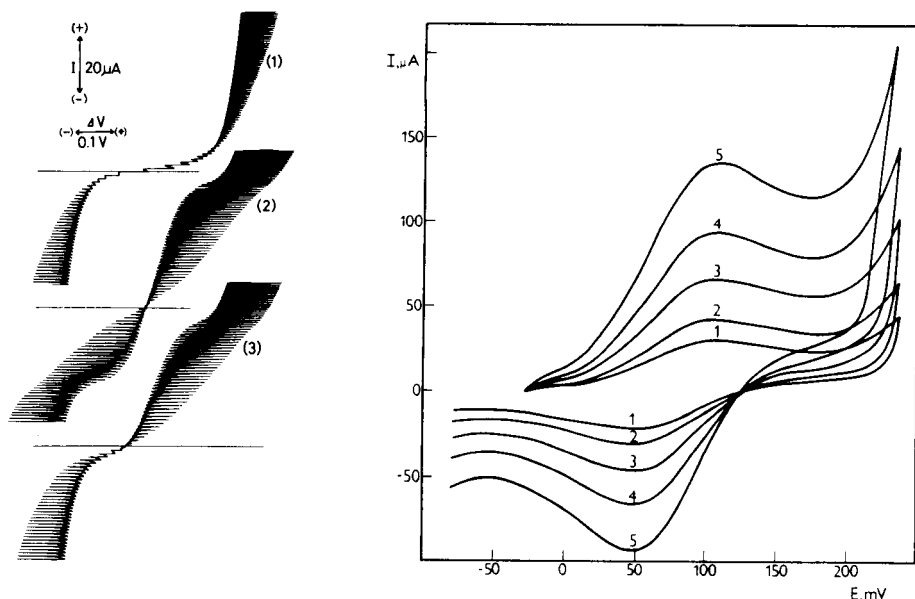


Fig. 4. Current-scan measurements of tetramethylammonium (TMA^+) cation at the aqueous electrolyte dropping electrode. Aqueous phase, 0.05 M $\text{LiCl} + 1 \text{ M MgSO}_4$; organic phase, 0.05 M tetrabutylammonium tetraphenylborate in nitrobenzene. Curves: (1) without TMA^+ ; (2) with 0.5 mM TMA^+ in each phase; (3) with 0.5 mM TMA^+ in the aqueous phase only [95].

Fig. 5. Potential-sweep voltammograms of monensin [169a]. Aqueous phase, 0.1 M HCl , 0.1 M NaNO_3 ; nitrobenzene phase, 0.01 M tetrabutylammonium tetraphenylborate, 1 mM monensin. Polarization rate (mV s^{-1}): (1) 5; (2) 10; (3) 25; (4) 50; (5) 100.

The influence of lowered temperatures on ion-selective electrode behavior has been described [211].

Potentiometric titrations of nitroform and perchlorate with cetylpyridinium chloride are possible with sensors which did not possess a typical selectivity for any of these ions [236]. Some success with this procedure claimed in the paper does not, however, prove its practical applicability.

FIXED-SITE ION-SELECTIVE ELECTRODES

As in Parts 2, 3 and 4 [1], all fixed site systems except the silicate glass electrodes are included in this section.

Silver halide electrodes and similar systems

The systems included here are the chloride, bromide, iodide, cyanide and thiocyanate ion-selective electrodes [266–328].

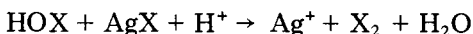
Halide-responsive electrodes have been used for the determination of halides in photographic emulsions [297], in rocks and soils [319] and of halogens bound in pharmaceuticals [313] and other organic substances

[281, 325]. Halide ion-selective electrodes have been constructed by using a conductive plastic as support [300]. Film electrodes for chloride, bromide and thiocyanate with a solid contact have been constructed [291].

A method for evaluation of equivalence points in potentiometric titration of halide mixtures has been suggested [277]. Simultaneous determination of bromide and chloride in natural waters by ion-exchange chromatography and direct potentiometry with ion-selective electrodes has been described [266].

Chloride- and bromide-selective electrodes based on silver halide/silver sulfide mixtures have been compared with the corresponding second-kind electrodes prepared by anodizing silver electrodes [294]. When the latter contain thick compact silver halide layers they show better resistance towards strong oxidizing agents.

The response of halide-selective electrodes to hypohalous acids has been studied in connection with the Belousov-Zhabotinsky oscillating reaction study [286, 304a, 305, 306] (cf. Parts 2–4). The hypohalous acid reacts with the membrane in the corroding reaction [276a]



The silver ions formed establish the potential of the ion-selective electrode. The balance of fluxes of HOX, Ag^+ and X_2 [305] has been calculated in an analogous way as in the theory of the cyanide-selective electrode (see Part 1). Figure 6 shows the calculated and experimental dependence for the response of the bromide-selective electrode to Ag^+ , Br^- and HOBr. The actions of the halous (HXO_2) and the halic ($\text{H}^+ + \text{XO}_3^-$) acid in the corroding process have also been studied [305].

Chloride-selective electrodes. Various applications of these electrodes

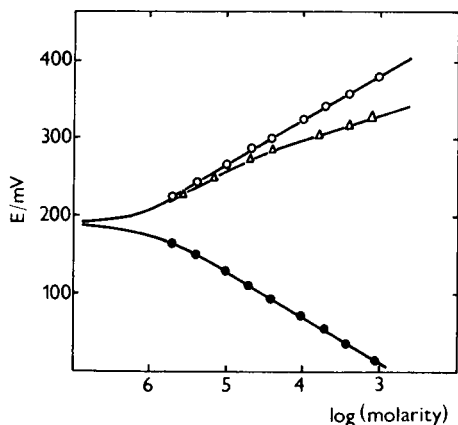


Fig. 6. Response of the bromide-selective electrode to the concentration of Ag^+ (\circ) and Br^- (\bullet) in 1.5 M H_2SO_4 and to the concentration of HOBr (\triangle) in 0.15 M H_2SO_4 . Full lines: theoretical curves. From [305].

are listed in Table 3. A film coverage in order to decrease bromide interference on the chloride-selective electrode has been suggested [284b]. The activity of hydrochloric acid has been measured by using the chloride-selective electrode [270, 271]. The stability of alkaline-earth metal complexes with fluoride at various temperatures [299] and of cobalt, nickel and zinc chloro complexes [284] has been determined by means of chloride-selective electrode measurements. The interferences in potentiometric determination of chlorides at the mg l^{-1} level have been studied [304].

The determination of chlorides in salted foodstuffs with a chloride-selective electrode and a dried-sample addition method has been compared with the titration method [280].

Bromide-selective electrode. This electrode has been used in the analysis of biochemical preparations and synthetic products [283]. Bromide impurities in potassium nitrate have been determined [275].

Iodide-selective electrodes. Diffusion of silver atoms in the solid electrolyte Ag_3SI and the conductivity of this membrane material have been studied [323]. Adsorption phenomena at the surface of the iodide-selective electrode have been investigated [290, 293]. An iodide-selective electrode supported with a graphite matrix has been prepared [310]. The preparation and evaluation of an iodide-selective electrode have been suggested as a student experiment [309].

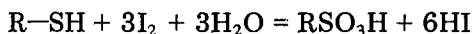
The iodide-selective electrode has been used for the determination of the consecutive formation constants of lead-iodide complexes and of the solubility product of lead iodide [279]. Traces of iodide in table salt have been determined by negative thermal ionization mass spectrometry and by ion-selective electrode potentiometry; agreement of the results was good [295].

TABLE 3

Applications of chloride-selective electrodes

Use	Reference
Chloride determinations	
in soils	268, 287
in waters	268, 278, 285, 296, 322, 324
in sweat	272
after PVC fires	274
in soluble salts (after preconcentration)	275
in concentrated H_2SO_4	276
in mineral waters	289
in cheese	292
in blood	303, 308, 317
in gas-chromatographic effluents	311
in rocks	320
in sea water	321
in amino-acid infusions	328

Microdeterminations of arsenic(III) ($0.1 \mu\text{g ml}^{-1}$) and of arsenic(V) after reduction are possible by iodimetric titration with an iodide-selective electrode for indication [282]. The iodide-selective electrode has been used in an indirect method for determination of sulfide in industrial waste waters after separation of sulfide as CdS [307]. Titrations of *N*-acetyl-L-cysteine, glutathione or D-penicillamine with silver ion and an iodide-selective indicator electrode [302] can be based on the reaction



Ethylmercaptan in natural gas can be determined after adsorption in a silver nitrate solution, precipitation of excess of silver with potassium iodide and coulometric back-titration of excess of iodide with the iodide-selective indicator electrode [288]. This electrode has also been used in potentiometric titrations of hydrazine and hydroxylamine in mixtures [301]; first, the sum of both is determined and then hydrazine is titrated after decomposition of hydroxylamine with nitric acid. Catalytic determinations of iron(III) and zirconium(IV) are based on their effects on the hydrogen peroxide/iodide reaction which is followed with an iodide-selective electrode [298].

Iodide-selective electrodes have also been used for direct potentiometric determinations of mercury(II) ions [269, 284a, 315, 318, 326]. Application of this electrode to determination of total residual chlorine in water has been evaluated [316] (cf. Part 3, p. 21).

Cyanide-selective electrode. A flow-injection method for cyanide determinations is possible with the cyanide-selective electrode [303]. Measurements of cyanides in waste waters from metal plating processes with this electrode are viable after separation by microdiffusion [267] or by distillation [314]. Cyanide ions in the presence of mercaptans have been determined with a cyanide-selective electrode after elimination of mercaptans by oxidation or distillation [273].

Other systems. The thiocyanate-selective electrode has been applied in sewage analysis [327]. Miscellaneous applications of the HgCl/HgS chloride-selective electrode have been described [312].

Silver sulfide ion-selective electrodes

Several papers have been devoted to sulfide-selective electrodes [329–346]. The ion and electron conductivity of β -Ag₂S and of samples saturated with silver has been measured [343, 344]. At an Ag₂S-membrane surface treated with alkaline ascorbic solutions, metallic silver has been detected by x-ray diffractometry [333].

A silver sulfide ion-selective electrode equipped with a printed circuit board has been described [339]. A silver sulfide electrode with a support based on a plastic with dispersed silver has been constructed [340]. A sensor consisting of a silver sulfide electrode and a pH glass reference electrode has been compared with a solid-state sensor based on a H₂S-sensitive semiconductor coating [332]; in acidic solution the sensor containing the ion-

selective electrode shows a better performance. A field electrode method for sulfide determination has been worked out [346].

Silver sulfide electrodes have been used for determinations of sulfide in environmental samples [345], in waters [330], in mineral raw materials [329] and in blood [338]. This electrode has also been applied in direct and titrimetric determination of sulfonamides [341] and in the titrimetric determination of dialkyldithiophosphates [334]. It can be used in analyses for silver in ores [342], and in measurements of the photosynthetic sulfide oxidation by *Chlorobium* [331]. Determinations of the disulfide (GSSH) and sulfhydryl (GSH) forms of glutathione and of glutathione reductase can be based on Ag_2S -electrode measurements [337]; GSSG is reduced to GSH by NADPH_2 in the presence of glutathione reductase and the Ag_2S -electrode responds to GSH (Fig. 7). The initial rate of GSSG reduction is a function of the glutathione reductase activity. As the Ag_2S -electrode also responds to rubeanic acid and to diethyldithiocarbamate, these species may also be used for titrations of mixtures of various heavy metals [335, 336]. For practical applications, of course, other methods are more advantageous.

Divalent metal chalcogenide electrodes

Significant work has appeared in this area [347–387]. Such ion-selective electrodes can also be viewed as electrodes of the third kind [365a].

Copper ion-selective electrodes. General papers on the construction and analytical evaluation of these electrodes have been published, see [358, 370, 379]. The detection limit of precipitate-based copper(II) ion-selective electrodes has been determined [382]. An attempt to decrease the detection limit has been made [354]. The response of the copper(II) ion-selective

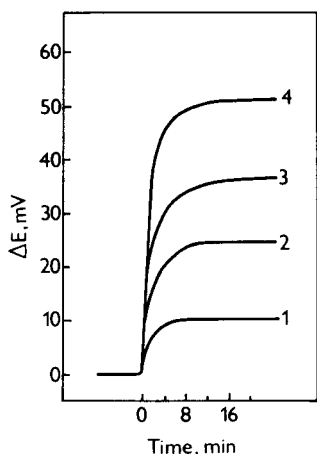


Fig. 7. Time-dependence of Ag_2S -electrode potential after addition of 1.2×10^{-5} M NADPH_2 to a mixture of glutathione reductase (1.4 IU) and different concentrations of GSSG at pH 8 and 25°C . GSSG: (1) 1.9×10^{-6} M; (2) 4.7×10^{-6} M; (3) 9.4×10^{-6} M; (4) 1.4×10^{-5} M. From [337].

electrode to mercury(II) [373], vanadate [367] and copper(I) [380] ions has been studied. The problems of the influence of chloride on the copper ion-selective electrode (cf. Parts 1 and 4) have been re-examined with non-stoichiometric electrodes [363--365]. The surface structure of the copper(II) ion-selective electrode has been studied by x-ray photoelectron spectroscopy [355] (cf. Part 4). The dissolution processes of the membrane have been investigated by anodic oxidation [359] and by cyclic voltammetry [349].

Calibration of copper(II) ion-selective electrode down to 10^{-19} M Cu^{2+} has been achieved in ethylenediamine metal buffers [348].

Copper ion-selective electrodes have been used for determinations of copper in zinc [347] and copper [383] plating baths, in waters [378] and in electrochemical reactors [384] and to determine fulvic acid [350]. Copper binding to serum albumin has also been studied with these electrodes [369]. The electrodes have been applied in the titrimetric assay of metallochromic dyes, such as calmagite, eriochrome blue black R, hydroxy naphthol blue, SNAZOXS, eriochrome blue SE, eriochrome black T, 1-(2-pyridylazo)-2-naphthol, methyl thymol blue, xylenol orange, alizarin complexone, tiron and thorin [366]. Some other titration methods based on this electrode have also been described [362, 375, 376].

Lead ion-selective electrode. The surface morphology of this electrode has been studied [371]. Studies by e.s.c.a. have proven the existence of a hydrated layer at the membrane surface [352, 386]. The adsorption and exchange reactions at the membrane have been investigated by radioactive tracers [353]. The effects of precipitating and complexing agents have also been studied [356].

The lead ion-selective electrode has been used for determinations of sulfate in magnesium oxide [360], of tungstate [385] and of the stability constants of iminodiacetic acid complexes with lead(II). A titrimetric determination of substituted catechols has also been proposed [377].

Cadmium ion-selective electrode. A cadmium ion-selective electrode has been prepared from various polycrystalline materials [351]. The response of the cadmium ion-selective electrode in the presence of complexing agents has been reported [372]. The influence of iron(III) ions on the electrode has been discussed [374]. The performance of the cadmium ion-selective electrode in metal buffers and the determination of stability constants of cadmium complexes has been described [387]. Titrations of nickel(II) with EDTA, in the presence of the Cd-EDTA complex so that a cadmium ion-selective indicator electrode could be used, has been reported [384]. Microamounts of americium can be determined by titration with DTPA using a cadmium ion-selective electrode [357]. Determination of nitrates can be based on their reduction by cadmium and titration of the Cd^{2+} formed [361].

Fluoride ion-selective electrode

As the applications of this ion-selective electrode are well established in several areas, the proportion of published papers on such topics has relatively decreased [178, 275, 278, 347–430]. The general properties of the fluoride electrode [348], the effect of pH [403] and the effect of adsorption, illumination and temperature [407] have been described. All-solid-state fluoride-selective electrodes have been described [395, 427] (cf. Part 4). The performance of the fluoride electrode in a flow-injection system has been described [420]. Bipolar pulse conductometric monitoring has been applied to this electrode [412].

Eleven buffers of the TISAB type have been examined [404–406]. The optimum buffer for fluoride determination in water was found to be TISAB III (M triammonium citrate), which contained 58 g of sodium chloride, 57 ml of anhydrous acetic acid, 243 g of triammonium citrate and 4 g of *trans*-1,2-diaminocyclohexanetetraacetic acid; both Al and Mg posed few interference problems. Another TISAB modification has also been suggested [413]. Rapid sample pretreatment by quinolin-8-ol removes aluminum ions before fluoride determination by ion-selective electrode [406]. Masking of Al(III), Ce(IV), Th(IV) and Zr(IV) can be achieved by nonylphenol ethoxylate [408].

Applications of the fluoride ion-selective electrode are listed in Table 4. Determination of fluoride in sodium chloride samples is based on preliminary separation by affinity chromatography with a zirconium(IV)-loaded cation exchange resin [401]. The electrode has been used for detection of fluorine-containing substances in air such as HF and hydrolyzed organophosphorus fluorides [393]. This electrode has also been used in titrations of sulfate [392] and oxalate [410]. A microdetermination of aluminum(III) [419] and a determination of aluminum oxide in rocks is based on the fluoride electrode (see also [415]). Enzyme-linked immunoassay of human immuno-

TABLE 4

Applications of fluoride-selective electrode

Use	Reference	Use	Reference
Fluoride determination			
in waters	278, 389, 400, 411	in bones	396
		in urine	411
in wastewaters	421	in aliphatic amine solutions	417
in pure salts after preconcentration	275	in dental tissues	418
in electroplating baths	347	in samples containing boron	422, 423
in milk	390	in organic compounds	424
in minerals and rocks	391, 409	in tea	425
in plants	394	in biological material	426
in phosphoric acid	399	in hair	428
in topaz	402	in D ₂ O	430

globulin G [388] and an assay of peroxidase [414] have been done with the fluoride-selective electrode.

A fluoride membrane electrode has been used to measure fluoride activity in low-melting fused salt systems [178] in cells of the type $\text{Ag}|\text{KSCN}(1), \text{Ag}_2\text{SO}_4(\text{sat.})|\text{KSCN}(1), \text{KF}(a_{\text{F}^-})|\text{LaF}_3 \text{ membrane}|\text{KSCN}(1), \text{Ag}_2\text{SO}_4(\text{sat.})\text{KF}(\text{sat.}, a_{\text{F}^-}^0)|\text{Ag}$.

Other systems

Various other systems have been reported [431–439]. A xanthate-selective electrode has been based on a membrane containing insoluble silver xanthate [431] and used for xanthate determination in flotation solutions [432, 439]. A tetraiodomercurate(II)-selective electrode membrane consists of a mixture of Ag_2HgI_4 and Ag_2S [436]. A thallium(I) ion-selective electrode contains a mixture of TII and HgI_2 in its membrane [438]. Vanadium oxide bronze ($\text{Li}_{1.6}\text{V}_{12}\text{O}_{29.7}$) has been suggested as a suitable material for a lithium ion-selective electrode [433]. A sodium ion-selective electrode based on a single crystal alumina wafer with implanted Li^+ and Si^+ ions has been constructed [434, 435]. Rare earth ion-selective electrodes with membranes prepared of EuB_2O_4 , $\text{Eu}_2\text{B}_2\text{O}_5$, EuB_4O_7 , $\text{Eu}_3\text{B}_2\text{O}_6$, EuNbO_3 , $\text{Eu}_{0.95}\text{NbO}_3$, $\text{Eu}_{0.90}\text{NbO}_3$, $\text{Eu}_{0.88}\text{NbO}_{2.31}$, $\text{Eu}_{0.73}\text{NbO}_{2.81}$, $\text{Eu}_{0.60}\text{NbO}_{3.03}$ and Pr_6O_{11} have been suggested [437].

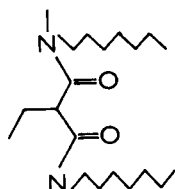
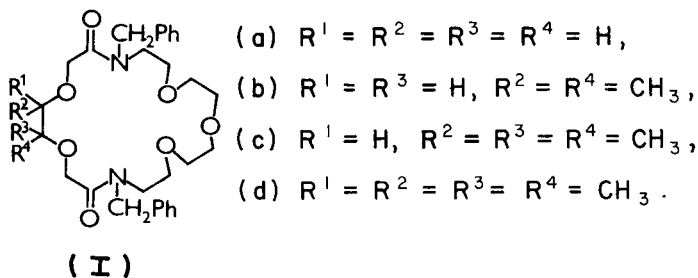
LIQUID-MEMBRANE ELECTRODES

This section deals with liquid-membrane ion-selective electrodes based on both liquid ion-exchangers and neutral ion-carriers (ionophores). The latter group has been the subject of several reviews [31, 31a, 66, 79], particularly with respect to application of crown polyethers in these sensors [64, 78, 87].

In the subsequent paragraphs, first the calcium and magnesium (both ionized ion-exchanger and neutral-carrier systems) [144, 154, 155, 396, 440–495], nitrate [278, 496–512], potassium (both ion-exchanger and neutral carrier systems) [138, 169, 215, 513–539], and sodium and lithium [167, 278, 449, 460, 533, 540–548] electrodes will be dealt with. Other systems based on ionized ion-exchangers [33, 58, 187, 187a, 222, 516, 549–637] and on neutral carriers [638–660] will be discussed separately.

Calcium ion-selective electrodes

Basic properties of Ca^{2+} - and Mg^{2+} -selective electrodes. A number of papers has been concerned with modification of the active sites of calcium electrodes. The Ca^{2+} -selective polymeric-membrane electrodes [144, 154, 155] were discussed on p. 7. Particular attention has been given to new neutral carriers [452, 457, 460, 467, 472, 477, 483–485]. These include N,N,N',N' -tetrasubstituted diamines [460, 452, 457, 472], monoamides of dicarboxylic acids [477], and polyetherdiamides (I) [483–485]. Trihexylphosphate and theonyltrifluoroacetone have been examined [467]. Of the tetrasubstituted diamides, N,N' -diheptyl- N,N' -dimethylethylmalonamide (II) shows suitable properties for Mg^{2+} -selective microelectrodes [460].



A gelatin-based alkaline earth ion-selective electrode for dimethylsulfoxide electrolytes has been described [480]. Other systems have been described [474, 476, 481, 489, 494]. End-point detection in complexiometric titrations using Ca^{2+} -selective electrode has been dealt with again [461]. Anion interferences with the Ca^{2+} -selective electrode increase with their hydrophobicity in the series $NO_3^- < SCN^- < ClO_4^-$ [469, 470]. In metal buffers, the Nernstian response of the calcium ETH-1001 ionophore-based electrode extends to activities as low as $10^{-8} \text{ mol l}^{-1}$ [475].

Biomedical applications with macroelectrodes. A review on calcium ion-selective electrodes in biology and medicine has been published [459], as has a general paper [468]. The problems of standards for automatic Ca^{2+} determinations with ion-selective electrodes have been discussed [453, 455, 464, 465, 493]. The interference of proteins with ionized calcium determinations has been emphasized [446, 447, 456a, 482, 487]. The Nova-2 analyzer has been evaluated for Ca^{2+} measurement [462]. The Nova-2 and Orion SS-20 analyzers show only small differences in the results of Ca^{2+} determinations in plasma and serum, while the differences in whole blood are larger [456]. The interfering effects on Orion SS-20 Calcium Ion Analyzer have been described [491]. The effects of sample freezing on serum calcium determinations with ion-selective electrodes have been discussed [486]. The values of calculated ionized calcium with those calculated from total calcium values have been compared favourably [466, 478]. The decrease in calcium activity caused by heparin has been studied with an Orion SS-20 Analyzer [443]. An ionized calcium analyzer with a built-in pH correction has been described [463]. The properties of ICA 1 Radiometer analyzer for Ca^{2+} activity and pH determination and for automatic recalculation of the calcium activity to pH 7.4 have been discussed [489a].

The calcium ion-selective electrode based on the neutral carrier ETH-1001 can measure total calcium in blood serum when the sample is acidified to pH 3.5 [441]. The membrane should contain, besides the ion carrier, potassium tetrakis(*p*-chlorophenyl)borate in bis(2-ethylhexyl)sebacate. Figure 8 shows the displacement of calcium from its complexes with serum components by hydrogen ions in diluted blood serum investigated with the described ion-selective electrode [441].

Calcium ion-selective electrodes have been used to determine calcium in human bile [421] and urine [442]. An automated stop-flow analyzer for total calcium and magnesium determination in blood has been designed [473]. Calcium movement in the early phase of neutrophil activation by phorbol myristate acetate has been studied with a calcium ion-selective electrode [479]. Determination of calcium in bones has been compared with activation analysis [396]. Assay of calcium in teeth has been described [444]. The arsenazo-III spectrophotometric method has been evaluated by comparison with the results obtained using a calcium ion-selective electrode [445].

Biomedical applications with microelectrodes. The neutral carrier-based calcium ion-selective microelectrodes have been critically evaluated [475]. The recommended ion-selective liquid consists of 10% (w/w) ETH-1001 ligand and 1% (w/w) sodium tetraphenylborate in 89% (w/w) *o*-nitrophenyloctyl ether; to the PVC-containing version, 14% (w/w) of poly(vinyl chloride) is added. The internal filling solution contains 0.1 mM CaCl₂, 1.1 mM nitrilotriacetic acid and 47 mM sodium tetraborate.

Calcium ion-selective microelectrodes have been used for intracellular measurements [449, 454, 492] and in a study of calcium efflux from muscle cells [488, 490]. A magnesium ion-selective microelectrode has been applied in a study of free magnesium in sheep, ferret and frog striated muscle at rest [467a].

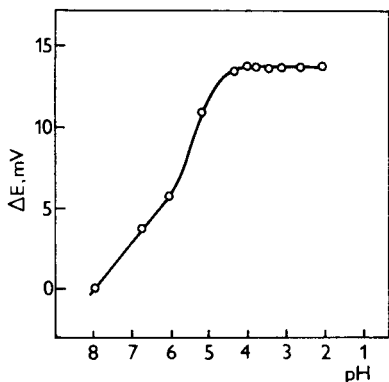


Fig. 8. Displacement of calcium ions from its complexes with serum components in a 20× diluted serum. From [441].

Further applications. By means of ion-selective electrodes, calcium has been determined in fruits [440], rocks [448], subsurface waters [451] and edible alginate solutions [495]. The formation and stability of calcium and magnesium phosphates has been studied at 37°C with ion-selective electrodes [450]. Association of calcium and magnesium benzoate, *o*-toluate, *o*-chlorobenzoate and salicylate has been investigated with the divalent-cation selective electrode [458].

Nitrate-selective electrodes

Several papers have been concerned with the general properties of nitrate-selective electrodes [496, 504, 506, 510a]. A coated-wire nitrate electrode has been described [512]. Nitrate complexes of uranium(VI) have been suggested as active components of a nitrate-selective electrode [510]. An anionic surfactant effect on the response of a nitrate electrode has been observed [499].

Nitrate-selective electrodes have been used for nitrate determinations in waters [278], palladium electroplating baths [500], soils [501, 509, 511], animal waste [502] and organs and tissues of farm animals [507]. Nitrate determinations in soils, plants and animal fodder by ion-selective electrodes has been recommended by the Czech Ministry of Agriculture [508]. The uncoupler-sensitive assimilatory nitrate uptake by *Rhodospseudomonas capsulata* has been directly observed with a nitrate-selective electrode [505].

A nitrite-selective electrode for determination of nitrite in waters has been designed [498] and simultaneous determinations of binary mixture of nitrate and nitrite by means of the ion-selective electrode have been described [503]. The nitrate-selective electrode also responds to hydrogen-molybdate [497].

Potassium ion-selective electrodes

Macroelectrodes. Various potassium ion-selective electrodes based on crown polyethers [138, 529, 533, 536, 538] have been described. The cryptand (2B2B2) has also been used for preparation of a potassium-selective electrode [517]. Another potassium electrode is based on a Nafion-120 membrane [215].

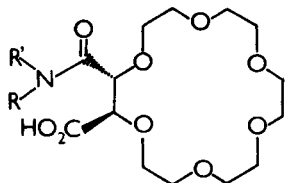
For the valinomycin-based electrodes, the effects of the membrane solvent [525, 526] and the concentration of free valinomycin in the membrane [524] and the transport processes [537] have been studied. A combination of potassium ion-selective electrode [532] and miniature K⁺ electrodes [518, 539] have been described. The inner solution has no effect on the performance of the electrode [520]. The valinomycin-based electrodes show a long-time shelf-life [169].

The potassium ion-selective electrodes have been used for determinations of potassium in drugs [514], sea water [515, 522], hemolyzed electrolytes [521], wine [530] and titanium production solutions [535]. Applications of potassium ion-selective electrodes in automated biomedical analyzers have been outlined on pages 10–12.

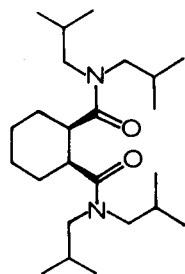
Microelectrodes. A general paper has been published [519]. Another potassium ion-selective electrode has been used as a reference electrode for potassium ion-selective microelectrode measurements [534]. The potassium microelectrode has been used to determine potassium in heart muscle [513, 528], kidney cells [516], rabbit gallbladder [523], the epithelium of the midgut of tobacco horn worms [527], and muscle fibers [523].

Sodium and lithium ion-selective electrodes

New versions of sodium ion-selective electrodes have been based on bis-(crown ether) compounds [533, 547] and on carboxylic acid derivatives of crown ethers (III) [167]. The effect of monensin concentration in the membrane on the performance of the sodium electrode has been studied [546].



(III)



(IV)

Active substances for lithium ion-selective electrodes are *cis-N,N,N',N'*-tetrakisobutyl-1,2-cyclohexanedicarboxamide (IV) [466] 1,5,9,13-tetraoxa-cyclohexadecane and its octamethyl derivative [540] and dioctylbenzene-dicarboxylate [544].

Sodium macroelectrodes have been used to determine sodium in surface water [278], biochemical products [541], milk [543] and sea water [548]. Sodium microelectrodes have been applied for sodium determinations in kidney cells [516], smooth muscle [542] and cerebrospinal fluid [545]. The sodium ligand ETH-227 has been used for intracellular application but attention must be paid to its response to Ca^{2+} ions [449].

Other systems based on ionized ion-exchangers

As was pointed out in Part 2, the possibilities of basing electrodes on hydrophobic ion-pairs formed between the species to be determined and a suitable counter-ion are almost endless. Only a fraction of these systems has found practical application.

Surfactant electrodes. Surfactant-sensitive electrodes (cf. Parts 2–4) have become an important topic; specialized reviews are available [33, 58, 549]. These electrodes have been used in the analysis of cosmetic products such as soaps, shampoos and toothpastes [551], and in determinations of long-chain quaternary ammonium species [561, 565] and of sodium alkylsulfate and alkyltrimethylammonium bromide in micellar solutions [597]. They have also been applied in studies of surfactant adsorption in colloidal suspensions [588], and of surfactant interaction with proteins [589, 628] and with synthetic polymers [598]. Surfactant-sensitive electrodes have also been used in titrations of ionic detergents [603, 630].

Biological membrane potential determinations. Membrane-permeable ions such as tetraphenylphosphonium, thiocyanate or tetraphenylborate distribute in the intracellular and extracellular space according to the Nernst equation which makes it possible to measure membrane potentials (cf. Part 3). Such procedures have been applied to the membranes of mitochondria [600], *Paracoccus denitrificans* [602, 614, 615], of *Azotobacter vinelandii* [608] and *Escherichia coli* [616, 617]; the methodology has been described [599, 601]. Analogous determinations with a microelectrode have been done for the *Rhodospseudomonas* chromatophore [558].

Ion-selective microelectrodes. Acetylcholine, choline [594] and hydrogen carbonate [596] microelectrodes have been described. The microelectrodes have been used to measure chloride and hydrogencarbonate in kidney cells [516].

Other systems. Quaternary ammonium-, phosphonium- and arsonium-based ion-selective electrodes are listed in Table 5; those based on tetra-

TABLE 5

Ion-selective electrodes based on tetraalkyl-ammonium, -phosphonium and -arsonium salts

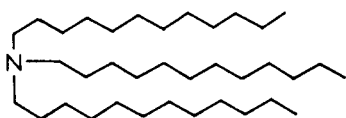
Type	Reference	Type	Reference
Sulfate	187	Nitrophenolate	581
Chloride	187a, 222	Phenolate	581
Chloroaurate(III)	552, 595, 578, 595	2,4-Dinitrophenolate	582
Dicyanoaurate(I)	552, 554, 624	Dinitrosalicylate	586
Oxalate	555	Thiocyanate	590, 607a, 611
Benzoate	556, 587	Naproxinate	591
Cholate	557	Trichloromercurate(II)	604, 605
Salicylate	560	Phosphate	613
Basic drug	564	Perrhenate	623
Perchlorate	579, 612	Azo compound	633
Carbonate	580	Anthraquinone anionic dyestuff	635

phenylborate and its derivatives are listed in Table 6. The tetrafluoroborate-selective electrode has been evaluated [559, 609] and used in the determination of boron in rocks [576]. Electrodes sensitive to phenolate [583], aromatic carboxylate [584], periodate [619], perchlorate [620] and bromomercurate [621] ions have been based on basic dyes. Further applications of the periodate-selective [566, 570, 610] and the picrate-selective [567–569, 571–574, 592, 593] electrodes have been described (cf. Part 4). Other suggested electrodes include a hexafluorophosphate-selective electrode [606], an ammonium-selective electrode based on the tris(2-nitroso-4-chlorophenol)iron(II) anion [607], a uranyl-selective electrode based on di(2-ethylhexyl)phosphate [626] and tetrachlorogallate and tetraphenylborate electrodes based on mixtures of alkyl derivatives of ferrocene [622]. Various systems in this category have been used in titrations of pharmaceuticals [631].

Other systems based on neutral ligands

Several interesting systems have been investigated [638–660].

Proton-selective electrodes. A H^+ -selective microelectrode has been based on a neutral ligand (V); its selectivities allows pH to be determined in the



(V)

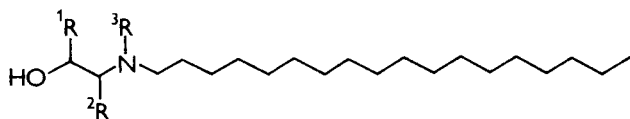
range less than 5.5 [638]. Blood pH measurement with this electrode has been compared with a glass electrode [639].

The pCO_2/pH combination electrode [643] is based on a system consisting of a polymeric membrane containing a proton carrier and an internal pH electrode. Simplification of this system has resulted in a hydrogen carbonate-sensitive electrode [647]. This new system contains a moderated polymer membrane with proton carriers (VI–VIII), which is also permeable to CO_2 .

TABLE 6

Ion-selective electrodes based on tetraphenylborate and its derivatives

Type	Reference	Type	Reference
Ethidium	553	Novocaine	618
Quaternary ammonium	562	Oxyphenonium	627
Alkylammonium	563	Ephedrine derivatives	625
Atropine	575, 585	Triarylmethane cationic dyestuff	629
Novatropine	575	Arenediazonium	632, 634
Nicotine	577	Alizarin	636



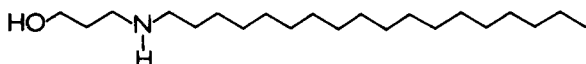
(a) (ETH-595) $^1R = C_6H_5$, $^2R = ^3R = CH_3$

(b) (ETH-1548) $^1R = ^2R = H$, $^3R = C_{18}H_{37}$

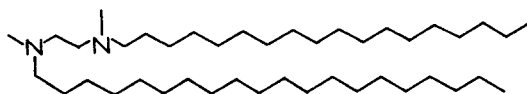
(c) (ETH-1591) $^1R = ^2R = ^3R = H$

(d) (ETH-1561) $^1R = CH_3$, $^2R = ^3R = H$

(VI)



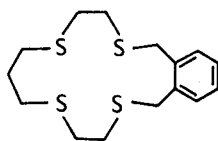
(VII)



(VIII)

Ammonium ion-selective electrodes. Meyerhoff and coworkers [644–646, 653–657] have used the nonactin-based ammonium ion-selective electrode in an ammonia gas sensor which is competitive with the conventional ammonia air-gap system, particularly because it eliminates the fragile internal pH glass electrode. In a continuous flow arrangement the interference from volatile amines is negligible [646]. Other studies of the nonactin-based ammonium ion-selective electrode have been reported [640, 641, 658–660].

The barium ion-selective electrode (cf. [648]) based on barium-polyethoxylate complexes can be used as a sensor for nonionic surfactants [649]. A copper(II)-selective electrode has been based on a macrocyclic polythiaether (IX), [650]. A PVC membrane containing dibenzo-18-crown-6 reacts with cationic surfactants such as 1-dodecylpyridinium ion (down to 10^{-6} M) [652]. The use of this ligand in electrodes for barium and nickel ions has also been attempted [651].



(IX)

Coated-wire ion-selective electrodes have been constructed for the determination of uranyl, neptunyl and plutonyl cations based on a substituted diamide as neutral ligand [642]. Another uranyl ion-selective electrode contains a combination of tri-n-butylphosphate, tri-n-octylphosphine and sodium tetraphenylborate in its membrane [651a].

If several chiral ionophores are present as active substances in the liquid membrane, the enantiomeric excess of ephedronium ion can be determined [642a].

POTENTIOMETRIC BIOSENSORS

This field has been reviewed several times [32, 60, 73, 74, 84] and new versions of the theory of biocatalytic membrane electrodes have been developed [96, 97]. Various new sensors of this type have been reported [661–675].

Enzyme electrodes for tyrosine [671] and histidine [672] have been designed. Bacterial electrodes for tyrosine [668], serine [667], L-arginine [670] and pyruvate [669] have been described. Animal tissues have been used in potentiometric sensors for adenosine [661], adenosine-5'-monophosphate [662], guanine [663] and glutamine [665]. Other sensors have been based on plant tissues [673, 674]. A model of a semiconductor biosensor similar to a taste bud has been proposed [675]. Substrate consumption by biocatalytic potentiometric membrane electrodes has been discussed [664].

An antigen-containing polymer membrane immunoelectrode has been critically evaluated [666]. Because of the low exchange current, the potential of this electrode is rather unstable so that its application seems rather doubtful.

Conclusion

The main sections of this review have dealt with various, partly new sensors, many of which show interesting potentialities. In contrast, various rather uninteresting systems have been suggested within the period of this review [676–681]; mainly, these have involved heterogeneous membrane systems, [676, 679, 680] or liquid-membrane systems based on heavy metal chelates [677, 678, 681]; in view of their low selectivity and other disadvantages, such systems can hardly be recommended for practical use. A partly sceptical review has already been presented [37].

The assistance of the Technical and Economic Research Institute of Chemical Industry, Prague, who supplied computerized Chemical Abstracts Condensates dealing with ion-selective electrodes, is highly appreciated. The author is obliged to Mrs. M. Kozlová of the Heyrovský Institute, for her help with ordering the material for this review. Colleagues from all over the world who send reprints and reports in the field of ion-selective electrodes provide invaluable assistance for these reviews; their continued help will be much appreciated.

REFERENCES

- 1 J. Koryta, *Anal. Chim. Acta*, 61 (1972) 329; 91 (1977) 1; 111 (1979) 1; 139 (1982) 1 (Parts 1—4).
- 2 T. Zeuthen (Ed.), *Applications of Ion-selective Microelectrodes*, Elsevier/North Holland/Biomedical Press, Amsterdam, 1981.
- 3 K. Cammann, *Rabota s ionselektivnymi elektrodami*, MIR, Moscow, 1980.
- 3 (a) V. V. Cosofret and J. D. R. Thomas, *Membrane Electrodes in Drug-Substances Analysis*, Pergamon Press, Oxford, 1982.
- 4 J. Zemel and P. Bergveld (Eds.), *Chemically Sensitive Electronic Devices*, Elsevier Sequoia, Lausanne, 1981.
- 5 E. Pungor and I. Buzás (Eds.), *Ion-selective Electrodes*, 3rd Symp., Mátrafüred, 1980, Akadémiai Kiadó, Budapest; Elsevier, Amsterdam, 1981.
- 6 J. Koryta and K. Štulík, *Ion-selective Electrodes*, 2nd edn., Cambridge University Press, Cambridge, 1983.
- 7 T. S. Ma and S. S. M. Hassan, *Organic Analysis Using Ion-selective Electrodes*, Vol. 1, Vol. 2, Academic Press, London, 1982.
- 8 W. E. Morf, *The Principles of Ion-selective Electrodes and of Membrane Transport*, Akadémiai Kiadó, Budapest; Elsevier Amsterdam, 1981.
- 9 D. W. Lübbers, H. Acker, R. P. Buck, G. Eisenman, M. Kessler and W. Simon (Eds.), *Progress in Enzyme and Ion-Selective Electrodes*, Springer-Verlag, Berlin, 1981.
- 10 J. Růžička and E. H. Hansen, *Flow-Injection Analysis*, J. Wiley, Chichester, 1981.
- 11 M. Whitfield and D. Jagner (Eds.), *Marine Electrochemistry: A Practical Introduction*, J. Wiley, Chichester, 1981.
- 11a *Handbook of Electrode Technology*, Orion Research, Cambridge, MA, 1982.
- 12 J. D. R. Thomas (Ed.), *Ion-Sel. Electrode Rev.*, 3 (1981), 4 (1982), 5 (1983).
- 13 K. Cammann, *Instrum. Forsch.*, 9 (1982) 1.
- 14 A. K. Covington, *Lab. Pract.*, 31 (1982) 239, 241, 243, 245, 247—248, 251.
- 15 M. R. Dhaneshwar and R. G. Dhaneshwar, *Indian Chem. Manuf.*, 18 (1980) 13.
- 16 T. Fujinaga, *Philos. Trans. R. Soc. London, Ser. A*, 305 (1982) 631.
- 17 H. B. Herman, *Pollut. Eng. Technol.*, 18 (1981) 151.
- 18 K. Hiirō, *Kagaku Gijutsushi Mol.*, 20 (1982) 41.
- 19 N. Ishibashi, *Kagaku Kogyo*, 33 (1982) 529.
- 20 E. Kretschmer, *Wiss. Fortschr.*, 32 (1982) 54.
- 21 C. R. Martin, *TRAC, Trends Anal. Chem.*, 1 (1982) 175.
- 22 M. E. Meyerhoff and Y. M. Fraticelli, *Anal. Chem.*, 54 (1982) R27.
- 23 F. Oehme, *Galvanotechnik*, 72 (1981) 373.
- 24 S. J. Pace, *Sens. Actuators*, 1 (1981) 475.
- 25 J. Tacussel and J. J. Fombon, *VIDE, Couches Minces*, 37 (1982) 311.
- 26 A. Takahashi, *Kogyo Yosui*, 285 (1982) 38.
- 27 J. D. R. Thomas, *Anal. Chem. Symp. Ser.*, 8 (1981) 123.
- 28 G. Wu, *Fenxi Huaxue*, 9 (1981) 748.
- 29 S. Yamaguchi, *Kensa to Gijutsu*, 9 (1981) 789.
- 30 Y. Zhang, *Fenxi Huaxue*, 10 (1982) 308.
- 31 D. Ammann, P. Anker, H. B. Jenny, P. Schulthess and W. Simon, in E. Kaiser, F. Gall, M. M. Müller and P. M. Bayer (Eds.), *XI Int. Congr. Clin. Chem.*, W. de Gruyter, Berlin, 1982, p. 1137.
- 31 (a) D. Ammann, W. E. Morf, P. Anker, P. C. Meier, E. Pretsch and W. Simon, *Ion-Sel. Electrode Rev.*, 5 (1983) 3.
- 32 M. Aizawa and S. Suzuki, *Kagaku to Kogyo (Osaka)*, 56 (1982) 46.
- 33 B. J. Birch and R. N. Cockcroft, *Ion-Sel. Electrode Rev.*, 3 (1981) 1.
- 34 R. P. Buck, *Ion-Sel. Electrode Rev.*, 4 (1982) 3.
- 35 R. P. Buck, *Sens. Actuators*, 1 (1981) 197.
- 36 D. J. Clarke, D. B. Kell, J. G. Morris and A. Burns, *Ion-Sel. Electrode Rev.*, 4 (1982) 75.

- 37 C. J. Coetzee, *Ion-Sel. Electrode Rev.*, 3 (1981) 105.
- 37 (a) A. K. Covington and M. J. F. Rebelo, *Ion-Sel. Electrode Rev.*, 5 (1983) 93.
- 38 C. H. Culberson, in M. Whitfield and D. Jagner (Eds.), *Marine Electrochemistry*, J. Wiley, Chichester, 1981, p. 187.
- 39 J. E. Davis, R. L. Solsky, L. Giering and S. Malhotra, *Anal. Chem.*, 55 (1983) 202R.
- 40 R. Dennhardt and J. G. Schindler, *Anaesthesiol. Intensivmed.* (Berlin), 141 (1981) 109.
- 41 A. A. Diggins, S. Lichtenstein, J. C. Synnott and S. J. West, *ASTM Spec. Tech. Publ.*, 742 (1981) 131.
- 42 M. B. A. Djamgoz and P. J. Laming, *Trends Neurosci.*, 4 (1981) 280.
- 42 (a) M. M. Emara, *Ion-sel. Electrode Rev.*, 4 (1982) 143.
- 43 M. Esashi, *Kagaku Kogyo*, 33 (1982) 481.
- 44 M. Fujimoto, K. Kotera, K. Kajino and S. Aoki, *Sogo Rinsho*, 29 (1980) 2699.
- 45 H. Galster, *GIT Fachz. Lab.*, 25 (1981) 32.
- 46 G. G. Guilbault, *Ion-Sel. Electrode Rev.*, 4 (1982) 187.
- 47 A. G. Hamza, *J. Fac. Sci., Riyad Univ.*, 10 (1979) 171.
- 48 H. B. Herman, in H. B. Mark and J. S. Mattson (Eds.), *Water Quality Measurement*, M. Dekker, New York, 1981.
- 49 D. Jagner, in M. Whitfield and D. Jagner (Eds.), *Marine Electrochemistry: A Practical Introduction*, J. Wiley, Chichester, 1981, p. 263.
- 50 G. J. Kakabadse, *Ion-Sel. Electrode Rev.*, 3 (1981) 127.
- 51 G. G. Kiselev, R. P. Lichko and Ya. G. Ryskov, *Pochvovedenie*, 9 (1981) 128.
- 52 J. Koryta, *Electrochim. Acta*, 29 (1984) in press.
- 53 J. Koryta, *Ion-Sel. Electrode Rev.*, 5 (1983) No. 2.
- 54 J. Koryta and P. Vanýsek, in H. Gerischer and C. W. Tobias (Eds.), *Advances in Electrochemistry and Electrochemical Engineering*, Wiley-Interscience, New York, NY, 1981, p. 113.
- 55 C. O. Lee, *Am. J. Physiol.*, 241 (1981) H 459.
- 56 P. Leroy, P. Garil and R. Rosset, *Analisis*, 10 (1982) 351.
- 57 E. Lindner, K. Tóth and E. Pungor, *Bunseki Kagaku*, 30 (1981) S 67.
- 58 R. A. Llenado and R. A. Jamieson, *Anal. Chem.*, 53 (1981) 174R.
- 59 E. Makleit-Szabo, *Acta Aliment. Acad. Sci. Hung.*, 10 (1981) 337.
- 60 M. Mascini, *Chim. Ind. (Milan)*, 64 (1982) 147.
- 61 J. Mašek and P. Ocelka, *Krmivářství Služby*, 16 (1980) 268.
- 62 D. Midgley, *Ion-Sel. Electrode Rev.*, 3 (1981) 43.
- 63 G. J. Moody and J. D. R. Thomas, *Ion-Sel. Electrode Rev.*, 3 (1981) 189.
- 64 H. Nakamura and K. Ueno, *Kagaku (Kyoto)*, 36 (1981) 758.
- 65 E. Niki, *Denki Kagaku*, 50 (1982) 13.
- 66 B. P. Nikolskii, E. A. Materova, O. K. Stefanova and V. E. Yurinskaya, *Radiokhimiya*, 24 (1982) 808.
- 67 R. Perez-Olmos, *Tech. Lab.*, 6 (1980) 1005.
- 68 O. H. Petersen and I. Findlay, *Tech. Life Sci.: Physiol.*, P1(2) (1982) p. 21.
- 69 T. C. Pinkerton and B. L. Lawson, *Clin. Chem.*, 28 (1982) 1946.
- 70 E. Pungor, *Kem-Kemi*, 9 (1982) 98.
- 71 E. Pungor, Z. Feher and G. Nagy, *CRC Crit. Rev. Anal. Chem.*, 14 (1983) 175.
- 72 Z. Qiu, D. Xu and Z. Chen, *Yaowu Fenxi Zazhi*, 2 (1982) 207.
- 73 G. A. Rechnitz, *J. Chem. Educ.*, 60 (1983) 282.
- 74 G. A. Rechnitz, *Science*, 214 (1981) 282.
- 75 S. Scholle and S. Scholle, Jr., *Chem. Prům.*, 32 (1982) 148.
- 76 W. Selig, *Fresenius Z. Anal. Chem.*, 312 (1982) 419.
- 77 Y. Shibazaki, *Kensa to Gijutsu*, 9 (1981) 714.
- 78 T. Shono, *Kagaku Kogyo*, 33 (1982) 524.
- 79 W. Simon, D. Ammann and P. C. Meier, *Hitachi Instrum. News*, 9 (1981) 1.
- 80 W. Simon, D. Ammann, W. Bussmann and P. C. Meier, in K. J. Laidler (Ed.), *Frontiers in Chemistry*, Pergamon Press, Oxford, 1982, p. 217.

- 81 R. L. Solsky, *CRC Crit. Rev. Anal. Chem.*, 14 (1982) 1.
- 82 O. K. Stefanova and M. M. Shultz, in D. A. Cadenhead and J. F. Danielli (Eds.), *Progress in Surface and Membrane Science*, Vol. 14, Academic Press, New York, NY, 1981, p. 131.
- 83 Y. Su, *Fen Hsi Hua Hsueh*, 9 (1981) 361.
- 84 S. Suzuki and I. Karube, in C. B. Weingard, E. Katchalsky-Katzir and L. Goldstein (Eds.), *Analytical Applications of Immobilized Enzymes and Cells*, Academic Press, New York, NY, 1981, p. 145.
- 85 R. C. Thomas, *Tech. Life Sci. : Physiol.*, P1(2) (1982) 12.
- 86 Yu. G. Vlasov, *Anal. Chem. Symp. Ser.*, 8 (1981) 147.
- 87 M. Yoshio and H. Noguchi, *Anal. Lett.*, 15 (1982) 1197.
- 88 G. J. Moody and J. D. R. Thomas, *Ion-Sel. Electrode Rev.*, 3 (1981) 209.
- 89 G. J. Moody and J. D. R. Thomas, *Ion-Sel. Electrode Rev.*, 4 (1982) 233.
- 90 S. Okazaki and T. Fujinagu, *Denki Kagaku*, 50 (1982) 115.
- 90 (a) K. U. Mesawa and Y. U. Mesawa, *Selectivity Coefficients for Ion-Selective Electrodes*, University of Tokyo Press, Tokyo, 1983.
- 91 R. Ahmad-Bitar, M. M. Abdul-Gader, A. M. Zihlit and A. M. Y. Jaber, *J. Electroanal. Chem.*, 143 (1983) 121.
- 92 R. G. Bates, *Anal. Chem. Symp. Ser.*, 8 (1981) 3.
- 93 B. Doyle, G. J. Moody and J. D. R. Thomas, *Talanta*, 29 (1982) 257.
- 94 B. Doyle, G. J. Moody and J. D. R. Thomas, *Talanta*, 29 (1982) 609.
- 95 T. Fujinaga, S. Kihara and Z. Yoshida, *Bunseki Kagaku*, 31 (1982) E301.
- 96 H. F. Hameka and G. A. Rechnitz, *J. Phys. Chem.*, 87 (1983) 1235.
- 97 H. F. Hameka and G. Rechnitz, *Anal. Chem.*, 53 (1981) 1586.
- 98 Le Q. Hung, *J. Electroanal. Chem.*, 115 (1980) 159.
- 99 Le Q. Hung, *J. Electroanal. Chem.*, 149 (1983) 1.
- 100 M. A. Ilyushchenko and V. A. Mirkin, *Vestn. Akad. Nauk Kazakh. SSR*, 4 (1981) 41.
- 101 M. A. Ilyushchenko and V. A. Mirkin, *Vestn. Akad. Nauk Kazakh. SSR*, 25 (1981) 160.
- 102 T. Kakiuchi and M. Senda, *Bull. Chem. Soc. Jpn.*, 56 (1983) 1322.
- 103 T. Kakiuchi and M. Senda, *Bull. Chem. Soc. Jpn.*, 56 (1983) 1753.
- 103 (a) F. M. Karpfen and J. E. B. Randles, *Trans. Faraday Soc.*, 49 (1953) 823.
- 104 J. Koryta, Le Q. Hung and A. Hofmanová, *Studia Biophys.*, 90 (1982) 25.
- 105 J. R. Luch, T. Higachi and L. A. Sternson, *Anal. Chem.*, 54 (1982) 1583.
- 106 O. R. Melroy, W. E. Bronner and R. P. Buck, *J. Electrochem. Soc.*, 130 (1983) 373.
- 107 O. R. Melroy and R. P. Buck, *J. Electroanal. Chem.*, 136 (1982) 19.
- 108 O. R. Melroy and R. P. Buck, *J. Electroanal. Chem.*, 143 (1983) 23.
- 109 O. R. Melroy, R. P. Buck, F. S. Stover and H. C. Hughes, *J. Electroanal. Chem.*, 121 (1981) 93.
- 110 V. A. Mikhailov, V. U. Osipov, E. N. Graf and I. A. Pushkareva, *Elektrokhimiya*, 17 (1981) 1464.
- 111 W. E. Morf, *Anal. Chem. Symp. Ser.*, 8 (1981) 267.
- 112 T. Osakai, T. Kakutani, T. Kakiuchi and M. Senda, *Rev. Polarogr. (Kyoto)*, 27 (1981) 51.
- 113 C. R. Powley and T. A. Nieman, *Anal. Chim. Acta*, 139 (1982) 61.
- 114 C. R. Powley and T. A. Nieman, *Anal. Chim. Acta*, 139 (1982) 83.
- 115 Z. Samec, D. Homolka and V. Mareček, *J. Electroanal. Chem.*, 135 (1982) 265.
- 116 Z. Samec, V. Mareček and D. Homolka, *J. Electroanal. Chem.*, 126 (1981) 121.
- 117 Z. Samec, V. Mareček, J. Weber and D. Homolka, *J. Electroanal. Chem.*, 126 (1981) 105.
- 118 E. J. W. Verwey and K. F. Niessen, *Philos. Mag.*, 28 (1939) 435.
- 119 H. Affolter and L. Carofoli, *Anal. Biochem.*, 115 (1981) 1.
- 120 T. G. Aityurina, V. V. Kiyanskii, N. A. Yaroslavtsev, Yu. I. Urusov and O. M. Petrukhin, *Zh. Anal. Khim.*, 37 (1982) 1326.

- 121 T. Akiyama, K. Komiya, Y. Okabe, T. Sugano and E. Niki, *Bunseki Kagaku*, 30 (1981) 754.
- 122 P. W. Alexander and P. Seegopaul, *Anal. Chem.*, 52 (1980) 2403.
- 123 W. Annan, N. A. Kirwan, W. S. Robertson, P. R. Teasdale and B. P. Ager, *J. Autom. Chem.*, 2 (1980) 212.
- 124 F. S. Apple, D. O. Koch, S. Graves and J. H. Ladenson, *Clin. Chem.*, 28 (1982) 1931.
- 125 D. N. Baron, *Clin. Chem.*, 27 (1981) 642.
- 126 M. A. Beg and A. Nabi, *J. Membr. Sci.*, 9 (1981) 197.
- 127 P. Bijster, H. L. Vader and C. L. J. Vink, *Ann. Clin. Biochem.*, 20 (1983) 116.
- 128 A. M. Bond, I. D. Heritage, G. G. Wallace and M. J. McCormick, *Anal. Chem.*, 54 (1982) 582.
- 129 A. M. Bond, H. A. Hudson, P. A. Van den Bosch, F. L. Watter and H. R. A. Exelby, *Anal. Chim. Acta*, 136 (1982) 51.
- 130 D. P. Brezinski, *Analyst (London)*, 108 (1983) 425.
- 131 R. P. Buck, *IEEE Trans. Electron Devices*, 29 (1982) 108.
- 132 R. G. Burr, *Clin. Chem.*, 28 (1982) 1710.
- 133 G. C. Cornfield, L. Ebdon and A. T. Ellis, *Org. Coat. Appl. Polym. Sci. Proc.*, 46 (1981) 445.
- 134 S. Caras and J. Janata, *Anal. Chem.*, 52 (1980) 1935.
- 135 D. W. Chan and J. White, *Clin. Chem.*, 27 (1981) 1111.
- 136 S. N. K. Chaudhari and K. L. Cheng, *Mikrochim. Acta*, II (1979) 411.
- 137 H. Chen, Z. Xiao and D. Tang, *Fen Hsi Hua Hsueh*, 9 (1981) 286.
- 138 H.-L. Chen, L.-F. Ting, Y.-M. Yang and Y.-F. Hu, *Fen Hsi Hua Hsueh*, 8 (1980) 303.
- 139 M. M. Civan, in A. Spitzer (Ed.), *Proc. Int. Works Hop. Den. Renol Physiol.*, 1982, p. 53.
- 140 H. K. Cho, Y. H. Lee, R. A. Couch, J. M. Jugadeesh and C. L. Olson, *Clin. Chem.*, 28 (1982) 1956.
- 141 J. F. Coetzee and C. W. Gardner, Jr., *Anal. Chem.*, 54 (1982) 2625.
- 142 R. L. Coleman and C. C. Young, *Clin. Chem.*, 27 (1981) 1938.
- 142 (a) R. L. Coleman and C. C. Young, *Clin. Chem.*, 28 (1982) 1703.
- 143 R. L. Coleman, C. C. Young and L. Sidoni, *Clin. Chem.*, 27 (1981) 1093.
- 144 G. C. Corfield, L. Ebdon and A. T. Ellis, *Polym. Sci. Technol.*, 16 (1982) 233.
- 145 P. Costello, N. P. Kubasik, B. B. Brody, H. E. Sine, J. A. Berttsch and J. P. D'Souza, *Clin. Chem.*, 29 (1983) 129.
- 146 A. M. Covault, E. W. Holmes, S. E. Kahn and E. W. Bermes, *Clin. Chem.*, 27 (1981) 1109.
- 147 A. K. Covington, T. R. Harbinson and A. Sibbald, *Anal. Lett.*, 15 (1982) 1423.
- 148 J. D. Czaban, A. D. Cormier and K. D. Legg, *Clin. Chem.*, 28 (1982) 1703.
- 149 J. D. Czaban and A. D. Cormier, *Clin. Chem.*, 26 (1980) 1921.
- 150 J. D. Czaban, A. D. Cormier and K. D. Legg, *Clin. Chem.*, 28 (1982) 1936.
- 151 E. Deak, *Anal. Chem. Symp. Ser.* 8 (1981) 203.
- 152 H. Degava, N. Shinozuku and S. Hayano, *Chem. Lett.*, (1983) 25.
- 153 G. A. East and I. A. Da Silva, *Anal. Chim. Acta*, 149 (1983) 277.
- 154 L. Ebdon, A. T. Ellis and G. C. Corfield, *Analyst, London*, 107 (1982) 288.
- 155 L. Ebdon, A. T. Ellis and G. C. Corfield, *Polym. Prepr. Am. Chem. Soc., Div. Polym. Chem.*, 21 (1980) 116.
- 156 C. E. Efstathiou and T. P. Hadjiioannou, *Anal. Chem.*, 54 (1982) 1525.
- 157 E. E. Epstein, *Clin. Chem.*, 27 (1981) 1111.
- 158 J. Fang, *Fen Hsi Hua Hsueh*, 9 (1981) 354.
- 159 Z. Figaszewski, Z. Koczorowski and G. Geblewicz, *J. Electroanal. Chem.*, 139 (1982) 317.
- 160 J. M. Flannery, *GIT Labor-Med.*, 5 (1982) 436, 439, 444.
- 161 J. Fligier, M. Gratzl, G. Nagy and E. Pungor, *Anal. Chem. Acta*, 134 (1982) 263.
- 162 J. G. Flood, A. L. Harris and R. E. Collins, *Clin. Chem.*, 27 (1981) 1110.
- 163 O. R. Flores, T. Belisle and M. Wensley, *Clin. Chem.*, 27 (1981) 1110.

- 164 O. Flores and E. Buzza, *Clin. Chem.*, 28 (1982) 1232.
165 O. R. Flores and C. G. Chittenden, *Lab. Prax. Med.*, 4 (1980) 1.
166 S. Fujiwara, T. Yusa and K. Vishiyama, *Bunseki Kagaku*, 31 (1982) E 135.
167 T. M. Fyles and C. A. McGavin, *Anal. Chem.*, 54 (1982) 2103.
168 G. Geblewicz, Z. Koczorowski and Z. Figaszewski, *Colloids Surf.*, 6 (1983) 43.
169 J. J. Griffin and G. D. Christian, *Talanta*, 30 (1983) 201.
169 (a) Guo Du, J. Koryta, W. Ruth and P. Vanýsek, *J. Electroanal. Chem.*, 159 (1983) 413.
170 A. Gustavsson and P. Nylén, *Anal. Chim. Acta*, 125 (1981) 65.
171 A. Haemmerli, J. Janata and H. M. Brown, *Anal. Chim. Acta*, 144 (1982) 115.
172 H. Hara, S. Okazaki and T. Fujinaga, *Bull. Chem. Soc. Jpn.*, 54 (1981) 2904.
173 G. H. Harff, *Clin. Chem.*, 28 (1982) 1232.
174 G. H. Harff and C. vanLeeuwen, *Clin. Chem.*, 28 (1982) 2003.
175 G. T. Hefter, *Anal. Chem.*, 54 (1982) 2518.
176 P. C. Hobby, G. J. Moody and J. D. R. Thomas, *Anal. Proc. (London)*, 19 (1982) 316.
177 A. Hofmanová, Le Q. Hung and W. Khalil, *J. Electroanal. Chem.*, 135 (1982) 257.
178 B. Holmberg and K. Jarring, *J. Electroanal. Chem.*, 146 (1983) 447.
179 S.-L. Hsieh, Fen Hsi Hua Hsueh, 8 (1980) 563.
180 A. Hulanicki, *Anal. Chem. Symp. Ser.*, 8 (1981) 103.
181 A. Hulanicki and A. Lewenstam, *Anal. Chem.*, 53 (1981) 1401.
182 A. Hulanicki and A. Lewenstam, *Talanta*, 29 (1982) 671.
183 A. Hulanicki, M. Trojanowicz and E. Poboży, *Analyst (London)*, 107 (1982) 1356.
184 B. Hundhammer, T. Solomon and B. Alemayehu, *J. Electroanal. Chem.*, 135 (1982) 301.
185 L. Q. Hung and A. Hofmanová, *Chem. Listy*, 76 (1982) 879.
186 S. Ishii, O. Flores and T. Belisle, *J. Clin. Lab. Autom.*, 2 (1982) 338.
187 H. Ishiwada, K. Suzuki, K. Kimura and T. Shirai, *Bunseki Kagaku*, 31 (1982) 346.
187 (a) H. Ishiwada, K. Suzuki and T. Shirai, *Bunseki Kagaku*, 31 (1982) 71.
188 G. J. Kakabadse, H. Abdul-Ahed, M. Khayat, G. Tassopoulos and A. Vahdati, in G. J. Kakabadse (Ed.), *Solvents — The Neglected Parameter*, UMIST Publication, Manchester, 1977.
189 G. J. Kakabadse, H. A. Maleila, M. N. Khayat, G. Tassopoulos and A. Vahdati, *Analyst (London)*, 103 (1978) 1046.
190 T. Kakutani, T. Osakai and M. Senda, *Bull. Chem. Soc. Jpn.*, 56 (1983) 991.
191 S. Hikara, Z. Yoshida and T. Fujinaga, *Bunseki Kagaku*, 31 (1982) E 297.
192 G. G. Kiselev, T. A. Mezhburd and V. N. Nikonov, *Zavod. Lab.*, 48 (1982) 3.
193 T. R. Kissel, J. R. Sandifer and N. Zumbulyadis, *Clin. Chem.*, 28 (1982) 449.
193 (a) Z. Koczorowski and G. Geblewicz, *J. Electroanal. Chem.*, 139 (1982) 177.
194 J. Koryta, Yu. N. Kozlov, A. Hofmanová, Le Q. Hung, W. Khalil, W. Ruth, P. Vanýsek and Guo Du, *Antibiotiki (Moscow)*, (1983) 810.
195 J. Koryta, W. Ruth, P. Vanýsek and A. Hofmanová, *Anal. Lett.*, 15B (1982) 1685.
196 Yu. N. Kozlov and J. Koryta, *Anal. Lett.*, 16B (1983) 255.
197 J. D. Kruse-Jarres, F. J. Schott and C. Trendelenburg, in E. Kaiser, F. Gabl, M. M. Müller and P. M. Bayer (Eds.), *11th Int. Cong. Clin. Chem.*, W. de Gruyter, Berlin, 1982, p. 1143.
198 J. H. Ladenson, D. Koch and F. S. Apple, *Clin. Chem.*, 27 (1981) 1094.
199 J. P. Leader, *Proc. Univ. Otago Med. Sch.*, 59 (1981) 80.
200 J. P. Leader, A. D. C. Macknight, D. R. Mason and W. M. Armstrong, *Proc. Univ. Otago Med. Sch.*, 59 (1981) 82.
201 G. B. Levy, *Clin. Chem.*, 27 (1981) 1435.
202 S. C. Lewis and K. W. Miller, *Clin. Chem.*, 27 (1981) 1111.
203 J. L. F. D. Lima and A. A. S. C. Machado, *Quim. Nova*, 3 (1980) 2.
204 J. L. C. Lima and A. A. S. C. Machado, *Anal. Tech. Environ. Chem.*, 2 (1981) 419.
205 J. L. C. Lima and A. A. S. C. Machado, *Rev. Port. Quim.*, 21 (1979) 15.

- 206 E. Lindner, K. Tóth and E. Pungor, *Anal. Chem.*, 54 (1982) 72.
207 E. Lindner, K. Tóth and E. Pungor, *Anal. Chem.*, 54 (1982) 202.
208 E. Lindner, K. Tóth and E. Pungor, *Magy. Kem. Foly.*, 88 (1982) 49.
209 E. Lindner, K. Tóth, E. Pungor and K. Nowakowski, *Magy. Kem. Foly.*, 88 (1982) 55.
210 P. Longhi, T. Mussini and S. Rondini, *Anal. Lett.*, 15 (1982) 1601.
211 I. N. Lyubimova, *Pochvovedenie*, 7 (1982) 61.
212 M. Maj-Žurawska and A. Hulanicki, *Anal. Chim. Acta*, 136 (1982) 395.
213 V. Mareček and Z. Samec, *Anal. Chim. Acta*, 141 (1982) 65.
214 V. Mareček and Z. Samec, *Anal. Lett.*, 15B (1981) 1241.
215 C. R. Martin and H. Freiser, *Anal. Chem.*, 53 (1981) 902.
216 H. Matsushita, N. Ishikawa and M. Okada, *Nippon Kagaku Kaishi*, 5 (1982) 775.
217 P. C. Meier, F. Lanter, D. Ammann, R. A. Steiner and W. Simon, *Pflugers Arch.*, 393 (1982) 23.
218 T. J. Mellor, M. Huskard and D. E. Mulcahy, *Anal. Lett.*, 15A (1982) 1549.
219 O. R. Melroy, W. E. Bronner and R. P. Buck, *Chem. Biochem. Environ. Instrum.*, 12 (1982) 77.
220 K. Nagy and T. A. Fjeldly, *Anal. Chem. Symp. Ser.*, 8 (1981) 287.
221 U. Oesch, S. Carus and J. Janata, *Anal. Chem.*, 53 (1981) 1983.
222 S. Oka, Y. Sibazazi and S. Tahara, *Anal. Chem.*, 53 (1981) 588.
223 S. Okazaki and H. Freiser, *Denki Kagaku*, 50 (1982) 117.
224 N. O'Leary, T. Hurley, M. Stapleton, B. Scully and P. F. Duggan, *Ann. Clin. Biochem.*, 18 (1981) 112.
224 (a) N. F. MacDonald, P. Z. Williams, J. I. Burton and J. G. Batskakis, *Am. J. Clin. Pathol.*, 76 (1981) 575.
225 C. J. Preusse and C. Fuchs, *J. Clin. Chem. Clin. Biochem.*, 17 (1979) 639.
226 R. F. Prini, C. R. DePattin, K. Tanaka and R. G. Bates, *J. Electroanal. Chem.*, 144 (1983) 422.
227 J. W. Ross, *Chem. Eng. News*, 59 (1981) 54.
228 J. Růžička and A. Ramsing, *Scand. J. Clin. Lab. Invest., Suppl.*, 42 (1982) 35.
229 Z. Samec, D. Homolka, V. Mareček and L. Kavan, *J. Electroanal. Chem.*, 145 (1983) 213.
230 Z. Samec, V. Mareček, J. Weber and D. Homolka, *J. Electroanal. Chem.*, 126 (1981) 105.
231 J. G. Schindler and M. v. Gülich, *Biomed. Technik*, 26 (1981) 43.
232 J. G. Schindler and M. v. Gülich, *Fresenius Z. Anal. Chem.*, 307 (1981) 105.
233 J. G. Schindler and M. v. Gülich, *J. Clin. Chem. Clin. Biochem.*, 19 (1981) 49.
234 J. G. Schindler, M. v. Gülich, H. Maier, G. Stork, W. Schäl, H.-E. Braun, W. Schmid and K.-D. Karaschinski, *Fresenius Z. Anal. Chem.*, 301 (1980) 410.
235 R. M. Seddon, P. H. Parker, M. R. Winton and A. W. Lansdell, *Clin. Chem.*, 29 (1983) 212.
236 W. Selig, *Mikrochim. Acta*, (I) (1983) 333.
237 G. Semenescu, *Rev. Chim. (Bucharest)*, 32 (1981) 170.
238 M. Senda, T. Kakutani and T. Osakai, *Denki Kagaku*, 49 (1981) 322.
239 J. Šenkýř and J. Petr, *Anal. Chem. Symp. Ser.*, 8 (1981) 327.
240 V. S. Shterman, I. V. Rosin, L. E. Mikhailova, V. V. Krasnoshchekov and N. P. Morozova, *Izv. Timirzayevsk. Shk. Akad.*, 2 (1982) 175.
241 F. Shu and T. Foley, *Clin. Chem.*, 27 (1981) 1094.
242 A. Sibbald, A. K. Covington, E. A. Cooper and R. F. Carter, *Clin. Chem.*, 29 (1983) 405.
243 J. Slanina, F. B. Bukker, P. A. C. Jongejan, L. van Lamsen and J. J. Möls, *Anal. Chim. Acta*, 130 (1981) 1.
244 K. Štulík and V. Pacáková, *Electrochemical Detection in High-performance Liquid Chromatography*, *CRC Crit. Rev. Anal. Chem.*, CRC Press, Boca Raton, 1983.
245 K. Štulík and V. Pacáková, *J. Electroanal. Chem.*, 129 (1981) 1.

- 246 K. Suzuki, H. Ishiwada, H. Inoue and T. Shirai, 1982 Pittsburgh Conf., Present. Abstr. No. 332.
- 247 K. Suzuki, H. Ishiwada, T. Shirai and S. Yanagisawa, *Bunseki Kagaku*, 30 (1981) 751.
- 248 S. Tahara, M. Yoshii and S. Olsa, *Chem. Lett.*, (1982) 307.
- 249 K. Tanaka and R. G. Bates, *Anal. Chem.*, 53 (1981) 1021.
- 250 K. Toth, E. Lindner and E. Pungor, *Anal. Chem. Symp. Ser.*, 8 (1981) 135.
- 251 A. Trojáněk, *Chem. Listy*, 76 (1982) 695.
- 252 M. Trojanowicz and R. Lewandowski, *Fresenius Z. Anal. Chem.*, 308 (1981) 7.
- 253 M. Trojanowicz and W. Matuszewski, *Anal. Chim. Acta*, 138 (1982) 71.
- 254 M. Trojanowicz, Z. Ungerstowska, W. Maluszewski, G. Moraczewska and A. Hulanicki, *Talanta*, 29 (1980) 113.
- 255 I. Uemasu and Y. Umezawa, *Anal. Chem.*, 54 (1982) 1198.
- 256 I. Uemasu and Y. Umezawa, *Anal. Chem.*, 55 (1983) 386.
- 257 Y. Umezawa, *Kagaku Kogyo*, 33 (1982) 505.
- 258 Y. Umezawa, I. Tasaki and S. Fujiwara, *Anal. Chem. Symp. Ser.*, 8 (1981) 359.
- 259 P. Vanýsek, W. Ruth and J. Koryta, *J. Electroanal. Chem.*, 148 (1983) 117.
- 260 R. Virtanen, *Anal. Chem. Symp. Ser.*, 8 (1981) 375.
- 261 Ch. H. Wang and T. R. Yu, *Z. Pflanzenernaehr. Bodenkd.*, 144 (1981) 514.
- 262 J. Yin and B. Cai, *Fenxi Huaxue*, 9 (1981) 548.
- 262 (a) S. L. Xie, *Ion Sel. Electrode Rev.*, 4 (1982) 133.
- 263 S. L. Xie, *Metrol. Assur. Meas. Environ. Control., Symp. IMEKO Tech. Comm. Metrol. — TC 8, 1st (1981) p. 316.*
- 264 V. A. Zarinskii, L. K. Shpigun and V. N. Yudin, *Zavod. Lab.*, 47 (1981) 23.
- 265 Z.-F. Zhao and X.-Y. Zhou, *Kao Teng Hsueh Hsiao Hua Hsueh Hsueh Pao*, 1 (1980) 113.
- 266 H. Akaiwa, H. Kawamoto and M. Osumi, *Talanta*, 29 (1982) 689.
- 267 K. Akiyama, M. Nagashima, Ch. Okumoto, K. Terashima and T. Hagiwara, *Bunseki Kagaku*, 31 (1982) 402.
- 268 G. M. Aleksandrova and Zh. L. Boriskova, *Visn. Silskogospod. Nauki*, 7 (1981) 73.
- 269 T. Aomi, *Denki Kagaku*, 48 (1980) 491.
- 270 Y. Awakura, S. Mitsuda and H. Majima, *Denki Kagaku*, 50 (1982) 494.
- 271 Y. Awakura, S. Mitsuda and H. Majima, *Denki Kagaku*, 50 (1982) 979.
- 272 R. G. Benson, D. M. Isherwood, F. A. McEvoy and A. Wood, *Clin. Chem.*, 28 (1982) 2447.
- 273 J. L. Bernal, R. Pardo and J. M. Rodriguez, *Anal. Chim. Acta*, 120 (1980) 367.
- 274 H. Bernhardt, *Schadenprisma*, 10 (1981) 51.
- 275 A. B. Blank and L. P. Eksperiandova, *Zh. Anal. Khim.*, 37 (1982) 1749.
- 276 K. D. Brown and G. A. Parker, *Analyst (London)*, 107 (1982) 1510.
- 276 (a) R. P. Buck, *Anal. Chem.*, 40 (1968) 1432.
- 277 D. T. Burns, B. K. Martin and G. Svehla, *Analyst (London)*, 108 (1983) 457.
- 278 L. F. Bystrova, V. B. Stradomskii and A. A. Nazarova, *Gidrokhim. Mater.*, 73 (1979) 49.
- 279 F. Ch. Chang and S. Ch. Wu, *J. Chin. Chem. Soc. (Taipei)*, 28 (1981) 203.
- 280 B. R. Chapman and I. R. Goldsmith, *Analyst (London)*, 107 (1982) 1014.
- 281 F. W. Cheng, *Microchem. J.*, 27 (1982) 401.
- 282 R. Christova and M. Ivanova, *Mikrochim. Acta*, 1981, II, 239.
- 283 A. Dimante, E. V. Lipets and A. Veveris, *Latv. PSR Zinat. Akad. Vestis, Kim. Ser.*, 5 (1982) 595.
- 284 H. Doe and T. Kitagawa, *Inorg. Chem.*, 21 (1982) 2272.
- 284 (a) G. A. East and I. A. Da Silva, *Anal. Chim. Acta*, 148 (1983) 41.
- 284 (b) R. J. Elin, E. A. Robertson and E. Johnson, *Clin. Chem.*, 27 (1981) 778.
- 285 W. Fischer, *Nachr. Mensch-Umwelt*, 9 (1981) 15.
- 286 N. Ganapathisubramanian and R. M. Noyes, *J. Phys. Chem.*, 86 (1982) 3217.
- 287 Z. Gao and M. Lu, *Huanjing Kexue*, 2 (1981) 376.
- 288 T. Garci, M. Szucs and J. Devay, *Magy. Kem. Foly.*, 86 (1980) 289.

- 289 B. Gorenc, D. Gorenc and B. Pihlar, *Vestn. Slov. Kem. Drus.*, 29 (1982) 5.
290 E. H. Graf, K. Toth, L. Polos and E. Pungor, *Magy. Kem. Foly.*, 88 (1982) 368.
291 A. L. Grekovich, K. N. Mikhailson, S. E. Didina, N. V. Garbuzova and E. A. Materova, *Ion. obmen i ionometriya (Leningrad)*, 3 (1982) 130.
292 H. F. Huggug and M. H. A. El-Salam, *Egypt. J. Dairy Sci.*, 9 (1981) 81.
293 E. G. Harsanyi, K. Toth, L. Polos and E. Pungor, *Anal. Chem.*, 54 (1982) 1094.
294 C. Harzdorf, *Anal. Chim. Acta*, 136 (1982) 61.
295 K. G. Heumann and W. Schnidmeier, *Fresenius Z. Anal. Chem.*, 312 (1982) 595.
296 L. H. Howe, R. E. Hadley and A. G. Fisher, Office of Naval Research, Washington, DC, Publ. No. TVA/ONR/NRO-82/4, EPA 600/7-82-005; Order No. DE 82904686, 196 pp., 1982.
297 W.-Ch. Hsu and Ch.-H. Chiu, *Fen Hsi Hua Hsueh*, 8 (1980) 219.
298 M. Kataoka, Y. Yoshizawa and T. Kambara, *Bunseki Kagaku*, 31 (1982) E 171.
299 V. Majer and K. Štulík, *Talanta*, 29 (1982) 145.
300 J. L. F. D. Lima and A. A. S. C. Machado, *Rev. Port. Quim.*, 21 (1979) 153.
301 J. Motonaka, S. Ikeda and N. Tanaka, *Bull. Chem. Soc. Jpn.*, 55 (1982) 2396.
302 J. Motonaka, S. Ikeda and N. Tanaka, *Bunseki Kagaku*, 31 (1982) 669.
303 H. Mueller, *Anal. Chem. Symp. Ser.*, 8 (1981) 279.
304 V. Narasimhan and G. Visalakshi, *J. Electroanal. Chem.*, 131 (1982) 325.
304 (a) Z. Nosticzius, *Acta Chim. Acad. Sci. Hung.*, 106 (1981) 347.
305 Z. Nosticzius, E. Nosticzius and Z. A. Schelly, *J. Am. Chem. Soc.*, 104 (1982) 6194.
306 Z. Nosticzius, E. Nosticzius and Z. A. Schelly, *J. Phys. Chem.*, 87 (1983) 510.
307 M. Novkirishka, G. Michailov and R. Christova, *Fresenius Z. Anal. Chem.*, 305 (1981) 411.
308 S. Oka, Y. Sibazaki and S. Tahara, *Anal. Chem.*, 53 (1981) 588.
309 D. S. Papastathopoulos and M. I. Karayannis, *J. Chem. Educ.*, 57 (1980) 904.
310 A. T. Pilipenko, E. M. Skobets, O. P. Ryabushko and Yu. S. Savin, *Ukr. Khim. Zh. (Russ. edn.)*, 48 (1982) 286.
311 C. B. Puchalsky, *Anal. Chem.*, 54 (1982) 1243.
312 L. Qi and S. Zhang, *Nanjing Daxue Xuebao Zivan Kexue*, 3 (1981) 347.
313 F. Rakias, K. Toth and E. Pungor, *Magy. Kem. Foly.*, 87 (1981) 88.
314 V. Říha, P. Vu Quat and K. Vytřas, *Česk. Hyg.*, 27 (1982) 212.
315 R. Sarin, *J. Inst. Chem. (India)*, 54 (1982) 69.
316 R. Sarin, *J. Inst. Chem. (India)*, 54 (1982) 77.
317 J. G. Schindler, M. v. Gülich and A. Bach, *Fresenius Z. Anal. Chem.*, 307 (1981) 404.
318 G. Somer, *Anal. Chem.*, 53 (1981) 2143.
319 K. Tan, *Fenxi Huaxue*, 9 (1981) 498.
320 K. Tan, *Fenxi Huaxue*, 9 (1981) 625.
321 S. Ya. Tarasenko, *Izv. Sib. Otd. Akad. Nauk SSSR. Ser. Khim. Nauk*, 2 (1982) 42.
322 A. Varduca, D. Virtosu, L. Popescu and O. Andrea, *Stud. Prot. Calitatii Apelor*, 19 (1979) 91.
323 Yu. G. Vlasov, Yu. E. Ermolenko and B. A. Nikolaev, *Elektrokhimiya*, 17 (1981) 1448.
324 J. Vorlíček and J. Plecítý, *Rudy*, 28 (1980) 227.
325 Ch.-Y. Wang and M.-Q. Su, *Hua Hsueh Hsueh Pao*, 38 (1980) 392.
326 Ch.-Y. Wang, *Kao Teng Hsueh Hsiao Hua Hsueh Hsueh Pao*, 2 (1981) 327.
327 A. Wreczycka, A. Wreczycki and N. Zelichowicz, *Mater. Semin. Nauk. Wyd. Mat. Przynr.*, 2 (1979) 140.
328 Z. Xiu and Z. Zhong, *Yaoxue Tongbao*, 17 (1982) 722.
329 G. I. Bebashko and O. N. Oleshko, *Zh. Anal. Khim.*, 37 (1982) 640.
330 O. V. Bibik and V. I. Gorokhovskaya, *Khim. Tekhnol. Pererab. Nefti Gaza*, (1981) 55.
331 D. C. Brune and I. Gonzalez, *Plant Cell Physiol.*, 23 (1982) 1323.

- 332 J. Gulens, H. D. Herrington, J. W. Thorpe, G. Mainprize, M. G. Cooke, P. Dal Bello and C. Macdougall, *Anal. Chim. Acta*, 138 (1982) 55.
- 333 J. Gulens and D. W. Shoemith, *J. Electrochem. Soc.*, 128 (1981) 811.
- 334 D. Haberland and W. Treichler, *Chem. Techn. (Leipzig)*, 34 (1982) 195.
- 335 S. S. M. Hassan and M. M. Habib, *Analyst (London)*, 106 (1981) 1281.
- 336 S. S. M. Hassan and M. M. Habib, *Fresenius Z. Anal. Chem.*, 307 (1981) 205.
- 337 S. S. M. Hassan and G. A. Rechnitz, *Anal. Chem.*, 54 (1982) 1972.
- 338 H. Jager and E. Tschager, *Dtsch. Molk. Ztg.*, 100 (1979) 1658.
- 339 A. Landet, P. Bogard, J.-C. Viré, G. J. Patriarce and G. D. Christian, *Anal. Lett.*, A14 (1981) 1135.
- 340 J. L. F. D. Lima and A. A. Machado, *Rev. Port. Quim.*, 21 (1979) 15.
- 341 F. Malecki and R. Starosćik, *Anal. Chim. Acta*, 139 (1982) 353.
- 342 S. Tong, *Fenxi Huaxue*, 10 (1982) 297.
- 343 Yu. G. Vlasov and Yu. E. Ermolenko, *Elektrokhimiya*, 17 (1981) 1301.
- 344 Yu. G. Vlasov and Yu. E. Ermolenko, *Ion. obmen i ionometriya (Leningrad)*, 3 (1982) 162.
- 345 B. L. Wilson, R. R. Schwarzer, C. O. Chukwuenye and J. Cyrous, *Microchem. J.*, 26 (1981) 402.
- 346 B. L. Wilson, R. R. Schwarzer and C. O. Chukwuenye, *Microchem. J.*, 27 (1982) 558.
- 347 T. G. Aityurina, V. V. Kikyanskii and A. F. Zhukov, *Khim. Promst. (Moscow)*, 1 (1981) 24.
- 348 A. Avdeef, J. Zabronsky and H. H. Stuting, *Anal. Chem.*, 55 (1983) 298.
- 349 R. Bertram and E. Hillrichs, *J. Electroanal. Chem.*, 129 (1981) 365.
- 350 G. A. Bhat, R. A. Saar, R. B. Smart and J. H. Weber, *Anal. Chem.*, 53 (1981) 2275.
- 351 H. Bourbognon, J.-J. Fombon, F. Lancelot, J. Paris, M. Roubin and J. Tacussel, *Analisis*, 9 (1981) 385.
- 352 S. N. K. Chaudhari, F. C. Chang, K. L. Cheng and V. Y. Young, *Anal. Chem.*, 52 (1981) 2048.
- 353 S. N. K. Chaudhari and K. L. Cheng, *Mikrochim. Acta*, 1980 II, 159.
- 354 M. Czae and T. Hong, *Taehan Chon'gi Hwahakhoe Chi*, 26 (1982) 427.
- 355 M. F. Ebel, *Anal. Chem. Symp. Ser.*, 8 (1981) 89.
- 356 M. F. El-Tarras, M. M. Amer and F. H. Mitwally, *Anal. Lett.*, A14 (1981) 1297.
- 357 M. Fan and B. Lu, *Fanxi Huaxue*, 9 (1981) 594.
- 358 F.-Ch. Fang, *J. Chin. Chem. Soc. (Taipei)*, 28 (1981) 15.
- 359 E. Ghali and A. Lewenstam, *Anal. Chem. Symp. Ser.*, 8 (1981) 235.
- 360 H. Gruber, *Metallurgie (Berlin)*, 36 (1982) 1072.
- 361 S. S. M. Hassan, *Talanta*, 28 (1981) 89.
- 362 S. S. M. Hassan and M. M. Habib, *Fresenius Z. Anal. Chem.*, 307 (1981) 413.
- 363 T. Hepel, *Anal. Chim. Acta*, 123 (1981) 151.
- 364 T. Hepel, *Anal. Chim. Acta*, 123 (1981) 161.
- 365 T. Hepel, *Anal. Chim. Acta*, 142 (1982) 217.
- 365 (a) M. A. Ilyushenko and V. A. Mirkin, *Issled. Ravnoves. Sistem (Alma-Ata)* 1982, p. 52.
- 366 B. Kratochevčí and C. Maitra, *Can. J. Chem.*, 60 (1982) 2387.
- 367 G. G. Lopachak and N. V. Bausova, *Zavod. Lab.*, 47 (1981) 9.
- 369 P. Mohanakrishnan and C. F. Chignell, *J. Pharm. Sci.*, 71 (1982) 1180.
- 370 D. Negoiu, M. S. Ionescu and C. Cristescu, *Rev. Chim. (Bucharest)*, 32 (1981) 67.
- 371 E. Pungor, K. Tóth, G. Nagy, L. Pólos, M. F. Ebel and I. Wernink, *Anal. Chim. Acta*, 147 (1983) 23.
- 372 D. Qi, T. Yin and X. Wu, *Huaxue Xuebao*, 40 (1982) 243.
- 373 Nj. Radić, *Anal. Lett.*, A14 (1981) 1125.
- 374 S. Sakura and R. Virtanen, *Bull. Chem. Soc. Jpn.*, 54 (1981) 1360.
- 375 W. Selig, *Microchem. J.*, 27 (1982) 102.

- 376 W. Selig, *Microchem. J.*, 28 (1983) 126.
377 W. Selig, *Mikrochim. Acta*, (1982) II, 141.
378 R. Stella and M. T. Ganzerli-Valentini, *Anal. Chem.*, 51 (1979) 2148.
379 J. Siemroth and I. Hennig, *Anal. Chem. Symp. Ser.*, 8 (1981) 339.
380 H. Stunzi, *Talanta*, 29 (1982) 75.
381 I. Uemasu and I. Iwamoto, *Anal. Chem.*, 54 (1982) 835.
382 Y. Umezawa, I. Uemasu and M. Watanabe, *Denki Kagaku*, 50 (1982) 109.
383 Yu. G. Vlasov, S. S. Mikhailova, V. V. Kolodnikov and Yu. E. Ermolenko, *Zh. Anal. Khim.*, 37 (1982) 2155.
384 F. C. Walsh and D. R. Gabe, *J. Appl. Electrochem.*, 11 (1981) 117.
385 G. Wunsch and B. Führer, *Fresenius Z. Anal. Chem.*, 313 (1982) 413.
386 V. Y. Young, S. N. Chaudhari and K. L. Cheng, *Surf. Interface Anal.*, 3 (1981) 176.
387 A. Yuchi, H. Wadu and G. Nakagawa, *Anal. Chim. Acta*, 149 (1983) 209.
388 P. W. Alexander and C. Maitra, *Anal. Chem.*, 54 (1982) 68.
389 W. R. Barnard and D. K. Nordstrom, *Atmos. Environ.*, 16 (1982) 99.
390 C. G. Beddows and D. Kirk, *Analyst (London)*, 106 (1981) 1341.
391 W.-L. Bie and G.-F. Dong, *Ti Chih K'o Hsueh*, 4 (1980) 399.
392 E. I. Bobrikova, T. B. Andreeva and V. V. Bardin, *Zh. Anal. Khim.*, 37 (1982) 2186.
393 A. Dolegal, D. Devilliers, G. Villard and M. Chemla, *Analisis*, 10 (1982) 377.
394 B. Eyde, *Fresenius Z. Anal. Chem.*, 311 (1982) 19.
395 T. A. Fjeldly and K. Nagy, *Anal. Chem. Symp. Ser.*, 8 (1981) 215.
396 D. Gawlik, W. Gatschke, D. Behne and P. Braetter, *J. Radioanal. Chem.*, 61 (1981) 313.
397 Y.-Ch. Ho M.-S. Mo, Y.-H. Chang and Ch.-H. Hsu, *Fen Hsi Hua Hsueh*, 8 (1980) 525.
398 L. Ilcheva, *Khim. Ind. (Sofia)*, 5 (1982) 230.
399 L. Ilcheva, K. Boshnakov and P. Bozadzniev, *Khim. Ind. (Sofia)*, 9 (1981) 402.
400 Y. Ji, *Huanjing Bachu (Beijing)*, 12 (1982) 10.
401 N. Kokubu, Y. Hayaside, T. Kobayasi and A. Yamasaki, *Denki Tsushin Daigaku Gakuho*, 31 (1980) 113.
402 H. Konno and M. Akizuki, *Neues Jahrb. Mineral. Monatsh.*, 10 (1982) 465.
403 S. N. Misra, *Vijnana Parishad Anusandhan Patrika*, 23 (1980) 383.
404 K. Nicholson and E. J. Duff, *Anal. Lett.*, A14 (1981) 493.
405 K. Nicholson and E. J. Duff, *Anal. Lett.*, A14 (1981) 887.
406 K. Nicholson and E. J. Duff, *Analyst (London)*, 106 (1981) 904.
407 K. Nicholson and E. J. Duff, *Analyst (London)*, 106 (1981) 985.
408 P. Pakalns, *Mikrochim. Acta*, 1983, I, 29.
409 A. Panaiotova, *Geokhim. Mineral. Petrol.*, 12 (1980) 83.
410 R. Pardo, J. L. Bernal and E. Barrado, *Anal. Lett.*, A14 (1981) 1541.
411 K. A. Phillips and C. J. Rix, *Anal. Chem.*, 53 (1981) 2141.
412 Ch. R. Powley and T. A. Nieman, *Anal. Chim. Acta*, 139 (1982) 83.
413 R. Sarin, *J. Inst. Chem. (India)*, 54 (1982) 116.
414 I. W. Siddiqi, *Clin. Chem.*, 28 (1982) 1962.
415 V. Simeonov, A. Voulgaropoulos, C. Apestopoulou and G. Vasilikiotis, *Fresenius Z. Anal. Chem.*, 311 (1982) 16.
416 V. Simeonov, A. Voulgaropoulos, M. Mihail and G. Vasilikiotis, *Fresenius Z. Anal. Chem.*, 314 (1983) 414.
417 R. A. Skorniyakova, L. V. Konyakhina and A. V. Grinevich, *Zavod. Lab.*, 47 (1981) 22.
418 D. J. Souganidis, T. M. N. Athanassouli and D. S. Papastathopoulos, *J. Dent. Res.*, 60 (1981) 103.
419 M. Trojanowicz and A. Hulanicki, *Mikrochim. Acta*, (1981) II, 17.
420 P. Van Der Winkel, G. De Backer, M. Vandeputte, N. Mertens, L. Dryon and D. L. Massart, *Anal. Chim. Acta*, 145 (1983) 207.
421 S. Vigoureaux, *Z. Wasser Abwasser Forsch.*, 15 (1982) 29.

- 422 H.-Ch. Wang, Fen Hsi Hua Hsueh, 8 (1980) 553.
423 H.-Z. Wang, Kang T'ieh, 15 (1980) 40.
424 Cheng-Yi Wang, Microchem. J., 27 (1982) 455.
425 F. Wu, L. Tang and Ch. Liu, Huanjing Kexue, 5 (1982) 46.
426 T. Ch. Yang and J. P. Tang, Ssu Ch'uan I Hsueh Yuan Hsueh Pao, 12 (1981) 237.
427 R. Yu, H. Gong and B. Chen, Gaodeng Xuexiao Huaxue Xuebao, 3 (1982) 55.
428 J. Yuan, Huanjing Kexue, 3 (1982) 58.
429 L. Xiang, Ch. Liu and Z. Hu, Fenxi Huaxue, 9 (1981) 698.
430 G. Zhu and H. Hua, Beijingdaxue Xuebao Zivan Kexue Ban, 4 (1981) 59.
431 A. Kowal, E. Krauss and A. Pomianowski, Chem. Anal. (Warsaw), 26 (1981) 441.
432 A. Kowal and R. Niewara, Paper 3, Int. Symp. Electroanal. Biomed. Environ. Ind. Sci., Cardiff 1983.
433 L. I. Manakova, N. V. Bausova and V. L. Volkov, Zh. Anal. Khim., 37 (1982) 539.
434 Y. Sanada, T. Akiyama and E. Niki, Bunseki Kagaku, 30 (1981) 678.
435 Y. Sanada, T. Akiyama, Y. Ujihira and E. Niki, Fresenius Z. Anal. Chem., 312 (1982) 526.
436 I. Sekerka and J. F. Lechner, Analyst (London), 106 (1981) 323.
437 Y. Suzuki, H. Itoh and T. Nakano, Rare Earths Mod. Sci. Technol., 3 (1982) 521.
438 Yu. G. Vlasov, V. V. Kolodnikov and V. G. Chernykh, Zh. Anal. Khim., 36 (1981) 1319.
439 Y. Yu, Huaxue Tongbao, 3 (1982) 148.
440 C. Agache and J. Alary, Bull. Trav. Soc. Pharm. Lyon, 23 (1979) 44.
441 P. Anker, E. Wieland, D. Ammann, R. E. Dohner, R. Asper and W. Simon, Anal. Chem., 53 (1981) 1970.
442 L. L. Beynon, Urinary Calculus, Int. Urinary Stone Conf., 1981, p. 363.
443 C. K. Biswas, J. M. Ramos and D. N. S. Kerr, Clin. Chim. Acta, 116 (1981) 343.
444 K. Bjorvath and T. Moerch, Acta Odontol. Scand., 37 (1979) 259.
445 H. M. Brown and B. Rydqvist, Biophys. J., 36 (1981) 117.
446 S. J. Butler and R. B. Payne, Clin. Chem., 29 (1983) 585.
447 Q. M. Chan, K. O. Ash, W. Hentschel and J. Wu, Clin. Chem., 27 (1981) 204.
448 Ch. Chen, Fenxi Huaxue, 10 (1982) 98.
449 M. Dagostino and O. Ch. Lee, Biophys. J., 40 (1982) 199.
450 P. G. Daniele, C. Rigano and S. Sammartano, Ann. Chim. (Rome), 72 (1982) 341.
451 V. G. Derkasova and L. I. Grigorova, Deposited Doc., SPSStl. 650 KHP-D 81, 7 pp., (1981).
452 S. E. Dibina, E. A. Materova, A. L. Grekovich and L. P. Vatlina, Elektrokimiya, 17 (1981) 598.
453 A. J. Diez, Laboratorio (Granada, Spain), 412 (1980) 301.
454 R. Di Polo, H. Rojas, J. Vergara, R. Lopez and C. Caputo, Biochim. Biophys. Acta, 728 (1983) 311.
455 L. J. Drop, D. R. Miscano and L. N. Tochka, Clin. Chem., 28 (1982) 2448.
456 L. J. Drop, L. N. Tochka and D. R. Misiano, Clin. Chem., 28 (1982) 129.
456 (a) P. H. Duncan, M. R. Wills, B. J. Smith and J. Savory, Clin. Chem., 28 (1982) 672.
457 V. M. Dziomko, I. S. Markovich, A. M. Kapustin, G. M. Sorokina, L. I. Blokhina, N. V. Kruglova, N. A. Bolotina and Yu. S. Ryabokobytko, Zh. Vses. Khim. Ova., 26 (1981) 466.
458 M. M. Emar, N. A. Farid and A. M. Waafi, Electrochim. Acta, 27 (1982) 647.
459 D. Erne and D. Ammann, Role Calcium Biol. Syst., 1 (1982) 71.
460 D. Erne, D. Ammann, A. F. Zhukov, F. Behm, E. Pretsch and W. Simon, Helv. Chim. Acta, 65 (1982) 538.
461 M.-N. Fan and P.-Ch. Lu, Fen Hsi Hua Hsueh, 8 (1980) 408.
462 P. Ferreira and B. E. Jacobson, J. Autom. Chem., 5 (1983) 40.
463 N. Fogh-Andersen, Clin. Chem., 27 (1981) 1264.
464 J. A. Fyffe, J. Autom. Chem., 4 (1982) 79.

- 465 J. A. Fyffe, A. S. Jenkins, C. J. Bolland, F. J. Dryburgh and M. D. Gardner, *Ann. Clin. Biochem.*, 18 (1981) 110.
- 466 M. D. Gardner, F. J. Dryburgh, J. A. Fyffe and A. S. Jenkins, *Ann. Clin. Biochem.*, 18 (1981) 106.
- 467 A. L. Grekovich, S. E. Didina and E. A. Materova, *Ion. obmen i ionometriya (Leningrad)*, 3 (1982) 123.
- 467 (a) P. Hess, P. Metzger and R. Weingart, *J. Physiol. (London)*, 333 (1982) 173.
- 468 T. Hirai, Y. Kurosawa, E. Mizuno, H. Kiyose, H. Naka and H. Ohta, *Eisei Kensa*, 31 (1982) 1027.
- 469 A. Hulanicki, M. Trojanowicz and Z. Augustowska, *Anal. Chem. Symp. Ser. 8*, (1981) 251.
- 470 A. Hulanicki, M. Trojanowicz and Z. Augustowska, *Chem. Anal., (Warsaw)*, 26 (1981) 115.
- 471 Z. Jiang, H. Hua, X. Fu, X. Zhou and W. Zhang, *Beijing Daxue Xuebao Ziran Kexueban*, 1 (1982) 56.
- 472 A. M. Kapustin, G. M. Sorokina, M. V. Ryazanova, I. A. Zaidenman, I. S. Markovich and V. M. Dziomko, *Elektrokimiya*, 18 (1982) 1435.
- 473 M. A. Koupparis, E. P. Diamandis and H. V. Malmstadt, *Clin. Chem.*, 28 (1982) 2149.
- 474 N. Lakshminarayanaiah, *J. Membrane Sci.*, 8 (1981) 255.
- 475 F. Lanter, R. A. Steiner, D. Ammann and W. Simon, *Anal. Chim. Acta*, 135 (1982) 51.
- 476 Ya. F. Lushchik, E. M. Rakhmanko, V. N. Muraveva and G. L. Starobinets, *Vestsi Akad. Nauk BSSR. Ser. Khim. Nauk*, 3 (1982) 8.
- 477 M. Maj-Żurawska, D. Erne, D. Ammann and W. Simon, *Helv. Chimica Acta*, 65 (1982) 55.
- 478 R. W. Marshall and A. Hodgkinson, *Clin. Chim. Acta*, 127 (1983) 305.
- 479 C. Mottola and D. Romeo, *J. Cell. Biol.*, 93 (1982) 129.
- 480 T. Nakamura, S. Morozumi and K. Izutsu, *Chem. Lett.*, 9 (1982) 1317.
- 481 V. V. Osipov, V. A. Mikhailov, V. A. Sergeeva and I. L. Novikova, *Izv. Sib. Otd. Akad. Nauk SSSR. Ser. Khim. Nauk*, 5 (1982) 46.
- 482 R. B. Payne, *Ann. Clin. Biochem.*, 19 (1982) 233.
- 483 J. Petránek and O. Ryba, *Anal. Chim. Acta*, 128 (1981) 129.
- 484 J. Petránek and O. Ryba, *Collect. Czech. Chem. Commun.*, 45 (1980) 1567.
- 485 J. Petránek and O. Ryba, *Tetrahedron Lett.*, (1977) 4249.
- 486 S. B. Plant and D. A. McCarron, *Clin. Chem.*, 28 (1982) 1362.
- 487 W. P. Shemerdiak, S. C. Kukrega, T. E. Lad, P. A. York and W. J. Henderson, *Clin. Chem.*, 27 (1981) 1621.
- 488 T. Shiba, T. Uruno, K. Kubota and K. Tagaki, *Jpn. J. Pharmacol.*, 31 (1981) 553.
- 489 K. Sykut, J. Dumkiewicz and R. Dumkiewicz, *Ann. Univ. Mariae Curie-Sklodowska, Sect. AA*, 33 (1979) 1.
- 489 (a) J. Thode, J. Wandrup, F. Aas and O. Siggaard-Anderson, *Scand. J. Clin. Lab. Invest.*, 42 (1982) 407.
- 490 T. Uruno, T. Shiba and K. Kubota, *J. Pharmacol. Methods*, 5 (1981) 127.
- 491 P. Vadgama, J. Mitchison, A. K. Covington and K. G. M. M. Alberti, *Clin. Chim. Acta*, 119 (1982) 249.
- 492 J. Voipio and K. Kaila, *Proc. 4th Natl. Meet. Biophys. Med. Eng. Finl.*, (1982) 121.
- 493 G. K. Worth, R. W. Retallack, R. D. Devlin, M. Jefferies and D. H. Gutteridge, *Clin. Chim. Acta*, 114 (1981) 283.
- 494 J. Xuan, *Turang (Nanjing)*, 14 (1982) 143.
- 495 B. Yan and G. Yao, *Shipin yu Faxiao Gongye*, 2 (1982) 17.
- 496 E. Barrado, J. L. Bernal and M. J. del Nozal, *Afinidad*, 38 (1981) 96.
- 497 J. L. Bernal, R. Pardo and E. Barrado, *Anal. Lett.*, 13 (A) (1980) 241.
- 498 L. Campanella, R. Marabito and L. Sorrentino, *Not. Met. Anal. Acq.*, 2 (1982) 1.
- 499 E. Campi, G. Saini and R. Castelli, *Ann. Chim., (Rome)*, 72 (1982) 471.
- 500 M. Geissler and R. Kunze, *Fresenius Z. Anal. Chem.*, 314 (1983) 560.

- 501 D. G. Hadjidemetrio, *Analyst* (London), 107 (1982) 25.
- 502 K. Haga, *Chikusan Shikenjo Kenkyu Hokoku*, 36 (1979) 111.
- 503 H. Hara, S. Okazaki and T. Fujinaga, *Bunseki Kagaku*, 30 (1981) 86.
- 504 E. Hopirtean, E. Stefanica and C. Liteanu, *Rev. Chim. (Bucharest)*, 33 (1982) 275.
- 505 M. A. Jackson, J. B. Jackson and S. J. Ferguson, *FEBS Lett.*, 136 (1981) 275.
- 506 C. Liteanu, E. Stefanica and E. Hopirtean, *Rev. Anal. Chem.*, (1981) 159.
- 507 V. K. Menkin, V. S. Shterman, M. A. Buryakova and V. V. Krasnoshchekov, *Osn. Povysh. Prod. S-Kh. Zhivotn.*, (1981) 108.
- 508 *Metody pro Zavádění Výsledků Výzkumu do Praxe, Stanovení Dusičnanů v Půdě, Rostlinách a Krmivech (Methods for Practical Applications of Research Results)*, Institute of Scientific and Technical Information for Agriculture, Prague, 1979, No. 23.
- 509 E. B. Schalscha, T. Schirado and I. Vergara, *Soil Sci. Soc. Am. J.*, 45 (1981) 446.
- 510 I. N. Semenova and O. M. Petrukhin, *Zh. Anal. Khim.*, 37 (1982) 761.
- 510 (a) M. Semler and M. Panoch, *Chem. Prům.*, 31 (1981) 478.
- 511 J. Staňa, *Agrochemia (Bratislava)*, 22 (1982) 119.
- 512 K. Suzuki, H. Ishiwada, T. Shirai and S. Yanagisawa, *Bunseki Kagaku*, 29 (1980) 816.
- 513 I. Cohen and R. Kline, *Circ. Res.*, 50 (1982) 1.
- 514 A. Dimante and A. Veveris, *Khim. Farm. Zh.*, 16 (1982) 510.
- 515 N. A. Fedotov, L. M. Khitrov, V. A. Zarinskii, I. Ya. Kolotyrkina and V. G. Lazarev, *Zh. Anal. Khim.*, 37 (1982) 80.
- 516 M. Fujimoto, K. Kajino, K. J. Peterson-Yantorno and K. Kotera, in M. Yoshida, Y. Hagihara and S. Ebashi (Eds.), *Adv. Pharmacol., Ther. Proc. 3rd Int. Cong.*, Pergamon Press, Oxford, 1982, p. 309.
- 517 J. Gajowski, B. Rieckemann and F. Umland, *Fresenius Z. Anal. Chem.*, 309 (1981) 343.
- 518 A. L. Grekovich, G. A. Troshina, K. N. Mikhelson and E. A. Materova, *Ion. obmen i ionometriya (Leningrad)*, 3 (1982) 138.
- 519 H. Hagberg and H. Haljamae, *Acta Physiol. Scand.*, 113 (1981) 535.
- 520 L. Jalkanen and R. Virtanen, *Anal. Lett.*, A14 (1981) 479.
- 521 J. Kopáč, Z. Drobníková, M. Panoch and M. Semler, *Čas. Lek. Česk.*, 121 (1982) 1255.
- 522 G. Marquis and J. Lebel, *Anal. Lett.*, A14 (1981) 913.
- 523 G. Meyer, S. Henin and D. Cremaschi, *Rend. Ist. Lomb. Accad. Sci. Lett. B*, 113 (1979) 55.
- 524 K. N. Mikhelson, A. L. Grekovich and E. A. Materova, *Elektrokhimiya*, 18 (1982) 1237.
- 525 K. N. Mikhelson, A. L. Grekovich, E. A. Materova and L. I. Dementyeva, *Elektrokhimiya*, 18 (1982) 1241.
- 526 K. N. Mikhelson, A. L. Grekovich, E. A. Materova and S. Yu. Filippov, *Elektrokhimiya*, 18 (1982) 59.
- 527 D. F. Moffett, R. L. Hudson, S. B. Moffett and R. L. Ridgway, *J. Membr. Biol.*, 70 (1982) 59.
- 528 M. Morad, *Fed. Proc., Fed. Am. Soc. Exp. Biol.*, 39 (1980) 1533.
- 529 Sh. K. Norov, A. K. Tashmukhamedova and N. Zh. Saifullina, *Zh. Anal. Khim.*, 37 (1982) 222.
- 530 T. L. Parfenteva, Ya. I. Turyan and S. A. Ovchinnikova, *Izv. vyssh. uchebn. zaved., Pishch. Tekhnol.*, 6 (1982) 108.
- 531 I. Shabunova and F. Vyskočil, *Pfluegers Arch.*, 394 (1982) 161.
- 532 O. K. Stefanova, A. P. Manzhos and M. M. Shults, *Elektrokhimiya*, 18 (1982) 423.
- 533 H. Tamura, K. Kimura and T. Shono, *Anal. Chem.*, 54 (1982) 1224.
- 534 R. C. Thomas and Ch. J. Cohen, *Pfluegers Arch.*, 390 (1981) 96.
- 535 S. M. Tkachenko, V. V. Suprunova and V. M. Pyartli, *Khim. Promst. (Moscow)*, 2 (1981) 27.

- 536 M. Yamauchi, A. Jyo and N. Ishibashi, *Anal. Chim. Acta*, 136 (1982) 399.
- 537 V. E. Yurinskaya, O. K. Stefanova and E. A. Materova, *Elektrokhimiya*, 17 (1981) 1628.
- 538 Z. Yu, Z. Huang, M. Zhang and X. Zhou, *Huaxue Xuebao*, 40 (1982) 1076.
- 539 G. Wu, X. Xue, C. Lu and S. Gao, *Fenxi Huaxue*, 9 (1981) 582.
- 540 K. M. Aalmo and J. Krane, *Acta Chem. Scand.*, A36 (1982) 227.
- 541 A. Dimante and A. Veveris, *Khim. Farm. Zh.*, 16 (1982) 116.
- 542 S. M. Friedman, R. A. McIndoe and G. Spieckermann, *Am. J. Physiol.*, 242 (1982) H 751.
- 543 J. Hall and J. T. Pearson, *J. Pharm. Pharmacol.*, 32 (1980) 69 P.
- 544 S.-W. Kao, Ch.-M. Lu, H.-H. Hsueh, K.-L.-Wu, Ch.-H.-Yan, Ch.-Ch. Kao, K.-Ch. Tan and Ch.-Ch. Yao, *K'o Hsueh T'ung Pao*, 25 (1980) 863.
- 545 J. M. Kapsha, *Exp. Neurol.*, 75 (1982) 320.
- 546 E. A. Materova, Z. S. Alagova and G. I. Shumilova, *Ion. obmen i ionometriya (Leningrad)*, 3 (1982) 92.
- 547 T. Shono, M. Okahara, I. Ikeda, K. Kimura and H. Tamura, *J. Electroanal. Chem.*, 132 (1982) 99.
- 548 A. Winkler, D. Siebers and K. Leweck, *GIT Fachz. Lab.*, 26 (1982) 228.
- 549 D. F. Anghel, *Inter. Symp. Electroanal.*, 13.—16.4.1981, Cardiff, Wales.
- 550 D. F. Anghel and Q. Popescu, *Mikrochim. Acta*, (1981) I, 441.
- 551 D. F. Anghel, G. Popescu and F. Niculescu, *Tenside Deterg.*, 17 (1980) 171.
- 552 E. N. Avdeeva, Yu. V. Shavnya and O. M. Petrukhin, *Zh. Anal. Khim.*, 37 (1982) 1434.
- 553 T. N. Blanton, J. B. Justice and G. B. Trowbridge, *Biochem. Biophys. Res. Commun.*, 102 (1981) 219.
- 554 E. S. Borovskii, E. M. Rakhman'ko, G. L. Starobinets and N. P. Labetskaya, *Zavod. Lab.*, 48 (1982) 20.
- 555 L. Campanella and T. Ferri, *Fresenius Z. Anal. Chem.*, 302 (1980) 304.
- 556 L. Campanella, T. Ferri and M. Gabrielli, *Rev. Roum. Chim.*, 27 (1982) 681.
- 557 L. Campanella, L. Sorrentino and M. Tomassetti, *Anal. Lett.*, 18B (1982) 1515.
- 558 R. Casadio, G. Venturoli and B. A. Melandri, *Photobiochem. Photobiophys.*, 2 (1981) 245.
- 559 K.-X. Chang, H.-Ch. Fu, W.-X. Chen, H.-Ch. Wang and Q. Yuan, *Hua Hsueh Hsueh Pao*, 38 (1980) 223.
- 560 K. K. Choi and K. W. Fung, *Anal. Chim. Acta*, 138 (1982) 385.
- 561 T. K. Christopoulos, E. P. Diamandis and T. P. Hadjiioannou, *Anal. Chim. Acta*, 143 (1982) 143.
- 562 C. J. Coetzee and A. J. Basson, *Anal. Chim. Acta*, 126 (1981) 217.
- 563 L. Cunningham and H. F. Freiser, *Anal. Chim. Acta*, 132 (1981) 43.
- 564 L. Cunningham and H. Freiser, *Anal. Chim. Acta*, 139 (1982) 97.
- 565 S. S. Davis and O. Olejnik, *Anal. Chim. Acta*, 132 (1981) 51.
- 566 E. P. Diamandis, C. E. Efstathiou, D. S. Papastathopoulos and T. P. Hadjiioannou, *Microchem. J.*, 28 (1983) 227.
- 567 E. P. Diamandis and T. P. Hadjiioannou, *Mikrochim. Acta*, (1980) II, 27.
- 568 E. P. Diamandis and T. P. Hadjiioannou, *Anal. Chim. Acta*, 123 (1981) 143.
- 569 E. P. Diamandis and T. P. Hadjiioannou, *Anal. Chim. Acta*, 123 (1981) 341.
- 570 E. P. Diamandis and T. P. Hadjiioannou, *Analyst (London)*, 107 (1982) 1471.
- 571 E. P. Diamandis and T. P. Hadjiioannou, *Clin. Chem.*, 27 (1981) 455.
- 572 E. P. Diamandis and T. P. Hadjiioannou, *Microchem. J.*, 27 (1982) 512.
- 573 E. P. Diamandis, M. A. Koupparis and T. P. Hadjiioannou, *J. Chem. Educ.*, 60 (1983) 74.
- 574 E. P. Diamandis, D. S. Papastathopoulos and T. P. Hadjiioannou, *Clin. Chem.*, 27 (1981) 427.
- 575 E. P. Diamandis, E. Athanasio-Malaki, D. S. Papastathopoulos and T. P. Hadjiioannou, *Anal. Chim. Acta*, 128 (1981) 239.
- 576 L. D. Dolaberidze, D. K. Kamkamidze, A. G. Dzhalishvili and T. M. Alkhazishvili, *Soobshch. Akad. Nauk Gruz. SSR*, 105 (1982) 297.

- 577 C. E. Efstathiou, E. P. Diamandis and T. P. Hadjiioannou, *Anal. Chim. Acta*, 127 (1981) 173.
- 578 M. Z. Gadashevich, I. A. Gurev, E. A. Gushchina, A. A. Kalugin and V. D. Selivanov, *Zavod. Lab.*, 47 (1981) 11.
- 579 Z.-F. Gao, Q. Yuan and H.-Y. Sheng, *Yu Chi Hua Hsueh*, 4 (1981) 259.
- 580 J. Greenberg and M. E. Meyerhoff, *Anal. Chim. Acta*, 141 (1982) 57.
- 581 E. A. Gribova, Z. I. Fodiman and A. A. Cherkasskii, *Zavod. Lab.*, 48 (1982) 20.
- 582 E. A. Gribova, Z. I. Fodiman, A. A. Cherkasskii and I. V. Fedotova, *Zavod. Lab.*, 48 (1982) 24.
- 583 I. A. Gurev and E. A. Gushchina, *Zh. Anal. Khim.*, 37 (1982) 1670.
- 584 I. A. Gurev, E. A. Gushchina and M. Z. Gadashevich, *Zh. Anal. Khim.*, 36 (1981) 1149.
- 585 I. A. Gurev, M. I. Drofa, A. A. Kalugin and E. V. Sankova, *Zh. Anal. Khim.*, 37 (1982) 315.
- 586 T. P. Hadjiioannou and P. C. Gridzatis, *Anal. Chim. Acta*, 126 (1981) 51.
- 587 H. Hara, S. Okazaki and T. Fujinaga, *Anal. Chim. Acta*, 121 (1980) 119.
- 588 K. Hayakawa, A. L. Ayub and J. C. T. Kwak, *Colloids Surf.*, 4 (1982) 389.
- 589 K. Hayakawa and J. C. T. Kwak, *J. Phys. Chem.*, 86 (1982) 3866.
- 590 K. Hiroy, A. Kawahara and T. Tanaka, *Bunseki Kagaku*, 31 (1982) E 33.
- 591 E. R. Hogue and W. C. Landgraf, *Anal. Lett.*, B14 (1981) 1757.
- 592 Z. Hu, X. Qian and J. Chen, *Fenxi Huaxue*, 10 (1982) 493.
- 593 Z. Hu, X. Qian, J. Chen, X. Yang and Q. Yuan, *Huaxue Xuebao*, 39 (1981) 719.
- 594 A. Jaramillo, S. Lopez, J. B. Justice Jr., J. D. Salamone and D. B. Neill, *Anal. Chim. Acta*, 146 (1983) 149.
- 595 H. Hua, M. Cao, Q. Zhou and G. Wei, *Fenxi Huaxue*, 10 (1982) 65.
- 596 K. Kajino, *Osaka Ika Daigaku Zasshi*, 40 (1981) 194.
- 597 K. M. Kale, E. L. Cussler and D. F. Evans, *J. Solution Chem.*, 11 (1982) 581.
- 598 K. Kale, G. C. Kresheck and J. Erman, *Theor. Appl. Aspects Surfactants, Proc. Int. Symp.*, 1 (1982) 665.
- 599 N. Kamo, *Seibutsu Butsuri*, 22 (1982) 59.
- 600 N. Kamo, M. Muratsugu, R. Hongoh and Y. Kobatake, *J. Membr. Biol.*, 49 (1979) 105.
- 601 P. Karlovský and V. Dadák, *Folia Microbiol. (Praha)*, 27 (1982) 460.
- 602 P. Karlovský, P. Zbořil, I. Kučera and V. Dadák, *Biologia (Bratislava)*, 37 (1982) 787.
- 603 M. Kataoku, Y. Kobayashi and T. Kambara, *Denki Kagaku*, 50 (1982) 882.
- 604 A. V. Kopytyin, P. Gábor-Klatsmányi, V. P. Izvikov and E. Pungor, *Anal. Chim. Acta*, 148 (1983) 35.
- 605 A. V. Kopytyin, P. Gábor-Klatsmányi, V. P. Izvekoy, E. Pungor and G. A. Yagodin, *Magy. Kem. Foly.*, 88 (1982) 122.
- 606 A. V. Kopytyin, P. Gábor-Klatsmányi, V. P. Izvekoy, E. Pungor, G. A. Jagodin and E. G. Iljin, *Magy. Kem. Foly.*, 89 (1983) 87.
- 607 T. Korenaga, *Anal. Chim. Acta*, 120 (1980) 361.
- 607 (a) T. Korenaga, *J. Autom. Chem.*, 3 (1981) 191.
- 608 S. Kumar and D. J. D. Nicholas, *Biochem. Int.*, 3 (1981) 581.
- 609 V. V. Kutsovskaya, I. A. Gurev and I. M. Korenman, *Izv. Vyssh. Uchebn. Zaved. Khim. Khim. Tekhnol.*, 25 (1982) 1350.
- 610 J. L. F. D. Lima and A. A. S. C. Machado, *Rev. Port. Quim.*, 20 (1978) 70.
- 611 V. L. Lomako, G. L. Starobinets and E. M. Rakhmanko, *Vesti Akad. Navuk B. SSR. Ser. Khim. Navuk*, 6 (1980) 5.
- 612 E. A. Materova, T. Ya. Bart and S. V. Billionkov, *Ion. obmen i ionometriya (Leningrad)*, 3 (1982) 155.
- 613 E. A. Materova, T. Ya. Bart and O. V. Yagodina, *Ion. obmen i ionometriya (Leningrad)*, 3 (1982) 146.
- 614 J. E. G. McCarthy and S. J. Ferguson, *Biochem. J.*, 196 (1981) 311.

- 615 J. F. G. McCarthy, S. J. Ferguson and D. B. Kell, *Biochem. J.*, 196 (1981) 311.
- 616 M. Muratsugu, N. Kamo, Y. Kobatake and K. Kimura, *J. Electroanal. Chem.*, 104 (1979) 477.
- 617 M. Muratsugu, N. Kamo and Y. Kobatake, *Bioelectrochem. Bioenerg.*, 9 (1982) 325.
- 618 D. Negoin, M. S. Ionescu and V. V. Cosofret, *Talanta*, 28 (1981) 377.
- 619 J. Pan and F. Hao, *Fenxi Huaxue*, 10 (1982) 469.
- 620 J. Pan and Y. Liu, *Fenxi Huaxue*, 9 (1981) 593.
- 621 J. Pan, L. Cai, J. Wu and X. Liu, *Fenxi Huaxue*, 9 (1981) 453.
- 622 A. A. Pendin, P. K. Leontevskaya, S. V. Stolyar, T. P. Vishnyakov, I. D. Vlasova and T. A. Sokolinskaya, *Ion. obmen. i ionometriya (Leningrad)*, 3 (1982) 205.
- 623 L. Peng, *Fenxi Huaxue*, 10 (1982) 70.
- 624 E. M. Rakhmanko, E. S. Borovskii, G. L. Starobinets and N. P. Labetskaya, *Zh. Anal. Khim.*, 37 (1982) 1966.
- 625 K. Selinger and R. Staroscik, *Chem. Anal. (Warsaw)*, 27 (1982) 223.
- 626 N. V. Serebrennikova, I. I. Kukushkina and N. V. Plotnikova, *Zh. Anal. Khim.*, 37 (1982) 345.
- 627 A. Smajkiewicz and L. Przyborowski, *Ann. Univ. Mariae Curie-Sklodowska, Sect. D*, 35 (1980) 243.
- 628 M. Vadnere and S. Lindenbaum, *Int. J. Pharm.*, 11 (1982) 57.
- 629 K. Vytřas and M. Dajková, *Anal. Chim. Acta*, 141 (1982) 377.
- 630 K. Vytřas, M. Dajková and V. Mach, *Anal. Chim. Acta*, 127 (1981) 165.
- 631 K. Vytřas, M. Dajková and M. Remeš, *Česk. Farm.*, 30 (1981) 61.
- 632 K. Vytřas, M. Remeš and H. Kubešová-Svobodová, *Anal. Chim. Acta*, 124 (1981) 91.
- 633 K. Vytřas, J. Kalous, Z. Kalábová and M. Remeš, *Anal. Chim. Acta*, 141 (1982) 163.
- 634 K. Vytřas, J. Latinák, T. Čapoun and H. Svobodová, *Chem. Prum.*, 32 (1982) 81.
- 635 K. Vytřas, J. Symerský, C. Dožru and A. Onur, *Anal. Chim. Acta*, 149 (1983) 217.
- 636 W. H. Yu, G. X. Zhang and H. J. Wang, *Acta Chim. Sin.*, 41 (1983) 229.
- 637 G. Zhang, H. Fu, W. Chen and H. Wang, *Huaxue Xuebao*, 39 (1981) 940.
- 638 D. Ammann, F. Lanter, R. A. Steiner, P. Schulthess, Y. Shijo and W. Simon, *Anal. Chem.*, 53 (1981) 2267.
- 639 P. Anker, D. Ammann and W. Simon, *Mikrochim. Acta*, 1983, I (1983) 237.
- 640 E. Barrado and J. L. Bernal, *Afinidad*, 39 (1982) 349.
- 641 E. Barrado, J. L. Bernal and R. Pardo, *Afinidad*, 39 (1982) 344.
- 642 P. A. Bertrand, G. R. Choppin, L. F. Rao and J.-C. G. Bunzli, *Anal. Chem.*, 55 (1983) 364.
- 642 (a) W. Bussmann and W. Simon, *Helv. Chim. Acta*, 64 (1981) 2101.
- 643 R. L. Coon, N. C. Lai and J. P. Kampine, *J. Appl. Physiol.*, 40 (1976) 625.
- 644 Y. M. Fraticelli and M. E. Meyerhoff, *Anal. Lett.*, 14B (1981) 415.
- 645 Y. M. Fraticelli and M. E. Meyerhoff, *Anal. Chem.*, 53 (1981) 992.
- 646 Y. M. Fraticelli and M. E. Meyerhoff, *Anal. Chem.*, 53 (1981) 1857.
- 647 R. J. J. Funck, W. E. Morf, P. Schulthess, D. Ammann and W. Simon, *Anal. Chem.*, 54 (1982) 423.
- 648 T.-P. Huang, T.-H. Tai, M.-H. Tan, Ch.-M. Cheu and M.-Ch. Wang, *Fen Hsi Hua Hsueh*, 8 (1980) 516.
- 649 D. L. Jones, G. L. Moody, J. D. R. Thomas and B. J. Birch, *Analyst (London)*, 106 (1981) 974.
- 650 S. Kamata, M. Higo, T. Kamibeppu and I. Tanaka, *Chem. Lett.*, (1982) 287.
- 651 U. S. Lal, M. C. Chattopadnyaya and A. K. Dey, *J. Indian Chem. Soc.*, 59 (1982) 493.
- 651 (a) C. S. Luo, E. C. Chang and Y. C. Yeh, *Anal. Chem.*, 54 (1982) 2333.
- 652 T. Maeda, M. Ikeda, M. Shibahara, T. Harata and I. Satake, *Bull. Chem. Soc. Jpn.*, 54 (1981) 94.

- 653 M. E. Meyerhoff, *Anal. Chem.*, 52 (1980) 1532.
654 M. E. Meyerhoff, *Anal. Lett.*, 13 (1980) 1345.
655 M. E. Meyerhoff, Y. M. Fraticelli, J. A. Greenberg, J. Rosen, S. J. Parks and W. N. Opdycke, *Clin. Chem.*, 28 (1982) 1973.
656 M. E. Meyerhoff and R. H. Robins, *Anal. Chem.*, 52 (1980) 2383.
657 M. E. Meyerhoff, Y. M. Fraticelli, W. N. Opdycke, L. G. Bachas and A. D. Gordus, *Anal. Chim. Acta*, 154 (1983) 17.
658 N. V. Rozhdestvenskaya and O. K. Stefanova, *Elektrokhimiya*, 18 (1982) 1379.
658 (a) F. Schams, *Arbeitsber. Okol. (Umwelttech)*, 5 (1981) 73.
659 O. K. Stefanova and I. V. Rusina, *Elektrokhimiya*, 14 (1978) 882.
660 O. K. Stefanova, N. V. Rozhdestvenskaya, M. V. Hefelova, A. N. Sverdlova and I. A. Skulskii, *Elektrokhimiya*, 17 (1981) 1082.
661 M. A. Arnold and G. A. Rechnitz, *Anal. Chem.*, 53 (1981) 515.
662 M. A. Arnold and G. A. Rechnitz, *Anal. Chem.*, 53 (1981) 1837.
663 M. A. Arnold and G. A. Rechnitz, *Anal. Chem.*, 54 (1982) 777.
664 M. A. Arnold and G. A. Rechnitz, *Anal. Chem.*, 54 (1982) 2315.
665 M. A. Arnold and G. A. Rechnitz, *Anal. Chim. Acta*, 113 (1980) 351.
666 S. Collins and J. Janata, *Anal. Chim. Acta*, 136 (1982) 93.
667 C. L. Di Paolantonio, M. A. Arnold and G. A. Rechnitz, *Anal. Chim. Acta*, 128 (1981) 121.
668 C. L. Di Paolantonio and G. A. Rechnitz, *Anal. Chim. Acta*, 141 (1982) 1.
669 C. L. Di Paolantonio and G. A. Rechnitz, *Anal. Chim. Acta*, 148 (1983) 1.
670 S. R. Grobler, N. Basson and C. W. Vanwyk, *Talanta*, 29 (1982) 49.
671 J. Havas and G. G. Guilbault, *Anal. Chem.*, 54 (1982) 1991.
672 P. M. Kovach and M. E. Meyerhoff, *Anal. Chem.*, 54 (1982) 217.
673 S. Kuriyama, M. A. Arnold and G. A. Rechnitz, *J. Membr. Sci.*, 12 (1983) 269.
674 S. Kuriyama and G. A. Rechnitz, *Anal. Chim. Acta*, 131 (1981) 91.
675 H. Matsuoka, I. Karube, Y. Kawana, S. Suzuki, Y. Miyahara and T. Moriizumi, *Bunseki Kagaku*, 50 (1982) 856.
676 E. J. Alarcon, G. C. Barrios and B. M. E. Carrera, *Bol. Chil. Quim.*, 27 (1982) 361.
677 S. S. M. Hassan and M. M. Habib, *Anal. Chem.*, 53 (1981) 508.
678 S. S. M. Hassan and M. M. Habib, *Microchem. J.*, 26 (1981) 181.
679 J. F. P. M. Inácio, J. L. F. C. Lima and A. A. S. C. Machado, *Rev. Port. Quim.*, 23 (1981) 133.
680 W. U. Malik, S. K. Srivasrava and A. Bansal, *Anal. Chem.*, 54 (1982) 1399.
681 E. V. Smirnova, O. M. Petrukhin and S. L. Rogatinskaya, *Zh. Anal. Khim.*, 37 (1982) 2137.

A MINIATURE FLOW-THROUGH CELL WITH A FOUR-FUNCTION CHEMFET INTEGRATED CIRCUIT FOR SIMULTANEOUS MEASUREMENTS OF POTASSIUM, HYDROGEN, CALCIUM AND SODIUM IONS

A. SIBBALD, P. D. WHALLEY and A. K. COVINGTON*

*Electrochemistry Research Laboratories, Department of Physical Chemistry,
University of Newcastle-upon-Tyne, Newcastle-upon-Tyne, NE1 7RU (Great Britain)*

(Received 21st November 1983)

SUMMARY

A miniature, flow-through cell with a four-function ChemFET integrated-circuit is described for the simultaneous measurement of K^+ , H^+ , Ca^{2+} and Na^+ in aqueous solutions. Depletion-mode field-effect devices with ion-implanted n^- channels are used, in conjunction with ionophore-doped, polymeric electroactive gates. A polyimide/photopolymer-based technique is employed for selective encapsulation of the devices, and an efficient, V-type, flow-through cell cap, suitable for application in blood analysis, is described. The ChemFET cell has a dead-space of $30 \mu l$ and a 100% response time of 20 s at a sample flow rate of $24.3 \mu l s^{-1}$, hence the effective dead space is approximately $486 \mu l$. The useful lifetime of the cell is typically 4–12 weeks. Electronic circuitry is described for multiplexing the individual channels rapidly and accurately, and for linearizing the resultant analogue output signal.

Chemical-sensing field-effect transistors (ChemFETs) are now a well established feature in the scientific literature [1, 2], although none seems to be commercially available yet, primarily because of the technical difficulties of selective encapsulation, and multiple gate deposition, on a large scale (vide infra). ChemFET devices have many unique advantages over conventional ion-selective electrodes (i.e., those having internal reference solution), namely their very small dimensions, their robust, solid-state nature, their low output impedance and their potential for low-cost mass-fabrication. These qualities are particularly well-suited for biomedical applications, hence much research and development has been stimulated by the early work of Bergveld [3–5] and others [6, 7], although this has been directed almost exclusively towards the goal of providing sensing elements intended for deployment on the tips of intravenous catheters for in-vivo monitoring of blood electrolytes.

This monitoring philosophy is fraught with numerous intractable difficulties which seem unlikely to be resolved. For example, each device must be connected to several leadout wires and adequately and selectively encapsulated into a narrow-bore (≈ 1.3 mm) flexible, blood-compatible cannula,

and a suitable reference electrode must be incorporated into the system. All these items must be *extremely* electrochemically stable in the presence of whole blood. Further, the devices, with a reference electrode must be insensitive to ambient temperature changes, and must be sterilized and non-thrombogenic.

Some of these difficulties are removed if suitable, miniature conventional ion-selective electrodes (rather than ChemFETs) are used for in-vivo monitoring. Such systems have been described by Cobbe and Poole-Wilson [8] for the measurement of pH in central arteries and veins, and by Lim, Linton and Band [9, 10] for the continuous intravascular measurement of plasma potassium, but this approach is not well-suited for monitoring more than a single ionic species.

Extra-corporeal ChemFET usage is considered here to be preferable to catheter-tip application. It should be possible to realise the full biomedical potential of such devices by using an approach similar to that described by Band and Semple [11]. Band and Semple designed and used a pH glass electrode, located on the arm of a subject, and connected with very small deadspace directly to an indwelling intravenous needle; blood was drawn through the sensor and then discarded. This is a powerful technique because the data obtained may be considered virtually to represent in-vivo values; and because intermittent calibration is possible and anti-coagulation fluids may be added to the system. The limiting factor for extended use in this instance is the quantity of blood which may be safely removed from the patient, and this is directly related to the deadspace of the sensor and of the sensor input tubing. ChemFET devices, in flow-through-cell configuration, should be ideally suited to this application.

Accordingly, a number of flow-through cells has been developed for ChemFET devices. An early design was used for the on-line measurement of K^+ in human blood [12], and a 5-channel cell, with five discrete $E_{\mu-146}$ ChemFETs [13], was fabricated for the measurement of H^+ , K^+ , Ca^{2+} , Na^+ and Cl^- in the laboratory. Some shortcomings present in these early cell designs necessitated further development work which has resulted in a superior type of ChemFET flow-through cell for 4-channel measurement (K^+ , H^+ , Ca^{2+} and Na^+), described here, which is fabricated from materials and by processes that are compatible with mass-production techniques.

CONSTRUCTION OF THE SYSTEM

ChemFET I.C. structure and geometry

The $E_{\mu-144}$ ChemFET I.C. (Fig. 1) has a die size of 2.52×2.52 mm, and is fabricated on 75-mm diameter, p-type, 14–20 ohm cm, (100) silicon wafers by using an n-channel metal gate process, featuring a composite gate dielectric of 90-nm Si_3N_4 on 50-nm SiO_2 . The devices presented here have a lightly-doped n^- channel (to provide depletion-mode operation); this was created by an arsenic ion-implant before gate oxide growth, and sets

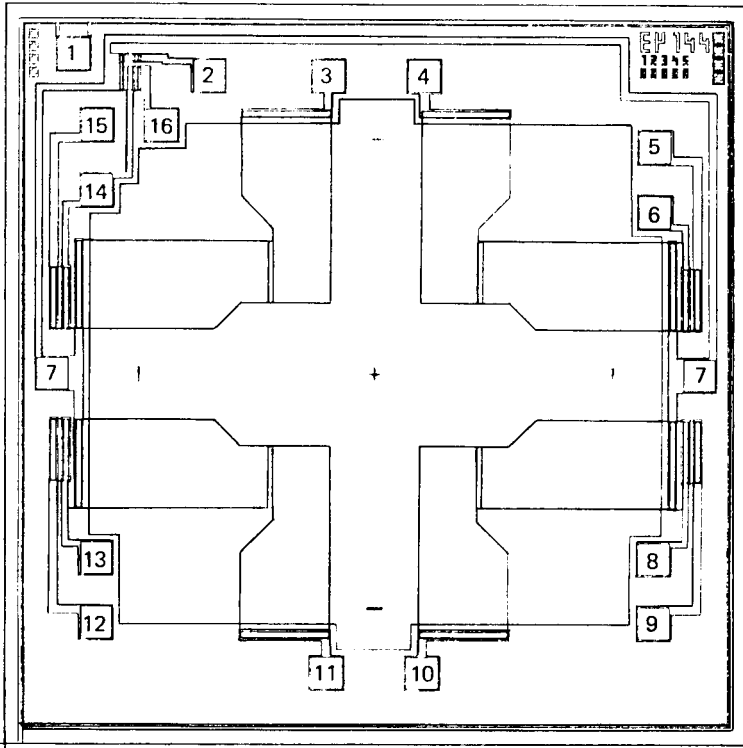


Fig. 1. Plan diagram of $E\mu$ -144 ChemFET I.C. (1) Bulk connection; (2) (test structure); (3) ChemFET A source; (4) ChemFET B source; (5) IGFET B source; (6) IGFET B gate; (7) common drain; (8) IGFET C gate; (9) IGFET C source; (10) ChemFET C source; (11) ChemFET D source; (12) IGFET D source; (13) IGFET D gate; (14) IGFET A gate; (15) IGFET A source; (16) (test structure).

the threshold voltage to approximately -0.9 V. Two process monitoring transistors are situated in the upper left corner and four ChemFET devices with low aspect-ratio source and drain diffusions (to minimise serial parasitic resistance) and $12 \times 206\text{-}\mu\text{m}$ channels are centrally located. Each ChemFET has a matched metal-gate IGFET located near the chip periphery, such that all eight devices (and both test transistors) share a common drain connection which is accessible by bonding pads on two sides of the chip; the common drain minimizes the number of leadout wires and therefore simplifies encapsulation procedures.

Encapsulation methodology

Miniature (20×7 mm), custom-designed printed circuit boards are used as chip-mounting substrates, configured to mate with 16-pin DIL socket adaptors (type 103-218, Farnell Electronic Components, Leeds). The copper tracks are gold-plated to ensure reliable wire bonding, and a centrally located recess (4 mm diameter, 0.5 mm deep) is milled out for locating the $E\mu$ -144

ChemFET I.C. The latter is attached with epoxy and then the substrate/I.C. assembly is cleaned. The cleanliness of the chip and the surrounding substrate are of paramount importance to successful encapsulation. The following successive, ultrasonic cleaning routine was adopted: detergent, distilled water ($\times 2$), propan-2-ol. After cleaning, the I.C. connections are wire-bonded to the substrate by using a gold-ball thermosonic bonder (Kulicke and Soffa, Horsham, PA; Type 2402-2), the I.C. is selectively encapsulated such that only the gate regions are exposed (see below), and the substrate is soldered to a 16-pin DIL socket adaptor. The individual electroactive gate films are then solvent-cast by using a cut-down pipette tip, and the flow-through cap is sealed into place with silicone rubber.

Previously described ChemFETs have been used with a variety of encapsulation agents. The most extensively used material is epoxy, although it is vital to choose a type which is not only suitable with regard to chemical inertness and low water absorption, but also has the correct degree of thixotropicity for selective encapsulation, i.e., which does not flow over the ChemFET gates during encapsulation. The Utah group use modified epoxy for this purpose [14], but a suitable epoxy which needs no modification was reported more recently [12].

Two types of encapsulation were successfully used in this work. Epo-Tek H54 epoxy is suitable for hand application over the I.C. periphery, metallization and bond-wires, followed by curing at 90°C for 1 h and a slow cooling cycle to minimize thermal shock; Epo-Tek 380 epoxy (non-flow), similarly cured, is ideal for partitioning the individual device gates. This technique is adequate for laboratory work on a small scale, but is not practicable for more extensive usage, which would need a suitable mass-encapsulation technique. For this reason, a novel encapsulation procedure utilising materials common to integrated circuit fabrication was developed, using a composite polymeric encapsulant. This comprises a thermally cured polyimide (Pyralin; Du-Pont (U.K.), Stevenage) and negative photoresist (Eastman-Kodak, Liverpool) and permits the selective exposure of the chemosensitive gate regions whilst ensuring adequate protection and electrical isolation of the remainder of the I.C. chip, the associated electrical connections, and the printed-circuit board on to which the I.C.s are mounted. The composite encapsulant has an estimated overall thickness of 30–50 μm .

The polyimide precursor is applied dropwise to the chip and surrounding substrate, and then partially cured as recommended by the manufacturer. After cooling, the substrates are dip-coated in negative photoresist and soft-baked. Optical masking of the chemosensitive gate regions is achieved by using black drawing ink applied with a 0.15-mm drafting pen, and the photoresist is polymerised by u.v. radiation in the usual way. A second coat of negative photoresist minimizes the possibility of pin-holes occurring in the encapsulation. The unexposed regions of the negative photoresist are developed with the appropriate developing solution as recommended by the manufacturer, and then a mixture of hydrazine hydrate and diaminoethane is used

to etch the underlying polyimide [15]. The small, and inevitable, amount of undercutting of the polyimide by the etchant is advantageous (Fig. 2) acting as a 'key' for the polymer-based electroactive gate membranes which would otherwise have relatively poor adherence to the Si_3N_4 surface of the I.C. The devices are finally baked at 180°C for 3 h to cure fully the composite encapsulant.

Electroactive gate materials

Ionophore-doped, polymeric gates were used for the fabrication of the K^+ , Ca^{2+} and Na^+ devices, whereas the Si_3N_4 surface of the composite gate dielectric of the remaining device was used directly as a pH-responsive material [2, 16, 17]; the details are given below.

Potassium ion-responsive gate. This preparation contained 5 mg of valinomycin, 165 mg of dioctyl adipate, 330 mg of PVC (B.P. Chemicals; Breon S110/10), and 3 ml of tetrahydrofuran (redistilled to remove stabilizers).

pH-Responsive gate. 90-nm Si_3N_4 was deposited at 800°C by low-pressure chemical vapour deposition, using dichlorosilane and ammonia (on top of 50-nm thermally-grown SiO_2) and etch-cleaned in buffered 5% hydrofluoric acid for 60 s immediately prior to bonding and encapsulation.

Calcium ion-responsive gate. Commercially available electrode membranes (Pye-Unicam type IS561- Ca^{2+}) were redissolved in approximately 0.5 ml redistilled tetrahydrofuran.

Sodium ion-responsive gate. Commercially available electrode membranes (Pye-Unicam type IS561- Na^+) were redissolved in approximately 0.5 ml of redistilled tetrahydrofuran.

The polymeric gates were formed by two-stage solvent-casting with an interval of 4 h between applications, and were estimated to be approximately $50\ \mu\text{m}$ thick. Devices were stored at ambient temperature and humidity for 24 h before the V-type flow-through cell cap was sealed in place, and then subsequently for a minimum of 48 h before use.

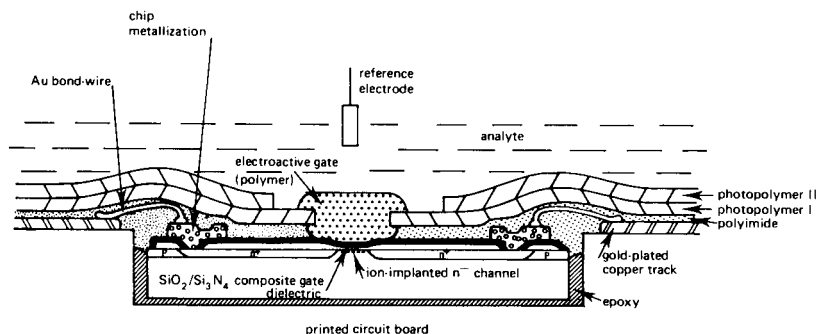


Fig. 2. Section diagram of polyimide/photopolymer-encapsulated, depletion-mode Chem-FET device.

The V-type flow-through cell design

Although other ChemFET devices have been used as discrete devices for incorporation into 'stand-alone' instrumentation [18, 19] by the Utah group and their collaborators, their I.C.s were mounted on to the tips of glass tubes and were then hand-encapsulated; no true flow-through ChemFET cells have been reported in the literature other than our early design. Whereas that particular sensor-cell was designed for 'high-speed' response (approximately 2 s for 100% response), some practical difficulties were encountered in subsequent work which necessitated the re-evaluation of the cell design. The problems were as follows: (1) the poor fluid dynamics with regard to bubble trapping; (2) the critical spacing necessary between the input port and the ChemFET surface (too large a separation severely degraded the cell response time whereas too short a separation resulted in pump-induced flow modulation of the electrical signal caused by the high fluid velocity over the electroactive gate film); (3) the difficulty in hand- (or machine-) fabricating the flow-through cell cap and its associated collars; and (4) the poor blood-compatibility of the plastic materials used for cap fabrication.

Consequently, pairs of smaller, $E\mu$ -146 devices (2.00×1.25 mm) were mounted and epoxy-encapsulated on to miniature (7 mm \times 20 mm) printed circuit boards suitable for soldering on to 16-pin DIL socket adaptors and made into miniature cells by suitable application of side-walls from printed circuit boards and a glass cover plate, with two 10 mm \times 1.5 mm diameter steel tubes fixed in place with epoxy to provide inlet and outlet ports such that the analyte flowed over (and parallel to) the surfaces of the devices. The response time was very poor, typically 30 s for 100% response, but this was not considered incompatible with the system which required a similar time period to flush its input deadspace. However, when blood was introduced to the system by using an active heparinization system for a 1.5-h on-line blood analysis [20], a stagnant boundary layer of red blood cells formed visibly over the ChemFET devices, because of the relatively inefficient flow characteristics, which resulted in very noisy output signals with substantial flow-modulation noise of 1–2 mV; this could not have been predicted by the earlier experiments using purely aqueous solutions. Nevertheless, bubble trapping was virtually eliminated and the encapsulation format based on a printed circuit board provided greater flexibility in flow-through cell design.

A significant further improvement was gained by the use of a V-type cell cap. This was made by bending a pyrex tube (1.5 mm bore, 4 mm outside diameter) through 90° , sectioning the tube at the elbow to expose the bore, and cutting both arms to approximately 10 mm in length. A stainless steel tube (1.5 mm diameter \times 8 mm) was glued into each arm with Epo-Tek H54 epoxy (Alpha Metals, Surrey) to provide push-fit tubing connections.

This type of cap was quick and simple to make, and the V-shape directs a flow of analyte directly on to the ChemFET surface, ensuring adequate flushing of the electroactive gate with fresh solution, and minimal bubble-trapping. The glass is relatively blood-compatible and clean in use, and the

chip surface is visible for inspection (although the cell is used with a clip-on cover because of the slight photosensitivity of the devices). The V-cell deadspace is approximately $30 \mu\text{l}$, and the cell response time, at a flow rate of $24.3 \mu\text{l s}^{-1}$ ($1.458 \text{ ml min}^{-1}$), is between 15 and 20 s (plus 5-s delay) when used with a heat exchanger/F-piece/valve input arrangement [13, 20]; the latter contributes a delay of several seconds to the response time because of analyte/carrier boundary-mixing during transport from the valve to the sensor cell. A downstream, side-entry, porous-plug reference electrode is used, connected directly to the ChemFET cell outlet port. An 'exploded' diagram of the complete ChemFET V-cell is shown in Fig. 3.

Electronic interfacing

It is advantageous to operate ChemFET sensors in such a way that the output signal is presented in the form of a voltage analogous to that of a conventional ion-selective electrode (i.e., having a logarithmic relationship with ionic concentration or activity) rather than use the drain current directly. This can be achieved by using the device in a constant-current mode, with an operational amplifier and the appropriate feedback circuitry [1], and this method is useful for operation at the athermal drain current level to minimise thermal sensitivity [2]. One disadvantage of this technique is the inherent circuit instability when the feedback loop is broken (which happens when a dip-type (board-mounted) sensor is moved from one solution to another), and also when switching or multiplexing between several devices which are being used together in the same solution. This results in a large voltage transient as the operational amplifier output switches to the positive power supply rail which, (a) injects charge into the system upon re-establishing the feedback loop (dipping back into solution or on completion of switching) and can polarise the reference electrode and electroactive gate, causing small, but significant, signal offsets (several mV) and hysteresis; and (b) can cause encapsulation breakdown. This is clearly an unsuitable feature for clinical

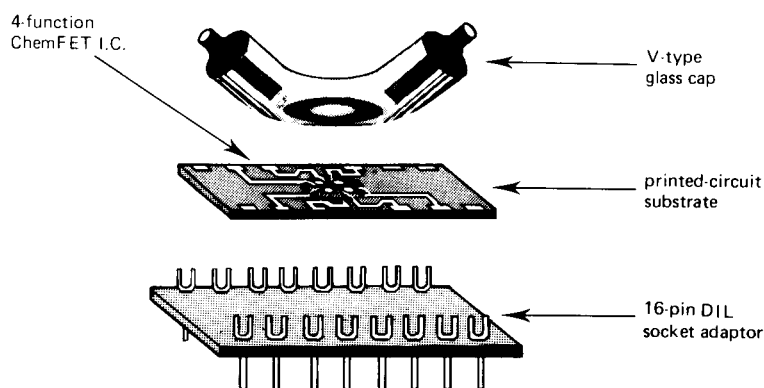


Fig. 3. V-type flow-through ChemFET cell.

analysis, where a 0.1-mV resolution is mandatory and rapid multiplexing between two or more channels is required; neither is this ideally compatible with the encapsulation materials described above.

It has been suggested that a complementary IGFET (i.e., geometrically similar to the ChemFET) can be used for signal 'linearization' and temperature compensation [21, 22] and such a circuit, in more complex form, has been used for the response-time evaluation of single-channel ChemFET-based microelectrodes [23].

A simpler electronic interfacing circuit which is also suitable for rapid multiplexing between four (or more) devices was devised; it is shown in Fig. 4. A stable +1-V drain voltage (V_{dd}) supplies both the E μ -144 quad-function ChemFET I.C. and a complementary IGFET (Q1) on a separate chip which is incorporated into the electronic circuitry as a discrete component after epoxy encapsulation and optical screening; this is preferable to using an IGFET on the same I.C. as the operational ChemFET sensors for three reasons: (1) voltage transients are still present on the IGFET gate and might threaten encapsulation integrity (although the other, previously noted, deleterious effects no longer obtain); (2) ChemFET encapsulation is simplified and improved by the reduced number of bonding wires; (3) a cause of thermal uncertainty is eliminated from the system (FET devices have a thermal coefficient of transconductance which is dependent on operating conditions and can be either positive or negative [24, 25]; the thermal characteristics of an enhancement-mode E μ -144 I.C. are available elsewhere [2]).

A suitable bias potential (V_{ref}), typically $0 \leq V_{ref} \leq +0.5$ V for depletion-mode devices, is applied to the reference electrode in order to set all device drain currents to, or near, the athermal level (in this case, approximately 500 μ A (for $V_{dd} = +1$ V), which are fed into a quad amplifier array, A1-A4 (Type 302-637; R.S. Components, London) in current-to-voltage conversion

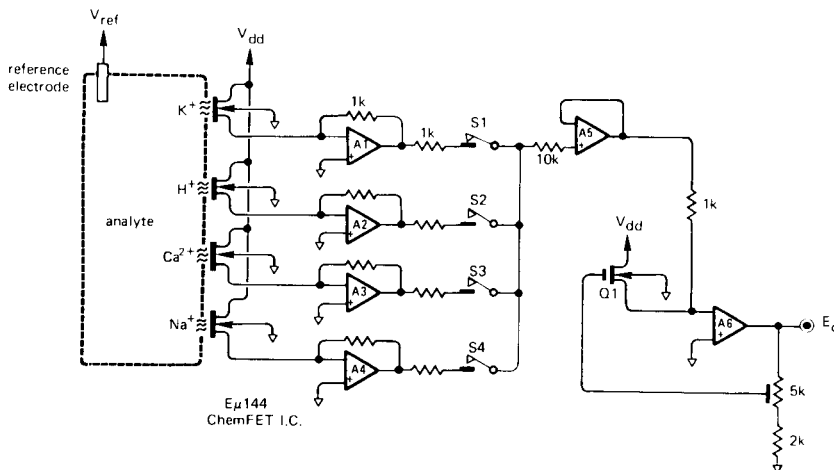


Fig. 4. Multiplexing and linearization circuitry for use with quadruple-function ChemFET I.C.

configuration. The amplifier outputs (-1 V per mA drain current) are fed via protective, current-limiting resistors through a computer-controlled array of miniature dual-in line relays, S1-S4 (Type 349-383; R.S. Components) into a buffer amplifier, A5. Amplifier A6 controls the current flowing in Q1 such that it is equal and opposite to that presented to its inverting port by A5. Gain can be introduced into the system and trimmed using a pre-settable potential divider network between A6 output and the gate of Q1; this can prove useful where other system elements, such as clinical electrical isolation units, do not have precisely unit gain and the latter is required for confirming Nernstian device response.

The effectiveness of this circuit was assessed over a wide range, using the computer-based system described above, to measure output potential, E , and bias potential (V_{ref}) over the voltage range $-1 \text{ V} \leq V_{\text{ref}} \leq +3 \text{ V}$ (Fig. 5), using a depletion-mode $E\mu$ -144 device with a bare Si_3N_4 (pH-responsive) gate in a MOPS buffer solution [13] at pH 6.86 and 23°C . The response was linear between bias potentials of -0.5 V and $+2.5 \text{ V}$, corresponding to drain current values of $304 \mu\text{A}$ and $1277 \mu\text{A}$, respectively, thus adequately bracketing the athermal operating point ($I_d \approx 500 \mu\text{A}$). Deviation from linearity when $V_{\text{ref}} < -0.5 \text{ V}$ is presumed to be due to a difference in ChemFET/IGFET threshold voltage, and for $V_{\text{ref}} > +2.5 \text{ V}$, to a difference in source/drain serial parasitic resistances.

RESULTS AND DISCUSSION

Encapsulation

To establish the ability of the encapsulating material (whether epoxy or polyimide/photoresist composite) to prevent spurious electrical leakage paths, the devices were mounted on to dip-type printed circuit boards and immersed in a phosphate buffer solution (pH 6.86), together with a single-junction porous-plug reference electrode; then connections to the ChemFET were short-circuited together and connected to electrical ground via a Keithley 616 digital electrometer in current-measuring (nA) mode. A bias

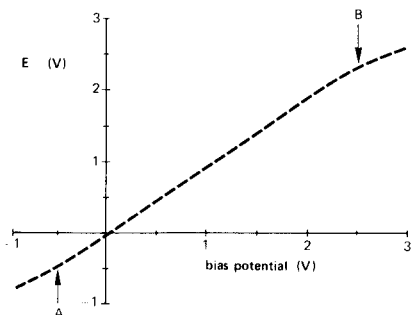


Fig. 5. Transfer characteristics of ChemFET linearization circuit showing linear range between A (-0.5 V) and B ($+2.5 \text{ V}$).

potential, sweeping from -1 V to $+3$ V in 20-mV increments (so as to bracket the linear region of operation of the device) was applied to the reference electrode under microcomputer control (Hewlett-Packard HP-85F), the latter being used to log bias voltage and leakage current from the electrometer via a high-resolution digital multimeter (Hewlett-Packard 3478A). Figure 6 shows the low leakage current (<10 pA) obtained with the composite materials after ten days in solution (curve A). This compares favourably with the recommendation that ChemFET leakage current levels should not be greater than 20 nA [16] or 30 nA [14]. However, a small proportion of the composite-encapsulated devices exhibited electrical breakdown of the encapsulation when the applied (positive) bias potential was in excess of 1.5–2 V (Fig. 6, curve B). This was attributed to high-field regions in the polymers where the encapsulation was anomalously thin because of the difficulty in regulating the thickness of the polymers, particularly over the gold bonding wires. Although comparatively high leakage currents (≈ 1 nA) were observed at high bias potentials (>2 V) for some devices, these subsequently reverted to a negligible value at normal operating potential differences, viz., the breakdown was not catastrophic. Throughout the development of this technique, the bonding wires proved to be the most difficult item to encapsulate successfully. (Leakage paths from the bond wires can be clearly seen by applying a high bias potential (3–9 V) and observing the localized bubble formation through a microscope.) To minimize the physical exposure of the bonding wires, the chips were mounted in shallow (0.5 mm) recesses in the printed circuit boards. The electronic circuit described previously in this paper is recommended for use with these composite-encapsulated devices, in order to eliminate voltage transients during switching or multiplexing and thus ensure that field-induced breakdown does not occur.

Measurement of the leakage current at a single fixed bias potential does not necessarily verify adequacy of encapsulation; the I/V leakage characteristics must be examined over a wide range. This is illustrated by the leakage characteristics of an epoxy-encapsulated nitrate-responsive polymer-gate ChemFET [26], shown in Fig. 7. Curve A was obtained with the gate membrane in place, and shows a relatively low leakage current throughout the applied bias range (0.14 nA at $+3$ V). However, on removal of the membrane a pronounced leakage current was obtained (curve B) and interference fringes were observed at the chip surface/epoxy interface, indicating solution penetration. Apparently the gate membrane, when in place, had acted as a leakage current limiter, but nevertheless, encapsulation failure was predicted by the x -axis displacement of both curves, because of the chip metallization having direct contact with the electrolyte solution.

Electrochemical responses

Potassium ions. A Nernstian response (58–59 mV/decade) was obtained over a wide operating range (10^{-1} – 10^{-5} mmol dm $^{-3}$), with no significant interferences from other ions commonly present in solution.

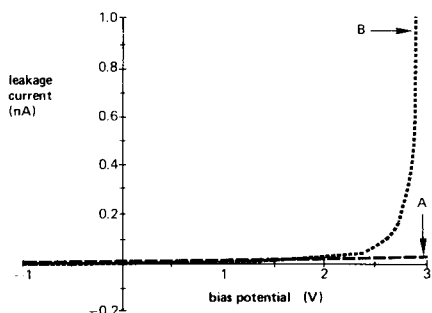


Fig. 6. Electrical leakage characteristics of polyimide/photopolymer-encapsulated device showing typical behaviour (A) and field-induced breakdown (B).

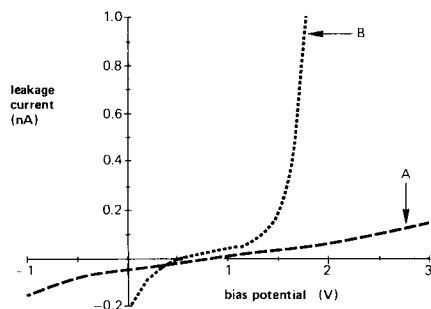


Fig. 7. Electrical leakage characteristics of epoxy-encapsulated device both (A) with, and (B) without, nitrate-responsive polymeric gate membrane.

Hydrogen ions. The response is dependent on the physical nature of the Si_3N_4 gate surface. It is known [1] that a thin SiO_2 (or mixed oxynitride) film forms spontaneously on the Si_3N_4 surface; SiO_2 exhibits a poor pH-response (≈ 35 mV/pH) in contrast to the near ideal response of a 'clean' Si_3N_4 surface [2], which is attributed to the presence of intrinsic H^+ ion-exchange sites arising from the inadvertent inclusion of small amounts of hydrogen [17] and oxygen [27] in the Si_3N_4 during the chemical vapour deposition.

Some H^+ -response slopes as low as 20 mV/pH were observed in this work, hence removal of any surface oxide is mandatory for optimum response. This was achieved by including a buffered 5% hydrofluoric acid etch for 60 s in the pre-encapsulation cleaning procedure (above), and devices thus treated had responses typically between 50 and 58 mV/pH over the range pH 1–14. There are no significant interferences from other ions in solution, although a small Na^+ -error is sometimes apparent at high pH levels (pH > 13). It seems likely that this is due to the presence of a residual, surface SiO_2 layer, permeable to sodium ions.

Calcium ions. A Nernstian response (28–29 mV/decade) was obtained over a wide operating range (10^{-1} – 10^{-5} mmol dm^{-3}), with no significant interferences from other ions in solution at clinical levels.

Sodium ions. Various commercially available materials, and a number of crown ethers, were investigated but a Na^+ -responsive electroactive gate really suitable for clinical application was not found. The ionophore ETH-227 (Fluka 71732, Fluka, Buchs, Switzerland) was tested, as described by Oesch et al. [14] but there were some problems [28]. The presently used material (Pye-Unicam type IS561- Na^+) generates a response of typically 53–56 mV/decade over the range 10^{-1} – 2.5×10^{-4} mmol dm^3 , but after exposure to solution for several hours it appears that a slight, sporadic H^+ -response (i.e., interference) is developed (several mV/pH). Although small, this is a significant interference for clinical applications where the

normal range of sodium concentration corresponds to a very small device response (ca. 2.4 mV).

Device lifetimes

Epoxy-encapsulated devices which are continuously exposed to solution generally have useful lifetimes between 15 and 90 days, and typically 30 days. Early failure is inevitably due to use of inadequate cleaning procedures during encapsulation and to rapid thermal cycling during the epoxy-curing stage. Late 'failure' is usually due to a gradual leaching out of the electro-active material from the polymeric gate with the plasticizer; this results in a slow decrease in the device response.

Polyimide/photopolymer-encapsulated devices appear to be more durable than devices which use epoxy; some have been used with a number of different PVC gate membranes and have withstood repeated peeling-off of the latter, which subjects the encapsulation/device bond to a substantial mechanical stress because of the undercut-keying of the structure (Fig. 2) providing high adherence between the encapsulation and the PVC membranes.

Response time

The flow-through cell assembly has a dead-space of only 30 μl , but a larger sample volume than this is required in order to ensure that the cell is completely flushed. The response time of the K^+ -device when subjected to a step change in K^+ concentration from 2 to 7 mmol dm^{-3} at a flow rate of $24.3 \mu\text{l s}^{-1}$ is shown in Fig. 8; the 95% response time is 15 s, and the 100% response time is approximately 20 s, hence the effective dead-space of the cell (at this flow rate) is 486 μl .

The response time could be substantially reduced by directing the inlet

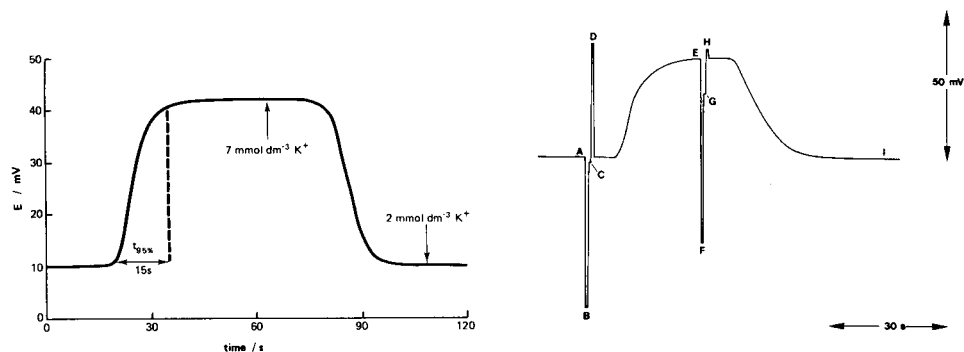


Fig. 8. Response-time characteristics of $E\mu\text{-144}$ ChemFET (K^+ -responsive channel) when used with the V-type flow-through cell.

Fig. 9. Analogue signal from a quadruple-function ChemFET device showing the multiplexing sequences before and during a sample cycle. For explanation of points A–I, see text and Table 1.

port directly on to the ChemFET gate surfaces [12], but in any practical system there will be an additional and similar dead-space volume associated with the input tubing (etc.) which would also require flushing. The present cell response time is therefore considered to be adequate for present requirements.

Stability

In order to provide accurate data despite slow, long-term drifts in the device outputs and particularly during the initial gate-hydration period, a technique of "analyte-chopping" has been established [12, 13] in which a "baseline" calibration solution (I) and the analyte sample are passed alternately through the ChemFET cell using a microcomputer-driven pinch valve system [20]. A second calibration solution (II) is substituted for the sample during an initial calibration routine. At present, a 25-s sampling period is used at intervals of either 90 or 120 s; the calibration solutions are: (I) 2 mmol dm⁻³ K⁺, 0.5 mmol dm⁻³ Ca²⁺, 156.5 mmol dm⁻³ Na⁺, pH 7.44; and (II) 7 mmol dm⁻³ K⁺, 3 mmol dm⁻³ Ca²⁺, 144 mmol dm⁻³ Na⁺, pH 7.01.

Figure 9 shows the ChemFET outputs during a calibration cycle and demonstrates the efficacy of the multiplexing circuitry shown in Fig. 4; Table 1 lists the data logged during that particular cycle. (There is a signal inversion and voltage offset because of the use of additional patient-isolation circuitry, but the scale (and hence the computed response slopes), is accurate. With the baseline (I) calibration solution passing through the cell, a multiplex logging cycle is initiated; after a software pause of 100 ms the mini-computer uses a digital multimeter (Hewlett-Packard Model 3478A) to read the K⁺-channel output 5 times in programmed fast-trigger mode with 0.1-mV resolution at a rate of 25 s⁻¹ (A, Fig. 9), then averages and stores the data. Channel 2 (H⁺) is then selected (B, Fig. 9) and the cycle is repeated, followed by channels 3 (C, Fig. 9), and 4 (D, Fig. 9), and reversion to channel 1 for visual monitoring. The sampling valve is immediately activated, then another multiplexing cycle is initiated after 25 s, and the valve is deactivated. The device outputs revert to their baseline values (I, Fig. 9) after approximately 25 s; the apparent 5-s propagation delay is due to the incorporation of a heat

TABLE 1

Individual ChemFET device outputs logged during the calibration cycle shown in Fig. 9

Channel	Ion	Solution I (V)	Solution II (V)	Difference (II - I) (mV)	Computed slope mV/decade
1	K ⁺	-1.0910 (A)	-1.0586 (E)	32.4	59.6
2	H ⁺	-1.1417 (B)	-1.1197 (F)	22.0	51.2
3	Ca ²⁺	-1.0925 (C)	-1.0699 (G)	22.6	29.0
4	Na ⁺	-1.0531 (D)	-1.0548 (H)	-1.7	47.0

exchanger between the sampling valve and the ChemFET cell [20]. There are no output offsets or transients generated during multiplexing.

The linearity and stability of the system are demonstrated in Fig. 10, which shows the results obtained by sampling a series of calibration I/ calibration II solutions mixed to provide unit stepped K^+ concentrations from 2 to 7 mmol dm^{-3} and associated incremental changes in Ca^{2+} and Na^+ . The system has recently been used for direct on-line blood analysis [28].

Thermal and optical responses

In common with all semiconductor-based sensors, ChemFET devices are both thermally and optically sensitive; but FET structures generally exhibit an athermal point or locus in their I_d/V_g characteristics [24, 25]. The thermal characteristics of the present I.C. (E μ -144) have been described elsewhere; the optimum drain-current for minimum thermal sensitivity is approximately 513 μA . Operation at (or near) this value, together with the use of a miniature heat exchanger, is sufficient to eliminate thermal sensitivity when sampling is done intermittently from a source at body temperature (37°C).

Optical sensitivity is due to photon absorption in the reverse-biased p-n junctions at the edges of the source and drain diffusions and underneath the channel, which generates a drain leakage current. This is avoided by painting the entire glass V-cap with matt black enamel except for a 2-mm square inspection window over the I.C., and fitting a loose, clip-on, black plastic cover during use.

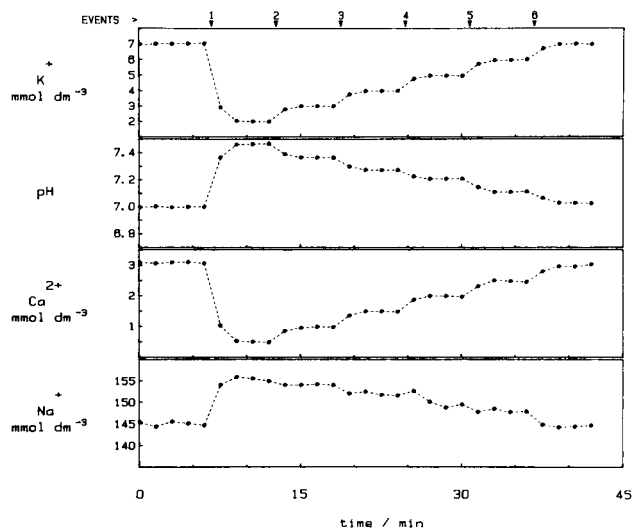


Fig. 10. Concentration data computed on-line from quadruple-function ChemFET I.C. sampling mixed calibration solutions I and II at 90 s intervals. The calibration I/calibration II solution ratios are: initially, 0/5; at event 1, 5/0; event 2, 4/1; event 3, 3/2; event 4, 2/3; event 5, 1/4; event 6, 0/5.

Conclusions

A miniature, flow-through cell has been developed using a quadruple-function ChemFET integrated-circuit for the simultaneous measurement of K^+ , H^+ , Ca^{2+} and Na^+ in aqueous solutions. Ionophore-doped polymers are used for the K^+ , Ca^{2+} and Na^+ electroactive gate films, while the pH-responsive Si_3N_4 gate insulator surface is used directly for the H^+ device. A novel polyimide/photopolymer encapsulation technique is described, which is superior to previously used methods and also has the potential for mass-production applications. The process may be also useful for the selective encapsulation of other microelectronic sensors (e.g., gas and enzyme sensors, pressure transducers, accelerometers, etc.).

The ChemFET cell has a dead-space of $30 \mu l$ and a 100% response time of 20 s at a sample flow rate of $24.3 \mu l s^{-1}$, hence the effective dead-space is approximately $486 \mu l$. The useful lifetime of the cell is typically 4–12 weeks.

Electronic circuitry is described, which permits the individual ChemFET device outputs to be rapidly multiplexed and logged with 0.1-mV precision without generating any voltage transients or offsets in the analogue signals, and which provides a linearized (i.e., analogous to conventional ion-selective electrodes) output over a wide range (-0.5 to $+2.5$ V). The reference electrode potential is invariant and transient-free, which ensures that there are no induced polarisation effects.

The flow-through analyser has been specifically engineered for blood analysis; use of a ChemFET integrated-circuit as the sensing element enables the sample volume to be minimized whilst providing multi-function capability, and therefore makes possible on-line analysis. It has been demonstrated that analysis of human blood, with blood drawn directly from the subject into the cell, can be done successfully over an extended period [28].

By the use of various different electroactive gate materials, including enzyme substrates and those suitable for detecting dissolved gases, it will eventually be possible to provide a comprehensive patient-monitoring system for clinical situations where fresh, reliable information is vital.

The authors acknowledge financial support from the Science and Engineering Research Council and the Water Research Council. We are grateful to the staff of the SERC Edinburgh Microfabrication Facility for device processing and particularly to Alan Gundlach for his advice; and to Du-Pont (UK) Ltd. and Eastman-Kodak Ltd. for samples of polyimide and photoresists.

REFERENCES

- 1 J. Janata and R. J. Huber, in H. Freiser (Ed.), *Ion-Selective Electrodes in Analytical Chemistry*, Vol. 2, Plenum Press, 1980, pp. 107–174.
- 2 A. Sibbald, *IEE Proc. I, Solid-State Electron Dev.*, 130 (1983) 233.
- 3 P. Bergveld, *IEEE Trans. Biomed. Eng.*, 17 (1970) 70.
- 4 P. Bergveld, *IEEE Trans. Biomed. Eng.*, 19 (1972) 342.

- 5 P. Bergveld, J. Wiersma and H. Meertens, *IEEE Trans. Biomed. Eng.*, 23 (1976) 136.
- 6 T. Matsuo and K. D. Wise, *IEEE Trans. Biomed. Eng.*, 21 (1974) 485.
- 7 S. D. Moss, J. Janata and C. C. Johnson, *Anal. Chem.*, 47 (1975) 2238.
- 8 S. M. Cobbe and P. A. Poole-Wilson, *Lancet*, (1979) 444.
- 9 M. Lim, R. A. F. Linton and D. M. Band, *Crit. Care Med.*, 10 (1982) 747.
- 10 R. A. F. Linton, M. Lim and D. M. Band, *Crit. Care Med.*, 10 (1982) 337.
- 11 D. M. Band and S. J. G. Semple, *J. Appl. Physiol.*, 22 (1967) 854.
- 12 A. Sibbald, A. K. Covington, E. A. Cooper and R. F. Carter, *Clin. Chem.*, 29 (1983) 405.
- 13 A. K. Covington and A. Sibbald, *Proc. NBS Workshop on Direct Potentiometric Measurements on Blood*, Washington, U.S.A., 1983, in press.
- 14 U. Oesch, S. Caras and J. Janata, *Anal. Chem.*, 53 (1981) 1983.
- 15 Y. Harada, F. Matsumoto and T. Nakakado, *J. Electrochem. Soc.*, 130 (1983) 129.
- 16 S. D. Moss, J. B. Smith, P. A. Comte, C. C. Johnson and L. Astle, *J. Bioeng.*, 1 (1976) 11.
- 17 Y. G. Vlasov, A. V. Bratov and V. P. Letavin, in E. Pungor and I. Buzas (Eds.), *Ion-Selective Electrodes (3rd Matrafured Symposium, Hungary, 1980)*, Elsevier, 1981, pp. 387-395.
- 18 A. V. Ramsing, J. Janata, J. Růžička and M. Levy, *Anal. Chim. Acta*, 118 (1980) 45.
- 19 J. Harrow, J. Janata, R. L. Stephen and W. J. Kolff, *Proc. EDTA*, 17 (1980) 179.
- 20 A. Sibbald, A. K. Covington and R. F. Carter, unpublished work, 1983.
- 21 J. Janata, personal communication, 1981.
- 22 B. A. McKinley, J. Saffle, W. S. Jordan, J. Janata, S. D. Moss and D. R. Westenskow, *Med. Instrum. (Baltimore)*, 14 (1980) 93.
- 23 A. Haemmerli, J. Janata and H. M. Brown, *Anal. Chim. Acta*, 144 (1982) 115.
- 24 O. Leistiko, *Phys. Scr.*, 18 (1978) 445.
- 25 L. Vadasz and A. S. Grove, *IEEE Trans. Electron Devices*, 13 (1966) 863.
- 26 P. D. Whalley, unpublished work, 1983.
- 27 M. Esashi and T. Matsuo, *IEEE Trans. Biomed. Eng.*, 25 (1978) 184.
- 28 A. Sibbald, A. K. Covington and R. F. Carter, *Clin. Chem.*, 30 (1984) 135.

LEAD-SELECTIVE ELECTRODES BASED ON LEAD(IV) OXIDE

DEREK MIDGLEY

Central Electricity Generating Board, Central Electricity Research Laboratories, Kelvin Avenue, Leatherhead, Surrey, KT22 7SE (Great Britain)

(Received 14th November 1983)

SUMMARY

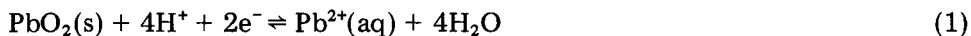
Lead(IV) oxide electrodes are shown to give near-theoretical calibration slopes for lead(II) ions over the range 10^{-8} – 10^{-5} mol l⁻¹, and to have near-theoretical standard potentials in different acidic media. They are compared with lead sulphide-silver sulphide membrane electrodes and shown to be more tolerant of acidity and copper(II), mercury(II) and iron(III) ions. Iron(II) and manganese(II), however, interfere significantly. Some of the advantages of the lead(IV) oxide electrode are brought out in the determination of the solubility product of lead sulphate; implications for constructing phosphate- and sulphate-sensitive electrodes are mentioned.

Reviews [1] reveal that lead chalcogenide-based electrodes have been prepared both commercially and experimentally in various forms (electrodes with homogeneous, heterogeneous, sintered and single-crystal membranes have been reported) but that there are scarcely any instances of the application of these electrodes to direct potentiometry for lead. Studies [2, 3] of these electrodes (mainly with lead sulphide/silver sulphide membranes) showed that the calibration slope and standard potential vary with time, that iron(III) and cadmium(II) ions interfere and that copper(II), silver and mercury ions must be absent. Such properties make these electrodes unattractive for direct potentiometric monitoring, because they would require frequent recalibration and at least two of the interferents (copper and iron(III)) are commonly present in real samples.

This paper examines the properties of lead(IV) oxide electrodes as direct potentiometric sensors and compares them with lead sulphide/silver sulphide electrodes. Hitherto, the only analytical use of lead(IV) oxide electrodes appears to have been as indicator electrodes in chelometric titrations [4, 5], although lead(IV) oxide/lead(II) sulphate paste electrodes have been used in thermodynamic studies [6, 7]. In the earlier electrodes, the lead(IV) oxide was either electrolytically deposited on platinum [4] or embedded in wax [5]; in this study it was rubbed into the surface of a Růžička Selectrode [8], which provides a robust and readily renewable membrane.

THEORY

Lead(IV) oxide reacts according to



The electrode potential for reaction (1) is

$$E = E^0 - 2s \text{ pH} - \frac{s}{2} \log [\text{Pb}^{2+}] \quad (2)$$

where $s = RT \ln(10)/F$ is the Nernst slope factor for a one-electron change. It follows from Eqn. 2 that the electrode is sensitive both to pH and to lead ions. Use of the electrode as a lead sensor demands, therefore, that the pH of the solution should be rigorously controlled, especially as the electrode is four times as sensitive to pH as to $\log [\text{Pb}^{2+}]$.

The pH should be controlled by an acidic medium (to avoid the formation of lead(II) hydroxide or hydroxo complexes) which does not interact strongly with lead ions. The media tested were 0.05 mol l⁻¹ nitric acid, pH 4.4 formate buffer and pH 4 acetate buffer. The stability constants [9, 10] of the lead-anion complexes are 10^{1.1} (nitrate), 10^{0.7} (formate) and 10^{2.7} (acetate).

EXPERIMENTAL

Apparatus

The e.m.f.'s were measured with a Beckman 4500 digital pH meter reading to 0.1 mV and were displayed on a chart recorder. A Techne C-100 thermostat was used to maintain the temperature of the solution and the electrodes at 25°C in a water-jacketed glass vessel. Solutions were stirred by a magnetic stirrer bar.

Lead(IV) oxide electrodes were prepared by impregnation of the PTFE/graphite substrate of a Radiometer F3012 Selectrode [8]. For comparison, conventional lead-selective electrodes were also tested: the Orion 94-82 with a homogeneous lead sulphide/silver sulphide membrane and the Radiometer F3004 in which a similar mixture is used to impregnate the PTFE-graphite substrate of the Selectrode. The reference electrode was a Radiometer K701 double-junction calomel electrode, the outer sleeve of which was fitted with whichever buffer solution was being used at the time, diluted to the same strength as that obtaining in the test solution.

Reagents

Lead(IV) oxide was of either BDH AnalaR grade (97%) or Ventron puratronic grade (99.9995%, as metal). The lead sulphide/silver sulphide mixture for the Radiometer F3004 was the S42215 powder supplied with the electrode.

A stock lead solution (0.1 mol l⁻¹) was prepared from lead nitrate. Other standard lead solutions were prepared by successive dilutions from this stock.

Solutions for pH adjustment (added 1:20, v/v) were as follows. A 1 mol l⁻¹ nitric acid was prepared from a BDH "Con-Vol" ampoule. Formic acid-formate buffer, pH 4.4, was prepared by dissolving 4.0 g of sodium hydroxide in about 50 ml of water, adding 5.1 ml of 90% formic acid and making up to 100 ml. Acetic acid-acetate buffer, pH 4.0, was prepared by dissolving 243 g of sodium acetate trihydrate in 400 ml of water, adding 480 g of anhydrous acetic acid and diluting to 1 l.

Interference tests were made with solutions of sulphate (iron(II), manganese(II), copper(II), cobalt(II)) or nitrate (zinc, nickel, mercury(II), iron(III)) salts.

Reagents were BDH AnalaR grade unless otherwise specified. Water was distilled and then demineralized on a mixed-bed ion-exchange resin.

RESULTS

Calibration slope

The slopes in 0.05 mol l⁻¹ nitric acid and pH 4 acetate media were sub-Nernstian at about -25 mV/decade, but were reproducible. In pH 4.4 formate medium, the slope was about -28 mV/decade. Figure 1 shows calibrations in the three media for the lead(IV) oxide and lead sulphide/silver sulphide electrodes. The latter were more sensitive than the lead(IV) oxide electrode in the two buffer solutions but less sensitive in nitric acid medium, which is below the operating pH specified for lead sulphide-based electrodes by the manufacturer (Orion).

Standard potential

The standard potential was calculated from

$$E^0 = E + \frac{s}{2} \log [\text{Pb}^{2+}] + \frac{s}{2} \log \alpha + \frac{s}{2} \log f_{\text{Pb}} + 2s \text{ pH} + E_{\text{ref}} - E_j \quad (3)$$

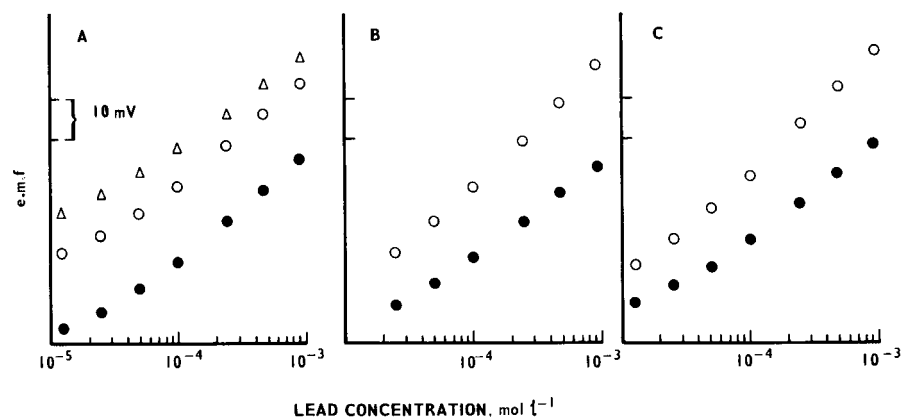


Fig. 1. Calibration of lead-selective electrodes: (A) in 0.05 mol l⁻¹ nitric acid; (B) in pH 4 acetate buffer; (C) in pH 4.4 formate buffer. (●) PbO₂ electrode; (○) Radiometer F3004; (Δ) Orion 94-82.

where E_{ref} is the half-cell potential of the saturated calomel reference electrode, E_j is the liquid junction potential calculated by the Henderson equation, f_{Pb} is the activity coefficient of lead ion calculated by the Davies equation [11], α is a term allowing for complexation with the anion in the medium, and $[\text{Pb}^{2+}]$ is the total lead concentration. The results in Table 1 show good consistency between the three media, but the values are low compared with the literature value [12] of 1455 mV. An irregular tendency for E^0 to decrease was observed over a period of days, which might account for the difference from the literature value. The potentials were, however, more stable than those for lead sulphide electrodes, which increased by 7–15 mV per day, accompanied by a decrease in the calibration slope and a change in the shape of the time response. (After a day, the potential of the lead sulphide electrodes overshoot the final equilibrium value when the lead concentration was changed; this was not observed with a fresh electrode.) No difference in standard potential could be attributed to the purity of the two types of lead(IV) oxide tested.

Response time

In 0.05 mol l⁻¹ nitric acid medium, the response of the lead(IV) oxide electrode to an approximately two-fold increase in concentration was complete within about 1 min (Fig. 2A). In pH 4.4 formate buffer (Fig. 2B) and pH 4 acetate buffer, however, these responses took 5–10 min. Lead sulphide/silver sulphide electrodes responded more quickly than the lead(IV) oxide electrodes in all the media.

Interferences

Figure 3 shows the response curves for various metal ions in the pH 4 acetate medium; the e.m.f.'s are displaced arbitrarily on the ordinate for the sake of clarity. Nickel, mercury(II), zinc and copper(II) ions had no significant interfering effect up to about 10⁻⁴ mol l⁻¹ but thereafter there was a response of about -5 mV per decade. Cobalt(II) had a more discernible effect even below 10⁻⁴ mol l⁻¹, with an almost linear response of about -14 mV per decade over the range 10⁻⁴–10⁻³ mol l⁻¹. Iron(III) produced a significant response; the curve in Fig. 3 represents an approximate response

TABLE 1

Standard potential of lead(IV) oxide electrodes

Medium	Ionic strength	E^0 (mV)	S.d. ^a	No. of measurements
Nitric acid	0.05	1448	1.4	42
pH 4 acetate	0.018	1446	2.5	24
pH 4.4 formate	0.05	1436	2.6	15

^aStandard deviation on mean.

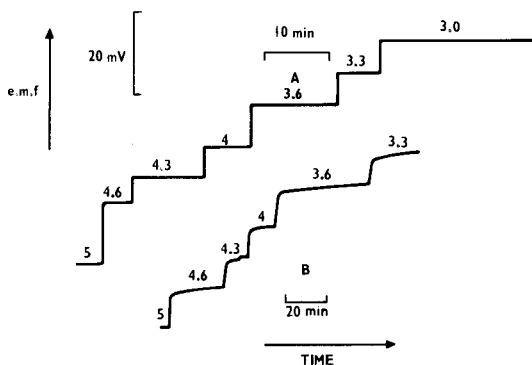


Fig. 2. Time response curves of lead(IV) oxide electrodes: (A) in 0.05 mol l^{-1} nitric acid; (B) in pH 4.4 formate buffer. Lead concentrations ($-\log [\text{mol l}^{-1}]$) are shown above the curves.

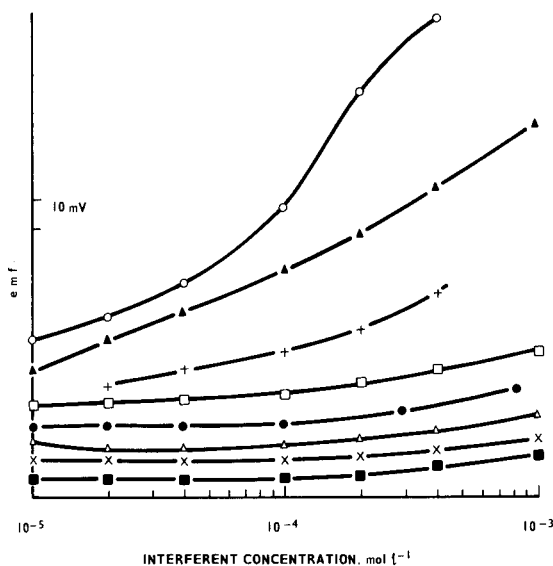


Fig. 3. Response of lead(IV) oxide electrode to interfering ions: (○) Fe^{2+} ; (▲) Mn^{2+} ; (+) Fe^{3+} ; (□) Co^{2+} ; (●) Cu^{2+} ; (△) Zn^{2+} ; (×) Hg^{2+} ; (■) Ni^{2+} .

of about -25 mV per decade, but this was constructed from readings taken arbitrarily about 1 h after the change of concentration, because the potentials were still drifting slowly at that time. At concentrations up to $10^{-4} \text{ mol l}^{-1}$, the electrode was slightly more sensitive (-32 mV per decade) to manganese(II) than to lead ions: at higher concentrations, the sensitivity to manganese ions increased markedly and steady potentials were not attained in 1 h. Iron(II) ions produced an even larger effect than manganese(II): the sensitivity was about -30 mV per decade up to $4 \times 10^{-5} \text{ mol l}^{-1}$, but the sensitivity then increased and equilibrium potentials were not reached in 1 h.

Selectivity coefficients were calculated by the separate solutions method for those ions giving an approximately Nernstian response, with the results shown in Table 2.

Compared with the lead sulphide/silver sulphide electrode [3], the lead(IV) oxide electrode is notably tolerant of copper and mercury ions, and is less affected by iron(III). The manganese(II) interference, however, is much worse. Iron(II) and cobalt(II) appear not to have been tested with the lead sulphide/silver sulphide electrode, but they would not be expected to interfere as much as they do with the lead(IV) oxide electrode. The iron(II) and manganese(II) interferences are presumably brought about by reduction of lead(IV) oxide with a consequent release of lead(II) ions.

Solubility product of lead sulphate

As a test of the accuracy of the lead(IV) oxide electrode, it was used to determine the solubility product of lead sulphate. The media used in the calibration studies were saturated with lead sulphate and the dissolved lead ion concentration was determined by reference to the calibration graphs. The solubility product was calculated from the equation $K_{so} = [\text{Pb}]^2 f_2^2 / \alpha_{\text{Pb}} \alpha_{\text{SO}_4}$, where $[\text{Pb}]$ is the experimentally obtained lead ion concentration, $\alpha_{\text{Pb}} = 1 + \sum_i \beta_i [A]$ corrects for complexing between lead and the background anion A, $\alpha_{\text{SO}_4} = 1 + 10^{1.94} \times 10^{-\text{pH}} \times f_2/f_1$ corrects for the protonation of sulphate, and f_1 and f_2 are the activity coefficients for singly and doubly charged ions, as calculated by the Davies equation [11].

The results in Table 3 show good agreement with the literature values [9] of 7.77–7.80. Similar results were obtained from laboratory-reagent-grade lead sulphate and from that prepared from lead nitrate and sodium sulphate (both analytical-reagent grade). This contrasts with attempts to use the lead sulphide/silver sulphide electrodes: steady potentials were not attained in saturated lead sulphate solutions, but much higher lead concentrations were being indicated than expected. Increasing the quantity of lead sulphate added increased the apparent lead concentration and the laboratory-reagent-grade material was worse in this respect. Analysis of the lead sulphate by x-ray fluorescence spectrometry revealed 0.0011% of copper in the laboratory reagent and 0.00027% copper in the material precipitated from analytical-

TABLE 2

Selectivity coefficients for lead(IV) oxide electrodes

Ion	Concentration range (mol l ⁻¹)	Selectivity coefficient
Fe ²⁺	10 ⁻⁵ –4 × 10 ⁻⁵	≈ 1
Fe ³⁺	10 ⁻⁵ –4 × 10 ⁻⁴	≈ 0.1
Mn ²⁺	10 ⁻⁵ –10 ⁻⁴	1–2
Co ²⁺	4 × 10 ⁻⁴ –10 ⁻³	4 × 10 ⁻²

TABLE 3

Solubility product of lead sulphate at 25.0°C

Medium	α_{Pb}	α_{SO_4}	K_{so}^0	Standard deviation ^a	No. of results
0.05 mol l ⁻¹					
nitric acid	1.63	2.95	7.83	0.04	3
pH 4 acetate	3.83	1.01	7.73	—	1
pH 4.4 formate	1.715	1.002	7.80	0.26	4

^aFor a single result.

reagent-grade chemicals. It is inferred that copper ions were selectively extracted from the lead sulphate and interfered with the lead sulphide-based electrodes.

DISCUSSION

The results show that the lead(IV) oxide electrode could be a significantly useful lead-selective electrode, even though its calibration slope and standard potential are not ideal. One of its chief merits is that ions such as copper(II) and mercury(II), which poison lead sulphide/silver sulphide membranes, do not interfere seriously. The lead(IV) oxide electrode can also withstand acidic conditions for much longer than the sulphide-based electrodes. A disadvantage of the lead(IV) oxide electrode is the need for precise control of pH but in practice little more is involved than in the use of ionic strength adjustment solutions in most potentiometric methods.

The advantages of the lead(IV) oxide electrode are illustrated by the determination of the solubility product of lead sulphate in a variety of acidic background media, in which literature values were reproduced with comparative ease, whereas sensible results could not be obtained with the sulphide-based electrodes. The solubility products of lead and copper sulphides imply that a 10¹¹-fold excess of lead over copper is required if copper interference is to be avoided with sulphide-based electrodes. Analytical-reagent-grade lead salts typically contain about 0.001% copper and it might seem, therefore, that an unambiguous calibration of an electrode with a lead sulphide membrane could hardly be obtained. Hulanicki and Lewenstam [13] showed, however, that the selectivity coefficient predicted on the basis of solubility equilibria is not reached within an hour, or much longer, depending on the concentration of copper, the temperature and the rate of stirring. On the basis of Hulanicki and Lewenstam's work, it would seem that interference by trace copper impurities might not be detectable within the time scale (minutes) of most potentiometric measurements. The solubility product study in this work suggests, however, that trace copper impurities could account for the drifts and short lifetimes of the phosphate-selective [14]

and sulphate-selective [15, 16] electrodes incorporating the lead salt, lead sulphide and silver sulphide, and the lead(IV) oxide electrode should be worthy of further investigation for such applications.

This work was carried out at the Central Electricity Research Laboratories and is published with the permission of the Central Electricity Generating Board.

REFERENCES

- 1 J. Koryta, *Anal. Chim. Acta*, 61 (1972) 329; 91 (1977) 1; 111 (1979) 1; 139 (1982) 1.
- 2 P. Kivalo, R. Virtanen, K. Wickström, M. Wilson, E. Pungor, G. Horvai and K. Tóth, *Anal. Chim. Acta*, 87 (1976) 401.
- 3 G. J. M. Heijne, W. E. van der Linden and G. den Boef, *Anal. Chim. Acta*, 100 (1978) 193.
- 4 C. Vandael, *Ind. Chim. Belge.*, 8 (1962) 932.
- 5 C. N. Wang, P. J. Kinlen, D. A. Schoeller and C. O. Huber, *Anal. Chem.*, 44 (1972) 1152.
- 6 W. C. Vosburgh and D. N. Craig, *J. Am. Chem. Soc.*, 51 (1929) 2009.
- 7 W. J. Hamer, *J. Am. Chem. Soc.*, 57 (1935) 9.
- 8 J. Růžička, C. G. Lamm and J. C. Tjell, *Anal. Chim. Acta*, 62 (1972) 15.
- 9 L. G. Sillén and A. E. Martell, *Stability Constants*, Special Publ. No. 17, Chem. Soc., London, 1971.
- 10 L. G. Sillén and A. E. Martell, *Stability Constants*, Suppl. No. 1, Special Publ. No. 25, Chem. Soc., London, 1971.
- 11 C. W. Davies, *Ion Association*, Butterworths, London, 1962, p. 41.
- 12 W. M. Latimer, *Oxidation Potentials*, 2nd edn., Prentice-Hall, Englewood Cliffs, 1952, p. 155.
- 13 A. Hulancki and A. Lewenstam, *Talanta*, 29 (1982) 671.
- 14 D. Midgley, *Talanta*, 26 (1979) 261.
- 15 M. S. Mohan and G. A. Rechnitz, *Anal. Chem.*, 45 (1973) 1323.
- 16 K. Nagy and T. A. Fjeldly, *Talanta*, 26 (1979) 811.

USE OF THE CLARK OXYGEN SENSOR WITH IMMOBILIZED ENZYMES FOR DETERMINATIONS IN FLOW SYSTEMS

VĚRA PACÁKOVÁ, KARLE ŠTULÍK* and DAGMAR BRABCOVÁ

Department of Analytical Chemistry, Charles University, Albertov 2030, 128 40 Prague 2, (Czechoslovakia)

JANA BARTHOVÁ

Department of Biochemistry, Charles University, Prague (Czechoslovakia)

(Received 11th September 1983)

SUMMARY

A small-volume cell has been constructed for amperometric flow measurements with a Clark oxygen sensor and its performance was tested. The Clark sensor can be combined with immobilized enzymes for determination of substances after enzymatic conversion during which oxygen is consumed or released. Two enzymes, glucose oxidase and tyrosinase, were used and two measuring techniques, employing the enzyme immobilized on the Clark sensor membrane and with the enzyme bound on a support in a preceding reactor, were tested and compared. It was found that, in the given system, measurement with the enzyme immobilized on the sensor membrane has better sensitivity, precision and response rate.

Determinations in flow systems are gaining ever-increasing importance, especially in clinical and environmental analysis. These measurements involve continuous-flow analysis, flow-injection analysis and the detection of substances eluted from chromatographic columns, in addition to continuous monitoring of substances. Several requirements must be satisfied, especially high sensitivity, low detection limit, signal stability and reproducibility, wide linear dynamic range, rapid response and a small detection volume to avoid excessive dispersion of the test substance zone; a detailed discussion of these aspects is available [1].

Enzyme electrodes are often used in flow systems because of their high selectivity [2, 3]. Enzyme electrodes may be potentiometric, based on ion-selective electrodes, or amperometric; the latter usually exhibit faster responses. Among the amperometric probes, the well-known Clark oxygen sensor [4] is especially advantageous, because it is sensitive, the measurement is reproducible, and the working electrode is protected against passivation in solution by a gas-permeable membrane. As many enzymatic reactions are accompanied by consumption or liberation of oxygen, the Clark sensor is well suited for combination with enzymes. Such enzyme probes have been used in both static [5–12] and dynamic [13] systems.

In flow systems, the enzyme must be immobilized, either on the electrode surface or in a preceding reactor. It has been claimed that the use of enzyme reactors [14–20] is preferable to enzyme immobilization on the sensor when the enzymatic reaction is slow, as a higher degree of substrate conversion is attained at a suitable flow rate and reactor length. However, the substrate diffusion within the reactor may cause dispersion of the substrate zone, resulting in a decrease in the measuring sensitivity and the sample throughput. The literature data are often contradictory on the relative merits of the two measuring techniques.

This paper describes a small flow-through cell with a Clark oxygen sensor. This cell was used for flow measurements with two enzymes, glucose oxidase and tyrosinase, immobilized either on the sensor surface or on an inert support packed in a precolumn. The performance of the two systems was studied.

EXPERIMENTAL

Chemicals and apparatus

The chemicals used were of analytical-reagent grade (Lachema, Czechoslovakia). Glucose oxidase (Reakhim, U.S.S.R.), tyrosinase (Koch-Light Laboratories, England) and Sepharose 4B, activated by cyanogen bromide (Pharmacia Fine Chemicals, Sweden) were used.

The flow-through cell is depicted in Fig. 1 and had an internal volume of $7 \mu\text{l}$. The Clark sensor was constructed by Dr. J. Čerkasov of the Department of Plant Physiology, Charles University, Prague; the working electrode surface area was 0.07 cm^2 (Fig. 2). All flow measurements were conducted

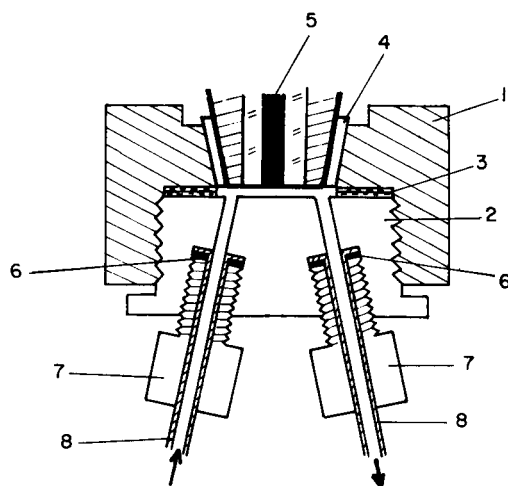


Fig. 1. The flow-through cell: (1, 2) plexiglas parts threaded for screwing together; (3) PTFE spacer (0.1 mm thick); (4) O-ring; (5) Clark sensor; (6) metal ring; (7) fixing screw; (8) PTFE tubing (0.8 mm i.d.).

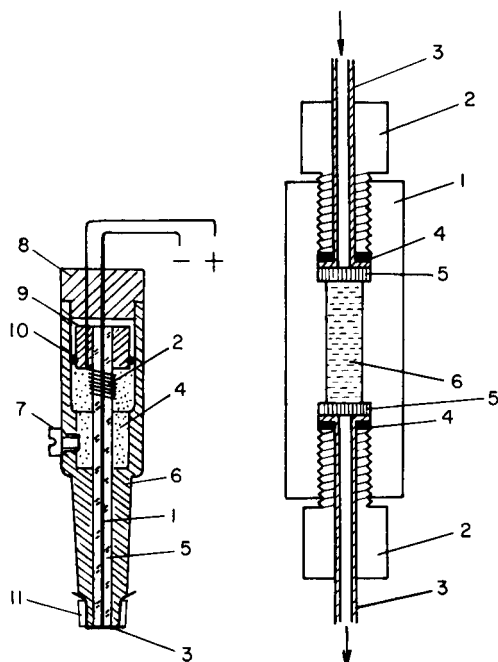


Fig. 2. Clark oxygen sensor: (1) Pt cathode; (2) Ag anode; (3) polypropylene membrane ($8 \mu\text{m}$ thick); (4) electrolyte ($0.1 \text{ M KCl}/0.1 \text{ M KHCO}_3$); (5) glass capillary; (6) electrode body (plexiglas); (7) opening for replenishment of the electrolyte; (8) electrode cap; (9) electrode lead seal; (10) O-ring; (11) plexiglas ring for fixing the membrane.

Fig. 3. The enzyme reactor: (1) plexiglas body with threaded holes; (2) hollow screw for fixing the tubing; (3) PTFE tubing (0.8 mm i.d.); (4) metal seals; (5) porous metal plug; (6) support with immobilized enzyme.

with a Model LC-XP liquid chromatograph (Pye-Unicam, England). The samples were introduced through a $20\text{-}\mu\text{l}$ loop.

The enzyme reactor used in some experiments was 15 mm long with an internal diameter of 3 mm and is shown in Fig. 3. For the amperometric measurements, a Model PA-3 polarographic analyzer was used with a Model TZ-4100 line recorder (both from Laboratorní Přístroje, Czechoslovakia).

Enzyme immobilization

Enzyme immobilization on the polypropylene membrane. The membrane, stretched over the sensor, was wetted with an aqueous 0.5% (w/v) solution of lauryl sulphate and dried. Then $50 \mu\text{l}$ of the gel-forming enzyme solution was applied to the membrane. This solution was prepared by dissolving gelatin (50 mg ml^{-1}) in distilled water at 50°C and adding the enzyme (1 mg ml^{-1}) to the solution at 25°C . The gel was allowed to dry on the membrane for 4 h at laboratory temperature and then the membrane was immersed for 2 min in a 2% solution of glutaraldehyde in 0.05 M phosphate buffer of pH 6.6 . The membrane was then allowed to dry at 5°C .

Enzyme immobilization on an inert support. Lyophilized Sepharose 4B activated with cyanogen bromide (1 g) was left to swell and then washed on a glass frit for 15 min with 200 ml of 10^{-3} M hydrochloric acid. The enzyme (glucose oxidase, 10 mg) was dissolved in 5 ml of a mixture 0.1 M in sodium hydrogencarbonate and 0.5 M in sodium chloride, mixed with the gel and gently stirred for 2 h at laboratory temperature. The unbound substance was washed out with the coupling buffer and the remaining active groups were blocked by reaction with 1 M ethanolamine at pH 8 for 1–2 h. Any protein that was not covalently bound was first washed out with a 0.1 M acetate/1 M sodium chloride buffer at pH 4, and then with a 0.1 M borate/1 M sodium chloride buffer at pH 8. This washing procedure was repeated three times.

Measuring procedure

For all measurements, the potential of the working electrode was held at -0.35 V (vs. Ag/AgCl electrode), i.e., at the beginning of the plateau on the current-potential dependence, where the highest signal-to-noise ratio was obtained. The whole measuring system was thermostatted at $24 \pm 1^\circ\text{C}$. In testing the performance of the flow cell (without enzymes), deaerated-distilled water (purged with nitrogen purified by passage through a column with heated copper filings, through traps containing alkaline solutions of pyrogallol and sodium anthraquinone- β -sulphonate and through a column containing molecular sieve) was used as the carrier liquid and samples of distilled water with the equilibrium concentration of atmospheric oxygen were injected into it. In measurements with the enzymes, a 0.1 M phosphate buffer (pH 7.0) in equilibrium with the air, was used as the carrier liquid and the samples were aqueous solutions of glucose (with glucose oxidase) or solutions of pyrocatechol in the 0.1 M phosphate buffer, pH 7.0 (with tyrosinase). When not in use, the enzyme sensors were stored in a solution of this phosphate buffer at 5°C .

RESULTS AND DISCUSSION

Testing of the flow-cell without enzyme

In evaluating the dependences given below, it must be borne in mind that the sensor is operated under non-stationary conditions in flow systems; the attainment of steady state requires times of the order of tens of seconds [4]. This fact leads to poorer reproducibility of response compared with stationary measurements and to greater differences in the numerical values of the operating parameters for various cell and sensor designs.

In the proposed system, both the electric current corresponding to the maximum of the response curve and the electric charge obtained as the area under the response curve were proportional to the amount of oxygen over the range studied, i.e., 1×10^{-7} – 8.5×10^{-10} g O_2 ; the latter value is the detection limit calculated as twice the absolute noise value. The calibration

regression lines exhibited acceptable linearity with slopes of 0.9 A g^{-1} (correlation coefficient 0.991) for the current dependence and 6.9 C g^{-1} (correlation coefficient 0.986) for the charge dependence, at a flow rate of 0.9 ml min^{-1} and at 24°C). The degree of electrochemical conversion of oxygen on the electrode is very low, corresponding to ca. 0.1% at a flow rate of 0.8 ml min^{-1} , as calculated from comparison of the peak area in coulombs with the charge required to reduce all the oxygen present.

The time constant of the cell system was obtained as the time required to attain 63.2% of the maximum response on a step change in the oxygen concentration. At a flow rate of 0.9 ml min^{-1} and a temperature of 24°C , the time constant was 3.0 s, which is a value sufficient for most common analytical purposes.

The signal dependence on the flow rate was measured from 0.1 to 2.5 ml min^{-1} . The signal decreased exponentially with increasing flow rate, with exponents of -0.9 and -1.45 for the current and charge dependences, respectively (obtained for oxygen amounts of 4.25×10^{-8} and $8.5 \times 10^{-8} \text{ g}$). Therefore, the peak height is less dependent on the flow rate, and to attain the highest possible sensitivity, the flow rates should be as low as possible; however, the peaks exhibit tailing and the reproducibility of measurement deteriorates at very low flow rates.

The signal dependence on the temperature is complex, because it is a combination of temperature effects not only on the solubility of oxygen in water, but on the rate of oxygen diffusion through the membrane and on the rate of oxygen reduction on the electrode. When the amount of oxygen added was kept constant at all the temperatures studied, then an increase in temperature from 24 to 40°C led to an increase in the maximum current from 0.85×10^{-8} to $1.39 \times 10^{-8} \text{ A}$, at a flow rate of 0.9 ml min^{-1} (i.e., the temperature factor was 3.38% per $^\circ\text{C}$). If the activation energy of the process is calculated from the Arrhenius equation, assuming that the process is controlled entirely by diffusion, then a value of ca. 18 kJ mol^{-1} is obtained, which is about three times the value for diffusion in aqueous solution without the membrane.

Measurement with the enzymes

The use of two enzymes, glucose oxidase and tyrosinase, was studied in the flow-through cell, with the enzymes immobilized either on the polypropylene membrane of the Clark sensor, or on Sepharose packed in a preceding reactor. The signal dependence on the flow rate, the time constants, the concentration dependences for glucose and pyrocatechol, the reproducibility of the measurement, and the effect of ageing of the enzyme systems on the sensor performance were examined. The advantages and drawbacks of the measurements of the peak height and area were compared.

Dependence on the flow rate and time constants. Both the peak height and area decrease exponentially with increasing flow rate; the values of the exponents are given in Table 1, compared with those for the Clark sensor

TABLE 1

The exponents of the signal dependence on the flow rate for the Clark sensor without an enzyme (A), for the Clark sensor with glucose oxidase (B) and tyrosinase (C) immobilized on the membrane, and for the Clark sensor with glucose oxidase deposited in a preceding reactor (D) and the values of the time constants

Measurement	Test substance	Exponent		Time constant ^a (s)
		Max. current	Peak area	
A	Oxygen	-0.9	-1.45	3.0 ^b
B	Glucose	-1.1	-1.36	10.5 ^c
C	Pyrocatechol	-0.78	-1.16	33.3 ^c
D	Glucose	-1.49	-1.27	26.7 ^d

^aTemperature, 24°C. ^bAt 0.9 ml min⁻¹. ^cAt 0.1 ml min⁻¹. ^dAt 0.3 ml min⁻¹.

without the enzyme. It can be seen that the presence of the enzymes does not have a large effect on the shape of the signal dependence on the flow rate and that the peak area is more dependent on the flow rate. The greatest dependence on the flow rate was found for the measurement with the enzyme reactor. In contrast, the time constant of the cell is strongly affected by the enzyme present (see Table 1) and it is larger for the measurement with the reactor, because of the considerable dispersion of the test substance zone. This dispersion is especially marked at very low flow rates (below 0.3 ml min⁻¹) and thus higher flow rates should be used; the peak dispersion is much smaller with the enzyme immobilized on the sensor membrane, so that low flow rates should be used to increase the measuring sensitivity. Typical response curves obtained with glucose oxidase immobilized on the sensor membrane and on the support in the reactor are given in Fig. 4.

Concentration dependence. The results are summarized in Table 2. It is evident that the sensors are sufficiently sensitive for analytical use. The linear dynamic range is wider and the calibration dependences have a better linearity with the enzymes immobilized on the electrode membrane than for the enzyme in the reactor. Although the degree of conversion in the reactor is higher, the measurement sensitivity is lower and the detection limit higher than in the measurement with the enzymes on the sensor membrane, as a result of the dispersion of the test substance zone in the reactor. Moreover, the use of the reactor leads to a considerable increase in the pressure in the system, which is disadvantageous from the experimental point of view.

Reproducibility and the time stability of the sensors. The precision of the measurement for various concentrations of test substances expressed in terms of the relative standard deviation, is summarized in Table 3. The peak current measurement is slightly more reproducible than the peak area measurement, except for the lowest concentrations. Measurements with the

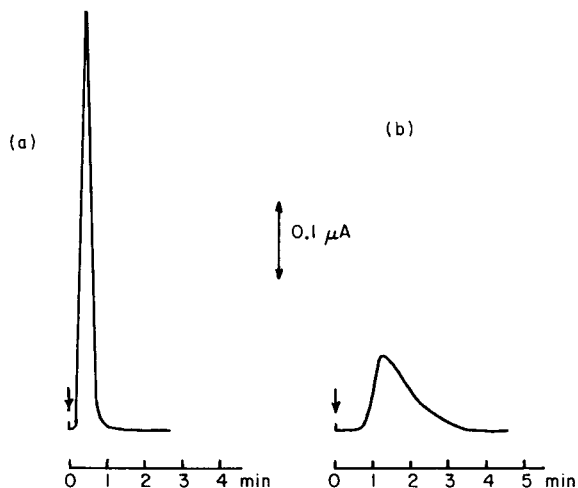


Fig. 4. Typical response curves obtained with glucose oxidase immobilized (a) on the sensor membrane and (b) on Sepharose in the preceding reactor. Glucose concentrations: (a) 5×10^{-3} M; (b) 5×10^{-2} M. Flow rates: (a) 0.1 ml min^{-1} ; (b) 0.3 ml min^{-1} .

enzyme on the sensor membrane have somewhat lower standard deviations than those with the enzyme in the reactor. The standard deviations are generally acceptable for analytical use.

The effect of ageing on the performance of the sensors is summarized in Table 4. It can be seen that the linear dynamic range is narrowed with increasing sensor age and the detection limit increases. The sensor with the enzyme immobilized on the membrane can be used for up to about 30 days, while the enzyme reactor lasts for up to about 50 days. This is the only advantage involved in using the enzyme reactor.

TABLE 2

Dependence of the sensor current on the concentration of the test substances and the detection limits^a

Substance/method	Linear dynamic range (M)	Slope (A mol^{-1})	Correl. coeff.	Detection limit ^b (M)
Glucose/enzyme on membrane ^c	6×10^{-7} — 5×10^{-3}	3.85×10^{-6}	0.998	6×10^{-7} (2.4×10^{-9} g)
Pyrocatechol/enzyme on membrane ^c	6×10^{-6} — 7×10^{-4}	4.03×10^{-6}	0.999	6×10^{-6} (1.32×10^{-8} g)
Glucose/reactor ^d	Poor linearity: ca. 10^{-3} — 10^{-2}	6.6×10^{-8}	0.942	3×10^{-4} (1.2×10^{-6} g)

^aTemperature, 24°C . ^bDetection limit defined as the signal for $S/N = 2$. The values in parentheses are the masses corresponding to the injection of $20\text{-}\mu\text{l}$ samples. ^cAt 0.1 ml min^{-1} . ^dAt 0.3 ml min^{-1} .

TABLE 3

Precision of measurements^a

Test substance	Concentration (M)	R.s.d. (%)	
		Current measurement	Peak area measurement
<i>Enzyme on the sensor membrane</i>			
Glucose	5×10^{-3}	0.90	2.63
	7×10^{-4}	3.52	4.68
	1×10^{-4}	21.23	17.30
Pyrocatechol	7×10^{-4}	1.10	0.90
	3×10^{-4}	0.87	2.00
	3×10^{-5}	20.10	15.60
<i>Enzyme in the reactor</i>			
Glucose	1×10^{-2}	1.85	2.67
	7×10^{-3}	4.20	5.21
	1×10^{-3}	18.84	40.54

^aStandard deviation calculated from five parallel measurements, $\alpha = 0.05$.

TABLE 4

The effect of ageing on the performance of the glucose oxidase sensor. Immobilization: A, on the sensor membrane; B, in the reactor

Age (days)	Immobilization	Linear dynamic range (M)	Detection limit (M)
0	A	6×10^{-7} — 5×10^{-3}	6×10^{-7}
	B	ca. 1×10^{-3} — 1×10^{-2}	3×10^{-4}
20	A	4×10^{-6} — 5×10^{-3}	4×10^{-6}
	B	ca. 1×10^{-3} — 1×10^{-2}	3×10^{-4}
40	A	5×10^{-3} — 1×10^{-2}	5×10^{-3}
	B	ca. 3×10^{-3} — 1×10^{-2}	1×10^{-3}
50	A	no response	
	B	ca. 5×10^{-3} — 1×10^{-2}	2×10^{-3}

It can be concluded from the above results that the systems will be useful quantitatively. In most cases, enzyme immobilization on the sensor membrane and measurement of peak heights at a low flow rate (ca. 0.1 ml min^{-1}) should be optimal. The expected sample throughputs, in view of the sample zone width, are ca. 60 and 20 samples per hour for glucose and pyrocatechol, respectively, when the enzymes are immobilized on the sensor membrane; the sample throughputs are about 15 and 5 h^{-1} when the enzyme reactor is used.

REFERENCES

- 1 K. Štulík and V. Pacáková, *CRC Critical Reviews in Analytical Chemistry*, CRC Press, Boca Raton, 1984.
- 2 G. G. Guilbault, in G. Svehla (Ed.), *Enzyme Electrodes in Analytical Chemistry*, Comprehensive Analytical Chemistry, Vol. 8, Elsevier, Amsterdam, 1977, p. 1.
- 3 G. G. Guilbault, *Appl. Biochem. Biotechnol.*, 7 (1982) 85.
- 4 See, e.g., M. L. Hitchman, *Measurement of Dissolved Oxygen*, J. Wiley, New York, NY, 1978.
- 5 L. Macholán and L. Šháněl, *Collect. Czech. Chem. Commun.*, 42 (1977) 3667.
- 6 L. Macholán, *Collect. Czech. Chem. Commun.*, 43 (1978) 1811.
- 7 L. Macholán, *Collect. Czech. Chem. Commun.*, 44 (1979) 3033.
- 8 P. Posádka and L. Macholán, *Collect. Czech. Chem. Commun.*, 44 (1979) 3395.
- 9 D. Pfeiffer, F. Scheller, M. Janchen and K. Bertermann, *Biochimie*, 62 (1980) 587.
- 10 M. Koyama, Y. Sato, M. Aizawa and S. Suzuki, *Anal. Chim. Acta*, 116 (1980) 307.
- 11 J. Havas, E. Borjesz, G. Nagy and E. Pungor, *Anal. Chem. Symp. Ser.*, 8 (1981) 241.
- 12 Y. Umezawa, S. Sofue and Y. Takamoto, *Anal. Lett.*, 15 (B2) (1982) 135.
- 13 L. Macholán, P. Londýn and J. Fischer, *Collect. Czech. Chem. Commun.*, 46 (1981) 2871.
- 14 D. J. Imman and W. E. Hornby, *Biochem. J.*, 129 (1972) 255.
- 15 W. Dritschilo and M. K. Weibel, *Biochem. Med.*, 9 (1974) 32.
- 16 G. Nagy and E. Pungor, *Hung. Sci. Instrum.*, 32 (1975) 1.
- 17 B. Watson, D. N. Stifel and F. E. Semersky, *Anal. Chim. Acta*, 106 (1979) 233.
- 18 T. T. Ngo, *Int. J. Biochem.*, 11 (1980) 459.
- 19 E. L. Gulberg, A. S. Altiyat and G. D. Christian, *J. Autom. Chem.*, 2 (1980) 189.
- 20 T. Hara, M. Toriyama and M. Imaki, *Bull. Chem. Soc. Jpn.*, 55 (1982) 1854.

DETERMINATION OF GLUTAMATE-PYRUVATE TRANSAMINASE ACTIVITY IN BLOOD SERUM WITH A PYRUVATE OXIDASE/POLY(VINYL CHLORIDE) MEMBRANE SENSOR

KUNIO KIHARA, EIKI YASUKAWA, MITSUHIRO HAYASHI and SACHIO HIROSE*

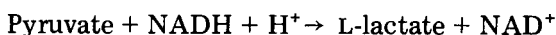
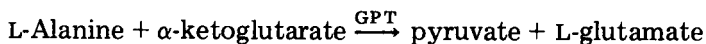
Central Research Laboratory, Mitsubishi Petrochemical Co. Ltd., Wakaguri, Ami, Inashiki-gun, Ibaraki 300-03 (Japan)

(Received 10th October 1983)

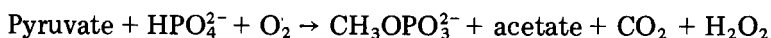
SUMMARY

Pyruvate oxidase (E.C. 1.2.3.3.) is immobilized by adsorption on a wet PVC membrane. Glutamate-pyruvate transaminase activity (5–1600 IU l⁻¹) in serum is determined by a pyruvate oxidase sensor consisting of the immobilized pyruvate oxidase coupled to a platinum electrode for measuring hydrogen peroxide, after an L-alanine- α -ketoglutarate reaction. The assay requires ≤ 60 s, and has a precision of 2–3%. Endogenous pyruvate should not interfere if measurements are made > 30 s after starting the reaction.

Glutamate-pyruvate transaminase (GPT) is of clinical significance, elevated values in serum indicating myocardial and hepatic diseases [1]. Spectrophotometric assays of GPT are used in most clinical laboratories [2–6], all based on a measurement of the decrease in absorbance of NADH, as a result of the following reaction sequence:



The method involves not only relatively large amounts of reagents and complicated procedures, but also positive errors because of endogenous pyruvate. Recently, an electrochemical method was introduced [7], based on the measurement of oxygen, after production of pyruvate as above, as a result of the following reaction, catalyzed by pyruvate oxidase:



However, GPT activity was not determined successfully, because of leakage of enzyme from the membrane of the sensor and because the conditions for use of the pyruvate oxidase sensor were not optimal. Finally, endogenous pyruvate in serum was not taken into account.

In order to develop a reliable method for the assay of GPT activity in serum, the immobilization of pyruvate oxidase and the optimization of the pyruvate oxidase sensor were studied, with particular attention to the effect

of endogenous pyruvate. The pyruvate oxidase was immobilized on a wet poly(vinyl chloride) (PVC) membrane, on which many other enzymes have successfully been immobilized [8–10] and the membrane was attached to an amperometric electrode for sensing hydrogen peroxide.

EXPERIMENTAL

Materials

The enzymes used were pyruvate oxidase (E.C. 1.2.3.3., from *Pediococcus sp.*, 21 IU mg⁻¹; Toyo Jozo Co.) and glutamate-pyruvate transaminase (GPT; E.C. 2.6.1.2., from porcine heart, 140 IU mg⁻¹; Boehringer Mannheim). Human control serum was purchased from Japan Travenol Co. (Tokyo); L-alanine, α -ketoglutarate, lithium pyruvate, thiamine pyrophosphate (TPP), flavine adenine dinucleotide (FAD) and 3-(*N*-morpholino)-propanesulfonic acid (MOPS) were obtained from Nakarai Chemical Co. (Kyoto). The poly(vinyl chloride) used had m.w. 48 400 (Kanegafuchi Kagaku Co., Tokyo). Deionized water was used for all procedures.

Pyruvate oxidase was determined by the method of Harger et al. [11], and GPT by the method of Wroblewski and LaDue [4].

Immobilization of pyruvate oxidase on a wet poly(vinyl chloride) membrane

A PVC solution (8% w/w) in dimethylformamide was cast on a glass plate (10 × 7 cm) and immersed in methanol at room temperature for 4 h. The wet PVC membrane (ca. 40 μ m thick) obtained was washed with distilled water and a portion of it (8 mm diameter) was added to 0.6 ml of a solution containing 3 mg ml⁻¹ pyruvate oxidase, 50 mM phosphate buffer (pH 7.0), 5 mM TPP, 50 mM MgCl₂, and 5 mM FAD. The mixture was incubated for 24 h at 4°C. The pyruvate oxidase/PVC membrane obtained was washed with a large volume of phosphate buffer and stored in phosphate buffer at 4°C. The activity of the pyruvate oxidase/PVC membrane was 0.2 IU cm⁻².

Assembly of the sensor

Figure 1 is a schematic diagram of the system. The sensor, consisting of the immobilized pyruvate oxidase/PVC membrane and a combined platinum electrode (TOA Electronics, Tokyo) was inserted into a small cell (1.0 ml) which was filled with a solution stirred magnetically. The electrode was maintained at -0.8 V vs. Ag/AgCl. The current from the sensor was converted to voltage by a 10-Mohm resistance and displayed on a recorder (Type 3066; Yokokawa Electric Works, Tokyo).

Procedures

For the determination of GPT activity, a buffer solution including L-alanine (500 mM), α -ketoglutarate (10 mM), FAD (0.1 mM), TPP (1 mM), MgCl₂ (10 mM), KH₂PO₄ (1 mM), KCl (100 mM) and MOPS (pH 7.3, 50 mM) was fed into the cell (1 ml) by peristaltic pump 7 (Fig. 1); pump 8

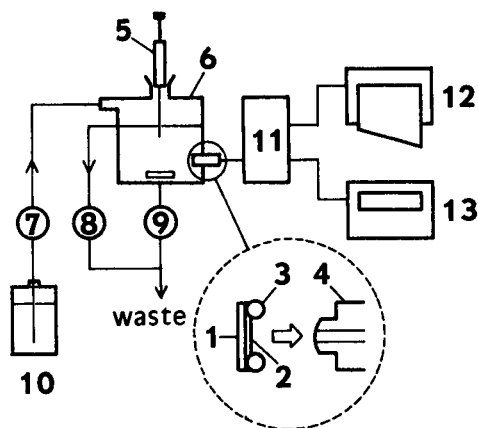


Fig. 1. Schematic diagram of the system (not to scale): (1) pyruvate oxidase/PVC membrane; (2) cellulose dialysis membrane; (3) O-ring; (4) platinum electrode; (5) micro-syringe; (6) cell; (7–9) peristaltic pumps; (10) buffer solution; (11) current converter and controller; (12) recorder; (13) digital meter.

was operated to remove the overflow. Then 50 μl of a lithium pyruvate solution (2 mM), a standard GPT solution (1060 IU l^{-1}) or serum was injected into the buffer solution in the cell. After the measurement of GPT activity, the buffer solution including the sample solutions was completely discarded by pump 9. The slope of a plot of voltage (based on current increase) against time was measured. The slopes obtained from various concentrations of GPT were plotted against the GPT activities determined by the method of Wroblewski and LaDue [4], in order to provide a calibration graph. The pyruvate oxidase/PVC membrane in the cell was washed with the buffer solution after each measurement and was kept in the buffer solution.

RESULTS AND DISCUSSION

Design of the sensor

In order to obtain a sensor for GPT, the pyruvate sensor, based on immobilized pyruvate oxidase was first studied with a lithium pyruvate solution. Preliminary experiments showed that the optimal concentrations of PVC in the casting solution and of pyruvate oxidase in the immersing solution were 8% (w/w) and 3.0 mg ml^{-1} , respectively, when a wet PVC membrane was used as carrier. No leakage of pyruvate oxidase from the wet PVC membrane was observed during the experiments. It is thought that pyruvate oxidase is adsorbed by hydrophobic interaction and remains in pores of appropriate size, controlled by the PVC concentration in the casting solution [8].

When this membrane was used with the amperometric electrode in the apparatus shown in Fig. 1, the initial output was constant when the buffer solution was fed into the cell. When 50- μl portions of solutions containing

0.5, 1.0 and 2.0 mM lithium pyruvate were injected into the system, the current increased as shown in Fig. 2. Production of hydrogen peroxide by the enzymatic reaction resulted in an increase in hydrogen peroxide concentration at the enzyme/PVC membrane, which began when the pyruvate solution was injected into the system. As a result, the electrode current increased markedly with time until a steady state was reached, within 30 s when the above standard solutions were used. No further change occurred after this time, which means that endogenous pyruvate in serum should have no influence on GPT activity measurements if measurements can be made after >30 s, as described below.

Pyruvate concentrations in lithium pyruvate solutions were determined by steady-state measurements. The calibration graph obtained under the standard conditions was linear over the range 0–4 mM; this corresponded to a maximum current difference of 200 nA. The minimum detectable concentration was 0.01 mM. Thus the pyruvate oxidase immobilized on the PVC membrane should be suitable for determining the GPT activity in serum, based on the conversion of L-alanine and α -ketoglutarate to pyruvate and L-glutamate.

Use of the sensor to determine GPT

The response of the sensor to pyruvate produced by the GPT-catalyzed reaction was examined. A standard GPT solution (1060 IU l^{-1}) was injected into the cell after the buffer solution, which included 500 mM L-alanine and

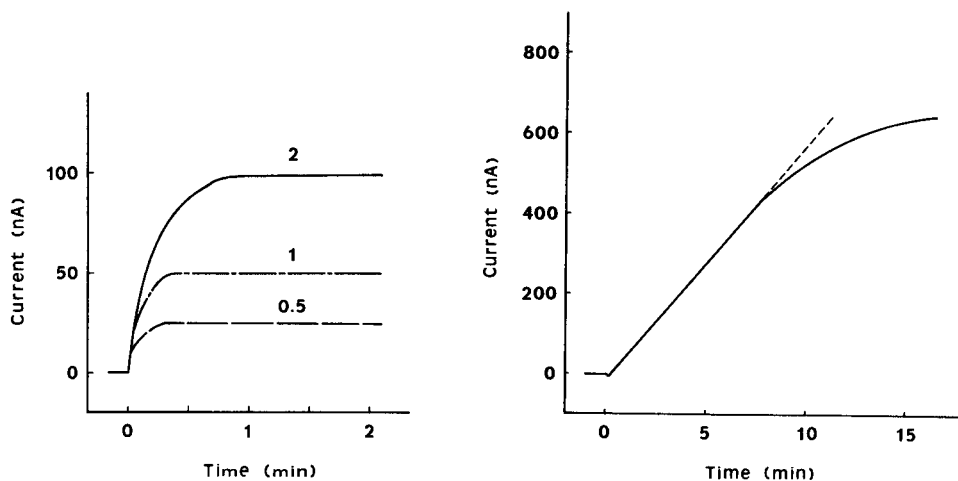


Fig. 2. Response curves of the pyruvate oxidase sensor for lithium pyruvate under the standard conditions for pyruvate determination. The numbers on the curves are the concentrations (mM) of pyruvate in the injected solutions.

Fig. 3. Response curve of the pyruvate oxidase sensor using a standard GPT solution (1060 IU l^{-1}), under the recommended conditions.

10 mM α -ketoglutarate as substrates for the enzymatic reaction, had been pumped into the cell. As shown in Fig. 3, the current increased with increasing reaction time, linearly for the first 7 min. The current increase indicated that pyruvate was produced enzymatically by GPT, as described above. A linear relation ($Y_1 = 0.044 X_1 - 0.12$; correlation coefficient 0.99, 12 assays) was obtained between the slope (Y , nA min^{-1}) of the output of the system in the initial linear region from 30 to 60 s and the activity of GPT (X_1 , IU l^{-1}) below 1600 IU l^{-1} . The minimum detectable concentration was 5 IU l^{-1} , which corresponded to 0.1 nA min^{-1} . Thus, a wide range of GPT activities, even the high activities found in hepatic diseases ($200\text{--}1500 \text{ IU l}^{-1}$), can be determined by this method.

Optimization of reagent concentrations

L-Alanine, α -ketoglutarate and phosphate (substrates) and TPP (coenzyme) are necessary for the enzymatic reactions. Therefore, the effects of variations of the concentrations of these species in the buffer solution on the output of the sensor were investigated. Some of the results are shown in Figs. 4 and 5; $50 \mu\text{l}$ of the standard GPT solution (1060 IU l^{-1}) was injected in each case. The output of the sensor increased gradually with increasing alanine concentration but became constant at 500 mM , which corresponds to about $10 K_m$ [12]. Thus, 500 mM L-alanine is recommended for use. As shown in Fig. 4, the highest output was obtained with $5\text{--}10 \text{ mM}$ α -ketoglutarate, so that 10 mM is used in the recommended procedure. Figure 5 shows that 1.0 mM phosphate is optimum. Further, it was found that the output became constant when the thiamine pyrophosphate concentration was $\geq 1.0 \text{ mM}$, which is therefore the recommended concentration.

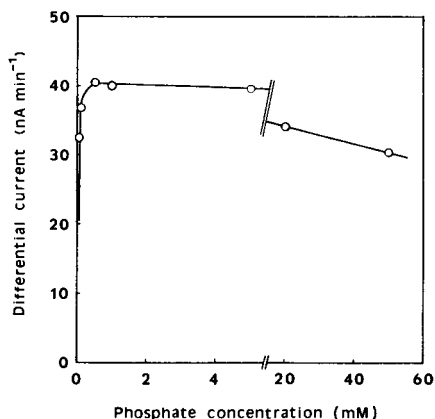
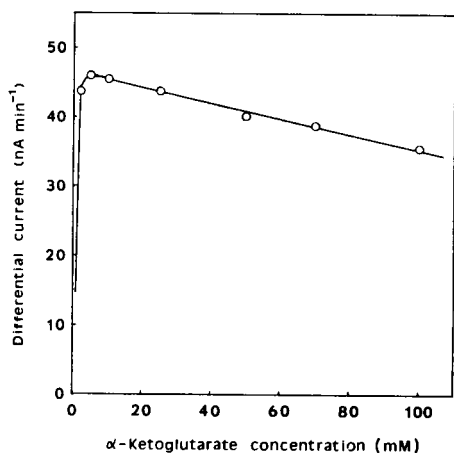


Fig. 4. Effect of α -ketoglutarate concentration (recommended conditions except for α -ketoglutarate concentration; $50 \mu\text{l}$ of GPT solution, 1060 IU l^{-1}).

Fig. 5. Effect of phosphate (KH_2PO_4) concentration (recommended conditions except for phosphate; $50 \mu\text{l}$ of GPT solution, 1060 IU l^{-1}).

Reproducibility, storage stability and accuracy

The reproducibility of GPT measurements was measured by making ten determinations of 30.8 IU l^{-1} and of 201 IU l^{-1} solutions. The coefficients of variation obtained from the initial rate of current increase were 2.4% and 2.3%, respectively. The immobilized enzyme retained 80% of its initial activity after storage for 6 months at 4°C and nearly 100% for 1 year at -20°C .

The GPT activity of human sera was determined by the conventional spectrophotometric method (X_2 , IU l^{-1}) [4] and by the proposed electrochemical method (Y_2 , IU l^{-1}). The results obtained were in satisfactory agreement ($Y_2 = 1.02 X_2 - 7.8$; correlation coefficient 0.99) for 26 assays of human sera over the range 5–1600 IU l^{-1} .

In conclusion, the results show that GPT in sera can be determined rapidly, precisely and accurately with the new sensor. Endogenous pyruvate (up to 1 mmol l^{-1} , which is 20 times the normal level) should also have no effect, because its response should reach a plateau within 30 s (Fig. 2). Therefore the slope of the current increase in the range above ca. 30 s indicates only the GPT activity, and does not involve contributions from endogenous pyruvate.

REFERENCES

- 1 B. Rietz and G. G. Guilbault, *Anal. Chim. Acta*, 77 (1975) 191.
- 2 A. Karmen, F. Wroblewski and J. S. LaDue, *J. Clin. Invest.*, 34 (1955) 126.
- 3 A. Karmen, *J. Clin. Invest.*, 34 (1955) 131.
- 4 F. Wroblewski and J. S. LaDue, *Proc. Soc. Exp. Biol. Med.*, 91 (1956) 569.
- 5 S. Reitman and S. Frankel, *Am. J. Clin. Pathol.*, 28 (1957) 56.
- 6 B. Rietz and G. G. Guilbault, *Clin. Chem.*, 21 (1975) 1544.
- 7 F. Mizutani, K. Tsuda, I. Karube, S. Suzuki and K. Matsumoto, *Anal. Chim. Acta*, 118 (1980) 65.
- 8 S. Hirose, E. Yasukawa, M. Hayashi and W. R. Vieth, *J. Membr. Sci.*, 11 (1982) 177.
- 9 S. Hirose, M. Hayashi, N. Tamura, T. Kamidate, I. Karube and S. Suzuki, *Anal. Chim. Acta*, 151 (1983) 377.
- 10 S. Hirose, E. Yasukawa and T. Nose, *J. Appl. Polym. Sci.*, 26 (1981) 1039.
- 11 L. P. Harger, D. M. Geller and F. Lipmann, *Fed. Proc. Fed. Am. Soc. Exp. Biol.*, 13 (1954) 11.
- 12 M. Saier and W. Jenkins, *J. Biol. Chem.*, 242 (1967) 101.

SELECTIVE DETERMINATION OF MICROBIAL CELLS BY GRAPHITE ELECTRODE MODIFIED WITH ADSORBED 4,4'-BIPYRIDINE

TADASHI MATSUNAGA* and YOICHI NAMBA

Department of Applied Chemistry for Resources, Tokyo University of Agriculture & Technology, Kaganei Tokyo 184 (Japan)

(Received 5th October 1983)

SUMMARY

The concentrations of microbial cells in suspensions can be measured with a graphite electrode modified with adsorbed 4,4'-bipyridine, by using cyclic voltammetry or differential pulse voltammetry. The relationship between the peak current and the cell concentration for *Saccharomyces cerevisiae* is linear over the range 0.03×10^8 – 2.0×10^8 cells ml^{-1} . Yeast, gram-positive bacteria and gram-negative bacteria gave different peak potentials, which may be useful for classification purposes. Electron transfer between the microbial cells and the 4,4'-bipyridine-modified electrode is mediated by coenzyme A in the cell wall.

Detection and enumeration of viable microbial cells are important for diagnosis, environmental assessment and food technology. Colony methods have been used [1] but these methods are time-consuming and demand complicated procedures. Therefore, various electrochemical methods have been developed for determining viable cell numbers [2–5]. For example, impedance measurements of culture media have been used to determine cell numbers [2, 3], although the cell numbers are measured indirectly from bacterial metabolites, and therefore, the results obtained sometimes do not correlate with true cell numbers. An electrode system has been developed for the continuous determination of cell numbers in fermentation media [4, 5]; although this system was shown to be convenient for the continuous determination of cell population, classification of micro-organisms was impossible. Recently, a novel method for detecting microbial cells has been developed, based on cyclic voltammetry at a basal-plane pyrolytic graphite electrode; electron transfer between cells and the graphite electrode is mediated by coenzyme A existing in the cell wall. Both enumeration and classification of microbial cells were possible from cyclic voltammograms by using an electrode system composed of a graphite electrode and a membrane filter retaining micro-organisms [6].

4,4'-Bipyridine is well-known for its ability to promote electron transfer in polynuclear transition metal complexes [7]. It has been shown [8] that 4,4'-bipyridine forms an adsorbed conducting monolayer on the surface of a gold electrode, enabling direct electron transfer to take place between the

electrode and cytochrome c. In this paper, a graphite electrode modified with 4,4'-bipyridine is used for the detection of microbial cells. The processes were followed by applying cyclic voltammetry or differential-pulse voltammetry.

EXPERIMENTAL

Materials

The materials used were 4,4'-bipyridine (Tokyo Kasei, Tokyo), phosphotransacetylase (E.C. 2.3.1.8; P. L. Biochemicals, Milwaukee, WI), co-enzyme A (Sigma Chemicals), acetylphosphate (Boehringer Mannheim), yeast extract (Difco Laboratories, Detroit, MI) and polypeptone (Kyokuto Pharmaceutical Co., Tokyo). Other reagents were of analytical-reagent or laboratory-grade and were used as received. Deionized water was used in all procedures.

Microbial cells

Saccharomyces cerevisiae was cultured aerobically at 30°C for 12 h in 100 ml of a medium (pH 7.0) containing 4 g of glucose, 1 g of polypeptone, 0.5 g of potassium dihydrogenphosphate and 0.2 g of magnesium sulfate heptahydrate. *Salmonella typhimurium* TA100 was grown aerobically at 30°C for 15 h in 100 ml of a medium (pH 7.0) containing 1 g of polypeptone, and meat extract. *Escherichia coli* K12 was cultured aerobically at 30°C for 12 h in 100 ml of a medium (pH 7.0) containing 0.1 g of glucose, 1 g of bacto-trypton, 0.5 g of yeast extract, and 5 g of sodium chloride. *Lactobacillus fermentum* ATCC 9338 was incubated anaerobically at 37°C for 16 h in 100 ml of a medium (pH 6.8) containing 1 g of trypticase, 0.3 g of tryptose, 0.5 g of yeast extract, 0.3 g of KH_2PO_4 , 0.3 g of K_2HPO_4 , 0.2 g of diammonium hydrogencitrate, 2 g of glucose, 0.1 g of Tween-80, 0.02 g of cysteine hydrochloride, and 0.5 ml of a salt solution (11.5% $\text{MgSO}_4 \cdot 7\text{H}_2\text{O}$, 0.68% $\text{FeSO}_4 \cdot 7\text{H}_2\text{O}$, 2.4% $\text{MnSO}_4 \cdot 2\text{H}_2\text{O}$, all w/v). *Bacillus subtilis* MI 112 was cultured aerobically at 30°C for 15 h in 100 ml of a medium (pH 7.0) containing 1.4 g of K_2HPO_4 , 0.6 g of KH_2PO_4 , 0.2 g of ammonium sulfate, 0.1 g of trisodium citrate, 0.5 g of Casamino acids (Difco Laboratories) 0.5 g of glucose and 0.02 g of magnesium sulfate heptahydrate.

Preparation of the 4,4'-bipyridine-modified electrode

A basal-plane pyrolytic graphite electrode with a surface area of 0.17 cm^2 was used. Before modification, the electrode was polished with an aqueous suspension of 0.3- μm alumina on a polishing cloth. 4,4'-Bipyridine (1.56 g) was dissolved in 100 ml of methanol, giving a 0.1 M solution. The graphite electrode was dipped in this solution for 1 min, with slow stirring. The electrode was polished and modified before each run to minimize undesirable electrochemical signals caused by surface-adsorbed species.

Procedures

Voltammetry. Cyclic voltammograms were obtained using a potentiostat (Hokuto Denko, Model HA301), a function generator (Hokuto Denko, Model HB104) and an X-Y recorder (Riken Denshi, F35). The glass cell (25-ml capacity) was fitted with a three-electrode system, comprising the 4,4'-bipyridine-modified graphite electrode, a platinum wire counter electrode and a saturated calomel reference electrode. The reference electrode was separated from the main cell compartment by immersion in a glass tube terminated by a sintered glass frit. Differential-pulse voltammograms were obtained by using a polarograph (Fuso Seisakusho, Model 312) and an X-Y recorder.

Preparation of protoplasts and sonicated cells. Protoplasts of *S. cerevisiae* were prepared by treatment with Zymolyase-5000 (Kirin Brewery Co., Tokyo). The cells were suspended in 10 ml of hypertonic phosphate buffer solution (pH 7.5) containing 0.6 M potassium chloride, and Zymolyase-5000 and 2-mercaptoethanol (0.3%) were added. The cell suspension was incubated at 30°C with shaking (30 strokes/min), centrifuged at 5°C and 8000 *g*, washed with hypertonic buffer, and resuspended in the hypertonic buffer. Sonicated cells were prepared by ultrasonic treatment of whole cells for 30 min in the phosphate buffer (pH 7.0). The cells were centrifuged at 5°C and 8000 *g* and the supernatant liquid containing the exudate from the cells was collected. The cell residues were resuspended in the buffer solution.

RESULTS

Cyclic voltammetry of microbial cells

Figure 1 shows the cyclic and differential-pulse voltammograms of a whole cell suspension of *Saccharomyces cerevisiae* at pH 7.0 obtained at the 4,4'-bipyridine-modified graphite electrode and the unmodified electrode in the potential range 0–1.0 V vs. SCE. Anodic waves appear at 0.74 V vs. SCE on the first scan in the positive direction for both electrodes; the peak potentials are consistent for the two types of measurement. The peak currents at the modified electrode are higher than those at the unmodified electrode; no peak current was obtained at either electrode in the absence of microbial cells. Figure 2 shows the relationship between the peak current of the cyclic voltammograms and the amount of 4,4'-bipyridine adsorbed on the graphite electrode. The peak current increased with increasing amount of 4,4'-bipyridine up to 10^{-11} mol. Formation of a 4,4'-bipyridine monolayer on the graphite electrode would be expected for this amount. The relationship between the peak current of the 4,4'-bipyridine-modified electrode and the scan rate was studied. The oxidation peak current increased linearly with the square root of the scan rate as expected for a diffusion-controlled electrode reaction; the slope of the line for the range 1–4 $\text{mV}^{1/2} \text{ s}^{-1/2}$ was 0.4 $\mu\text{A mV}^{-1/2} \text{ s}^{1/2}$. The effect of pH on the peak potentials of the voltammograms is indicated in Fig. 3. The slope of the potential vs. pH plot was

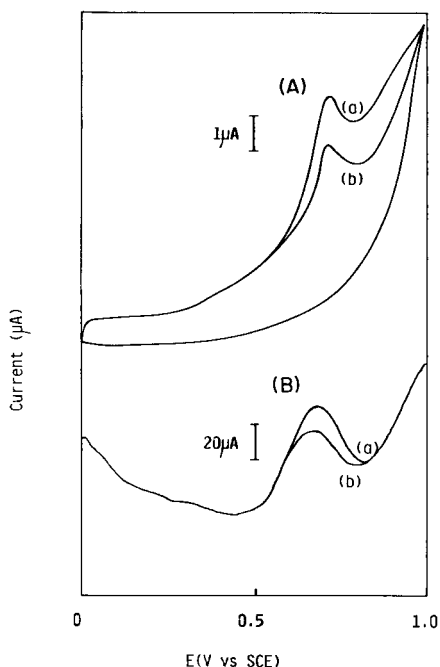


Fig. 1. Cyclic voltammograms (A) and differential-pulse voltammograms (B) of a suspension of *S. cerevisiae*: (a) 4,4'-bipyridine-modified electrode; (b) unmodified electrode. The cell concentration was 2.2×10^8 cells ml^{-1} . For cyclic voltammetry, the scan rate was 10 mV s^{-1} . For differential-pulse voltammetry, the conditions were: scan rate 10 mV s^{-1} , pulse height 100 mV , pulse width 20 ms .

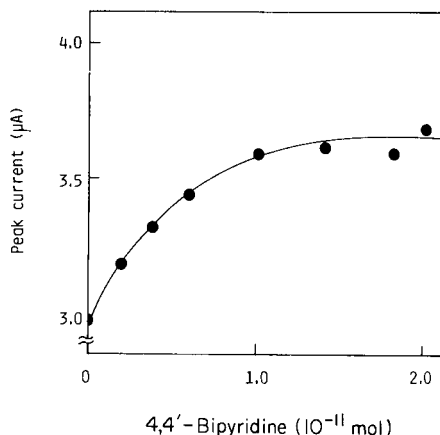


Fig. 2. Relationship between the peak current of cyclic voltammograms and the amount of 4,4'-bipyridine adsorbed on the electrode. Conditions as Fig. 1. Peak heights were measured at 0.74 V vs. SCE.

60 mV in the pH range 5.5 – 8.5 , but the linear relation was distorted at pH 5.5 and the slope was 30 mV below pH 5.5 .

Figure 4 shows the relationship between the peak currents of cyclic voltammograms and the cell concentration of *S. cerevisiae* for the 4,4'-bipyridine-modified electrode and the unmodified electrode. The peak current increased linearly with increasing cell concentration for both electrodes, but the modified electrode provided about 1.4 times better sensitivity. The peak currents from the modified electrode were reproducible with an average relative error of 5% when a microbial suspension containing 10^8 cells ml^{-1} was employed. The minimum detectable cell concentration of *S. cerevisiae* was 3×10^6 cells ml^{-1} . These results indicate that cell numbers can be determined by using the 4,4'-bipyridine-treated electrode. In further tests, the cell populations were determined at various incubation times. The cells were sampled, centrifuged and resuspended in the buffer solution, because the culture media interfered with the measurements. The peak currents

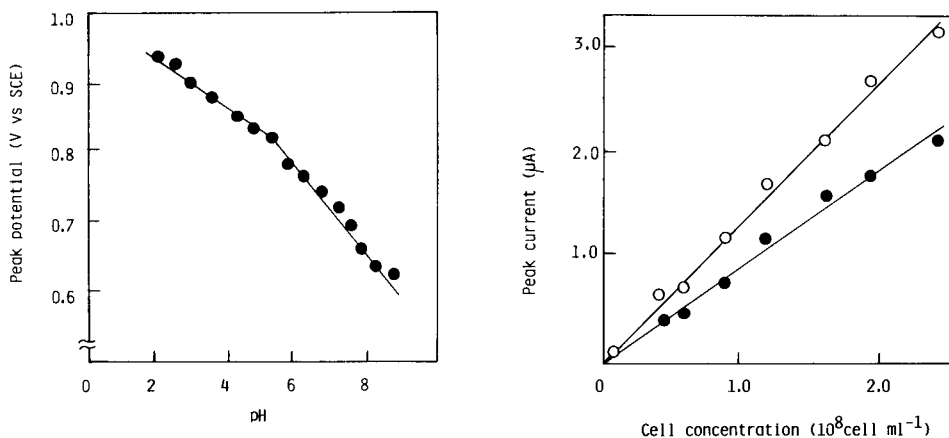


Fig. 3. Plots of peak potentials vs. pH with the 4,4'-bipyridine-modified electrode. The cell concentration was 1.3×10^8 cells ml^{-1} . Conditions as for Fig. 1 except for pH; the pH was adjusted with 0.1 M NaOH or 0.1 M HCl.

Fig. 4. Relationship between peak current and cell concentration with (○) the 4,4'-bipyridine-modified electrode; (●) the unmodified electrode. The experiments were performed under the standard conditions. Cyclic voltammograms were obtained at a scan rate of 10 mV s^{-1} . Peak heights were measured at 0.74 V vs. SCE.

increased with increasing cell populations; the peak currents per 10^8 cells were almost constant ($1.2\text{--}1.4 \mu\text{A}$) for cells incubated for 10–20 h.

Classification of microbial cells with the 4,4'-bipyridine-modified electrode

The plasma membrane of yeast cells, *S. cerevisiae*, is surrounded by a cell wall (50–200 nm thick) composed of glycan, chitin and a mannoprotein complex. The plasma membrane of gram-negative bacteria such as *E. coli*, and *S. typhimurium* is surrounded by a peptidoglycan wall (3 nm thick), which in turn is covered by an outer membrane (8 nm thick) that is a mosaic of protein lipid and lipopolysaccharide. Gram-positive bacteria such as *B. subtilis* and *L. fermentum* have simpler cell envelopes; their plasma membrane is surrounded by a cell wall, typically 25 nm wide, composed of peptidoglycan and teichoic acid.

Cyclic voltammograms of cell suspensions of yeasts and gram-positive and negative-bacteria were obtained by using the 4,4'-bipyridine-modified electrode in the same conditions as described above for *S. cerevisiae*. The cell concentrations were 1.0×10^{10} cells ml^{-1} for *E. coli*, 6.0×10^8 cells ml^{-1} for *S. typhimurium*, 2×10^8 cells ml^{-1} for *B. subtilis* and 5×10^8 cells ml^{-1} for *L. fermentum*, respectively. The suspensions of *E. coli*, *S. typhimurium*, *B. subtilis* and *L. fermentum* gave peak currents at 0.72 V, 0.70 V, 0.68 V and 0.68 V vs. SCE, respectively. The peak potentials for these bacteria were reproducible within a deviation of ± 0.01 V (10 runs on each). These results suggest that the structure of the cell wall affects the peak

potentials of cyclic voltammetry. The peak current of gram-negative bacteria appeared at more positive potentials than those of gram-positive bacteria. Yeast cells gave higher peak potentials than these bacteria.

Mechanism of electron transfer between microbial cells and the 4,4'-bipyridine-modified electrode

Table 1 summarizes the peak currents obtained from whole cells, protoplasts and sonicated cells, and the effects of antibiotics and metabolic inhibitors. Only small peak currents were obtained from protoplasts and sonicated cells. When arsenite was added to the whole cell suspension, the peak current decreased whereas rotenone, antimycin A and cyanide, which inhibit the mitochondrial electron-transport chain, had no effect on the peak current.

Table 2 summarizes the peak potentials of whole cells, the exudate of sonicated cells, coenzyme A, NADH and cysteine and the increase in the peak current obtained with the modified electrode compared to the original graphite electrode. The peak potentials of the exudate of sonicated cells and coenzyme A were the same. The increases in peak current are significant in all cases except NADH which was unaffected by modification of the electrode.

The concentration of coenzyme A in the dissolved exudate from sonicated cells, determined by the phosphotransacetylase method of Stadtman et al. [9], was found to be 3.6 mM.

DISCUSSION

Electron transfer from microbial cells to graphite electrode is expected to be closely correlated with the formation and generation of coenzymes. The metabolic pathway of *S. cerevisiae* is well known: in aerobic conditions, glucose is decomposed to pyruvate in the cytosol by the glycolytic pathway; pyruvate is converted to acetyl coenzyme A with reduction of NAD^+ and enters the citric acid cycle. In this Krebs cycle, 2 mol of ATP, 6 mol of NADH

TABLE 1

Peak currents obtained from whole cells, protoplasts and sonicated cells and the effect of antibiotics and metabolic inhibitors

Sample	Relative peak current (%)	Sample	Relative peak current (%)
Whole cells (<i>S. cerevisiae</i>)	100	Whole cells + rotenone (7.6 mM)	100
Protoplasts	21	Whole cells + antimycin A (5.9 mM)	100
Sonicated cells	6 ^a	Whole cells + cyanide (10.8 mM)	100
Whole cells + arsenite (10 mM)	66		

^aMeasured at 0.74 V vs. SCE for whole cells and sonicated cells, and at 0.67 V vs. SCE for protoplasts.

TABLE 2

Increase in peak current for various compounds and a cell suspension and the peak potentials with the 4,4'-bipyridine-modified electrode

Sample	Increase in peak current ^a (%)	Peak potential (V vs. SCE)
Whole cells (<i>S. cerevisiae</i>)	50	0.74
Exudate of sonicated cells	55	0.65
Coenzyme A (3.7 mM)	45	0.65
NADH (5 mM)	0	0.40
Cysteine (2.5 mM)	20	0.45

^aPeak current with the modified electrode—peak current with the unmodified electrode.

and 2 mol of FADH₂ are formed; electrons from NADH₂ and FADH₂ are transferred to molecular oxygen with generation of ATP by oxidative phosphorylation; the Krebs cycle and oxidative phosphorylation occur inside mitochondria. Rotenone, antimycin A and cyanide are known to inhibit the mitochondrial electron-transport chain, but these compounds had no effect on the peak currents here (Table 1). These results suggest that the generation of peak current is not correlated with oxidative phosphorylation. Arsenite is known to inhibit pyruvate dehydrogenase, and the peak current decreased when arsenite was added to the cell suspension (Table 1). Thus, the generation of current is probably correlated with pyruvate dehydrogenase. Little peak current was obtained from protoplasts and sonicated cells (Table 1), whereas a higher current was obtained from the dissolved exudate of sonicated cells than from whole cells. Coenzyme A was enzymatically detected in the exudate solution and the peak potentials were the same (Table 2). These results suggest that coenzyme A mediates the electron transfer between microbial cells and the 4,4'-bipyridine-modified electrode. The peak currents of coenzyme A, whole cells and their dissolved exudate increased when the electrode surface was modified with 4,4'-bipyridine, whereas the peak current for NADH remained the same. These facts also support the idea of an electron transfer mediated by coenzyme A. The peak current obtained from cysteine was also enhanced by 4,4'-bipyridine. Both coenzyme A and cysteine have a sulfhydryl group, which is probably involved in the electron transfer, but the detailed mechanism requires further study.

As shown in Fig. 2, the peak current increased with increasing amounts of 4,4'-bipyridine up to around 10⁻¹¹ mol, which suggests monolayer formation on the electrode surface. When 4,4'-bipyridine is added to a cell suspension, the surface coverage would be expected to be governed by the Langmuir adsorption isotherm, where the fraction covered, θ , is related to the concentration of 4,4'-bipyridine, C , by $\theta^{-1} = 1 + kC^{-1}$. The peak current increased with increasing concentration of 4,4'-bipyridine, and a plot of $1/\Delta I$ (increase of peak current) against $1/C$ was linear: this is consistent with

the existence of a monolayer on the electrode surface. 4,4'-Bipyridine has been reported to form an adsorbed conducting monolayer on the surface of a gold electrode and to enhance a direct electron transfer between the electrode and cytochrome c [8]. However, cytochrome c is electro-inactive at an unmodified gold electrode whereas microbial cells are electrochemically oxidized even at the unmodified graphite electrode.

As described above, coenzyme A mediates an electron transfer between whole cells of *S. cerevisiae* and the 4,4'-bipyridine-modified electrode. This mediated electron transfer was also observed for other microorganisms. Accordingly, the difference of peak potential in yeast, gram-positive bacteria and gram-negative bacteria is attributed not to species of electroactive substances but to the micro-environment surrounding coenzyme A in the cell walls, which differ in these bacteria. The peak potentials depend on factors such as pH (Fig. 3). The differences in peak potential may serve for classification of some microbial cells, and further work is in progress on application of the modified electrode to classification of other microbial cells.

This work was partially supported by Grant-in-Aid for Scientific Research No. 58 550515, from the Ministry of Science and Culture.

REFERENCES

- 1 J. R. Postgate, in J. R. Norris and D. W. Ribbons (Eds.), *Methods in Microbiology*, Vol. 1, Academic Press, New York, 1969, pp. 611-621.
- 2 W. K. Hadley and G. Senyk, in D. Schlessinger (Ed.), *Microbiology-1975*, American Society for Microbiology, Washington, DC., 1975, pp. 12-21.
- 3 Y. Zafari and W. J. Martin, *J. Clin. Microbiol.*, 5 (1977) 545.
- 4 T. Matsunaga, I. Karube and S. Suzuki, *Appl. Environ. Microbiol.*, 37 (1979) 117.
- 5 T. Matsunaga, I. Karube and S. Suzuki, *Eur. J. Appl. Microbiol. Biotechnol.*, 10 (1980) 125.
- 6 T. Matsunaga and H. Gomyo, *Denki Kagaku*, 51 (1983) 143.
- 7 H. Fisher, G. M. Tom and H. Taube, *J. Am. Chem. Soc.*, 98 (1976) 5512.
- 8 M. J. Eddowes and H. A. O. Hill, *J. Am. Chem. Soc.*, 101 (1979) 4461.
- 9 E. R. Stadtman, G. D. Novelli and F. Lipman, *J. Biol. Chem.*, 191 (1951) 367.

POTENTIOMETRIC STRIPPING ANALYSIS AND ANODIC STRIPPING VOLTAMMETRY WITH CARBON FIBER ELECTRODES

G. SCHULZE* and W. FRENZEL

Institut für Anorganische und Analytische Chemie, Technische Universität Berlin, Straße des 17. Juni 135, 1000 Berlin 12 (Germany)

(Received 20th September 1983)

SUMMARY

High-modulus carbon fibers are used as working electrodes in differential-pulse stripping voltammetry and potentiometric stripping analysis. Different types of electrodes (particularly single-fiber and brush electrodes) are compared with regard to reproducibility, sensitivity, and practical aspects. Zinc, cadmium, and lead are determined in the $100 \mu\text{g l}^{-1}$ to 1 mg l^{-1} range and optimum experimental parameters are described. The cut single-fiber electrode has the best general characteristics.

Carbon fibers have recently been used as electrodes in normal voltammetry [1, 2] as well as in anodic stripping voltammetry (a.s.v.) [3]. It has been shown that in differential-pulse a.s.v. (d.p.a.s.v.) carbon fibers preplated with a thin mercury film give very low background currents, better peak resolution when compared to the HMDE, and good reproducibility. The d.p.a.s.v. was done with low-modulus fibers about 0.5 cm in length. The electrode surface was mainly defined by the axial area of the fiber.

In this study high-modulus fibers are used for d.p.a.s.v. and also for potentiometric stripping analysis (p.s.a.) [4, 5]. Normally, p.s.a. is used in connection with a mercury film electrode on a glassy carbon substrate. The use of fiber electrodes for p.s.a. does not seem to have been described in the literature; but their application seems to be very promising, because a smaller electrode surface is thought to diminish the background problems associated with p.s.a. [5]. Another advantage is the possibility of working with very small volumes.

Four different types of electrodes are compared using both techniques. One primary interest is the application of a cut-fiber electrode similar to that reported by Dayton et al. [2].

EXPERIMENTAL

Apparatus and reagents

All a.s.v. was done with a polarographic analyzer (PAR, Model 174 A) in connection with a three-electrode set up. The potentiometric stripping mea-

surements were made with a potentiostatic device (PAR, Model 173). The electrolytic cell for a.s.v. and p.s.a. was a 50-ml glass vessel with a plexiglas cover in which holes were drilled for the electrodes and nitrogen purge. The solutions were stirred magnetically.

Standard solutions were prepared from 1 g l^{-1} metal ion stock solutions (Merck) by diluting with doubly distilled water. All other reagents were of reagent grade or better.

Electrodes

The working electrodes were constructed by inserting the carbon fibers (Sigrü Elektrographit, Meitingen; $8\text{--}10 \mu\text{m}$ diameter) into standard pipet tips. One drop of a cyanacryl glue (Acculite, Cotronics Corp.) was carefully slid into the top of the pipet tip, so that the tip became filled with a few millimeters of glue by capillarity action, the remainder forming a small droplet around the fiber. The glue was then cured overnight at 60°C . Electrical contact between the carbon fiber and a silver wire was made by introducing one drop of mercury into the tip. To prevent outflow of mercury it was sealed in with an epoxy resin which was left to harden for at least 1 h. This preparation is simple and yields reproducible electrodes. The electrodes were found to be free of leakage. The four different working electrodes are shown schematically in Fig. 1.

Types A and B are similar to those proposed by Pouchon et al. [1] and

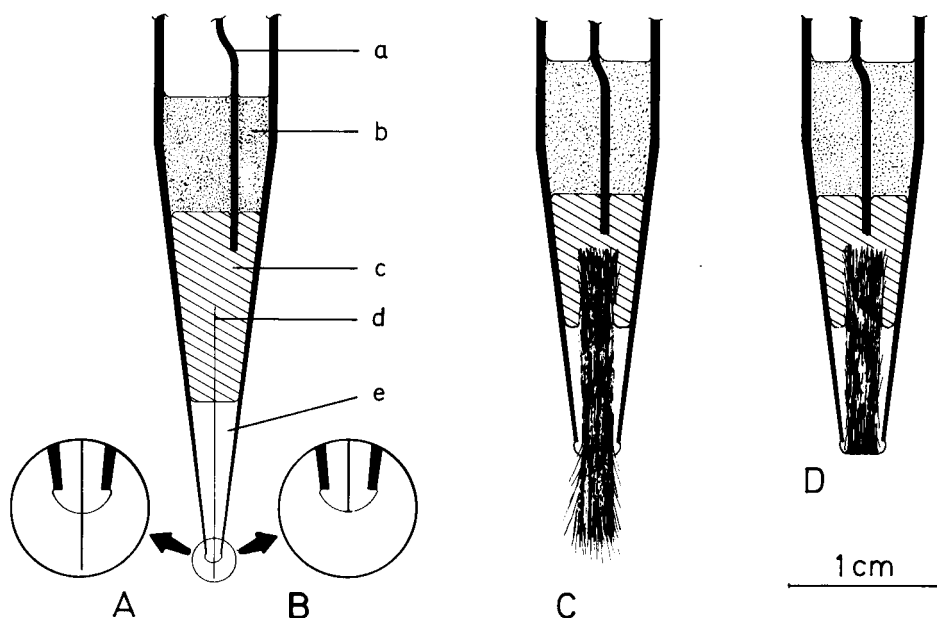


Fig. 1. The four electrode types used: (A) single fiber electrode; (B) cut-fiber electrode; (C) fiber bundle electrode; (D) cut-bundle electrode. (a) Silver wire; (b) epoxy resin; (c) mercury; (d) carbon fiber; (e) cyanacryl glue.

Dayton et al. [2], respectively. The other two electrodes are not single fiber electrodes, but carbon fiber bundles. For comparison, a PAR HMDE and a Tecator glassy carbon electrode (Tecator AB, Höganäs, Sweden) were examined. A platinum wire served as the auxiliary electrode; the reference electrode was a SCE. All potentials are reported vs. SCE.

Conditioning of electrodes. Mechanical cleaning and polishing of fiber electrodes is of course impossible; therefore, different chemical and electrochemical procedures were tested. The best results were obtained by chemically cleaning the electrodes with an iodine/iodide mixture to dissolve the unwanted mercury. The use of strong oxidants (e.g., nitric acid) should be avoided as it leads to irreproducible electrode response. Conditioning by applying a positive potential is not advisable, because this may cause the destruction of the carbon fiber. For both a.s.v. and p.s.a. it proved advantageous to preplate the working electrodes with mercury for at least 3 min at -1.0 V before recording the first scan. Once preplated, the electrodes may be used for several hours. Calomel formation has to be prevented by applying a sufficiently negative potential. The a.s.v. method is much more sensitive than p.s.a. to disturbances caused by the condition of the electrode. Some of the electrodes prepared were usable for p.s.a. but inadequate for a.s.v.; therefore, all the electrodes were tested by scanning a d.c. voltammogram from -1.4 V to $+0.4$ V in a 0.1 M HCl electrolyte. Only electrodes with sufficiently high overpotential and smooth response were used (see Fig. 2).

Procedures

For d.p.a.s.v. the solutions were prepared by the addition of $500\ \mu\text{l}$ of 30% hydrochloric acid (high purity) and $500\ \mu\text{l}$ of mercury(II) nitrate stock solution ($1\ \text{g l}^{-1}\ \text{Hg}^{2+}$) to 25 ml of water, followed by the addition of appropriate analyte aliquots from $100\ \text{mg l}^{-1}$ stock solutions. Sample solutions were purged with nitrogen for 10 min and kept under nitrogen during the measurement. For conditioning, a potential of -1.0 V was applied to the working electrode for 3 min while the solution was stirred; the potential was then switched off and the codeposited metals were chemically stripped by the excess of Hg^{2+} . Immediately after the preplating step, a suitable deposition potential was set at the working electrode and maintained during the deposition time (generally 60–600 s). Stirring was then stopped and an anodic scan was started at a rate of $5\ \text{mV s}^{-1}$ up to $+50$ mV. Subsequent measuring steps were done without renewed conditioning. Measured currents were divided by ten to allow for the gain in the PAR 174 A differential pulse mode.

The same solutions were used for p.s.a. Purging with nitrogen was not required and the stripping was done in stirred solution. In contrast to a.s.v., the electronic circuitry was disconnected at the end of the deposition time and the potential-time curve was recorded. Both peak currents and stripping times on the chart were evaluated.

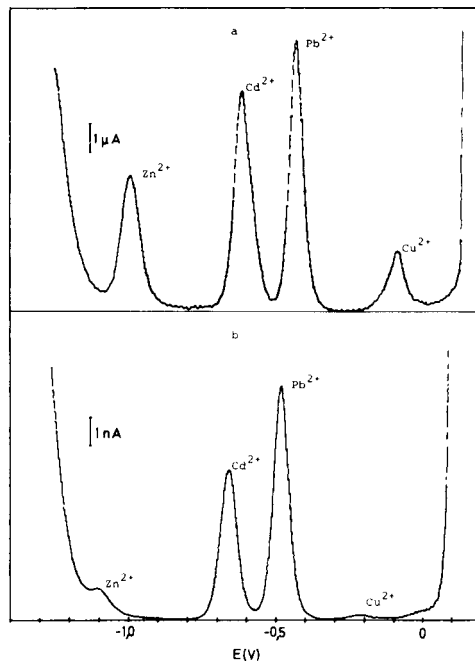
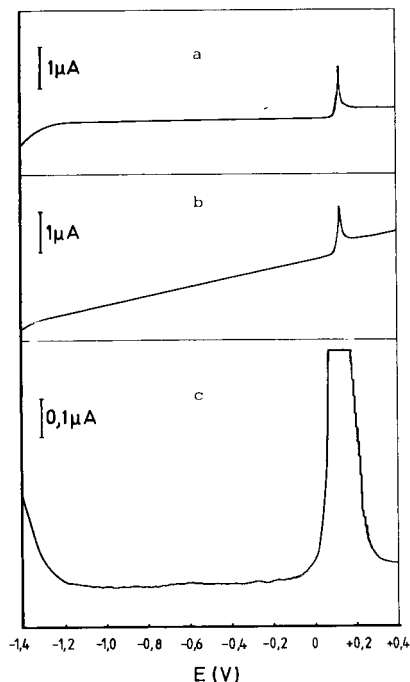


Fig. 2. Background electrolyte scans for the single fiber electrode (type A): (a) d.c. scan of an electrode in good condition; (b) d.c. scan of an electrode in bad condition; (c) d.p.a.s.v. run at 5 mV s^{-1} , 50 mV pulse, 0.5 s drop time at the electrode used in (a).

Fig. 3. D.p.a.s.v. of a solution containing $250 \mu\text{g l}^{-1}$ Cd^{2+} , Pb^{2+} , and Zn^{2+} each, and 10 mg l^{-1} Hg^{2+} in 0.1 M HCl at the electrodes of type A (a) and B (b). The copper signal is due to impurities.

RESULTS AND DISCUSSION

Comparison of different fiber electrode types

A test solution containing 1 mg l^{-1} Pb^{2+} and 10 mg l^{-1} Hg^{2+} in 0.1 M HCl was used; the electrolysis time was 120 s , and the plating potential was set to -1.0 V .

The sensitivity of d.p.a.s.v. is distinctly influenced by electrode area [6]. As a consequence of their small area, carbon fibers exhibit considerably decreased peak currents as shown in Table 1. Therefore, it makes no sense to compare the sensitivity of electrodes of different size. The background currents, however, are also lowered with decreasing electrode area [6]. The background currents at three selected potentials at the various electrodes are also given in Table 1. From an analytical point of view, the utility of an electrode depends on the signal-to-background ratio. For comparison, the peak current was divided by the background current measured at -1.0 V for the electrode in question. The highest value for this ratio was obtained for the mercury film glassy carbon electrode (MFGCE), but fiber electrodes of type A and type B also showed excellent results.

TABLE 1

D.p.a.s.v. and p.s.a. data for Pb^{2+} (1 mg l^{-1}) for the various electrode types tested. Electrolysis time, 120 s; plating potential, -1.00 V^a

Electrode type	D.p.a.s.v.				P.s.a.			
	I_p (μA)	I_r^b (μA) at			I_p/I_r^c	Half-peak width ^d (mV)	t_s (s)	Background signal (s) at -0.1 V
		-1.3 V	-1.0 V	-0.2 V				
HMDE	3.0	1.75	0.13	0.10	23.1	75	—	—
MFGCE	82.5	2.50	0.20	0.45	412.5	60	1.20	0.020
Fiber A	1.9	0.06	0.005	0.01	380.0	50	1.14	0.005
type B	0.0015	0.00012	0.00001	0.00001	150.0	45	1.08	n.d.
C	250	1000	250	150	1.0	110	0.98	0.100
D	5.5	1.60	0.18	0.15	30.6	70	1.23	0.025

^aAll data are the average of three measurements; n.d. = not detectable. ^bBackground current. ^cBackground current taken at -1.0 V . ^dEstimated from the first scan after conditioning.

Electrodes of type A showed a surprisingly low background current over a wide potential range. The signal-to-background ratio suggests that the determination of lead in the lower $\mu\text{g l}^{-1}$ range is possible. This agrees approximately with the results reported by Cushman et al. [3]. Electrodes with a fiber length varying from 0.2 mm to 15 mm were built and compared. The fiber length has little influence on the response. The cut single-fiber electrode (type B) had no measurable background current between -1.0 V and -0.1 V ; also the signal-to-background ratio, calculated from the minimum detectable current, for this electrode is excellent. This electrode is preferable as it cannot break during stirring or handling and may be easily cleaned by wiping with a wet tissue. One limitation in the use of the cut-fiber electrode is that picoampere currents have to be measured at low sample concentrations (about $1 \mu\text{g l}^{-1}$). Both kinds of bundle electrodes (types C and D) showed relatively high background currents. Electrodes of type C cannot be used for a.s.v., because the peak currents are not reproducible and resolution is very poor. Cushman et al. [3] reported an increase in resolution obtained at the fiber electrodes used by them. This was also observed in the present studies. Table 1 includes the half-peak width values.

In p.s.a., the electrode area has no influence on the stripping time, because the same law of diffusion is valid for both the deposition and reoxidizing step. One of the main problems in p.s.a is the capacitance background from the discharge of the electrode [7]. As the double-layer charge is proportional to the electrode area, a decrease in discharge time would be expected when fiber electrodes are used. Because a microprocessor was not available to record the potential-time curves, the background values were estimated from the chart recording. The same solution ($1 \text{ mg l}^{-1} \text{ Pb}^{2+}$) as for d.p.a.s.v. was used to examine the stripping time (t_s) after preconcentration for 120 s in stirred solution. In p.s.a. all the electrodes showed quite similar stripping times, but background was evidently best at the fiber electrodes of types A and B. The p.s.a. data are given in Table 1.

The remainder of this work was done with electrodes of types A and B.

Differential-pulse a.s.v. of lead and cadmium

The results presented in Table 2 show that the peak current is proportional to metal ion concentration in the 0.1–1 mg l⁻¹ range. As expected, the response also varies linearly with deposition time (see Table 3). Typical voltammograms are given in Fig. 3 for electrodes of types A and B. Repeatability (relative standard deviation) calculated from ten consecutive scans without renewed conditioning was better than 3% for Cd and Pb, but the reproducibility was >5% (five samples). This requires the use of the standard addition method. The negative potential shift in relation to the HMDE, described by Cushman et al. [3], was also observed in this work. At the type B electrode it is more distinct than at the type A electrode. The plating of zinc and cadmium was found to be very sensitive to the plating potential. For cadmium the optimum potential is -1.30 V, but for zinc it depends on the type of electrode. At the type A electrode, zinc can also be deposited at -1.30 V, yielding reproducible peak currents, whereas at the type B electrode a high overpotential occurs. To obtain a stripping signal, potentials

TABLE 2

D.p.a.s.v. peak current in relation to lead and cadmium concentration ($t_e = 120$ s, set potential, -1.30 V)^a

Conc. (mg l ⁻¹)	Electrode type A		Electrode type B	
	I_p (Pb) (μ A)	I_p (Cd) (μ A)	I_p (Pb) (nA)	I_p (Cd) (nA)
0.1	0.21	0.14	0.15	0.14
0.3	0.60	0.46	0.39	0.45
0.5	1.04	0.68	0.73	0.71
0.7	1.51	0.99	1.07	0.89
1.0	1.90	1.60	1.51	1.30

^aAll data are the average of five measurements.

TABLE 3

D.p.a.s.v. peak currents in relation to electrolysis time for 500 μ g l⁻¹ Pb²⁺^a

Electrolysis time (s)	60	120	240	360	480	600	1200
I_p (μ A) for type A	0.50	1.40	2.01	3.10	3.97	5.23	10.41
I_p (nA) for type B	0.41	0.73	1.40	2.09	2.73	3.47	6.81

^aAll data are the average of five measurements.

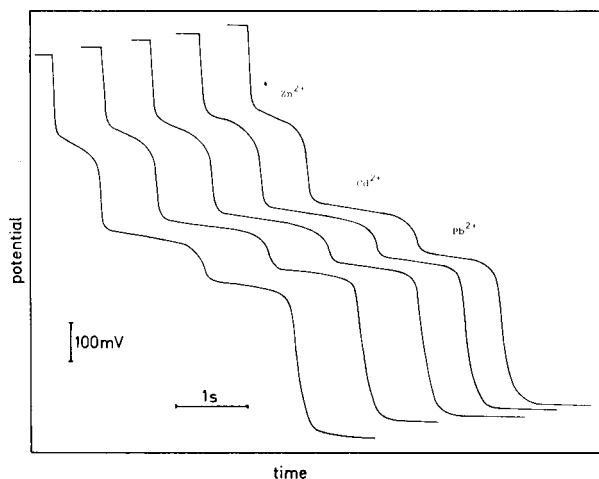


Fig. 4. Five consecutive potentiometric stripping curves of a solution containing $500 \mu\text{g l}^{-1}$ Cd^{2+} , Pb^{2+} , and Zn^{2+} each after in-situ preplating of the mercury film. Electrolysis time, 120 s; electrolysis potential, -1.30 V .

more negative than -1.50 V have to be set, but poor reproducibility is then caused by hydrogen formation.

Potentiometric stripping analysis for lead, cadmium, and zinc

For both electrode types, the repeatability (10 runs) as well as the reproducibility (5 samples containing $500 \mu\text{g l}^{-1}$ Cd, Pb, and Zn each) was better than 5%. A set of five consecutive runs is shown in Fig. 4. When the standard addition method was used, linear calibration plots through the origin were obtained for each element within the $0.1\text{--}1 \text{ mg l}^{-1}$ concentration range (see Table 4). Deposition times between 1 and 10 min were investigated, with the results tabulated in Table 5. It is apparent that the stripping times for lead are proportional to the deposition time. The nega-

TABLE 4

Dependence of stripping time on concentration in the p.s.a. for zinc, cadmium, and lead. ($t_e = 120 \text{ s}$, set potential, -1.30 V)^a

Conc. (mg l^{-1})	Electrode type A			Electrode type B		
	t_s (Pb)	t_s (Cd)	t_s (Zn)	t_s (Pb)	t_s (Cd)	t_s (Zn)
0.1	0.12	0.18	0.15	0.12	0.16	0.11
0.2	0.23	0.34	0.31	0.21	0.30	0.20
0.4	0.50	0.67	0.57	0.48	0.62	0.43
0.6	0.71	1.04	0.89	0.68	1.00	0.61
0.8	0.96	1.31	1.16	0.89	1.27	0.85
1.0	1.14	1.64	1.38	1.08	1.51	1.02

^aAll data are the average of five measurements.

TABLE 5

Dependence of stripping time on electrolysis time for $1 \text{ mg l}^{-1} \text{ Pb}^{2+}$ solution in p.s.a.^a

Electrolysis time (s)	60	120	240	360	480	600
t_s (s) for type A	0.58	1.14	2.23	3.38	4.50	5.63
t_s (s) for type B	0.53	1.08	2.11	3.20	4.27	5.32

^aAll data are the average of five measurements.

tive potential shift found in d.p.a.s.v. also appeared in p.s.a., its extent differing from electrode to electrode. The shift was more distinct at electrodes of type B than at the others.

The decreased background signal at the fiber electrodes leads to sharply pronounced breaks at the equivalence points in the potential vs. time curves. This is especially important for the determination of elements with stripping potentials close to that which occurs after the stripping is completely finished, e.g. copper and bismuth. The stripping curves for lead and copper obtained with a normal GCE and a cut-fiber electrode are given in Fig. 5(a and b). In addition, there arises the possibility of selectively determining copper and bismuth simultaneously (Fig. 5c).

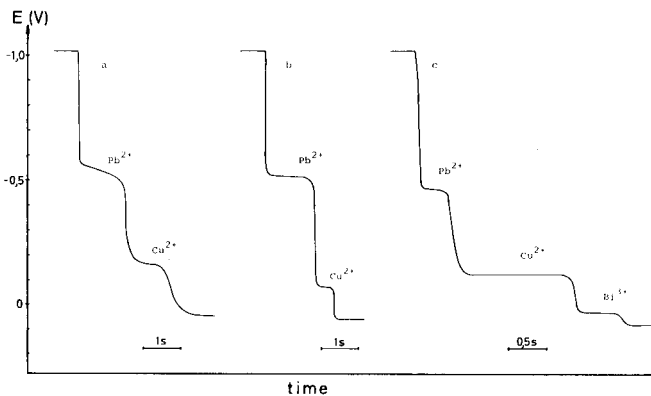


Fig. 5. Potentiometric stripping curves of lead, copper, and bismuth. (a, b) Comparison of the normal MFGCE (curve a) with the cut-fiber electrode (curve b). Solution containing $500 \mu\text{g l}^{-1} \text{ Pb}^{2+}$, $100 \mu\text{g l}^{-1} \text{ Cu}^{2+}$, and $10 \text{ mg l}^{-1} \text{ Hg}^{2+}$ in 0.1 M HCl ($t_e = 300 \text{ s}$, set potential, -1.00 V). (c) Simultaneous determination of $250 \mu\text{g l}^{-1} \text{ Pb}^{2+}$, $500 \mu\text{g l}^{-1} \text{ Cu}^{2+}$, and $500 \mu\text{g l}^{-1} \text{ Bi}^{3+}$ at the cut-fiber electrode ($t_e = 120 \text{ s}$, set potential, -1.00 V).

Conclusions

Carbon fiber electrodes appear to be really useful in stripping analysis. The response is linear to both concentration and electrolysis time. The small background signals obtained lead to excellent signal-to-background ratios. Because of their small size, fiber electrodes, and especially the cut-fiber electrode, offer advantages when small sample volumes have to be analyzed. Their applications in flow-through detectors for flow injection analysis and h.p.l.c. seems very promising.

Valuable discussions with Mr. K. Seider are highly appreciated. Thanks are also expressed to Sigri Elektrographit GmbH for the provision of carbon fibers.

REFERENCES

- 1 J. L. Pouchon, R. Cespuaglio, F. Gonon, M. Jouvét and J.-F. Pujol, *Anal. Chem.*, 51 (1979) 1483.
- 2 M. A. Dayton, J. C. Brown, K. J. Stutts and R. M. Wightman, *Anal. Chem.*, 52 (1980) 946.
- 3 M. R. Cushman, B. G. Bennett and C. W. Anderson, *Anal. Chim. Acta*, 130 (1981) 323.
- 4 D. Jagner and A. Graneli, *Anal. Chim. Acta*, 83 (1976) 19.
- 5 D. Jagner, *Analyst (London)*, 107 (1982) 593.
- 6 T. R. Copeland and R. K. Skogerboe, *Anal. Chem.*, 46 (1974) 1257A.
- 7 J. Mortensen and D. Britz, *Anal. Chim. Acta*, 131 (1981) 159.

ADSORPTIVE STRIPPING VOLTAMMETRIC DETERMINATION OF THIOUREA AND THIOUREA DERIVATIVES

V. STARÁ and M. KOPANICA*

The J. Heyrovský Institute of Physical Chemistry and Electrochemistry, Czechoslovak Academy of Sciences, Prague (Czechoslovakia)

(Received 2nd September 1983)

SUMMARY

Adsorptive stripping voltammetry of thiourea, α -naphthylthiourea and diphenylthiourea is discussed. In perchlorate solution, these compounds are adsorbed at the hanging mercury drop electrode at positive potentials (or at open circuit) and can be stripped in a cathodic scan. Detection limits are 2.5 ng l^{-1} for thiourea, 80 ng l^{-1} for α -naphthylthiourea and 50 ng l^{-1} for diphenylthiourea. The method is applicable in the determination of thiourea in cattle-feed and in the direct analysis of urine.

Thiourea and several thiourea derivatives have found wide application in agriculture because of their fungicidal, herbicidal and rodenticidal activity. These compounds are toxic; thiourea appeared on a list of carcinogens in 1983 [1]. Methods for the determination of low amounts of thiourea and related compounds are therefore important. In this respect, titrimetric and colorimetric methods are unsuitable because of their limited sensitivity. Electrochemical methods are of greater importance.

Polarographic methods based on measurement of the catalytic current caused by thiourea in the presence of copper(II) ions [2] and on measurement of the hydrogen overvoltage [3] offer low detection limits (ca. $10 \mu\text{g l}^{-1}$). Higher sensitivity is obtained by pulse voltammetric methods. Differential pulse polarography can be used for the resolution of mixtures containing thiourea, α -naphthylthiourea and diphenylthiourea; detection limits then reach the values of about $10 \mu\text{g l}^{-1}$ [4]. Because thiourea and its derivatives form insoluble mercury salts [5], these compounds can be determined by cathodic stripping voltammetry (c.s.v.) at a hanging mercury drop electrode (HMDE). The detection limit of c.s.v. for thiourea and the derivatives mentioned, in 1 M sodium hydroxide is about 1 ng ml^{-1} [4]. In this paper, it is shown that the detection limits of these c.s.v. procedures can be dramatically diminished if the analyte is accumulated on the surface of the HMDE under the conditions when adsorption of the mercury salt prevails.

EXPERIMENTAL

Equipment and chemicals

A polarographic analyzer (PA-4; Laboratorní přístroje, Prague) was used in the three-electrode configuration. A static mercury drop electrode (SMDE 1; Laboratorní přístroje, Prague) served as the working electrode in either the hanging mercury drop electrode (HMDE) mode or the dropping mercury electrode (DME) mode. A saturated calomel electrode was used as the reference electrode and platinum wire as the auxiliary electrode. Dissolved oxygen was removed from the test solutions by prepurified nitrogen.

Thiourea was of reagent grade (Lachema, Czechoslovakia). Samples of α -naphthylthiourea and diphenylthiourea were obtained from the Institute of Hygiene and Epidemiology, Prague. Stock solutions (10^{-2} M) of these compounds were stored at 4°C. All solutions used were prepared from twice-distilled water in quartz apparatus.

Procedures

The electroanalytical techniques used were cyclic voltammetry at the HMDE, d.c. polarography or voltammetry, normal pulse polarography or voltammetry (n.p.p./n.p.v.), differential pulse polarography or voltammetry (d.p.p./d.p.v.) and fast-scan differential pulse voltammetry; in the last technique, five pulses per second are applied with sampling identical as in d.p.p. [6].

For adsorptive stripping voltammetry, the test solution was deaerated with oxygen-free nitrogen for 10 min. The HMDE was kept at the accumulation potential E_{acc} in stirred solution (mechanical stirring with constant rate). During stirring, a fresh mercury drop was dialed on the SMDE and from that instant the accumulation time t_{acc} was counted. After the stirrer had been switched off, the solution was allowed to come to rest for another 15 s. The solution was then scanned in the cathodic direction at scan rates of 20–100 mV s⁻¹ in the d.c. mode and 20 mV s⁻¹ in the fast-scan d.p.v. mode. When the analyte was accumulated with disconnected electrode circuitry, the circuitry was re-connected simultaneously with switching off the stirrer. The sequence of all the described operations (with preselected timing and potential values) was done automatically by means of the PA-4 analyzer.

RESULTS AND DISCUSSION

On the cyclic voltammogram of thiourea recorded in 0.1 M sodium perchlorate (pH 5.6) at the HMDE, a sharp, cathodic peak was observed at -0.65 V (vs. SCE) (Fig. 1). The height of this peak increased with prolongation of the period during which the HMDE was kept at +0.25 V before scanning; simultaneously the peak potential shifted to more negative values. A small anodic peak appeared at a potential of -0.55 V. Practically identical cyclic voltammograms were obtained under identical conditions with α -naphthylthiourea and diphenylthiourea.

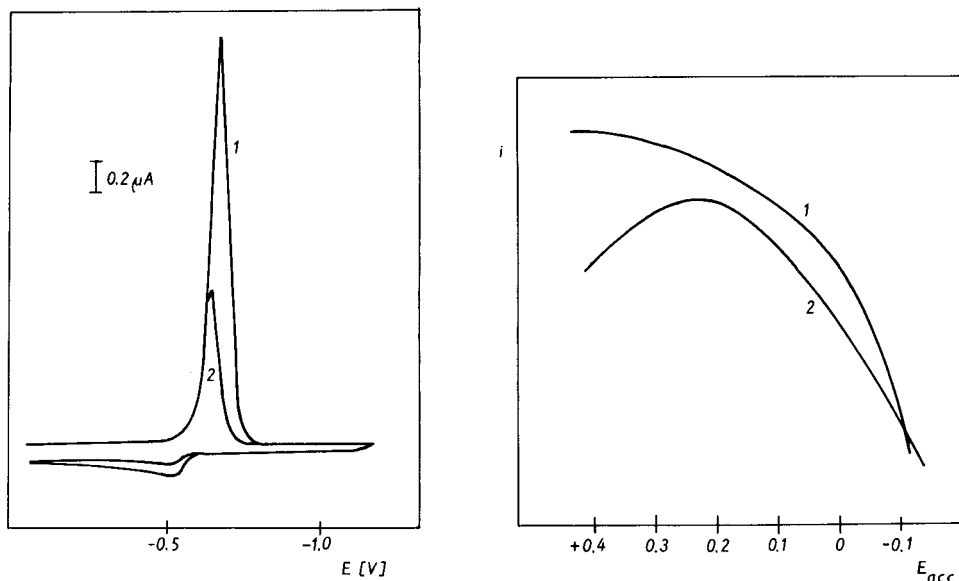


Fig. 1. Cyclic voltammograms of thiourea. Conditions: HMDE, d.c., 1×10^{-6} mol l⁻¹ thiourea in 0.1 M NaClO₄; polarization from -0.20 V to negative values and back. Accumulation time at -0.20 V: (1) 20 s; (2) 0 s.

Fig. 2. Dependence of the adsorptive s.v. peak current of thiourea and α -naphthylthiourea on the accumulation potential. Conditions: fast-scan d.p.v., HMDE, $t_{\text{acc}} = 60$ s, $t_{\text{R}} = 15$ s. Curves: (1) 5×10^{-7} mol l⁻¹ thiourea; (2) 5×10^{-7} mol l⁻¹ α -naphthylthiourea.

Compared with the cyclic voltammogram of thiourea obtained in alkaline medium (1 M sodium hydroxide), the results presented here show a higher degree of reversibility of the system studied and remarkable suppression of the anodic peak, the height of which is only about 4% of the height of the cathodic peak in slightly acidic medium, whereas in alkaline medium the height of the anodic peak corresponds to about 80% of the height of the cathodic peak. These findings correspond with the results of Dhaktode et al. [7], who reported a reversible, diffusion-controlled electrode process of thiourea in acidic or neutral media and an irreversible process in alkaline medium at the HMDE. The products of the reversible process are the soluble species $[\text{Hg}(\text{thiourea})_2]^{2+}$ whereas insoluble HgS is the product formed in alkaline medium. The cathodic peak current recorded in perchlorate medium is much higher than the corresponding current obtained in alkaline medium and thus more suitable for analytical application.

Normal pulse voltammograms of thiourea at the HMDE recorded in perchlorate media showed different waves with half-wave potentials, currents and shape depending on the value of the initial potential. A wave with a maximum at $E_{1/2} = -0.70$ V was obtained when the initial potential was in the range $+0.30$ to $+0.10$ V; with more negative initial potential values

(0 to -0.30 V), the n.p. wave was shifted to more negative potentials and the corresponding current decreased substantially. These findings suggest that the soluble $[\text{Hg}(\text{thiourea})_2]^{2+}$ species formed in the reaction between thiourea and mercury(II) ions are adsorbed on the surface of the HMDE and subsequently stripped by scanning in a negative direction. In this way, a sensitive determination of thiourea can be achieved by using the method of adsorptive stripping voltammetry [8].

Adsorptive stripping voltammetry of thiourea and its derivatives

It follows from the n.p.v. data that adsorptive stripping voltammetry of thiourea is influenced by the value of the accumulation potential E_{acc} . The dependences of the stripping current on the accumulation potential for the determination of thiourea and α -naphthylthiourea are shown in Fig. 2. In both cases, maximum current was obtained when the E_{acc} value was in the range $+0.40$ to $+0.20$ V, which is in agreement with the n.p.v. data. It was observed that the accumulation was possible when the electrode circuitry was disconnected during the accumulation interval. Under these conditions, the formation of mercury ions is suppressed; the potential of the working electrode is established by the composition of the supporting electrolyte. Further experiments showed that the determination of thiourea is slightly more sensitive when the accumulation is completed in open circuit; the signal measured is three times higher under these conditions and the results are readily reproducible. In ten determinations of 2.00×10^{-7} mol l^{-1} thiourea done with open circuit during the accumulation and rest time (t_{R}), the mean value was found to be 1.98×10^{-7} mol l^{-1} and the standard deviation was 0.054×10^{-7} mol l^{-1} .

The peak current increased with prolonged accumulation time, the corresponding dependence having the nature of an adsorptive isotherm. The region in which the current increases linearly with time depends on the analyte concentration and covers the intervals 0–60 s for thiourea concentrations up to 4×10^{-7} mol l^{-1} , 0–600 s for α -naphthylthiourea concentrations up to 1×10^{-6} mol l^{-1} or up to 8×10^{-8} mol l^{-1} diphenylthiourea.

In the interval between pH 4 and 7, the adsorptive voltammetric behaviour of the compounds studied is only slightly influenced by changes of pH. It was observed that above pH 7, the peak current increased and, above pH 8, a double peak was observed.

As expected, this determination of thiourea and the derivatives is influenced by the presence of surface-active substances. Triton X-100, dodecylsulphate and gelatine caused a decrease in the peak current and a shift of the peak potential to more negative values. This decrease is however time-dependent; at $2 \times 10^{-4}\%$ Triton X-100 the peak current of thiourea decreased by 20% immediately after the addition of this surfactant and during next 10 min, gradually increased to its original value. At higher surfactant concentration, this process was slower and the peak current did not return to the original value within 60 min. Experiments showed that up to the

amount corresponding to $10^{-3}\%$ Triton X-100, the peak current decreased to about 20% of its original current value 10 min after the addition of the surfactant.

Because thiourea, α -naphthylthiourea and diphenylthiourea are adsorbed on the surface of the HMDE under practically identical conditions, their simultaneous presence in the test solution cannot be distinguished by the method described. It was observed that the peak currents did not increase linearly when a mixture of, e.g., thiourea and diphenylthiourea was added to the supporting electrolyte. The thiourea derivatives can be differentiated by d.p.p. at a DME as reported by Smyth and Osteryoung [4].

Sodium sulphide was found to behave similarly to thiourea; the E_p value was -0.85 V and thus thiourea and its derivatives can be determined as described above when the sodium sulphide concentration does not exceed that of the thiourea. The presence of metal ions (Cu^{2+} , Pb^{2+} , Cd^{2+} , Co^{2+}) does not have a serious influence on the determination of thiourea, α -naphthylthiourea or diphenylthiourea, but these metal ions may affect the E_p and i_p values of thiourea. If the sample solution contains a high concentration of these metal ions ($>10^{-5}$ mol l^{-1}), the method of standard addition should be applied for evaluation of the results.

The greatest advantage of the adsorptive stripping voltammetry of thiourea and the derivatives is the high sensitivity of the determination compared with the sensitivity of c.s.v. in alkaline medium [4]. With the d.c. or fast-scan d.p.v. techniques and a 600-s accumulation time, the detection limits were evaluated as 2.5 ng l^{-1} for thiourea, 80 ng l^{-1} for α -naphthylthiourea and 50 ng l^{-1} for diphenylthiourea. The current vs. analyte concentration dependences are linear in a wide concentration range: up to 4×10^{-6} mol l^{-1} for thiourea and α -naphthylthiourea and up to 8×10^{-7} mol l^{-1} for diphenylthiourea. The correlation coefficients of the calibration lines (i_p vs. concentration) were calculated as 0.9983 for thiourea, 0.9980 for α -naphthylthiourea and 0.9981 for diphenylthiourea in the concentration interval 10^{-8} – 10^{-7} mol l^{-1} .

In the determination of trace amounts of these compounds ($<10^{-9}$ mol l^{-1}), it is preferable to use adsorptive stripping voltammetry with d.c. measurements, because the background interferences are then limited, as can be seen from the curves in Fig. 3.

Analytical applications

Analysis of aqueous extracts of cattle-feed. The proposed method was applied for the determination of thiourea in aqueous extracts of various types of cattle-feed which contained thiourea as a toxic impurity. An aliquot of the extract was mixed with an appropriate amount of sodium perchlorate, the pH value was adjusted to 5–6 if necessary and the given procedure was applied with disconnected circuitry. The results obtained (10–100 $\mu\text{g ml}^{-1}$ thiourea) were in good agreement with the reported data.

Direct analysis of urine. The proposed method for the direct determination

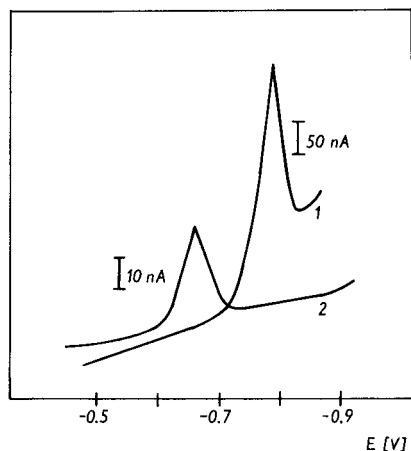


Fig. 3. Adsorptive stripping voltammetry for low concentrations of thiourea; (1) 4×10^{-9} mol l⁻¹ thiourea, HMDE, fast-scan d.p.v., disconnected circuitry, $t_{\text{acc}} = 120$ s, $t_{\text{R}} = 15$ s; (2) 4×10^{-11} mol l⁻¹ thiourea, d.c., $E_{\text{acc}} = +0.20$ V, $t_{\text{acc}} = 600$ s, $t_{\text{R}} = 15$ s.

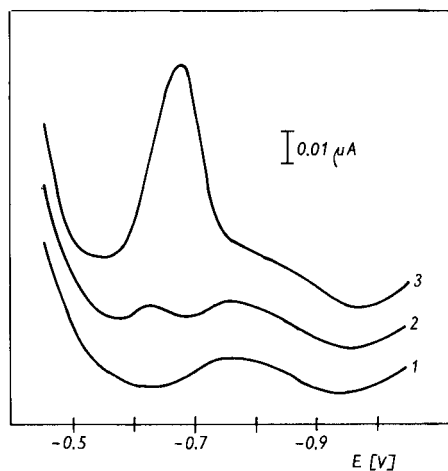


Fig. 4. Adsorptive stripping voltammetry applied to normal urine: (1) 5 ml of urine and 5 ml of 0.5 sodium perchlorate, HMDE, fast-scan d.p.v. $E_{\text{acc}} = +0.10$ V, $t_{\text{acc}} = 60$ s, $t_{\text{R}} = 15$ s; (2) solution as in (1) spiked with 1.2 ng ml⁻¹ thiourea; (3) solution as in (1) spiked with 28 ng ml⁻¹ thiourea.

of thiourea in urine is an improvement on the procedure in alkaline medium; in the latter method, an interfering substance present in urine is stripped at the same potential as thiourea. It was found that in the proposed determination of thiourea, the choice of the accumulation potential is very important because urine contains several surface-active compounds. If the determination was done with open circuit, urine diluted in the ratio 1:1 with 0.5 M sodium perchlorate yielded three peaks in the potential range between -0.35 and -0.80 V and the determination of thiourea became impossible. If, however, the accumulation potential was $+0.10$ V, the diluted urine gave a peak at -0.42 V while the added thiourea gave a peak at -0.68 V (Fig. 4). The sensitivity of the method made it possible to detect 1 ng ml⁻¹ thiourea after an accumulation time of 60 s. The proposed method can be applied for screening of patients exposed to foreign sulphur compounds in the context of defects in sulphur metabolism.

REFERENCES

- 1 3rd Ann. Rep. Carcinogens, U.S. Dept. Health and Human Services, Washington, DC, 1983.
- 2 H. Sohr and K. Wienhold, *Anal. Chim. Acta*, 83 (1976) 415.
- 3 P. E. Holland, J. T. Peeler and A. J. Wehby, *Anal. Chem.*, 41 (1969) 153.
- 4 M. R. Smyth and J. G. Osteryoung, *Anal. Chem.*, 49 (1977) 2310.
- 5 M. Fedorenko, O. Manoušek and P. Zuman, *Chem. Listy*, 49 (1953) 1494.
- 6 V. Gajda and K. Horák, *Anal. Chim. Acta*, 134 (1982) 219.
- 7 S. S. Dhaktode, M. M. Palpecha and R. G. Dhaneshwar, *J. Electrochim. Soc. (India)*, 30 (1981) 142.
- 8 R. Kalvoda, *Anal. Chim. Acta*, 138 (1982) 11.

DIFFERENTIAL-PULSE POLAROGRAPHY OF TRICHOHECENE MYCOTOXINS

Determination of Deoxynivalenol, Nivalenol and Fusarenone-X in Maize

A. VISCONTI and A. BOTTALICO

Istituto Tossine e Micotossine da Parassiti Vegetali, Consiglio Nazionale delle Ricerche, Via Amendola 197/F, 70126-Bari (Italy)

F. PALMISANO* and P. G. ZAMBONIN

Laboratorio di Chimica Analitica, Dipartimento di Chimica dell'Università, Via Amendola 173, 70126-Bari (Italy)

(Received 5th July 1983)

SUMMARY

The polarographic behaviour of representative trichothecenes is described. Compounds characterized by an α,β -unsaturated carbonyl group or by a macrocyclic lactonic ring were found to be electroactive in a methanolic Britton–Robinson buffer. Differential pulse polarography provides detection limits of the order of 40 nmol l⁻¹ with linear ranges extending up to 9 μ mol l⁻¹. The application of differential pulse polarography is described for the determination of nivalenol (3 α ,4 β ,7 α ,15-tetrahydroxy-12,13-epoxytrichothec-9-en-8-one), deoxynivalenol (3 α ,7 α ,15-trihydroxy-12,13-epoxytrichothec-9-en-8-one) and fusarenone-X (3 α ,7 α ,15-trihydroxy-4 β -acetoxy-12,13-epoxytrichothec-9-en-8-one) in infected maize. A suitable liquid/liquid extraction and chromatographic cleanup procedure is reported. Detection limits for the overall procedure and for a sample size of 50 g are of the order of 50 ng g⁻¹ while average recoveries range from 20 to 70% at the 1 μ g g⁻¹ level. Polarographic results are compared with those obtained by a gas-chromatographic method.

Trichothecenes [1–3] are a group of chemically correlated fungal metabolites characterized by high toxicity towards microorganisms, plants, animals and humans. Many of the fungi that produce trichothecenes, and in particular the *Fusarium* species, colonize various foodstuffs and have been implicated several times as causative agents in mycotoxicoses associated with the ingestion of moldy foods and feeds. The development of precise, selective and sensitive methods for trichothecenes determination in naturally contaminated foodstuffs is then of fundamental importance for environmental and health protection. Thin layer chromatography [4], gas-liquid chromatography [4], high performance liquid chromatography [5, 6] and radioimmunoassay [7] are the currently available methods for determination of trichothecenes. Scott [4] has critically evaluated these methods for accuracy, precision and limit of detection.

Modern polarographic techniques have been little used for mycotoxins,

and trichothecenes in particular [8]. In this context, a systematic investigation has recently been initiated [9, 10] in order to assess the potentialities of differential pulse polarography (d.p.p.) as an accurate and sensitive means of determining trichothecenes. In this paper, the polarographic behaviour of HT-2 toxin (3 α ,4 β -dihydroxy-15-acetoxy-8 α -[3-methyl-butyryloxy]-12,13-epoxytrichothec-9-ene), diacetoxyscirpenol (3-hydroxy-4,15-diacetoxy-12,13-epoxytrichothec-9-ene), nivalenol (3 α ,4 β ,7 α ,15-tetrahydroxy-12,13-epoxytrichothec-9-en-8-one), fusarenone-X (3 α ,7 α ,15-trihydroxy-4 β -acetoxy-12,13-epoxytrichothec-9-en-8-one), monoacetoxydeoxynivalenol (3 α -acetoxy-7 α ,15-dihydroxy-12,13-epoxytrichothec-9-en-8-one), verrucarins-A and roridin-A is reported, to complete the previous work. The application of the polarographic method for the determination of deoxynivalenol, nivalenol and fusarenone-X in artificially and naturally contaminated maize samples is described and the results are compared with those obtained by a gas-chromatographic (g.c.) method.

EXPERIMENTAL

Apparatus, reagents and samples

The apparatus and the experimental set-up were the same as previously reported [9] unless otherwise specified.

All the compounds and solvents used were of analytical-reagent grade.

The supporting electrolyte for polarographic measurements was a Britton-Robinson buffer/methanol (9 + 1) mixture. The pH of the buffer was adjusted to the desired value by dropwise addition of 2 M sodium hydroxide.

Sep-Pak C₁₈ cartridges (Water Associates) were used for the purification of the extracts. Tri-sil-TBT (Pierce Eurochemie) was used as silylating agent for g.c.

HT-2 toxin and deoxynivalenol standards were supplied by Prof. C. J. Mirocha (Minnesota University). Fusarenone-X and nivalenol standards were supplied by Prof. Y. Ueno (Tokyo University). Diacetoxyscirpenol was obtained from Calbiochem, verrucarins-A and roridin-A from Makor. 3-Acetyldeoxynivalenol was extracted from a culture of *Fusarium graminearum* Schw. (ITM 126) on maize. Standard solutions (0.1 or 1 $\mu\text{g } \mu\text{l}^{-1}$) of these toxins were prepared in methanol and stored in the dark under refrigeration.

Real samples (naturally infected maize ears) came from field crops picked in Austria and northern Italy.

Procedures

Artificially infected corn samples were obtained by growing different strains of *Fusarium* on 200 g of maize kernels at 27°C for 4 weeks. The cultures were then dried and finely ground.

The toxins were extracted and purified by the following procedure. Ground samples (50 g) were extracted with 200 ml of methanol/1% NaCl (55 + 45) and 100 ml of hexane. After filtration, the hexane layer was dis-

carded and the methanol layer was extracted again with 60 ml of hexane. The methanol portion was then extracted with three 50-ml portions of chloroform; the chloroform extracts were combined and concentrated to near dryness. The residue was then reconstituted in 2 ml of methanol/water (60 + 40), passed through a Sep-Pak C₁₈ cartridge and eluted with a new 2-ml portion of the methanol/water mixture (fraction A). Further elution with two 2-ml portions of methanol gave fraction B. Fractions A and B were evaporated nearly to dryness, reconstituted with 200 μ l of methanol and purified by preparative t.l.c.; the plates were developed with chloroform/methanol (9 + 1). The toxin bands, detected by fluorescence quenching, were scraped off and eluted with methanol. Fraction A was used for the determination of nivalenol, deoxynivalenol and fusarenone-X; fraction B can be used for the determination of T-2 toxin and diacetoxyscirpenol.

Experimental conditions for g.c. and polarographic analysis were those previously reported [9] unless otherwise specified.

RESULTS AND DISCUSSION

Polarographic behaviour

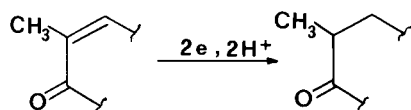
The trichothecene mycotoxins can be classified on the basis of the similarity of their structures, in four different groups (Table 1). Each group presents a different polarographic behaviour.

Group A. Compounds belonging to group A (HT-2 toxin, diacetoxyscirpenol and the previously investigated T-2 toxin) were electro-inactive in the methanolic Britton–Robinson buffer used.

In contrast, a well defined polarographic activity characterizes the mycotoxins of group B and C and can be related to the presence of activated double bonds such as the α,β enone system of the group B and the diene system present in the lactone ring of compounds belonging to group C.

Group B. The differential pulse polarographic behaviour of monoacetoxydeoxynivalenol, nivalenol and fusarenone-X was substantially similar to that previously reported for deoxynivalenol. A single reduction peak was observed at pH 7–8; this was followed, at higher pH, by a second reduction peak at more negative potential values. As expected on the basis of the small structural differences between the examined toxins, the observed peak potentials were very close to each other (see Table 2). This implies that when a mixture of these toxins is to be analyzed a prior separation is necessarily required (*vide infra*).

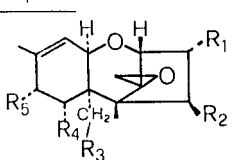
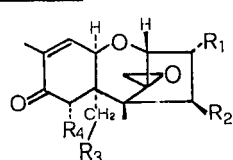
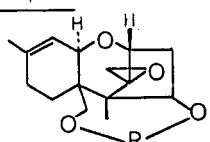
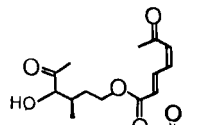
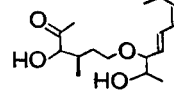
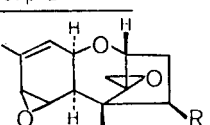
A mechanism for the reduction of these compounds has been suggested elsewhere [11]. It was shown that the first reduction peak corresponds to the overall process



which leads to the formation of the corresponding trichothecane.

TABLE 1

Chemical structures of trichothecene toxins investigated by d.p.p. and their classification according to Ueno [2]

Group A	R ₁	R ₂	R ₃	R ₄	R ₅	
	Diacetoxy-scirpenol	OH	OAc	OAc	H	H
	T-2 toxin	OH	OAc	OAc	H	OCOCH ₂ CH(CH ₃) ₂
	HI-2 toxin	OH	OH	OAc	H	OCOCH ₂ CH(CH ₃) ₂
Group B	R ₁	R ₂	R ₃	R ₄		
	Deoxynivalenol	OH	H	OH	OH	
	Nivalenol	OH	OH	OH	OH	
	Fusarenone - X	OH	OAc	OH	OH	
	Monoacetoxy-deoxynivalenol	Ac	H	H	H	
Group C	R					
	Verrucaric-A					
	Roridin-A					
Group D						

Group C. Verrucaric-A and roridin-A were chosen as representative compounds of Group C which contains six members similar to verrucaric and six members similar to roridin. A typical d.p.p. polarogram of verrucaric-A recorded at pH 7.5 is shown in Fig. 1. In the pH range 4–8, a single reduction step was observed; the peak potential shifted towards more negative values when the pH was increased to a value of 6 and then remained practically unchanged (Fig. 2). Potential-controlled (at -1.3 V vs. SCE) coulometry of verrucaric-A indicated that two electrons are involved in the overall electrode reaction. The electrolyzed product, which was electroinactive, was extracted with chloroform, and then concentrated to dryness and redissolved in methanol.

In contrast to the original toxin, which showed an absorption maximum

TABLE 2

Peak potentials of some group B trichothecenes at different pH values in Britton—Robinson buffer/10% methanol supporting electrolyte
(Concentration of each toxin $3.3 \mu\text{g ml}^{-1}$. Instrumental conditions: drop time 1 s; scan rate 5 mV s^{-1} ; pulse amplitude 50 mV. Values in parentheses indicate the peak potential of the second reduction peak)

pH	Peak potential (V vs. SCE)		
	Nivalenol	Fusarenone-X	3-Acetoxydeoxynivalenol
7	-1.35	-1.360	-1.355
8	-1.36	-1.375	-1.375
9	-1.375	-1.390	-1.385
10	-1.395 (-1.59)	-1.41 (-1.61)	-1.410 (-1.60)
11	-1.40 (-1.60)	-1.415 (-1.62)	-1.420 (-1.62)
12	-1.41 (-1.61)	-1.420 (-1.63)	-1.420 (-1.64)

at 259 nm characteristic of an $\alpha,\beta,\gamma,\delta$ -unsaturated dicarbonyl compound, the u.v. spectrum of the electrolysis product did not show any absorption peak.

The electroactive site is thus certainly confined to the muconic acid moiety of this molecule. The considerably less cathodic peak potentials (compared to Group B) shown by the toxins similar to verrucarins is then readily explained on the basis of the more extended conjugation present in the electroactive site of these molecules.

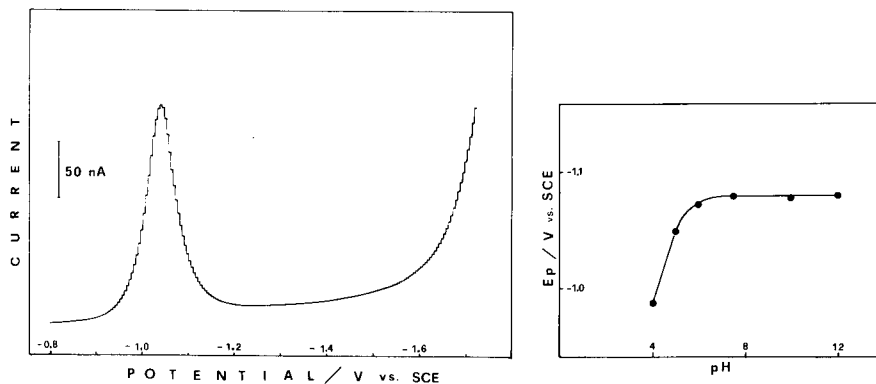
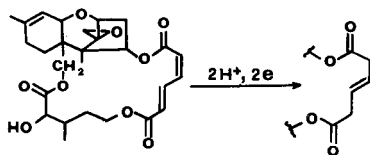


Fig. 1. Differential pulse polarogram of verrucar-A in a Britton—Robinson buffer pH 7.5/methanol (9 + 1) supporting electrolyte. Pulse amplitude 100 mV, drop time 1 s, scan rate 5 mV s^{-1} ; toxin concentration $24 \mu\text{mol l}^{-1}$.

Fig. 2. Plot of the peak potential (E_p) of verrucar-A vs. the pH of the supporting electrolyte.

The overall electrode reaction



may be suggested as the more probable but further investigation is needed for a detailed mechanistic formulation.

At pH values higher than 8, a quite rapid decay of the reduction peak previously described was observed with the appearance of new reduction waves (compare, for example, the curves given in Fig. 3). This behaviour could be ascribed to a base-catalyzed hydrolysis [12] of the lactonic ring present in the molecule with the formation of electroactive products.

Roridin-A was found to be electroinactive in the acidic pH range while at pH around 7 a double shoulder was observed on the background discharge. This is not surprising if one considers that the diene system of roridin-A is less activated than in toxins like verrucar-A. In alkaline solution (e.g., pH 10.5), two distinct peaks occur at -1.44 and -1.65 V. The nature of these peaks was not investigated because at this pH the base-catalyzed hydrolysis of the lactone moiety (as observed for the parent compound verrucar-A) would again intervene.

Group D. None of the three toxins belonging to group D was investigated because of lack of standards.

At the present stage of investigation, it appears that trichothecenes of group B and the verrucar-A type trichothecenes of group C are well suited

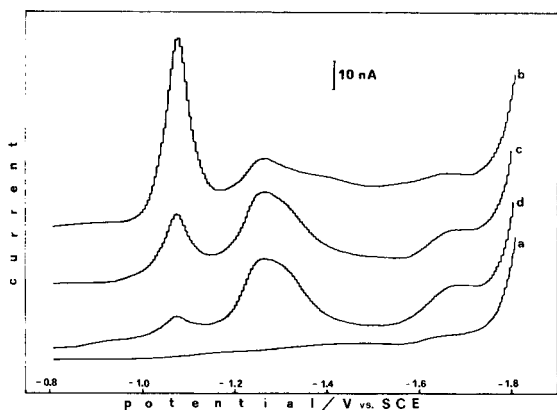


Fig. 3. Differential pulse polarograms run in a Britton—Robinson buffer pH 12/methanol (9 + 1) supporting electrolyte at different times after the addition of verrucar-A ($15 \mu\text{g ml}^{-1}$). Curves: (a) supporting electrolyte; (b, c, d) polarograms taken 5, 18 and 32 min after the addition of the toxin. Instrumental conditions: pulse amplitude 50 mV; scan rate 5 mV s^{-1} ; drop time 1 s.

for polarographic procedures. It is likely that a proper derivatization reaction (e.g., nitro-derivatives) would enable all types of these mycotoxins to be measured polarographically.

Analytical applications

Calibration curves. Calibration graphs for representative toxins were obtained over the concentration range 5×10^{-8} – 9×10^{-6} mol l⁻¹ by adding authentic standards to 3 ml of the mentioned supporting electrolyte at pH 8. The instrumental conditions were: scan rate 5 mV s⁻¹, drop time 1 s, pulse amplitude 100 mV. These calibration graphs were linear in the given concentration range; Table 3 lists the calibration parameters and the detection limits calculated as three times the standard deviation of the intercept.

Recovery study. The recovery of the overall procedure was evaluated from measurements on spiked maize samples at an analyte concentration of 1 µg g⁻¹ by both the g.c. and d.p.p. methods; the results were not significantly different. The recoveries obtained are reported in Table 4. In the course of this work, the average recovery for deoxynivalenol (50%) was found to be twice the value already published [9]; the previous lower recovery can be ascribed to a toxin loss at the Sep-Pak purification stage. This loss was avoided by eluting the cartridge twice with 2 ml of the methanol/water mixture each time (see Experimental). The recovery for nivalenol remains unsatisfactory; higher values (up to 50% in the g.c. method) can be obtained by replacing chloroform with ethyl acetate but this introduced some co-extracted electroactive interference which partly masked the reduction peak of nivalenol.

Analysis of infected maize. Artificially infected maize samples were analyzed for their contents of deoxynivalenol, nivalenol and fusarenone-X by g.c. and d.p.p. (Table 5). The *Fusarium tricinatum* isolate produced both nivalenol and fusarenone-X. In this case, the t.l.c. step (see Procedure) was used both to purify the extract and to separate the two toxins which would mutually interfere in the d.p.p. method. For this purpose, the bands at the

TABLE 3

Calibration parameters and detection limits for some trichothecenes^a

Toxin	Intercept (nA)	Slope (nA µmol ⁻¹)	Correlation coefficient	Standard error of fit (nA)	Detection limit ^b (nmol l ⁻¹)
Nivalenol	0.32 ± 0.05	3.38 ± 0.03	0.9994	0.45	44
Fusarenone-X	0.25 ± 0.04	2.97 ± 0.03	0.9995	0.27	40
Verrucaric-A	1.83 ± 0.09	7.45 ± 0.04	0.9998	0.25	36

^aSupporting electrolyte was BR buffer pH 8/methanol (9 + 1); drop time 1 s, scan rate 5 mV s⁻¹, pulse amplitude 100 mV. ^bThree times the standard deviation of the intercept [9].

TABLE 4

Recovery of the overall procedure obtained on 50 g of corn spiked with 1 $\mu\text{g g}^{-1}$ of each toxin

Toxin	Recovery (%)	R.s.d. ($N = 5$) (%)
Deoxynivalenol	50	10
Fusarenone-X	70	6
Nivalenol	20	10

TABLE 5

Polarographic and gas-chromatographic determination of deoxynivalenol, nivalenol and fusarenone-X in extracts from maize samples, artificially or naturally infected

Sample	Trichothecene ($\mu\text{g g}^{-1}$) ^a					
	Deoxynivalenol		Nivalenol		Fusarenone-X	
	D.p.p.	G.c.	D.p.p.	G.c.	D.p.p.	G.c.
Culture of						
<i>F. graminearum</i> (ITM 126)	1.18	1.20	—	—	—	—
<i>F. equiseti</i> (ITM 5)	ND	ND	—	—	—	—
<i>F. tricinctum</i> (ITM 16)	ND	ND	9.80	10.50	2.00	2.10
<i>Fusarium</i> -infected maize from						
Austria	—	—	0.50	0.70	0.44	0.66
			1.78	2.00	0.95	1.10
Northern Italy	20.00	18.00	—	—	—	—

^aResults are mean values of three replicates. ND, not detected.

same R_f values as the authentic toxins were scraped off and processed individually. Some results obtained on real samples, *Fusarium*-infected maize, are also reported in Table 5. Detection limits for the overall procedure were in the range 40–50 ng g^{-1} for a sample size of 50 g.

REFERENCES

- 1 Y. Ueno, in M. H. Draper (Ed.), *Advances in Nutritional Research* Vol. 3, Plenum, New York, NY, 1980.
- 2 Y. Ueno, in J. V. Rodricks, C. W. Hesseltine and M. A. Mehlman (Eds.), *Mycotoxins in Human and Animal Health*, Pathotox Publisher, Park Forest South, IL, 1977.
- 3 R. F. Vesonder and C. W. Hesseltine, *Process Biochem.*, 16 (1981) 12.
- 4 P. M. Scott, *J. Assoc. Off. Anal. Chem.*, 65 (1982) 876 and references therein.
- 5 M. E. Stack and R. M. Eppley, *J. Assoc. Off. Anal. Chem.*, 63 (1980) 1278.
- 6 A. Visconti and A. Bottalico, *Chromatographia*, 17 (1983) 97.
- 7 S. Lee and F. S. Chu, *J. Assoc. Off. Anal. Chem.*, 64 (1981) 156.
- 8 M. R. Smyth, D. W. Lawellin and J. G. Osteryoung, *Analyst (London)*, 104 (1979) 73.
- 9 F. Palmisano, A. Visconti, A. Bottalico, P. Lerario and P. G. Zambonin, *Analyst (London)*, 106 (1981) 992.
- 10 A. Visconti and F. Palmisano, *J. Chromatogr.*, 252 (1982) 305.
- 11 R. Pizzigallo, Graduate Thesis, Institute of Analytical Chemistry, University of Bari, 1981.
- 12 W. Breinstein and C. Tamm, *Helv. Chim. Acta*, 60 (1977) 1523.

THE OXIDATIVE VOLTAMMETRIC BEHAVIOUR OF SOME SULPHONAMIDES AT THE GLASSY CARBON ELECTRODE

ASTRID MOMBERG V., MARÍA E. CARRERA B., DIETRICH VON BAER and CARLOS BRUHN F.

Departamento de Análisis Instrumental, Facultad de Farmacia, Universidad de Concepción, P.O. Box 237, Concepción (Chile)

MALCOLM R. SMYTH*

School of Chemical Sciences, National Institute for Higher Education, Glasnevin, Dublin 9 (Eire)

(Received 21st September 1983)

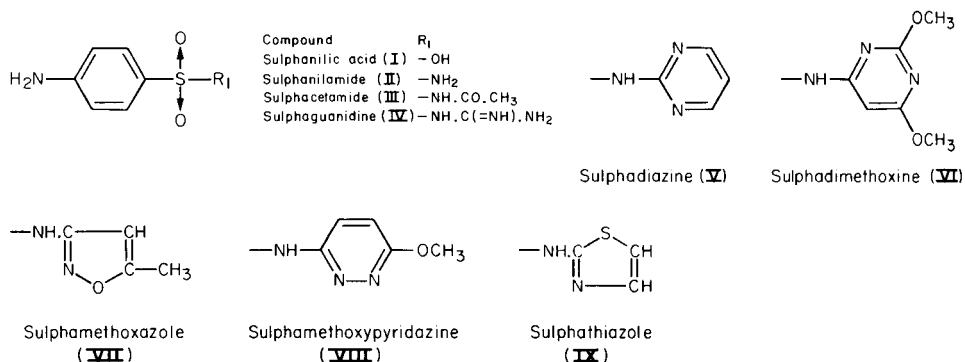
SUMMARY

The voltammetric behaviour of sulphanilic acid and eight sulphonamides at the glassy carbon electrode is discussed. These compounds were found to undergo a $2e^-$ process which appeared to involve the formation of iminobenzoquinone as the final product. The pK_a values relating to the deprotonation of the *p*-amino substituent on the phenyl ring, evaluated from the voltammetric data, were found to be in good agreement with those obtained from ultraviolet spectroscopic data. Voltammetric methods were applied to the analysis of selected mixtures, to the determination of sulphaguanidine in a drug formulation, and as a method for the detection of sulphonamides after high-performance liquid chromatography.

Sulphonamide drugs are widely prescribed for the treatment of bacterial infections of the gastrointestinal tract. These compounds are usually determined by thin layer or paper chromatography followed by colorimetry based on the Bratton–Marshall procedure [1–3]. Recently, several papers have been published on the application of high-performance liquid chromatography (h.p.l.c.) with ultraviolet detection [4–6], which has improved both the selectivity and the sensitivity of sulphonamide determinations. The separation and determination of sulphonamides is also possible by gas chromatography, but this generally involves a prior derivatization [7].

This study is concerned with the oxidative voltammetric behaviour of sulphanilic acid (I) and eight sulphonamides (II–IX) at a glassy carbon electrode, with a view to developing methods for their determination based on linear sweep voltammetry and h.p.l.c. with voltammetric detection. This latter technique provides sensitive, selective determinations of many phenolic and amino-containing compounds of biological significance [8].

These compounds were chosen to represent the various structures which can be present in this class of compound.



EXPERIMENTAL

Apparatus, samples and solutions

Ultraviolet spectra were recorded with a Carl-Zeiss DMR-22 scanning ultraviolet spectrophotometer. Voltammetric curves were recorded in a 3-electrode cell having a platinum counter electrode, a saturated calomel reference electrode and a glassy carbon working electrode (PAR Model G0021). The potential waveforms were applied from a PAR Model 170 Electrochemistry System. Chromatographic separation of the sulphonamides was achieved on a Waters C₁₈-Radial Pak reverse-phase column (5 μm, 8 mm × 100 mm) in a Perkin-Elmer Model Series 2/1 liquid chromatograph at a flow rate of 1.0 ml min⁻¹. The compounds were detected in the eluent (7:3 0.067 M phosphate buffer (pH 6.7): methanol) by using a Perkin-Elmer Model LC-85 spectrophotometric detector at 258 nm and a Metrohm Model 656/641 electrochemical detection system at +1.0 V, connected in series.

Samples of the sulphonamides studied were synthesized by the standard methods described in the Merck Index (9th edition); the purities of these samples were checked by t.l.c. and melting points. *p*-Aminophenol and 4-aminothiophenol (Aldrich Chemical Co.) were used as received. All other compounds were of analytical grade. A stock Britton-Robinson buffer solution (pH ≈ 1.8), composed of a mixture of boric acid, acetic and orthophosphoric acid (each 0.04 M) was prepared and buffer solutions of varying pH were obtained by the addition of 0.2 M sodium hydroxide. All distilled water used in this study was obtained from a Millipore Milli-Q system.

Procedures

Ultraviolet spectra were recorded on 1 × 10⁻⁴ M solutions of the sulphonamides in the pH range 0–6, and pK_a values were obtained from plots of absorbance vs. pH at selected wavelengths. Linear sweep and cyclic voltammograms were generally obtained using the following conditions: initial potential -0.2 V, final potential +1.2 V, scan rate 50 mV s⁻¹. For differential pulse voltammetry, the pulse height was 50 mV, the scan rate 2 mV s⁻¹ and the drop time 1 s.

For the determination of sulphaguanidine in "Carbon-Sulphaguanidine" tablets (Lab. Valma, Santiago, Chile), the tablets were crushed and extracted twice with 10-ml volumes of 1 M hydrochloric acid for 5 min at 90°C and the solution was diluted to 50 ml with distilled water. The sulphaguanidine content was then determined both by ultraviolet detection at 260 nm and differential pulse voltammetry at +0.85 V in Britton-Robinson buffer pH 7.0.

RESULTS AND DISCUSSION

Voltammetric behaviour of sulphonamides

Sulphonamides are electrochemically reducible in aprotic media [9, 10] but this behaviour has not been found useful for analytical purposes. In order to determine sub-micromolar concentrations of sulphonamides, Fogg and Ahmed [11] devised a derivatization procedure based on diazotization and coupling with 1-naphthol, but this polarographic method showed no real advantage over the standard colorimetric procedure with which it was compared. The oxidative behaviour of sulphonamides at the glassy carbon electrode was therefore investigated, in order to see if a direct voltammetric method could be applied to their determination.

All the *p*-amino-substituted sulphonamides and sulphanilic acid exhibited an irreversible 2-electron oxidation wave at the glassy carbon electrode, the potential of which was found to depend on pH. The pH dependences of the peak potential of the waves obtained for sulphanilic acid (I), sulphanilamide (II), sulphacetamide (III) and sulphathiazole (IX) when linear sweep voltammetry was used, are shown in Fig. 1. From this it can be seen that sulphanilic acid and sulphanilamide show four regions of linearity, whereas sulphacetamide and sulphathiazole show only three. In the case of sulphanilic acid, the break in the E_p vs. pH curve at 3.2 is in very good agreement with the

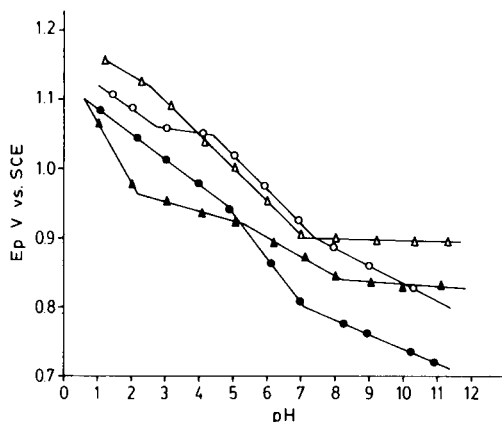
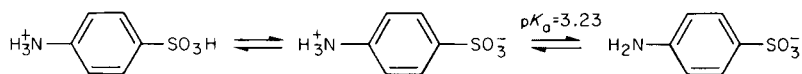


Fig. 1. Plots of E_p vs. pH for selected sulphonamides: (Δ) sulphacetamide; (▲) sulphanilic acid; (○) sulphanilamide; (●) sulphathiazole.

pK_a value of 3.23 cited in the literature [12], and corresponds to the deprotonation of the *p*-amino substituent on the phenyl ring



Deprotonation of the $\text{---SO}_3\text{H}$ substituent occurs at very low pH values, as in benzenesulphonic acid ($pK_1 = 0.70$) [12]. The absence of such a break in the E_p vs. pH plots at the low pH values for sulphacetamide and sulphathiazole indicates that the deprotonation of the ---NH_3^+ substituent in their molecular structures occurred at pH values lower than for the other two compounds. In order to test this, the ultraviolet spectra for compounds (III)–(IX) were recorded in solutions of pH 0–5, and pK_a values relating to this equilibrium were determined from plots of absorbance vs. pH. The results are shown in Table 1, from which it can be seen that the pK_a values obtained for those compounds that did not exhibit a break in their respective E_p vs. pH plots at low pH values (i.e., sulphacetamide, sulphamethoxazole and sulphathiazole) were all <2.0 . For those compounds which had spectrophotometrically determined pK_a values exceeding 2.0, breaks were found in the E_p vs. pH plots which were in good agreement with the spectroscopic data.

The second breaks in the E_p vs. pH plots for compounds I, II, IV, V, VI and VIII and the first break in the E_p vs. pH plots for compounds III, VII and IX, all reflect a change from lesser to greater slope, and correspond to pK_a values of the $\text{---NH}_3^+ \rightleftharpoons \text{---NH}_2$ equilibrium. The subsequent break in the plots for all the compounds studied corresponds to a change to lesser slope, and reflects the polarographic dissociation constant (pK'). The breaks at around pH 7.0, however, appears to reflect a change in electrochemical behaviour. At pH > 7.0 , the waves for all compounds began to decrease in size and occurred over a larger range of potential, indicating an increasing degree of irreversibility of the processes involved. From these results, it would

TABLE 1

Comparison of pK_a values relating to the $\text{---NH}_3^+ \rightleftharpoons \text{---NH}_2$ equilibrium of sulphonamides obtained by u.v. spectroscopy and voltammetry

Compound	pK_a value		Compound	pK_a value	
	U.v.	Voltammetry ^b		U.v.	Voltamm
Sulphanilic acid	3.23 ^a	3.2 (5.8)	Sulphadimethoxine	2.05 ^e	2.3 (4.2)
Sulphanilamide	2.36 ^a	2.7 (4.4)	Sulphamethoxazole	1.65 ^c	ND (2.5)
Sulphacetamide	1.40 ^c	ND (2.5)	Sulphamethoxy pyridazine	2.10 ^c	2.2 (4.8)
Sulphaguanidine	2.20 ^d	2.8 (5.4)	Sulphathiazole	1.70 ^f	ND (4.7)
Sulphadiazine	2.20 ^d	2.3 (5.5)			

^aLiterature value [12]. ^bThe values in parentheses are the pK' values; ND, not determined.

^cAt 280 nm. ^dAt 270 nm. ^eAt 260 nm. ^fAt 255 nm.

appear that protonation of the R-NH₂ group at the electrode surface is required before oxidation can proceed.

In solutions of pH < 7.0, all the compounds studied exhibited a small double wave on the reverse scan in cyclic voltammetry. This is illustrated for sulphanilic acid in Britton-Robinson buffer pH 5.0 in Fig. 2(a). Thus, although the electrochemical process giving rise to the oxidation wave for sulphonamides is irreversible, one (or more) of the products of the electro-oxidation must undergo reduction on the reverse scan. It was believed that the sulphanilic acid moiety was responsible for the voltammetric behaviour of the sulphonamides, and so the behaviour of model compounds related to this structure was investigated. The first compound studied was benzenesulphonic acid which was shown not to be oxidized under the conditions employed here. In previous studies at platinum and PbO₂ anodes [13, 14], benzenesulphonic acid was shown to be oxidized in aqueous solutions, to give various products, including 3,4-dihydroxy-*p*-hydroxy-benzenesulphonic acid, benzoquinone, fumaric acid and succinic acid. This indicates that the *p*-amino substituent of the sulphonamides studied is involved in the electrode process. From a study [15] on the oxidation of 2,4,6-tri(*t*-butyl)aniline at the platinum electrode in acetonitrile by controlled potential electrolysis, 3,5-di(*t*-butyl)-4-imino-2,5-cyclohexadienone was identified as the final product of the electrode reaction.

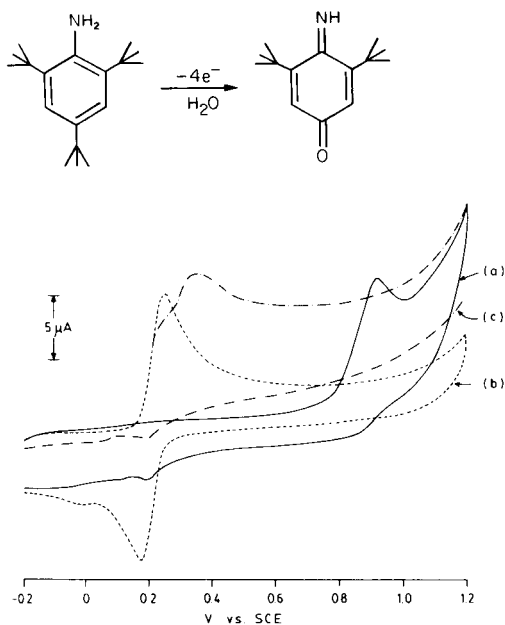


Fig. 2. Cyclic voltammetry behaviour in Britton-Robinson buffer pH 5.0: (a) 1×10^{-4} M sulphanilic acid; (b) 1×10^{-4} M *p*-aminophenol; (c) 1×10^{-4} M *p*-aminophenol + 1×10^{-4} M $S_2O_3^{2-}$.

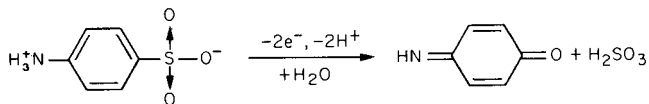
In order to test the idea that a similar mechanism might be involved in the oxidation of sulphonamides, the voltammetric oxidation of *p*-aminophenol was studied; iminobenzoquinone is known to be the main oxidation product of this compound. The cyclic voltammogram of *p*-aminophenol in Britton–Robinson buffer, pH 5.0 (Fig. 2, curve b) shows the double wave associated with reduction of the products of the electrode reactions at about the same potentials as those for sulphanilic acid (Fig. 2, curve a), though the latter peaks are much smaller. Because the proposed mechanism leading to the formation of iminobenzoquinone would involve the formation of SO_2 (or HSO_3^-), the effect of these species on the cyclic voltammetric behaviour of *p*-aminophenol was examined. Sulphite and sulphur dioxide were produced in situ from potassium metabisulphite



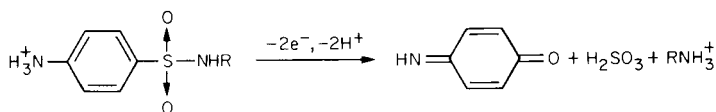
The results (Fig. 2, curve c) show that the peak heights on the reverse scan were dramatically reduced by the addition of metabisulphite. It was further shown that the pH-dependence of the oxidation product of sulphanilic acid was similar to that of iminobenzoquinone. The oxidation of 4-aminothiophenol was also investigated, because the iminothiobenzoquinone formed is a conceivable intermediate in the oxidation of sulphonamides; the cyclic voltammetric behaviour of this compound showed no similarities, however, with those of the sulphonamides investigated. As the *p*-amino substituent is obviously important in determining the oxidation behaviour of sulphonamides, the voltammetric behaviour of phthalylsulphathiazole (X) was investigated; this compound underwent a 1-electron oxidation at potentials similar to that of sulphathiazole, but it did not give a cyclic voltammetric peak relating to the reduction of the product of the electro-oxidation.



Based on the above results, the overall electrode process for sulphanilic acid appears to be



A more detailed study involving controlled-potential electrolytic and spectroelectrochemical techniques would be required to characterize the products more fully. In the case of the sulphonamides studied, the overall mechanism may be



Differential-pulse voltammetric resolution of mixtures

Based on the results obtained for the pH dependence of the E_p values of the various compounds studied, it is possible to use differential pulse voltammetry to resolve partly certain mixtures of sulphonamides, provided that the separation of their E_p values exceeds 100 mV. This is illustrated in Fig. 3 for a mixture of sulphacetamide and sulphanilic acid at pH 3.0 and for a mixture of sulphaguanidine and sulphathiazole at pH 10.0. It would obviously be difficult to obtain quantitative results using this approach.

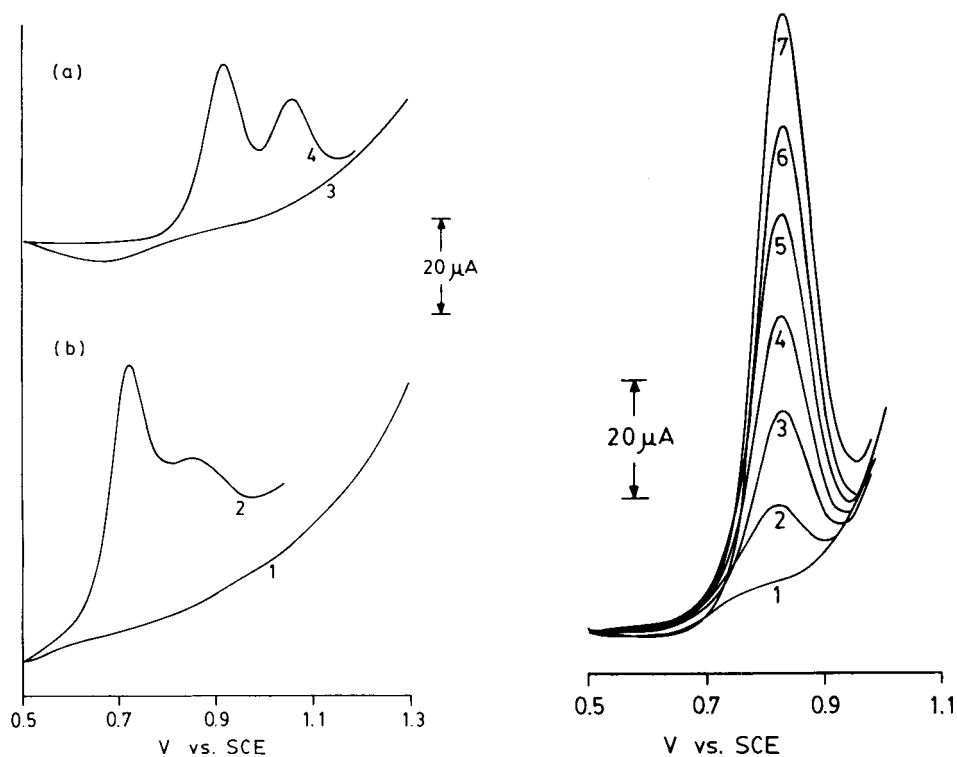


Fig. 3. Differential-pulse voltammetric resolution of mixtures: (a) Britton-Robinson buffer pH 3.0 (1) and a mixture of sulphacetamide and sulphanilic acid (2); (b) Britton-Robinson buffer pH 10.0 (3) and a mixture of sulphaguanidine and sulphathiazole (4).

Fig. 4. Calibration for sulphaguanidine in Britton-Robinson buffer pH 7.0. (1) Buffer alone; (2) 9.90×10^{-6} M, (3) 1.96×10^{-5} M, (4) 2.91×10^{-5} M, (5) 3.85×10^{-5} M, (6) 4.76×10^{-5} M, (7) 5.66×10^{-5} M sulphaguanidine.

Differential pulse voltammetric determination of sulphaguanidine in Carbon-Sulphaguanidine tablets

Differential pulse voltammetry (d.p.v.) was used to quantify sulphaguanidine in Carbon-Sulphaguanidine tablets. Calibration graphs obtained at pH 7.0 were linear within the concentration range $1-8 \times 10^{-5}$ M (Fig. 4), which is suitable for the quality control of this pharmaceutical formulation. The limit of detection was 5×10^{-6} M. The precision, expressed as relative standard deviation, was $\pm 4\%$ in duplicate extract determinations.

A recovery study of sulphaguanidine by interpolation in the calibration graph yielded a mean of $107 \pm 3\%$ in four tablets. By the standard addition method, the recovery was lower and less reproducible ($85 \pm 25\%$ in five tablets) and so this approach was disregarded. A comparison with u.v. spectrophotometric results at pH 7.0 (260 nm) indicated a mean recovery of $97 \pm 4\%$ in four tablets. The relatively higher recovery obtained by d.p.v.

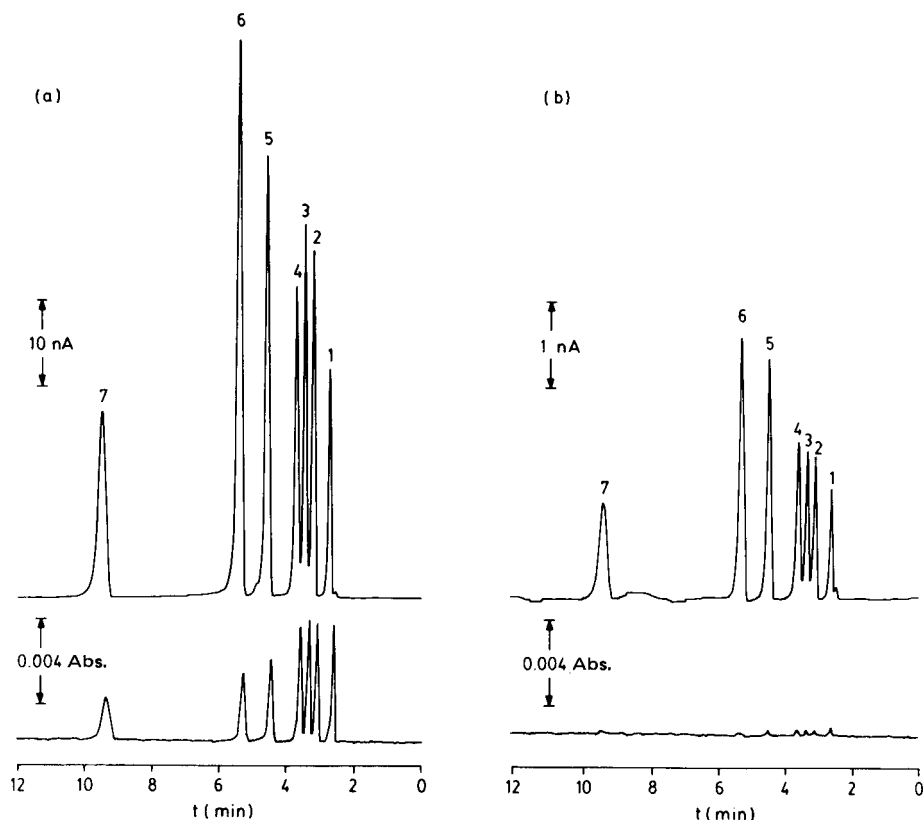


Fig. 5. H.p.l.c. of sulphenamides. Upper curves correspond to voltammetric detection and lower curves to u.v.-detection. Concentration of each compound: (a) 1×10^{-5} M; (b) 4×10^{-7} M. Injection volume $6 \mu\text{l}$. Compounds: (1) sulphacetamide; (2) sulphaguanidine; (3) sulphanilamide; (4) sulphadiazine; (5) sulphamethoxazole; (6) sulphathiazole; (7) sulphamethoxy-pyridazine.

may be attributed to a change in the baseline, associated with the surface condition of the glassy carbon electrode.

H.p.l.c. of some sulphonamides with u.v. and voltammetric detection

Based on the results obtained for the voltammetric oxidation of sulphonamides at the glassy carbon electrode, the voltammetric detection of a mixture of seven sulphonamides after separation by h.p.l.c. was investigated and compared with u.v.-detection [5, 6]. Figure 5(a) shows that each sulphonamide detected by u.v. at a concentration of 1×10^{-5} M was also detected by the voltammetric method. The employment of the voltammetric detector as the second detector in series was not found to contribute significantly to peak broadening. Figure 5(a) also indicates how voltammetric detection of sulphonamides significantly increases the sensitivity after h.p.l.c. separation. At the 0.4×10^{-7} M level, sulphonamides could not be quantified by u.v.-detection (Fig. 5b) but the voltammetric detector was satisfactory. The limit of detection of the latter technique was 1×10^{-7} M (or 1 pmol for a 6- μ l injection) for each sulphonamide studied.

Studies on the determination of these compounds in body fluids will be the subject of a later communication.

The authors are grateful to the Faculty of Pharmacy of the University of Concepción (Chile), the National Institute for Higher Education (NIHE), Dublin, and Higher Education for Development Cooperation (HEDCO, Ireland) for support of Dr. M. R. Smyth's visit to Chile.

REFERENCES

- 1 A. C. Bratton and E. K. Marshall, *J. Biol. Chem.*, 128 (1939) 573.
- 2 United States Pharmacopeia, 19th rev. edn., Mack Publishing Co., Easton, PA, 1975.
- 3 Official Methods of Analysis, 12th edn., Assoc. Offic. Anal. Chem., Washington DC, 1975, p. 700.
- 4 S. C. Su, A. V. Hartkopf and B. L. Karger, *J. Chromatogr.*, 119 (1976) 523.
- 5 T. B. Vree, Y. A. Hekster, A. M. Baars, J. E. Damsma and E. van der Kleijn, *J. Chromatogr. (Biomed. Appl.)*, 146 (1978) 103.
- 6 K. Harzer, *J. Chromatogr.*, 155 (1978) 399.
- 7 K. Beyermann, *Organische Spurenanalyse*, G. Thieme Verlag, Stuttgart, 1982, pp. 118, 133.
- 8 M. R. Smyth, C. G. B. Frischkorn and H. W. Nürnberg, *Anal. Proc.*, 18 (1981) 215.
- 9 L. Horner and H. Neumann, *Chem. Ber.*, 98 (1965) 3462.
- 10 L. Benedetti, R. Andreoli, C. B. Gavioli and G. Grandi, *J. Electroanal. Chem.*, 68 (1976) 243.
- 11 A. G. Fogg and Y. Z. Ahmed, *Anal. Chim. Acta*, 70 (1974) 241.
- 12 Handbook of Chemistry and Physics, 61st edn., CRC, Cleveland, OH, 1980-81, p. D161.
- 13 F. Fichter and E. Stocker, *Helv. Chim. Acta*, 7 (1924) 1064.
- 14 R. Tonoli, in F. Fichter (Ed.), *Organische Elektrochemie*, Steinhof, Dresden, 1942, p. 123.
- 15 G. Cauquis, G. Fauvelot and J. Rigaudy, *C.R. Acad. Sci.*, 264 (1967) 1758.

LINEAR-SWEEP VOLTAMMETRY AT A DROPPING MERCURY ELECTRODE IN CONTINUOUS FLOW SYSTEMS

Z. KOWALSKI* and W. KUBIAK

Institute of Materials Science, Academy of Mining and Metallurgy al. Mickiewicza 30, Kraków (Poland)

(Received 9th November 1983)

SUMMARY

Linear-sweep voltammetry at a dropping mercury electrode is examined in flowing systems with parallel, opposite and normal mercury and fluid flow. The influence of fluid velocity ($0\text{--}12\text{ cm s}^{-1}$) on current and potential parameters of linear-sweep voltammograms is described. The ranges of fluid velocity in which current parameters are independent of flow, were determined by analysis of variance. It is shown that at certain sweep rates, the current does not depend on fluid velocity up to 12 cm s^{-1} .

Detectors based on dropping or hanging drop mercury electrodes have been applied in liquid chromatography [1] and in more general flowing systems [2]. The possibility of using voltammetric detection in high-performance liquid chromatography [3, 4] and in flow-injection systems [5] has become of great interest. The main reasons are the high sensitivity, selectivity and wide linear range of voltammetric detectors. One serious disadvantage of such detectors when used in flowing systems is the dependence of the limiting current on solution flow velocity. Thus it is necessary to ensure precise measurement and stabilization of fluid flow. Most frequently, when a voltammetric detector is operated at a fixed potential, the limiting current is proportional to the square root of the mean linear velocity of the fluid (in the case of opposite and normal flows of mercury and fluid) or to the cubic root (in the case of parallel mercury and fluid flows). The general equations for these cases have been given recently by Hanekamp and De Jong [6].

Under laminar flow conditions, a hydrodynamic boundary layer [7] is formed at a mercury drop. In this layer, the flow-velocity vector changes its magnitude from that at the mercury surface to that in the bulk fluid flow of the solution. If the directions of the flow at the drop surface and the bulk fluid flow are not the same, or if the surface is curved, boundary layer separation will occur. The boundary layer affects the diffusion layer formed at the electrode, thus changing the ion-transport conditions and the limiting current. This picture is complicated by the facts that the thickness of the boundary layer varies at different points of a mercury drop, and that the

mercury drop is growing. This situation makes exact mathematical descriptions impossible in practice. However, there are some cases in which this difficulty may be overcome.

Four cases can be described qualitatively. First, if the diffusion layer is so thick that it reaches the region of the boundary layer where the flow-velocity vector is large, then the bulk solution flow will have a strong influence on the diffusion layer. The limiting current then depends on the mean linear velocity of fluid. The equation given by Hanekamp and De Jong [6] provides a good approximation of this dependence. In the second case, the diffusion layer is so thin that it reaches only the region of the boundary layer where the flow velocity vector is small, and the diffusion layer will then only be affected insignificantly by the bulk flow. This case occurs when short potential pulses are used for electrode polarization. In the third possible case, the electrode itself affects the diffusion layer so strongly that any perturbation induced by the fluid flow can be neglected over a certain range of flow rates. The rapidly dropping mercury electrode, the streaming mercury electrode and the rotated dropping mercury electrode have such properties. In the fourth case, the linear flow rate near the electrode is considerably reduced by the construction of the flow detector, so that the hydrodynamic conditions near the electrode approximate stationary conditions.

In the first case, the limiting current depends on the mean linear flow velocity, whereas in the other three cases the limiting current is independent of the linear velocity up to a certain value. From the points of view of construction of flow systems and data interpretation, these three cases have peculiar significance. An example of the third case is found in a paper by Tamamushi et al. [8], the fourth case occurs partially in a paper by Bond et al. [9] and the second case occurs when normal-pulse polarography is applied [9, 10] or when linear-sweep voltammetry is applied, as in the present work, the whole voltammogram being obtained on a single drop. Linear-sweep voltammetry makes it possible to determine some depolarizers simultaneously and to establish electrode reaction parameters by the interpretation of data obtained from flow systems.

The basic aim of the present paper is to verify the usefulness of linear-sweep voltammetry in investigations of flow systems. For this purpose, the range of fluid velocities in which linear-sweep voltammetry is independent of flow, and the effects of voltage scan rate, were studied experimentally.

EXPERIMENTAL

The dropping mercury electrode flow detector

Two detectors were used (Fig. 1), one for parallel and opposite flow (A) and the other for normal flow (B). The detectors were made of glass. The mean linear velocity of fluid flow was constant over the whole detector. The working electrode was a dropping mercury electrode (DME) with a 20-cm

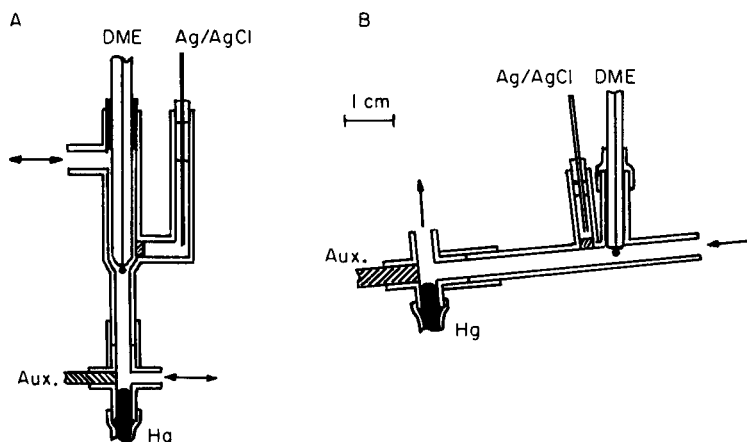


Fig. 1. The flow-through detectors. See text for details.

long glass capillary and a drop time of 3.6 s. The end of the capillary used in the parallel detector (A) was conically shaped. The reference electrode was a silver/silver chloride wire connected with the flowing solution by a salt bridge. The auxiliary electrode was a steel rod.

Equipment and chemicals

The system consisted of a Radiometer ABU-13 autoburet used as a pump and a flow detector connected by plastic tubes. After passing the detector, the solution was turned back to the solution reservoir. Oxygen was removed by bubbling argon through the solution in the reservoir. For linear-sweep voltammetry, a Digiscope polarograph (type OP-5; Telpod, Poland) was used for electrode polarization and recording. With this instrument, the sweep rate can be changed continuously within the range $0.3\text{--}40\text{ V s}^{-1}$, and currents and potentials can be displayed digitally [11]. The delay time can be fixed as seconds or as fractions of the drop time. The instrument has an inner circuit for detecting the moment that the drop falls off.

In all measurements, cadmium(II) ion in 0.1 M potassium chloride was used as depolarizer. The concentration of cadmium(II) was $2.5 \times 10^{-4}\text{ M}$ in the opposite flow-arrangement and 10^{-4} M in the parallel and normal flow systems. All chemicals were of analytical grade and were used as received. Water was distilled twice.

RESULTS AND DISCUSSION

Statistical approach

To define the extent to which the parameters of linear-sweep voltammetry are independent of flow, it is necessary to formulate the criterion of independence and to choose a method of interpreting the results. The criterion

was established as the interval $\bar{x} \pm 1.25\sigma$ (where \bar{x} is the mean value and σ is the standard deviation); interpretation was based on analysis of variance [12]. The conditions for using the analysis of variance are the normality of distribution of results and the equality of variance. Normality of distribution was checked for 84 results of cathodic peak current measurements by the χ^2 test. Equality of variance was checked in each series by the Cochran test. If non-equality of variance is found at high flow velocity, it is caused by perturbations of the laminar boundary layer. Thus, the limiting flow velocity at which the current measurement is undisturbed, can be established by a variance equality test. Next, the calculations of the power of the F-test were done by using Hartley—Pearson charts [12]. To establish the size of the sample confidence limit, the values $\alpha = 0.05$ and test power $\beta \geq 0.95$ were assumed. To reach this test power, eight observations for each of nine flow rates are required; if less than nine flow rates are considered, the test power is greater. The calculations for analysis of variance were applied first for measurements at all flow velocities. If the test for the equality of mean values failed, the measurements for the highest linear velocity were rejected and the calculations were repeated. This procedure was applied until the test for the equality of mean values was successful. At this point, the range of fluid velocity at which the current parameter is independent of flow was established.

Cathodic and anodic peak current

The cathodic peak current was measured between the points A and B (Fig. 2). The starting potential was -0.420 V and the scan finished at -0.900 V; the delay time was 1.8 s and the drop time 3.6 s.

A plot of the cathodic peak current, measured for normal flow, versus the square root of the linear flow velocity for different values of scan rate is presented in Fig. 3A. The range for the independence of current from flow velocity is marked by a broken line. For opposite and parallel flows, the plots are similar, but the ranges over which current is independent of flow are different. These are presented in Table 1. The widest range of independence is obtained for a scan rate of 5 V s^{-1} . If the kind of flow is considered, the widest range is for parallel flow and the narrowest for normal flow. Measurements are possible up to certain limiting values of linear flow rate defined by the test of equality of variance. These limiting values of fluid velocity were 3.72 cm s^{-1} for normal flow, 5.59 cm s^{-1} for opposite flow and 10.87 cm s^{-1} for parallel flow. For high voltage scan rates, these limiting values are sometimes greater.

The anodic peak current was measured between points E and F (Fig. 2). A plot of anodic peak current for parallel flow versus the square root of the fluid velocity is shown in Fig. 3B. For small scan rates, the current strongly depends on the fluid velocity. The ranges over which the anodic peak current is independent of flow rate (Table 1) are narrower than the ranges for the cathodic peak current. The widest range is for a scan rate of 20 V s^{-1} .

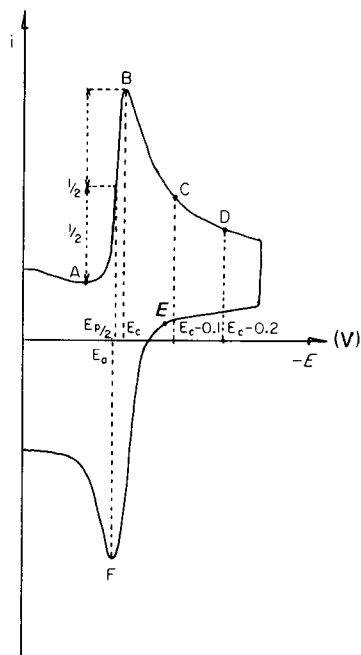


Fig. 2. The linear-sweep (cyclic) voltammogram and the measuring points.

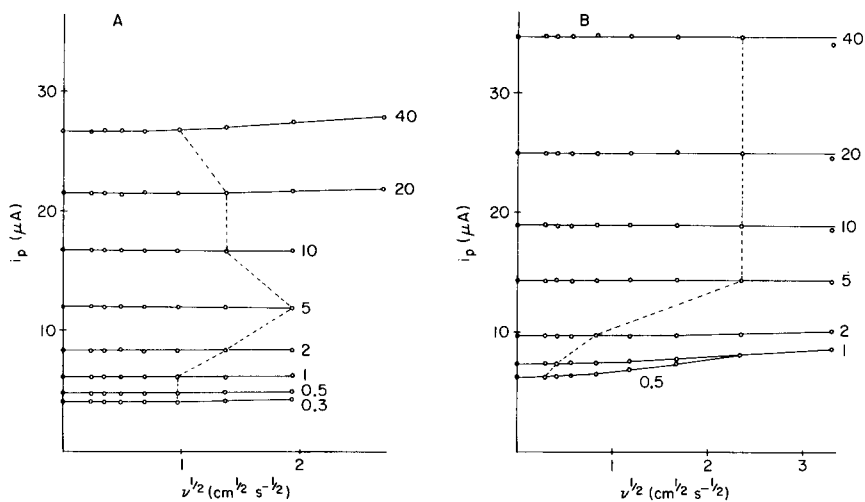


Fig. 3. Peak current (i_p) vs. square root of mean linear flow velocity: (A) cathodic peak current for normal mercury and fluid flows; (B) anodic peak current for parallel mercury and fluid flows. The numbers on the plots are the scan rates in $V s^{-1}$. For explanation, see text.

TABLE 1

Mean linear flow velocity up to which the cathodic and anodic peak currents are independent of flow rate

Scan rate (V s ⁻¹)	Flow velocity (cm s ⁻¹)		
	Opposite	Parallel	Normal
<i>Cathodic peak</i>			
0.3	—	10.87	0.94
0.5	1.11	5.59	0.94
1.0	1.11	10.87	0.94
2.0	1.11	5.59	1.87
5.0	4.38	10.87	3.72
10.0	2.21	5.59	1.87
20.0	0.14	10.87	1.87
32.0	0.56	10.87	—
40.0	—	—	0.94
<i>Anodic peak</i>			
0.6	0.18	0.09	0.00
1.0	0.18	0.18	0.24
2.0	0.35	0.71	0.47
5.0	0.71	5.59	0.94
10.0	5.59	5.59	3.72
20.0	10.87	5.59	7.24
40.0	1.42	5.59	1.87

Other parameters for current and potential

The currents at potentials 0.1 and 0.2 V more negative than the cathodic peak potential ($i_{0,1}$ and $i_{0,2}$, respectively) were measured between points A and C ($i_{0,1}$) and between A and D ($i_{0,2}$), as shown on Fig. 2. The influence of fluid velocity on these currents (Fig. 4) is very strong at small scan rates.

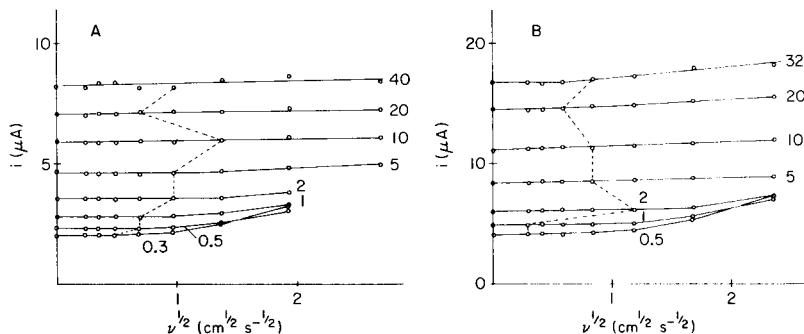


Fig. 4. Plots of current vs. square root of mean linear flow velocity. (A) Current measured at a potential 0.1 V more negative than the cathodic peak potential for normal mercury and fluid flows. (B) Current measured at a potential 0.2 V more negative than the cathodic peak potential for opposite mercury and fluid flows. The numbers on the plots are the scan rates in V s⁻¹.

TABLE 2

Mean linear flow velocity up to which the currents measured at a potential 0.1 V more negative than the cathodic peak potential are independent of flow rate

Scan rate (V s ⁻¹)	Flow velocity (cm s ⁻¹)		
	Opposite	Parallel	Normal
0.3	—	0.71	0.24
0.5	0.00	1.42	0.47
1.0	0.09	5.59	0.47
2.0	0.18	10.87	0.94
5.0	2.82	1.42	0.94
10.0	1.42	2.82	1.87
20.0	0.71	0.71	0.47
40.0	0.71	0.18	0.94

Table 2 shows the ranges of the $i_{0.1}$ current that are independent of fluid velocity.

The cathodic peak potential, anodic peak potential and half-peak potential are independent of flow over the full range of fluid velocity.

The influence of flow on the linear-sweep voltammograms

The influence of flow velocity on the linear-sweep voltammogram for a scan rate of 0.5 V s⁻¹ is shown in Fig. 5A. The cathodic part of this curve is constant up to a linear flow rate of 1.4 cm s⁻¹. For greater flow velocities, the part of the curve after the cathodic peak is raised. If the concentration is small (5×10^{-6} M), and flow velocity is high, the shape of the curve

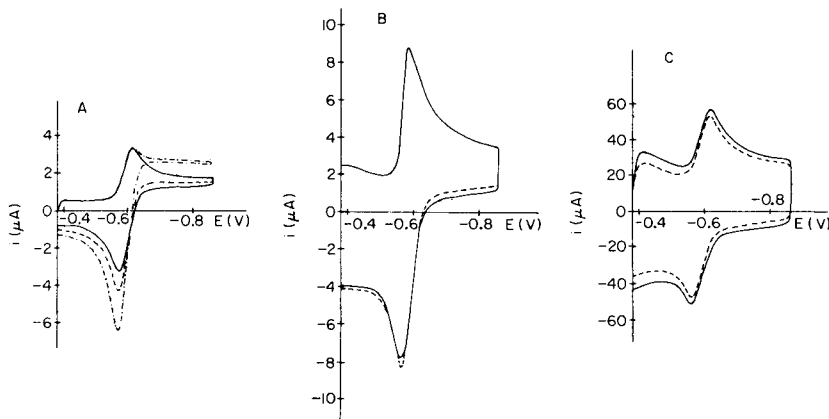


Fig. 5. Influence of fluid velocity on linear-scan voltammograms. (A) Scan rate 0.5 V s⁻¹; flow rate (—) 0 cm s⁻¹, (- - -) 1.4 cm s⁻¹, (- · - ·) 5.6 cm s⁻¹. (B) Scan rate 5 V s⁻¹; flow rate (—) 0 cm s⁻¹, (- - -) 5.6 cm s⁻¹. (C) Influence of fluid velocity on fast sweep cyclic curve. Scan rate 40 V s⁻¹; flow rates as in (B).

changes from a peak to a wave. The anodic part of the curve is raised before the peak and lowered at and after the peak. This causes a strong increase of the anodic peak current. The voltammogram for a scan rate of 5 V s^{-1} (Fig. 5B) is changed somewhat in the anodic scan by a high flow velocity. The curve for a scan rate of 40 V s^{-1} (Fig. 5C) is changed at high flow rates because of a reduction of the capacity current. This effect can also be observed for low scan rates, when the concentration is about $5 \times 10^{-6} \text{ M}$ and the ratio of capacity to faradaic current is greater.

Linearity of response

Solutions containing 5×10^{-6} , 10^{-5} , 5×10^{-5} , 10^{-4} , $5 \times 10^{-4} \text{ M}$ cadmium ion in 0.1 M potassium chloride were examined at different flow velocities. The calibration graphs were computed by linear regression. For a scan rate of 1 V s^{-1} (flow velocity range $0\text{--}0.71 \text{ cm s}^{-1}$), a sensitivity of $0.0691 \mu\text{A } \mu\text{M}^{-1}$ was found with a correlation coefficient of 0.9984. For a scan rate of 5 V s^{-1} (flow velocity range $0\text{--}5.59 \text{ cm s}^{-1}$), a sensitivity of $0.145 \mu\text{A } \mu\text{M}^{-1}$ was found with a correlation coefficient of 0.9969. The ranges over which cathodic peak currents are independent of flow at these lower concentrations are basically the same as at 10^{-4} M , but the limiting flow velocity at $5 \times 10^{-6} \text{ M}$ was only 2.82 cm s^{-1} .

Rate criterion

To evaluate the nature of the current in linear-sweep voltammetry, the slope of the regression line of the dependence of the cathodic peak current on scan rate should be considered in logarithmic coordinates. If the DME is used and the delay time is constant, current density instead of current should be applied [13]. For opposite flow and a fluid velocity of 1.11 cm s^{-1} , this slope of the regression line was found to be 0.496 with a correlation coefficient 0.9990. This value is in good conformity with the theoretical value of 0.5 for the diffusion current.

Conclusion

The results presented here show that linear-sweep voltammetry can be useful in flowing systems. The currents are independent of fluid velocity over a wide range at an appropriate scan rate. Because the currents and potentials are independent of flow velocity over certain ranges, the results obtained in the flow systems can be used to calculate electrode reaction parameters according to the theory of linear-sweep voltammetry.

REFERENCES

- 1 W. Kemula, *Rocz. Chem.*, 26 (1952) 281.
- 2 L. F. Cullen, H. P. Brindle and G. J. Papariello, *J. Pharm. Sci.*, 62 (1973) 1708.
- 3 B. Fleet and C. J. Little, *J. Chromatogr. Sci.*, 12 (1974) 747.
- 4 S. K. Vohra, *Am. Lab.*, 13 (1981) 66.
- 5 P. Maitoza and D. C. Johnson, *Anal. Chim. Acta*, 118 (1980) 233.

- 6 H. B. Hanekamp and H. G. De Jong, *Anal. Chim. Acta*, 135 (1982) 351.
- 7 H. Schlichting, *Boundary Layer Theory*, McGraw-Hill, New York, NY, 1979.
- 8 R. Tamamushi, S. Momiyama and N. Tanaka, *Anal. Chim. Acta*, 23 (1960) 585.
- 9 A. M. Bond, H. A. Hudson and P. A. Van Den Bosch, *Anal. Chim. Acta*, 127 (1981) 121.
- 10 H. B. Hanekamp, W. H. Voogt and P. Bos, *Anal. Chim. Acta*, 118 (1980) 73.
- 11 Z. Kowalski and J. Szednicki, Patent PL 86052, 1978.
- 12 H. Scheffe, *The Analysis of Variance*, J. Wiley, New York, NY, 1961.
- 13 I. I. Vataman and V. T. Mierian, *Elektrokhimiya*, 11 (1975) 298.

LARGE-VOLUME WALL-JET CELLS AS ELECTROCHEMICAL DETECTORS FOR HIGH-PERFORMANCE LIQUID CHROMATOGRAPHY

H. GUNASINGHAM

Department of Chemistry, National University of Singapore, Kent Ridge, 0511 (Singapore)

(Received 21st October 1983)

SUMMARY

The wall-jet electrode is an attractive configuration for electrochemical detectors for high-performance liquid chromatography (h.p.l.c.) on account of its high convective mass-transfer characteristics. Another important, though less recognized, feature is its small effective cell volume, which is shown to be almost independent of the geometric cell volume. The effective volume is less than the volume of the hydrodynamic boundary layer, or only a few microlitres. The practical use of the wall-jet detector in both normal-phase and reverse-phase h.p.l.c. is discussed with particular reference to the distance between the jet and the electrode. A new cell design is proposed.

A common misconception prevalent with regard to the use of electrochemical detectors for high-performance liquid chromatography (h.p.l.c.) is that the geometric cell volume should be minimized in all cases. The assumption is that the smaller the cell volume, the less band spreading and so the greater the efficiency of detection [1]. However, this reasoning is, in the main, applicable only to detectors having electrode geometries where the solute band flows parallel to the electrode surface, at zero incidence; the parallel plate and tubular electrodes are examples in this category. When the electrode area is significantly larger than the cell inlet dimensions (as is usually the case), only a limited path across the electrode surface is exposed to the solute band as it passes through the cell. The width of the path is of the order of the inlet diameter; and, as a consequence, the current efficiency is low. In order to maximize the exposure of the electrode surface to the solute, it is necessary to use a thin-layer cell in which the working electrode is confined to a thin channel having a volume between 0.1 and 1 μl [1]. For thin-layer cells, then, the active (or effective) volume is the geometric cell volume. Apart from increasing the exposure of the electrode surface to the eluted solute band, constriction of flow by means of a thin-layer cell increases the linear flow rate of the solute band, so that the mass-transfer rate is also enhanced. Finally, the thin-layer cell is also assumed to serve the purpose of limiting band spreading. But, as will be shown later, this is not a vital function.

In the case of detectors based on the wall-jet principle, the need for a thin-layer cell does not arise. However, this is not often recognised and the usual practice has been to use thin-layer cells. As an example of this view, van der Linden and Dieker [2] indicated the desirability of using wall-jet cells with geometric volumes less than $0.5 \mu\text{l}$ (effectively, a thin-layer cell) in a recent review.

THEORY

When a fluid flows over a surface, a thin layer is formed near the surface. In that layer, large velocity gradients occur, starting from zero at the surface to a value which corresponds to external frictionless flow. The velocity profiles within the boundary layer can be quite complex.

In the wall-jet configuration, the jet of fluid impinges perpendicularly on the working electrode and flows radially over the surface [3]. Recently, the equation for boundary-layer thickness was derived [4] based on correlations deduced by Glauert [3]. For the purpose of derivation, the boundary layer was defined as the region adjacent to the wall wherein the major portion of the radial flow profile of the wall jet is found. The equation for the boundary-layer thickness is

$$\delta_{bl} = 5.8 \pi^{3/4} a^{1/2} \nu^{3/4} R^{5/4} V^{-3/4} \quad (1)$$

where a is the inlet radius, ν the kinematic viscosity, R the radius of the electrode, and V the volume flow rate. It can be seen that the boundary-layer thickness increases rapidly downstream from the jet origin. Equation 1 does not show any dependence on the inlet/electrode distance. The assumption made is that the free jet, as it emerges from the inlet, remains intact. A necessary condition for this assumption is that the flow of the jet is laminar. In fact, for aqueous solutions, it was found that laminar flow conditions hold for volume flow rates upto $5\text{--}6 \text{ ml min}^{-1}$. This easily covers the flow-rate range usual in h.p.l.c. work [4].

Spreading of the eluted solute band is slight in the flow of the free jet and occurs mainly downstream from the wall jet, because of radial velocity gradients in the boundary layer. Spreading can take place radially (upstream and downstream) and outward from the electrode. Glauert [3] showed that the radial velocity profile reaches a maximum a short distance from the wall, and then rapidly diminishes to a limiting value (corresponding to the frictionless flow of the bulk solution surrounding the wall jet). As the jet flows downstream from the wall, the radial velocity profile broadens and the boundary-layer thickness increases, as indicated by Eqn. 1.

In the context of h.p.l.c. detection, the distribution profile of the solute band in the radial flow of the jet is governed by the radial velocity profile. Thus the major part of the solute band passing through the cell is found a short distance from the electrode surface. In fact, more than 70% of the solute band is found within half the width of the boundary layer. Because

the flow of the jet after striking the electrode takes place radially in three dimensions, the entire electrode area is exposed to the solute band as it passes through the cell.

Accordingly, the effective cell volume of the wall-jet detector can be considered to be significantly less than the volume of the boundary layer formed over the electrode surface.

The boundary-layer volume can be estimated simply; a plot of boundary-layer volume against flow rate is shown in Fig. 1. As can be seen, in the flow rate range normally used in h.p.l.c., the boundary-layer volume is only a few microlitres. The volume decreases rapidly with increasing flow rate.

The use of the wall-jet in a thin-layer arrangement could actually result in a loss of current efficiency, because of the interference of the back wall or nozzle body. This effect has been described as being the result of reduction in momentum transfer because of the surface drag effect of the body within the boundary layer. Of course, reduction of the cell volume to a value less than the boundary-layer thickness results in increased linear flow rate, which can partly compensate for the loss of momentum transfer caused by surface drag. However, the trade-off is not very significant and it is usually preferable to have the back wall and nozzle body well clear of the boundary layer. In fact, as long as the back wall (or nozzle body) is outside the boundary layer, the actual geometric cell volume is immaterial to the efficacy of the wall-jet detector. There are also other advantages, in certain applications, to have a large volume cell. These will be discussed below.

Figure 2 shows the difference between the flow patterns over the electrode for a parallel-plate detector and wall-jet detector. The difference in electrode surface exposure is obvious. Figure 3 compares the boundary layers formed on a flat plate with parallel flow at zero incidence and on the wall-jet detector. In both cases, the boundary layer increases downstream, but the boundary layer for the wall jet increases more rapidly. The radial-velocity profile of the wall jet and the velocity profile of flow over the flat plate are also indicated.

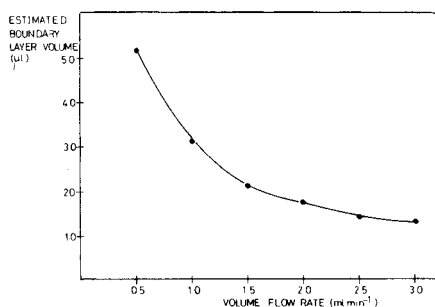


Fig. 1. Plot of estimated boundary-layer volume (over electrode surface) against flow rate for the wall-jet electrode. $R = 1.5$ mm, $a = 0.1$ mm, $\nu = 10^{-2}$ cm² s⁻¹.

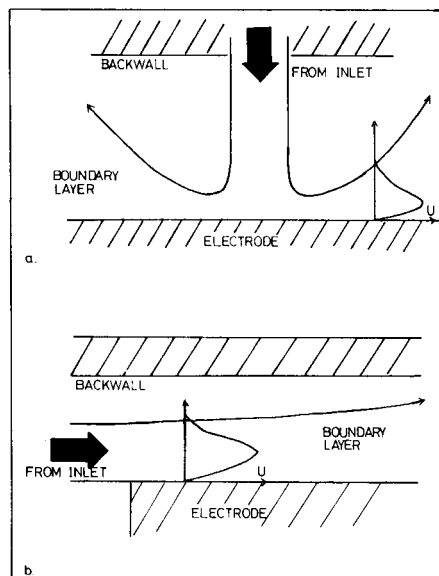
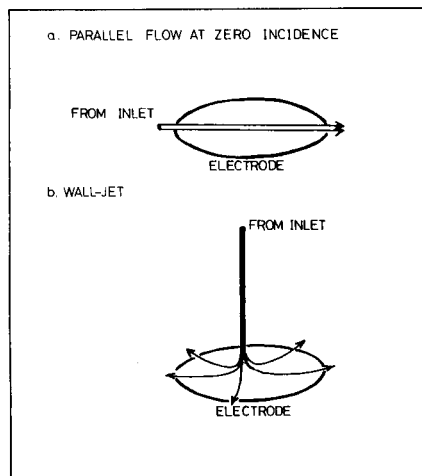


Fig. 2. Flow patterns: (a) parallel flow at zero incidence; (b) wall jet.

Fig. 3. Boundary layers: (a) at the wall jet; (b) at a flat electrode with parallel flow at zero incidence. U is the flow rate parallel to the electrode surface, which is the radial-flow velocity in the case of the wall jet.

EXPERIMENTAL

Wall-jet cell

Two types of cell design were used. The first was similar to the original Fleet-Little design [5] and is made of Kel-F (3M Company). This cell is suitable for use in normal-phase h.p.l.c. with non-aqueous eluents; a modified Ag/AgCl reference electrode with a hydroxyethylcellulose salt bridge was used [6]. This reference system afforded reasonably stable and reproducible (± 20 mV) potentials.

The second wall-jet cell used was a ring-disk system [4]. In this design, two outlets, made of stainless steel, were used (to minimize eddy formation at high flow rates) and the reference electrode was positioned opposite the working electrode. The geometric cell volume was much larger than that of the first cell. The working electrode was made of glassy carbon (Tokai, Japan). One or other of the stainless tube outlets served as the counter electrode.

The h.p.l.c. system

The high-pressure pump was a purpose-built system with nitrogen applied to a solvent reservoir which was connected with a 0.25-in stainless-steel tube. The solvent was vacuum-degassed prior to operation.

The column for normal-phase chromatography was a Zorbax 6 × 0.25-in. silica column (particle size 8 μm; Dupont). For reverse-phase work, an ODS-Permaphase column (particle size 10 μm; Dupont) was used. Typically, the pressures applied were in the range 300–500 psi, resulting in solvent flow rates of 0.2–1.0 ml min⁻¹. Samples were injected through a septum with a 10-μl syringe.

In order to make the eluent conducting a supporting electrolyte was used. For the normal-phase work, 0.05 M tetrabutylammonium fluoroborate was necessary. In the case of the reverse-phase separations, 0.1 M potassium nitrate was used.

RESULTS

Comparison of resolution with a u.v. detector placed in series

The wall-jet detector (of the Fleet–Little design) was placed in series after a u.v. detector. The two detectors were connected by 20 cm of 1/16-in. teflon tubing. Figure 4 shows two traces obtained with the u.v. and wall-jet detectors for the normal-phase separation of the antihypertensive drug,

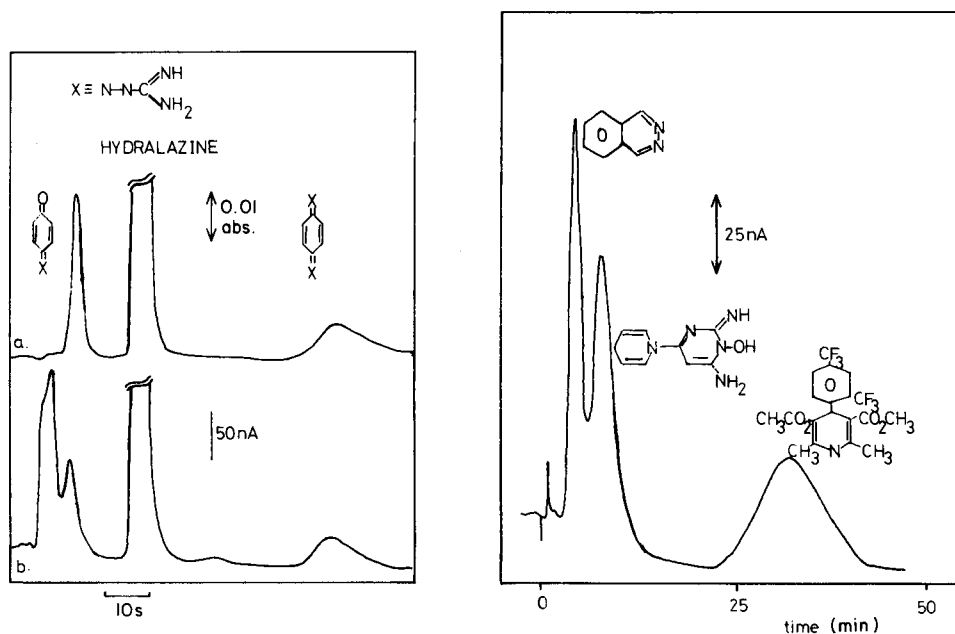


Fig. 4. Comparison of u.v. and wall-jet detectors for the determination of hydralazine and its metabolites. Eluent: hexane/ethanol (4:1) 0.05 M in $(C_4H_9)_4NBF_4$. (a) U.v. detector, 260 nm; (b) wall-jet detectors at +1.0 V vs. modified Ag/AgCl.

Fig. 5. Wall-jet trace for the reverse-phase separation of three antihypertensive drugs. Eluent: 25% (1:3) methanol/water made 0.1 M in KNO_3 . Working potential = +1.0 V vs. Ag/AgCl.

hydralazine, and its intermediates. In this example, the inlet-electrode separation for the wall jet was 4 mm, thus the inlet body and cell wall, opposite the working electrode, were well clear of the hydrodynamic boundary layer. The wall-jet detector at such large separations can be considered as a large-volume cell (as opposed to a thin-layer cell). As can be seen, not only are the sensitivities of the wall-jet and u.v. detectors similar, but the wall-jet trace shows negligible loss of resolution, despite the dead-volume of the first detector and the length of connecting tubing. It is of interest that the wall-jet trace shows impurities which were not picked up by the u.v. detector.

Figure 5 shows a trace obtained with the wall-jet detector for the reverse-phase separation of four drugs. The corresponding u.v. trace was virtually identical with regard to resolution. The poorer resolution obtained for the last two peaks was caused by the chromatography rather than band spreading in the detector.

Effect of inlet-electrode distance

Figure 6 shows the effect of changing the inlet-electrode distance on the normal-phase chromatography of six phenols. The important point is that, as the distance increases, there is little loss of resolution. Yet, although resolution is little affected, the peak heights change substantially as the inlet-electrode distance is increased. Figure 7 shows the peak currents plotted against the inlet-electrode distance for each of the six phenols. Interestingly, the peak heights for the first three phenols (in order of elution) increase to limiting values, whereas the peak heights for the last three decrease to limiting values. The trends observed may be related to the presence of the nozzle body and the cell wall (opposite the working electrode) within the boundary layer. The difference between the first three phenols and last three phenols may be explained in terms of differences in their mobilities, which causes an alteration of the radial velocity profile [3]. The effect of inlet-electrode distance has been discussed in detail [4]. This example clearly shows that increasing the inlet-electrode distance may result in increased peak heights, without loss of resolution.

Figure 8 shows plots of peak current against inlet-electrode distance for the modified ring-disk wall-jet detector, for the reverse-phase separation of hydroquinone. Sample injections were of pure hydroquinone dissolved in methanol. Again, the trend for the disk and ring electrodes may be explained in terms of the disturbance of the hydrodynamic boundary layer. However, here the radii of the disk and ring electrodes are much larger; thus the boundary layer volume will be correspondingly larger. Figure 9 shows the effect of changing the inlet-electrode distance on the peak resolution for the same hydroquinone measurements. As can be seen, the disk electrode shows negligible band spreading, whereas the ring electrode shows a slight loss of resolution because of band spreading in the downstream radial flow; the increased boundary layer thickness is more significant for the ring electrode.

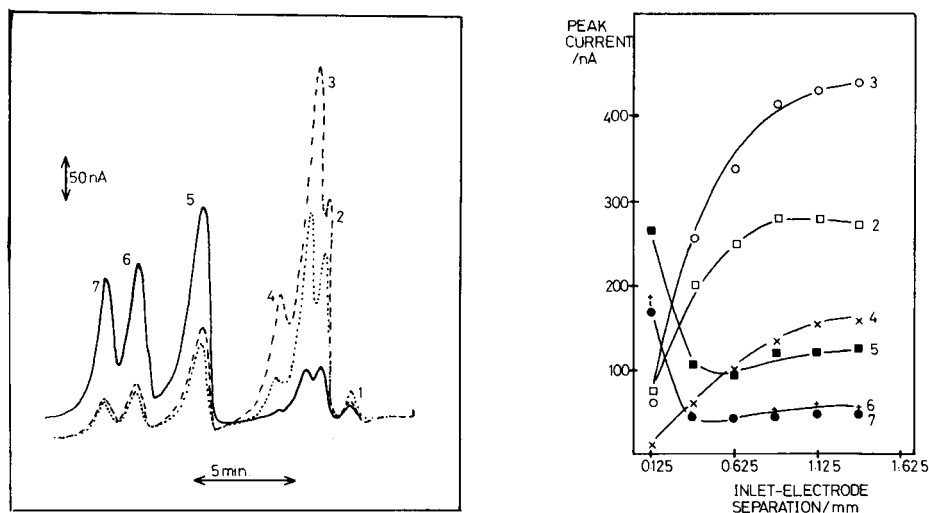


Fig. 6. Effect of inlet-electrode distance on the normal-phase chromatography of a phenol mixture. Eluent: (7:3) hexane/ethanol, 0.05 M in $(C_4H_9)_4NBF_4$ with 0.5% (v/v) ammonia added. Peaks: (1) impurity; (2) 2,6-diisopropylphenol; (3) 3-isopropylphenol; (4) phenol; (5) *o*-aminophenol; (6) *p*-aminophenol; (7) *p*-phenylenediamine. Working potential +0.8 V vs. modified Ag/AgCl; flow rate 0.2 ml min⁻¹. Inlet-electrode distance: (—) 0.125 mm; (···) 0.375 mm; (---) 1.125 mm.

Fig. 7. Plots of peak current vs. inlet-electrode distance for the separation of phenols. The numbers on the curves correspond to those in the legend to Fig. 6.

DISCUSSION

The results presented show that, in contrast to the parallel-plate detector, the wall-jet detector can be efficient if a cell of comparatively large volume is used rather than a thin-layer cell. Apart from the high current efficiency and resolution, a large-volume cell provides a means for new types of measurements. For example, it can be used effectively for detection in gradient-elution h.p.l.c. [7]. A thin-layer cell would be prone to deleterious effects from changing eluent composition, particularly when the eluent changes from a partly aqueous to a totally non-aqueous system. The need for electrolyte compatibility in mixed eluent systems is also avoided.

The large-volume wall-jet detector affords a number of benefits in flow-injection analysis, particularly for post-injection chemical treatment prior to amperometric determination; this will be described at a later date.

The sensitivity of the wall-jet detector is high, and, on theoretical grounds, it should perform better than thin-layer cells with parallel flow. As an example of sensitivity, hydralazine can be determined in the picogram range; moreover, a linear response can be obtained from picogram to microgram amounts of sample injected.

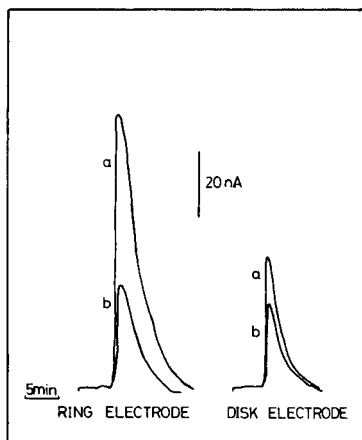
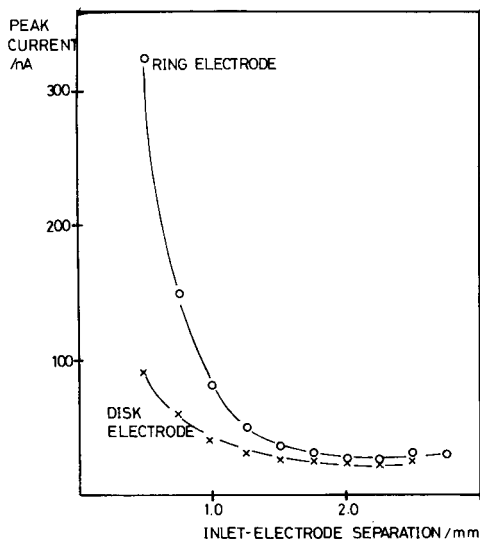


Fig. 8. Plots of peak current vs. inlet-electrode distance for hydroquinone ($1 \text{ ng } \mu\text{l}^{-1}$) detected at a modified wall-jet ring-disk electrode. Ring dimensions: 7.0 mm i.d., 10 mm o.d. Disk diameter 5 mm; inlet diameter 0.3 mm. Working electrode potentials, +1.0 V vs. Ag/AgCl for both ring and disk. Eluent: (1:3) methanol/water made 0.1 M in KNO_3 . Flow rate 0.4 ml min^{-1} .

Fig. 9. Effect of inlet-electrode distance on peak resolution for the hydroquinone injections shown in Fig. 8. Inlet-electrode distance: (a) 2.0 mm; (b) 1.0 mm.

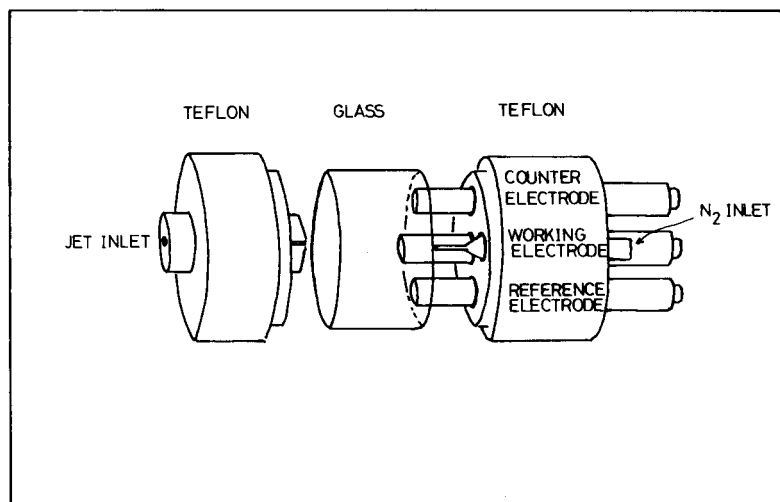


Fig. 10. Large-volume wall-jet cell design.

A final practical benefit of a large-volume cell is that it is easy to fabricate. A simple system has been designed for use in conjunction with the PAR model 303 electrode assembly [7]. Figure 10 is a schematic diagram of a simple, large-volume cell which should be useful for most hydrodynamic voltammetric applications such as h.p.l.c., anodic stripping voltammetry and flow-injection analysis. Attractive features of this cell are that it is suitable for aqueous as well as non-aqueous work, and that the electrode system is easily visible, which is not feasible with an all-teflon or Kel-F cell. The glass cylinder is press-fitted to the teflon base holding the nozzle; the other teflon piece is loosely fitted to the other end of the cylinder. The cell need not be completely filled with solution, as only ends of the three electrodes have to be covered with solution.

REFERENCES

- 1 P. T. Kissinger, *J. Chem. Educ.*, 60 (1983) 308.
- 2 W. E. van der Linden and J. W. Dieker, *Anal. Chim. Acta*, 119 (1980) 1.
- 3 M. B. Glauert, *J. Fluid Mech.*, 1 (1956) 625.
- 4 H. Gunasingham and B. Fleet, *Anal. Chem.*, 55 (1983) 1409.
- 5 B. Fleet and C. J. Little, *J. Chromatogr. Sci.*, 12 (1974) 747.
- 6 H. Gunasingham and B. Fleet, *J. Chromatogr.*, 43 (1983) 261.
- 7 H. Gunasingham, B. T. Tay, K. P. Ang and L. L. Koh, *J. Chromatogr.*, 285 (1984) 103.

THE ACIDITY OF SUPERACIDIC MEDIA DERIVED FROM FLUOROSULFURIC ACID AND TRIFLUOROMETHANESULFONIC ACID

BERNARD CARRE

Laboratoire de Chimie Générale et Minérale, Faculté des Sciences, Parc Grammont, 37200 Tours (France)

JACQUES DEVYNCK*

Laboratoire d'Electrochimie Analytique et Appliquée (associé au CNRS, LA 216), Ecole Nationale Supérieure de Chimie de Paris, 11, rue Pierre et Marie Curie, 75231 Paris Cedex 05 (France)

(Received 29th July 1983)

SUMMARY

The acidity level of superacidic media derived from fluorosulfuric acid and trifluoromethanesulfonic acid (TFMS) was determined by using the potentiometric indicators tetrachloroquinone and tetrafluoroquinone. A voltammetric and potentiometric study of these indicators was conducted to evaluate their pH indicator range, from the strongest acid media (SbF₅ solution) to the strongest base media (H₂O or KF solution). The R_0 function in 1 M strong base medium was found to be $R_0 = -17.2$ (fluorosulfuric acid) and $R_0 = -16$ (TFMS). The autoprotolysis constant (pK_t) was evaluated in both solvents; $pK_t = 6.1$ (fluorosulfuric acid) and $pK_t = 6$ (TFMS).

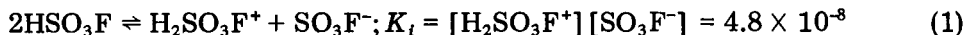
Fluorosulfuric acid has been used, alone or mixed with antimony pentafluoride, as a superacidic medium, to achieve the activation of hydrocarbons, especially the isomerization of alkanes [1–9]. The derived perfluoroalkanesulfuric acids have also been considered for such an application. Among the latter, trifluoromethanesulfonic acid (TFMS) has a high acidity level, and has been offered in the monohydrate form for making fuel cell electrolytes [10, 11]. Although the properties of these acids are well known, very few results are available concerning their relative acidity levels; H_0 functions have been determined for fluorosulfuric acid [12, 13], but only one H_0 function is known for TFMS [14].

The most important properties of these media are known to depend on their acidity level when "neat", but when the medium also contains acidic (e.g., SbF₅) or basic (e.g., H₂O) solutes, this level also depends on the autoprotolysis constant [15]. Therefore, precise correlation is necessary between these media and other superacidic media, especially those derived from hydrofluoric acid which have been extensively studied [15]. In the work reported here, potentiometric indicators with an acidity of a type similar to those

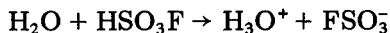
already described were studied in order to define their $R_0(H)$ functions [16] and to relate them to each other and to other superacidic media, as well as to evaluate their autoprotolysis constants.

Fluorosulfuric acid

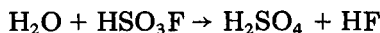
Fluorosulfuric acid (HSO_3F) dissociates according to the reaction [17]



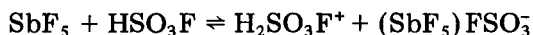
Although water is basic, it can react in two different ways [18], either as a strong base at low temperature



or roughly by destroying the solvent when added carelessly



No elementary protonic acids are known to be strong in fluorosulfuric acid. The strongest acids known are fluorosulfonate-accepting Lewis acids [12]

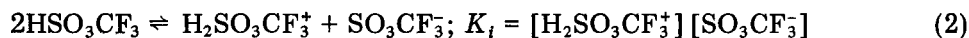


There is an internal dissociation of the solvent from its constituent elements: $\text{HSO}_3\text{F} \rightleftharpoons \text{HF} + \text{SO}_3$ ($K = [\text{SO}_3][\text{HF}] = 10^{-8}$). The presence of sulfur trioxide affects the reactions because sulfur(VI) is a strong oxidizing agent.

The H_0 functions have been determined by Gillespie and Peel [12]: $H_0 = -15.07$ for "neat" fluorosulfuric acid; $H_0 = -11.5$ for $\text{HSO}_3\text{F} + 1\text{M KSO}_3\text{F}$; and $H_0 = -18.9$ for $\text{HSO}_3\text{F} + 1\text{M SbF}_5$ [13]. Sommer et al. [19] have checked the protonation of the Hammett indicators through n.m.r. spectrometry.

Trifluoromethanesulfonic acid

The acidic properties of trifluoromethanesulfonic acid (HSO_3CF_3 ; TFMS) have not been studied extensively and very few constants have been determined. The acid dissociation would be



The solvent $\text{p}K_t$ has never been determined. Water and alkaline trifluoromethanesulfonates are strong bases [20], and like fluorosulfuric acid, the strongest acids have to be Lewis acids of the MF_5 type (SbF_5). Only the H_0 function of the supposedly "neat" acid, $H_0 = -14.1$, is known [14].

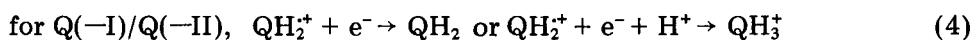
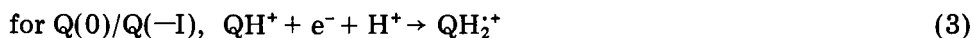
EXPERIMENTAL

The equipment used was similar to that described earlier [21, 22].

Selection of acidity indicators

The use of electrochemical acidity indicators dissolved in these solvents is of considerable interest. The standard hydrogen electrode does not act

properly. In fluorosulfuric acid, the H^+/H_2 system at a platinized platinum electrode is not reversible (slow system) and hydrogen is oxidized by sulfur(VI) (SO_3 is produced by the internal dissociation of the solvent). The electrochemical behaviour of hydrogen is similar in TFMS. As described earlier [21, 22], quinone systems give reversible electrochemical systems which are pH indicators and are stable in these strongly acidic media. The weakly basic quinones, tetrachloro-*p*-benzoquinone (TCQ) and tetrafluoro-*p*-benzoquinone (TFQ), were used, as well as the corresponding hydroquinones. The protonation of quinones can be monitored by n.m.r. [23]. Both quinones were studied in hydrofluoric acid: in basic medium, they reduce in a unique single step $Q(0)/Q(-II)$: $Q + 2e^- + 2H^+ \rightarrow QH_2$. One proton is exchanged by one electron. In strongly acidic medium (SbF_5), quinones reduce in two one-electron steps. A semiquinone formation $Q(-I)$ has also been demonstrated. The reactions are as follows



depending on the pH.

Reference system

The most suitable reference electrode used was a silver electrode (Ag/Ag^+) [24] in TFMS or a copper electrode (Cu/Cu^{2+}) [25] in fluorosulfuric acid. All potentials are measured by comparison with a system supposedly independent of the solvent. It has been shown that perylene [25, 26, 27] and octafluoronaphthalene [28] may serve as such references in very acidic medium.

Perylene. Perylene quickly oxidizes to a monocationic form in these acidic solvents. When yellow perylene is dissolved, the solution turns green first and purple quickly afterwards, a colour characteristic of the monocation, which can be oxidized to the dication in a reversible one-electron process (Fig. 1). With a rotating platinized platinum electrode in a 1 M strong base medium, the half-wave potentials found were $E_{1/2} = 0.300$ V for fluorosulfuric acid and $E_{1/2} = 0.280$ V for TFMS.

Octafluoronaphthalene. This compound is oxidized giving three different oxidation waves: the first wave corresponds to a reversible one-electron process over the whole accessible pH range in both solvents: $C_8F_8 \rightarrow C_8F_8^+ + e^-$. The cationic radical prepared by controlled potential electrolysis is stable and turns green (as in hydrofluoric acid [28]). The first wave is readily reversible, while the other two are not and have a stronger intensity. With a rotating platinized platinum electrode in 1 M strong base, the half-wave potentials obtained for the first oxidation wave were $E_{1/2} = 0.850$ V in fluorosulfuric acid and $E_{1/2} = 0.830$ V in TFMS. Octafluoronaphthalene was chosen as the reference in the present work. Its oxidation potential is very high and its chemical stability is remarkable in these acidic solvents.

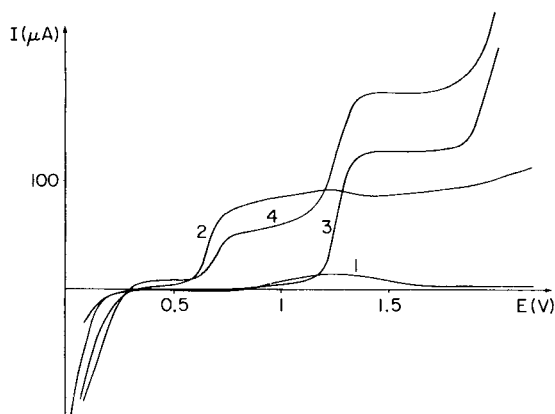


Fig. 1. Voltammetric curves of octafluoronaphthalene and perylene in trifluoromethanesulfonic acid: (1) residual current; (2) 0.5 mM perylene; (3) 1 mM octafluoronaphthalene; (4) 1 mM octafluoronaphthalene + 0.4 mM perylene.

Voltammetric study of quinones

Several electrodes were considered (platinum, gold, glassy carbon) but the best results were obtained on platinized platinum (Table 1). Figures 2 and 3 show the evolution of the voltammograms of the quinones as a function of pH over the whole acidity range. The decrease of the limiting diffusion current in strongly basic media (Fig. 2, curves 3–8 and Fig. 3, curves 1–3) corresponds to a decrease in the solubility. Table 1 shows the $E_{1/2}$ values and the slopes of E vs. $\log[(I_d - I)/I]$ plots for the reduction wave of the tetrachloroquinone and tetrafluoroquinone in basic and in neutral (neat solvent) media. The reduction proceeded in one reversible wave. The slope of the variation of $E_{1/2}$ vs. logarithm of base concentration for both quinones in strong base (H_2O) media in fluorosulfuric acid, is reported in Table 2. The same variation was observed with fluoride ion as the strong base. The slopes of the variation

TABLE 1

Voltammetric data for tetrachloroquinone (TCQ) and tetrafluoroquinone (TFQ) in fluorosulfuric acid and in trifluoromethanesulfonic acid

Medium		TCQ		TFQ	
		HSO_3F^a	$H_2SO_3CF_3^b$	HSO_3F^a	$H_2SO_3CF_3^b$
"Neutral"	$E_{1/2}$ (V)	0.630	0.360	0.470	0.220
	S^c	55	75	80	90
Basic	$E_{1/2}$ (V)	0.510	0.270	0.330	0.110
	S^c	55	65	70	70

^a1 M sodium fluoride. ^b1 M water. ^cSlope of the linear plot for the wave: E vs. $\log[(I_d - I)/I]$.

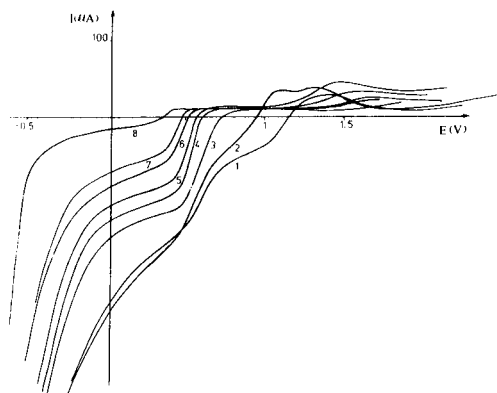


Fig. 2. Voltammetric curves of 1 mM tetrachloroquinone in trifluoromethanesulfonic acid at various acidity levels: (1) 0.64 M SbF_5 ; (2) 0.12 M SbF_5 ; (3) "neutral" media; (4) 0.25 M H_2O ; (5) 0.76 M H_2O ; (6) 1.26 M H_2O ; (7) 2.5 M H_2O ; (8) 7 M H_2O .

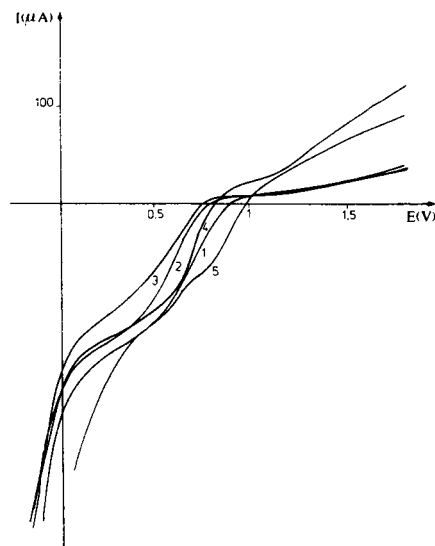


Fig. 3. Voltammetric curves of 1 mM tetrafluoroquinone in fluorosulfuric acid at various acidity levels: (1) "neutral" media; (2) 5×10^{-2} M NaF ; (3) 10^{-1} M NaF ; (4) 0.13 M SbF_5 ; (5) 0.54 M SbF_5 .

of $E_{1/2}$ are also close to the theoretical value (59 mV) in the case of trifluoromethanesulfonic acid (Table 2). These variations imply an exchange of 1 electron per H^+ in the redox reaction $\text{Q} + 2\text{H}^+ + 2\text{e}^- \rightleftharpoons \text{QH}_2$. The equation of the voltammetric curve is

$$E = E^0 - 0.06 \text{ pH} - 0.06 \log [(I_d - I)/I]$$

The results are less simple in "acidic" media and depend on the SbF_5 concentration. Tetrachloroquinone presents two irreversible reduction waves in both solvents; the waves shift to more positive potentials as the antimony pentafluoride concentration increases (Fig. 2, curves 2 and 3). The quinone is dark purple in acidic solution. Tetrafluoroquinone also gives two waves in dilute antimony pentafluoride solution (<0.4 M SbF_5 in fluorosulfuric acid or <0.2 M in trifluoromethanesulfonic acid; see Fig. 3, curve 4 and Fig. 4, curve 2) and two waves in more concentrated antimony pentafluoride solution (e.g., Fig. 3, curve 5). By analogy with the results obtained in hydrofluoric acid where the same kind of behavior has been observed [23], the two-wave system indicates two one-electron steps corresponding to the semiquinone stabilization. The two reduction steps of the quinone correspond to the redox equilibria, $\text{QH}^+ + \text{H}^+ \rightleftharpoons \text{QH}_2^+$ and $\text{QH}_2^+ + \text{e}^- \rightleftharpoons \text{QH}_3^+$.

Voltammograms of a 1:1 mixture of tetrafluoroquinone and tetrafluoro-

TABLE 2

Half-wave reduction potential shift of tetrachloroquinone (TCQ) and tetrafluoroquinone (TFQ) with base concentration (C) in fluorosulfuric acid and trifluoromethanesulfonic acid (TFMS)

($E_{1/2} = a \log C + b$; $C = \text{H}_2\text{O}$ or F^- concentration $10^{-4} \text{ M} < C < 10^{-1} \text{ M}$)

		Fluorosulfuric acid	Trifluoromethane sulfonic acid
TCQ	a (mV)	57 ± 3^a	60 ± 2^a
	b (mV)	516 ± 5	291 ± 4
TFQ	a (mV)	63 ± 3	68 ± 3
	b (mV)	328 ± 5	103 ± 3

^aConfidence limits, probability: 95%.

hydroquinone were obtained in trifluoromethanesulfonic acid (Fig. 4); the equilibrium potential of a platinum electrode at which the system is reversible is directly linked to the pH of the solution by $E = E^0 - 0.06 \text{ pH}$. The voltammograms are well defined in basic and in neutral media (curves) but distortion appears in acidic media, probably because of the oxidizing power of antimony(V) fluoride.

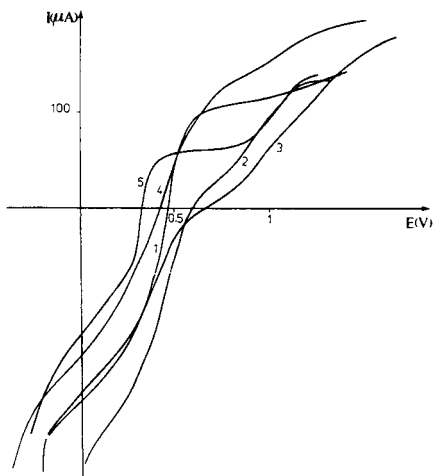


Fig. 4. Voltammetric curves of a mixture of 5 mM tetrafluoroquinone and 5 mM tetrafluorohydroquinone in trifluoromethanesulfonic acid at various acidity levels: (1) 10^{-2} M H_2O ; (2) 0.13 M SbF_5 ; (3) 0.4 M SbF_5 ; (4) 0.7 M H_2O ; (5) 5 M H_2O .

RESULTS AND DISCUSSION

Determination of the $R_0(H)$ acidity functions

The evaluation of the reduction half-wave potential of quinones (or equilibrium potential of a mixture of the quinone and hydroquinone) allows calculation of the $R_0(H)$ acidity function. The expression for $R(H)$ is

$$R(H) = F(2.3 RT)^{-1} (E_{1/2(\text{aq})} - E_{1/2(\text{s})})$$

where $E_{1/2(\text{aq})}$ refers to the potential of the pH indicator in water and $E_{1/2(\text{s})}$ refers to the potential of the same pH indicator in the solvent, both potentials being expressed by reference to the half-wave potential of a reversible system supposed to be independent of the solvent [16]. The solvent-independent system is octafluoronaphthalene (OFN/OFN⁺) which was previously studied in hydrofluoric acid [28]. Because this compound is insoluble in water, its half-wave potential must be evaluated by using an intermediate compound which is soluble in the solvent and in water. Perylene/perylene⁺ can be used for this purpose.

Tetrachloroquinone was used to evaluate the $R(H)$ function of the strongly basic solution. The reduction of this quinone proceeds by the same scheme in water and in TFMS or fluorosulfuric acid solution. The $E_{1/2}$ values for the reduction of tetrachloroquinone in aqueous solution are as follows: 0.260 V vs. ferrocene (Fe/Fe⁺), 0.840 V vs. perylene (Pe⁺/Pe²⁺) and 1.390 V vs. octafluoronaphthalene (OFN/OFN⁺). The corresponding calculated values of $R_0(H)$ in sodium fluoride or water solutions are reported in Table 3. These values correlate with the $R_0(H)$ function obtained with the same quinone in hydrofluoric acid, which was $R_0(H) = 14.2$ (1 M KF) [22, 29].

The tetrafluoroquinone reduction presents the same one-step, two-electron reversible reduction in strongly basic solution and in dilute strong acid solution ($\text{SbF}_5 < 0.4$ M in fluorosulfuric acid and < 0.2 M in TFMS).

TABLE 3

$R_0(H)$ acidity function of basic (H_2O or NaF) and acidic (SbF_5) media in fluorosulfuric and trifluoromethanesulfonic acid.

Potential reference: octafluoronaphthalene (OFN/OFN⁺). Acidity indicators: tetrachloroquinone (TCQ) and tetrafluoroquinone (TFQ)

Medium	$E_{1/2}$ (V)	Indicator	$R_0(H)$
$\text{HSO}_3\text{F} +$	0.360	TCQ	-17.2
1 M NaF	0.330	TFQ	-17.2
$\text{HSO}_3\text{F} +$	0.694	TFQ	-23.4
1 M SbF_5			
$\text{HSO}_3\text{CF}_3 +$	0.430	TCQ	-16
1 M H_2O	0.210	TFQ	-16
$\text{HSO}_3\text{CF}_3 +$	0.572	TFQ	-22.1
1 M SbF_5			

Thus, the same system can be used to calculate the acidity function of the strongest acid solution. Extrapolated values (corresponding to a 1 M SbF_5 solution) are reported in Table 3.

Calculation of apparent autoprotolysis constants

According to the autoprotolysis equilibria (Eqns. 1 and 2) reported above, the evaluation of the acidity function of a strong acid and a strong base (NaF or H_2O) with the same electrochemical pH indicator leads to the determination of the autoprotolysis constant, pK_i . The values obtained with tetrafluoroquinone are $pK_i = R_0(\text{H}) (1 \text{ M } \text{SbF}_5) - R_0(\text{H}) (1 \text{ M } \text{NaF}) = 6.2 \pm 0.5$ for fluorosulfuric acid, if SbF_5 is considered as a strong acid as in hydrofluoric acid, and $pK_i = R_0(\text{H}) (1 \text{ M } \text{SbF}_5) - R_0(\text{H}) (1 \text{ M } \text{H}_2\text{O}) = 6.1 \pm 0.5$ for trifluoromethanesulfonic acid. The value for pK_i in fluorosulfuric acid is one unit lower than that obtained by Barr et al. [17] by conductimetric measurements because they have considered SbF_5 as only partially ionized ($pK = 2.15$). There is no published value in the case of trifluoromethanesulfonic acid.

Comparison between acidity ranges

Figure 5 shows the three fluorinated acid solvents, hydrofluoric, fluorosulfuric and trifluoromethanesulfonic acids, related to the R_0 scale. The correspondence with the H_0 scale is represented, and the results confirm the 6-unit deviation between R_0 and H_0 functions already observed in

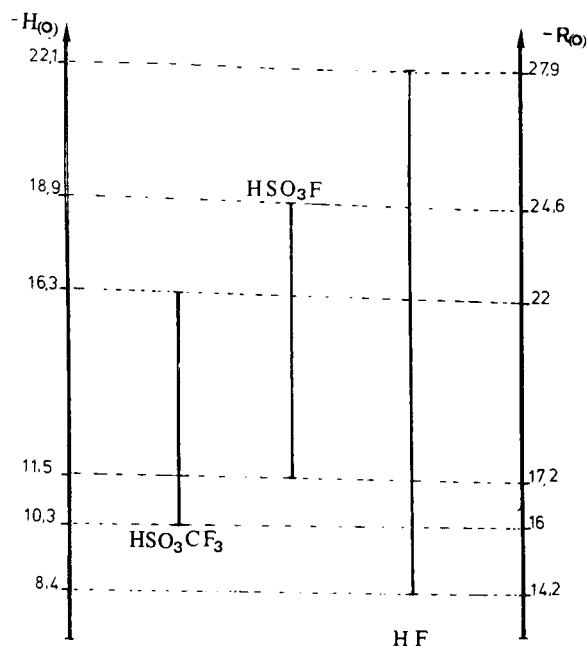


Fig. 5. Relative position of the acidity scales of fluorosulfuric, trifluoromethanesulfonic and hydrofluoric acids, and the relationship between the $R_0(\text{H})$ and H_0 acidity functions.

hydrofluoric acid [14]. It can be seen that hydrofluoric acid has the widest acidity range, which enables the most acidic and the most basic media to be reached ($pK_t = 13.7$).

Conclusion

As in hydrogen fluoride, tetrachloroquinone and tetrafluoroquinone appear to be suitable pH indicators; they are sufficiently stable and their protonation allows the pH to be evaluated in the whole acidity range of the solvents. These quinones are the two electrochemical pH indicators useful in very acidic media.

Comparison between the values determined for R_0 and H_0 shows that the difference between these two functions is almost constant. The difference found is the same as in hydrofluoric acid. The pK_t values determined for fluorosulfuric and trifluoromethanesulfonic acid through R_0 measurements are of the same magnitude. The accessible pH range covers 6 units. Thus superacid media based on these two acids makes it possible to reach very acidic media by addition of antimony(V) fluoride ($R_0 = -25$), but the acidity range is not as wide as that of hydrofluoric acid.

The presence of S(VI), from the sulfur trioxide produced secondarily to their internal dissociation, differentiates these two acids from hydrofluoric acid. Sulfur trioxide is a potent oxidizing agent which participates directly in oxidations. It oxidizes hydrogen so that it becomes impossible, in practice, to use a hydrogen electrode in sulfur-containing superacids, as in sulfuric acid.

REFERENCES

- 1 G. A. Olah and J. Lukas, *J. Am. Chem. Soc.*, **89** (1967) 2227.
- 2 H. Hogeveen and J. Gaasbeek, *Rec. Trav. Chim.*, **88** (1969) 703.
- 3 G. A. Olah, Y. Halpern, J. Shen and Y. K. Mo, *J. Am. Chem. Soc.*, **95** (1973) 4960.
- 4 J. W. Larsen, P. A. Bovis, C. R. Watson and R. M. Pagni, *J. Am. Chem. Soc.*, **96** (1974) 2284.
- 5 C. Pitti, F. Bobillart, A. Thiebault and M. Herlem, *Anal. Lett.*, **8** (1975) 241.
- 6 M. Herlem, F. Bobillart, A. Thiebault and A. Jobert, *Anal. Lett.*, **10** (1978) 767.
- 7 C. Pitti, M. Cerles, A. Thiebault and M. Herlem, *J. Electroanal. Chem.*, **126** (1981) 163.
- 8 G. M. Kramer, *J. Org. Chem.*, **40** (1975) 5173.
- 9 D. Brunel, A. Germain and A. Commeyras, *Nouv. J. Chim.*, **2** (1978) 275.
- 10 V. B. Hughes, B. D. McNicol, M. R. Andrew, R. B. Jones and R. T. Short, *J. Appl. Electrochem.*, **7** (1977) 161.
- 11 A. A. Adams and R. T. Foley, *J. Electrochem. Soc.*, **126** (1979) 775.
- 12 R. J. Gillespie and T. E. Peel, *J. Am. Chem. Soc.*, **95** (1973) 5173.
- 13 H. H. Hyman, M. Kilpatrick and J. J. Katz, *J. Am. Chem. Soc.*, **79** (1957) 3668.
- 14 J. Grondin, R. Sagnes and A. Commeyras, *Bull. Soc. Chim. Fr.*, **11** (1976) 1779.
- 15 P. L. Fabre, J. Devynck and B. Trémillon, *Chem. Rev.*, **82** (1982) 591.
- 16 H. Strehlow and H. Wendt, *Z. Phys. Chem. (Frankfurt am Main)*, **30** (1960) 141.
- 17 J. Barr, R. J. Gillespie and R. C. Thompson, *Inorg. Chem.*, **3** (1964) 1149.
- 18 G. Adhami, *Thèse de doctorat d'état, Paris VI* (1972).
- 19 J. Sommer, P. Canivet, S. Schwartz and P. Rimmelin, *Nouv. J. Chim.*, **5** (1981) 45.

- 20 D. C. Russel and J. D. Senior, *Can. J. Chem.*, 52 (1974) 2975.
- 21 J. Devynck, A. Ben Hadid, P. L. Fabre and B. Trémillon, *Anal. Chim. Acta*, 100 (1978) 343.
- 22 J. P. Masson, J. Devynck and B. Trémillon, *J. Electroanal. Chem.*, 64 (1975) 193.
- 23 A. Ben Hadid, P. Rimmelin, J. Sommer and J. Devynck, *J. Chem. Soc. Perkin Trans. 2*, (1982) 269.
- 24 J. Verastegui, Thèse 3ème cycle, Université Pierre et Marie Curie, Paris VI (1973).
- 25 A. Jobert, Thèse docteur ingénieur, Université Pierre et Marie Curie, Paris VI (1979).
- 26 D. Bauer and M. Bouchet, *C. R. Acad. Sci., Sér. C*, (1972) 274.
- 27 D. Bauer, J. P. Beck and P. Texier, *Collect. Czech. Chem. Commun.*, 36 (1971) 360.
- 28 A. Ben Hadid, Thèse d'état, Université Pierre et Marie Curie, Paris VI (1980).
- 29 J. P. Masson, J. Devynck and B. Trémillon, *J. Electroanal. Chem.*, 64 (1975) 175.

THE USE OF PATTERN RECOGNITION TECHNIQUES IN CHEMICAL DIFFERENTIATION BETWEEN BORDEAUX AND BOURGOGNE WINES

HILKO VAN DER VOET* and DURK A. DOORNBOS

Laboratory for Pharmaceutical and Analytical Chemistry, Research Group Optimization, State University, Antonius Deusinglaan 2, NL-9713 AW Groningen (The Netherlands)

MENNO MEEMS and GERRIT VAN DE HAAR

Food Inspection Service, P.O. Box 465, NL-9700 AL Groningen (The Netherlands)

(Received 18th October 1983)

SUMMARY

Forty French red wines from the Bordeaux and Bourgogne regions were analyzed by twelve chemical procedures, which provided twenty features per sample. Chemical differences between these two types of wine were found and with pattern recognition techniques the number of variables that must be measured for this differentiation, is minimized. Feature selection and classification methods are evaluated on the basis of this data set.

Wines are very complex mixtures of many organic and inorganic compounds. Factors that have an influence on the composition are many, but among the most important is certainly the geographic origin, which is responsible for such important variables as soil and climate. For this reason, it can be expected that wines from two distinct geographic regions will have different characteristics. Unfortunately, the chemical nature of this difference still remains poorly understood. Because of this complexity, the application of multivariate data analysis and especially pattern recognition seems valuable. Previous work has been done on distinguishing between French and two types of American wines based on atomic emission spectrometry, gas chromatography and sensory evaluation [1–4].

In this study, an attempt was made to distinguish between French Bordeaux and Bourgogne wines on the basis of a number of very different constituents and properties. The data were analyzed by pattern recognition techniques in order to find the most useful features for discrimination between these two wine regions. An equally important objective was to evaluate the usefulness of the different methods of data analysis in problems concerning the authenticity of food products. In this article, the principles of certain pattern recognition techniques used for the classification are first outlined, and special attention is given to some points that are not often mentioned in the literature (e.g., the fundamental equality of SLDA and multiple regression analysis). A more general review of the possibilities of pattern recognition has been given by Kryger [5].

EXPERIMENTAL

Forty red wines, 21 from the Bordeaux region and 19 from the Bourgogne region, were selected. All these wines were quality wines (Appellation Contrôlée). Details of their origin are given in Table 1.

Twelve methods of chemical analysis were applied (for details, see Meems [6]). The pH was measured potentiometrically. Total acid was determined by potentiometric titration to pH 7.0 after boiling under reflux. Volatile acid was determined by steam distillation and titration to a phenolphthalein end-point. Organic acids were examined by h.p.l.c. with u.v. detection at 210 nm; peaks were obtained for citric, tartaric, malic, succinic, lactic and acetic acids and another peak was not identifiable. Sodium and potassium were measured by atomic emission spectrometry and iron by atomic absorption spectrometry. Anthocyanines were measured by two methods: (a) the difference in absorption at 520 nm between solutions at different pH values; (b) the difference in absorption at 520 nm with and without addition of sodium hydrogensulphite. Malvine was quantified by ion-pair h.p.l.c. and fluorescence spectrometry. The absorption was measured at the maximum near 520 nm (A520). Ethanol was determined by distillation and density measurement. Sugars and glycerol were determined by h.p.l.c. with a refractive index detector. All these analyses were done at the laboratory of the Food Inspection Service, Groningen.

TABLE 1

Origin of wine samples. All wines were quality wines (Appellation Contrôlée)

Bordeaux wines	Bourgogne wines
1. Chateau la Cabanne 1979	22. Palais des Ducs 1976
2. Chateau des Cabannes 1978	23. Macôn rouge supérieur
3. Domain de l'église 1979	24. Bourgogne Grand Ordinaire 1978
4. Chateau Lalène 1976	25. Bourgogne Passe-Tout-Grains 1979
5. Bordeaux supérieur	26. Bourgogne Passe-Tout-Grains 1976
6. Chateau la Croix de Miot 1976	27. Bourgogne Grand Ordinaire 1979
7. Chateau la Gravette 1978	28. Bourgogne Passetoutgrains 1979
8. Chateau le Peuy-Saincrit 1975	29. Bourgogne Grand Ordinaire 1979
9. Chateau Bellevue-Lugagnac 1978	30. Macôn 1976
10. Chateau la Croix de Miot 1976	31. Macôn 1980
11. Chateau Canteloiseau 1978	32. Macôn Rouge Supérieur 1979
12. Chateau Bayard Lancade 1979	33. Macôn 1980
13. Chateau la Croix St. Jean 1979	34. Bourgogne Grand Ordinaire 1979
14. Chateau de Viens 1978	35. Macôn Rouge Henri Darviot 1978
15. Cru Cantemerle 1974	36. Macôn Supérieur 1979
16. Chateau Bourdicotte 1978	37. Macôn 1978
17. Rineau 1978	38. Bourgogne Rouge 1979
18. Bordeaux Supérieur	39. Bourgogne 1979
19. Chateau Courson 1978	40. Bourgogne Passetoutgrains 1979
20. Chateau la Ramonette 1979	
21. Chateau Timberlay 1978	

TABLE 2

Set of 20 features extracted from 12 determinations (mean and standard deviation) for Bordeaux and Bourgogne wines

	Bordeaux	Bourgogne	Order ^a
Total acid (meq l ⁻¹)	70 ± 7	80 ± 7	2
Volatile acid (meq l ⁻¹)	8.9 ± 1.8	10.0 ± 1.8	12
Ethanol (% v/v)	11.7 ± 0.5	11.8 ± 0.2	19
pH	3.40 ± 0.10	3.42 ± 0.08	18
Glycerol (g l ⁻¹)	7.0 ± 0.7	6.9 ± 0.4	17
Ratio glycerol/ethanol	7.4 ± 0.6	7.3 ± 0.5	16
Citric acid (g l ⁻¹)	0.12 ± 0.15	0.30 ± 0.32	10
Tartaric acid (g l ⁻¹)	2.3 ± 0.4	2.7 ± 0.3	5
Malic acid (g l ⁻¹)	0.10 ± 0.10	0.10 ± 0.15	20
"Succinic acid" ^b (g l ⁻¹)	8.1 ± 2.8	6.0 ± 1.4	8
Lactic acid (g l ⁻¹)	3.5 ± 0.7	4.1 ± 0.7	7
Acetic acid (g l ⁻¹)	0.37 ± 0.14	0.44 ± 0.16	14
Unknown h.p.l.c. peak (cm)	7.3 ± 3.2	4.6 ± 1.7	4
Absorbance at 520 nm	1.0 ± 0.4	0.3 ± 0.5	1
Sodium (mg l ⁻¹)	23 ± 10	16 ± 10	11
Potassium (g l ⁻¹)	0.90 ± 0.07	0.81 ± 0.13	9
Malvine (mg l ⁻¹)	1.9 ± 0.8	1.6 ± 0.7	15
Anthocyanines method 1 (mg l ⁻¹)	86 ± 34	54 ± 34	6
Anthocyanines method 2 (mg l ⁻¹)	85 ± 30	51 ± 34	3
Iron (mg l ⁻¹)	7.2 ± 1.6	6.3 ± 2.0	13

^aThe relative order of importance for the discrimination between Bordeaux and Bourgogne, from variance weighting. ^bThe values found are calculated as succinic acid, but as such they are extraordinarily high, so presumably also some other acid is measured (gluconic acid?).

From the results of the chemical analyses, twenty features (Table 2) were extracted for computer analysis. Glucose and fructose were not detected in the 40 wine samples. The feature list includes the ratio of glycerol to ethanol, which is a commonly used criterion in quality control. Twelve very outlying measurements were deleted and replaced with the class mean for that variable.

The computer programs used for the data analysis were the general pattern recognition package ARTHUR [7], the well-known statistical package SPSS [8] and the ALLOC programs [9]. All programs were run on the CYBER 170/760 computer of the Groningen State University.

CLASSIFICATION TECHNIQUES

The 40 wines were classified as either Bordeaux or Bourgogne by using six different methods and some variations, which are described briefly below. Detailed mathematical descriptions are not given. For this purpose, the 40 wine samples can be considered as 40 object points in a multidimensional space, the measurements made on each sample being the coordinates of the

object point. Most techniques can then be viewed as straightforward extensions to the multidimensional case of discrimination on the basis of one or two measurements.

In supervised pattern recognition, there is always a set of objects (wine samples) of known origin. These objects constitute the training set and are used for the construction of a classifier. Evaluation of the results must not be based on the classification of these training samples, but on an independent test or prediction set. In previous work [1, 2], only the training set itself was classified, leading to over-optimistic success rates for the performance of the classifier (see, e.g. Coomans [10]).

Because only 40 known wine samples were available here, the leave-one-out method was used. Thus a classifier is constructed on the basis of 39 samples and the remaining sample is classified; then this sample is replaced in the training set, another sample is removed, a new classifier is developed on this training set and the deleted sample is classified. The procedure continues until all samples have been deleted and classified once.

The classification methods can be divided in three groups, which are discussed below.

Methods constructing a separating surface

Statistical discriminant analysis (SDA) and the linear learning machine (LLM) construct a separating surface in the multidimensional space, such that Bordeaux wines fall on one side of this surface and Bourgogne wines on the other.

In statistical discriminant analysis, a discriminant axis situated in the multidimensional space is computed so that the projections of the data points of the two classes on this axis are separated maximally. When the two classes are assumed to have the same intrinsic structure (i.e., equal variance-covariance matrices), the separating surface, perpendicular to the discriminant axis, is linear and the procedure is known as statistical linear discriminant analysis (SLDA). If the variance-covariance structure of the two groups is different, the separating surface is curved and the method is statistical quadratic discriminant analysis (SQDA). Exactly the same results as with SLDA can be obtained by using multiple linear regression. If a categorical variable y , that can assume only two values (e.g., 1 for Bordeaux and 2 for Bourgogne) is defined, then regression of y on the variables measured yields the same result as SLDA. This SLDA is implemented in several routines of the ARTHUR package (LEAST, REGRES, LEDISC, LESLT) and in the routine DISCRIMINANT of SPSS. The results of LEAST may differ slightly from those of REGRES and DISCRIMINANT, because the separating plane is adjusted empirically somewhere on the discriminant axis. The SQDA is easily performed as a special option of DISCRIMINANT. Another advantage of the SPSS routine is that results are in a probabilistic form, i.e., for each classified point a posteriori group probabilities are given.

A linear learning machine (LLM) or binary adaptive classifier also constructs

a separating surface, but by an empirical method with no use of statistical properties (means, variances, covariances) of the training groups. A randomly chosen $(m - 1)$ -dimensional hyperplane is situated in the m -dimensional space and then all wines are classified with this plane. When a wine is incorrectly classified, the hyperplane is adjusted by taking its mirror image with respect to the misclassified point. This process is repeated and is known to converge if the two groups are indeed linearly separable. It is continued until all wines are correctly classified or a maximum number of iterations is reached. Implementations of the LLM are the ARTHUR routines PLANE and MULTI, the latter separating one training group from all other groups, while PLANE separates each pair of groups. For binary problems (2 training groups) the two methods are identical.

Potential and nearest-neighbour methods

Most of these methods start by computing the distance matrix, which contains all interpoint distances in the multidimensional space. One can then classify a data point from the test set into the same class as its nearest neighbour in this hyperspace. This method (the 1 nearest neighbour or 1NN method) can be extended to more neighbouring data points. Classification is then done on the basis of a majority vote of the k nearest neighbours (KNN method). This method is implemented in the ARTHUR routine KNN, and computes classifications for $k = 1$ and $k = 3-10$.

Extending the ideas behind the KNN method, it seems more logical to consider not 1 or k , but all data points, while letting their influence on classification decrease as their distance from the test point to be classified increases. This may be visualized by supposing that all training group points represent an electrical charge, positive for group 1 and negative for group 2. The (uncharged) test point receives influences from all training set points and its classification is determined by the electrical potential at its coordinates being net positive or negative. This method, with a Gaussian model for the potential distribution around each point, is found in the program package ALLOC [9]. Classification results are, as with SLDA, in a probabilistic form.

Another way to obtain a potential distribution for each class is to use the relative frequency distributions on each separate variable of the training groups. This is called the histogram method (HIST). By extending the histogram idea to more dimensions, a multidimensional "chess-board" is obtained. The multivariate relative frequency in each field is calculated by multiplication of the univariate relative frequencies. This is done for each class separately and a test point will be assigned to the class that has the highest multivariate relative frequency in the field where the test point lies. In fact, this procedure assumes that the variables are not correlated with each other (only then is multiplication of probabilities allowed); but this is often not true. Theoretically, it would be preferable therefore to transform the variables to independent features by some decorrelating technique. The histogram method can be found in ARTHUR as the BAYES method (routines BASET and

BACKLAS). Decorrelation can be achieved in various ways, e.g., by using the routine SELECT (see under "Feature selection").

Hyperboxes or multivariate confidence regions

These methods construct a model for each class separately. The best known method is SIMCA (soft independent modelling of class analogy or statistical isolinear multi-category analysis). Principal component methods are applied to each class to calculate a new set of coordinate axes which can have fewer dimensions than the original hyperspace. The optimal number of dimensions is established by a technique called cross-validation. Along each of these new axes, a confidence region is constructed, which results in an envelope or hyperbox for each class. The distance to these hyperboxes determines the classification of test points. Implementation is available in the SIMCA package of Wold [11] and as the method SIMCA (routines SICVA, SIPRINCO and SICLAS) in ARTHUR.

CLUSTER ANALYSIS

Before classification techniques (i.e., supervised pattern recognition) were applied in this work, some tests were done with cluster analyses, based on the routines HIER and TREE of ARTHUR. These unsupervised pattern recognition methods assume no prior knowledge of the origin of the samples, but try to find "natural" clusters in the multidimensional space. Although there was a strong tendency for most samples to cluster with samples from the same class, no "natural" separation was obtained in this way.

One can also represent the multidimensional space by mapping it onto two dimensions. In this way, one can exploit the fact that the human eye is the best available pattern recognizer in 2 or 3 dimensions. The commonest projection, the eigenvector projection, employs principal components analysis and projects all data points onto the plane spanned by the first two eigenvectors of the data, corresponding to directions in the hyperspace with maximal variance of the data points. The eigenvector projection of the 40 wine samples is shown in Fig. 1. Here, as with cluster analysis, it can be seen that several samples disturb a neat clustering of Bordeaux and Bourgogne, respectively.

A rather different method of representing multivariate data is based on two-dimensional pictures of human faces [12]. Each feature is represented as a characteristic feature of the face, e.g., size of the eyes or the form of the chin. Some of these "personified" wines are shown in Fig. 2 for illustration. But this method of cluster analysis also did not give a definite separation between the two types of wine.

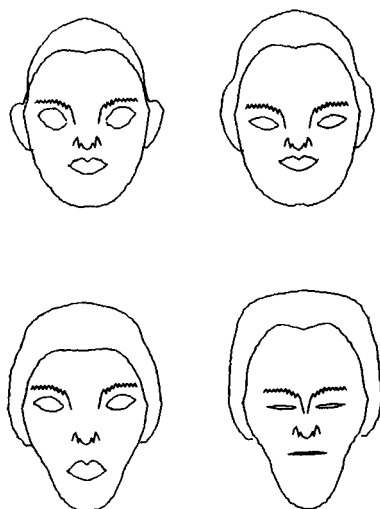
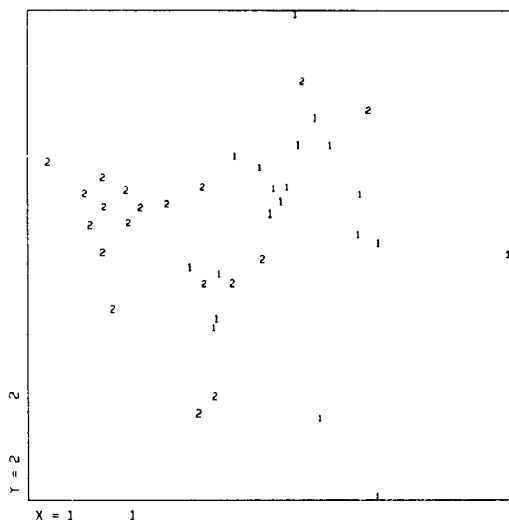


Fig. 1. Eigenvector plot of 40 wine samples. Class 1 = Bordeaux; class 2 = Bourgogne.

Fig. 2. Some wine samples represented as faces. Above are two typical Bourgogne wines; below are two typical Bordeaux wines.

FEATURE SELECTION

For classification based on geographic origin, the data set included all the available features. However, there are several reasons for reducing the number of features used. In the first place, feature selection is often one of the major aims in pattern recognition analysis. The analysis indicates which features are most important; often, the number of measurements that have to be made on future test samples can be reduced. This was certainly true in this investigation, where twelve chemical procedures were applied to obtain 20 features. Another important reason for feature reduction is to avoid nonsense classifications. The ratio n/d (number of data points to number of features) should be over 3 and preferably even higher (see, e.g., Varmuza [13]).

The simplest mode of feature selection is to judge each feature separately on its discriminating ability as expressed in, for instance, the variance weight (i.e., the ratio of the interclass variance to the intraclass variance). The relative order of importance of the 20 features in the present investigation is shown in Table 2. Best discriminating variables are absorption at 520 nm (A520), total acid, anthocyanines, the unknown h.p.l.c. peak, and tartaric acid. However, when more than one feature has to be selected, this method is not optimal: anthocyanines and absorption, for example, are strongly correlated, and it appears that the discriminating information contained in both variables is about the same. Therefore, if the absorption at 520 nm

is selected first, little additional information is obtained by selecting anthocyanines in the next step. But the opposite can also occur. A variable which in itself is useless for classification, e.g., the pH [Bordeaux pH 3.40 ± 0.10 (standard deviation) and Bourgogne pH 3.42 ± 0.08], turns out to be very useful in combination with another variable, with which it is correlated, i.e., total acid. This is illustrated in Fig. 3, which for clarity is a somewhat idealized version of the real situation. It can be seen that, although total acid cannot discriminate absolutely between the two classes, its performance is greatly improved by including the pH in the feature selection. The correlation between these two variables was -0.88 for Bordeaux and -0.74 for Bourgogne. Chemically Fig. 3 may be interpreted as a larger buffering capacity of Bourgogne wines, as more alkali is needed for neutralization for wines with equal pH.

For the above-mentioned reasons, the variance weight selection order was not used here to obtain a reduced set of features. Instead, more sophisticated techniques were preferred because these take into account all features selected previously. The methods used were the stepwise forward selection procedures of the SELECT and STEP routines in ARTHUR, the DISCRIMINANT analysis of SPSS and the ALLOC-1 program. The results are summarized in Table 3. The STEP and DISCRIMINANT selections are basically the same and operate with the same kind of distance criteria as used in SLDA. In both methods, a feature that is indicated to be significant in an early stage of the selection procedure, but insignificant after the addition of several other features, is eliminated before addition of another feature. In the present case, this happened with three features (lactic acid, tartaric acid and A520). The resulting set of six features will be called the SLDA selection hereafter.

The SELECT method is in fact based on the same principles as the SLDA selection with the difference that it lacks the possibility of dropping previously selected variables. The criterion for importance of the features is the variance

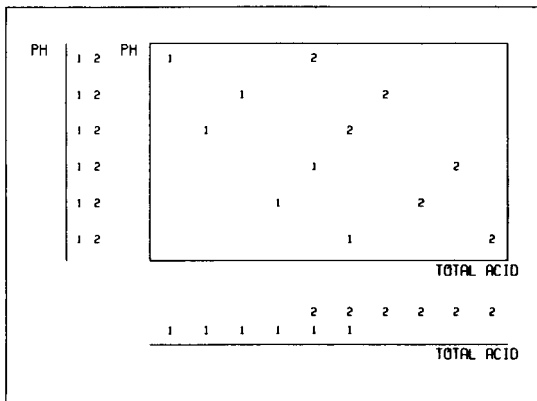


Fig. 3. Discrimination between Bordeaux (1) and Bourgogne (2) based on total acid alone, pH alone and both variables together.

TABLE 3

Reduction of the number of variables by feature selection (n is the resulting number of features)

SLDA selection $n = 6^a$	SELECT selection $n = 11$	ALLOC selection $n = 4$	Heuristic selection $n = 8$
"Succinic acid"	A520	Total acid	Total acid
Citric acid	Tartaric acid	A520	A520
Total acid	"Succinic acid"	Potassium	Potassium
pH	Lactic acid	Tartaric acid	Tartaric acid
Malvine	Citric acid		pH
Acetic acid	Unknown h.p.l.c. peak		Citric acid
	Total acid		"Succinic acid"
	pH		Unknown h.p.l.c. peak
	Volatile acid		
	Acetic acid		
	Potassium		

^aA520, tartaric acid and lactic acid were chosen in the first instance, but removed at a later stage of the selection process.

weight, the Fisher weight or the correlation-to-property weight (the last option leading to similar results as SLDA selection without deleting features). With variance weighting, eleven features were chosen (SELECT selection).

A quite different method, finally, is to use the classification results as a guide in the selection process. This is done in ALLOC-1, where at each step a classification is done by using every combination of previously selected features with a new feature. An advantage is that the selection criterion (classification rate) and the stopping criterion (change in classification rate when adding the next variable) are easily interpretable. This allows some heuristic manipulation by the user of the program. In our case, ALLOC-1 needed nine features before a minimum error rate was obtained, but it first passed through a local minimum at three selected features. After the unexpected selection of malic acid as the third feature, the error rate increased when the next variable was added. This suggested that malic acid was not such a good feature after all, and after some preselection trials it became possible to reach the same minimum error rate with only four instead of nine features (ALLOC selection).

CLASSIFICATION

All classifications were done by using the complete set of 20 features, each of the three subsets obtained by feature reduction methods, and an additional self-chosen selection of eight variables which was really an attempt

to combine what seemed to be the most important variables from the other methods (heuristic selection) (see Table 3). The results of the classifications, all done by the leave-one-out method, are given in Table 4, which shows the number of wine samples classified erroneously. In general, it can be seen that by choosing the appropriate techniques, prediction rates of 90% or more are easily achieved, which indicates that a chemical differentiation between Bordeaux and Bourgogne wines is certainly possible. Predictions done by the usual panel of the Food Inspection Service in a small organoleptic investigation were correct only in about 50% of all cases. It has to be noted, however, that the wine samples were obtained in licensed victualler's shops and not in the region of origin. Although all the wines were indicated as quality wines, the true origin of the samples cannot be guaranteed. The wines misclassified by pattern recognition methods were about equally often Bordeaux and Bourgogne wines.

One of the six investigated methods (HIST) always performed very badly compared to other methods. A decorrelation of the features as indicated by theory in case of dependency among the variables did not improve the results (HIST(orth)). It has to be remarked that in our version of ARTHUR (version 07-01-78), we have corrected some errors. The results shown are those obtained after correction and were about equally bad as those before correction.

TABLE 4

Number of wrongly classified wines (out of 40) when different feature selection and classification methods were used. Best results (prediction rate $\geq 90\%$) are underlined

Classification method ^a	Feature selection method ^b				
	— (20)	SLDA (6)	SELECT (11)	ALLOC (4)	Heuristic (8)
<i>Separating plane</i>					
1. SLDA	5	<u>2</u>	<u>3</u>	<u>4</u>	<u>4</u>
SQDA	6	<u>3</u>	<u>3</u>	<u>4</u>	<u>4</u>
2. LLM ^c	8-9	<u>1-3</u>	6-8	5	4-5
<i>Potential methods</i>					
3. KNN ($k = 1$)	5	7	<u>3</u>	<u>2</u>	<u>4</u>
KNN ($k = 3$)	7	6	5	<u>2</u>	<u>2</u>
KNN ($k = 10$)	7	9	5	<u>3</u>	<u>4</u>
4. ALLOC	<u>3</u>	8	<u>3</u>	<u>2</u>	<u>1</u>
5. HIST	9	12	8	9	12
HIST (orth)	17	11	12	9	13
<i>Hyperboxes</i>					
6. SIMCA (2)	8	8	8	<u>3</u>	<u>3</u>

^aAll classifications were done by using the leave-one-out method. ^bNumber of features in parentheses. ^cResults of LLM are variable because of a random initialization of the separating plane.

The methods KNN and ALLOC are somewhat related (as explained above). This was confirmed by the classification results, which were bad for the SLDA selection and better for the ALLOC selection and the heuristic selection. However, almost everywhere, the results obtained with ALLOC were better than, or at least as good as, those obtained with KNN. Moreover, there was no optimum value of k in the KNN method, where best results were alternatively obtained with 1, 3 or 4 neighbours (see Fig. 4A).

The SLDA and LLM techniques, both of which construct a separating plane between the two classes, also showed a somewhat similar trend, i.e., best prediction rates with SLDA feature selection and worst with the use of all 20 features. The ratio n/d is only 2 when 20 features are used and so it

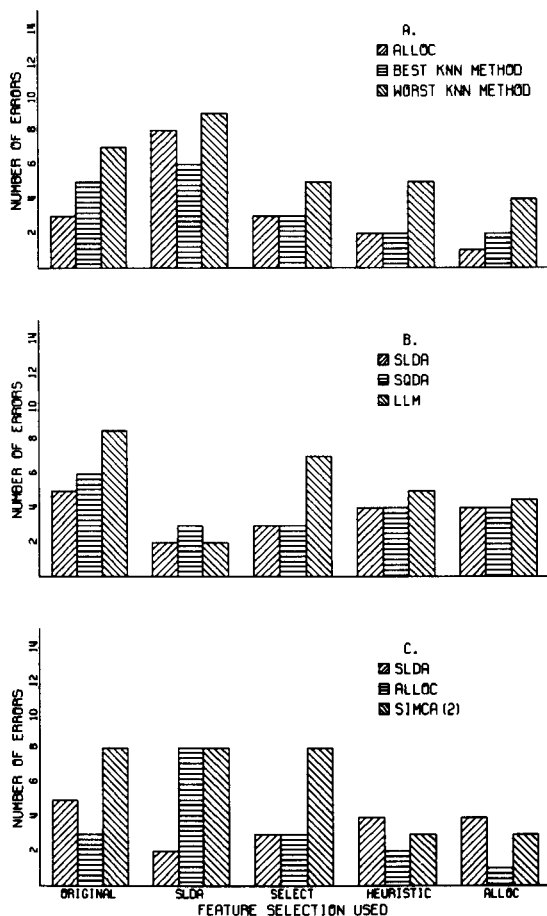


Fig. 4. Number of errors for some classification methods: (A) comparison of ALLOC and KNN ($k = 1-10$); (B) comparison of SDA and LLM; (C) comparison of SLDA, ALLOC and SIMCA. From left to right, the results relate to the situations before feature selection and after SLDA, SELECT, Heuristic and ALLOC feature selection.

can be expected that classifiers with little predictive power will be constructed on the training set. The SLDA classification was nearly always superior to LLM classification (see Fig. 4B). Results of the latter method are variable because the separating hyperplane is randomly initialized. The quadratic modification of SLDA, SQDA, never had advantages over SLDA. For this reason, it can be concluded that the structures of the Bordeaux and the Bourgogne classes do not differ very much.

The last method examined, SIMCA, could not be judged properly, because of some errors in the ARTHUR routines that were used. The routine SICSVA for cross-validation did not work properly, so that each class was invariably modeled by a 2-principal-component factor model. The results obtained were good when the number of features was small (4 or 8). For larger sets of features, the number of components was probably insufficient.

From Table 4 it can be seen that feature selection is clearly a useful procedure: in almost every case a reduction of the error rate was accomplished. Which feature selection method should be used depends on the classification technique that is used in combination with it. The SLDA selection turns out to be especially suitable for methods that construct a separating surface in the hyperspace, i.e., SLDA, SQDA and LLM. Other classifications do not improve or even get worse (ALLOC) by applying SLDA feature selection. The ALLOC feature selection procedure gives best results with ALLOC and KNN classifications. But SLDA and SIMCA(2) also perform rather well, so that ALLOC classification seems to be quite generally useful, as already suggested by Hermans et al. [9].

The eight features chosen by heuristic selection (and including the four features from ALLOC selection) gave about the same results. With SELECT, finally, good results were obtained by using the SLDA, SQDA, 1NN and ALLOC classifications. This feature selection technique therefore seems quite generally useful, but it has the tendency to select more features than other methods; this can of course be changed by modifying the default values of the stopping criterion.

CONCLUSIONS

A chemical differentiation between Bordeaux and Bourgogne wines can be made with a prediction rate of 90.0–97.5% by choosing the appropriate pattern recognition techniques. Use of all twenty available features (resulting from twelve chemical procedures) is unnecessary and even undesirable, because the use of variables with no extra discriminating information only introduces noise in the pattern recognition process. Feature selection is therefore essential, but the method used should always be chosen in combination with the classification technique applied.

From theoretical considerations and from the results presented above, the following methods seem most promising: SLDA selection with SLDA classification; ALLOC selection with ALLOC classification (or possibly

SLDA or SIMCA classification); SELECT selection with SLDA or ALLOC classification. The SIMCA method was somewhat handicapped in this study, so that its performance is probably underestimated.

The advantages of SLDA are its wide availability in computer programs and the possibility of expressing the results as a multiple regression equation from which the origin of future test samples can be predicted. For example, the combination of ALLOC selection with SLDA classification leads to the equation

predicted class number = $-0.1285 + 0.01326 \text{ total acid (meq l}^{-1}\text{)}$

+ $0.4672 \text{ tartaric acid (g l}^{-1}\text{)} - 0.4594 \text{ A520} - 0.2842 \text{ potassium (g l}^{-1}\text{)}$

where class 1 = Bordeaux wines and class 2 = Bourgogne wines. It should be stressed, however, that these results may be specific to the data set used. A method such as SQDA, for instance, may turn out to be superior to SLDA when the classes are asymmetric. For understanding the true nature of complex mixtures such as wines and indeed many food products, it is useful to use different methods of multivariate data analysis (cluster analysis, projection onto 2 dimensions, various feature selection and classification techniques, correlation analysis, etc.).

REFERENCES

- 1 W. O. Kwan, B. R. Kowalski and R. K. Skogerboe, *J. Agric. Food Chem.*, 27 (1979) 1321.
- 2 W. O. Kwan and B. R. Kowalski, *J. Agric. Food Chem.*, 28 (1980) 356.
- 3 W. O. Kwan and B. R. Kowalski, *J. Food Sci.*, 45 (1980) 213.
- 4 W. O. Kwan and B. R. Kowalski, *Anal. Chim. Acta*, 122 (1980) 215.
- 5 L. Kryger, *Talanta*, 28 (1981) 871.
- 6 M. Meems, *Het chemisch karakteriseren van wijn met behulp van patroonherkenning*, Rep. 82-19, Food Inspection Service Groningen, 1982.
- 7 A. M. Harper, D. L. Duewer, B. R. Kowalski and J. L. Fasching, in B. R. Kowalski (Ed.), *Chemometrics: Theory and Application*, ACS Symposium Series 52, American Chemical Society, Washington, DC, 1977.
- 8 N. H. Nie, C. H. Hull, J. G. Jenkins, K. Steinbrenner and D. H. Bent, *SPSS: Statistical Package for the Social Sciences*, 2nd edn., McGraw-Hill, New York, 1975.
- 9 J. Hermans and J. D. F. Habbema, *Manual for the ALLOC Discriminant Analysis Programs*, University of Leiden, 1976.
- 10 D. Coomans, *Doctoral thesis*, Free University of Brussels, 1982, p. 236.
- 11 S. Wold and M. Sjöström, in B. R. Kowalski (Ed.), *Chemometrics: Theory and Application*, ACS Symposium Series 52, American Chemical Society, Washington, DC, 1977.
- 12 H. Chernoff, *J. Am. Stat. Assoc.*, 58 (1973) 361.
- 13 K. Varmuza, *Pattern Recognition in Chemistry*, Springer Verlag, Berlin, 1980, pp. 114-117.

BEWERTUNG VON GLÄTTUNGSEXPERIMENTEN

E. SORKAU, K. DOERFFEL* and T. REIHER

*Sektion Chemie der Technischen Hochschule "Cari Schorlemmer" Leuna-Merseburg,
4200 Merseburg (D.D.R.)*

P. C. MEIER

*Laboratorium für Organische Chemie der Eidgenössischen Technischen Hochschule
Zürich, CH-8092 Zürich (Schweiz)*

(Eingegangen den 24 Oktober 1983)

SUMMARY

(Evaluation of curve-smoothing techniques)

Conditions for curve smoothing can be compared experimentally by simulation or theoretically by applying information theory. Simulation experiments provide the conditions either for optimization of the signal/noise ratio or for minimizing the systematic error; the results presented are easily evaluated in practice. Information theory assumes that loss of information will not be caused by the smoothing procedure. Conditions for maximal noise improvement for a preset systematic error are then obtainable; the regularities are easily interpreted from graphs.

ZUSAMMENFASSUNG

Bedingungen für Glättungsprozeduren lassen sich experimentell durch Simulation finden oder theoretisch m.H. der Informationstheorie abschätzen. Aus Simulationsexperimenten folgen Bedingungen entweder für maximale Verbesserung des Signal-Rausch-Verhältnisses oder für Minimierung des systematischen Fehlers. Diese tabellarisch niedergelegten Ergebnisse lassen sich praktisch sehr einfach auswerten. Die Informationstheorie setzt voraus, daß bei der Glättungsprozedur kein Informationsverlust eintreten darf. Dann liefert sie bei vorgegebenen systematischen Fehlern Glättungsbedingungen für maximal mögliche Rauschverbesserung. Diese Gesetzmässigkeiten sind graphisch leicht auswertbar.

Zur Verbesserung des Signal-Rausch-Verhältnisses (SRV) setzt man oft die von Savitzky und Golay [1, 2] vorgeschlagene Polynomglättung ein. Die Anwendung dieses Verfahrens führt zwar einerseits zu der erwünschten Rauschminderung, andererseits aber auch zu einer unerwünschten systematischen Verfälschung des Mess-signals; das Signal wird kleiner und breiter (Abb. 1). Die Wahl des Filteralgorithmus ist abhängig von der Signal-form und -überlappung, von der Fragestellung und von Randbedingungen wie z.B. Anzahl der Messpunkte je Halbwertsbreite FWHM und vorliegendem SRV. Obwohl bereits verbreitet kommerzielle Lösungen angeboten werden, gibt es zur Wahl optimaler Glättungsbedingungen hinsichtlich Fensterbreite

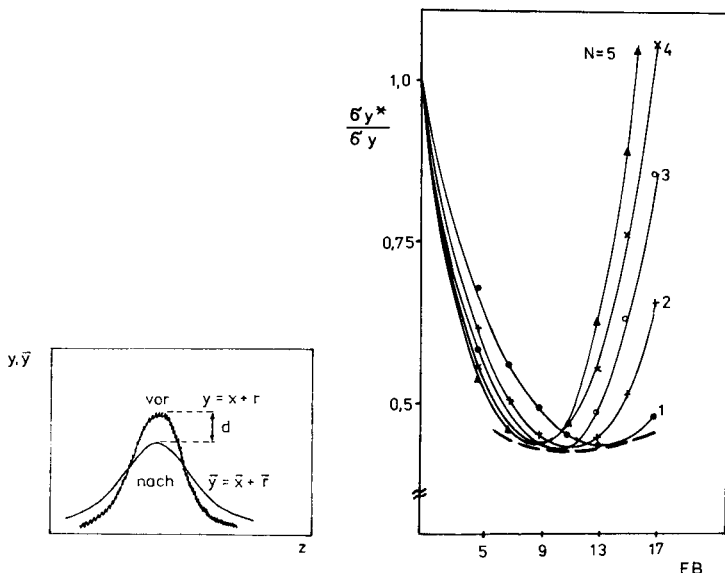


Abb. 1. Mess-signal vor und nach dem Glätten. y = Mess-signal; x = Nutzsinal; r = Rausch-signal; d = systematischer Fehler; z = Wellenzahl o.ä.

Abb. 2. Rauschminderung σ_{y^*}/σ_y in Abhängigkeit der Fensterbreite und Anzahl der Glättungen N (FWHM = 23; $\sigma_y/y = 0,68\%$).

FB (Anzahl der Mess-punkte je Glättungsintervall) sowie des Polynom-grades k noch teilweise unterschiedliche Empfehlungen. Dabei werden die Glättungsbedingungen entweder für ein maximales SRV [3–5] oder für eine geringe systematische Verfälschung d [6, 7] optimiert. Alle diese Empfehlungen setzen eine mehr oder weniger redundante Abtastung des Mess-signals voraus. Dies ist, besonders bei schmalen Signalen, nicht immer realisierbar. Dann sind Glättungsprozeduren zu finden, die mit möglichst wenigen Mess-punkten bei tragbarem systematischem Fehler eine hohe Effektivität in der Rauschunterdrückung bringen.

GLÄTTUNGSBEDINGUNGEN AUS SIMULATIONSEXPERIMENTEN

Maximales Signal-Rausch-Verhältnis

Zu den Simulationsexperimenten wird ein verrauschtes Lorentz-Signal y mit FWHM = 4 . . . 15 vorgegeben. Die Standardabweichung des Rauschens, bezogen auf die Peakhöhe, variiert in den Grenzen $\sigma_y/y_{\max} = 0,25 \dots 8\%$. Die Fensterbreite des Savitzky-Golay-Polynoms beträgt $FB = 5 \dots 17$. Vom geglätteten Signal \bar{y} wird das unverrauschte Nutzsinal x subtrahiert. Den Differenzvektor $D = \bar{y} - x = \bar{x} - x + \bar{r}$ benutzt man im Intervall $\pm 2,5$ FWHM, um mit σ_y^* eine Standardabweichung zu definieren, die sowohl des residuelle Rauschen \bar{r} als auch die systematische Signalverzerrung $d = \bar{x} - x$ erfasst.

erfassungssystem automatisch den besten Algorithmus auswählt. Ähnliche Tabellen lassen sich für höhere Polynomgrade erstellen. Somit ist auch die Wahl eines geeigneten Polynomgrades möglich. Solch eine Vorgehensweise garantiert für das schnelle praktische Arbeiten die bestmögliche Verbesserung des SRV, garantiert aber nicht einen minimalen systematischen Fehler, da σ_y^* residuelles Rauschen und systematische Verzerrungen erfasst.

Minimale systematische Verzerrung

Für die Ermittlung des systematischen Fehlers wird die Polynomglättung auf ein unverraushtes Lorentz-Signal x angewandt. Der Fehler im Signalmaximum ergibt sich aus der Differenz $d = x - \bar{x}$. Erwartungsgemäss steigt er mit zunehmender Fensterbreite und abnehmenden Polynomgrad (Abb. 3). Ist nur ein systematischer Fehler von $d = d_{\max}$ zulässig, so darf das Verhältnis Glättungsintervall/Halbwertsbreite $[(FB - 1)/(FWHM - 1)]$ eine aus Abb. 3 ablesbare Schranke nicht überschreiten. Der Wert dieser Schranke ist abhängig vom Polynomgrad. Bei vorgegebenen FWHM erhält man demzufolge alternative Lösungen von Fensterbreiten und Polynomgraden. Die optimalen Parameter ergeben sich aus dem minimalen residuellen Rauschen, charakterisiert durch das Verhältnis $\sigma_{\bar{y}}/\sigma_y$.

Die Standardabweichung $\sigma_{\bar{y}}$ des geglätteten Signals kann durch Anwendung des Fehlerfortpflanzungsgesetzes auf die Glättungsvorschrift [1] ermittelt werden. (Es wird vorausgesetzt, dass der zufällige Fehler normal verteilt ist und jeder Messwert die gleiche Standardabweichung σ_y aufweist.) Mit zunehmender Fensterbreite und abnehmenden Polynomgrad sinkt das residuelle Rauschen (Abb. 4). Die optimale Fensterbreite ist gekennzeichnet durch das minimale $\sigma_{\bar{y}}/\sigma_y$. Unterscheiden sich die Fehlerminima nicht, so ist der kleinere Polynomgrad zu wählen, da dieser weniger Rechenoperationen erfordert. Diese Vorgehensweise garantiert, dass die Polynomglättung einen vorgegebenen systematischen Fehler nicht überschreitet. Das Ergebnis ist jedoch nicht in jedem Fall eine bestmögliche Verbesserung des SRV.

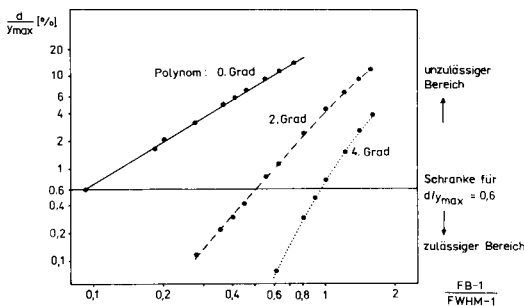


Abb. 3. Systematische Verfälschung des Signalmaximums.

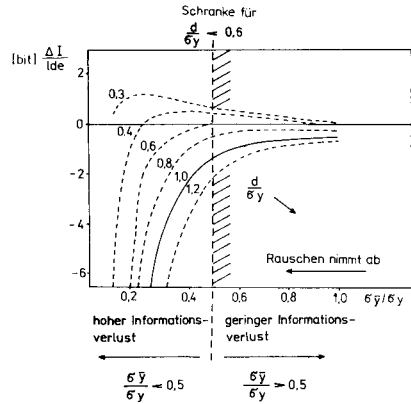
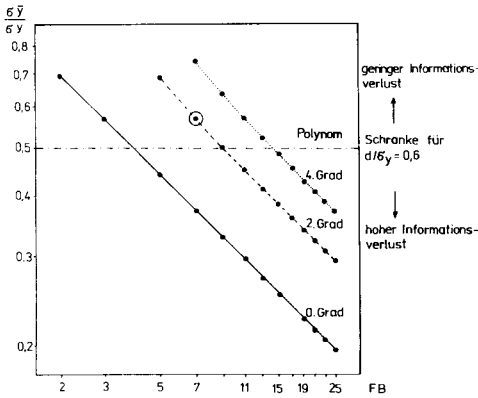


Abb. 4. Verkleinerung des zufälligen Fehlers. o: Bedingungen für $d_{max}/y_{max} \leq 1\%$, $\sigma_y/y_{max} = 1\%$ (Optimum für FWHM = 10).

Abb. 5. Informationsgehalt in Abhängigkeit von Standardabweichung σ_y und systematischem Fehler d .

INFORMATIONSGEHALT DER POLYNOMGLÄTTUNG

Der Informationsgehalt I eines Mess-signals y an der Stelle z im Intensitätsbereich $[y_{min}; y_{max}]$ ist nach Eckschlagler [8] gegeben durch

$$I = \text{ld} [(y_{max} - y_{min}) / (2\pi e)^{1/2} \sigma_y] - 1/2 \text{ld} e(d/\sigma_y)^2 \tag{1}$$

Hierbei sind e die EULER'sche Zahl, d der systematische Fehler, σ_y die Standardabweichung des gemessenen Wertes y , y_{min} die untere Grenze des Meßbereiches bzw. die Nulllinie.

Das Auftreten systematischer Fehler führt nach Gl. 1 zu einem Informationsverlust. Dieser kann bei systematischen Fehlern $d/\sigma_y < 1$ als tragbar angesehen werden. Deshalb sollte die mit der Glättung verbundene systematische Verfälschung diesen Wert nicht überschreiten. Vor dem Glätten wird das Mess-signal als frei von systematischen Fehlern angesehen ($d = 0$). Sein Informationsgehalt ergibt sich aus

$$I_{vor} = \text{ld} [(y_{max} - y_{min}) / (2\pi e)^{1/2} \sigma_y] \tag{2}$$

Nach dem Glätten tritt ein systematischer Fehler d auf und der zufällige Fehler σ_y vermindert sich auf $\sigma_{\bar{y}}$. ($\sigma_{\bar{y}}$ berücksichtigt nur das residuelle Rauschen im Unterschied zu σ_y^*).

Den Informationsgehalt berechnet man zu

$$I_{nach} = \text{ld} [(y_{max} - y_{min}) / (2\pi e)^{1/2} \sigma_{\bar{y}}] - 1/2 \text{ld} e(d/\sigma_{\bar{y}})^2 \tag{3}$$

Die Differenz $\Delta I = I_{nach} - I_{vor}$ gibt die Informationsänderung in Abhängig-

keit vom systematischen Fehler und von der Rauschminderung $\sigma_{\bar{y}}/\sigma_y$ wieder. Man bezieht $\sigma_{\bar{y}}$ und d auf σ_y und erhält dadurch dimensionslose, reduzierte Grössen. Die Subtraktion der Gln. 2 und 3 ergibt

$$\Delta I/\text{ld } e = -\ln(\sigma_{\bar{y}}/\sigma_y) - [1/2 (d/\sigma_y)^2] (\sigma_{\bar{y}}/\sigma_y)^{-2} \quad (4)$$

Nach Gl. 4 bringt jede Glättung ($\sigma_{\bar{y}}/\sigma_y < 1$) mit einem systematischen Fehler $d/\sigma_y > 0,6$ prinzipiell einen Informationsverlust. Dieser ist mit abnehmenden Rauschen zunächst nur gering, nimmt dann aber rapide zu (Abb. 5).

Bei Kenntnis der Standardabweichung des ungeglätteten Signals (σ_y/y_{\max}) und nach Vorgabe des noch zulässigen systematischen Fehlers (d/y_{\max}) kann man das Verhältnis d/σ_y berechnen und somit eine Schranke $\sigma_{\bar{y}}/\sigma_y$ festlegen, oberhalb deren der Informationsverlust noch tragbar, unterhalb jedoch unvertretbar gross ist (Abb. 5).

SCHLUSSFOLGERUNGEN

Für die Bewertung von Glättungsprozeduren ist das Verhältnis d/σ_y eine entscheidende Grösse. Ein Informationsgewinn ist nur für $d/\sigma_y \leq 0,6$ zu erwarten (Abb. 5), für $d/\sigma_y > 0,6$ ist jede Glättung mit einem Informationsverlust verbunden. Im Fall $d/\sigma_y = 0,6$ kann die Glättung ohne Informationsverlust bis zu einem Verhältnis $\sigma_{\bar{y}}/\sigma_y = 0,5$ erfolgen. Für kleinere Werte d/σ_y darf die Glättung noch weiter getrieben werden.

Setzt man $\sigma_y/y_{\max} = 0,01 = 1\%$, so muss für das geforderte Verhältnis $d/\sigma_y \leq 0,6$ der systematische Fehler $d/y_{\max} < 0,6\%$ sein. Nach Abb. 3 ergibt sich bei einem Glättungspolynom 2. Grades, dass die Breite des Glättungsintervalls maximal 50% der Halbwertsbreite betragen sollte. Der minimal zulässige Wert $\sigma_{\bar{y}}/\sigma_y = 0,5$ wird mit $\text{FB} = 9$ ($k = 2$) (Abb. 4) und $\text{FWHM} = 17$ erreicht.

Eine Erhöhung von FWHM bei gleichbleibendem Verhältnis von Glättungsintervall zu Halbwertsbreite erhöht auch FB. Damit verbunden ist eine stärkere Rauschminderung und ein Unterschreiten von $\sigma_{\bar{y}}/\sigma_y = 0,5$. Das bedeutet Informationsverlust, da jetzt der Informationsgehalt durch den systematischen Fehler bedingt ist. Es ist deshalb bei konstantem Verhältnis Glättungsintervall/Halbwertsbreite zwecklos, FWHM vergrössern zu wollen.

Falls $\sigma_{\bar{y}}/\sigma_y$ unterschritten werden soll, muss der systematische Fehler verringert werden. Das kann man durch Vergrössern des Verhältnisses FWHM/FB erreichen, d.h., die Zahl der Messpunkte je Halbwertsbreite muss schneller wachsen als die Fensterbreite. Auf diese Weise wird es möglich, die Schranke $\sigma_{\bar{y}}/\sigma_y = 0,5$ ohne Informationsverlust beliebig zu unterschreiten. Es muss lediglich die Unabhängigkeit zweier benachbarter verauschter Messpunkte gewahrt bleiben.

LITERATUR

- 1 A. Savitzky und M. J. E. Golay, *Anal. Chem.*, 35 (1964) 1627.
- 2 J. Steinier, Y. Termonia und J. Deltour, *Anal. Chem.*, 44 (1972) 1906.
- 3 C. G. Enke und T. A. Nieman, *Anal. Chem.*, 48 (1976) 705A.
- 4 J. P. Porchet und H. H. Günthard, *J. Phys. E*, 3 (1970) 261.
- 5 M. U. A. Bromba und H. Ziegler, *Anal. Chem.*, 53 (1981) 1583.
- 6 G. Marx, V. Hopfe, R. Rost und P. Lehm, *Wiss. Ztschr. Friedrich-Schiller-Univ. Jena, Math.-Nat. R.*, 25 (1976) 825.
- 7 H. Ziegler, *Appl. Spectrosc.*, 35 (1981) 88.
- 8 K. Eckschlager, *Anal. Chem.*, 49 (1977) 1265.

ENHANCEMENT OF THE PERFORMANCE OF ANALYTICAL LABORATORIES BY A DIGITAL SIMULATION APPROACH

T. A. H. M. JANSE and G. KATEMAN*

Department of Analytical Chemistry, Faculty of Sciences, University of Nijmegen, Toernooiveld, 6525 ED Nijmegen (The Netherlands)

(Received 26th October 1983)

SUMMARY

A laboratory for water quality monitoring, with 9 technicians working on 60 procedures, is modelled. The computer simulation model based on queueing theory is validated, giving further proof that this theory is applicable to existing laboratory organisations. Important parameters in the model are descriptions of the sample input and the existing work capacity of the laboratory and the relationships between batch intake and batch processing of samples. Various simulation experiments demonstrate the possibilities of investigating organisational features which could lead to enhanced performance with increased yield of analytical information.

An analytical laboratory can be viewed in different ways: as a means of obtaining solutions to problems, as a means of making money, or as the maintenance of an essential, probably uneconomic, service department. Analytical laboratory management has to deal with many aspects. Basically, information is obtained from samples by applying analytical procedures. The organisation created must supply the required information, using the available means and methods; this includes purely technical structures (administration, coordination, service facilities) and the creation of a good social and psychological climate [1]. The performance of the laboratory, i.e., the throughput of analytical information, is influenced by organisational decisions at all levels.

This paper is mainly concerned with the analytical performance. An earlier theoretical modelling [2] has shown that, in addition to the traditional analytical items such as accuracy, precision and detection limit, waiting times should be considered; they reflect laboratory capacity. However, theoretical queueing models oversimplify real laboratory organisation, which is better described by the operations research technique of digital simulation [3–5]. Many practical aspects might be so investigated; only some are considered here. The construction and results of a digital simulation model from a small laboratory for water quality monitoring are presented.

Description of the laboratory

The laboratory considered deals with water quality monitoring and is situated near a municipal potable-water plant (G.E.B., Dordrecht). Analyses

are done for this plant and for many external customers, e.g., from sewage purification plants, swimming pools, and other facilities. The management plans carefully to ensure a steady sample load: a sample program is arranged annually and updated continuously. All samples entering the laboratory are distributed among the different analytical sections, in order to obtain a maximum batch size. Results are mostly collected weekly, re-checked and, if complete, reported.

Apart from these routine analyses, other jobs include quality-control problems, maintenance and research projects. In the general plan about 15% of the working time is available for these projects. The staff consists of twelve men (1979 situation); nine are available for analytical jobs. The workers rotate around the different groups of analytical methods. The organisation is such that 37,000 routine analyses as well as other tasks can be handled yearly.

Formulation of the problem

Theoretical laboratory models indicate how the information obtainable is influenced by limited laboratory capacity. More realistic models allow extrapolation of some organisational effects on this information. How far digital simulation models could contribute could be important.

The main difference between the theoretical models and the laboratory investigated here is the batch-input/batch-processing way of sample handling; grouped samples enter the laboratory, and are regrouped for batch processing. Obviously, the more samples per batch, the smaller the overhead per sample. Maximal batch size will obviously be limited by the available equipment, space and technical skill. Minimal batch sizes are established particularly where the batch processing involves a long initial period; samples may be collected over a period of days or weeks for efficient processing, which obviously affects waiting times. Within certain limits, the laboratory capacity is strongly influenced by the minimal and maximal batch sizes, and this affects the total yield of information. This problem has been considered [6] but is treated further here.

A concrete problem in the laboratory considered was that the time reserved by the management for research projects (15%) was never actually achieved. Too often, research projects had to be cancelled, because of lack of capacity. Organisational measures were ineffective in improving this situation. A simulation model might provide a solution. Another problem was the increasing number of routine analyses requested (e.g., 37,000 in 1979, 41,000 in 1982) and the increasing complexity of the work (60 procedures in 1979, 77 in 1982). Decisions had to be taken on equipment purchase, and automation projects demanded organisational adaptation. A simulation model as a management tool, or just the presentation of the parameters involved, could be helpful in these management decisions.

The modelling

Many textbooks on modelling and simulation are available [7–10]; details

need not be repeated here. One of the main characteristics of this operations research technique is a continuous search for detailed information, which confronts the laboratory management with unexpected questions.

The main information for the systems analysis was extracted from the administration files for 1979. The records contained the required information on sample submission date, reporting date and the analytical procedures performed per sample. The personnel records contained information on absences, as well as detailed information on daily activities. Information on the analytical procedures was already collected for laboratory planning purposes. During synthesis and verification of the model, other detailed information was necessary, but the aim was always to keep the model as simple as possible. Basically, the simulation model is a queueing model, consisting of jobs and workers, constructed in order to visualize the laboratory organisation and its impact on waiting lists and idle times.

THE MODEL

A rough outline of the laboratory throughput is shown in Fig. 1; it includes only the four main analytical sections and the analyses assigned to them. Other activities were not considered in the model, partly to keep the model simple and partly because they interfered insignificantly with the routine activities (e.g., sampling, cleaning and administration). The first characteristic of the system, which requires adequate description, is the way that samples are submitted to the laboratory and are routed for processing.

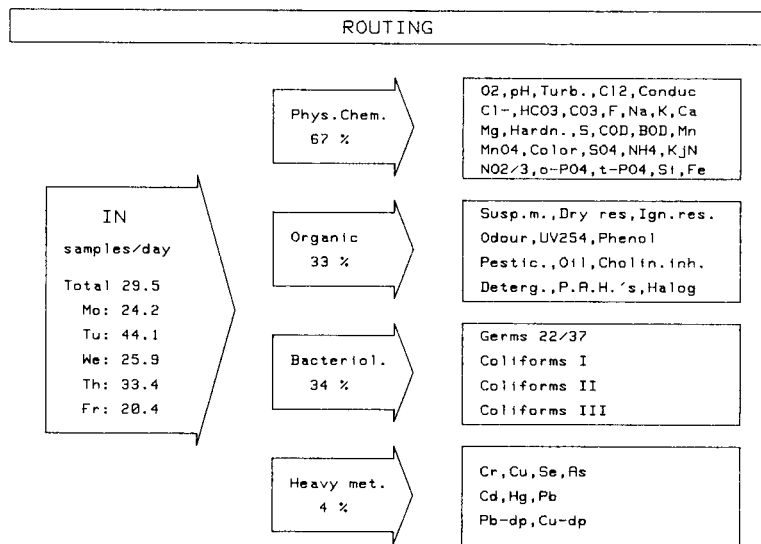


Fig. 1. The design of the laboratory, showing the sample flow; the analytical procedures are listed in Table 3.

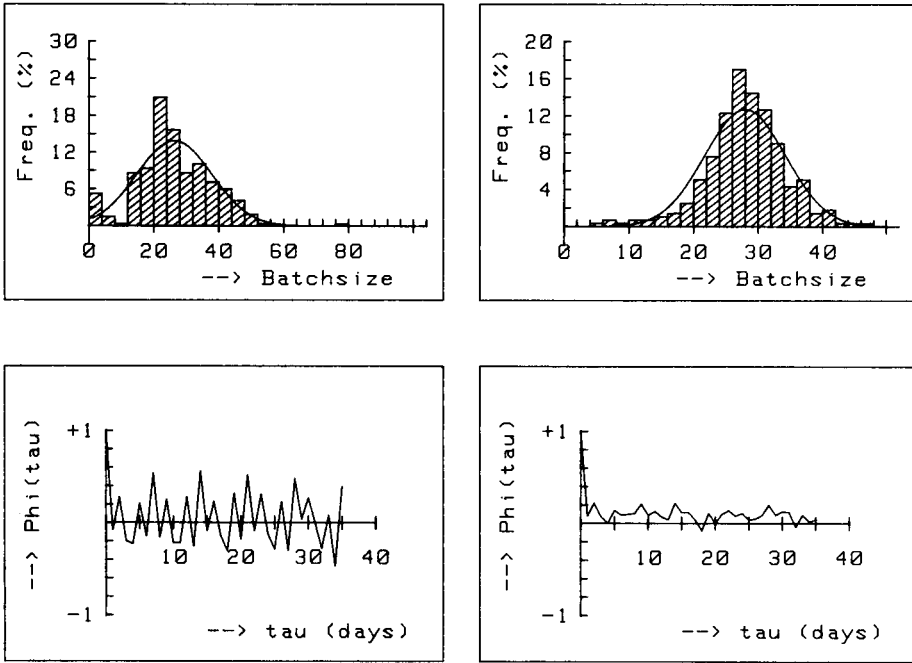


Fig. 2. Histograms, with fit functions, and autocorrelograms, computed from the daily batch size of samples entering the laboratory. Left; without correction. Right: after correction for daily variation.

Figure 2A shows the distribution of the input sample batch size. The autocorrelation plot shows a significant weekly periodicity in the arrival pattern; in the planning scheme, samples arrive preferably on Tuesdays and Thursdays (Fig. 1). This pattern is also observable at the analytical sections, and at the work sites, where the actual profit from the established pattern is found. After correction for this weekly periodicity, only a minor fortnightly fluctuation remains. As shown in Fig. 2B, the corrected time series of the daily incoming batch size shows no significant autocorrelation. The distribution of this corrected batch size is not significantly different from a Gaussian distribution (Kolmogorov-Smirnov test at the $\alpha = 0.05$ level). This means that the input batch size is correctly described by a daily mean and a residual variance.

Routing of the samples

The simplest way to simulate the routing of the samples, is to investigate the probability of samples entering every section. This is correct provided that these probabilities are independent; but a relationship was clearly present. Instead of investigating all possible conditional probabilities, it is easier to represent the routing to the sections by investigating the probability of all combinations. From the fifteen possibilities, eleven are relevant. Table 1

TABLE 1

Routing; the probabilities of samples being processed in one or more sections

Section							
Physical chemistry	Yes	Yes	Yes	Yes	Yes	—	—
Organic	—	—	Yes	Yes	Yes	Yes	—
Bacteriology	—	Yes	—	Yes	Yes	—	Yes
Heavy metals	—	—	—	—	Yes	—	—
Percentages	39	15	7	5	3	20	11

shows the seven principal routings to the sections, with their probabilities. In the same way, the problem for all possible combinations of analyses for every sample is investigated. For the organic, bacteriology and heavy metals sections with a limited number of combinations, this is no problem. As an example, the requests for the organic section are shown in Table 2. Description of the physical chemistry section is more complicated; for the thirty available procedures, $>10^9$ combinations are possible. Only 192 combinations were found; 11 combinations covered almost 60% of the samples, minor deviations from these eleven combinations included. The other 40% can be described in terms of individual probabilities over the individual procedures, as no further significant probability interactions were indicated.

Those eleven combinations were found by using pattern recognition techniques (ARTHUR [11]). All analytical combinations occurring for more than 10 samples, were used as patterns with thirty binary features indicating the need for an analytical procedure to be applied to the sample. Hierarchical clustering produced 11 clusters at the 0.7 similarity level. These 11 combinations were compared in subsequent clustering experiments with the other samples processed in the physical chemistry section. About 40% of the

TABLE 2

Routing; the probabilities of requests for organic analysis in the organic section

Method							
Suspend. Mat.	—	—	—	—	Yes	Yes	—
Tot. residue, dry	—	Yes	—	—	—	—	—
Odour	—	—	—	Yes	—	Yes	—
Phenol	—	—	—	—	—	—	Yes
Oil	—	—	—	—	—	—	Yes
Pesticides	—	—	Yes	—	—	—	Yes
Cholinest. inh.	—	—	Yes	—	—	—	Yes
Detergents	—	—	—	—	—	Yes	—
PAH	—	—	—	—	—	—	Yes
U.v.-254	—	—	—	Yes	—	Yes	—
Organic halog.	Yes	—	Yes	—	—	—	Yes
Percentage	16	13	2	34	23	9	3

samples could not be assigned to any of these 11 main analytical packages, indicating no further correlations. These analytical combinations were not distinguishable from random trials.

The eleven frequently occurring combinations were clearly recognized by the laboratory management and related to particular objects.

Laboratory capacity

The laboratory capacity was recorded daily by representing the activities of every member of the laboratory by means of a color code; translation of this code produced a file which gave a one-year view of all activities with a two-hour resolution. Thus the daily capacity (in hours) assigned to every section as well as the total capacity, was known. Statistical investigation again showed a one week periodicity. The distributions are shown in Fig. 3. After correction for this periodicity, a strong frequency with a period of two weeks remained for the heavy metals section, because samples for that section were collected over 2 or 4 weeks for batch processing. This is also visible in the histogram from the daily capacities allocated to the heavy metals section (Fig. 3). Further studies showed no other significant fluctuations or other autocorrelation values. The remaining distributions were statistically normal distributions; like the sample input, the capacity present in each section is adequately described by a daily mean and a variance. For the heavy metals section, the characteristics for the odd and even weeks are obviously different. The time spent in research activities gives another

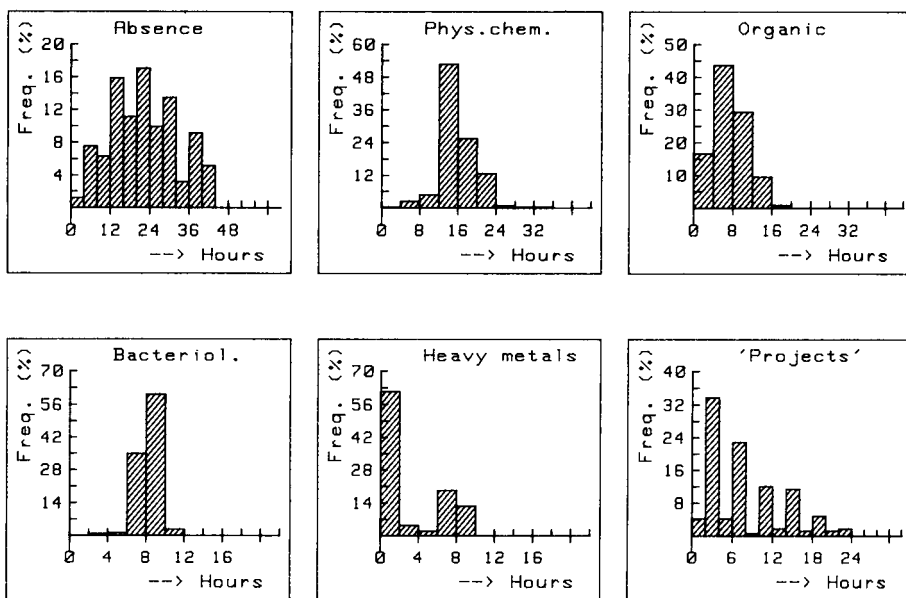


Fig. 3. Histograms, showing the distribution from absence and presence of the analysts with the various activities, in man-hours/day.

picture; a weekly fluctuation is again visible, with Mondays and Fridays being favoured. However, the distribution shows a strong skewness, more an exponential than a Gaussian distribution. A correct fit was not possible because of the way the data were recorded (mostly rounded off to periods of at least 4 h). This distribution indicates that queueing aspects are really present. If research activities are really given lower priority than routine activities, they are actually an "idle-time" distribution. In the simplest queueing model (the M/M/1-model), these are exponentially distributed.

Organisation: correlation between workload and capacity

An important feature is the relation between daily workload and the available capacity (man-hours). If a daily re-allocation of capacity over the four sections is possible, depending on the number of samples entering each section, there should be a significant correlation between these parameters. Because of the weekly periodicity in both sample input and the capacity, the cross-correlations show the same pattern for all sections. No time lag is observable, not even for the heavy metals section, mainly because of the low capacity and low sample input on Fridays. After the correction for periodicities, the cross-correlations were recalculated. Only for the physical chemistry section was there a significant correlation between the daily sample input and the allocated capacity (Fig. 4A). However, this correlation is very low (0.50) and shows that the laboratory planning is mainly based on the weekly periodicity. For the heavy metals section, the remaining pattern is mainly fortnightly, particularly in the capacity assignment: minor fortnightly fluctuations, with some time lag, are visible in the cross-correlation after the week correction, as shown in Fig. 4B. This confirms the observed weekly pattern for total sample input; no specific sample input planning is possible for samples that require analysis for some heavy metals.

Further correlation analysis showed no other unexpected significant correlations between all variables. A significant, but low, negative correlation

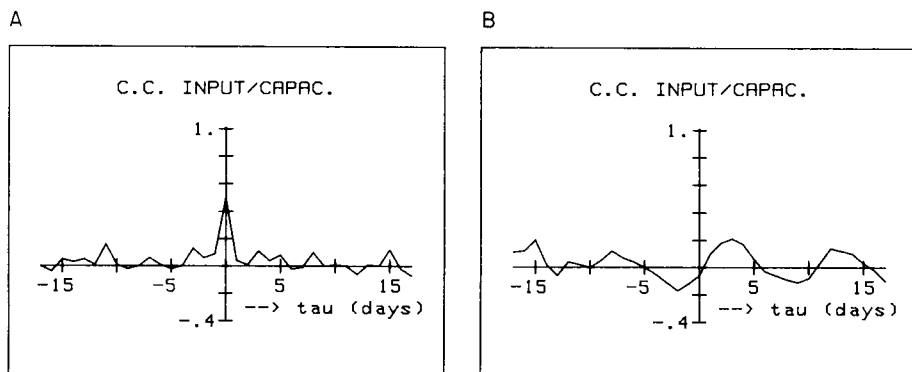


Fig. 4. Cross-correlograms (CC) showing lagged correlations between the number of required analyses and the allocated capacity (in man-hour) for two sections: (A) physical chemistry; (B) heavy metals.

of -0.42 was found between the research capacity and the absence of workers, confirming the idea of 'idle time' being used for the relatively low-priority 'research' activities.

The analytical procedures

The most important characteristics of the analytical procedures in the context of this work are the batch time $C1$, and the sample time $C2$; the time required to process a batch of N samples is $AT(N) = C1 + N \times C2$. In this way, the processing time is a function of batch size only. In reality, this processing time is a stochastic variable, influenced by many sources, as it is a human activity with many man/machine interactions. No attempt was made to describe the actual work-time requirement for the batch processing of the samples in more detail, statistically or otherwise, as this would demand a classical Taylor mode of collecting real job times. The laboratory management knew by experience that the main stochastic feature in the batch-processing time was most probably the daily batch size. Table 3 shows a list of all the analytical procedures used in the four sections, with the batch-processing and sample times. The minimal and maximal batch sizes are also shown; most of them are related to equipment and official procedure instructions.

Some of the procedures are separated in time by subprocedures. All samples processed for metals must be preserved immediately after entering the laboratory; this averages 15 min per sample. Extraction procedures (e.g., for gas chromatography) averages 30 min per sample. All the bacteriological tests take at least two days. For the biological oxygen demand (BOD) the time between the two subprocedures has to be seven days (BOD-7). All these factors are included in the simulation model. Time spent on other jobs (e.g., preparation of reagents, discussions of work, and standardisations) are not included in the $C1$ and $C2$ times, and are mostly done once a week; a survey of these jobs, with the times needed, was obtained from the laboratory management and included in the model.

Priorities

Table 3 contains a priority factor for the procedures: these refer to the speed with which processing must be done and is related to the stability of samples. Thus "0" means that the sample must be processed as soon as possible, without delay; "1" means processing within 24 h; "2" means that a delay of some days is permitted, provided that the sample can be refrigerated if necessary; "3", "4" and "5" represent different periods of sample collection (1, 2 and 4 weeks, respectively). In order to simulate the actual sequence of processing the samples, this priority is of great importance. Other parameters involved in this sequence algorithm are the current batch size and the time that the oldest sample in the batch has waited.

More priorities concerning jobs to be done are also present. For obvious reasons, the highest priority is assigned to jobs such as the preparation of reagents. The next highest priority is given to a number of samples taken

TABLE 3

Analytical procedures and their characteristics

	<i>C1</i> ^b	<i>C2</i> ^b	Min	Max	<i>PF</i> ^a		<i>C1</i> ^b	<i>C2</i> ^b	Min	Max	<i>PF</i> ^a
<i>Physical chemistry</i>						<i>Organic</i>					
Oxygen	6	3	0	—	0	Suspended mat.	0	15	0	—	1
pH	9	3	0	—	0	Tot. residue(dry)	0	10	0	—	1
Turbidity	3	3	0	—	0	Odour	10	40	0	5	0
Chlorine	2	2	0	—	0	U.v.-254 abs.	5	5	0	—	1
Carbonate	3	3	0	—	0	Phenol	80	20	4	—	3
COD	20	10	0	16	1	Oil	40	10	4	—	4
Permang. cons.	5	5	0	—	1	Pesticides	120	10	8	—	4
Color	3	3	0	—	1	Cholinst. inh.	160	10	8	—	4
BOD	0	20	0	—	0	Detergents	45	15	4	—	2
Ammonium I	12	8	0	—	0	PAH	30	80	4	—	4
Ammonium II	0	8	0	—	0	Organic halog.	0	15	0	—	3
Kjeldahl-N	10	10	0	16	1	<i>Bacteriology</i>					
Nitrite	3	3	0	—	0	Germ 22	7	7	0	—	0
Nitrate	16	4	0	—	0	Germ 37	7	7	0	—	0
Orthophosphate	20	5	0	—	0	Coliforms I	8	8	0	—	0
Total phosphate	15	15	0	—	1	Coliforms II	8	8	0	—	0
Silicate	12	3	0	—	1	Coliforms III	0	26	0	—	0
HCO ₃ ⁻	4	4	0	—	0	<i>Heavy metals</i>					
Sulfide	4	7	0	4	2	Chromium	95	7	5	—	5
Conductivity	6	3	0	—	2	Copper	95	7	5	—	4
Chloride	8	4	0	—	2	Selenium	170	7	8	—	5
Sulfate	4	7	0	—	2	Arsenic	155	7	8	—	5
Fluoride	15	5	4	—	3	Cadmium	145	7	5	—	4
Sodium	25	5	4	—	3	Mercury	160	5	5	—	5
Potassium	25	5	4	—	3	Lead	155	7	5	—	4
Calcium	0	5	0	—	2	Lead solub.	70	1	2	—	4
Magnesium	0	1	0	—	2	Copper solub.	155	7	2	—	4
Tot. hardness	5	5	0	—	2						
Manganese	4	4	0	—	2						
Iron	16	4	0	—	2						

^aPriority factor. ^bTime in min.

from streams in the water preparation plant to be monitored (e.g., for total hardness). This is an object-orientated priority; information is required within a given period. Actually, these samples are generated separately in the model input description: most of them enter the laboratory daily.

Conflict between these different kinds of priorities is almost unavoidable. However, this was of minor importance, because no object-orientated priority was given to samples which had a priority factor exceeding 2 (i.e., storable for ≥ 1 week). In this way, a simulation of all the activities of the workers could be placed in sequence, with a minimal number of details concerning all the possible daily activities.

THE DIGITAL SIMULATION MODEL

The computer simulation model was written in FORTRAN-IV for an IBM-370/158 computer system. A standard simulation subroutine package (GASP [12]) was included. This package was extended with standard statistics such as goodness-of-fit tests and autocorrelation routines, and sub-routines for generating independent uniform, gaussian, exponential and erlang-k distributed random numbers. No advanced variance reduction techniques were used: common random numbers were used in the simulation experiments. All the simulations were done over a total time of 350 working days (with 10 hours a day), with a short prurun.

The model works as follows. Samples, with their requests for analysis, are generated by the appropriate parameters and random number generators, and positioned in a virtual "administration" queue. Every analysis to be done is copied and placed, according to an analytical sequence number, in the proper section queue to form batches again. The worker capacity is generated in the same way; every "worker" checks the waiting line for activities and removes the one selected, according to the priority sequence algorithm mentioned above. After the time needed to complete the "job", the sample in the administration queue is updated and the next task can be chosen. Periodically (daily, weekly or even monthly), the administration queue is checked to remove the finished samples.

The simulation output consists of pictures of over-all and section delay times, waiting times and idle times, as well as a survey of input and tracer parameters. An output of "daily reports" is also possible; this shows the numbers of samples entered, present and finished, results collected in batches, jobs done, and capacities used. Actually, a very realistic picture of a laboratory with a completely automated administration was obtained, despite the simulation.

VALIDATION

The key step in the modelling procedure is the validation stage. First, partial validation was done during the model construction, concerning only the description of the sample input stream. No statistically significant difference was observed between the simulated and actual input batch-size distribution (K.S.-test, $\alpha = 0.01$).

The main validation test was executed on the overall delay times (i.e., the time between sample entrance date and reporting date). A representation of the actual values is given in Fig. 5; simulation results are shown in Fig. 6. Although some differences are visible, the total delay time distribution gives no significant difference between the actual and simulated data, according to the K.S.-test ($\alpha = 0.01$). Table 4 shows the mean delay times for every section; there is no significant difference between the model and the real laboratory data. Finally, the idle-time distribution is shown in Fig. 7; although

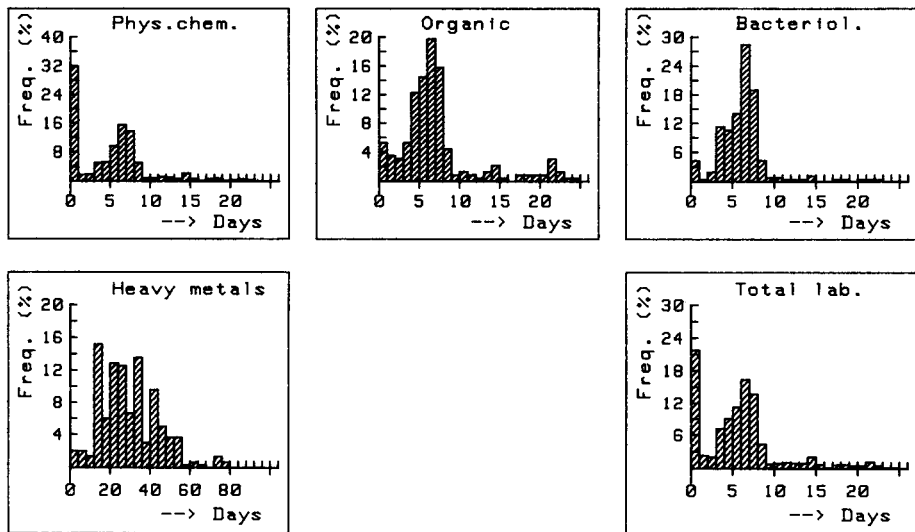


Fig. 5. The actual distributions of delay times for the four sections and the total laboratory.

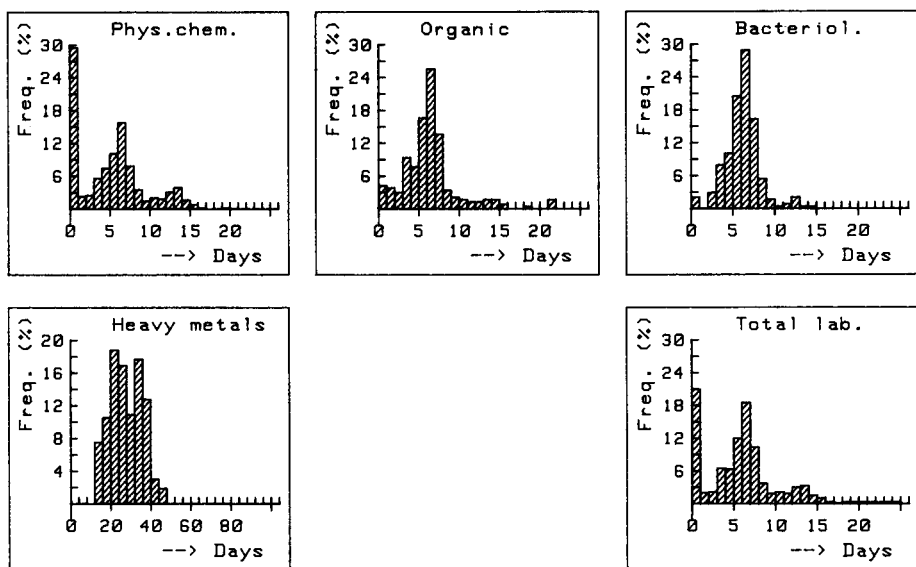


Fig. 6. The simulated distributions of delay times for the four sections and the total laboratory.

no correct test procedure was possible, the resemblance of the simulated idle-time distribution and the research-activity distribution (Fig. 3) confirms, at least, that the daily job assignment is close to reality.

At this stage, the validation step was completed. Of course, more validation tests would be preferable. Some validation tests were impossible because

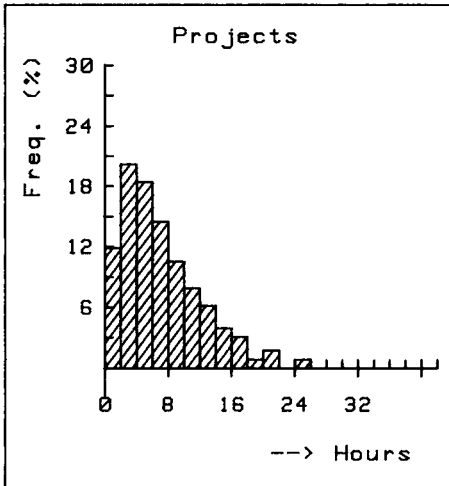


Fig. 7. The simulated daily idle-time distribution for the total laboratory.

comparative real data were not available (e.g., waiting times instead of delay times), whereas other, more detailed, tests would probably show significant differences between actual data and the simulation results (e.g., testing correlation values). This would require addition of more details into the simulation model and so would complicate matters. Actually, the model constructor may decide to add more details depending on the kind of experiments he wants to perform, and the available time for the modelling procedure. However, this means that the experimental results should be treated with care in order to avoid erroneous conclusions.

RESULTS

With the model, various experiments were done, for theoretical and practical reasons. Parameters far off their actual values were not included in these experiments. First, because the model is only partly a reflection of reality, and because the validation is only based on the situation with the actual parameter values; the more deviation from reality is introduced, the

TABLE 4

Mean delay times (days) for the sections: validation

Section	Real	Simulation	St. dev.
Phys. chem.	5.5	6.1	0.2
Organic	9.2	9.2	0.8
Bacteriology	6.2	6.6	0.12
Heavy metals	29.2	27.8	0.5

less confidence can be placed in the resulting output. Secondly, if in reality a large parameter change actually did occur, it is very likely that measures would be taken to adapt the organisation to the new circumstances.

The utilization factor is the main parameter to consider in the simplest theoretical queueing models. A value of 0.84 was computed for the laboratory using the real data given in Table 5. This is in good agreement with the annual laboratory survey report from which the effective working capacity per day was calculated as 6.5 h, resulting in an almost equal utilization factor of $6.5/8 = 0.81$.

According to the simple theoretical queueing models, an increased workload should result in an exponential increase in waiting and delay times, and consequently in a decrease of the analytical information yield. Figure 8A shows the consequences for the mean delay times arising from a 20% variation in the average sample-input batch size. The batch-processing mechanism acts like a buffer on the increased batch sizes: the mean processing time per sample is automatically lowered by processing in larger batches, thus preventing a proportional increase in the utilization factor. The mean delay time does increase, but far from exponentially. An interesting observation is the slight decrease in mean delay-time for the heavy metals section; this happens because all such samples are collected over two or four weeks; the minimal batch size is obtained earlier when the arrival rate of the samples increases. In Fig. 8B, no sample delays are shown, but the waiting times before the requested results are obtained. The mean waiting times for the different processing-priority classes (see also Table 3) are shown. At first sight, the class "3" and "4" priorities are most sensitive to the increased sample input. However, the class "0", "1" and "2" priorities allow storage for no longer than, respectively, some hours, one day or two days. And although the increase in simulated waiting time for the group "0" samples is only from 0.44 day to 0.71 day, this results in an increased violation of the "no day delay" rule from 4.7% to 18.4% of the total processing demand. For class "1" samples, this violation increases from 17.6% to 60.5%; for class "2" samples, it increases from 6.7% to 27.1%. However, these percentages cannot be directly trans-

TABLE 5

The 1979 overall survey (hours) for the real laboratory

Section	Workload	Capacity
Phys. chem.	3471	4486
Organic	2027	2318
Bacteriology	1747	2192
Heavy metals	718	731
Research proj.	(1478)	1478
Total	9441	11205

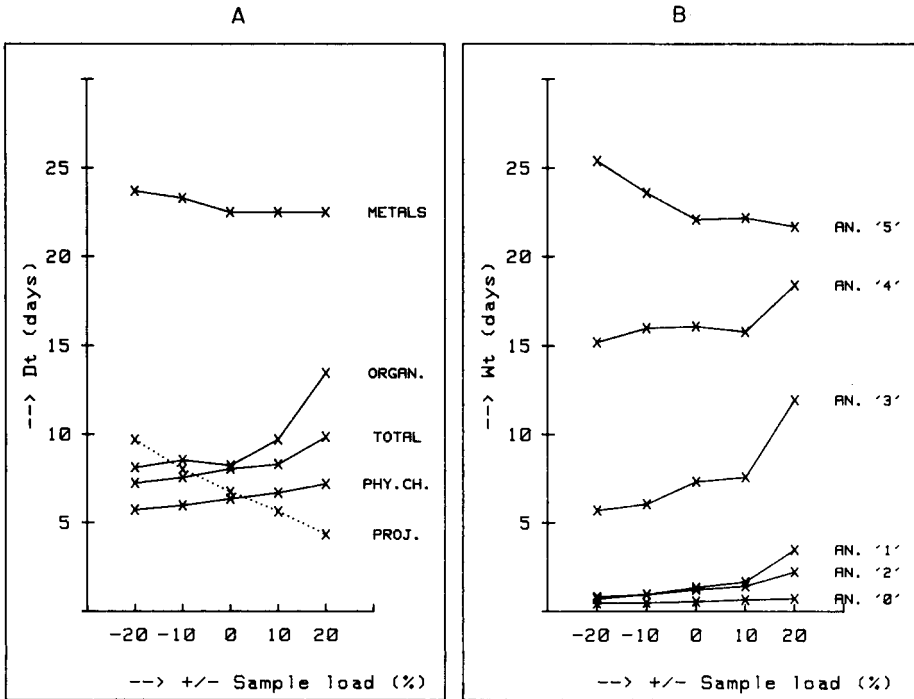


Fig. 8. Simulations: effect of increasing sample load on mean delay time (Dt), mean waiting time (Wt) and mean idle time (dashed line). The vertical scale is in hour/day for the idle times. (A) For various sections; (B) for procedures with different priorities.

ferred to the real situation: without doubt, proper organisational actions will lower them. But the mechanism is present, and the information yield is influenced negatively by it; the storage of water samples is a difficult matter, frequently mentioned in literature (see, e.g. [13, 14]). The longer the storage period, the greater the uncertainty about the final result. Thus the information yield can be expressed in terms of standard deviations of the analytical results. The class "3" and "4" samples show the largest increase in waiting times, because of the lower priority; storage is allowed for the preserved samples. In contrast to the group "5" samples, the pre-fixed minimal batch size is low so that less waiting time is needed to reach this batchsize.

Figure 8A also indicates how the idle-time behaves with increasing workload. If the batch-processing mechanism were absent, a 20% increase of the input-stream would result in almost no idle-time. Clearly, the situation now is less dramatic: the model indicates about 17% decrease in the time available for research activities with every 10% increase in sample input.

The research activity

The research activities are organisationally the most difficult to plan, because of the low priority. The very nature of such work demands adequate

time; an "idle" time of < 2 h is too short even to start. Actually, the management system prevents the occurrence of many scattered short periods of "idle" time over all workers, and tries to concentrate it on one section or worker, which gives time for some supplementary activity. In order to simulate this translation of "idle" time to available time for research activity, the following routine was built in: all idle-times left daily were rounded off to the lower integer and then summed over all workers present. This results in the histogram shown in Fig. 7. The simulated research-time is 1458 ± 34 (standard deviation) h over a total 350-day run. The actual amount was 1478 h. All the other relatively short idle-times are really idle or are devoted to numerous smaller jobs in the laboratory. An action that might be taken to increase the time available for research activities, is simply to increase their priority. A simulation experiment was done with the highest possible priority for the research activities. The result was very similar to the effect of a 20% input increase. Only the minimal batch-size effect was absent; all sections showed an increasing mean delay time. The consequences for the analytical information yield were explained above, and were accordingly unacceptable to the management.

The input batch-size variance

The annual sample planning scheme produces the input batch-size distributions shown in Fig. 2. The influence of such planning schemes on laboratory performance is undoubtedly favourable. A comparison can be made with the theoretical M/G/1 and D/G/1 queueing models [2] having, respectively, an unpredictable Poisson input, and an input with a fixed arrival pattern, without stochastic fluctuations. Waiting times in the latter might be completely absent. In the simulation model, this effect is considered by means of a change in the residual input batch-size variance, as mentioned in the sample input description (see also Fig. 2B). In combination with the weekly pattern in the sample load, this results in a standard deviation for incoming batch sizes, as reported in Table 6, together with the other main simulation results: none of the changes in the resulting delay times is significant. For the idle-times, there is even a slight increase, though it is not significant, according to the measured uncertainty in the output result. The absence of an effect on

TABLE 6

Simulation results for a change in the input sample batch size (days)

Stand. dev. input	15.7	16.0	16.9	17.9	18.3	
Total mean delay time	8.09	8.08	8.41	8.31	8.34	$\pm 0.3^a$
Mean research time	6.63	6.78	6.66	7.05	6.88	$\pm 0.3^a$
Mean waiting time						
for "0" samples	0.51	0.54	0.56	0.58	0.60	$\pm 0.03^a$
for "1" samples	1.37	1.35	1.62	1.78	1.67	$\pm 0.3^a$

^aStandard deviation.

the delay times might be explained as follows: the sample input is controlled by the planning schemes in such a way that further control enhances laboratory performance slightly or not at all. The delay times are probably more influenced by variations in the available capacity. A decreasing input batch-size variance (more input control) might even result in less time available for research activities.

Maximal batch size

Some batch sizes for sample processing are limited because of equipment (Table 3); this is an essential parameter on model construction. All procedures without a maximal batch size were given a maximum batch size of 40. The effects of decreasing this batch size are shown in Fig. 9; it can be seen that the maximal batch-size level starts to interfere with performance at about 10 samples per batch. Of course, the increase in waiting and delay times is due to a limited number of procedures, with a relatively high demand. This model could trace these nodal points. But care is needed, as this would require more detailed experimentation; no "equipment" nodes were implemented in the simulation model. For example, the purchase of an automatic analyser might be considered. Important factors in this decision are: the sample input and related organisation to ensure large batches for processing,

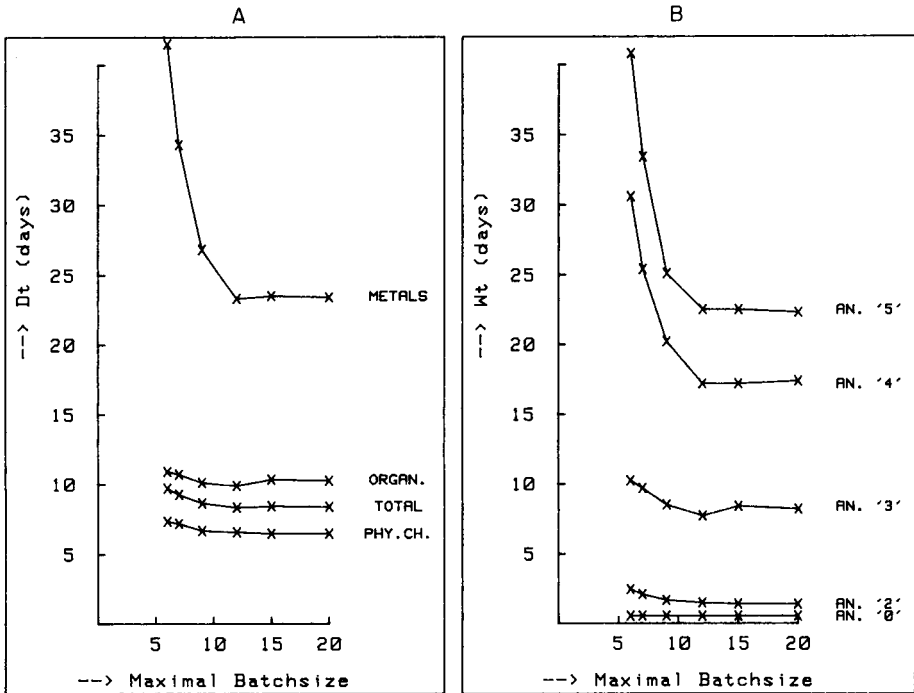


Fig. 9. Simulations: effect of decreasing maximal batch size on mean delay time and mean waiting time. (A) For various sections; (B) for procedures with different priorities.

and a comparison between the available equipment and the automatic analyser in the actual laboratory environment. This simulation model might be used to give a computer-aided decision with respect to the former aspect, but the latter aspect requires a more detailed simulation. However, the simulations show that at a certain level of maximal batch sizes, the buffering capacity of the laboratory could be considerably reduced. Reconsideration of the length of the periods for sample collection or other organisational measures might enhance the laboratory performance.

CONCLUSIONS

Laboratory organisation can be described in terms of queueing theory, based on workload and capacity. By pure theoretical modelling, it was shown [2] that without any organisation, a utilisation factor of 0.5 is optimal. If more "organisation factors" are added, the "optimal" utilisation factor is higher. In a real situation, a high utilisation factor leaves little room for other planned activities: additional jobs, such as "research projects", are within reach, up to a utilisation level of about 0.85, provided that they are given lower priority. An increase in this priority will almost unavoidably result in increased waiting times elsewhere, thus influencing the information yield with respect to sample processing. More detailed research is required to compute the latter effect. Storage of samples causes a decrease of information, related to the decreased reliability of the analytical result. However, the purpose of the analysis must also be considered; delays of results required for process control will clearly be far more important than delays for samples taken for annual surveys. Organisationally, the batch-input/batch-processing mechanism acts as a buffer: to some extent, the more samples enter the laboratory, the less time is needed per sample for processing. The simulation model allows the effects of minimal and maximal batch sizes to be investigated. The modelling technique is thus shown to be valuable for management decisions. However, the model construction requires intensive bookkeeping, including not only sample features (e.g., sample input) and handling (e.g., batch processing) but also worker features (e.g., allocation of capacity) and processing characteristics (e.g., $C1$ and $C2$ times, minimal and maximal batch size).

More detailed simulation requires still more detailed information (e.g., equipment and its type, quantity and downtimes). Such system information is more readily available when an appropriate data-acquisition system is implemented. Of course, attention must be given to social and psychological aspects in the use of such system information, but computerisation of some administrative aspects is now almost unavoidable. The considerations outlined above could be helpful in a more systematic approach to laboratory management.

We thank Ir. E. A. v. Naerssen and Ing. J. A. v. d. Bom for their cooperation in this research; we also thank Drs. P. C. Thijssen and Mr. C. Baerwaldt for their contribution in processing the large amount of data.

REFERENCES

- 1 R. Goulden, *Analyst* (London), 99 (1974) 929.
- 2 T. A. H. M. Janse and G. Kateman, *Anal. Chim. Acta*, 150 (1983) 219.
- 3 B. G. M. Vandeginste, *Anal. Chim. Acta*, 112 (1979) 253.
- 4 B. G. M. Vandeginste, *Digital Simulation of a Laboratory for Structural Analysis*, thesis, Catholic University of Nijmegen, 1980.
- 5 I. K. Väänänen, S. Kivitikko, J. Koskenniemi, J. Koskimies and A. Relander, *Method. Inf. Med.*, 13 (1974) 158.
- 6 J. G. Vollenbroek and B. G. M. Vandeginste, *Anal. Chim. Acta*, 122 (1980) 435.
- 7 G. A. Mihram, *Simulation: Statistical Foundations and Methodology*, Academic Press, New York, NY, 1972.
- 8 T. H. Naylor, J. L. Balintfy, D. S. Burdick and Kong Chu, *Computer Simulation Techniques*, Wiley, New York, NY, 1966.
- 9 D. Gross and C. M. Harris, *Fundamentals of Queueing Theory*, Wiley, New York, NY, 1974.
- 10 F. F. Martin, *Computer Modelling and Simulation*, Wiley, New York, NY, 1968.
- 11 B. R. Kowalski and C. F. Bender, *J. Am. Chem. Soc.*, 94 (1972) 5632; 95 (1973) 686; 96 (1974) 916.
- 12 J. A. G. M. Kerbosch and R. W. Sierenberg, *Discrete Simulatie*, Samsom, Alfen aan de Rijn, 1973.
- 13 F. J. Sprenger, *Z. Wasser Abwasser Forsch.*, 11 (1978) 128.
- 14 C. L. Chakrabarti, K. S. Subramanian, J. E. Sueiras and D. J. Young, *J. Am. Water Works Assoc.*, 70 (1978) 560.

RAPID RADIOCHEMICAL SEPARATION IN NEUTRON ACTIVATION ANALYSIS

Part 1. The use of C₁₈-Bonded Silica Gel and Selective Complexation for Determinations of Manganese, Copper and Zinc in Biological Materials

J. J. FARDY*, G. D. McORIST and T. M. FLORENCE

CSIRO Division of Energy Chemistry, Lucas Heights Research Laboratories, Private Mail Bag 7, Sutherland, NSW, 2232 (Australia)

(Received 21st September 1983)

SUMMARY

A rapid radiochemical separation method based on the removal of metal ions by columns of C₁₈-bonded silica gel after selective complexation by 8-quinolinol, ammonium pyrrolidinedithiocarbamate or cupferron is described for the determination of manganese, copper and zinc in neutron-activated biological materials. The removal of the metal ions, either by adsorption or by a combination of filtration and adsorption on columns of C₁₈-bonded silica gel, was investigated to optimise the separation procedure. Analysis of several National Bureau of Standards and International Atomic Energy Agency biological reference materials demonstrated the effectiveness of this technique. The method is simple and reliable and readily adaptable in all radiochemical laboratories. Furthermore, columns of C₁₈-bonded silica gel have been successfully recycled a number of times without deterioration.

Neutron activation analysis (n.a.a.), is widely used to measure the concentration of many elements in an extensive range of materials. Although instrumental n.a.a. is the preferred version of this technique, its use for some types of sample, including biological materials, is seriously hampered by the quantities of interfering radionuclides produced by the matrix (²⁴Na, ³²P, ³⁸Cl, ⁴²K and ⁸²Br). Subsequent radiochemical separations are usually based on a combination of distillation, ion-exchange and/or solvent extraction procedures [1, 2] or on the use of inorganic absorbents [3] or liquid-liquid extraction alone [4]. The first procedure is time-consuming, the second is subject to serious product losses, and the last method involves manipulations that result in unnecessary radiation exposure to the operator.

Activated carbon has been used successfully to preconcentrate trace metal ions from sea water in the absence and presence of complexing agents [5, 6] and was later used on water samples in analyses for trace metals [7–11]. It was recently introduced into radiochemical procedures for concentrating a number of trace elements from dissolved, irradiated, biological material before measurement of the activated carbon fraction by high-resolution γ -spectrometry [12].

Similarly, C₁₈ chemically bonded silica gel has been used to separate metal chelates [13, 14] and later studies have shown that trace metal pre-concentration from water and sea water could be effected by a combination of chelation and subsequent adsorption on this material [15, 16]. In view of the ready availability of C₁₈-bonded silica gel in short (10 mm) preppacked columns, their use in radiochemical procedures has now been studied and a new separation method for the determination of manganese, copper and zinc in irradiated biological materials has been developed. The method involves complexation of these metal ions with 8-quinolinol (oxine), ammonium pyrrolidinethiocarbamate (APDC) or cupferron (ammonium nitroso- β -phenylhydroxylamine) followed by removal on a column of C₁₈-bonded silica gel and then activity measurements on either the column or the effluent from the stripped column by high-resolution γ -spectrometry.

EXPERIMENTAL

Neutron irradiation and radioactivity measurements

Neutron irradiation of biological materials were done for 10 h, using the X-6 pneumatic tube of the Australian Atomic Energy Commission's 15-MW materials testing reactor, HIFAR, at a thermal flux of 5×10^{12} n cm⁻² s⁻¹. Suitable radioactive tracers were prepared from their sulphate salts by activation in the X-176, self-service, pneumatic tube of this reactor for 5–30 min at a thermal neutron flux of 5×10^{13} n cm⁻² s⁻¹.

Gross γ -ray measurements were taken for all radioactive tracer experiments, with a 2-in. NaI(Tl) well scintillation counter.

Simultaneous determinations of manganese, copper and zinc in biological materials were made with a 100-cm³, 20%, coaxial Ge(Li) detector (Ortec Series 8000, FWHM 1.8 keV at 1.332 MeV) coupled to a Canberra CI8180 4096-channel pulse-height analyser. Subsequent data reduction was achieved with a series of Fortran-IV computer programs written by the staff of these laboratories.

Reagents

All reagents were of analytical-reagent grade. The carrier solutions for the radiochemical separation procedures were prepared from the sulphate salts of manganese, copper and zinc as individual solutions and as a combined carrier solution containing 0.5 g l⁻¹ of each element in 0.2 M sulphuric acid.

Irradiation standards were prepared by pipetting 10- μ l aliquots of the combined carrier solution onto Whatman No. 541 filter papers (2 cm), which were then dried for 16 h in a vacuum desiccator over silica gel and packed into 0.8-ml polythene containers (washed in nitric acid and ethanol and air-dried) for irradiation.

Columns of C₁₈-bonded silica gel, and silica were purchased (Waters Associates Pty Ltd, Sydney) as Sep-Pak C₁₈ and silica cartridges.

Radioactive tracer solutions (0.2 M sulphuric acid) were: ⁵⁴Mn as man-

ganese(II) sulphate, ^{64}Cu as copper(II) sulphate and $^{69\text{m}}\text{Zn}$ and ^{65}Zn as zinc(II) sulphate.

8-Quinolinol was used as a 5% solution in ethanol, APDC as a 1% solution in water and cupferron as a 5% solution in water. All reagents were stored in dark glass bottles and kept under refrigeration when not in use. Solutions were kept for one week before fresh solutions were prepared.

Apparatus

The Sep-Pak cartridges have luer fittings and were used with 10-, 20- and 50-ml hypodermic syringes (Terumo Corp.). For most of these studies, the plungers were removed and the hypodermic syringe barrels were located in a perspex frame and fitted with bored rubber stoppers through which compressed air was injected via plastic needle valves (Cole-Parmer) and plastic and glass tubing. Solutions were then forced through the Sep-Pak cartridges at flow rates of 10–20 ml min⁻¹.

Biological samples

National Bureau of Standards standard reference Orchard Leaves (SRM-1571) and Bovine Liver (SRM-1577), and IAEA standard reference milk powder (A-11) and blood (A-2) were used to test the development of this separation procedure. These samples (70–150 mg) were weighed into 0.8-ml polythene or 1.2-ml polypropylene containers and irradiated with standards for 10 h. The irradiated samples were cooled for two hours before implementing the radiochemical procedure.

Removal of elements by C₁₈-bonded silica gel columns

The removal of manganese, copper and zinc by C₁₈-bonded silica gel was investigated by radioactive tracer experiments. Studies were confined to sulphate medium because most separation procedures associated with biological materials involve dissolution in H₂SO₄/HNO₃ or H₂SO₄/H₂O₂ mixtures. Based on the use of 1–2 ml of 18 M sulphuric acid per 100 mg of biological materials and dilution of solutions to a total volume of 25–100 ml, studies were confined to 0.18 M and 1.44 M sulphate solutions.

The solutions studied contained 0.25 or 2 ml of 18 M sulphuric acid, 5–100 μg of total carrier concentration of each element and their radioactive tracer, 13 ml of water, 3 ml of 2 M ammonium acetate solution and 10–100 μl of 8-quinolinol, 0.1–1 ml of cupferron or 1–5 ml of APDC solutions. After adjustment of the pH with 6–15 M ammonia solution, solutions were diluted to 25 ml with water. The activities of the solutions were measured by gross γ-ray counting before and after passage through columns of C₁₈-bonded silica gel at flow rates between 10 and 20 ml min⁻¹.

Column elution experiments with ethanol, methanol and 3–7 M nitric acid were followed by a gross γ-ray count of each column before and after elution.

Radiochemical separation procedure for biological samples

Samples, irradiated for 10 h and cooled for 2 h, were transferred to a 100-ml beaker to which was added 2 ml of 18 M sulphuric acid, 5 ml of 15 M nitric acid and 10 μ l of combined carrier solution. The solutions were heated on a hot plate to fumes of sulphur trioxide. If the solutions were not clear, a further 5 ml of 15 M nitric acid was added and the evaporation repeated. The solutions were cooled before diluting to about 10 ml with water, then 3 ml of 2 M ammonium acetate and 4 ml of 15 M ammonia solution were added and the solutions were again cooled before addition of the chelating agent (100 μ l of 8-quinolinol, 1 ml of cupferron or 5 ml of APDC). A wash solution was prepared in the same manner and at the same time as the sample solutions, but without carrier and irradiated sample. The additional quantity of ammonia solution required to adjust the pH to 8.5–9.0 was determined on the wash solution. The same volume of alkali was added to each sample solution: the solutions were then diluted to about 30 ml.

The Sep-Pak C₁₈ columns were prepared for all column studies, as recommended by the manufacturer, by passing 2 ml of methanol followed by 5 ml of water. The beaker and the hypodermic syringe barrel were washed with 5 ml of wash solution and the washings were passed through the column. If high-resolution γ -spectrometry was performed on the columns, they were removed from the perspex separation apparatus, carefully dried, and encapsulated in polystyrene containers (6 ml) before measurement. Alternatively, the columns were stripped consecutively with 5 ml of methanol/3 M nitric acid, 2 ml of 7 M nitric acid and 5 ml of methanol into 70-ml polystyrene containers, and manganese, copper and zinc measurements were made on these solutions by high-resolution γ -spectrometry.

RESULTS AND DISCUSSION

Pre-irradiation or post-irradiation separation

Most researchers favour post-irradiation separation procedures because blank problems from reagents are eliminated. We considered the possibility of adsorbing the elements onto C₁₈-bonded silica gel, irradiating the columns and measuring the elements on the columns by γ -spectrometry, then subtracting the contribution from reagents and the column components. The trace element profile of a Sep-Pak C₁₈ column was measured by standard instrumental n.a.a.; elements present in concentration exceeding 0.1 μ g g⁻¹ are listed in Table 1. Concentrations of V, Ga, As, Sb, Cs, La, Ce, Nd, Sm, Dy, Yb, Lu, Hf, Ta, Th and U were less than 0.1 μ g g⁻¹. The concentrations of manganese in the C₁₈-bonded silica gel and zinc in the support plug were of the same magnitude as those measured in many biological materials, which, therefore, precluded the use of pre-irradiation separation procedures with these columns.

TABLE 1

Trace element profile of Sep-Pak C₁₈ cartridge components ($\mu\text{g g}^{-1}$)

Element	C ₁₈ material	Plastic column	Support plugs
Na	17.1 ± 0.7	1.5 ± 0.1	6.0 ± 0.3
Al	117 ± 21	ND ^a	ND
Cl	18 ± 3	4.6 ± 0.4	ND
Ti	156 ± 25	< 4	ND
Cr	0.81 ± 0.06	0.12 ± 0.02	0.20 ± 0.05
Mn	0.21 ± 0.03	0.024 ± 0.008	ND
Fe	23 ± 2	ND	< 4
Zn	2.6 ± 0.1	2.1 ± 0.5	19 ± 2

^aND, not detected.*Chelating agents and carrier concentrations*

Most sulphur and nitrogen donors that are selective chelating agents form metal complexes of low solubility. For example, the intrinsic solubility of most metal 8-quinolinolates is in the range 10^{-6} – 10^{-9} M [17]. This not only favours many analytical procedures involving filtration but also those based on adsorption processes because the organic structure prefers hydrophobic substrates to the highly polar water solvent. However, if maximum flow rates are to be maintained and the removal is to be controlled by an adsorption mechanism, the nature and extent of the metal chelate precipitation must be controlled for it to be used successfully with columns of C₁₈-bonded silica gel.

The concentrations of manganese, copper and zinc found in biological materials vary from sub- $\mu\text{g g}^{-1}$ for manganese to several hundred $\mu\text{g g}^{-1}$ for copper. Therefore, the need for carrier addition differed from element to element. When the concentrations exceeded $50 \mu\text{g g}^{-1}$, no carrier was required for that element.

Carrier additions were tested individually for each element at the two sulphate concentrations and in the pH range 6.0–9.0 for the various chelating agents. In 0.18 M sulphate, 8-quinolinol (1.38×10^{-3} M) could support 10 μg of copper, 50 μg of manganese and 20 μg of zinc in a solution volume of 25 ml before the onset of precipitation. Increasing the sulphate concentration to 1.44 M increased the solubility to 25 μg per 25 ml for copper and greater than 100 μg for manganese and zinc. Although cupferron solutions (1.29×10^{-2} M) contained greater than 100 μg of manganese and zinc in solution, the addition of only 5 μg of carrier produced light precipitation. Changes to the sulphate concentrations did not significantly alter the solubility of the cupferron chelates. The APDC reagent (1.22×10^{-2} M) itself precipitates heavily from acidic solution at pH values less than 4.0; above pH 4.5, most of the precipitate dissolves. However, copper and zinc chelates precipitated from solution after the addition of only 5 μg of each carrier, whereas manganese remained soluble up to 100 μg per 25 ml. Again, in-

creased sulphate concentration did not produce a significant change in the solubility.

In view of the limited solubility of the various copper chelates, but the need for a holdback carrier when the copper content of a biological sample is less than $1 \mu\text{g g}^{-1}$, subsequent studies were made with an additional $5 \mu\text{g}$ of the element(s) under investigation.

The pH dependence of metal chelate removal

The results for the removal of manganese, copper and zinc as various chelates by columns of C_{18} -bonded silica gel are shown in Fig. 1. Manganese, copper and zinc were removed quantitatively from an aqueous phase of 8-quinolinol and 0.18 M sulphate at pH 3.0, 5.0 and 7.0, respectively. These quantitative separations agree closely with the published data for this liquid-liquid extraction system [18]. When the sulphate concentration was increased to 1.44 M, the pH value for quantitative removal increased by one pH unit for each of the metal/8-quinolinolate species. Although neither zinc nor manganese was precipitated from 8-quinolinol solutions in these tracer studies, their removal being by adsorption processes, solutions of copper appeared cloudy at pH values greater than 5.0 and its removal in the pH range 5.0–9.0 was by both filtration and adsorption.

The study of APDC chelation was complicated by the heavy precipitation

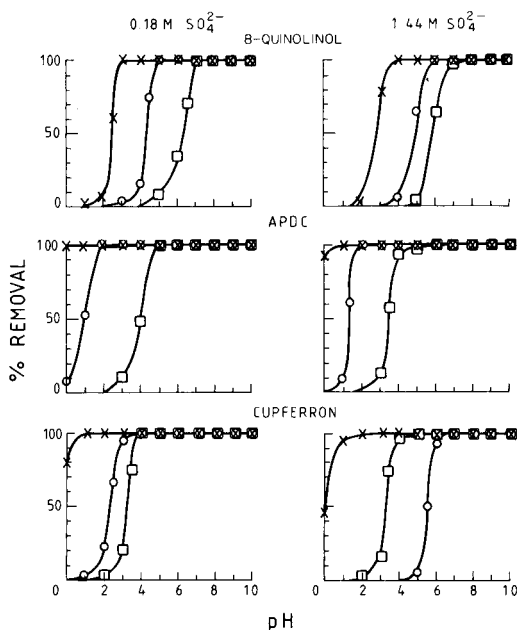


Fig. 1. The removal of Mn, Cu and Zn by C_{18} -bonded silica gel from 8-quinolinol (1.38×10^{-3} M), APDC (1.22×10^{-3} M) or cupferron (1.29×10^{-2} M) solutions as a function of pH and sulphate concentrations. (x) Cu; (o) Zn; (□) Mn.

of this reagent in the pH region below 4.5; this impeded column studies. However, Fig. 1 shows that copper was removed quantitatively over the whole pH range, zinc above pH 2.0 and manganese above pH 5.0. Again, these data closely followed literature data for liquid-liquid extraction in APDC systems [18]. Sulphate had only a minor influence on the chelation system. The solubility of APDC and its metal chelates dictated that filtration was the major mode of separation.

The cupferron system was characterised by a very large shift in the pH dependence of zinc removal with changing sulphate concentration (Fig. 1). In 0.18 M sulphate, zinc was removed quantitatively above pH 4.0 but required pH values above 7.0 to achieve the same result in 1.44 M sulphate. Neither copper nor manganese displayed the same effect, copper being removed quantitatively in the pH range 1.0–2.0 and manganese in the range 4.0–5.0, independent of the sulphate concentration. The cupferron reagent precipitated at pH values below 2.0. At higher pH, the mechanism for removal of each ion paralleled that of the 8-quinolinol system; filtration and adsorption dictated copper removal, but adsorption processes accounted for the removal of manganese and zinc.

Studies were made on the chemical speciation of the metals in the various solutions and its relation to metal ion removal by C₁₈-bonded silica gel. The speciation in these solutions could be determined by incorporating total metal and ligand concentrations and known stability constant data into a revised version of the computer program SIAS [19]. Unfortunately, there are no reliable published data for the stability constants of metal APDC or cupferron complexes but data for metal 8-quinolinol, hydroxide, hydrogen-sulphate and acetate are available [20–22]. A summary of the relationship between the amount of metal ion as the 8-quinolinolates and the separation on C₁₈-bonded silica gel is given in Table 2. Excluded from this table are the results for the contributions of sulphate, acetate and hydroxy species to the total speciation in solution because these hydrophilic complexes have no affinity with the hydrophobic matrix of the Sep-Pak C₁₈ cartridges. In 0.18 M sulphate solutions, quantitative removal was observed if 20% or more of the metal ion was present as the metal 8-quinolinolate. Surprisingly, at higher sulphate concentrations, removal of manganese increased at lower fractions of metal 8-quinolinolate formation.

Chelating agent concentration and ethanol addition

Detailed studies were made of the minimum concentration of chelating agent required to achieve quantitative removal of the three metal ions. Table 3 lists the concentration range for each ligand at the minimum optimum pH given in Fig. 1. Only the results for manganese are tabulated, because copper and zinc were totally removed for all systems over the concentration range examined. From these investigations, it was concluded that the addition of 1.4×10^{-3} M 8-quinolinol, 1.28×10^{-2} M APDC or 3.2×10^{-3} M cupferron was sufficient to obtain a quantitative recovery of manganese, copper and zinc on columns of C₁₈-bonded silica gel.

TABLE 2

Speciation and percentage removal from 8-quinolinol solution (1.38×10^{-3} M) as a function of pH and sulphate concentration

pH	0.18 M Sulphate			1.44 M Sulphate		
	% Metal/8-quinolinol		Removal (%)	% Metal/8-quinolinol		Removal (%)
	1:1	1:2		1:1	1:2	
<i>Copper</i>						
2.0	0.5	0	5.9	0.09	0	2.8
3.0	27.9	9.6	>99	7.1	2.4	79.9
4.0	3.2	96.8	>99	3.0	96.4	>99
<i>Zinc</i>						
4.0	1.8	0	14	0.07	0	0
5.0	44.1	8.8	>99	4.1	0.8	66
6.0	19.8	79	>99	16.2	64.7	>99
<i>Manganese</i>						
5.0	0.4		8	0		0
6.0	6.9		34.5	0.24		67
7.0	44.7		>99	2.5		97
8.0	88.9		>99	21		>99
9.0	98.4		>99	68		>99

TABLE 3

Adsorption of manganese on C_{18} -bonded silica gel as a function of the concentration of chelating agent in 0.18 M sulphate solution

8-Quinolinol concn. (10^{-4} M)	Removal ^a (%)	APDC concn. (10^{-3} M)	Removal ^b (%)	Cupferron concn. (10^{-3} M)	Removal ^b (%)
1.38	30.5	1.22	27.8	1.29	98.6
3.45	59.6	2.44	64.9	3.23	>99
6.90	74.6	6.10	92.2	6.45	>99
13.8	>99	12.2	>99	12.9	>99

^aAt pH 7.0. ^bAt pH 6.0.

Although the extent of precipitation of the metal ion as the metal chelates could be carefully controlled in the early tracer studies, there was concern for the degree of control possible when multielement biological materials are added to these ligand systems. Some control was gained by minimising the weight of biological sample, but qualitative tests showed that the addition of ethanol could enhance column operation by increasing the solubility of the metal chelate and favouring the more rapid adsorption mechanism, or by changing the nature of the precipitate. However, tracer studies, summarised in Table 4, revealed that while up to 30% (v/v) ethanol could be tolerated in the copper and zinc systems with 8-quinolinol or APDC, and

TABLE 4

Influence of ethanol addition on the removal of Mn, Cu and Zn in the presence of various chelating agents

Ethanol (% v/v)	Removal (%)			Ethanol (% v/v)	Removal (%)		
	Mn	Cu	Zn		Mn	Cu	Zn
<i>8-Quinolinol, pH 7.0</i>				<i>Cupferron, pH 6.0</i>			
0	>99	>99	>99	0	>99	>99	>99
10	>99	>99	>99	10	>99	>99	>99
20	96	>99	>99	20	97	>99	>99
30	76	>99	>99	30	48	99	67
40	4.4	98	98	40	10.6	75	13.1
<i>APDC, pH 6.0</i>							
0	>99	>99	>99				
10	72	>99	>99				
20	70	>99	>99				
30	65	>99	>99				
40	60	99	98				

20% (v/v) in these cupferron systems, the removal of manganese was adversely affected by any ethanol addition to the APDC solution and by more than 10% (v/v) ethanol in the 8-quinolinol or cupferron systems.

Recycling C₁₈-bonded silica gel columns

The possibility of recycling Sep-Pak C₁₈ cartridges was examined. Where adsorption was the sole process for metal ion removal (e.g., trace copper in 8-quinolinol solutions in the pH range 3.0–4.5), all activity was readily removed from the column with 5 ml of methanol. However, if the metal chelates were partially precipitated from solution and then separated by both filtration and adsorption, methanol failed to remove the activity quantitatively. Only the use of a nitric acid (2 ml of 7 M) eluant followed by a methanol wash (5 ml) yielded clean columns for all chelate systems.

Adverse effects from these strong nitric acid solutions as a result of the removal of some or all the octadecyl-bonded groups on the silica gel columns was measured by taking a single column of C₁₈-bonded silica gel through ten cycles of an adsorption step with copper in 8-quinolinol solution at pH 4.0 and an elution step with 2 ml of 7 M nitric acid, 3 ml of water and 5 ml of methanol. Copper was removed quantitatively from solution and then from the column in each cycle. Substitution of a Sep-Pak silica cartridge in the above investigation failed to remove copper ion from solution quantitatively after any cycle. With the Sep-Pak C₁₈-bonded silica gel column, the experiment was repeated for zinc from cupferron solutions at pH 6.0, where the zinc/cupferron chelate does not precipitate from solution; the results were the same as for copper.

Elution studies on columns used to separate manganese, copper and zinc from biological materials showed that where the time between the adsorp-

tion and elution was significant, the activity was best removed with successive washes of 5 ml of methanol/3 M nitric acid, 2 ml of 7 M nitric acid and 3 ml of methanol. Columns were successfully recycled up to three times for radiochemical separations from irradiated biological materials.

Analytical results and conclusions

This radiochemical separation procedure was used to determine manganese, copper and zinc in standard milk powder, blood, bovine liver and orchard leaves. The results are compared in Table 5 with the values certified by IAEA and NBS; agreement between them was good and the precision satisfactory.

These results demonstrate the effectiveness of this technique for determining manganese, copper and zinc in biological materials. The method is simple and reliable and is readily adaptable in all radiochemical laboratories with the commercial availability of C₁₈-bonded silica gel in short prepacked columns. Furthermore, these columns can be recycled successfully a number of times without deterioration.

The technique is not confined to these metal ions or chelating agents, and studies are being undertaken to extend both groups.

The authors express their gratitude to Mrs. Y. J. Farrar for assisting with the high-resolution γ -spectrometric measurements and subsequent data reduction.

TABLE 5

Determinations of Mn, Cu and Zn in NBS and IAEA standard reference materials ($\mu\text{g g}^{-1}$)

Reference material	Element	Metal concentration ($\mu\text{g g}^{-1}$)			Certified value
		Chelating ligand at pH 8.5–9.0 ^a			
		Cupferron	8-Quinolinol	APDC	
IAEA Milk Powder (A-11)	Mn	0.38 ± 0.01	0.30 ± 0.03	0.33 ± 0.02	0.38 ± 0.08
	Cu	0.70 ± 0.02	0.75 ± 0.02	0.70 ± 0.03	0.84 ± 0.17
	Zn	36 ± 3	37 ± 1	36 ± 2	38.9 ± 2.3
IAEA Blood (A-2)	Mn	104 ± 1	98 ± 3	107 ± 1	123 ± 22
	Cu	48.3 ± 1.2	41 ± 2	40 ± 2	45 ± 3
	Zn	84 ± 5	74 ± 10	73 ± 6	89 ± 12
NBS Bovine Liver (SRM-1577)	Mn	9.4 ± 0.1	10.5 ± 0.1	10.5 ± 0.1	10.3 ± 1
	Cu	183 ± 2	201 ± 1	185 ± 3	193 ± 10
	Zn	123 ± 8	133 ± 4	121 ± 10	130 ± 13
NBS Orchard Leaves (SRM-1571)	Mn	88 ± 3	90 ± 4	88 ± 3	91.6 ± 1.1
	Cu	13.5 ± 0.6	13.6 ± 0.5	13.4 ± 0.5	12.6 ± 0.9
	Zn	24 ± 1	24 ± 2	24 ± 1	25.1 ± 0.8

^aMean and standard deviation based on counting statistics.

REFERENCES

- 1 P. S. Tijoe, J. J. M. de Goeij and J. P. W. Houtman, *J. Radioanal. Chem.*, 16 (1973) 153.
- 2 J. Shuhmucher, W. Maier-Borst and H. J. Hauser, *J. Radioanal. Chem.*, 37 (1977) 503.
- 3 G. Torok, R. Schelenz, E. Fisher and J. F. Diehl, *Fresenius Z. Anal. Chem.*, 263 (1973) 110.
- 4 H. Nakahara, Y. Nagame, Y. Yoshizawa, H. Oda, S. Gotoh and Y. Murakami, *J. Radioanal. Chem.*, 54 (1979) 183.
- 5 W. B. Kerfoot and R. F. Vaccero, *Limnol. Oceanogr.*, 18 (1973) 689.
- 6 H. A. van der Sloot, R. Masee and H. A. Das, *J. Radioanal. Chem.*, 25 (1975) 99.
- 7 S. Jensen, L. Renberg and L. Reutergardh, *Anal. Chem.*, 49 (1977) 316.
- 8 R. Masee, H. A. van der Sloot and H. A. Das, *J. Radioanal. Chem.*, 35 (1977) 157.
- 9 H. A. van der Sloot, G. D. Wals and H. A. Das, *Anal. Chim. Acta*, 90 (1977) 193.
- 10 J. Wijkstra and H. A. van der Sloot, *J. Radioanal. Chem.*, 46 (1978) 379.
- 11 B. M. Vanderborcht and R. E. van Grieken, *Anal. Chem.*, 49 (1977) 311.
- 12 H. A. van der Sloot, G. D. Wals, C. A. Weers and H. A. Das, *Anal. Chem.*, 52 (1980) 112.
- 13 P. C. Uden, D. M. Parees and F. H. Walters, *Anal. Lett.*, 8 (1975) 795.
- 14 H. Hoshino, T. Yotsuyanagi and K. Aomura, *Bunseki Kagaku*, 27 (1978) 1203.
- 15 G. L. Mills and J. G. Quinn, *Mar. Chem.*, 10 (1981) 93.
- 16 H. Watanabe, K. Goto, S. Taguchi, J. W. McLaren, S. S. Berman and D. S. Russell, *Anal. Chem.*, 53 (1981) 738.
- 17 I. M. Kolthoff, E. B. Sandell, E. J. Meehan and S. Bruckenstein, *Quantitative Chemical Analysis*, Macmillan, London, 1969.
- 18 G. H. Morrison and H. Freiser, *Solvent Extraction in Analytical Chemistry*, Wiley, New York, NY, 1957.
- 19 R. M. Sylva and J. J. Fardy, SIAS — A computer program for generalised calculation of speciation in mixed-ligand aqueous systems, AAEC/E445, Aust. Atomic Energy Comm. Report, 1978.
- 20 R. M. Smith and A. E. Martell, *Critical Stability Constants. Vol. 2, Amines*, Plenum Press, New York, NY, 1975.
- 21 A. E. Martell and R. M. Smith, *Critical Stability Constants. Vol. 3, Other Organic Ligands*, Plenum Press, New York, NY, 1977.
- 22 R. M. Smith and A. E. Martell, *Critical Stability Constants. Vol. 4, Inorganic Complexes*, Plenum Press, New York, NY, 1976.

A POST-COLUMN PHOTOCHEMICAL DETECTOR FOR USE IN THE DETERMINATION OF TRACE METALS WITH *n*-BUTYL-2-NAPHTHYLMETHYLDITHIOCARBAMATE BY HIGH-PERFORMANCE LIQUID CHROMATOGRAPHY

Y. T. SHIH^a and PETER W. CARR*

University of Minnesota, Department of Chemistry, Minneapolis, MN 55455 (U.S.A.)

(Received 19th August 1983)

SUMMARY

The determination of traces of metals by high-performance liquid chromatography of their *n*-butyl-2-naphthylmethyldithiocarbamate (BNMDTC) complexes on a nonpolar stationary phase, with a post-column photochemical detector is described. Metal complexes of this ligand are thermodynamically stable and kinetically inert towards dissociation. To provide low detection limits, a photochemical reactor was developed to generate a fluorescent product. A major product of the photolysis of BNMDTC complexes is identified as the highly fluorescent *n*-butyl-2-naphthyl-methylamine. Detection of metal ions as BNMDTC complexes at the 10^{-8} M level is feasible. Iron, nickel, mercury and cobalt complexes are readily determined.

The application of high-performance liquid chromatography (h.p.l.c.) for quantifying metal ions has received great interest over the past decade [1–4]. In a previous report [5], *n*-butyl-2-naphthylmethyldithiocarbamate (BNMDTC) was used as a pre-column derivatization reagent for trace metal ions. To be competitive with other methods such as anodic stripping voltammetry, atomic absorption spectrometry, and neutron activation, detection of sample concentrations as low as 1×10^{-7} – 1×10^{-8} M is required. To reach this objective, a method with lower detection limits than ultraviolet (u.v.) absorption is needed.

In general, dithiocarbamate complexes are electrochemically active and can be both oxidized and reduced. Because of possible exchange reactions between the dithiocarbamate complexes and metal electrodes, only carbon electrodes are useful although their utility in reductive processes is limited by the small negative potential range [6, 7] available on such surfaces. In some preliminary work, the possibility of using the electrochemical detector in the oxidation mode for measuring BNMDTC complexes was tested at 1.0 V vs. Ag/AgCl; it was found that the high background current under the experimental conditions and the poor reproducibility of the measurement combined

^aPresent Address: 3M Company, St. Paul, MN, U.S.A.

to yield detection limits which were no better than those obtained with a u.v. detector.

Recently, Bond and Wallace [8] studied the use of diethyldithiocarbamates (DDTC) as complexing agents for the determination of copper by h.p.l.c. with an electrochemical detector and observed the same problems. In addition, Kissinger and Bratin [9] found that carbon-based electrodes used at potentials of +1.0 V or more are subject to severe loss in sensitivity and selectivity in the aqueous solvents used in liquid chromatography. It is possible that irreversible adsorption of species containing sulfur alter the chemistry of the electrode surface and make long-term reproducibility even more difficult to achieve. This limits the use of electrochemical detection for BNMDTC complexes, especially at trace levels.

Lower detection limits should be attainable by fluorescence measurements but the BNMDTC complexes do not fluoresce directly despite the presence of the naphthyl group. It is well known that some u.v.-absorbing substances may be converted to fluorescent materials by irradiation with u.v.-energy [10]. This phenomenon is useful as a derivatization method by use of a post-column reactor. The chief advantages of this approach are the possibility of improved detectability and the fact that there is no dilution of the effluent. Several groups [11–14] have shown the utility of this technique. Dialkyldithiocarbamate complexes are known to undergo photochemical reactions [15]. It was expected that photodecomposition of BNMDTC would result in a fluorescent product by analogy to the acid decomposition process which produces a secondary amine. In fact, in the case of BNMDTC, any fragment from photodecomposition containing a naphthyl group might offer a very useful method for the fluorescent detection of BNMDTC at low concentrations.

EXPERIMENTAL

Chromatography system

The h.p.l.c. system has been described [5]. Several different and commonly used h.p.l.c. detectors were investigated to quantify the BNMDTC complexes after their separation on columns with a nonpolar stationary-phase. An LDC 254-nm fixed wavelength absorbance detector and an Hitachi (Model 100-10) variable-wavelength absorbance detector were used for preliminary experiments. An electrochemical detector (LC-304T; Bioanalytical System, IIV) was used for electrochemical detection; glassy carbon was used as the working electrode with the potential fixed at +1.0 V vs. Ag/AgCl. Fluorimeters used were a Perkin-Elmer 650-10LC and a Schoeffel FS-970. Because of the non-fluorescent nature of the BNMDTC complexes, a photochemical post-column reactor was designed and placed before the fluorimeter so that fluorescence measurements were possible. In the photochemical post-column derivatization experiments, an u.v. absorbance detector was placed before the post-column reactor to obtain more information.

Photochemical measurements

In bulk solutions. A medium-pressure 175-W mercury lamp (Target Store, St. Paul, MN) was positioned into a $12 \times 8 \times 6$ -in. aluminum box. The outside glass envelope of the lamp was removed so that u.v. energy would directly irradiate the sample. The samples were kept in a fluorescence photometric cell and irradiated from the side of the cuvette at about 15 cm from the light source. After irradiation, the samples were cooled to room temperature and mixed before any measurements were made.

In a flow system. Studies in a flow system were conducted in the chromatographic system described earlier [5] with and without a column and with a home-made photochemical post-column reactor (see Fig.1) placed upstream of the fluorimeter. The reaction coil was made of teflon tubing and was supported by four teflon rods. The diameter of the coil was ca. 6 cm; further details are given in later paragraphs. It was very simple to make a connection between the reactor and the chromatographic column or the detector with a normal Altex to Swagelok connector. However, for small tubing (i.d. < 0.01 -in.), it was difficult to make a flange with a normal flanging tool. The

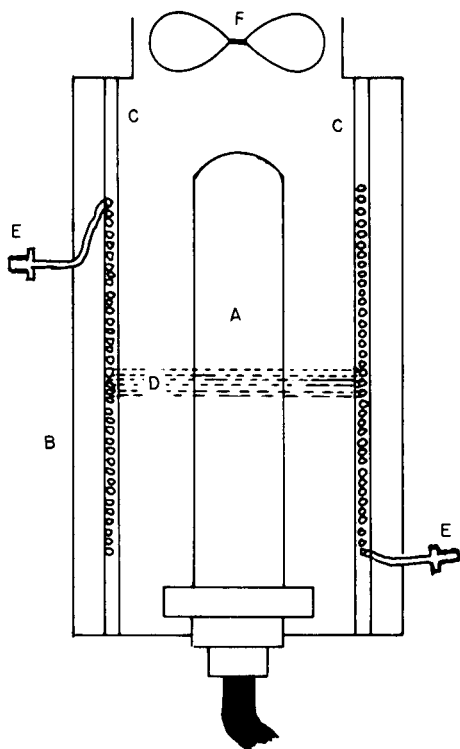


Fig. 1. Photochemical reactor. (A) medium-pressure mercury lamp; (B) lamp housing; (C) teflon rod (coil holder); (D) coiled teflon tubing; (E) Altex to Swagelok connectors; (F) cooling fan.

tubing was sealed into a larger diameter teflon tube which could then be easily flanged. Teflon tubes were first etched by Chemgrip treating agent (Chemplast, NJ) before being sealed with an epoxy glue. This connection could withstand pressures corresponding to normal h.p.l.c. flow rates (less than 4 ml min^{-1}) without leaking. The walls of the lamp housing were covered with aluminum foil to reflect the light back into the reactor. A fan was placed at one end of the lamp housing to remove heat. This is essential to prevent solvent from boiling at low flow rates. The reactor must be placed in a hood because the mercury lamp generates ozone.

Detection limit

A $90 \times 4.6\text{-mm}$, $10\text{-}\mu\text{m}$, μ Bondapak C_{18} column was used for the simultaneous determination of $\text{Fe}(\text{BNMDTC})_3$, $\text{Ni}(\text{BNMDTC})_2$, $\text{Hg}(\text{BNMDTC})_2$, and $\text{Co}(\text{BNMDTC})_2$. The mobile phase was 93/7 methanol/water with 1.0 mM Tris at pH 8.25. The flow rate was 1 ml min^{-1} as delivered by an IBM LC9533. A $200\text{-}\mu\text{l}$ injection loop was used for all samples. Concentrations of the samples were in the range 1.0×10^{-8} – $1.0 \times 10^{-6} \text{ M}$. Six standard solutions were used to generate a calibration graph. Four different standards at $1 \times 10^{-8} \text{ M}$ were prepared separately so that personal errors of sample handling would be included. Only one standard at $1 \times 10^{-7} \text{ M}$ and $2 \times 10^{-7} \text{ M}$ was needed according to the procedures of Hubaux and Vos [16]. Results reported are the average of three or four injections at each concentration. The photochemical post-column reactor used was the Model III device described later. Chromatograms were recorded on a strip chart recorder and a Hewlett-Packard 3390A integrator (Palo Alto, CA).

RESULTS AND DISCUSSION

A preliminary study of photochemical post-column detection of BNMDTC was done with a Tracor photoconductivity detector (Tracor 965, Tracor, Inc., IL). However, only the quartz cell and the low-pressure mercury lamp (4.4 mW cm^{-2} at 0.75 in. from source) in the Tracor detector were used. Under normal h.p.l.c. conditions, an injection of BNMDTC complexes did not give any fluorescent response. However, when the mercury lamp in the reactor was turned on, a normal chromatogram of the BNMDTC complexes was recorded on the downstream fluorimeter. The fluorescence yield was very low. It then became important to find conditions to improve and to optimize the fluorescent signal.

Effect of light sources

As a part of the preliminary study, the mercury lamp in the Tracor detector was replaced by a zinc lamp which had an output of $2.4 \text{ mW ster-cm}^{-2}$ and an emission maximum at 214 nm . The results showed that the fluorescent yields were much less than when a mercury lamp was used. This indicates that the photodecomposition was not caused by the absorbance of

the naphthyl group at 210–220 nm. In general, an increase in the intensity of the light source will increase the yield of the photochemical products. Thus, a medium-pressure mercury lamp was used for studying the photochemistry of BNMDTC complexes.

A scan of the fluorescence spectrum of the photodecomposed BNMDTC complexes showed that the products had the same excitation and emission wavelength maxima as did BNM amine. The wavelengths causing the decomposition were further defined by using a series of filters. The results are summarized in Table 1. It was concluded that the photochemistry is controlled by absorption of radiation between 220 and 300 nm.

Identification of photolysis products

As mentioned above, the photolysis products have the same fluorescence spectrum as the BNM amine, and wavelengths from 220 to 300 nm are responsible for the photodecomposition. These wavelengths also overlap the absorption bands of the NCS_2 group in the dithiocarbamate molecules. Thus a possible mechanism of photodecomposition is as follows



It is believed that u.v. energy is absorbed by the NCS_2 group and breaks the $\text{N}=\text{C}$ bond to produce the fluorescent BNM amine. To test this hypothesis, the u.v. absorption and fluorescence spectra of different BNMDTC complexes, BNM amine, and naphthalene, were examined more closely. The fluorescent properties of these substances are shown in Table 2. Complexes of BNMDTC do not fluoresce, thus no data for these compounds prior to photolysis are included. The maximum excitation and emission wavelengths of BNMDTC complexes after irradiation are the same as of the BNM amine before and after photolysis and are consistently different from the wavelengths of naphthalene before and after irradiation. Note that there are some impurities in the blank that give a fluorescent background although it is different from the

TABLE 1

Effects of wavelength on the photolysis of BNMDTC complexes

Metal	Fluorescence intensity (relative)		
	300–400 nm ^{a,b} band pass	400 nm ^{b,c} cut-off	No filter ^d
Blank	10	10	10.2
Zn(II)	12.5	15.6	137
Ni(II)	10.5	11.0	70
Cu(II)	10.8	10.8	90
Hg(II)	10.5	10.6	132

^aMaximum at 50% T at 365 nm. ^bIrradiation time, 1 min. ^c85% T above 400 nm, 0% T below 360 nm. ^dIrradiation time, 20 min.

TABLE 2

Fluorimetric data of selected BNMDTC related substances

Substances ^a	Before photolysis			After photolysis ^b		
	λ_{ex} (nm)	λ_{em} (nm)	Inten- sity	λ_{ex} (nm)	λ_{em} (nm)	Relative intensity
Blank	223	445	1.7	223	445	1.7
Naphthalene	218	327	64	218	327	63
BNM amine	221	330	58	221	330	51.4
Zn(BNMDTC) ₂	221	330	3.0	221	330	56
Hg(BNMDTC) ₂	—	—	—	221	330	53
Cu(BNMDTC) ₂	—	—	—	221	330	43
Ni(BNMDTC) ₃	—	—	—	221	330	26
Co(BNMDTC) ₂	—	—	—	221	330	43
Fe(BNMDTC) ₃	—	—	—	221	330	50

^a 1×10^{-5} M. ^b Irradiation time, 30 min.

emission wavelengths of the BNM amine or naphthalene. In spite of the blank problem, the excitation and emission wavelengths of the BNM amine are not changed by irradiation; the fluorescence intensity decreases about 12% after photolysis for 30 min. This decrease also occurs in the u.v. absorbance and is not fully understood as yet.

The u.v. absorption spectra of naphthalene and BNM amine before and after photolysis are shown in Fig. 2. Naphthalene is not sensitive to u.v. irradiation. After irradiation, the BNM amine has a slightly different u.v. spectrum which is again different from the spectrum of naphthalene. This indicates that the BNM amine is not photodecomposed to naphthalene. The u.v. spectra of the BNMDTC complexes after irradiation are identical to the spectrum of BNM amine after irradiation. The typical absorption by NCS₂, or the charge-transfer bonds of some BNMDTC complexes, essentially disappeared after irradiation. The u.v. spectra of the zinc-BNMDTC complex before and after irradiation are shown in Fig. 3. The absorption band at 265–270 nm caused by the absorption of the NCS₂ group vanishes after photolysis. The spectra are the same as that of BNM amine and different from that of naphthalene. The above results strongly support the view that the main product of the photochemical decomposition of the metal complexes is the BNM amine. This was further confirmed by injection of the BNMDTC complexes (after irradiation) into an h.p.l.c. system. Only one major peak having a retention volume equal to that of the BNM amine was observed. This also rules out naphthylmethylamine as the product. Thus, it is concluded that BNM amine is the principal product of the photochemical decomposition.

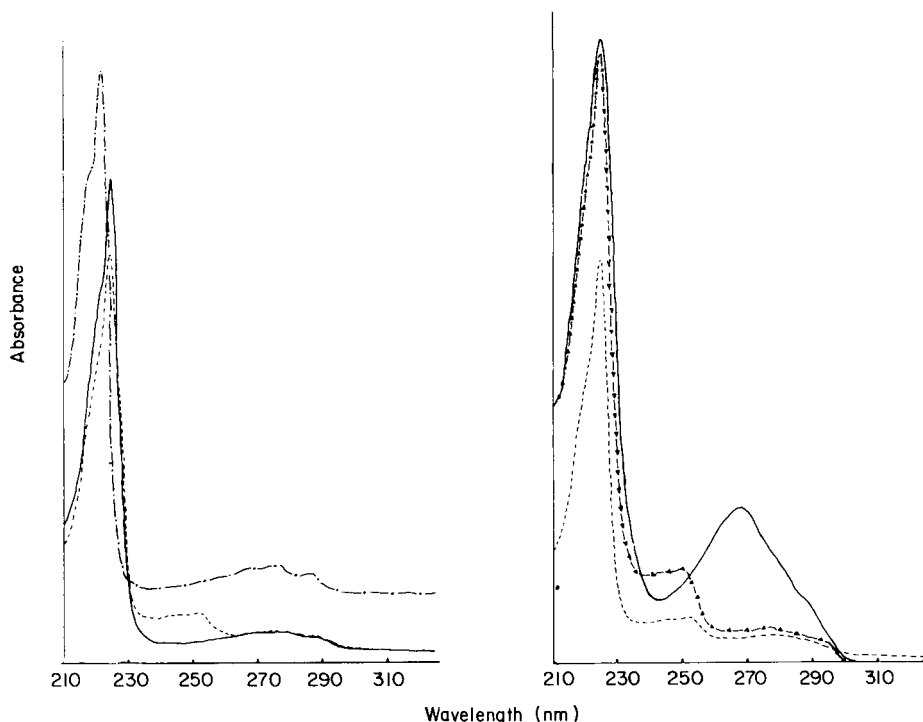


Fig. 2. Absorption spectra of naphthalene and BNM amine before and after photolysis. Concentrations, 1×10^{-5} M; solvents, 95/5 methanol/water, 1 mM Tris at pH 8.25; GCA spectrometer, 500 signal averaging, 2.0 AUFS, scan rate 50 nm/div. irradiation time, 20 min. (---) Naphthalene before and after photolysis; (—) BNM amine before photolysis; (---) BNM amine after photolysis.

Fig. 3. Absorption spectra of zinc BNMDTC and BNM amine before and after photolysis. Conditions: see Fig. 2. (—) $\text{Zn}(\text{BNMDTC})_2$ before photolysis; (—△—) $\text{Zn}(\text{BNMDTC})_2$ after photolysis; (---) BNM amine after photolysis.

Rate of photolysis

The rates of the photodecomposition (the increase of the fluorescence intensities) of BNMDTC complexes are rather fast (see Fig. 4). After irradiation for 5 min, fluorescence is nearly at steady state. Within that time, BNM amine is not noticeably decomposed. In the case of BNMDTC complexes, the electron density on the NCS_2 group is modified by the presence of the different metals. Thus they have different absorptivities in the 220–300-nm range. The rates of appearance of the fluorescent products correlate with the absorptivities of the metal complexes in this wavelength range.

Ideally, complete photolysis of one mole of 2:1 complex, e.g., $\text{Zn}(\text{BNMDTC})_2$, should yield twice the fluorescence of 1 mole of BNM amine. However, all of the BNMDTC complexes have a net fluorescence significantly

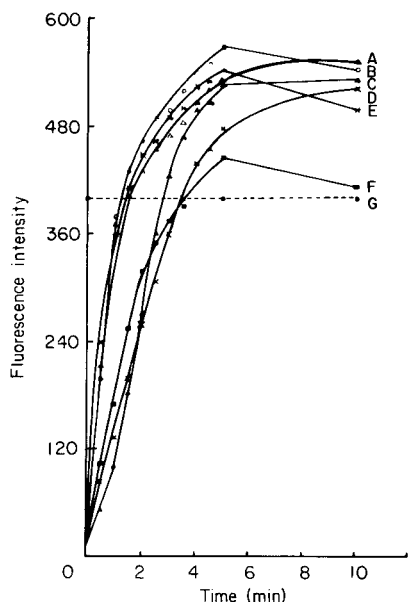


Fig. 4. Rate of photolysis in bulk solutions. Concentrations, 1×10^{-5} M; Solvents, 95/5 methanol/water, 1.0 mM Tris at pH 8.25; Varian SF-330, $\lambda_{ex} = 233$ nm, 10-nm slit, $\lambda_{em} = 330$ nm, 20-nm slit, selector $\times 1$, sensitivity $\times 1$, time constant 0.25 s; photolysis, Hg medium-pressure lamp. Curves: (A) $\text{Fe}(\text{BNMDTC})_3$; (B) $\text{Zn}(\text{BNMDTC})_2$; (C) $\text{Ni}(\text{BNMDTC})_2$; (D) $\text{Co}(\text{BNMDTC})_2$; (E) $\text{Hg}(\text{BNMDTC})_2$; (F) $\text{Cu}(\text{BNMDTC})_2$; (G) BNM amine.

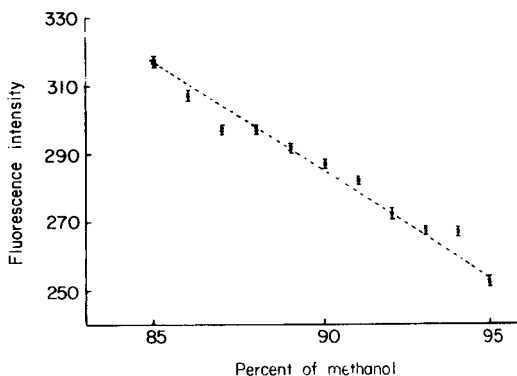


Fig. 5. Effect of water in the solvent on the fluorescence of BNM amine. (1×10^{-5} M). Conditions: Varian SF-330, $\lambda_{ex} = 233$ nm, slit 10 nm, $\lambda_{em} = 330$ nm, slit 20 nm, selector $\times 1$, sensitivity $\times 1$, time constant 0.25 s. Y-intercept = 272.7 ± 3.7 , $\sigma = 2.02$; slope 5.35 ± 0.5 , $\sigma = 0.27$; correlation coefficient 0.987 at 90% confidence level.

lower than expected. In fact, the complexes of mercury, zinc and copper show a decrease in their fluorescence intensities after 10 min of irradiation. It is not surprising that excessive irradiation leads to decreased fluorescence, because of a follow-up photochemical process [13, 17].

Effect of chemical conditions

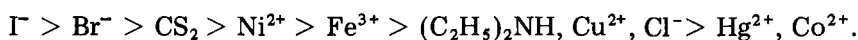
Although temperature and oxygen content may be significant variables, no attempt was made to control their effects in this work. It should be noted that oxygen is not an easily controlled factor, especially when a photochemical reactor is made of teflon. Nevertheless, it is concluded from the measurements made in bulk solution that oxygen is not a major variable. In addition, the solubility of oxygen in the solvents used is probably diminished by the increased temperature.

Because the best mobile phase for the separation of BNMDTC complexes is a methanol/water mixture [5], the study of solvent effects was restricted to 95/5 to 85/15 methanol/water (Fig.5). The fluorescence intensity of BNM

amine increased by about 12% as the water content increased from 5% to 15%. It was also found that in these solvents, pH changes from 8.25 to 5.5 increased the fluorescence intensity of BNM amine by about 60%. Guilbault [18] has stated that increasing the "proticity" of the solvent can increase the fluorescence yield if a nonbonding energy level exists between the π and π^* level. This is probably the case with BNMDTC complexes. On addition of polar or H-bonding solvents, it is possible to stabilize the nonbonding energy level and increase the fluorescence intensity ($\pi \rightarrow \pi^*$). Free protons have the same effect as H-bonding solvents, but to a greater extent.

Based on the above, a mobile phase with either low pH or high water content should be used to optimize the measurement of fluorescence. However, these conditions have considerable chromatographic disadvantages. First, low pH increases the dissociation and chemical decomposition rate of the complexes [19] during the separation. Second, high water content (>5%) will increase the separation time.

According to the photodecomposition mechanism, free metal ions and carbon disulfide are the principal possible coproducts. The effects of these species on the fluorescence intensity of the BNM amine are summarized in Table 3. The reported data are the relative change of intensities upon the addition of free metal ions, carbon disulfide, and other solutes to the solution of BNM amine which is predissolved in 95/5 methanol/water containing 1 mM acetate buffer at pH 5.5. The ratios of the concentration of BNM amine to solute are 2:1 for the free metal ions and 1:1 for the other solutes. The EDTA was added to see if it could act as a masking reagent to reduce quenching by free metal ions. Diethylamine was tested as a possible masking or competing reagent for quenching by carbon disulfide. The order of observed quenching strength is as follows:



Clearly, heavy-atom quenching will be a problem in this work, the only exception being chloride. Free metal ions quench the fluorescence as in many

TABLE 3

Quenching of fluorescence of BNM amine by selected solutes

Solute ^a	Change in FI ^b (%)	Solute ^a	Change in FI ^b (%)	Solute ^a	Change in FI ^b (%)
H ₂ O	<-0.1	Co(II)	-5.7	Cu(II)/EDTA	+2.9 ^c
CH ₃ OH	<-0.1	Ni(II)	-11.4	Cl ⁻	-6.5
Cu(II)	-6.1	CS ₂	-13.7	Br ⁻	-37
Hg(II)	-5.5	(C ₂ H ₅) ₂ NH	-6.3	I ⁻	-96
Fe(III)	-11.5	Hg(II)/EDTA	+1.6 ^c	CS ₂ /(C ₂ H ₅) ₂ NH	-6.0

^a0.5 × 10⁻⁵ M. ^bChange in fluorescence intensity. ^cChange of fluorescence intensity on the addition of EDTA to metal and BNM amine mixture.

other fluorescent processes; EDTA can be used as a masking reagent for metals even though the effect is small. Unfortunately, diethylamine did not reduce the quenching by carbon disulfide. Initially it was thought that this happened because diethylamine does not react with carbon disulfide in acidic solution; but in alkaline solution, diethylamine still did not reduce the quenching by carbon disulfide and, in fact, it quenched the fluorescence of the BNM amine. It is well known that aromatic and aliphatic amines quench many fluorescent processes through an electron- or charge-transfer reaction during the formation of an exciplex [18, 20]. The efficiency of this quenching process depends on the structure of the amine, the fluorescent substance, and the solvent medium. In a polar solvent, cationic and anionic radicals can be obtained from the quencher (amine) and the fluorescent species, respectively. In alkaline solution, amines have higher electron-donating abilities than in acidic solution and thus are stronger quenchers. Because the BNM amine is a much larger molecule than diethylamine, self-quenching of BNM amine through the same mechanism is sterically hindered.

The main conclusion then is that quenching of fluorescence by the side products, metal ions, and carbon disulfide limits the maximum fluorescence yield and establishes an upper limit on the reaction time. Once the rate of generation of BNM amine cannot compensate for the follow-up photochemical processes, the fluorescence yield will decrease upon further irradiation. EDTA can be used to improve the yield by complexing metals but the full yield equivalent to BNM amine cannot be obtained because of the presence of carbon disulfide. All in all, there are not very many chemical parameters that one can adjust to enhance greatly the fluorescence yield or signal.

Design of the flow photochemical reactor

Use of any post-column reactor invariably involves a compromise between obtaining a complete reaction and excessive dispersion by band broadening (Taylor dispersion). As shown above, short irradiation times result in an insufficient yield of fluorescent product and excessive irradiation times lead to a decrease in fluorescence because of subsequent reactions. The reaction time is constant for any reactor at a given flow rate, but the optimum reaction time will vary from compound to compound. Although the flow rate should be optimized for the best chromatographic results in terms of the separation efficiency, one must also optimize the size and shape of the reactor for the optimum reaction time and minimum band dispersion.

According to Atwood and Golay [21], under certain conditions the dispersion of peaks, as measured by peak variance produced in straight open tubes in chromatographic systems can be approximated as

$$\sigma_v^2 = \pi d^4 FL / 384D \quad (1)$$

where σ_v is the standard deviation of a Gaussian peak in volume (cm^3), D is the diffusivity of the sample (typically, $D \approx 10^{-5} \text{ cm}^2 \text{ s}^{-1}$) in the mobile phase, F is the flow rate in units of $\text{cm}^3 \text{ min}^{-1}$, L is the length of the tube (cm) and

d is the inside diameter of the tube (cm). This equation indicates that the total volume and also the dimensions of a reactor will affect the performance of the reactor.

Quartz capillaries have good transparency, but are fragile, expensive, and not readily available; leak-proof connections are often difficult to obtain. Recently, teflon tubing has been used for photochemical reactors by several authors [12, 22, 23] because teflon is transparent to u.v. radiation. Therefore, teflon tubing was used here, primarily because of its excellent mechanical properties.

Model I (Long and wide reaction coil). As a starting point, a 1-ml volume reactor was made from 500 cm of 0.02-in. i.d. teflon tubing. Bulk-solution results indicated that, after one minute of irradiation, most of BNM-DTC complexes will be only 50% decomposed in terms of their maximum fluorescence (see Fig. 4). This is quite different from the results obtained in a flow reactor (Fig. 6). In the flow system, the fluorescent yields are high after irradiation for 1 min, and are almost maximized. This high efficiency of the photochemical reaction is a consequence of the short optical path length of the small tubing. However, the peak broadening caused by this reactor was much too large to allow its use in a viable system.

Model II (Short and wide reaction coil). It was not clear whether a decrease in reactor size would lead to a decrease in peak height, but it would certainly produce a narrower peak. Therefore, the effect of using a shorter reactor was studied (see Table 4). Obviously, at the same flow rate, the shorter the reaction coil, the lower will be the fluorescence yield. These yields are shown in columns 1 and 3 in Table 4 as the product of peak area and flow rate ($A \times F$). Using the same reactor, the yields are less at higher flow rate. In any case, the yields should be, and are, the same if the residence times in the reactor are equal (see columns 3 and 5).

Peak heights behave quite differently than peak areas in such a reactor. For a concentration detector, the peak height (ϕ) of a Gaussian peak is inversely proportional to the standard deviation of the peak

$$\phi = \alpha W / (2\pi)^{1/2} \sigma_v, \quad (2)$$

where W is the total amount of substance injected. It is also well known that the standard deviation in volume units is proportional to both the flow rate and the length of the tubing (Eqn. 1). Thus, in the same reactor, high flow rates decrease the fluorescence yield and increase the peak broadening such that peak height will decrease (see columns 2 and 6). However, when the residence time in the photochemical reactor is held constant, a lower flow rate and shorter reaction coil will make the peak-height measurements better than the area measurements (see columns 4 and 6). This was proved with BNM amine as the solute (see columns 2 and 6); it should be pointed out that the fluorescence of the BNM amine is independent of the length of the reactor. However, the fluorescence intensity from the BNMDTC complexes increases with the length of the reactor. In a shorter reactor, the yield from

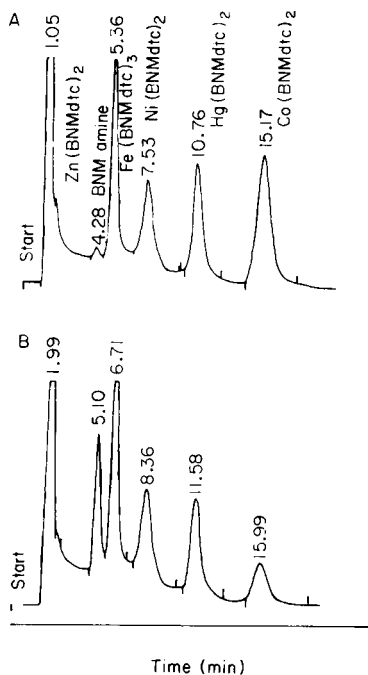
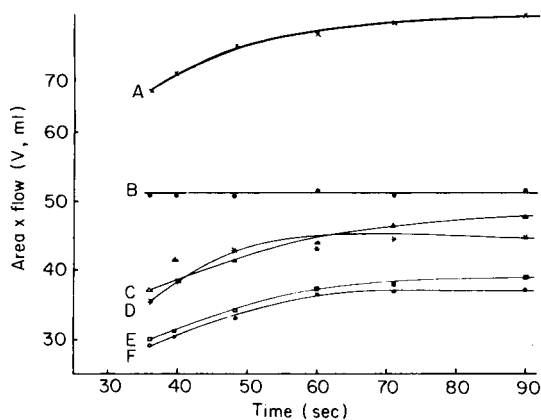


Fig. 6. Photolysis of BNMDTC complexes in flow system. Teflon coil of 6-cm diameter (Model I); Perkin-Elmer 650-10LC, sensitivity $\times 0.3$; λ_{ex} 233 nm, slit 10 nm; λ_{em} 330 nm, slit 20 nm. Mobile phase, 95/5 methanol/water, 1 mM acetate buffer pH 5.5; sample concentration, 1×10^{-5} M. H.p.l.c. system without packed column. Curves: (A) Zn(BNMDTC)₂; (B) BNM amine; (C) Ni(BNMDTC)₂; (D) Hg(BNMDTC)₂; (E) Cu(BNMDTC)₂; (F) Co(BNMDTC)₂.

Fig. 7. Chromatograms of BNMDTC complexes with and without photochemical reactor (Model III). Mobile phase 95/5 methanol/water, 1 mM Tris, pH 8.25, at 1 ml min^{-1} ; samples, 1×10^{-6} M of each component, 200- μl injection; Column, $90 \times 4.6 \text{ mm}$, μ Bondapak C₁₈, 10 μm ; Model III reactor. Detector: (A) IBM fixed wavelength 254 nm, 0.01 AFS; (B) Schoeffel FS-970, 220 nm, 1×10^{-6} AFS.

area measurement is less, but the peak height responses are higher because dilution is less; this is true only for complexes which decompose rapidly (e.g., zinc and mercury BNMDTC). For the photochemically more stable complexes (e.g., copper and cobalt BNMDTC) the peak-height responses are less in a shorter reactor than in a longer reactor because of the lower yield of fluorescent product.

A separation of BNMDTC complexes was tried at low concentration. Although the signal-to-noise ratio was good, the peaks were excessively broad.

Model III (Long narrow reaction coil). In the Model II system, the effect of the length of the reactor on peak broadening was studied. According to Eqn. 1, the inside diameter of a reactor should have a strong influence on peak broadening. If the volume of the reactor, V , is kept constant, Eqn. 1 can be written as

TABLE 4

Comparison of the photolysis yield^a in different sizes of reactor

Compound ^b	Reactor volume 1.20 ml				Reactor volume 0.54 ml	
	1.2 min/1 ml min ⁻¹ ^c		0.6 min/2 ml min ⁻¹ ^c		0.54 min/1 ml min ⁻¹ ^c	
	A × F	Pk. ht.	A × F	Pk. ht.	A × F	Pk. ht.
	(1)	(2)	(3)	(4)	(5)	(6)
BNM amine	200	90	198	90	199	106
Zn(BNMDTC) ₂	261	117	220	97	220	123
Cu(BNMDTC) ₂	195	83	128	53	112	61
Co(BNMDTC) ₂	277	125	200	87	178	99
Hg(BNMDTC) ₂	236	107	196	86	190	113

^aFluorescence intensity from integrator. ^bConcentration is 1×10^{-5} M, except for the Co and Hg complexes at $1-2 \times 10^{-6}$ M. ^cResidence time/flow rate.

$$\sigma_v^2 = V_T F d^2 / 96D \quad (3)$$

$$\text{or } \sigma_v^2 = V_T^2 F / 24\pi DL \quad (4)$$

This equation indicates that a reactor with long, narrow tubing has less peak broadening than a reactor with short, wide tubing provided that both reactors have the same volume. Reactor Model III was, therefore, made from a 10-m long, 0.01-in. i.d. teflon tube which had about the same volume as the Model II reactor. An overall comparison of the peak broadening in the three different reactors is summarized in Table 5. Theoretical values of σ_v were calculated from the equation [21]: $\sigma_v/V_T = n^{-1/2}(1 + 3/n)^{-1/4}$, where n is the number of theoretical plates of a tube of length L and is expressed as $n = 24\pi DL/F$. The volumes of the reactors were obtained experimentally from the solute transit time. They are somewhat different from the values calculated from the length and inside diameter of the reaction coil because of the non-uniformity of the tubes.

Clearly, peak broadening in the connectors is negligible. The values of σ_v for the different reactors are all much smaller than the calculated values because the Aris-Taylor equation for peak broadening in straight tubes is not valid for coiled tubes [17].

By halving the i.d. of the tube, a σ_v of about $42 \mu\text{l}$ was achieved in the Model III system; this is less than half the value of the previous system. The extra benefit probably results from the geometry of the coil. In Model III, many coils cross over each other and around the tubing mounts. It is well known that a few sharp bends along a length of tubing will augment radial mixing. Recently, a striking example of this knitted coil effect was presented by Uihlein and Schwab [17], which was much better than any of our models. However, their "knitted" reactor has a high pressure drop. Model III was judged to be quite acceptable in terms of the separation (resolution) for the

TABLE 5

Peak broadening caused by the different designs of photochemical reactors

Model	I.d. (in.)	Length (cm)	V_T (ml)	n	σ_v (μ l)			HETP (cm)
					Theor.	Found	Ratio ^a	
I	0.02	500	1.2	22.6	252	138	0.55	6.6
II	0.02	260	0.54	11.8	151	95	0.63	8.1
III	0.01	1000	0.69	45.2	102	42	0.41	3.7
Connector	0.01	6	—	2.72	2	7.5	—	—

^aRatio of σ_v (found)/ σ_v (theoretical).

BNMDTC complexes. Figure 7 shows a chromatogram obtained for the separation of the BNMDTC complexes with and without the Model III photochemical reactor. The peak widths of the chromatogram (A) recorded by a u.v. absorption detector located before the post-column reactor are about the same as those of the chromatogram (B) recorded by a fluorimeter located after the reactor. It may be noted that only the resolution of the free amine and iron(III) may be compromised by the broadening in the reactor. It is evident that the peak broadening in the photochemical reactor is insignificant and that the resolution between pairs of BNMDTC complexes is excellent.

Detection limits

The detection limits of some selected BNMDTC complexes, including the iron, nickel, mercury and cobalt complexes, were studied by the photochemical post-column derivatization method. These complexes can be simultaneously separated under the conditions outlined for Fig. 7 with very good resolution. Calibration graphs of these complexes and BNM amine are plotted as the ratio of signal to concentration vs. the log of concentration or amount injected (see Fig. 8). Effectively, this is a plot of the sensitivity vs. logarithmic concentration. The linearity of detector response is very good for BNM amine. Decreased sensitivities at high concentrations of most BNMDTC complexes (except nickel) are not caused by nonlinearity of the detector or by self-quenching of the BNM amine; more likely they are caused by carbon disulfide and metal ions. At low concentrations, the iron and cobalt complexes have higher sensitivities because of contamination or reaction between sample and metal components of the column. The negative deviations of nickel and mercury at low concentrations indicate that these complexes dissociate slightly. In general, the linearity should be quite acceptable for determinations of trace metals, provided that the response factor is within $\pm 5\%$ of the mean. The linear ranges for BNM amine, and the iron, nickel, mercury and cobalt complexes are 2–400, 10–400, 40–400, 20–400 and 40–400 pmol, respectively.

Detection limits estimated by the method of Hubaux and Vos [16] and other data are presented in Table 6. It is evident that the precision of the

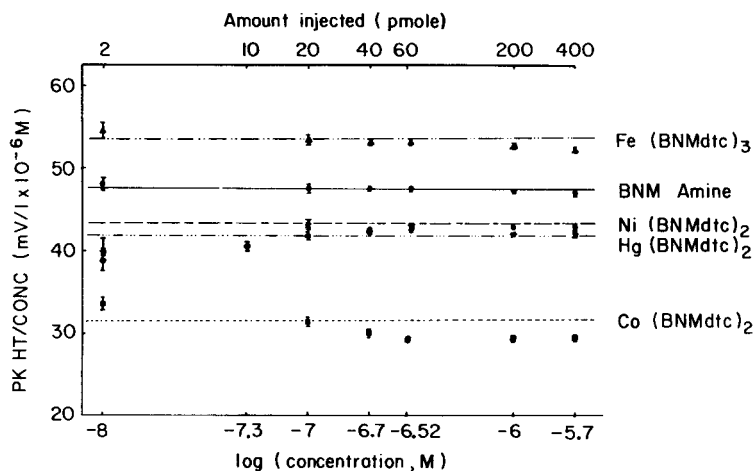


Fig. 8. Effects of concentration on sensitivity for selected BNMDTC complexes. Solvent, 93/7 methanol/water, 1 mM Tris at pH 8.25 at 1 ml min⁻¹; 200- μ l samples. Column as for Fig. 7; Model III reactor; Schoeffel FS-970, 221 nm, detector.

TABLE 6

Precision of peak-area and peak-height measurements of BNMDTC complexes

Metal	Relative standard deviation (%) at different concentrations (M)											Estimated detection limit (10 ⁻⁸ M)			
	2 × 10 ⁻⁶		1 × 10 ⁻⁶		3 × 10 ⁻⁷		2 × 10 ⁻⁷		1 × 10 ⁻⁷		1 × 10 ⁻⁸		C ^c	D ^d	E ^e
	A ^a	B ^b	A	B	A	B	A	B	A	B	A	B			
Fe	0.1	0.1	0.1	0.1	1.6	1.0	3.0	1.5	3.2	1.8	7.0	2.6	0.5	0.3	1.0
Ni	1.5	1.0	2.0	2.0	4.0	2.8	5.7	4.0	6.2	4.6	8.1	7.2	5.0	4.0	2.0
Hg	0.1	0.1	0.1	0.1	1.0	1.0	3.8	2.0	4.0	2.5	6.3	8.2	3.5	0.6	2.0
Co	0.1	0.1	0.1	0.1	0.6	0.6	2.5	1.1	2.9	1.2	9.5	1.5	1.3	0.8	2.0
BNM amine	0.1	0.1	0.1	0.1	0.5	0.5	2.0	0.5	2.0	0.5	6.2	1.0	0.8	0.5	1.0

^aPeak area. ^bPeak height. ^cFrom peak-area measurement. ^dFrom peak-height measurement. ^eFrom S/N measurement.

peak-height measurements is better than that of the peak-area measurements, especially at low concentration. Thus, detection limits estimated from peak-height measurements are better.

Usually, this estimation method is more precise and conservative from the statistical point of view than is the conventional method which defines the detection limit as the concentration or amount at which the signal-to-noise ratio is 2:1 or 3:1. However, if the calibration graph is not linear, this method will not be preferred. This is demonstrated by the nickel complex. The best detection limits for iron, nickel, mercury and cobalt are 0.6, 8.0, 1.2 and 1.6 pmol or 0.2, 1.2, 1.2 and 0.5 μ g l⁻¹, respectively.

Survey of chromatographic properties of BNMDTC complexes

The metal-DDTC complexes can be separated by both normal-phase and reversed-phase liquid chromatography [2]. This indicates that interactions between the samples and the silanol groups on the solid stationary surface and the hydrophobic liquid stationary phase both play important roles. Because the stationary phases in nonpolar-phase systems actually possess both silanol groups and bound ligands, only the results from nonpolar-phase systems were closely examined.

It is well known that the resolution of a particular set of samples can vary as the column (stationary phase) and the mobile phase are varied. Normally, the effects are small with a small change in separation conditions. In the case of DDTC, however, it has been shown that the separation is extremely sensitive to the conditions. The particle sizes [24, 25] and support materials [24, 26] have been shown to alter the elution order of the complexes. Obviously, the organic modifiers in the mobile phase can influence the separation [27]. Schwedt [24, 27] found that a change in the methanol/water compositions from 68/32 to 70/30 caused an inversion of the elution order of the lead and nickel complexes. He has also found that under identical separation conditions, the separation of DDTC and tetramethylenedithiocarbamate complexes have very different resolution but the same elution order for the cadmium, lead, nickel, cobalt, zinc, copper and mercury complexes [2, 24]. This indicates that the selectivity of the separation is dependent upon the inner part of the molecules as well as the hydrophobic alkyl components.

In the case of the BNMDTC complexes, the separation was assessed in a variety of mobile phases (acetonitrile-water, THF-water, isopropanol-water and methanol-water). Preliminary experiments indicated that methanol-water mixtures gave the best chromatographic selectivities and therefore the most easily optimized resolution. Because of the presence of the bulky butyl and naphthyl groups, a very strong mobile phase is needed (i.e., 95/5 methanol/water). Actual retention (k') is very sensitive to the mobile-phase composition, but the elution order is invariant. The chromatographic results differ considerably between different nonpolar stationary-phase columns as in the case of the DDTC complexes. The selectivity of this separation is probably controlled by the differences in the interactions of the NCS_2 group with the surface and the mobile phase as moderated by the metal. The interactions between amines and the silanol groups on the packing material can be very strong [28]. Here, it was observed that heavily loaded (22% weight carbon) C_{18} columns gave very poor selectivity and diminished retention of the BNMDTC complexes. Also, a PRP column (150 \times 4.1 mm, 8–12 μm , polystyrenedivinylbenzene), which is extremely hydrophobic and has no free silanol group, had very long retention, but essentially no selectivity for the different BNMDTC complexes.

The present separation is possible on a variety of commercial columns. Table 7 shows the optimal chromatographic conditions and results for some selected BNMDTC complexes which are separable on three different reversed-phase columns. The Supelco C_8 column has the highest carbon loading and

TABLE 7

Chromatographic results for $M(\text{BNMDTC})_n$

- [I. Column: Waters RCM-100 C_{18} , 5% carbon loading, 10- μm particles, 100 \times 8 mm. Mobile phase: 95/5 methanol/water, 1 mM Tris, pH 8.25, at 2.0 ml min^{-1} .
 II. Column: Supercosil LC-8, 20% carbon loading, 5- μm particles, 150 \times 4.6 mm. Mobile phase: 85/15 methanol/water, 1 mM Tris, pH 8.25, at 2.5 ml min^{-1} .
 III. Column: Waters $\mu\text{Bondapak } C_{18}$, 10% carbon loading, 10- μm particles, 90 \times 4.6 mm. Mobile phase: 93/7 methanol/water, 1 mM Tris, pH 8.25, at 1.0 ml min^{-1} .]

Metal	Retention (k')			Asymmetry (a/b)			Reduced plate height (h)		
	I	II	III	I	II	III	I	II	III
Fe(III)	3.9	4.6	2.3	0.9	1.0	1.1	12.0	15.5	10
Ni(II)	6.2	6.4	3.6	1.2	1.2	1.2	8.7	16.3	13.2
Cu(II)	8.5	9.2	5.2	1.1	1.0	1.1	6.7	15.7	9.4
Hg(II)	10.1	10.9	5.5	1.0	1.2	1.1	5.3	13.8	9.3
Co(II)	12.1	—	8.1	1.0	—	1.0	6.7	—	13.4
Toluene ^a	4.2	3.2	3.9	1.2	0.98	1.1	4.8	7.2	8.0

^a60/40 methanol/water at flow rate indicated in each column.

possibly the lowest number of free silanol groups of any of the stationary phases. This column required a relatively weak mobile phase such as 85/15 methanol/water to separate the BNMDTC complexes. The RCM-100 C_{18} and $\mu\text{Bondapak } C_{18}$ columns are very similar. However, the separation of copper— and mercury—BNMDTC complexes was not achieved under the conditions investigated here. The peak shapes of the BNMDTC complexes are all excellent; the highest asymmetry value was only 1.2. However, the separation efficiencies (h) are all below what can be achieved under optimal conditions. It should be noted that this may not be a fair evaluation because all three columns had been used extensively before the separation of the BNMDTC complexes. The RCM-100 C_{18} column had been used for other studies at pH 10.0 and the column beds of the Supelco C_8 and $\mu\text{Bondapak } C_{18}$ columns had been disturbed by placing silanized metal frits in the end-fittings of the columns [29]. Thus, the separation results for toluene are also included in the table for comparison purposes.

Although dithiocarbamate complexes have been reported for nearly 60 elements, the above technique was applied to a much more limited set. For the method described here to work, the metal must replace zinc because the zinc salt of BNMDTC was used. Secondly, the complex must be either thermodynamically very stable or kinetically inert toward dissociation so as to provide acceptable peak width and shape. Finally, in order to achieve the detection limits reported here, the BNMDTC complex must be photochemically decomposed to a fluorescent product. Thus far we have been able to demonstrate either by chromatographic means or by direct chemical observation that BNMDTC complexes can be formed for Fe(II, III), Co(II), Ni(II), Cu(I, II), Zn(II), Mo(VI), Ag(I), Cd(II), Sn(II), La(III), Ce(III), Pt(II), Au(III), Hg(II), Ti(III), Pb(II), Bi(III) and U(VI). Formation of complexes could not be detected for Ti(IV), V(V), Cr(III, VI), In(III), Sn(IV), Sb(III), W(VI), Ce(IV) or Th(IV).

Additional complexes might form if a salt other than zinc(II)-(BNMDTC)₂ were available. To test this conjecture, the BNMDTC was generated using sodium or potassium hydroxide in the synthetic procedure [29]. The reagent is sufficiently hydrophobic to allow extraction of these cations into nonpolar solvents such as chloroform. Addition of calcium ion prevented the extraction of the sodium and potassium, from which it can be inferred that a fairly strong ion-pair exists between calcium and BNMDTC. Thus, if a more reactive salt of the complexing agent were available, one should be able to detect either an ion-pair or complex with a very wide variety of metals.

This work was supported by a grant from the National Institute of Occupational Safety and Health. (1RO1-OH00876-01).

REFERENCES

- 1 G. Schwedt, *Chromatographic Methods in Inorganic Analysis*, Dr. Alfred Huethig Publishers, New York, 1981.
- 2 G. Schwedt, *Chromatographia*, 12 (1979) 613.
- 3 M. Moriyasu and Y. Hushimoto, *Bull. Chem. Soc. Jpn.*, 54 (1981) 2470.
- 4 J. W. O'Laughlin and T. P. O'Brien, *Anal. Lett.*, A11 (1978) 829.
- 5 Y. T. Shih and P. W. Carr, *Anal. Chim. Acta*, 142 (1982) 55.
- 6 K. S. Stulik and V. Pacakova, *J. Electroanal. Chem.*, 129 (1981) 1.
- 7 P. Kissinger and K. Bratin, *Talanta*, 29 (1982) 365.
- 8 A. M. Bond and G. G. Wallace, *Anal. Chem.*, 29 (1982) 365.
- 9 P. Kissinger and K. Bratin, *Recent Developments in the Reductive LCEC of Organic Compounds Using Mercury Film and Glassy Carbon Electrodes*, presented at the Eastern Analytical Symposium, New York, Sept., 1980.
- 10 A. Stoll and W. Schlientz, *Helv. Chim. Acta*, 38 (1955) 585.
- 11 P. Hajdú, M. Uihlein and D. Damm, *J. Clin. Chem. Clin. Biochem.*, 18 (1980) 209.
- 12 P. J. Twitchett, P. L. Williams and A. C. Moffat, *J. Chromatogr.*, 149 (1978) 683.
- 13 A. H. M. T. Scholten and R. W. Frei, *J. Chromatogr.*, 176 (1979) 349.
- 14 M. F. Lefevre, R. W. Frei, A. H. M. T. Scholten and U. A. Th. Brinkman, *Chromatographia*, 15 (1982) 459.
- 15 G. L. Miessler, G. Stuk, T. P. Smith, K. W. Given, M. C. Palazzotto and L. H. Pignolet, *Inorg. Chem.*, 15 (1976) 1982.
- 16 A. Hubaux and G. Vos, *Anal. Chem.*, 42 (1970) 849.
- 17 M. Uihlein and E. Schwab, *Chromatographia*, 15 (1982) 140.
- 18 G. G. Guilbault, *Practical Fluorescence Theory, Methods and Techniques*, 2nd edn., M. Dekker, New York, 1973, Ch. 2.
- 19 E. B. Sandell and H. Onishi, *Photometric Determination of Trace Metals*, 4th edn., Wiley-Interscience, New York, 1978, pp. 512-532.
- 20 W. A. Yee, D. G. Lishan and G. S. Hammond, *J. Phys. Chem.*, 85 (1981) 3435.
- 21 J. G. Atwood and M. J. E. Golay, *J. Chromatogr.*, 218 (1981) 98.
- 22 A. H. M. T. Scholten, P. L. M. Willig, U. A. Th. Brinkman and R. W. Frei, *J. Chromatogr.*, 199 (1980) 239.
- 23 P. Ciccio, R. Tappa and A. Guiducci, *Anal. Chem.*, 53 (1981) 1309.
- 24 G. Schwedt, *Chromatographia*, 12 (1979) 289.
- 25 N. Häring and K. Ballschmiter, *Talanta*, 27 (1980) 873.
- 26 G. Schwedt, *Z. Anal. Chem.*, 288 (1977) 50.
- 27 G. Schwedt, *Chromatographia*, 11 (1978) 145.
- 28 B. A. Bidlingmeyer, J. K. Del Rios and J. Korpi, *Anal. Chem.*, 54 (1982) 442.
- 29 Y. T. Shih and P. W. Carr, *Talanta*, 28 (1981) 411.

LIQUID ADSORPTION CHROMATOGRAPHY OF CHELATES

The Effect of Structure on the Thin-layer Chromatographic Behaviour of Chelates

A. R. TIMERBAEV* and O. M. PETRUKHIN

V. I. Vernadskii Institute of Geochemistry and Analytical Chemistry, U.S.S.R. Academy of Sciences, Kosigina 19, Moscow (U.S.S.R.)

(Received 29th September 1983)

SUMMARY

The thin-layer chromatographic behaviour of chelates belonging to different classes is discussed. The major adsorption interactions of chelates are hydrogen bonding between the ligand donor atoms and the surface hydroxyl groups and reactions between the metal atom and the electron-donor active centres of the sorbent. Predominance of either of these general mechanisms depends on the chelate structure and particularly on the coordination saturation of the chelate. Coordination-saturated chelates are retained because of hydrogen bonding, while the metal atom does not participate directly but can influence sorption by affecting the electron density distribution in the chelating ring. Atomic electronegativity is used as a measure of the electron-acceptor ability of the metal. Electronegative atoms located outside the functional group of the chelate can participate in the adsorption either directly or by affecting the proton-acceptor ability of the donor atoms as a result of induction and steric effects. The relationship between chelate retention factors and the parameters characterizing the electron and spatial structure of ligands can be described quantitatively by an equation of the type $\log [(1/R_f) - 1] = A + \Sigma\sigma$. In the case of coordination-unsaturated chelates, adsorption interactions with participation of the metal atom predominate, either by ion exchange (with ligand replacement) or by a donor-acceptor mechanism (with introduction of the adsorption centre into the coordination sphere without decomposition). In general, the adsorbability of chelates is directly related to the proton-acceptor ability of donor atoms and the acceptor ability of the metal atom. Classification of chelates by their adsorption interactions is proposed. Recommendations are given for selecting the optimal chelating reagent for the separation of metals by liquid-adsorption chromatography.

The liquid chromatography of chelates has become an important technique in inorganic analysis [1–3]. Pre-extraction with chelating reagents ensures simultaneous separation of a group of metals; thus it allows a wider application of the major chromatographic advantage (i.e., an effective separation of multi-component mixtures) and improves the separation by means of selective extraction. High-performance liquid chromatography (h.p.l.c.) of chelates also provides effective determinations of traces of metals, because pre-extraction used for concentration reduces the detection limits to the picogram level. This fact has caused considerable interest in the h.p.l.c. of chelates in recent years [4–7].

However, literature data indicate that the chromatography of many chelates involves many difficulties in choosing separation conditions. These difficulties depend mainly on the complicated nature of many chelates themselves as well as the technique. The choice of chelating reagents is usually made empirically. Little attention has been given to theoretical aspects such as studies of general regularities in chromatographic behaviour, and of the mechanism of chelate separation. This undoubtedly impedes the development of the method.

A systematic study of the dependence of the chromatographic properties of chelates on their structure (the nature of the metals, type of donor atoms and ligand structure as a whole) was therefore undertaken. In the present paper, liquid chromatography means primarily liquid-adsorption chromatography (l.a.c.) which, along the reversed-phase variant, has gained wide application for chelate separation. Thin-layer chromatography (t.l.c.) was used in the investigation because of its characteristics of convenience, technical simplicity, and rapidity.

EXPERIMENTAL

Chelates and chromatographic materials

The complexes were prepared according to known methods by precipitation from an aqueous-alcohol medium (β -diketonates, thio- β -diketonates), or by mixing aqueous solutions of metal salts and the reagent (diethyldithiocarbamates, dialkyldithiophosphates, dialkyldithiophosphinates), or by extraction (8-quinolinolates and some others). The chelates were purified chromatographically, and after recrystallization from appropriate mixtures of solvents, were characterized by melting points, elemental analyses, and spectroscopic techniques (i.r., n.m.r. etc.).

The ligands tested are listed in Table 1.

The following sorbents were used for chromatography: silica gel L (5–40 μ m; Lachema, CSSR), Silpearl (Sklarny Kavalier, CSSR), aluminium oxide (neutral, Brockman II activity; Reanal, Hungary), microcrystalline cellulose LK

TABLE 1

The ligands tested and their abbreviations

AA	Acetylacetone	DHDTP	Dicyclohexyldithiophosphate
BA	Benzoylacetone	DPDTPN	Dipropyldithiophosphinate
DBM	Dibenzoylmethane	DPDTP	Dipropyldithiophosphate
DBDTPN	Dibutyldithiophosphinate	DTAA	Dithioacetylacetone
DBDTP	Dibutyldithiophosphate	HFAA	Hexafluoroacetylacetone
DEDTC	Diethyldithiocarbamate	Q	8-Quinolinol
DEDTP	Diethyldithiophosphate	TBA	Monothiobenzoylacetone
D2EHDTP	Di-2-ethylhexyldithiophosphate	TTFA	Thenoyltrifluoroacetone
D2EHP	Di-2-ethylhexylphosphate	TFAA	Trifluoroacetylacetone
DMDTP	Dimethyldithiophosphate		

(Lachema) and some others, as well as commercially available Silufol chromatographic plates (Kavalier). The t.l.c. plates were usually prepared by applying an unbonded layer of the sorbent (thickness, 0.5 or 1.0 mm) onto glass plates (9 × 12 or 13 × 18 cm). The organic solvents used as mobile phases were purified by standard procedures, dried, and distilled.

Chromatographic conditions

The experiments were done at constant temperature ($25 \pm 0.25^\circ\text{C}$) with the chromatographic chamber placed in a thermostat. Constant humidity in the chamber was maintained by means of a hygostat (i.e., a saturated solution of a salt over its crystals). Samples (1–10 μl) of 0.025–0.1% (w/v) solutions of the chelates in chloroform or ethanol, or their mixture (1 + 1), were applied with a calibrated capillary (EVA-Chrom, F.R.G.) or a microsyringe. The development time was kept constant at 10 min. The developed zones were detected by using iodine vapour or from their characteristic colours. Certain weakly coloured complexes were detected by means of selective reagents.

To obtain highly reproducible results, special importance was attached to standardization of the experimental conditions in determining the R_f values. It was shown in preliminary investigations that the procedures of layer preparation and sample application, as well as the sorbent layer thickness and the sample size (in the region of low loading where the deviations of the adsorption isotherms from linearity were insignificant) did not appreciably affect the reproducibility of R_f values. The factors most discernibly affecting the mobility of substances included the degree of sorbent saturation with water vapour, and to a lesser extent, with the vapours of the mobile phase. The latter mainly affect the kinetic factors of the process. Chromatographic separations were therefore done under equilibrium conditions, the surface of the sorbent being saturated with both moisture and the organic solvent vapour.

In these studies of the dependence of chelate retention on the duration of sorbent contact with water and solvent vapours, it was found that simultaneous saturation for 1.5–2 h sufficed to establish the corresponding equilibria and to obtain reproducible results, irrespective of the chelate type, the nature of the solvent, or the adsorptive properties of silica gel (initial moisture content). Typical dependences are presented in Fig. 1. Longer contact times did not affect the chelate mobility. Accordingly, the chromatographic properties of the complexes were studied under standardized conditions of plate preparation, i.e., the plates with the applied chelates were kept over the vapours of the mobile phase and hygostat for 2 h prior to development. As a result of the optimized chromatographic conditions and the above precautions, the reproducibility of the R_f values was better than 0.02, which is close to the optimum for conventional t.l.c.

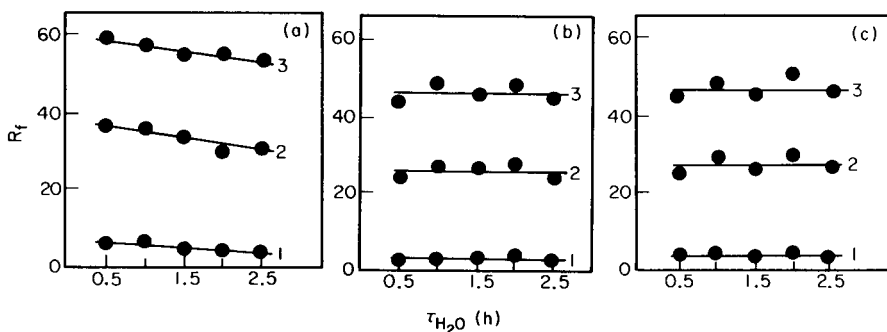


Fig. 1. Dependence of the R_f values of (1) Co(AA)₃, (2) Co(DBM)₃, (3) Cr(DBM)₃ on the time of silica gel contact with water vapour (t_{H_2O}) and the mobile phase vapour (chloroform) (t_{MP}). t_{MP} : (a) 1 h; (b) 1.5 h; (c) 2 h.

RESULTS AND DISCUSSION

Preliminary theoretical considerations

The chromatographic properties of chelates, like those of any other compound, depend primarily on their structure. According to the classification of molecules with regard to their ability to undergo different types of interaction in molecular adsorption chromatography, which was proposed by Kisilev [8], chelates can be generally assigned to group C, in conformity with their electronic structure. This group includes molecules which have a localized positive charge (on the metal atom for chelates), whereas the excess electron density is distributed on the adjacent bonds (donor atoms of ligands). Further, most chelates have atoms and bonds with locally concentrated electron density (e.g., free electron pairs or π -bonds), and they can be regarded in the same way as molecules of group B. Thus, in the case of molecular adsorption of chelates on the specific sorbents used in l.a.c., specific interactions of electron-active atoms of the chelates with the corresponding active centres on the surface make the predominant contribution to the overall adsorption energy.

In investigating the chromatographic behaviour of chelates, one must take into account participation of the central metal atom, the donor atoms of the chelating group, and the peripheral electronegative atoms located outside the active site of the chelate in the adsorption interactions. The immediate contribution to adsorption of those parts of the organic molecule that do not interact specifically depends on the type of the ligand and is generally rather small.

In separation on hydroxyl-containing sorbents, which are the most widely used for l.a.c. of chelates, the two following types of interactions make the main contribution to adsorption: (1) hydrogen bonding between the electronegative atoms of ligands and the surface hydroxyl groups, and (2) the interaction of metal atoms with electron-donor adsorption centres. The latter can occur as a result of coordination of the metal atom followed by ligand

substitution, or by introduction to the coordination sphere without its destruction, i.e., a donor-acceptor mechanism. In both cases, the adsorption interactions are not of molecular, but of chemical nature and are practically irreversible.

Depending on the extent to which the electron environment of the metal corresponds to its coordination capacity, the neutral chelates are divided into coordination-unsaturated and coordination-saturated which exhibit, respectively, higher or lower acceptor ability towards the electron-donor centres. Accordingly, coordination-saturated and coordination-unsaturated chelates differ considerably in their chromatographic behaviour, and the results obtained for them can conveniently be discussed separately.

Coordination-unsaturated chelates

Investigations of the chromatographic behaviour of coordination-unsaturated chelates mainly involved β -diketonates of divalent transition and trivalent rare-earth metals, and the 8-quinolinolates of certain metals. Because of partial uncompensation of the positive charge on the central atom and therefore additional interactions with the electron-donor active centres, these chelates adsorb significantly on hydroxyl-containing sorbents. In practice, on elution with non-polar solvents, the complexes do not move from the origin (irreversible adsorption) and, when the elution ability of the mobile phase is increased, they are chromatographed as broad bands.

In the case of β -diketonates, the interactions of the metal atom are sometimes so strong that the electronegative surface groups of silica gel ($-\text{OH}$, $-\text{O}-$ and, possibly, $-\text{O}^-$) partially or completely replace the ligands, destroying the chelate. This usually occurs with nonpolar solvents, when adsorption is accompanied by replacement of the molecules of mobile phase from the monolayer adsorbed on the surface of the sorbent. This produces irreversible formation of the surface compounds located at or near the start; the chromatograms show the zones belonging to the free reagent.

Strong retention of coordination-unsaturated β -diketonates is not necessarily decreased by introduction of voluminous substituents into the reagent in order to screen the active site of the chelate, e.g., phenyl in benzoylacetates and dibenzoylmethanates, or trifluoromethyl in thenoyltrifluoroacetates.

Complexes of cobalt(II) and nickel display a higher acceptor ability than the analogous copper chelates, and so are adsorbed more strongly, being decomposed completely (if at all) with the loss of both ligands. With copper β -diketonates, the destruction process apparently takes place stepwise. Similar chromatographic properties are displayed by diketonates of lanthanides (and lanthanum and yttrium), which have high acceptor abilities because of vacant $4f$ -shell orbitals.

8-Quinolinolates are chromatographically more stable, but the highly ionic character of the metal-ligand bond means that they exhibit heightened acceptor and, hence, adsorption ability (Table 2).

TABLE 2

 R_f values of 8-quinolinolates on Silufol^a

Complex	R_f value			
	Chloroform	Acetone	Methanol	Dioxane
Cu(Q) ₂	0.03	0.65	0.66	0.77
Fe(Q) ₃	0.00	0.15	0.08	0.78
Mg(Q) ₂	0.12	0.12	0.22	0.77
Ni(Q) ₂	0.07	0.15	0.09	0.75
Pb(Q) ₂	0.11	0.07	0.15	0.77

^aT.l.c. was done under unconventional conditions.

The chromatography of coordination-unsaturated chelates requires the presence of polar components in the mobile phase. Even so, the results may be unsatisfactory, although adsorption of the complexes may be decreased and rather mobile and symmetric zones obtained. The major disadvantage of increased polarity of the mobile phase is the lowered selectivity of separation caused by bonding of the sorbent active centres by the polar molecules of the solvent. The specific solvation of solutes also levels off differences in their chromatographic behaviour so that the complexes have similar R_f values.

No success was achieved in attempts to chromatograph β -diketonates of divalent transition metals with mobile phases containing organic donor-active compounds capable of decreasing coordination-unsaturation (acceptor ability) via adduct formation; tests with prepared adducts were also unsuccessful. For example, the addition of up to 4% (w/w) of pyridine (an amount quite sufficient to cover the silica gel with a monomolecular layer) did not decrease the adsorption of the acetylacetonates and thenoyltrifluoroacetates of Co, Cu and Ni. The adducts of copper and nickel β -diketonates were destroyed during chromatography because the interaction of the chelate with sorbent was much stronger than that with the organic base. Also destroyed were such stable adducts as those of thenoyltrifluoroacetates of rare earth metals with tri-*n*-octylphosphine oxide.

Thus, the use of coordination-unsaturated chelates for the separation of metals by l.a.c. is limited because of their high affinity for specific sorbents and inadequate stability.

Coordination-saturated chelates

Coordination-saturated chelates are more suitable for separation. In these complexes, the central atom has no energetically favorable orbitals and does not participate directly in adsorption interactions. That is why most coordination-saturated chelates are readily chromatographed on specific sorbents even with solvents of moderate polarity and are usually rather stable during chromatography.

Yet, the behaviour of such chelates is far from being unambiguous. Complexes with strongly electronegative atoms in the chelating group (e.g., oxygen in β -diketonates or cupferronates, and nitrogen and oxygen atoms in 8-quinolinolates) are adsorbed mainly by hydrogen bonding, which is the commonest adsorption interactions for chelates. Therefore, the mobility of such chelates is relatively weak, depending only slightly on the nature of metal. For example, β -diketonates with similar ligands almost always have similar retention values (Table 3), which makes separations difficult.

Because the adsorption interactions with participation of ligand donor atoms predominate, the adsorption of such coordination-saturated chelates depends on the structure of the organic part of the molecule. Hence, such chelate adsorption is governed by the same general regularities as occur for organic compounds, i.e., the relations between the retention values and the parameters describing the electron and spatial structure of the compounds. Thus, those substituents in β -diketonates that produce electron-acceptor effect lower the negative charge on the oxygen atoms and increase the mobility of the complexes (Table 3). A similar effect can be produced by spatial hindrance caused by voluminous substituents near the active site of the chelate. On the whole, the mobility of β -diketonates increases in the ligand sequence $AA < BA < DBM < TTFA \approx TFAA < HFAA$.

Quantitatively, the effect of substituents on the adsorbability of chelates can be described through the correlation equation based on the linearity principle in changes of free energies [8]. The general formula is $\log K = \log K_0 + \sum_k \sum_i \rho_i \sigma_{i,k}$, where K is the equilibrium constant in the presence of

TABLE 3

R_f values of β -diketonates of trivalent metals in t.l.c. on Silpearl ($n = 4-8$; $\alpha = 0.05$)

Complex	$R_f \times 100$		Complex	$R_f \times 100$	
	Chloroform	Diisopropyl ether		Chloroform	Diisopropyl ether
Co(AA) ₃	3.3 ± 0.5	1.1 ± 0.2	Cr(TTFA) ₃	40.6 ± 2.0	34.1 ± 0.5
Co(BA) ₃	4.3 ± 0.7	18.2 ± 1.4 ^a 34.7 ± 1.4 ^b	Cr(HFAA) ₃	77.2 ± 0.8	71.7 ± 0.8
			Fe(AA) ₃	— ^c	— ^c
			Fe(BA) ₃	— ^c	— ^c
Co(DBM) ₃	26.9 ± 1.4	37.2 ± 1.8	Fe(DBM) ₃	0-10 ^d	31.2 ± 1.3
Co(TFAA) ₃	39.8 ± 1.7	60.9 ± 1.1	Fe(TTFA) ₃	0-10 ^d	30.7 ± 0.7
Co(TTFA) ₃	38.9 ± 2.6	35.8 ± 0.7	Al(AA) ₃	— ^c	— ^c
Co(HFAA) ₃	75.8 ± 0.6	78.1 ± 1.4	Al(TTFA) ₃	0-8 ^d	35.1 ± 1.8
Cr(AA) ₃	2.3 ± 0.5	3.0 ± 0.1	Ga(AA) ₃	— ^c	— ^c
Cr(BA) ₃	3.8 ± 0.3	38.9 ± 0.7	Ga(TTFA) ₃	0-29 ^d	40.3 ± 2.0
Cr(DBM) ₃	45.9 ± 1.3	50.0 ± 0.6	In(AA) ₃	— ^c	— ^c
Cr(TFAA) ₃	19.1 ± 0.9 ^a 39.7 ± 2.1 ^b	43.5 ± 2.4 ^a 61.8 ± 0.9 ^b	In(TTFA) ₃	0-32 ^d	40.1 ± 2.0

^aCis-isomer. ^bTrans-isomer. ^cThe complexes are decomposed during chromatography.

^dThe mobility depends on the sample size.

substituent of index k , and K_0 is the equilibrium constant in the absence of any substituent; i is the index of the interaction type characterized by constant σ_i ; ρ_i serves as a measure of reaction sensitivity to the effects of the corresponding substituent actions. If the process of chelate adsorption in l.a.c. is regarded as a reversible heterogeneous reaction with a sorbent (S): $(ML_n)_M + S \rightleftharpoons (ML_n)_S$, and if the equations $K = k(V_S/V_M)$ and $k = (1 - R_f)/R_f$ are introduced, then the equation obtained is

$$\log [(1/R_f) - 1] = A + \rho^* \sum_k \sigma_k^* + \delta \sum_k E_{S_k}$$

where σ^* and E_S are Taft's induction and steric constants; k is the index of the substituent; ρ^* and δ serve as measures of adsorption sensitivity to the effects of induction and steric actions, respectively; A designates a sum of constant members.

The graphic relationships obtained through this equation are presented in Fig. 2. As can be seen, the correlation of the adsorption ability of β -diketonates and the sum of induction and steric constants of substituents is approximately linear. The proximity of the slopes of the plots for the complexes of cobalt(III) and chromium(III) (-0.66 and -0.67 , respectively) confirmed the slight dependence of the behaviour of coordination-saturated β -diketonates on the nature of the metal. The absolute values of the slopes of the plots indicate that the adsorption process is rather sensitive to the effect of substituents, i.e., it is controlled primarily by the structural features of the ligand.

Similar dependences were obtained for each effect separately, when it was assumed that the principle of additivity was observed and that the various types of interactions were independent (Fig. 3). The corresponding mono-parametric equations are

$$\log [(1/R_f) - 1] = A_1 + \rho^* \sum_k \sigma_k^*$$

$$\log [(1/R_f) - 1] = A_2 + \delta \sum_k E_{S_k}$$

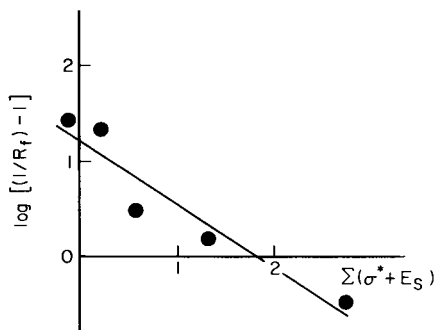


Fig. 2. Dependence of the adsorbability of cobalt(III)- β -diketonates on the sum of induction and steric constants of substituents (silica gel/chloroform). $t = 0.94$; $S = 0.50$.

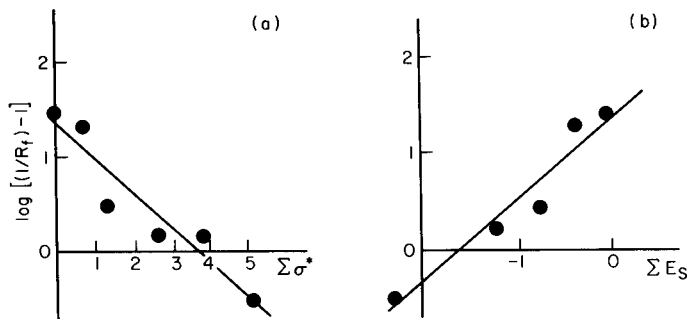


Fig. 3. Relationships for cobalt(III) β -diketonates: (a) $\log [(1/R_f) - 1] = f(\Sigma\sigma^*)$ for $t = 0.93$ and $S = 0.50$; (b) $\log [(1/R_f) - 1] = f(\Sigma E_s)$ for $t = 0.95$ and $S = 0.48$.

As can be seen from Fig. 3, the retention values of complexes are in good correlation with those of the total induction (a) and steric (b) effects of the substituents. The negative slope of the dependence, characterizing a purely inductive interaction ($\rho^* < 0$), signifies that the chelate mobility increases as the electron-acceptor ability of the substituents increases. In l.a.c. terms, the negative sign of ρ^* means that, during chromatography, the chelate ring exhibits proton-acceptor properties while interacting with the surface silanol groups.

These findings, in addition to the linear relations obtained (which mean that chelate adsorption is governed by the principle of linearity of free energy changes), indicate that the adsorption of coordination-saturated chelates on hydroxyl-containing sorbents can indeed be ascribed to the formation of hydrogen bonds. Furthermore, the R_f values of similar complexes can be predicted from the values of the corresponding constants of substituents. A comparison of the chromatographic mobility of β -diketonates with the same central atom implies that the atoms and bonds of the ligand outside the chelate ring play a minor role in the adsorption process.

Kinetically labile β -diketonates of Al(III), Fe(III), In(III) and Ga(III) differ considerably in their chromatographic behaviour (Table 3). In chromatography on specific sorbents, they are less stable and are often irreversibly adsorbed or destroyed if the ligand is replaced by the active site of the sorbent in the inner coordination sphere of the metal, similarly to coordination-unsaturated chelates. However, the ligand structure affects even the chromatographic properties of labile complexes. Thus, although acetylacetonates and benzoylacetonates, despite their higher thermodynamic stability, are destroyed on silica gel when eluted with moderately polar solvents, the spatial screening of the active site of the chelate in dibenzoylmethanates and thenoyltrifluoroacetonates impedes the interaction of the metal atom and increases the chromatographic stability of the complexes.

Coordination-saturated chelates with weaker electronegative donor atoms of the S,S,N,S, and even O,S type were studied, including thio- β -diketonates, diethyldithiocarbamates and dialkyldithiophosphates. In such chelates, the

proton-acceptor ability, and so the strength of hydrogen bonding with surface hydroxyl groups, are much lower. Moreover, in such chelates, the metal-ligand bond is essentially covalent, the charge on the central atom is much weaker, and energies of vacant orbitals are lower. Naturally, the acceptor ability of such chelates with respect to electronegative atoms and groups is lower.

Thioderivatives of β -diketonates and dialkylphosphates exhibit high mobility even when eluted with apolar solvents. The effect of the replacement of one or, particularly, both donor oxygens by sulphur is well illustrated in Table 4. These complexes are mobile even on the strongly polar aluminium oxide. However, for coordination-saturated chelates, sorbents other than silica gel are of little use. When solvents of low polarity are used as the mobile phase, the mobility of the complexes on thin layers of aluminium oxide is low, the R_f values are similar (Table 5). When more polar solvents are used,

TABLE 4

R_f values of nickel and cobalt(III) β -diketonates and copper di-2-ethylhexylphosphate and their thioderivatives on a thin layer of silica gel ($n = 5-6$; $\alpha = 0.05$)

Complex	$R_f \times 100$	
	Chloroform	Diisopropyl ether
Ni(AA) ₂	— ^a	— ^a
Ni(DTAA) ₂	73.6 ± 1.8	44.4 ± 1.1
Ni(BA) ₂	— ^a	— ^a
Ni(TBA) ₂	40.4 ± 2.9	51.8 ± 2.3
Co(BA) ₃	4.3 ± 1.1	18.8 ± 0.1; 36.9 ± 1.3
Co(TBA) ₃	60.1 ± 1.5	52.0 ± 2.2
Cu(D2EHP) ₂	0.0	0—3 ^b
Cu(D2EHDTP) ₂	82.8 ± 0.7	83.6 ± 2.0

^aThe complexes were decomposed during chromatography. ^bThe mobility depends on the sample size.

TABLE 5

R_f values of benzoylacetates and monothiobenzoylacetates on a thin layer of aluminium oxide^a

Complexes	R_f				
	Hexane	Carbon tetrachloride	Toluene	Diisopropyl ether	Chloroform
Cu(BA) ₂	0.00	0.00	0.00	0.00	0.00
Ni(BA) ₂	0.00	0.00	0.00	0.00	0.00
Co(BA) ₃	0.09	0.06	0.18	0.29	0.45—0.70
Ni(TBA) ₂	0.05	0—0.07	0—0.45	0—0.45	0.60—0.90
Co(TBA) ₃	0.00	0.11	0.50—0.75	0.62	0.75—0.95

^aT.l.c. was carried out under unconventional conditions.

the chromatographic zones become diffuse; even chloroform is totally unsuitable for chromatography. Cellulose cannot be used because it is a weakly polar sorbent; complexes move near the solvent front (R_f 0.8–0.9) even on elution with nonpolar hydrocarbons.

The weaker energy of adsorption interactions (hydrogen bonding) with donor atoms for chelates of the S,S,N,S, and O,S types has two consequences. First, their chromatographic behaviour is affected by the nature of the metal which is very important for selective separation. In the case of coordination-saturated chelates, the metal acts on the electron density distribution at the active site of the chelate; this can be regarded as particular to this class of compounds in studies of the principles of chelate adsorption. The proton-acceptor ability of donor atoms must depend on the extent of the ionic character of the metal-ligand bond, and should thus be predetermined by the effective positive charge localized on the metal atom. For qualitative evaluation of the effective charges of metal atoms, the values of their atomic electronegativity were used. Obviously, the lower the electronegativity of the atom, the higher will be the effective charge, the electron density on the donor atoms, and, consequently, the adsorbability of the chelate.

Indeed, the mobility of monothio- β -diketonates, dialkyldithiophosphates and dialkyldithiophosphinates approximately correlates with the electronegativity values of the central atoms: complexes with lower electronegativity are more strongly adsorbed. For diethyldithiocarbamates, this correlation is less strict (see below). (It should be noted here, however, that for coordination-saturated β -diketonates, which are chelates with strongly electronegative donor atoms, the dependence between the R_f and electronegativity values is not observed at all.)

Nonetheless, the ligand structure has a strong influence on the chromatographic behaviour of coordination-saturated chelates of this type. Thus, for dialkyldithiophosphates, the R_f values of the complexes increase from the methyl derivatives through diethyl to the dipropyl derivatives (Table 6). As the alkyl chain becomes longer, the specific interactions of the complexes with the sorbent remain practically unchanged, but the orientation of molecules to the sorbent surface which is advantageous for adsorption is impeded, while the role of the chelate-eluent interactions is intensified. However, further elongation of the substituent has little effect on the adsorbability of complexes, even for ramified or cyclic substituents. That is why the adsorption of palladium and nickel dialkyldithiophosphates (and to a lesser degree, the lead complexes) obeys the linearity principle in free energy changes (see above) only for linear alkyl substituents (Fig. 4). The slopes of the linear regions of the dependences of retention values on the total steric effect of substituents differ considerably for complexes of different metals, which confirms the dependence of the chromatographic properties of these complexes on the nature of the central metal atom. However, beginning from the butyl substituents, the spatial hindrances near the active site of the chelate tend to counteract the effect of the metal, and the resolution of the complexes diminishes.

TABLE 6

R_f values of dialkyldithiophosphates and dialkyldithiophosphinates on a thin layer of Silpearl ($n = 5-8$; $\alpha = 0.05$)

Complex	$R_f \times 100$		Complex	$R_f \times 100$	
	Chloroform	Diisopropyl ether		Chloroform	Diisopropyl ether
Ni(DMDTP) ₂	0-22 ^a	8-42 ^a	Pb(D-s-BDTP) ₂	33.4 ± 1.4	68.2 ± 1.5
Ni(DEDTP) ₂	0-27 ^a	39-53 ^a	Pb(DHDTP) ₂	46.5 ^b	67.7 ^b
Ni(DPDTP) ₂	0-54 ^a	63 ^a	Pb(DPDTPN) ₂	37.3 ± 3.3	60.9 ± 2.1
Ni(D-i-BDTP) ₂	—	70 ^a	Pb(DBDTPN) ₂	52.3 ± 1.0	69.3 ± 1.0
Ni(D-s-BDTP) ₂	67 ^a	69.7 ± 1.2	Pd(DMDTP) ₂	55.4 ± 1.0	52.2 ± 0.9
Ni(DHDTP) ₂	—	70 ^a	Pd(DEDTP) ₂	62.4 ± 0.8	59.2 ± 2.5
Ni(DPDTPN) ₂	48.8 ^b	57.6 ± 1.0	Pd(DPDTP) ₂	72.2 ± 0.7	69.6 ± 1.5
Ni(DBDTPN) ₂	62.3 ^b	57.4 ± 1.4	Pd(D-i-BDTP) ₂	72.7 ± 0.5	73.8 ± 0.9
Pb(DMDTP) ₂	11.5 ± 0.5	18.7 ± 0.5	Pd(D-s-BDTP) ₂	73.8 ± 0.4	70.6 ± 1.1
Pb(DEDTP) ₂	21.7 ± 3.3	40.2 ± 1.1	Pd(DHDTP) ₂	73.6 ± 1.3	71.1 ± 2.3
Pb(DPDTP) ₂	23.6 ± 2.3	56.1 ± 1.3	Pd(DPDTPN) ₂	50.8 ± 2.3	60.3 ± 1.0
Pb(D-i-BDTP) ₂	40.6 ^b	65.3 ± 1.2	Pd(DBDTPN) ₂	65.1 ± 1.0	68.8 ± 1.1

^aThe mobility depends on the sample size. ^b $n < 3$.

Another consequence of decreased proton-acceptor ability of the chelating functional group is the fact that electronegative atoms located away from the functional group in the ligand, especially nitrogen atoms in diethyldithiocarbamates, can contribute considerably to hydrogen bonding with silanol groups. To confirm the participation of such atoms in adsorption interactions, infrared (i.r.) spectroscopy was used. It is known that in most

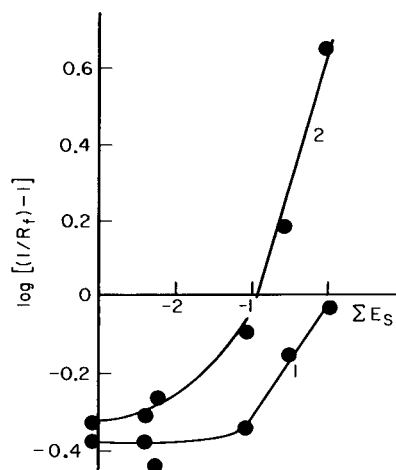


Fig. 4. Dependence of the adsorbability of dialkyldithiophosphates on the size of the alkyl substituents (silica gel/diisopropyl ether): (1) palladium; (2) lead.

dithiocarbamates the free electron pair of nitrogen is shifted toward the chelate ring, and that the C—N bond is partly double-bond in character. Naturally, this shift affects the proton-acceptor ability of the nitrogen atom; while it defines the probability of participation of the nitrogen in the adsorption of complexes, it also depends on the nature of the central metal atom. The latter fact is one of the reasons for the high selectivity of diethyldithiocarbamate separations (see below). Indeed, the position of the adsorption band related to the stretching vibrations of the C—N bond in the i.r. spectra of the complexes (Table 7) confirms intensification of the double-bond character of the bond, and a corresponding decrease in the proton-acceptor ability of the nitrogen atom. The chromatographic mobility of the complexes increases in accord with the shift of the ν_{CN} band to the high-frequency region: the larger the ν_{CN} values, the larger the R_f values (Table 8). The additional contribution of nitrogen atoms to the formation of hydrogen bonds with the surface hydroxyl groups produces quite selective adsorption

TABLE 7

Frequencies of the vibrations of the CN bond in the i.r. spectra of diethyldithiocarbamates

Complex	ν_{CN} (cm^{-1})	Complex	ν_{CN} (cm^{-1})	Complex	ν_{CN} (cm^{-1})
Bi(DEDTC) ₃	1485	Fe(DEDTC) ₃	1492	Ni(DEDTC) ₂	1518
Cd(DEDTC) ₂	1501	Hg(DEDTC) ₂	1497	Pb(DEDTC) ₂	1484
Co(DEDTC) ₃	1492	In(DEDTC) ₃	1499	Sb(DEDTC) ₃	1487
Cr(DEDTC) ₃	1493	Mn(DEDTC) ₃	1493	Zn(DEDTC) ₂	1504
Cu(DEDTC) ₂	1507				

TABLE 8

R_f values of diethyldithiocarbamates on a thin layer of Silpearl ($n = 6-10$; $\alpha = 0.05$)

Complex	$R_f \times 100$		Complex	$R_f \times 100$	
	Benzene	Dichloro- methane		Benzene	Dichloro- methane
Ag(DEDTC)	0	0-2 ^a	Mn(DEDTC) ₃	23.2 ± 2.7	37.9 ± 3.2
As(DEDTC) ₃	38.2 ± 2.0	61.3 ± 1.4	Mo ₂ O ₄ (DEDTC) ₂	0	0
Bi(DEDTC) ₃	0-6 ^a	0-10 ^a	MoO ₂ (DEDTC) ₂	0	0
Cd(DEDTC) ₂	13.9 ± 0.2 ^a	43.7 ± 2.1 ^a	Ni(DEDTC) ₂	21.8 ± 1.0	58.3 ± 0.6
Co(DEDTC) ₃	11.3 ± 2.1	44.8 ± 1.2	Pb(DEDTC) ₂	6-27 ^a	0-46 ^a
Cr(DEDTC) ₃	14.8 ± 1.3	53.0 ± 2.4	Pd(DEDTC) ₂	31.2 ± 1.5	69.5 ± 1.1
Cu(DEDTC) ₂	33.8 ± 1.9	61.8 ± 1.2	Sb(DEDTC) ₃	0-8 ^a	0-12 ^a
Fe(DEDTC) ₃	0-2 ^a	0-6 ^a	Sn(DEDTC) ₂	0	0-3 ^a
Ga(DEDTC) ₃	0-45 ^a	0-48 ^a	Sn(DEDTC) ₄	0	0-3 ^a
Hg(DEDTC) ₂	32.0 ± 1.1	59.0 ± 1.5	VO(DEDTC) ₂	19.3 ± 1.0	38.8 ± 1.3
In(DEDTC) ₃	21.0 ± 1.5 ^a	46.7 ± 3.0 ^a	Zn(DEDTC) ₂	38.3 ± 2.1 ^a	59.2 ± 3.2 ^a

^aThe mobility depends on the sample size.

of diethyldithiocarbamates on silica gel. Of interest is the lower mobility of some complexes compared with other coordination-saturated chelates and even the tendency of some of them to undergo irreversible adsorption.

In the study of dialkyldithiophosphates, which also have electronegative atoms capable of participation in specific interactions, there was no indication of direct participation of such atoms in adsorption. The mobility of these complexes is much higher than that of their dialkyldithiophosphate analogues with the same alkyl substituents (Table 6). Moreover, all the dithiophosphates studied, irrespective of ligand size, are less strongly adsorbed than the diethyldithiocarbamates.

Thus, a comparison of the chromatographic behaviour of coordination-saturated chelates of different types prompts the conclusion that the effects of peripheral electronegative atoms on the adsorbability of chelates depend essentially on the ligand type. Such effects can be related to participation in adsorption interactions, or to changes in the proton-acceptor ability of donor atoms by induction or steric hindrance.

In general, coordination-saturated chelates, particularly those with a low total electronegativity of the donor atoms (S,S,N,S and O,S types) are quite suitable for the separation of metals by l.a.c. Their chromatographic behaviour is not complicated by high adsorbability, and the complexes are quite stable during chromatography. The selectivity of separation of chelates of this type is quite high even when one-component mobile phases are employed. Sometimes, selectivity can be improved by introducing an electronegative atom near the chelating group of the ligand so that it can participate in adsorption interactions. The peripheral structure of the ligand, i.e., the electron-active and steric properties of substituents, also affects the relative mobility of chelates. Thus, the optimum chelating reagent for separating metals in l.a.c. is one with low electronegativity of the donor atoms, with substituents having average induction and steric effects, and peripheral electronegative atoms.

CONCLUSIONS

The complexity of the chromatographic behaviour of chelates in separations based on adsorption mechanisms is associated with the simultaneous participation of several electron-active atoms in adsorption. There are very few examples in which adsorption is governed predominantly by interactions with only one type of atom. Thus, considerations of the interrelations between chromatographic properties and chelate structure really require a multiparametric approach. Nevertheless, the methods employed here, essentially a consideration of the peculiarities of chelate behaviour in l.a.c. from the point of view of coordination chemistry, make it possible to systematize the experimental data, to establish the peculiarities of chelate chromatographic behaviour, and to propose classification of chelates according to the types of adsorption interaction. The adsorbability of the chelates

studied depends on the proton-acceptor ability of the complexes and on their acceptor ability with respect to the electron-donor active centres, thus all these chelate systems can be divided into three groups (Table 9).

Most useful in l.a.c. are coordination-saturated chelates of S,S,N,S and O,S types, such as dithiocarbamates and monothio- β -diketonates. The available literature data confirm this conclusion.

The correlation shown between the chromatographic properties and the structure of chelates ensures not only the establishment of optimum chelating reagents for the separation of metals. Understanding of the nature of

TABLE 9

Classification of chelates according to the types of adsorption interactions on hydroxyl-containing sorbents in liquid-adsorption chromatography

Chelate type	Major types of adsorption interactions	Chromatographic behaviour (adsorption nature) of chelates	Possibility of use in l.a.c.
Coordination-unsaturated	Interaction of the metal atom with electron-donor adsorption centres according to the ion-exchange or donor-acceptor mechanism with the formation of surface compounds. Hydrogen bonding of donor atoms of ligands with the surface hydroxyl groups.	Strong and often irreversible adsorption, in certain cases with decomposition of complexes during chromatography.	Limited use because of high adsorption ability and insufficient stability.
Coordination-saturated of the O,O and N,O types	Hydrogen bonding of donor atoms of ligands with the surface hydroxyl groups. Interaction of the metal atom with electron-donor adsorption centres, with replacement of ligands (for kinetically labile complexes).	Rather mobile on elution with solvents of moderate polarity, and stable; the chromatographic properties are mainly determined by structure of ligand.	Rather limited use because of the weak effect of the nature of the metal and close retention values of complexes with identical ligands.
Coordination-saturated of the O,S,N,S and S,S types	Hydrogen bonding of donor atoms of ligands, as well as of peripheral electronegative atoms with the surface hydroxyl groups.	High mobility; the chromatographic behaviour is greatly affected by the nature of the metal; the ligand structure also affects the chromatographic properties.	Most applicable for the separation of metals.

adsorption interactions and the mechanism of chelate adsorption facilitates the choice of conditions for the separation, and offers the possibility of predicting them. Thus, for chromatography of complexes with low total electronegativity of the donor atoms on hydroxylated silica gel, the mobile phases should have moderate elution ability, e.g., chlorine-containing and aromatic hydrocarbons or their mixtures with saturated hydrocarbons. A more detailed choice of separation conditions depends on the actual chelate system and the number of the complexes to be separated. Obviously, in some cases, the separation problem can be solved more easily by changing the ligand rather than the chromatographic system.

Further progress in the theory of l.a.c. of chelates requires the determination of the energy of all the adsorption interactions with the participation of different atoms and groups of complexes, and the establishment of their relative contributions to the overall adsorption energy at a quantitative level.

The authors express their gratitude to Prof. Yu. A. Zolotov for valuable discussions and practical recommendations.

REFERENCES

- 1 G. Schwedt, *Top. Curr. Chem.*, 85 (1979) 85.
- 2 G. Schwedt, *Chromatographische Methoden in der Anorganischen Analytik*, Springer-Verlag, Heidelberg, 1980.
- 3 P. C. Uden, *Proc. Anal. Div. Chem. Soc.*, 15 (1978) 4.
- 4 G. Schwedt, *Chromatographia*, 12 (1979) 613.
- 5 H. Veening and B. R. Willeford, *Rev. Inorg. Chem.*, 1 (1979) 281.
- 6 A. R. Timerbaev, O. M. Petrukhin and Yu. A. Zolotov, *Zh. Anal. Khim.*, 36 (1981) 1160.
- 7 B. R. Willeford and H. Veening, *J. Chromatogr.*, 251 (1982) 61.
- 8 A. V. Kisilev, *Zh. Fiz. Khim.*, 41 (1967) 2470.
- 9 V. A. Palm, *The Bases of the Quantitative Theory of Organic Reactions*, Khimia, Leningrad, 1977.

LIQUID-LIQUID EXTRACTION OF GROUP IB METAL IONS BY THIOETHERS

AKIRA OHKI and MAKOTO TAKAGI*

Department of Organic Synthesis, Faculty of Engineering, Kyushu University 36, Hakozaki, Higashi-ku, Fukuoka 812, (Japan)

KEIHEI UENO

Department of Industrial Chemistry, Kumamoto Institute of Technology, Ikeda 4-22-1, Kumamoto 860, (Japan)

(Received 5th September 1983)

SUMMARY

Liquid-liquid extraction of metal ions by means of organic extractants possessing divalent sulfur (thioethers) is discussed. It is shown that 1,2-bis(hexylthio)ethane (BHTE) and 13,14-benzo-1,4,8,11-tetrathiacyclopentadecane (TTX) are powerful extractants for soft metal ions such as copper(I), silver(I), and gold(I). The same is true for the trivalent phosphorus compounds, triphenylphosphine and phosphite triesters, which were studied for comparison. Copper(II) and gold(III) are efficiently extracted with thioethers in combination with reducing agents. From an equilibrium study for the extraction of copper(I) and silver(I) by BHTE (L), a complex of the type ML_2X (M^+ , metal ion; X^- , anion) was proved to be extracted. In the extraction of gold, the combined use of a thioether and phosphite enhanced the extractability of the metal, compared with the independent use of these extractants; the synergism is discussed. Further, the reductive extractions of copper(II) and gold(III) were coupled with a photo-redox reaction, leading to light-induced extraction of these metal ions.

Liquid-liquid extraction of metal ions from natural and industrial waters is regarded as a versatile method for hydrometallurgy and waste-water treatment processes. Various selective extractants have been developed for many metal species. Extractions based on ligands with *O*- or *N*-donor atoms are widely known, but relatively few studies have been reported on extractants possessing sulfur or phosphorus as electrically neutral donor atoms (thioethers, phosphines, phosphite esters).

Trivalent phosphorus compounds such as trialkyl- or triaryl-phosphites and phosphines are reported to extract transition metals selectively in their low valence states (copper(I), silver(I), gold(I), palladium(II), platinum(II), etc.) because of a so-called soft-soft interaction [1–4]. Thioether-containing extractants have been less studied. Russian workers have reported extractions by thioethers, which proved to be efficient for gold(III), palladium(II), platinum(IV), and some other metal ions [5, 6].

In this study, it was found that thioethers are especially powerful extrac-

tants for copper(I), silver(I), and gold(I). The behavior of thioethers for metal extraction was studied in detail with an emphasis on the redox conditions of the system. A photo-redox reaction was introduced to effect a light-induced extraction of metal ions. Trivalent phosphorus extractants were also studied under similar conditions for comparison. Further, by taking advantage of the difference in extractability between differently charged states of metal ions, an efficient extraction and back-extraction system was constructed.

EXPERIMENTAL

Reagents

1,2-Bis(hexylthio)ethane (BHTE) was prepared from 1-hexanethiol and 1,2-dibromoethane by the conventional method. [Found, 64.0% C, 11.5% H; calculated for $C_{14}H_{30}S_2$, 64.1% C, 11.5% H.] 13,14-Benzo-1,4,8,11-tetra-thiacyclopentadecane (TTX) was synthesized as described by Rosen and Busch [7]. Other chemicals were of reagent grade, and further purifications were effected through recrystallization or distillation when necessary. The absence of pentavalent species ($\geq P=O$) in the trivalent phosphorus reagents was confirmed by infrared spectroscopy.

Procedures

An aqueous solution (10 ml) containing metal salts ($Cu(NO_3)_2$, $AgNO_3$, $NaAuCl_4$), appropriate buffering agents, and any other reagents required was shaken with a solution (10 ml) of the extractant in 1,2-dichloroethane or toluene in a stoppered centrifuge tube at 25°C. After phase separation, the metal concentrations both in the aqueous phase and in the organic phase were measured by atomic absorption spectrometry using a Nippon Jarrell-Ash AA-1 instrument.

The back-extraction experiments were done as follows: an aliquot (6 ml) from the separated organic solution was shaken with an aqueous stripping solution (10 ml) at 25°C, and the metal ion in the aqueous solution was measured.

For the light-induced extractions, a photosensitizer system (a combination of glucose and titanium oxide of the anatase type) was added to the aqueous phase, and the extraction vessel (a stoppered, pyrex tube with 50-ml capacity) was irradiated by a 500-W xenon lamp (Ushio Denki) without filter.

RESULTS AND DISCUSSION

Extraction of Group IB metal ions by organic sulfur and phosphorus compounds

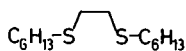
The extractions of Group IB metal ions by sulfur- and phosphorus-containing extractants are summarized in Table 1. Copper was easily extracted from aqueous to organic solution under reducing conditions by BHTE, TTX, dihexyl sulfide (DHS) (only at a high extractant concentration), triphenyl-

TABLE 1

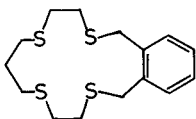
Extraction of Group IB metal ions by organic sulfur- and phosphorus-containing extractants^a

Run	Metal	Extractant ^b	(mM)	Solvent ^c	Metal extracted (%)
1-1	Cu	BHTE	(5)	D	100
1-2	Cu	BHTE	(5)	T	4
1-3	Cu	BHTE	(0.4)	D	66
1-4	Cu	TTX	(0.4)	D	99
1-5	Cu	DHS	(5)	D	3
1-6	Cu	DHS	(500)	D	96
1-7	Cu	TPPN	(5)	T	99
1-8	Cu	TBPT	(5)	T	98
1-9	Ag	BHTE	(5)	D	100
1-10	Ag	BHTE	(5)	T	5
1-11	Ag	TTX	(5)	D	100
1-12	Ag	DHS	(5)	D	1
1-13	Ag	TPPN	(2)	T	95
1-14	Au	BHTE	(2)	T	98
1-15	Au	DHS	(2)	T	99
1-16	Au	TPPN	(1)	T	100
1-17	Au	TPPT	(1)	T	78

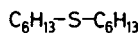
^aFor copper, the aqueous phase was 0.2 mM in $\text{Cu}(\text{NO}_3)_2$ (1 M = 1 mol dm⁻³), 5 mM in $(\text{NH}_3\text{OH})_2\text{SO}_4$ and 0.1 M in $\text{CH}_3\text{COONH}_4$ (pH 5.9); in runs 1–6, 10 mM NaClO_4 was also present in the aqueous phase. For silver, the aqueous phase was 0.2 mM in AgNO_3 and 0.1 M in $\text{CH}_3\text{COONH}_4$ (pH 6.6); in runs 9–12, 10 mM NaClO_4 was also present. For gold, the aqueous phase was 0.2 mM in NaAuCl_4 and 0.14 M in HNO_3 (pH 1.1); in run 17, 0.5 M KCl was also present. In all cases, the shaking time was 15 min. ^bBHTE, 1,2-bis(hexylthio)ethane; TTX, 13,14-benzo-1,4,8,11-tetrathiacyclopentadecane; DHS, dihexyl sulfide; TPPN, triphenylphosphine; TBPT, tributyl phosphite; TPPT, triphenyl phosphite. ^cSolvent D, 1,2-dichloroethane; solvent T, toluene.



BHTE



TTX



DHS

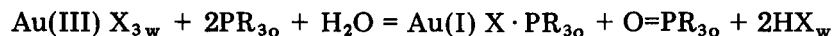
phosphine [TPPN; PPh_3], and tributyl phosphite [TBPT; $\text{P}(\text{OC}_4\text{H}_9)_3$] (runs 1, 4, 6–8). When the reducing agent was not added to the aqueous phase, copper was extracted scarcely at all with any of these extractants. The results indicate that these extractants possessing soft donor atoms preferentially extract soft metal species [copper(I)] over relatively hard species [copper(II)]. It is known that tetradentate thioethers such as TTX and an open-chain thioether (5,8,12,15-tetrathianonadecane) can serve as a copper carrier in liquid-membrane ion-transport systems [8, 9]. The extraction behavior of thiocrowns has been investigated in detail for several metal ions [10].

It is noteworthy that even a dithioether, BHTE, which has two donor sulfur atoms, efficiently extracted copper(I), although the extractability was somewhat inferior to that of TTX (runs 3, 4). The monothioether, DHS, was less effective as an extractant, so that a high concentration was required for quantitative extraction of copper (runs 5, 6).

Trivalent phosphorus compounds extracted copper(I) efficiently in spite of their monodentate nature (runs 7, 8). In this case, the addition of a lipophilic anion such as perchlorate to the aqueous phase was not required, whereas thioethers could hardly extract copper in the absence of such an anion. Another difference between the sulfur and phosphorus compounds was the solvent needed to effect the extraction. The phosphorus extractants were effective in either toluene or 1,2-dichloroethane solutions, whereas the sulfur extractants behaved very poorly in toluene solution (run 2).

The extraction behavior of silver(I) ion was similar to that of copper(I) (runs 9–13). The sulfur extractants did not function favorably in the absence of perchlorate, and the monodentate extractant (DHS) showed only a limited extraction ability (run 12). Moreover, toluene was not a suitable solvent for the sulfur extractants (run 10).

Gold [as tetrachloroaurate(III)] was extracted without the addition of a reducing agent (runs 14–17); this result is in contrast to the extraction of copper. The addition of reducing agent (ascorbic acid, hydroxylamine) to the aqueous phase caused deposition of the metal. Pronin et al. [6] suggested that gold was extracted by thioethers in the form $[(R_2S)_2Au(III)-X_2]^+ \cdot X^-$, where R_2S is a dialkyl sulfide and X^- is an anion. In the case of phosphorus extractants, Healy et al. [2] mentioned that the extractants simultaneously served as reducing agent according to the reaction



where PR_3 and $O=PR_3$ represent trivalent and pentavalent phosphorus compounds, respectively, and the subscripts w and o indicate the aqueous phase and organic phase, respectively. Even a monodentate thioether (DHS) served as a good extractant for gold, which was quite different from its behavior with copper and silver. Further, it was noted that when a thioether (e.g., DHS) and triphenyl phosphite (TPPT) were present together in the organic phase, a synergistic extraction was observed (see below).

Other metal ions such as iron(II), iron(III), cobalt(II), nickel(II), and zinc(II) were hardly extracted by these sulfur and phosphorus compounds under conditions similar to those outlined in Table 1.

Equilibrium study of the extraction of copper and silver by BHTE

If the extracted species have a molecular composition ML_mX_n (M^+ , monovalent metal ion; L, BHTE; X^- , anion), the reaction and the extraction constant (K_{ex}) can be defined as follows



or, expressed logarithmically,

$$\log D = \log K_{\text{ex}} + n \log [X^-]_{\text{w}} + m \log [L]_{\text{o}} \quad (1)$$

where $D = [\text{ML}_m\text{X}_n]_{\text{o}}/[\text{M}^+]_{\text{w}}$. The distribution ratio (q) of the total metal species between the two phases, defined by $q = (\text{total metal concentration in organic phase})/(\text{total metal concentration in aqueous phase})$, is easily evaluated. The extractant L is highly lipophilic and does not distribute to the aqueous phase. Similarly, the concentration of the metal complex ML_mX_n in the aqueous phase is negligibly small. Under these conditions and if the pH (buffering reagent) and redox conditions (in the case of copper extraction) are kept constant, D is proportional to q . Therefore, Eqn. 1 can be given as

$$\log q = \log K_{\text{ex}}' + n \log [X^-]_{\text{w}} + m \log [L]_{\text{o}} \quad (2)$$

where K_{ex}' is a conditional extraction constant defined by $K_{\text{ex}}' = [\text{ML}_m\text{X}_n]_{\text{o}}/[\text{M}]_{\text{w, total}} [X^-]_{\text{w}}^n [L]_{\text{o}}^m$.

A plot of $\log q$ against $\log [L]_{\text{o}}$ at constant $[X^-]_{\text{w}}$ is shown in Fig. 1. Similarly, a plot of $\log q$ against $\log [X^-]_{\text{w}}$ at constant $[L]_{\text{o}}$ is shown in Fig. 2; perchlorate was used as the anion X^- , and its concentration was varied. For both copper and silver extractions, a slope of ca. 2 in Fig. 1 and the slope of ca. 1 in Fig. 2 were obtained, indicating that $m = 2$ and $n = 1$ in the above scheme. Consequently, the extraction reactions can be formulated for copper or silver as

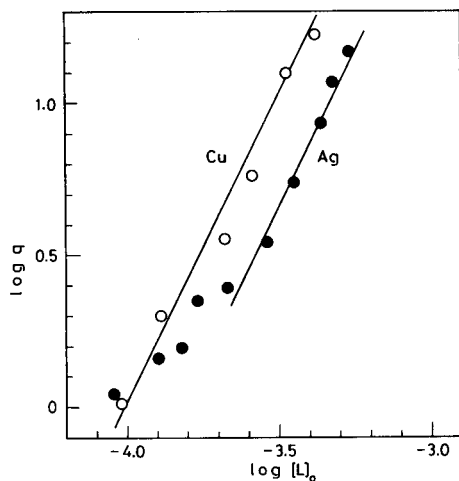


Fig. 1. A plot of $\log q$ against $\log [L]_{\text{o}}$. The conditions are the same as those of run 1-1 (○) and run 1-9 (●) in Table 1 except that the concentration of BHTE in the organic phase was varied.

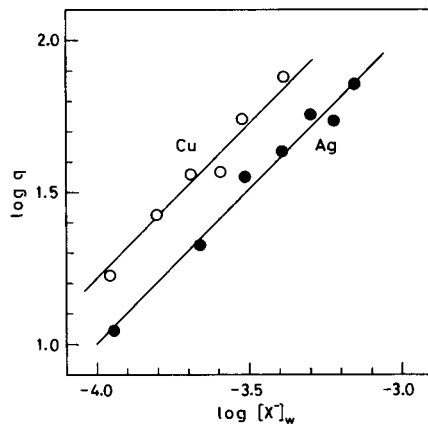


Fig. 2. A plot of $\log q$ against $\log [X^-]_{\text{w}}$. The conditions are the same as those of run 1-1 (○) and run 1-9 (●) in Table 1 except that the concentration of perchlorate ion in the aqueous phase was varied.



The value of $\log K_{ex}'$ is 9.9 for copper and 9.6 for silver. The observed departure from slope 2 for silver in Fig. 1 at low $[L]_o$ values may be ascribed to some extraction of $AgLX$ complex.

The effect of anion X^- was investigated. The copper extraction was promoted in the order, perchlorate \approx thiocyanate $>$ bromide $>$ chloride \approx nitrate, indicating that lipophilic anions are effective in the extraction reaction. This suggests that the structure of the metal complex extracted is of an ion-pair type, $[ML_2^+] \cdot X^-$. This is most probable for $X = ClO_4^-$.

Synergism in the gold extraction

The extraction of gold by triphenyl phosphite was strongly affected by extra chloride added to the aqueous phase; when chloride was not added, extraction was unfavorable (Table 2, run 1). The use of both DHS and TPPT in the organic phase led to a considerable enhancement in the gold extraction compared with those runs (runs 5–7) in which DHS and TPPT were used independently. It should be emphasized that in all these cases gold was extracted as colorless complexes.

When only the thioether was used in the organic phase, the organic solution became yellow, with an absorption maximum at 325 nm. The absorbance was found to be proportional to the amount of gold in the organic phase, suggesting that the absorption is due to the gold(III)–thioether complex; the structure $[Au(III) L_2Cl_2]^+ \cdot Cl^-$ (L, DHS) seems likely. In contrast, with the combined use of DHS and TPPT, the extracted complex is most probably not a gold(III) complex, but a gold(I)–thioether complex. In this case, the TPPT serves primarily to reduce gold(III) to gold(I) (compare runs 5 and 7).

TABLE 2

Synergism in the gold extraction^a

Run	TPPT (mM)	KCl (M)	Au extracted (%)	Run	TPPT (mM)	DHS (mM)	Au extracted (%)
2-1	1	0	7	2-5 ^b	2	0.2	94
2-2	1	0.1	47	2-6 ^b	0	0.2	37
2-3	1	0.5	78	2-7 ^b	2	0	31
2-4	2	0.5	89	2-8	2	0.2	54
				2-9	0	0.2	37
				2-10	2	0	14
				2-11 ^c	2	1	75
				2-12 ^c	0	1	37
				2-13 ^c	2	0	14

^aAqueous phase was 0.2 mM in $NaAuCl_4$ and 0.14 M in HNO_3 , and organic phase (toluene) contained TPPT; KCl was added to the aqueous phase in runs 2–4 and DHS was added to the organic phase in runs 5–13 as noted. Shaking time, 15 min. ^bShaking time, 45 min. ^c1 mM $NaAuCl_4$ was used.

The extraction of the gold(III)—thioether complex came quickly to equilibrium. In contrast, when reduction was involved, the extraction was established only slowly, so that the extent of extraction increased with longer shaking times (compare runs 8 and 5). With a different concentration of gold, a similar tendency to synergism was observed (runs 11–13). It might appear that the role of TPPT as a reductant could be taken by other common reducing agents. The use of *N,N,N',N'*-tetramethylbenzidine (in the organic phase) or ascorbic acid (in the aqueous phase), however, resulted in the deposition of gold metal. Thus, the phosphite ester is peculiar as a reducing agent in the reductive extraction of gold(III).

Light-induced extraction

Reducing species can be generated photochemically by the use of titanium oxide semiconductor suspensions. It has been reported that dichromate ion is reduced to chromium(III) [11] and copper(II) ion to the metal [12] in aqueous solutions. The reduction of copper(II) to copper(I) and a selective membrane transport and separation of copper ion by the combined use of bathocuproine or tetrathioethers have been described [8, 9].

In the present work, an aqueous feed solution (containing copper(II) nitrate, glucose and titanium oxide) and an organic extractant solution were placed in a centrifuge tube and stirred magnetically under photoirradiation. The amounts of copper ion in the separated aqueous and organic phases were measured, with the results summarized in Table 3. The balance of the copper ion was found to be adsorbed on the titanium oxide suspension, and so there was no other serious side reactions such as the deposition of copper(0). The new extractant, BHTE, was found to extract copper(I) with the aid of

TABLE 3

Light-induced copper extraction^a

Run	Glucose (mM)	TiO ₂ (mg)	Extractant	Light	Distribution of copper (%)	
					Aqueous	Organic
3-1	5	10	BHTE	on	0	100
3-2	5	10	BHTE	off	74	6
3-3	5	0	BHTE	on	98	0
3-4	5	0	BHTE	off	100	0
3-5	0	10	BHTE	on	54	31
3-6	5	10	TPPN	on	14	76
3-7	5	10	TPPN	off	79	6
3-8	5	10	TBPT	on	3	87
3-9	5	10	TBPT	off	75	5

^aAqueous phase (10 ml) contained 0.2 mM Cu(NO₃)₂, glucose, TiO₂, and 0.1 M CH₃COONH₄; the organic phase (1,2-dichloroethane) contained 5 mM extractant. Irradiation (stirring) time, 15 min.

the photochemically assisted reducing agent (run 1). When the same extraction was done in the dark, the fraction of copper extracted was small (run 2). In the absence of the photosensitizer, copper was not extracted at all whether the illumination was applied or not (runs 3, 4). When glucose was eliminated from the photosensitizing system, the copper extraction was considerably retarded but did take place (run 5). It is known that essentially any organic material can replace the role of glucose, and it is possible that 1,2-dichloroethane or the extractant served as a photosensitized reductant.

In the case of phosphorus extractants, the light-induced extraction could be done similarly (runs 6–9), but was much less effective than when BHTE was used.

An attempt was made to extract gold under photosensitized conditions; titanium oxide was dispersed in the aqueous phase while benzoin was added in the organic phase as a reductant. On illumination, a considerable deposition of gold metal was observed, and the extraction occurred to only a limited extent.

The idea of light-induced extraction of metal ions may offer new possibilities in the utilization of solar energy in separation chemistry.

Back-extraction of Group IB metal ions

The Group IB metal complexes in the organic solution could be stripped into the aqueous solution under appropriate conditions, as shown in Table 4. Copper ion was completely stripped under oxidizing conditions (run 1), reverting to the original divalent state. In the absence of explicit oxidizing agents, the back-extraction was retarded but did take place to a considerable extent (runs 2, 3). Presumably, aerobic oxygen served as the oxidizing agent. The back-extraction of silver ion was favored by use of an ammoniacal

TABLE 4

Back-extraction of Group IB metal ions^a

Run	Metal	Organic feed solution	Aqueous stripping solution	Metal stripped (%)
4-1	Cu	1-1	5 mM Ce(SO ₄) ₂ , 0.25 M H ₂ SO ₄	100
4-2	Cu	1-1	0.25 M H ₂ SO ₄	49
4-3	Cu	1-1	0.1 M CH ₃ COONH ₄	52
4-4	Ag	1-9	1 M NH ₃	100
4-5	Ag	1-9	20 mM N(C ₂ H ₄ OH) ₃ , 1 M NH ₃	100
4-6	Au	2-4	1 M NH ₃	70
4-7	Au	2-4	50 mM N(C ₂ H ₄ OH) ₃ , 1 M NH ₃	100
4-8	Au	2-5	20 mM N(C ₂ H ₄ OH) ₃ , 1 M NH ₃	100
4-9	Au	2-5	0.1 M CH ₃ COONH ₄	2

^aOrganic feed solutions containing Group IB metal complexes are from the extraction in Tables 1 and 2 (indicated by the run numbers). Feed solution, 6 ml; stripping solution, 10 ml. Shaking time, 15 min.

stripping solution (runs 4, 5). The extracted gold(I) ion was also stripped by the ammoniacal solution (run 6), and the addition of triethanolamine to the stripping solution facilitated the reaction (runs 7, 8). Triethanolamine tends to stabilize the trivalent state of metal ions and may have aided the aerobic oxidative back-extraction.

The authors thank Mr. Koichi Tanaka for his help in the extraction experiments. The present work was supported by a Grant-in-Aid for Scientific Research from the Ministry of Education, Science, and Culture of Japan.

REFERENCES

- 1 T. H. Handley and J. A. Dean, *Anal. Chem.*, 33 (1961) 1087.
- 2 T. V. Healy, C. J. Barton and I. Windeatt, *J. Inorg. Nucl. Chem.*, 36 (1974) 2575.
- 3 T. V. Healy and C. J. Barton, *J. Inorg. Nucl. Chem.*, 36 (1974) 2578.
- 4 M. Mojski, *Talanta*, 27 (1980) 7.
- 5 P. I. Artyukhin, E. A. Startseva, L. Ya. Marochkina, V. I. Andrievskii, V. G. Mazur, L. M. Gindin and I. L. Kotlyarevskii, *Izv. Sib. Otd. Akad. Nauk SSSR. Ser. Khim. Nauk*, (1972) 90.
- 6 V. A. Pronin, M. V. Usol'tseva, Z. N. Shastina, N. K. Gusarova, E. P. Vyalykh, S. V. Amosova and B. A. Trofimov, *Russ. J. Inorg. Chem.*, 18 (1973) 1016.
- 7 W. Rosen and D. H. Busch, *J. Am. Chem. Soc.*, 91 (1969) 4694.
- 8 A. Ohki, T. Takede, M. Takagi and K. Ueno, *Chem. Lett.*, (1982) 1529.
- 9 A. Ohki, T. Takede, M. Takagi and K. Ueno, *J. Membr. Sci.*, 15 (1983) 231.
- 10 K. Saito, Y. Masuda and E. Sekido, *Anal. Chim. Acta*, 151 (1983) 447.
- 11 H. Yoneyama, Y. Yamashita and H. Tamura, *Nature*, 282 (1977) 817.
- 12 H. Reich, W. W. Dunn and A. J. Bard, *J. Phys. Chem.*, 83 (1979) 2248.

SEPARATION OF MOLYBDENUM FROM TUNGSTEN WITH DI(2-ETHYLHEXYL)-PHOSPHORIC ACID AS EXTRACTANT

N. R. DAS, B. NANDI and S. N. BHATTACHARYYA*

Nuclear Chemistry Division, Saha Institute of Nuclear Physics, 92 Acharya Prafulla Chandra Road, Calcutta — 700 009 (India)

(Received 7th February 1983)

SUMMARY

The use of di(2-ethylhexyl)phosphoric acid (HDEHP) as an extractant for the separation of molybdenum from tungsten was examined with the help of molybdenum-99 and tungsten-187 as radiotracers. Effective separation was obtained when the aqueous phase contained phosphoric acid at pH 0.8–2 or pH 3–3.5, depending on the amounts of metal. The method is applicable to both tracer and milligram amounts of molybdenum. The structure of the extracted species was examined by infrared spectroscopy.

Molybdenum and tungsten form one of the critical pairs of elements that have very close chemical similarities [1]; thus their mutual separation has always been of interest. Liquid-liquid extraction is one of the most efficient general methods for complex separation. In a continuation of attempts to apply the well-known extractant, di(2-ethylhexyl)phosphoric acid (HDEHP) for the mutual separation of various congeneric pairs of elements [2, 3], the separation of molybdenum and tungsten is discussed here. The extraction of molybdenum with HDEHP has been described from different mineral acid media [4–15], but the separation of molybdenum and tungsten with HDEHP [15–17] from such aqueous acidic media has received little attention. Laskorin et al. [15] used a 0.1 M nitric acid medium with extraction into kerosene.

In the study reported here, it was found that the extraction of tungsten is less efficient than that of molybdenum in various mineral acid media, the extent of extraction of both elements being dependent on the acidity of the aqueous solution. However, the percentage extraction of tungsten was greatly decreased when orthophosphoric acid was added to the aqueous medium. Hence the present paper offers a detailed study of the extraction of molybdenum and tungsten (tracer to milligram levels) by HDEHP for the effective separation of molybdenum and tungsten.

EXPERIMENTAL

Reagents

The solvents (carbon tetrachloride, benzene, n-heptane, cyclohexane, chloroform) and other chemicals used were of analytical grade. The

di(2-ethylhexyl)phosphoric acid (ICN Pharmaceuticals, Plainview, NY) was purified as described by Peppard et al. [18]; the procedure involves hydrolysis of mono and pyro esters with hydrochloric acid, which is removed by washing with water, partitioning between diethyl ether and ethylene glycol, and recovery of HDEHP by evaporation of the ether fraction.

The radiotracers molybdenum-99 (as molybdate) and tungsten-187 (as tungstate) were obtained from BARC (Trombay, India).

General procedure

The metal ions were extracted from 25-ml portions of aqueous orthophosphoric acid solutions containing the ions as molybdate or tungstate at definite concentrations, along with the respective radiotracers in the same chemical form. The pH of the resulting solution was measured (pH meter). This aqueous solution was equilibrated with equal volumes of organic phase containing a defined concentration of HDEHP at room temperature. The activities were measured with a GM counter, so that the activity from the daughter ^{99}Tc in the case of ^{99}Mo was avoided [4]. An Ortec Ge(Li) detector (25% efficiency) with an 8K multichannel analyzer was used to measure the γ -spectra. A Beckman IR-20A spectrophotometer was used for infrared measurements.

RESULTS AND DISCUSSION

The extraction behaviour of molybdenum and tungsten at tracer levels from various acidic media with HDEHP is summarized in Table 1, which shows that the percentage extraction of the metal ions decreases as the acidity is increased. The distribution ratios of molybdenum are always higher than those of tungsten, and the general trend of decreasing extraction with increasing acidity is most pronounced for tungsten, when orthophosphoric acid is present in the aqueous phase.

The distribution ratios for the extraction of the metal ions at tracer levels from orthophosphoric acid medium by 0.1 M HDEHP in n-heptane over a wide pH range are shown in Fig. 1. The distribution ratio of molybdenum

TABLE 1

Extraction (%) of molybdenum and tungsten at tracer levels from different acids with 0.1 M HDEHP in n-heptane

Acid (N)	HCl		HNO ₃		H ₂ SO ₄		HClO ₄		H ₃ PO ₄	
	Mo	W	Mo	W	Mo	W	Mo	W	Mo	W
0.1	98.0	68.8	95.2	72.7	92.7	56.7	98.6	67.2	94.5	29.1
1.0	84.0	62.3	94.3	70.0	91.0	54.2	97.2	62.6	89.6	10.1
5.0	78.0	57.9	93.3	69.0	90.3	50.4	97.2	61.2	15.0	— ^a

^aNegligible.

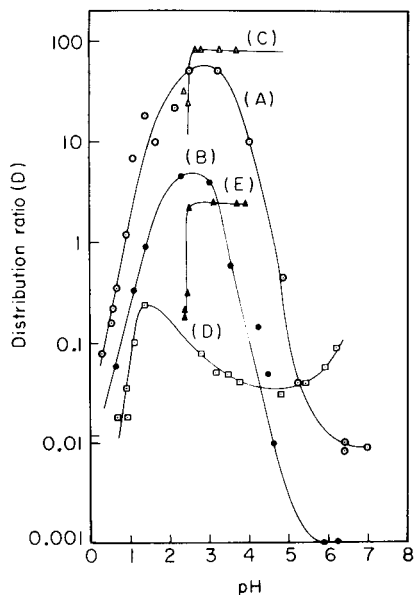


Fig. 1. Effect of pH on the distribution ratios for molybdenum and tungsten extractions: (A) ^{99}Mo tracer in H_3PO_4 medium with HDEHP in n-heptane; (B) ^{99}Mo tracer in H_3PO_4 medium with HDEHP in chloroform; (C) ^{99}Mo tracer in H_3AsO_4 medium with HDEHP in n-heptane; (D) ^{187}W tracer in H_3PO_4 medium with HDEHP in n-heptane; (E) ^{187}W tracer in H_3AsO_4 medium with HDEHP in n-heptane. A 0.1 M solution of HDEHP was used in all cases.

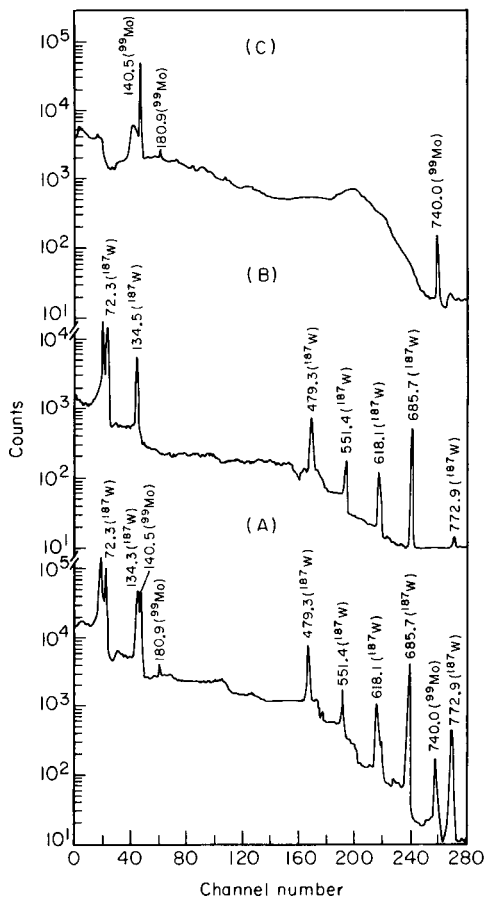
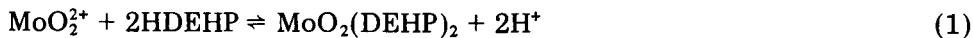


Fig. 2. γ -Spectra: (A) ^{99}Mo and ^{187}W mixture; (B) aqueous fraction left after extraction of ^{99}Mo ; (C) the HDEHP extract.

increases linearly as the pH increases to about 2 and then decreases above pH 3.2 (Fig. 1, curve A). In this pH range, molybdenum(VI) mainly exists in the cationic form, such as MoO_2^{2+} , $\text{MoO}(\text{OH})_2^{2+}$ or $\text{Mo}_2\text{O}(\text{OH})_8 \cdot \text{H}_2\text{O}^{2+}$ [1]. In a strongly acidic solution, molybdenum(VI) is mainly present as MoO_2^{2+} species [1, 19] which can exchange with HDEHP,



Therefore, a linear increase in the distribution ratio with pH is expected. The straight line observed in the pH range 0.5–2.0 (Fig. 1, curve A) has a

slope of 2, which agrees with that required by Eqn. 1. As the pH is increased above 3.2, the molybdenum species in the aqueous phase change. In the pH range 3.2–7, the decreasing distribution ratios for molybdenum are consistent with the aggregation of molybdenum to form the heteropoly anion, $\text{H}_3\text{PMo}_{12}\text{O}_{40}$ [1]. In alkaline solution, of course, the MoO_4^- ion present is not extracted with HDEHP.

Tungsten shows a similar trend of extraction (Fig. 1, curve D). The WO_4^{2-} ion prevails in the aqueous solution and the distribution ratios increase up to pH 1.4, the slope being about 2. Further increase of pH decreases the distribution ratio, probably because of gradual formation of $\text{H}_3\text{PW}_{12}\text{O}_{40} \cdot x\text{H}_2\text{O}$ [20]. However, in the pH range 4–7, the distribution ratio for tungsten again increases; in this pH range, tungsten exists as paratungstate, $[\text{HW}_6\text{O}_{21}]^{5-}$ [21]. This anionic form should not be extracted with HDEHP, but the increasing distribution ratios indicate that some interaction does occur, despite the high charge on the anion. It could be argued that there is an ion–dipole interaction between paratungstate and an –OH group of HDEHP in the pH range 4–7, though it is then difficult to see why the heteropolytungstate anion undergoes no such interaction.

In addition to the characteristic variation in the distribution ratios with pH, it should be noted that the distribution ratios for molybdenum are much larger than those for tungsten, probably because the heteropoly anion of tungsten is more stable than that of molybdenum [1]. That this heteropoly anion formation plays an important role in these extractions is clear from curves C and E in Fig. 1, which shows the distribution ratios when the arsenate ion replaces phosphate in the solution, forming the corresponding heteropoly anion. Molybdophosphoric acid is well known to be more stable than the corresponding arsenic acid [1] which agrees well with the present results that the distribution ratios for both elements are higher in arsenic acid than in orthophosphoric acid medium. Incidentally, it was shown that phosphorus in the aqueous phase does not exchange with that in the organic phase, by making appropriate extractions with radioactive ^{32}P in the aqueous phase; no ^{32}P was detected in the extract with HDEHP.

The remarkable decrease in the distribution ratios for tungsten in orthophosphoric acid medium is very important for the separation. Molybdenum is extracted at the tracer level almost free from tungsten at pH 3–3.5 from orthophosphoric acid medium with 0.1 M HDEHP in n-heptane. The decontamination factor, calculated as $D_{\text{Mo}}/D_{\text{W}}$ (D = distribution ratio) [22] was >500 in the pH range 3–3.5 (curves A and C, Fig. 1). The absence of significant contamination from ^{187}W in the organic phase was verified by γ -ray spectrometry (Fig. 2). As can be seen, the spectrum of the organic layer (curve C) shows no significant amount of ^{187}W , while the aqueous phase (curve B) is free from ^{99}Mo [22].

This separation was extended to extractions of milligram amounts of the two elements. It was found that the distribution ratios decreased as the concentration of the metal ions increased throughout the pH range studied

(Fig. 3). The distribution ratio for 0.0025 M molybdenum(VI) in the aqueous solution increases initially upto about pH 2, then decreases; for 0.02 M molybdenum(VI), this ratio increases only upto pH 1.1. The point of maximum extraction shifts towards lower pH with increasing metal ion concentration in the aqueous solution (Figs. 1 and 3). This observed shift can be explained if one considers the chemistry of formation of hydrolytic polymeric species of molybdenum(VI) [23, 24]; the consumption of hydrogen ions naturally increases with increasing molybdenum concentration, to provide the MoO_2^{2+} ions needed for the extraction by HDEHP.

The case of tungsten(VI) at milligram levels is shown in Fig. 3, curve C. The formation of WO_2^{2+} occurs at $\text{pH} < 1$ [20]; at about pH 1, tungsten is mainly present as hydrated tungstic oxide, $\text{WO}_3 \cdot 2\text{H}_2\text{O}$ and $\text{WO}_3 \cdot \text{H}_2\text{O}$ [1]. Therefore, extraction of 0.0014 M tungsten(VI) at pH 1–2.5 may be considered as being due to dipole–dipole interaction with an OH group of the HDEHP molecule rather than to WO_2^{2+} formation as on the tracer scale. Above pH 2.5, heteropolyacid aggregation becomes pronounced and so extraction decreases; the later increases in extraction at pH 6 may be explained in the same way as curve D in Fig. 1. In this larger-scale work, the efficiency of separation was estimated by measuring, by γ -ray spectrometry, the extent of coextraction of the two metal ions. The results (Table 2) indicate that contamination by tungsten in the separation of molybdenum does not exceed about 1%.

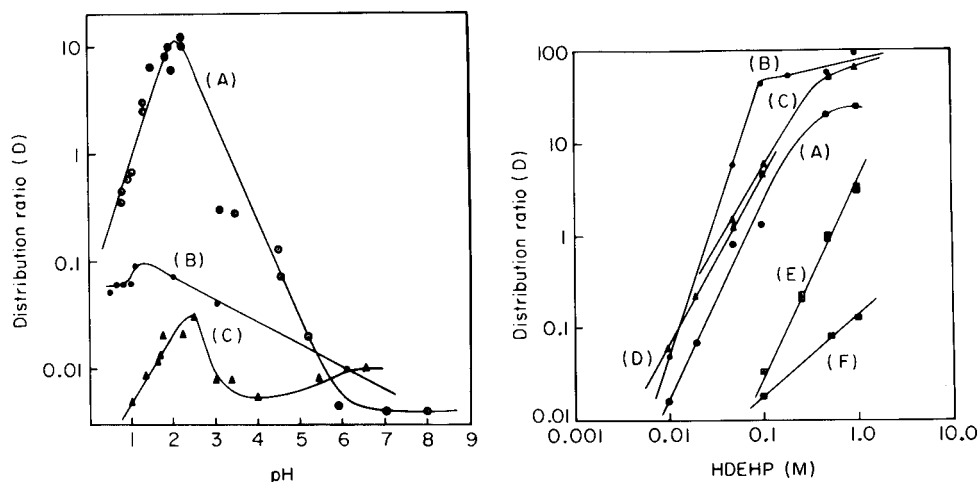


Fig. 3. Variation of distribution ratios with pH in the $\text{H}_3\text{PO}_4/0.1\text{ M HDEHP}/n\text{-heptane}$ system. Concentration of metal ion: (A) 2.5×10^{-3} M Mo(VI); (B) 2.0×10^{-2} M Mo(VI); (C) 1.4×10^{-3} M W(VI).

Fig. 4. Dependence of the distribution ratios for Mo and W in H_3PO_4 medium on HDEHP concentration. Extractions: (A) ^{99}Mo tracer at pH 1–1.2, (B) 5×10^{-5} M Mo at pH 2.1; (C) 2.5×10^{-3} M Mo at pH 2.8; (D) ^{99}Mo tracer at pH 1.2; (E) ^{187}W tracer at pH 1.2; (F) 1.4×10^{-3} M W at pH 2.8. The HDEHP solution was in *n*-heptane, except for curve D, for which chloroform was used.

TABLE 2

Contamination by tungsten in the extraction of 2.5×10^{-3} M molybdenum in phosphoric acid media by 0.1 M HDEHP at pH 1.4 and pH 2.1

Tungsten conc. ($\times 10^{-3}$ M)	Distribution ratios			
	$D_{\text{Mo/pH 1.4}}$	$D_{\text{W/pH 1.4}}$	$D_{\text{Mo/pH 2.1}}$	$D_{\text{W/pH 2.1}}$
0.3	2.27	0.026	10.0	0.025
0.6	2.45	0.004	10.0	0.02
0.9	2.50	0.004	10.0	0.023
1.2	2.49	0.004	10.0	0.02
1.7	2.50	0.004	10.0	0.02

The effect of the HDEHP concentration on the extractibility of the metal ions was examined (Fig. 4). The distribution ratio for molybdenum increases with increasing HDEHP concentration, starting from 0.01 M HDEHP in n-heptane, and tends to level off at different values, depending on the amount of molybdenum. Extraction of tracer tungsten(VI) starts only at a higher concentration of HDEHP (0.1 M) and steadily increases with increase in the concentration of HDEHP.

From the above studies, the whole process of extraction by HDEHP may be postulated as follows. First, the metal ion interacts with HDEHP at the interface of the organic and aqueous layers, where the monomeric HDEHP molecules are orientated with their polar end towards the aqueous phase, the selectivity of the interaction depending on the formation constant of the complex produced. At 0.001–0.1 M HDEHP, the slopes of the curves are about 2, which indicates that two molecules of HDEHP are associated with the metal ion complex. On further increase of the concentration of HDEHP, these slopes decrease (Fig. 4), possibly because of aggregation; aggregation of the extractant depends on such factors as HDEHP concentration, nature of the metallic species and type of the apolar diluent used [25]. The distribution ratio values were found to decrease with increase in the dielectric constant of the diluents used (Table 3).

Infrared studies

The infrared spectra were examined over two regions covering 700–3000 cm^{-1} . The spectrum of an extract of 0.02 M Mo(VI) from aqueous orthophosphoric acid into 0.1 M HDEHP in carbon tetrachloride is compared with the spectrum of free HDEHP in the same solvent in Fig. 5. Carbon tetrachloride was chosen because it has no alkyl group. With HDEHP alone, the broad intense band round 1000 cm^{-1} can be ascribed to the superimposition of P–O(C), C–O(P), (P)–OH, P–O–(H) groups [26]. In the molybdenum complex, this band is split up and the symmetric and antisymmetric stretching vibrations of the MoO_2 group [27] were observed at 960 cm^{-1} .

TABLE 3

Distribution ratios (D) for molybdenum or tungsten on extraction from aqueous 0.1 M phosphoric acid at pH 2.37 by 0.1 M HDEHP in different diluents

Diluent	Dielectric constant	D_{Mo}^{a}	D_{W}^{b}	D_{Mo}^{c}	D_{W}^{d}
n-Heptane	1.9	19.01	0.700	11.00	0.020
Cyclohexane	2.052	18.06	0.200	10.05	0.020
Carbon tetrachloride	2.240	10.62	0.060	0.13	0.008
Benzene	2.283	8.02	0.054	0.12	0.008
Toluene	2.387	7.09	0.040	0.12	0.008
Chloroform	5.05	4.60	0.005	0.11	0.005

^aFor 10^{-8} M Mo(VI). ^bFor 10^{-8} M W(VI). ^cFor 2.5×10^{-3} M Mo(VI). ^dFor 1.4×10^{-3} M W(VI).

In the spectrum of HDEHP, the P=O stretching vibration is observed at 1220 cm^{-1} [28] whereas the spectrum of the complex exhibits a strong band around 1170 cm^{-1} , which may be ascribed to the involvement of P=O group in forming a coordinate bond with MoO_2^{2+} , as suggested by Kolarik [6]. The maximum at 1360 cm^{-1} is ascribed to the deformation mode of hydrogen atoms in the $-\text{CH}_3$ group and that at 1465 cm^{-1} is due to the $-\text{CH}_2$ group

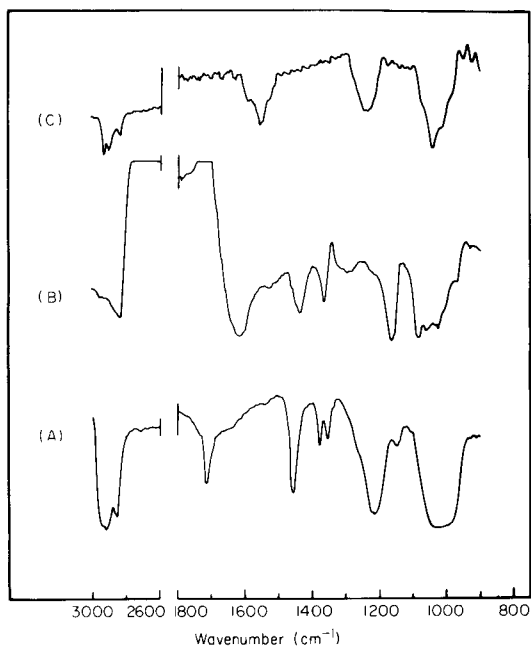
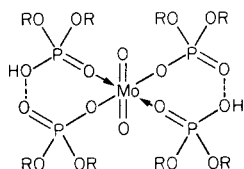


Fig. 5. Infrared spectra of samples in carbon tetrachloride (0.1 mm cells): (A) 0.1 M HDEHP; (b) Mo-HDEHP complex; (C) deuterated HDEHP.

of HDEHP [28]. These bands shift only slightly in the complex. The absorption band at 1710 cm^{-1} for free HDEHP is ascribed to the deformed —OH bond [28], which is known to be affected by hydrogen bonding. In the metal complex, this band appears as a broad shallow band around 1620 cm^{-1} [28]; deuteration of the free ligand shifts this deformation mode to 1555 cm^{-1} . From this, it can be concluded that the —OH group remains hydrogen-bonded in the metal complex, although this does not agree with the structure proposed by Zelikman and Nerezov [7]. The P—OH stretching vibration around 2840 cm^{-1} arises from a dimeric structure (hydrogen bonding) [28]. The band from free HDEHP is less intense from the metal complex, suggesting that the metal cation replaces hydrogen in the complex, breaking the hydrogen-bonded structure and affecting the phosphoryl oxygen.

From these observations, it appears that the molybdenum-HDEHP complex extracted from aqueous phosphoric acid solution, has a closed ring structure:



This structure does not agree with that reported by Zelikman and Nerezov [7] but closely agrees with that put forward by Kolarik [6].

Grateful acknowledgement is due to Dr. S. Ghosh, Reader, Department of Inorganic Chemistry, Indian Association for the Cultivation of Science, Calcutta-700 032, for his help with i.r. spectroscopy.

REFERENCES

- 1 Comprehensive Inorganic Chemistry, J. C. Bailar, H. J. Emeleus, Sir Ronald Nyholm and A. F. Trotman-Dickenson (Eds.), Pergamon Press, Oxford, 1973, Vol. 3, Ch. 36; Vol. 4, Ch. 51.
- 2 N. R. Das, B. Nandi and S. N. Bhattacharyya, *Int. J. Appl. Radiat. Isot.*, 32 (1981) 205.
- 3 N. R. Das, B. Nandi and S. N. Bhattacharyya, *Radioanal. Chem.*, 62 (1981) 53.
- 4 T. S. Urban'ski, M. Chojecki and R. Kaczyn'ska, *Radioanal. Chem.*, 30 (1976) 369.
- 5 A. A. Palant and V. A. Rejnickenko, *J. Appl. Chem. USSR*, 46 (1973) 1124; *Zh. Prikl. Khim. (Leningrad)*, 46 (1973) 1062.
- 6 Z. Kolarik, *J. Inorg. Nucl. Chem.*, 35 (1973) 2025.
- 7 A. N. Zelikman and V. M. Nerezov, *Zh. Neorg. Khim.*, 14 (1969) 1307.
- 8 T. D. Titkova and V. I. Levin, *Radiokhimiya*, 17 (1975) 55.
- 9 V. L. Bychovtsov, *Radiokhimiya*, 13 (1971) 657.
- 10 Yu. B. Kletnik, I. A. Bykhovskaya and L. V. Sekretova, *Zh. Anal. Khim.*, 24 (1969) 707.
- 11 F. Cerrai and G. Ghersini, *J. Chromatogr.*, 24 (1966) 383.
- 12 A. N. Zelikman, *Molybdenum* (in Russian), Atomizdat, Moscow, 1972.
- 13 I. L. Jenkins and A. G. Wain, *J. Appl. Chem.*, 14 (1964) 449.
- 14 S. M. Karpacheva, V. S. Smelov, Yu. I. Vereshchagin, I. V. Davydov, V. T. Moskaleva, M. N. Ryzhov and A. V. Strakhova, *Zh. Neorg. Khim.*, 12 (1967) 1925.
- 15 B. N. Laskorin, V. S. Ul'yanova and R. A. Sviridova, *Zh. Prikl. Khim. (Leningrad)*, 35 (1962) 2409.

- 16 G. M. Vol'dman, A. N. Zelikman and I. Sh. Khutoretskaya, *Izv. Vyssh. Uchebn. Zaved. Tsvet. Metall.*, No. 2 (1974) 97.
- 17 F. Esnault, M. Robaglia, J. M. Latard and J. M. Demarthe, *International Solvent Extraction Conference*, Lyon, France, Sep. 1974.
- 18 D. F. Peppard, G. W. Mason, I. L. Maier and W. J. Driscoll, *J. Inorg. Nucl. Chem.*, 4 (1957) 334.
- 19 Stephen J. Lippard (Ed.), *Progress in Inorganic Chemistry*, Vol. 22, Interscience, NY, 1977, p. 35.
- 20 H. J. Emeleus and J. S. Anderson, *Modern Aspects of Inorganic Chemistry*, 2nd edn., Routledge & Kegan Paul, London, 1954, p. 212.
- 21 J. F. Duncan and D. L. Kepert, *J. Chem. Soc.*, (1961) 5317; (1962) 205.
- 22 F. Adams and R. Dams, *Applied Gamma-ray Spectrometry*, Pergamon Press, Oxford, 1972, pp. 549, 627.
- 23 M. L. Freedman, *J. Inorg. Nucl. Chem.*, 25 (1963) 575.
- 24 K. B. Yatsimirskii and I. I. Alekseeva, *Izv. Vyssh. Uchebn. Zaved. Khim. Khim. Tekhnol.*, 1 (1958) 53.
- 25 J. H. Fendler, *Acc. Chem. Res.*, 9 (1976) 153.
- 26 V. I. Spiriyakov, P. G. Kurtikov, V. M. Barinov, A. S. Solovkin and G. N. Yakovlev, *Radiokhimiya*, 14 (1972) 574.
- 27 F. A. Cotton and R. M. Wing, *Inorg. Chem.*, 4 (1965) 867.
- 28 L. J. Bellamy, *The Infrared Spectra of Complex Molecules*, Methuen, London, 1959, pp. 21-23, 312, 319.

SURVEY OF REACTION TYPES IN LOW-ENERGY COLLISIONAL ACTIVATION OF PROTONATED METHYL ALKYL KETONES

MAURICE M. BURSEY* and JEFFREY A. NYSTROM^a

Department of Chemistry, University of North Carolina at Chapel Hill, Chapel Hill, NC 27514 (U.S.A.)

J. RONALD HASS

Laboratory of Molecular Biophysics, National Institute of Environmental Health Sciences, P.O. Box 12233, Research Triangle Park, NC 27709 (U.S.A.)

(Received 30th September 1983)

SUMMARY

In contrast to high-energy collisions, where simple cleavages are commoner, rearrangements typically account for 96–100% of products in low-energy collisions of the $[M + 1]^+$ ions of aliphatic methyl ketones. Rules for predicting low-energy helium collisional-activated decomposition (CAD) spectra of the ketones are based on proton affinities of fragments formed by simple rearrangements. The commonest reaction is equivalent to the energetically improbable four-center 1,3-H or 1,3-R shift; other rearrangements equivalent to processes with five-, six-, or seven-center activated complexes are less important. In larger ions, loss of water followed by loss of alkene dominates. *O*-Protonated enol forms either lose water to give a carbonium ion that rearranges to forms capable of losing olefin fragments, or rearranges to an intermediate in the formation of acetyl ion and an alkane. *O*-Protonated keto forms rearrange to alkanes and protonated smaller carbonyl compounds. The ion kinetic energies necessary to produce several intense daughter ions at threshold establish the order of sequential fragmentations. When helium is the collisional gas and the ion energy is 30 eV in the laboratory frame (the maximum value studied), the ion energy is only 0.8–1.9 eV in the center-of-mass frame depending on its size. Only a fraction of this kinetic energy is converted to internal energy, so that onsets of reaction channels differing by several tenths of an electron-volt are easily studied. Some isomers of methyl ketones can be easily distinguished by He-CAD spectra of their $[M + 1]^+$ ions.

The increasing use of ionization by protonation or cationization, combined with the separation of these ions from background and other components by mass-analyzed ion kinetic energy spectrometry (m.i.k.e.s.), has prompted surveys of fragmentations of $[M + H]^+$ ions from several typical functional groups [1–3]. As would be expected [4, 5] for even-electron ions, their m.i.k.e. spectra are dominated by rearrangement processes in which even-electron ions are formed; odd-electron ion products are not excluded and often are useful in interpretation. The m.i.k.e.s. technique imposes high-energy collisions on ions; in contrast, the tandem quadrupole

^aPresent address: Department of Chemistry, Queens College, Charlotte, NC 28274, U.S.A.

technique for mass spectrometry/mass spectrometry (m.s./m.s.) imposes low energy. The acceptance of tandem quadrupole instruments for m.s./m.s. intensifies the need to establish general fragmentation patterns for typical functional groups, because the energy distribution in excited ions formed by the low-energy collision processes in these instruments may not contain the high-energy tail of the m.i.k.e.s. product distribution. This high-energy tail is the portion which accents the simple cleavage processes that often lead to the odd-electron product ions, among others [6]. Accordingly, fragmentation processes in tandem quadrupole instruments may be dominated even more by low-energy processes with tight transition states. In this study, this effect is accentuated by the choice of helium as the collisional gas. That choice reduces the center-of-mass (COM) energy of the accelerated ion to low values, according to the equation

$$E_{\text{COM}} = [m/(M + m)]E_{\text{LAB}} \quad (1)$$

Here E_{COM} is the center-of-mass energy of the ion of mass M that collides with a collision gas of mass m after acceleration to E_{LAB} in the laboratory frame. Thus an ion of m/z 100 accelerated through 50 V collides with helium with a COM energy of only 2 eV. From thresholds for appearance of fragment ions from a few molecules, including 2-pentanone, a model for compounds reported here, it has been concluded that some 15–40% of this translational energy may be converted into internal energy [7, 8].

The N_2 collisional activation spectra of protonated 2-hexanone [9] and 3-hexanone [2] have been discussed briefly. Dominant fragmentations there were summarized as alkane loss, alkene loss, alkyl loss, and water loss. The present study reports the helium low-energy collisional-activation spectra of several methyl alkyl ketones to identify products.

EXPERIMENTAL

Low-energy collisional-activation spectra were obtained with a tandem quadrupole system (Extranuclear Laboratories) previously described [10]. Samples were introduced through a direct probe equipped with a needle valve. The source pressure of the sample was sufficient to convert virtually all of the molecular ions to $[M + 1]^+$ ions by ion–molecule reactions (self-ionization). The source temperature was $245 \pm 5^\circ\text{C}$. Ions were accelerated through 30 V to give them 30-eV kinetic energy before mass separation in the first quadrupole to pass only $[M + 1]^+$ ions to the collision cell. Helium was introduced into the collision cell at a pressure measured by an ion gauge as between 1×10^{-6} and 7×10^{-6} torr for various studies, although the location of the gauge was not sufficiently close to the cell to claim that this reading reflects the pressure in the cell; it served to ensure experimental reproducibility. These pressures were known to be in the single-collision region [8]. Helium pressure and cell voltages were adjusted to optimize total fragment ion current.

TABLE 1

Helium collisional-activation mass spectra of the $[M + 1]^+$ ions of aliphatic ketones

m/z	Acetone	Butanone	Cyclopropyl methyl ketone	3-Methyl-2-pentanone	4-Methyl-2-pentanone	2-Hexanone	4,4-Dimethyl-2-pentanone	5-Methyl-2-hexanone	3-Ethyl-2-pentanone	2-Heptanone	2-Octanone	5-Ethyl-2-heptanone	2-Nonanone
29	2.1	0.57	—	—	—	—	—	—	—	—	—	—	—
31	100	7.1	—	—	—	—	—	—	—	—	—	—	—
32	—	0.10	—	—	—	—	—	—	—	—	—	—	—
39	—	0.16	—	—	—	—	—	—	—	—	—	—	—
41	26	—	—	—	—	0.35	—	—	—	—	—	—	—
42	1.8	—	—	—	—	—	—	—	—	0.23	—	—	1.6
43	2.7	10.4	100	—	17	0.36	—	—	1.9	0.69	1.9	—	—
44	1.6	0.37	—	—	—	—	—	—	—	—	—	—	—
45	—	—	—	100	28	13	—	1.9	16	3.6	3.3	—	—
53	—	0.11	—	—	—	—	—	—	—	—	—	—	—
54	—	0.24	—	—	—	—	—	—	—	—	—	—	—
55	—	100	—	8.4	—	30	—	13	12	22	6.9	0.12	2.5
56	—	0.59	—	—	—	—	—	—	—	—	—	—	—
57	—	0.23	0.74	39	100	8.9	84	2.4	7.0	0.73	2.3	1.2	7.6
58	—	0.51	—	—	—	—	—	—	—	—	—	—	—
59	—	—	—	66	27	11	—	1.9	69	3.6	1.9	—	—
60	—	—	—	—	—	0.27	—	—	—	—	—	—	—
61	—	—	—	—	—	—	—	—	0.19	—	—	—	—
67	—	—	11	—	—	—	—	—	—	—	—	—	—
68	—	—	—	—	—	0.13	—	—	—	—	—	—	—
69	—	—	—	—	—	—	100	3.8	6.2	7.6	100	14	100
70	—	—	0.38	—	—	—	—	—	—	—	2.3	—	—
71	—	—	—	—	—	0.54	4.3	1.9	43	16	2.2	0.16	1.5
72	—	—	—	—	—	0.41	—	—	—	—	1.4	0.08	—
73	—	—	—	—	—	1.4	—	0.44	100	5.6	3.3	—	1.4
79	—	—	—	—	—	—	—	—	—	—	0.39	—	—
80	—	—	—	—	—	—	—	—	—	—	0.63	—	—
81	—	—	—	—	—	—	—	—	—	—	3.7	—	—
82	—	—	—	—	—	—	—	—	—	—	2.0	—	—
83	—	—	—	29	42	100	—	—	—	0.59	33	18	—
84	—	—	—	—	—	1.1	—	—	—	—	3.1	—	—
85	—	—	—	—	—	0.71	—	—	—	1.0	8.8	0.51	19
86	—	—	—	—	3.3	1.5	0.23	—	4.0	0.91	0.51	—	—
87	—	—	—	—	—	—	—	—	—	0.82	—	0.32	3.7
92	—	—	—	—	—	—	—	—	—	—	0.29	—	—
93	—	—	—	—	—	—	—	—	—	—	0.57	—	—
95	—	—	—	—	—	—	—	—	—	—	0.58	—	—
97	—	—	—	—	—	—	0.67	100	53	100	—	0.16	—
99	—	—	—	—	—	—	—	—	—	—	2.7	0.40	3.3
100	—	—	—	—	—	—	—	—	—	0.56	0.5	—	—
101	—	—	—	—	—	—	—	—	—	—	0.77	0.26	4.4
102	—	—	—	—	—	—	—	—	—	—	—	—	3.0
103	—	—	—	—	—	—	—	—	—	—	—	—	5.8
111	—	—	—	—	—	—	—	—	—	—	27	—	—
112	—	—	—	—	—	—	—	—	—	—	0.84	—	—
113	—	—	—	—	—	—	—	—	—	—	1.4	—	—
114	—	—	—	—	—	—	—	—	—	—	0.68	—	—
115	—	—	—	—	—	—	—	—	—	—	—	0.53	1.7
125	—	—	—	—	—	—	—	—	—	—	—	100	5.8
MH ⁺	>800	300	300	790	800	130	>800	190	525	180	265	330	390

TABLE 2

Relative abundances of ions formed by indicated neutral losses

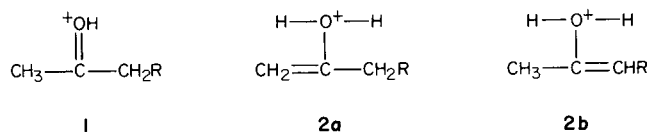
	Acetone	Butanone	Cyclopropyl methyl ketone	3-Methyl-2-pentanone	4-Methyl-2-pentanone	2-Hexanone	4,4-Dimethyl-2-pentanone	3-Ethyl-2-pentanone	5-Methyl-2-hexanone	2-Heptanone	2-Octanone	5-Ethyl-2-heptanone	2-Nonanone
H ₂ O	25	100	11	29	42	100	0.69	53	100	100	27	100	5.8
H ₂ O +	—	—	—	8.4	—	30	100	6.2	3.8	7.6	33	0.16	—
C ₂ H ₄	—	—	—	—	—	—	—	—	—	—	—	—	—
H ₂ O +	—	—	—	—	—	0.35	—	12	13	22	100	18	—
C ₃ H ₆	—	—	—	—	—	—	—	—	—	0.28	6.0	14	100
H ₂ O +	—	—	—	—	—	—	—	—	—	—	—	0.12	2.5
C ₂ H ₁₀ ^o	—	—	—	—	—	—	—	—	—	—	—	—	—
C ₂ H ₄	100	5.0	0.73	—	—	1.4	—	—	—	0.82	0.77	0.53	1.7
C ₂ H ₆	—	—	100 ^a	66	27	11	—	100	0.44	5.6	—	0.26	4.4
C ₂ H ₈	—	—	—	—	28	13	—	69	1.9	3.6	3.1	0.32	3.7
C ₂ H ₁₀	—	—	—	—	—	—	—	16	1.9	3.6	1.9	—	1.4
C ₂ H ₁₂	—	—	—	—	—	—	—	—	—	—	3.3	—	1.4
CH ₄	2.7	0.23	—	3.0	—	0.71	—	—	—	—	1.4	—	—
C ₂ H ₆	2.1	10.4	—	—	—	0.54	—	—	—	1.0	2.7	—	—
C ₂ H ₈	—	0.57	—	39	100	8.9	4.3	43	1.8	16	8.8	0.40	3.8
C ₂ H ₁₀	—	—	—	—	17	0.36	—	7.0	2.4	0.73	2.2	0.51	19.2
C ₂ H ₁₂	—	—	—	—	—	—	—	1.9	—	0.69	2.3	0.26	1.3
C ₂ H ₁₄	—	—	—	—	—	—	—	—	—	—	1.9	1.2	7.6

^aCyclopropane?

Ketones were all commercial samples of high purity, found not to contain detectable impurities by mass spectrometry.

RESULTS AND DISCUSSION

Table 1 contains the He-CAD spectra of the [M + H]⁺ ions of the ketones studied. Table 2 isolates the superficially parallel fragmentations of each [M + H]⁺ ion. Almost all decompositions are consistent with an [M + H]⁺ ion protonated on oxygen; there are two such ions, the protonated keto form 1 and the protonated enol forms 2a and 2b.



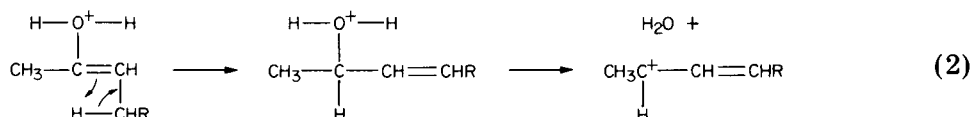
Evidence for cationized enol forms can be found in ion cyclotron resonance studies, where decompositions of the cationized enol form of ketones account for many fragment ions when Cu⁺ is the cation [11]. There is some evidence from chemical ionization studies that ketones with more than six carbons sometimes protonate on the alkyl chain [12].

Each major type of fragmentation is discussed in sequence below. The "mechanisms" are unsupported by labeling or other methods for ion structures and mechanisms, and their merit is for bookkeeping. For the sake of brevity many "mechanisms" are presented as four-center, concerted processes even though it is recognized [13] that these processes involve high-energy pathways unlikely to be accessible to these ions. Such reactions surely proceed by combinations of other pathways, confirmation of which will be a subject of future research.

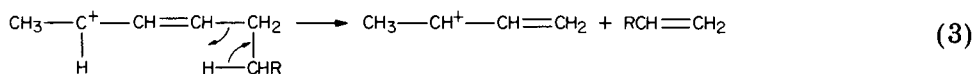
Initial loss of water

The principal fragmentation of the protonated ketones, except for acetone, is by loss of water and then an alkene. Its occurrence is consistent with the dominant metastable processes in similar ions generated by dissociative electron ionization [14–16]. In our examples, these processes account for 63% to 80% of fragments. For acetone and butanone, only water is lost; for 2-hexanone and 2-heptanone, $[\text{MH} - \text{H}_2\text{O}]^+$ is the base peak; for 2-octanone and 2-nonanone, $[\text{MH} - \text{H}_2\text{O} - \text{C}_2\text{H}_{2n}]^+$ is the base peak.

A mechanism for loss of water consistent with thermochemistry may be outlined as



For sufficiently long R, an olefin is eliminated. The products may be



Alkenyl ions which undergo such decompositions on the metastable time scale or longer are of course in equilibrium with many of their isomers [17–19].

The alternative formation of $[\text{MH} - \text{H}_2\text{O} - \text{C}_n\text{H}_{2n}]^+$ by loss first of the alkene, then of water, can be discounted in at least the case of 2-octanone because the intermediate $[\text{MH} - \text{C}_3\text{H}_6]^+$ is absent. More generally, studies of the dependence of fragmentation on ion kinetic energy (for example, Figs. 1–4) show that usually $[\text{MH} - \text{H}_2\text{O} - \text{C}_n\text{H}_{2n}]^+$ forms at higher energies than $[\text{MH} - \text{H}_2\text{O}]^+$ (which is the principal fragment at low collision energies) but at lower energies than $[\text{MH} - \text{C}_n\text{H}_{2n}]^+$. Hence the low-energy route to $[\text{MH} - \text{H}_2\text{O} - \text{C}_n\text{H}_{2n}]^+$ is through the initially dehydrated ion, though some may also be formed from the $[\text{MH} - \text{C}_n\text{H}_{2n}]^+$ intermediate at higher energies.

Protonated acetone (Fig. 3A) must of course lose water by a different mechanism. In this spectrum there are only two fragments, m/z 41 (25%, by loss of water) and m/z 31 (100%, by loss of ethylene), as in the case of the same ion produced by dissociative electron ionization [14, 16]. If it is assumed that the loss of water involves the intervention of *O*-protonated

enol 3, the $[C_3H_5]^+$ ion so formed is less stable than the allyl ion [20], and the low-energy pathway to $[C_3H_5]^+$ may be a multistep process composed of dissociation and a 1,2-H migration; the following two steps may be

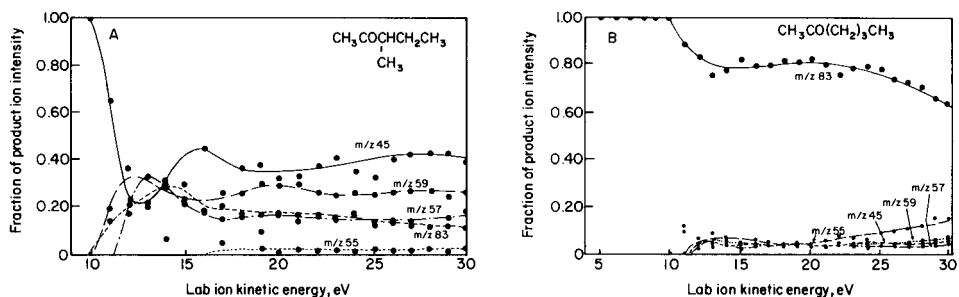


Fig. 1. Kinetic energy dependence of daughter ion currents for (A) protonated 3-methyl-2-pentanone and (B) protonated 2-hexanone. As is typical of larger unbranched or singly branched ketones studied, $[M - H_2O]^+$ (m/z 83) is formed at lower energy than $[M - H_2O - C_2H_4]^+$ (m/z 55), and $[M - C_2H_4]^+$ is not intense enough to be plotted at any kinetic energy.

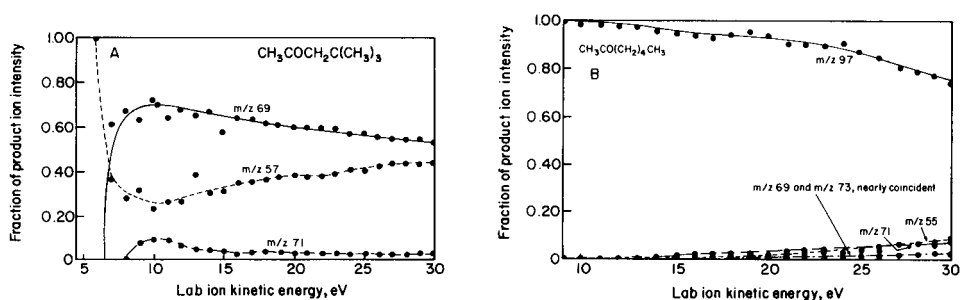


Fig. 2. Kinetic energy dependence of daughter ion currents for (A) protonated 4,4-dimethyl-2-pentanone and (B) protonated 2-heptanone.

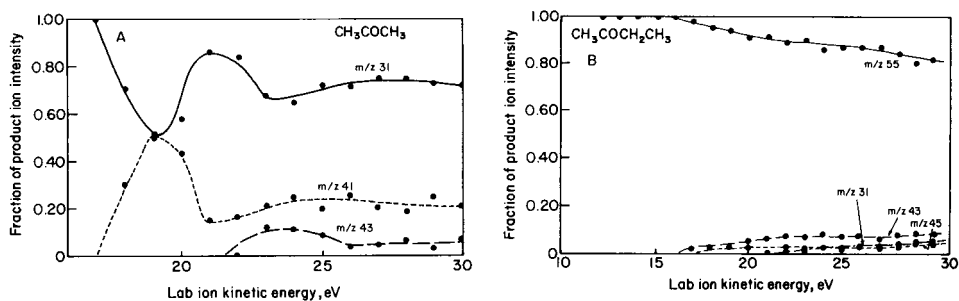


Fig. 3. Kinetic energy dependence of daughter ion currents for (A) protonated acetone and (B) protonated butanone. Water loss dominates the spectrum in B.

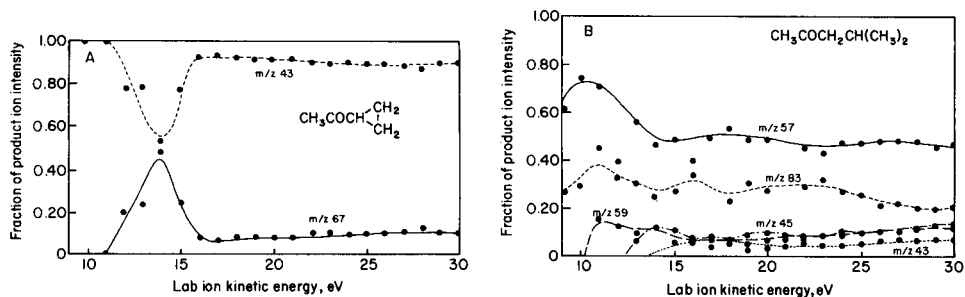
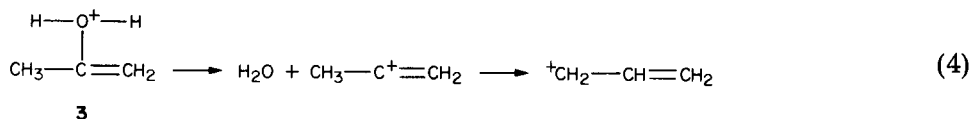
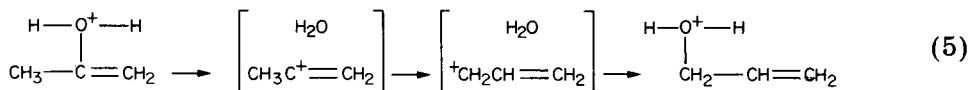


Fig. 4. Kinetic energy dependence of daughter ion currents for (A) protonated cyclopropyl methyl ketone and (B) protonated 4-methyl-2-pentanone.

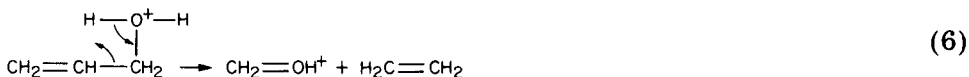
suggested



The loss of ethylene may point to the formation of a third isomer of m/z 59 from 3. Intermediate to the formation of this isomer is a complex described (by reference to the proton affinities of C_3H_4 , 176 kcal mol⁻¹ [21], and H_2O , 170 kcal mol⁻¹ [22]) as a solvate of $[\text{C}_3\text{H}_5]^+$ by water



The intermediate *O*-protonated allyl alcohol may decompose to protonated formaldehyde and ethylene by the equivalent of a four-center process. (Other mechanisms are possible.)

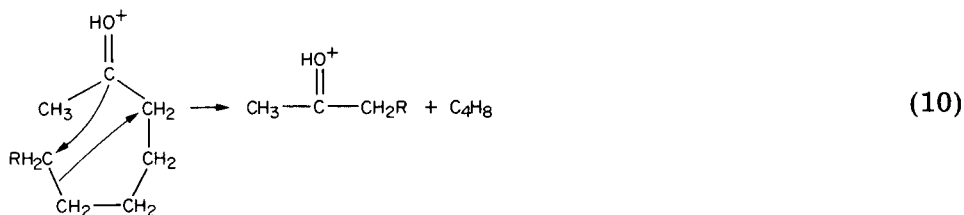


Proton affinities of CH_2O (182 kcal mol⁻¹ [22]) and C_2H_4 (160 kcal mol⁻¹ [23]) at 298 K are inconsistent with observed products; this observation suggests that a proton-bound complex of formaldehyde and ethylene is not intermediate to the reaction. The accessibility of this form and related forms of $\text{C}_3\text{H}_7\text{O}^+$ has been discussed [15, 24]. The behavior of protonated butanone (Fig. 3B) is analogous to that of protonated acetone.

These decompositions are not general models for the reactions of the heavier ketones. For example, consider 2-hexanone for a further model. Loss of water from the protonated enol form is more nearly consonant with the further reactions of the ion if it proceeds through a form of slightly higher energy that results from the equivalent of a 1,3-H transfer (Eqn. 2, R = C_2H_5). Further loss of ethylene suggests an equivalent of a four-center process (Eqn. 3, R = H). The separation of products corresponds to a competition of ethylene (proton affinity 160 kcal mol⁻¹ [23]) and 1,2-butadiene for a proton, with the expected product $\text{CH}_3\text{CH}^+\text{CH}=\text{CH}_2$.

stability of the neutral olefin in Eqn. 7, consistent with electron ionization-induced fragmentation reactions.

Finally, there is an analogous process for loss of C_4H_8 from larger ions that could proceed through a seven-membered ring

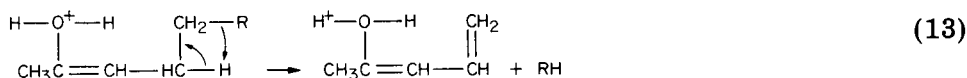


Loss of alkane

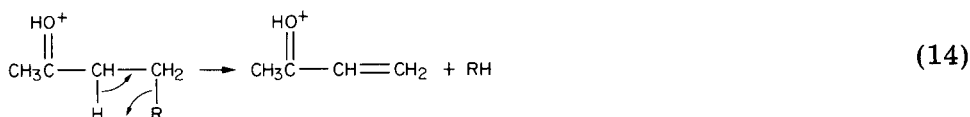
In general, loss of an alkane accounts for only a small fraction of daughter ions; the exceptions are 2-nonanone, cyclopropyl methyl ketone (taking loss of C_3H_6 as cyclopropane loss and equivalent there to alkane loss, Fig. 4A), and 4-methyl-2-pentanone (Fig. 4B). Possibly 2-nonanone is protonated on the alkyl chain [12] to an extent great enough to account for its behavior. The behavior of most smaller ketones can be rationalized as equivalent to the four-center processes of Eqns. 11 and 12, though, as in 4-methyl-2-pentanone, other processes can dominate the spectrum.



The larger ketones have important losses of alkanes rationalized by the equation



Presumably, the formation of the extended conjugation is favorable enough to accentuate the process. The formation of conjugated systems may also be used to rationalize a set of losses summarized for brevity as



Conclusions

As expected, collisions of low-energy ketone ions with helium induce fragmentations with low thresholds and tight activated complexes, predominantly four-center processes. Product intensities are often governed

by proton affinities, as if weakly associated proton-bound clusters were intermediates. Loss of water, often followed by an olefin, usually dominates the fragmentations. Other major losses are those of olefins and alkanes.

REFERENCES

- 1 J. R. Hass, D. J. Harvan and M. M. Bursey, *Anal. Chim. Acta*, 105 (1979) 129.
- 2 M. L. Sigsby, R. J. Day and R. G. Cooks, *Org. Mass Spectrom.*, 14 (1979) 273.
- 3 M. L. Sigsby, R. J. Day and R. G. Cooks, *Org. Mass Spectrom.*, 14 (1979) 556.
- 4 F. W. McLafferty, *Interpretation of Mass Spectra*, 3rd edn., University Science Books, Mill Valley, CA, 1980, p. 48.
- 5 M. Karni and A. Mandelbaum, *Org. Mass Spectrom.*, 15 (1980) 53.
- 6 M. M. Bursey, *Mass Spectrom. Rev.*, 1 (1982) 3.
- 7 D. J. Douglas, *J. Phys. Chem.*, 86 (1982) 185.
- 8 J. A. Nystrom, M. M. Bursey and J. R. Hass, *Int. J. Mass Spectrom. Ion Proc.*, 55 (1983) 263.
- 9 G. R. Glish, P. H. Hemberger and R. G. Cooks, *Anal. Chim. Acta*, 119 (1980) 137.
- 10 M. W. Siegel, *Anal. Chem.*, 52 (1980) 1790.
- 11 R. C. Burnier, G. D. Byrd and B. S. Freiser, *Anal. Chem.*, 52 (1980) 1641.
- 12 F. H. Field, *J. Am. Chem. Soc.*, 90 (1968) 5649.
- 13 D. H. Williams and G. Hvistendahl, *J. Am. Chem. Soc.*, 96 (1974) 6753.
- 14 F. W. McLafferty and I. Sakai, *Org. Mass Spectrom.*, 7 (1973) 971.
- 15 R. D. Bowen, D. H. Williams, G. Hvistendahl and J. R. Kalman, *Org. Mass Spectrom.*, 13 (1978) 721.
- 16 U. I. Zákorsky, *Org. Mass Spectrom.*, 17 (1982) 253.
- 17 K. Levsen, *Org. Mass Spectrom.*, 10 (1975) 55.
- 18 F. Borchers, K. Levsen, H. Schwarz, C. Wesdemiotis and H. U. Winkler, *J. Am. Chem. Soc.*, 99 (1977) 6359.
- 19 M. A. Shaw, R. Westwood and D. H. Williams, *J. Chem. Soc., Part B*, (1970) 1773.
- 20 J. O. Lay, Jr., and M. L. Gross, *J. Am. Chem. Soc.*, 105 (1983) 3445.
- 21 D. H. Aue, W. R. Davidson and M. T. Bowers, *J. Am. Chem. Soc.*, 98 (1976) 7600.
- 22 J. F. Wolf, R. H. Staley, I. Koppel, M. Taagepera, R. T. McIver, Jr., J. L. Beauchamp and R. W. Taft, *J. Am. Chem. Soc.*, 99 (1977) 5417.
- 23 D. H. Aue and M. T. Bowers, in M. T. Bowers, (Ed.), *Gas Phase Ion Chemistry*, Vol. 2, Academic Press, New York, 1979, Ch. 9.
- 24 J. L. Holmes, R. T. B. Rye and J. K. Terlouw, *Org. Mass Spectrom.*, 14 (1979) 606.
- 25 F. P. Lossing and G. P. Semeluk, *Can. J. Chem.*, 48 (1970) 955.
- 26 R. M. A. Refaey and W. A. Chupka, *J. Chem. Phys.*, 48 (1968) 5205.

SURVEY OF REACTIONS OF PROTONATED ACETATE ESTERS INDUCED ON LOW-ENERGY COLLISIONS WITH HELIUM AND NITROGEN

MAURICE M. BURSEY* and JEFFREY A. NYSTROM^a

Department of Chemistry, University of North Carolina at Chapel Hill, Chapel Hill, NC 27514 (U.S.A.)

J. RONALD HASS

Laboratory of Molecular Biophysics, National Institute of Environmental Health Sciences, P.O. Box 12233, Research Triangle Park, NC 27709 (U.S.A.)

(Received 30th September 1983)

SUMMARY

The major fragmentations induced by collisions of 30-eV (laboratory coordinate) protonated acetate esters with helium and nitrogen are the rearrangements observed in earlier high-energy collisional activation studies, except for the diagnostic loss of alkane observed in the high-energy process, which is missing. The kinetic energy dependence of fragmentation is reflected in peak intensities at 30 eV. As proposed earlier, helium collisions are useful for categorization of the compounds, and nitrogen for their identification.

Two studies of collisional activation of protonated esters have appeared [1, 2]. Some, but not all, of the fragmentations under these conditions are similar to those of protonated esters under chemical ionization conditions in the source. The acyl group is generally identifiable because one of the major losses is that of the alcohol molecule; other fragmentations are losses of alkane, alkene, and alkyl or aryl groups.

These collisional activation studies were performed on mass-separated ion kinetic energy spectrometers, in which the ion is accelerated through several thousand volts before the collision. Under this condition, there is a significant fraction of ions that receives high internal energy [3]. The last decomposition, loss of a radical instead of a molecule, is more characteristic of high-energy processes than the other decompositions, losses of molecules requiring only low energy. Many such reactions are observed in the fragmentation of $[M + 1]^+$ ions produced by chemical ionization [4], which have only low internal energy.

In collisions of ions accelerated only through low potentials, such reactions should be absent. This prediction is most likely to be true when the center-of-mass kinetic energy of the ion in the collision is minimized. That

^aDepartment of Chemistry, Queens College, Charlotte, NC 28274, U.S.A.

condition will be met when the collision gas has a low mass [5]. Accordingly, this paper describes a study of the fragmentations of acetate esters upon collision with helium, in which a very small amount of internal energy is imparted to the ion, and with nitrogen, in which more energy is deposited in the ion.

EXPERIMENTAL

The esters were reagent-grade materials obtained from commercial sources. They were free from impurities easily identified by mass spectrometry. A hybrid instrument consisting of a Finnigan Instruments 3300 EI/CI source mounted on an Extranuclear Laboratories tandem quadrupole stack, and described earlier [5], was used. Samples were introduced through a direct probe equipped with a needle valve. The recorded sample pressure in the source was $1-6 \times 10^{-6}$ torr; the ion gauge is not placed for accuracy and the true value of the pressure is higher, so that $[M + 1]^+$ ions were formed by self-protonation. Ion-gauge pressure of collision gas in the collision region was $1-8 \times 10^{-6}$ torr, although the gauge was again not well placed for accuracy. Ions were accelerated by a source voltage, although spectra differed only slightly (apparently as a result of the change in residence time in the collision cell) when the kinetic energy was the result not of a single acceleration from the source voltage but was the sum of two accelerations, the first in the source and the second from the potential applied to the collision cell between the quadrupole stacks. Spectra reported here are those from ions with a kinetic energy of 30 eV (accelerated only in the source). The source temperature was 190–200°C. Spectra are the average of at least three scans.

RESULTS AND DISCUSSION

The spectra of protonated methyl acetate (Table 1) differ qualitatively from those of the other esters and are discussed separately. The helium collisional activation spectrum contains only one daughter, m/z 43, characteristic of the chemical ionization spectra of acetate esters [4]. A mechanism such as



has the form of lowest energy as reactant but proceeds through an energetically unlikely four-center complex. The actual process is likely only equivalent, and for example may be stepwise. The nitrogen collisional activation spectrum has m/z 43 as the base peak, with CH_3^+ as the second most intense peak. Figure 1 shows the dependence of the major ion intensities on kinetic energy. The other peaks are minor: CHO^+ , CH_3O^+ , CH_5O^+ , $\text{C}_2\text{H}_5\text{O}^+$, $\text{C}_2\text{H}_7\text{O}^+$. Some of them present interesting examples of low-energy equivalents of processes with high-energy four-center activated complexes as well as intuitive

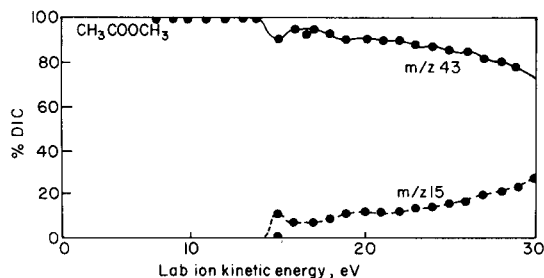
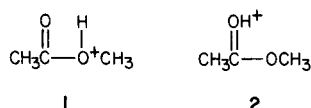


Fig. 1. Dependence of daughter ion currents (DIC) of methyl acetate on ion kinetic energy.

evidence for the role of an ether-*O*-protonated form of protonated ethyl acetate 1.



The probable reactions are



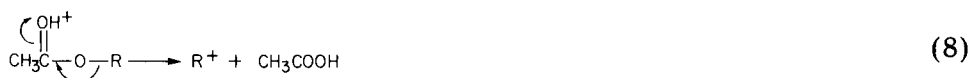
The site of ester protonation has been studied by several authors; either *O* can be protonated to yield 1 and 2, and there is disagreement on which form is the more stable [6, 7].

Of the heavier aliphatic acetates, those up to butyl acetate are dominated by *m/z* 61, protonated acetic acid, which can in principle be formed by the low-energy equivalent of a high-energy four-center process, illustrated for carbonyl-protonated ester (Eqn. 6) or by a McLafferty rearrangement, illustrated for ether-protonated ester (Eqn. 7). This behavior mirrors the known

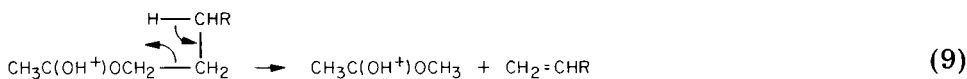
fragmentation of protonated ester ions in chemical ionization [8].



The formation of the acyl ion by nominal elimination of alcohol, similar to Eqn. 1, is also found in all esters; from studies noted below, the formation may proceed through two steps, loss of olefin and then water. The production of the alkyl ion remains important in the lighter esters and is the base peak in the heavier ones



Fragmentation of these alkyl ions, e.g., the production of C_2H_3^+ from C_2H_5^+ and the production of C_2H_5^+ from $\text{CH}_3\text{CH}_2\text{CH}_2\text{CH}_2^+$, is also observed, reflecting behavior of protonated esters in dissociative chemical ionization [8]. Decarbonylation similar to Eqn. (5) may account for $[\text{M} - 28]^+$ peaks. There are also ions derived from loss of olefins with fewer carbons than the entire R group: $[\text{M} - \text{C}_3\text{H}_6]^+$ from n-butyl acetate and $[\text{M} - \text{C}_4\text{H}_8]^+$ from n-amyl acetate presumably are related processes. Equation 9 accounts for the similarity, though it is intended only as an approximate guide because its concerted nature makes it inaccessible to low-energy ions



Loss of water was observed in only one case, from n-butyl acetate. There is not enough information to postulate a mechanism but the reaction could proceed through the McLafferty intermediate.

There is little evidence of loss of alkane, observed in high-energy spectra [2]. The loss of 44 from n-butyl acetate and 72 from i-amyl acetate could be alkane losses but they clearly are unrelated mechanistically. The general alkane losses found earlier apparently require higher energy than was attained in these collisions, even with nitrogen.

The principal fragmentations of protonated phenyl acetate yield m/z 93, protonated phenol; m/z 77, C_6H_5^+ ; and m/z 43. These may be formed by analogy to the processes found in methanol.

The dependence of fragmentation induced by collision with nitrogen upon ion kinetic energy is illustrated for the heavier esters in Figs. 2 and 3. (Because

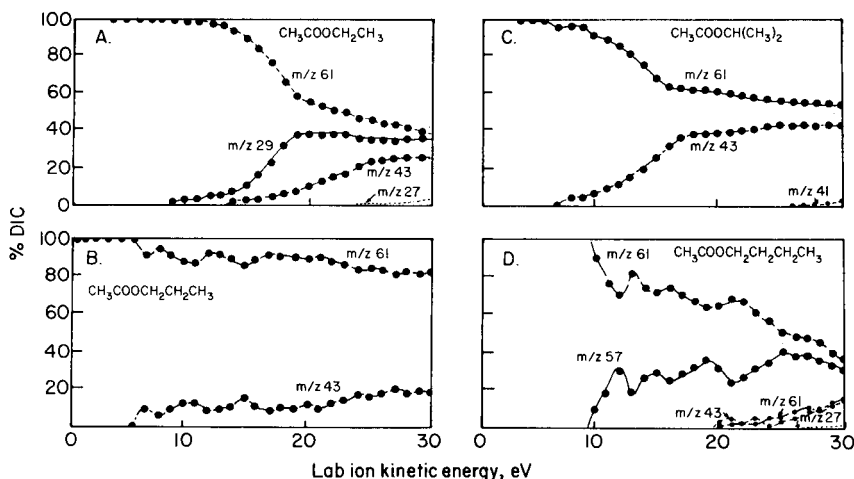


Fig. 2. Dependence of daughter ion currents on ion kinetic energy: (A) ethyl acetate; (B) n-propyl acetate; (C) i-propyl acetate; (D) n-butyl acetate.

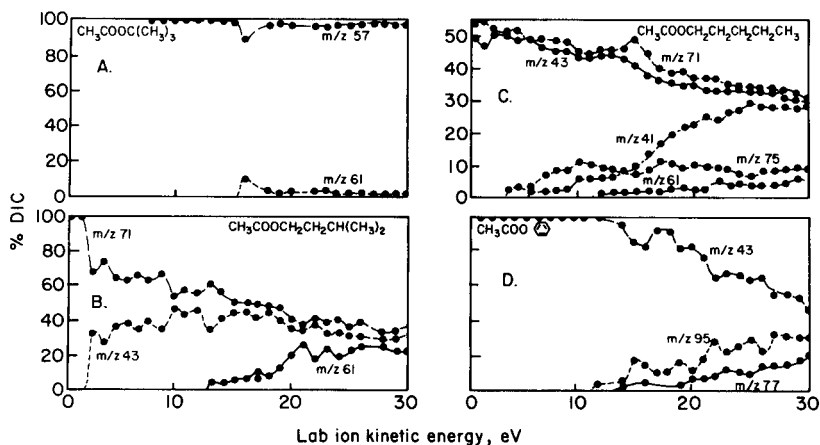
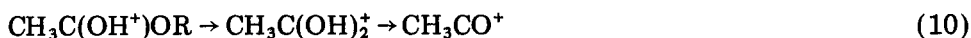


Fig. 3. Dependence of daughter ion currents on ion kinetic energy: (A) t-butyl acetate; (B) n-amyl acetate; (C) i-amyl acetate; (D) phenyl acetate.

collision with helium at the laboratory energies used rarely provides more than one intense fragment, these data are not plotted; those that do produce two or more fragments yield more detailed information on the closely spaced onsets.) The major qualitative conclusion is that ions formed at higher energies have lower relative intensities at 30 eV. This conclusion suggests in turn that the activated complexes for most processes are roughly equally tight. Inferences can also be made about the origins of the smaller ions: they demonstrate generally that m/z 43 may be formed by the intermediate protonated acetic acid. Thus



Although the carbonyl-protonated form is written, this is only the dominant form and the other ether-protonated form is also possible [9]. Comments on the origins of smaller hydrocarbon ions are also possible based on the data shown in the figures. For example, in *i*-amyl acetate (Fig. 3), the shapes of the curves for m/z 71 and m/z 61 ions suggest that both are precursors to m/z 43, so that m/z 43 is likely a mixture of C_3H_7^+ and CH_3CO^+ . This possibility can be investigated once an instrument capable of high resolution of the daughter ions is available.

Conclusions

Collision with helium only occasionally provides more fragments than the $\text{CH}_3\text{C}(\text{OH})_2^+$ and R^+ ions, and therefore would be useful for the routine classification of aliphatic acetates and their distinction from aromatic acetates. More structural information is available from collision with nitrogen. Reactions are almost all rearrangements, usually the equivalent of four-centered processes, and the helium collisions provide interesting fundamental information to identify the slow decompositions of ions with low internal energies. It is expected that most of the simple cleavages that accompany these rearrangements in high-energy m.i.k.e. spectrometry are missing here; it is intriguing that one of the major types of rearrangements there, alkane loss, is also missing. This may indicate that the precursor for this product is particularly stable so that a large activation barrier must be overcome before the fragmentation can occur.

The reactivity of protonated acetate esters under the conditions used here resembles their reactivity in the ion cyclotron resonance spectrometer [7], and, to a lesser extent, fragmentation after simple chemical ionization [8]. However, the reactivities are not identical; decarbonylation, further fragmentation of alkyl ions, and the extrusion of small olefins exemplified by Eqn. 9 were not found in the ion cyclotron resonance spectra. Thus, although both experiments represent conditions of low internal energy and long lifetime, they are clearly dissimilar in detail, because the energy and lifetime conditions are not identical.

Finally, the processes uncovered offer opportunity to gather evidence for the true mechanisms of the processes summarized by the equations given above.

REFERENCES

- 1 J. R. Hass, D. J. Harvan and M. M. Bursey, *Anal. Chim. Acta*, 105 (1979) 129.
- 2 M. L. Sigsby, R. J. Day and R. G. Cooks, *Org. Mass Spectrom.*, 14 (1979) 556.
- 3 F. W. McLafferty, P. F. Bente, III, R. Kornfeld, S.-C. Tsai and I. Howe, *J. Am. Chem. Soc.*, 95 (1973) 2120.
- 4 F. H. Field, *J. Am. Chem. Soc.*, 88 (1966) 4337.
- 5 J. A. Nystrom, M. M. Bursey and J. R. Hass, *Int. J. Mass Spectrom. Ion Proc.*, 55 (1983) 263.

- 6 F. M. Benoit and A. G. Harrison, *J. Am. Chem. Soc.*, 99 (1977) 3980.
- 7 C. V. Pscheck and S. E. Buttrill, Jr., *J. Am. Chem. Soc.*, 96 (1974) 6027.
- 8 J. A. Herman and A. G. Harrison, *Can. J. Chem.*, 59 (1981) 2133.
- 9 N. E. Middlemiss and A. G. Harrison, *Can. J. Chem.*, 57 (1979) 2827.

FLOW FLUORIMETRY OF TRACE AMOUNTS OF URANIUM(VI) AFTER PRECONCENTRATION ON A TRI-*n*-OCTYLPHOSPHINE OXIDE/POLYETHYLENE COLUMN AND ELUTION WITH HYDROGENPHOSPHATE SOLUTION

HITOSHI WATARAI^a and NOBUO SUZUKI*

Department of Chemistry, Faculty of Science, Tohoku University, Sendai 980 (Japan)

(Received 27th May 1983)

SUMMARY

The fluorescence of uranyl ion is enhanced in phosphoric acid medium and in hydrogenphosphate medium. The pH dependence of the fluorescence intensity showed maxima at pH 1–2 and pH 7–8. The concentration of phosphoric acid which gave maximum intensity was around 1 M, but in the hydrogenphosphate media an increase in the concentration lowered the intensity. The procedure was used in combination with preconcentration on a tri-*n*-octylphosphine oxide/polyethylene column. This simple system provided a limit of detection of 0.04 μg for uranium and the calibration graph was linear for the range 0.08–0.8 μg of uranium when 4–15 ml of sample solution was passed through the column. The flow fluorimetric method was applied to the determination of uranium in a spinel.

The most commonly accepted photometric method of determining trace amounts of uranium is based on measuring the fluorescence of the uranyl ion in alkali metal fluoride glass beads [1]. This method can provide high sensitivity but requires very careful preparation of homogeneously fused glass under strictly controlled conditions, because the fluorescence yield of the glass beads is highly dependent on their composition. In comparison with the high yield of the solid-state luminescence, the rather low yield of fluorescence of uranyl ion in solution has rarely been utilized. Yet the solution method has significant advantages such as easy preparation of homogeneous media and the possibility of direct connection with various separation and/or enrichment techniques.

Enhancement of uranyl fluorescence by phosphoric acid was reported by Sill and Peterson [2]. The lifetime of the uranyl fluorescence in phosphoric acid was measured as 189 μs in 1 M phosphoric acid which is about twenty times longer than the lifetimes in perchloric acid or sulfuric acid [3]. This was utilized to improve the detection limit for uranyl ion by discriminating uranyl fluorescence from the short-lived fluorescence of common organic

^aPresent address: Department of Chemistry, Faculty of Education, Akita University, Akita 010, Japan.

compounds (10^{-9} s) [4]. These studies indicate that phosphoric acid is the preferred medium for solution fluorimetry of uranyl ion.

For the determination of trace amounts of uranium in natural or industrial materials, simple and reproducible separation and preconcentration techniques are usually needed prior to the final measurement. For this purpose, extraction chromatography with tri-*n*-octylphosphine oxide (TOPO) on polyethylene was used. TOPO is known as a powerful extractant for uranium [5] and polyethylene seems preferred as the solid support because its solubility parameter ($7.7\text{--}8.2 \text{ cal}^{1/2} \text{ cm}^{-3/2}$) [6] is closer to that of *n*-octane ($7.6 \text{ cal}^{1/2} \text{ cm}^{-3/2}$), the inert moiety of TOPO, than those of other polymers such as polytetrafluoroethylene and polystyrene. A column of Microthene (microporous polyethylene) supporting a solution of TOPO in cyclohexane has been used for collection of uranium from urine and the total amount was determined by spectrophotometry [7]. In the present study, pure TOPO powder was found to be well supported by polyethylene in the presence of nitric acid.

In this paper, the fluorescence characteristics of uranyl-phosphate solutions and a simple fluorimetric procedure for uranium based on collection on a TOPO/polyethylene column and elution with hydrogenphosphate solution are reported.

EXPERIMENTAL

Chemicals and equipment

Aqueous solutions of uranyl ion were prepared from uranyl nitrate or U_3O_8 of analytical-reagent grade. All other reagents used were G.R. grade. Redistilled water was used throughout.

Fluorescence spectra and excitation spectra were measured by means of a Hitachi MPF-4 or a JASCO FP-550X fluorescence spectrophotometer at 25°C . To eliminate the influence of the strong excitation light at 270 nm, a Toshiba Y45 filter was inserted between the cell and the photomultiplier tube. The spectra and chromatograms were recorded on TOA FBR-251A flat-bed recorder.

Chromatographic system for flow fluorimetry

The TOPO/polyethylene column was prepared as follows: 2 g of polyethylene powder (100–200 mesh), as supporting material, was shaken for >12 h with 0.40 g of TOPO and 10 ml of 2 M nitric acid. The TOPO powder turned oily on contact with nitric acid, so that an organic solvent like cyclohexane was not needed to dissolve TOPO. The TOPO-coated polyethylene was packed in a 4 mm i.d. \times 20 cm long Kusano CIG glass column. The pump used was a Kyowa Seimitsu KHU-26H minimicro pump or a JEOL P-2705S constant flow pump with a pressure gauge. The JASCO spectrofluorimeter was used with a $15\text{-}\mu\text{l}$ flow cell.

For examination of eluents, 0.75 ml of 6.3×10^{-5} M uranyl ion solution

in 2 M nitric acid was introduced into the TOPO/polyethylene column, washed in with 4 ml of 2 M nitric acid, and then eluted with a phosphate-containing solution (see below).

The linearity between the elution peak height and the concentration of uranyl ion was examined by loading 4–15 ml of 1.05×10^{-7} M or 2.10×10^{-7} M uranyl ion solution, washing in with 4 ml of 2 M nitric acid, and then eluting with 1 M potassium dihydrogenphosphate at a flow rate of 0.75 ml min^{-1} . The volume of uranyl solution loaded on the column or the volume of washing solution has no effect on the result between 4 and 114 ml.

Determination of uranium in spinel

The powdered sample had the composition MgAl_2O_4 . A portion (0.2 g) of the powder (>60 mesh) was mixed with 0.8 g of sodium tetraborate and 0.8 g of sodium carbonate, and fused in a platinum crucible. The melt was dissolved in 2 M nitric acid, and ammonia solution was added until precipitation of aluminium hydroxide was complete. The precipitate was collected by filtration, dissolved in 2 M nitric acid and loaded on the TOPO/polyethylene column which was then washed. The uranium was then eluted as described above.

RESULTS AND DISCUSSION

Fluorescence of uranyl ion in phosphate solution

Fluorescence spectra of uranyl ion in 0.1 M phosphoric acid and 0.1 M dipotassium hydrogenphosphate solutions with excitation at 270 nm are shown in Fig. 1. The spectrum in phosphoric acid solution shows maxima at 494 nm and 516 nm in agreement with the reported maxima [8], while the

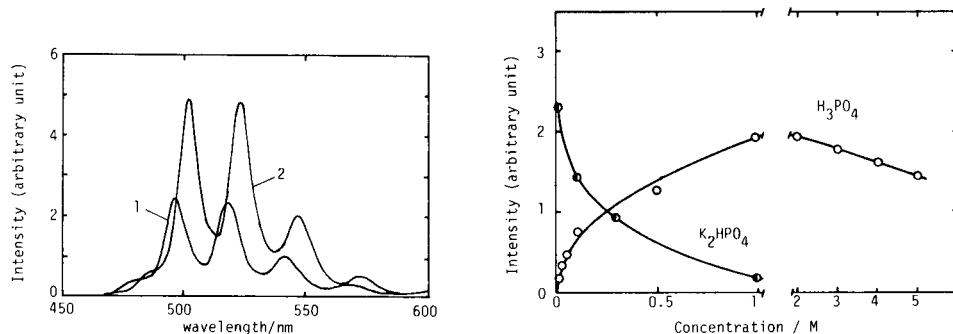


Fig. 1. Fluorescence spectra of 6.3×10^{-5} M uranyl ion: (1) in 0.1 M H_3PO_4 ; (2) in 0.1 M K_2HPO_4 . Excitation at 270 nm.

Fig. 2. Variation of fluorescence intensity of uranyl ion (10^{-4} M) with H_3PO_4 or K_2HPO_4 concentration.

peaks observed in the hydrogenphosphate solution shift toward longer wavelength. This suggests that different species contribute to the spectra in the two systems. The fluorescence intensity also gave a different dependence on the phosphate concentration in the two media (Fig. 2). An increase of phosphoric acid concentration up to 1 M enhanced the intensity, whereas an increase in dihydrogenphosphate concentration caused a rapid decrease. The pH dependences of the fluorescence intensity at constant phosphate concentrations of 1.0, 0.5 and 0.1 M are shown in Fig. 3. At each phosphate concentration, the fluorescence spectrum shifted toward longer wavelength in the pH region above 5, and the variation of the intensity at the maximum wavelength with pH showed two maxima around pH 1–2 and pH 7–8. The fluorescence intensity was linearly proportional to the uranyl ion concentration at pH 1.0 or pH 8.5. This indicates that the fluorescent species contains one uranium atom in its composition.

The predominant role of phosphate in the enhancement effect is to form a complex with the uranyl ion, depressing the quenching effect of solvating water [9, 10]. Thus the pH dependences shown in Fig. 3 may correspond to the distribution curve of certain uranyl-phosphate complexes. The fractions of uranyl-phosphate complexes with change in pH can be calculated in the acidic region by using the reported values of the formation constants, $10^{1.58}$ for $\text{UO}_2(\text{H}_2\text{PO}_4)^+$, $10^{1.58}$ for $\text{UO}_2(\text{H}_3\text{PO}_4)^{2+}$, $10^{1.18}$ for $\text{UO}_2(\text{H}_2\text{PO}_4)_2$ and $10^{2.30}$ for $\text{UO}_2(\text{H}_2\text{PO}_4)_2(\text{H}_3\text{PO}_4)$ [11], and the acidity constants of phosphoric acid, $K_1 = 10^{-2.161}$, $K_2 = 10^{-7.207}$ and $K_3 = 10^{12.325}$ [12]. The calculated results are depicted in Fig. 4. A comparison between the pH dependence of the fraction of $\text{UO}_2(\text{H}_2\text{PO}_4)_2(\text{H}_3\text{PO}_4)$ and that of the fluore-

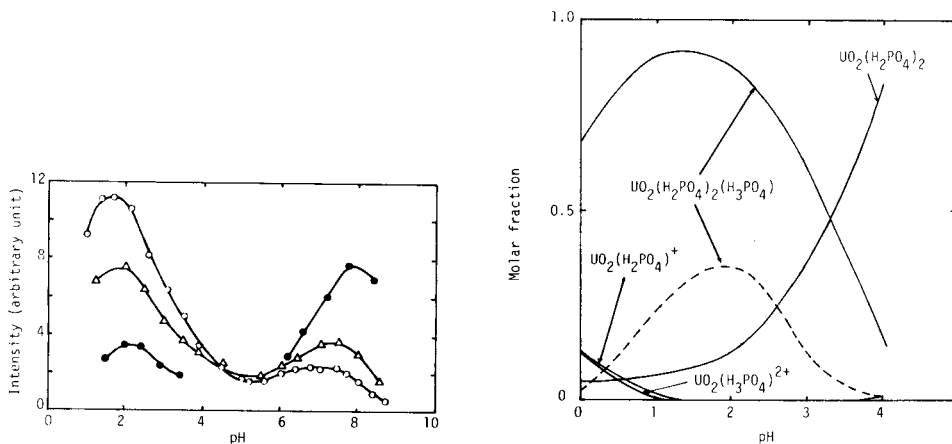


Fig. 3. Variation of fluorescence intensity of uranyl ion (6.3×10^{-5} M) with pH in $\text{H}_3\text{PO}_4/\text{K}_2\text{HPO}_4$ media. Total phosphate concentration: (○) 1.0 M; (△) 0.5 M; (●) 0.1 M. Excitation at 270 nm.

Fig. 4. Molar fraction of uranyl phosphate complexes in the acidic region. Total phosphate concentration: (—) 1.0 M, (---) 0.1 M.

scence intensity suggests a dominant influence of this type of complex. At neutral pH, reliable formation constants allowing the calculation of the distribution curve are not available, but the predominance of the monohydrogenphosphate ion in this region suggests the formation of UO_2HPO_4 [13]. The above evidence indicates the possible utility of hydrogenphosphate solution for enhancing the fluorescence of the uranyl ion.

Preconcentration flow fluorimetry

The fluorescence enhancement caused by phosphate media was examined further by using a phosphate solution as an eluent after uranyl ion had been collected on the TOPO/polyethylene column. Three kinds of eluents, 1 M solutions of H_3PO_4 , KH_2PO_4 and K_2HPO_4 , were examined; the results are shown in Fig. 5. The elution curve with 1 M phosphoric acid gives the largest peak area, but the peak tails badly. The 1 M monohydrogenphosphate eluent gives the highest peak height with the shortest elution time; a 2 M solution gave no improvement on the peak height compared to a 1 M solution, whereas a 0.1 M solution lowered the peak height and increased tailing. For the purpose of quick preconcentration for fluorimetry, a 1 M monohydrogenphosphate media seems to be the best.

The reproducibility of the peaks, when eluted by 1 M monohydrogenphosphate, is shown in Fig. 6. The five peaks measured successively gave only

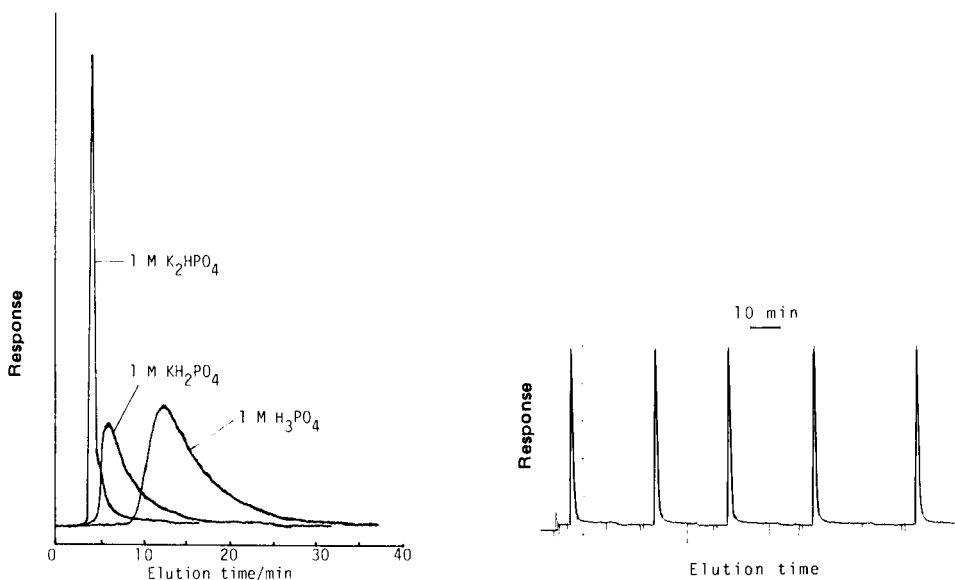


Fig. 5. Elution curves of uranyl ion, for additions of $11 \mu\text{g}$ U(VI). $\lambda_{\text{ex}} = 270 \text{ nm}$, $\lambda_{\text{em}} = 494 \text{ nm}$. Flow rate, 0.75 ml min^{-1} .

Fig. 6. Reproducibility of elution curve of uranyl ion for $8.9 \mu\text{g}$ U(VI). Eluent, 1 M K_2HPO_4 at 0.82 ml min^{-1} . $\lambda_{\text{ex}} = 270 \text{ nm}$; $\lambda_{\text{em}} = 494 \text{ nm}$.

1% relative standard deviation, in spite of slight splits in the peaks because of pulsation of the pump. The recovery of uranyl ion on the TOPO/polyethylene column was found to be $98.9 \pm 1.0\%$ from triple experiments; this was checked by collecting the nitric acid wash after the column had been loaded with 100 ml of 1.3×10^{-7} M uranyl ion, and reloading the wash after the initially extracted uranium had been eluted. The calibration graph for uranyl ion gave a linear equation in the range 0.08–0.8 μg of uranium(VI) in various volumes between 4 and 15 ml: peak height (cm) = $(14.5 \pm 0.3) \text{U(VI)} (\mu\text{g}) + (0.16 \pm 0.13)$, with a correlation coefficient of 0.997. The detection limit defined as twice the noise was 0.04 μg . This method thus promises to serve as a convenient means of determining uranium at the $\mu\text{g l}^{-1}$ level.

Interference of foreign metal ions on the elution peak height was examined, because various transition metals and closed-shell type ions may act as quenchers of uranyl fluorescence [14]. The influence of 25.6 mg of Fe(III), 22.0 mg of Al(III), 12.6 mg of Mn(II), 10.9 mg of Th(IV), 10.2 mg of V(V) or 8.3 mg of Cr(III) coexisting with 8.9 μg of uranium was completely eliminated by washing with less than 50 ml of 1 M sulfuric acid after the loading of the sample on the column.

The flow fluorimetric method proposed here was examined for the determination of traces of uranium in a spinel (MgAl_2O_4). A mean value of $0.70 \pm 0.10 \mu\text{g g}^{-1}$ was obtained from duplicate experiments; this value was in reasonable agreement with reported values of $0.80 \mu\text{g g}^{-1}$ and $0.50 \mu\text{g g}^{-1}$ obtained by neutron activation analysis and by secondary ion mass spectrometry, respectively [15].

REFERENCES

- 1 G. L. Booman and J. E. Rein, in I. M. Kolthoff and P. J. Elving (Eds.), *Treatise on Analytical Chemistry*, Pt. II, Vol. 9. Interscience, New York, 1962, p. 102.
- 2 C. W. Sill and H. E. Peterson, *Anal. Chem.*, 19 (1947) 646.
- 3 M. Moriyasu, Y. Yokoyama and S. Ikeda, *J. Inorg. Nucl. Chem.*, 39 (1977) 2199.
- 4 R. Kaminski, F. J. Purcell and E. Russanage, *Anal. Chem.*, 53 (1981) 1093.
- 5 T. M. Florence and Y. J. Farrar, *Anal. Chem.*, 42 (1970) 271.
- 6 A. F. M. Barton, *Chem. Rev.*, 75 (1975) 731.
- 7 C. Testa, *Anal. Chim. Acta*, 50 (1970) 447.
- 8 A. Danielsson, B. Ronnholm, L-E. Kjellstrom and F. Ingman, *Talanta*, 20 (1973) 18.
- 9 M. Moriyasu, Y. Yokoyama and S. Ikeda, *J. Inorg. Nucl. Chem.*, 39 (1977) 2211.
- 10 M. D. Marcantonatos, *J. Chem. Soc., Faraday Trans. 1*, 75 (1979) 2273.
- 11 C. F. Baes, Jr. and J. M. Schreyer, Report ORNL-1579 (1953).
- 12 J. Bjerrum, G. Schwarzenbach and L. G. Sillen, *Stability Constants*, Vol. 2, The Chemical Society, London, 1958, p. 7.
- 13 A. I. Moskvin, *Zh. Neorg. Khim.*, 12 (1967) 3319.
- 14 M. Moriyasu, Y. Yokoyama and S. Ikeda, *J. Inorg. Nucl. Chem.*, 39 (1977) 2205.
- 15 K. Kudo, H. Anayama, T. Shigematsu, S. Hirai, T. Nozaki, M. Aratani, H. Otsuka, S. Okano, S. Okamoto, T. Nakanishi, M. Sakanoue, N. Suzuki and M. Koyama, *Radioisotopes*, 31 (1980) 490.

SYNTHESIS OF *o,o'*-DIHYDROXYAZO COMPOUNDS AND THEIR APPLICATION TO THE DETERMINATION OF MAGNESIUM AND CALCIUM BY FLOW INJECTION ANALYSIS

H. WADA* and G. NAKAGAWA

Laboratory of Analytical Chemistry, Nagoya Institute of Technology, Showa-ku, Nagoya (Japan)

K. OHSHITA

Laboratory of Chemistry, Daido Institute of Technology, Minami-ku, Nagoya (Japan)

(Received 6th September 1983)

SUMMARY

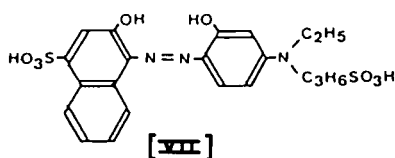
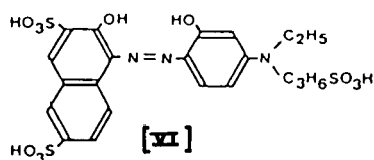
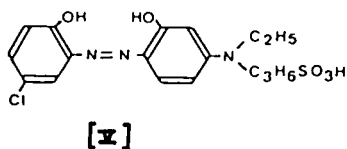
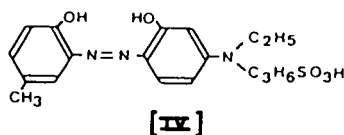
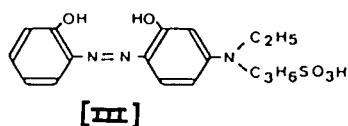
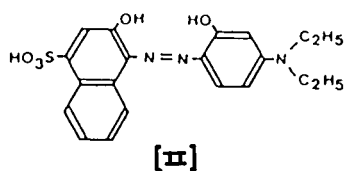
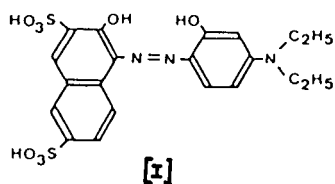
Seven *o,o'*-dihydroxyazo dyes were synthesized and examined as spectrophotometric reagents for magnesium and calcium. These reagents are highly sensitive for magnesium ($\epsilon = 47\,000$) and calcium ($\epsilon = 39\,000\text{ l mol}^{-1}\text{ cm}^{-1}$). Of the reagents synthesized, 2-(2-hydroxy-3,6-disulfo-1-naphthylazo)-5-(*N,N*-diethylamino)phenol was the best because of its ease of preparation and purification, and its stability in alkaline solution. This dye was applied in the determination of magnesium and calcium by flow injection analysis. The total concentration of magnesium (0.1–1.2 mg l⁻¹) and calcium (0.4–4.0 mg l⁻¹) was determined by masking iron(III), aluminium(III), copper(II), zinc(II), manganese(II) and cadmium(II) with 2,3-dimercapto-1-propanol (DMP) and triethanolamine (TEA). Magnesium was determined by masking calcium and the other metal ions with a ligand buffer containing barium(II)–EGTA, DMP and TEA. The amount of calcium was obtained as the difference between the two peak heights. Results for the determination of magnesium and calcium in potable water and serum are presented.

Various organic reagents have been proposed for the spectrophotometric determination of magnesium and calcium. Previously, 1-(2-hydroxy-3-sulfo-5-chloro-1-phenylazo)-2-naphthol-3,6-disulfonic acid was applied to the spectrophotometric determination of magnesium by flow injection analysis [1]. This reagent and its magnesium chelate are very soluble in water, but the sensitivity is not very high for magnesium ($\epsilon = 24\,000\text{ l mol}^{-1}\text{ cm}^{-1}$). The introduction of an alkylamino group at the *p*-position to the azo group should markedly enhance the sensitivity of the chelates, and the introduction of a sulfonic acid group into the alkylamino group should improve their solubility in water [2, 3]. In this study, seven *o,o'*-dihydroxyazo dyes having dialkylamino or alkyl and sulfoalkylamino group were synthesized. This paper describes the properties of the reagents synthesized, and their application in the determination of magnesium and calcium by flow injection analysis. Satisfactory results were obtained for the determination of magnesium and calcium in potable water and serum.

EXPERIMENTAL

Synthesis of dyes

Reagents [I]—[VII] were synthesized.



- [I] 2-(2-Hydroxy-3,6-disulfo-1-naphthylazo)-5-(*N,N*-diethylamino)phenol
 [II] 2-(2-Hydroxy-4-sulfo-1-naphthylazo)-5-(*N,N*-diethylamino)phenol
 [III] 2-(2-Hydroxy-1-phenylazo)-5-[*N*-ethyl-*N*-(3-sulfopropyl)amino]phenol
 [IV] 2-(2-Hydroxy-5-methyl-1-phenylazo)-5-[*N*-ethyl-*N*-(3-sulfopropyl)amino]phenol
 [V] 2-(2-Hydroxy-5-chloro-1-phenylazo)-5-[*N*-ethyl-*N*-(3-sulfopropyl)amino]phenol
 [VI] 2-(2-Hydroxy-3,6-disulfo-1-naphthylazo)-5-[*N*-ethyl-*N*-(3-sulfopropyl)amino]phenol
 [VII] 2-(2-Hydroxy-4-sulfo-1-naphthylazo)-5-[*N*-ethyl-*N*-(3-sulfopropyl)amino]phenol

[I] and [II]. Disodium 1-nitroso-2-naphthol-3,6-disulfonate (nitroso R salt) was reduced with tin(II) chloride as described previously [4]. The amino compound or sodium 1-amino-2-naphthol-4-sulfonate was diazotized with sodium nitrite solution in the usual way. The diazo compound obtained by salting out was coupled with *N,N*-diethyl-*m*-aminophenol in 2 M sodium hydroxide at 0°C. The solution was allowed to stand for 1 h and then acidified with dilute hydrochloric acid. The crude dye was dissolved in a small amount of aqueous 20% ethanol and concentrated hydrochloric acid was added slowly. After one day, the precipitate was obtained. This recrystallization was repeated several times.

Elemental analysis gave the following results. [I]: calcd. for $C_{20}H_{21}N_3O_8S_2 \cdot 3H_2O$, 43.7% C, 4.9% H, 7.7% N; found 43.5% C, 4.4% H, 7.6% N. [II]: calcd. for $C_{20}H_{21}N_3O_5S \cdot H_2O$, 55.4% C, 5.4% H, 9.7% N; found 55.2% C, 5.4% H, 9.5% N.

[III], [IV] and [V]. 2-Aminophenol, 2-amino-4-methylphenol or 2-amino-4-chlorophenol was dissolved in 4 M hydrochloric acid and diazotized with sodium nitrite solution at 0°C in the usual way. The diazo compound was coupled with *N*-ethyl-*N*-(3-sulfopropyl)-*m*-aminophenol, which was synthesized as previously [3], in 2 M sodium hydroxide at 0°C. The solution was allowed to stand for 1 h and then acidified with dilute hydrochloric acid. To this solution, ethanol was added to precipitate the crude dye, which was recrystallized from ethanol containing a little water (ca. 5%). This recrystallization was repeated several times.

Elemental analysis gave the following results. [III]: calcd. for $C_{17}H_{20}N_3O_5SNa \cdot 2H_2O$, 46.7% C, 5.5% H, 9.6% N; found 46.1% C, 5.4% H, 9.8% N. [IV]: calcd. for $C_{18}H_{22}N_3O_5SNa \cdot H_2O$, 49.9% C, 5.6% H, 9.7% N; found 49.5% C, 5.6% H, 9.7% N. [V]: calcd. for $C_{17}H_{19}N_3O_5SNa \cdot 3H_2O$, 41.7% C, 5.1% H, 8.6% N; found 41.9% C, 5.1% H, 9.0% N.

[VI] and [VII]. The diazo compound obtained from 1-amino-2-naphthol-3,6-disulfonic acid or 1-amino-2-naphthol-4-sulfonic acid was coupled with *N*-ethyl-*N*-(3-sulfopropyl)-*m*-aminophenol in 2 M sodium hydroxide at 0°C. The solution was allowed to stand for 1 h and then acidified with hydrochloric acid. Addition of ethanol to this solution precipitated the crude dye. These dyes were highly water-soluble and were recrystallized several times from a propanol-ethyl acetate-water (5 + 5 + 4) solution.

Elemental analysis gave the following results. [VI]: calcd. for $C_{21}H_{20}N_3O_{11}S_3Na_3 \cdot 4H_2O$, 34.6% C, 3.9% H, 5.8% N; found 34.7% C, 3.8% H, 5.5% N. [VII]: calcd. for $C_{21}H_{21}N_3O_8S_2Na_2 \cdot 4H_2O$, 40.3% C, 4.6% H, 6.7% N; found 40.2% C, 4.1% H, 6.7% N.

Reagents

Each azo compound was dissolved in water.

The standard solutions of magnesium and calcium were prepared from magnesium chloride and calcium carbonate; these solutions were standardized by EDTA titration. Other metal ion solutions were prepared by dissolving their nitrate, sulfate or chloride salts. All reagents used were of analytical-reagent grade.

2,3-Dimercapto-1-propanol (DMP) solution (0.1 M) was prepared by adding a deaerated solution containing twice the required molar quantity of sodium hydroxide to the weighed amount of DMP and diluting with the necessary amount of deaerated water. This solution was prepared daily.

The buffers used were acetic acid-sodium acetate (2 M, pH 3-7), ammonia-ammonium chloride (2 M, pH 8-11). All water used was redistilled from a hard-glass vessel.

Apparatus

A Union Giken Model SM-401 spectrophotometer and a Hitachi-Horiba Model F-7 pH meter were used.

A diagram of the flow-injection manifold is shown in Fig.1. The teflon tubing used was of 0.5 mm i.d. except for the back-pressure coil which was of 0.25 mm i.d. (50-cm long). A chromogenic reagent solution and a buffer solution (B_1 or B_2) containing masking reagents were delivered each at 0.81 ml min^{-1} with a peristaltic pump (Gilson HP 4). The sample was injected into the buffer stream via a rotary valve (Oyo-Bunko Kiki) to which a loop of appropriate volume was attached. Sample and the reagent solutions were mixed in the 300-cm coil. A flow cell (Oyo-Bunko Kiki; 10-mm light path, $20\text{-}\mu\text{l}$ volume) situated in a spectrophotometer (Oyo-Bunko Kiki; Uvilog-7), and a recorder (Rika Denki R-31) were used for recording the absorbance.

Recommended procedure for the determination of magnesium and calcium

A portion of the sample solution containing $0\text{--}1.2 \text{ mg l}^{-1}$ magnesium and $0\text{--}4 \text{ mg l}^{-1}$ calcium was injected into the stream of B_1 buffer which contains 10^{-2} M DMP and 10^{-2} M triethanolamine (TEA). The peak height, corresponding to the sum of the concentrations of magnesium and calcium, was measured. Then, valve V was switched to B_2 buffer containing 10^{-2} M DMP, 10^{-2} M TEA, barium nitrate ($1.04 \times 10^{-3} \text{ M}$) and ethyleneglycol-bis(2-aminoethylether)tetraacetic acid (EGTA; $1.00 \times 10^{-3} \text{ M}$), and another portion of the sample solution was injected into this stream. This peak height corresponded to the concentration of magnesium. By subtracting this peak height from that for the sum of magnesium and calcium, the concentration of calcium was obtained.

RESULTS AND DISCUSSION

Properties of the reagents and their metal chelates

The absorption maxima of the azo dye solutions are given in Table 1; the absorption spectra of I and VI, II and VII or III, and IV and V were almost

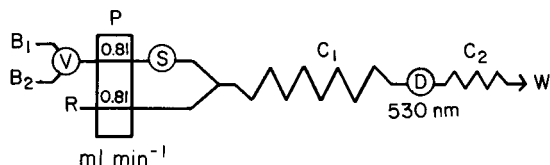


Fig. 1. Flow diagram: P, peristaltic pump with indication of flow rate (ml min^{-1}); S, sample injector with loop ($40 \mu\text{l}$); V, three-way valve for buffer solution (B_1 and B_2); C_1 , mixing coil (0.5 mm i.d., 300 cm long); C_2 , back-pressure coil (0.25 mm i.d., 50 cm long); D, spectrophotometer equipped with flow cell (volume $20 \mu\text{l}$, light path 10 mm); R, color-forming reagent ($5 \times 10^{-5} \text{ M}$); B_1 , ammonia-ammonium chloride buffer (0.1 M, pH 10.5) containing DMP (10^{-2} M) and TEA (10^{-2} M); B_2 , ammonia-ammonium chloride buffer (0.1 M, pH 10.5) containing DMP (10^{-2} M), TEA (10^{-2} M), Ba(II) ($1.04 \times 10^{-3} \text{ M}$) and EGTA ($1.00 \times 10^{-3} \text{ M}$).

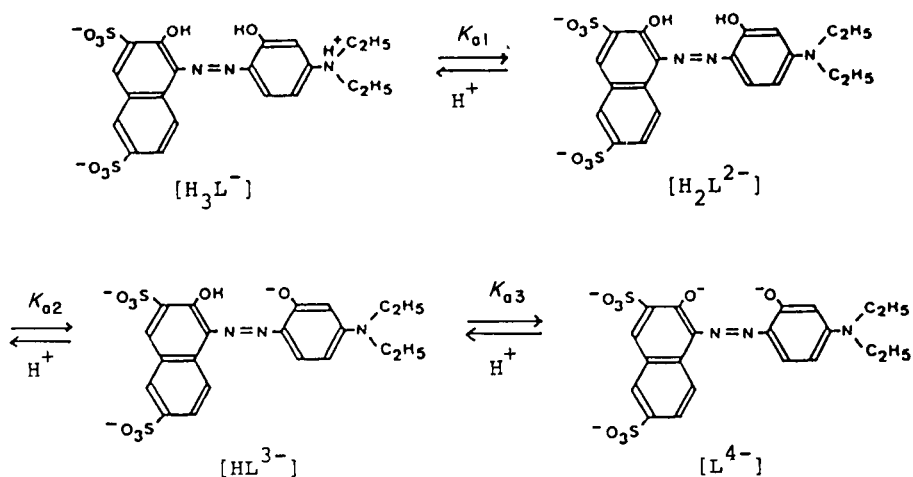
TABLE 1

Absorption maxima of the azo compounds and their magnesium and calcium chelates

Compound	Absorption maxima (nm)					
	H ₃ L	H ₂ L	HL	L	Mg chelate	Ca chelate
I	500	502	622–628	525	560	550
II	516	507	575, 608	512	563	550
III	504	481	525	497	496	497
IV	508	484	534	505	503	508
V	501	481	532	505	505	508
VI	503	516	640–644	540	560	551
VII	523	510	610	510	562	550

the same. Reagents I, VI and VII are highly soluble in water, whereas II, III, IV and V are less soluble. The absorption spectra of I at different pH values are shown in Fig. 2.

The dissociation equilibria of reagent I, taken as an example, can be written as



The acidity constants of these reagents were determined by Hildebrand and Reilly's method [5]; for the determination of K_{a1} and K_{a2} , the hydrogen activities were measured with a pH meter, while for K_{a3} the concentrations of hydrogen ion were calculated from the concentration of sodium hydroxide added. The values are given in Table 2.

All the reagents synthesized react with magnesium and calcium to give orange (III, IV and V) or purple (I, II, VI and VII) chelates above pH 8. The absorption spectra of the magnesium and calcium chelates with reagent I are shown in Fig. 3. The absorption maxima of the magnesium and calcium chelates are listed in Table 1. The molar absorptivities of the magnesium and

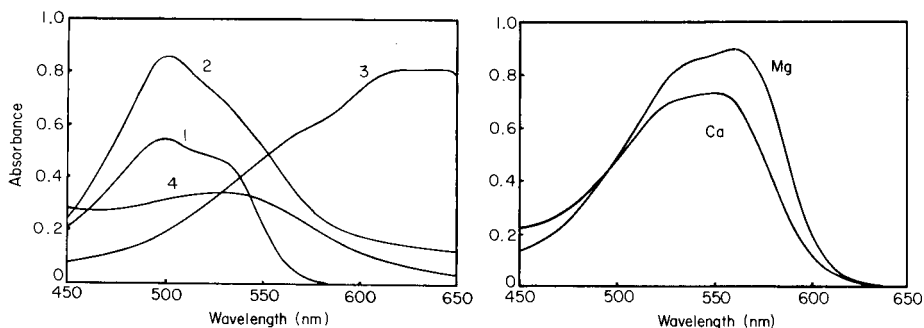


Fig. 2. Absorption spectra of reagent I (2×10^{-5} M) at different pH values: (1) 1; (2) 6; (3) 11; (4) 14. ($\mu = 0.1$, 25°C).

Fig. 3. Absorption spectra of the chelates of magnesium (2×10^{-3} M) and calcium (2×10^{-3} M) with reagent I (2×10^{-5} M) at pH 10.5.

calcium chelates of these reagents were almost the same: 4.7×10^4 l mol $^{-1}$ cm $^{-1}$ for magnesium and 3.9×10^4 l mol $^{-1}$ cm $^{-1}$ for calcium. These are about twice the values for the chelates reported earlier [1]. The magnesium or calcium chelates of these reagents are soluble in water, but gradually decompose in alkaline solution (pH 10); the chelates of reagent II are the least stable. Therefore, the spectra of the reagents and their chelates were measured immediately after the solutions had been prepared.

Because of its ease of preparation and purification, and its high solubility and relative stability in alkaline solutions, reagent I is the best for the spectrophotometric determination of magnesium and calcium.

Application in flow-injection analysis

Detecting wavelength. The absorption maxima of the magnesium and calcium chelates of reagent I appear at 560 and 550 nm, respectively, and that

TABLE 2

Acidity constants^a of the azo compounds at $\mu = 0.1$ and 25°C

Compound	$\text{p}K_{a1}$	$\text{p}K_{a2}$	$\text{p}K_{a3}$
I	4.35	8.25	13.2
II	3.65	8.50	12.6
III	2.90	8.65	12.8
IV	3.05	8.75	12.7
V	2.80	8.05	12.6
VI	3.50	7.85	13.3
VII	2.60	8.30	12.6

^a $K_{a1} = (\alpha_{\text{H}^+}) [\text{H}_2\text{L}]/[\text{H}_3\text{L}]$, $K_{a2} = (\alpha_{\text{H}^+}) [\text{HL}]/[\text{H}_2\text{L}]$, $K_{a3} = [\text{H}^+] [\text{L}]/[\text{HL}]$ (charges are omitted).

of the reagent itself at 622–628 nm in the pH range 10–11.5 (Figs. 2 and 3). The difference between the absorbances of the reagent and the magnesium and calcium chelates is large around 530 nm, which was therefore preferred for measurements.

Optimal reaction conditions. As seen in Fig. 4, the peak height for magnesium was constant and largest in the pH range 10.3–10.8 (ammonia–ammonium chloride) whereas the peak height for calcium kept increasing. Above pH 11, of course, magnesium is hydrolyzed, so a pH value of 10.5 was chosen. Increasing the concentration of the color-forming reagent will provide higher peaks and increase the determinable amounts of magnesium and calcium, but this will also cause larger reagent blanks. Therefore, a 5×10^{-5} M solution was used for the determination of 0.1–1.2 mg l⁻¹ magnesium and 0.4–4 mg l⁻¹ calcium.

The effect of mixing coil length on the peak height for magnesium was examined for the range 1–5 m. The peak height decreased with increasing coil length, but the reproducibility was poor with a coil less than 2 m, and a 3 m coil is recommended.

The same flow rates were used for the buffer and reagent channels. When the two flow rates were varied over the range 0.5–1.5 ml min⁻¹, the peak heights were similar but reproducibility deteriorated at flow rates higher than 1 ml min⁻¹. For a reasonable sampling rate, flow rates of 0.80–0.85 ml min⁻¹ are recommended. The peak heights increased with increasing sample volumes; for the apparatus employed, 40 μ l was most suitable.

Calibration graphs. As shown in Fig. 5 (A, B), calibration graphs were linear for 0.1–1.2 mg l⁻¹ of magnesium and 0.4–4.0 mg l⁻¹ of calcium.

Effects of other ions. Iron(III), aluminum(III), copper(II), zinc(II), cadmium(II) and manganese(II) react with the reagent and would interfere. Various masking reagents such as TEA, triethylenetetramine, diethylenetriamine, potassium cyanide, sulfosalicylic acid, DMP and *N*-(dithiocarboxy)-

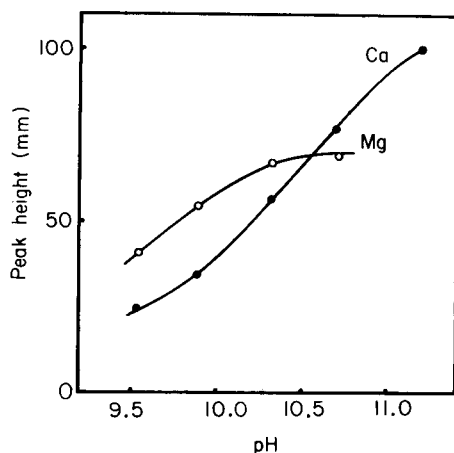


Fig. 4. Effect of pH, Ca: 2.0 mg l⁻¹, Mg: 0.48 mg l⁻¹.

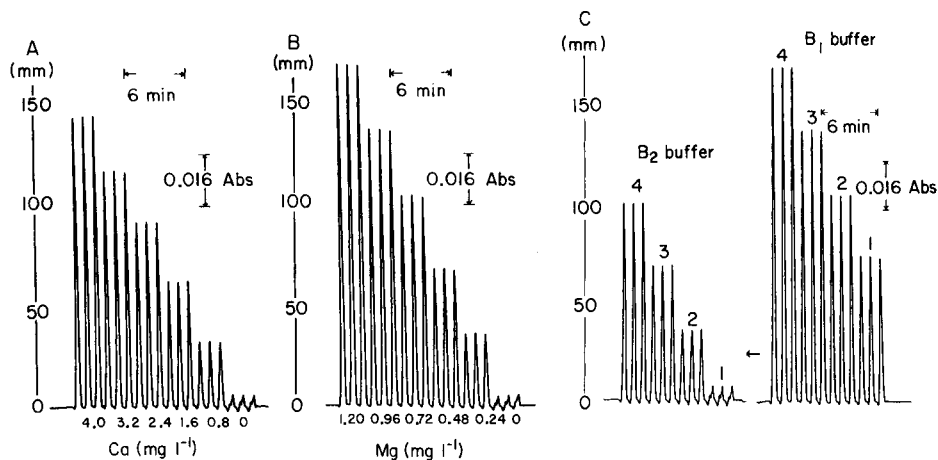


Fig. 5. (A) Calibration output for magnesium. (B) Calibration output for calcium. (C) Determination of calcium and magnesium in synthetic samples in buffers B₁ and B₂: (1) 2.0 mg l⁻¹ Ca only; (2) 2.0 mg l⁻¹ Ca + 0.24 mg l⁻¹ Mg; (3) 2.0 mg l⁻¹ Ca + 0.48 mg l⁻¹ Mg; (4) 2.0 mg l⁻¹ Ca + 0.72 mg l⁻¹ Mg.

sarcosine were examined. The interferences from these ions could be eliminated by masking with DMP (10⁻² M) and TEA (10⁻² M). The tolerable amounts of these metals with this masking solution are listed in Table 3. Phosphate, carbonate or sulfate did not interfere up to 10⁻³ M.

Determination of magnesium in the presence of calcium

The calcium—EGTA complex ($\log K_{\text{CaY}} = 11.0$) is much more stable than that of magnesium ($\log K_{\text{MgY}} = 5.2$), and magnesium chelate of reagent I ($\log K_{\text{MgL}} = 7.2$) is more stable than that of calcium ($\log K_{\text{CaL}} = 6.5$). Therefore, calcium may be masked with EGTA. In fact, calcium was completely masked by injecting samples into a 0.1 M ammonia—ammonium chloride buffer containing EGTA (10⁻³ M), but at the same time the peak height of magnesium diminished. However, when a ligand buffer containing EGTA and barium in 4% excess was used, calcium was completely masked without any significant decrease in the peak height for magnesium.

The total peak heights for magnesium and calcium in various synthetic

TABLE 3

Tolerable amounts of diverse metal ions

Ion	Maximum tolerated (mg l ⁻¹)	Ion	Maximum tolerated (mg l ⁻¹)
Fe(III)	1.5	Zn(II)	70
Al(III)	2.5	Cd(II)	110
Cu(II)	30	Mn(II)	1.0

TABLE 4

Determination of Mg and Ca in potable waters and in a serum (all results are given as mg l⁻¹)

	F.i.a. ^a		A.a.s.		EDTA titration	
	Mg	Ca	Mg	Ca	Mg	Ca
Tap water 1	0.75	5.62	0.70	5.66	0.7	5.9
2	0.66	5.24	0.67	5.21	0.7	5.3
3	0.93	5.25	0.87	5.36	0.9	5.6
4	0.75	5.62	0.70	5.51	0.7	5.6
Serum ^b	19	92	—	—	—	—

^aProposed method. ^bCertified values are 21 ± 3 and 91 ± 5, respectively.

samples (constant calcium concentration and varying magnesium concentrations) were measured by using the 0.1 M ammonia—ammonium chloride buffer containing DMP (10⁻² M) and TEA (10⁻² M). The peak heights for magnesium in these samples were then measured when the 0.1 M ammonia—ammonium chloride buffer contained DMP (10⁻² M), TEA (10⁻² M), Ba(II) (1.04 × 10⁻³ M) and EGTA (1.00 × 10⁻³ M), i.e., the B₂ buffer. Good results were obtained (Fig. 5C).

Application to potable water and serum

This method was applied to the determination of magnesium and calcium in four tap waters and a standard serum (ORTHO Normal Control Serum). Water samples were diluted 2–4 times, and 40 μl portions were injected. In the case of serum, the standard freeze-dried serum was dissolved in 5 ml of water and then the solution was diluted fifty times. Again, 40-μl portions were injected. The mean values of five injections are shown in Table 4.

The results for the water samples were compared with those obtained by atomic absorption spectrometry (a.a.s.) and by EDTA titration. In the case of a.a.s., lanthanum oxide was added to the samples. The results by the proposed method are in good agreement with those obtained by the other methods. For serum, the results agreed well with the certified values. Clearly, this method, which is highly sensitive and selective, can be applied to the determination of trace amounts of magnesium and calcium in various samples.

The authors thank Mr. T. Nishiyama for the atomic absorption spectrometric measurements and acknowledge a Grant-in-Aid for Scientific Research (No. 58540356) from the Ministry of Education, Science and Culture, Japan.

REFERENCES

- 1 H. Wada, A. Yuchi and G. Nakagawa, *Anal. Chim. Acta*, 149 (1983) 291.
- 2 H. Wada, T. Ishizuki and G. Nakagawa, *Anal. Chim. Acta*, 135 (1982) 333.
- 3 K. Ohshita, H. Wada and G. Nakagawa, *Anal. Chim. Acta*, 149 (1983) 269.
- 4 H. Wada and G. Nakagawa, *Anal. Chim. Acta*, 121 (1980) 265.
- 5 G. P. Hildebrand and C. N. Reilley, *Anal. Chem.*, 29 (1957) 258.

SIMULTANEOUS SPECTROPHOTOMETRIC DETERMINATION OF HUMIC ACID AND IRON IN WATER

P. D. CARPENTER and J. D. SMITH*

Marine Chemistry Laboratory, School of Chemistry, University of Melbourne, Parkville, 3052 (Australia)

(Received 15th November 1983)

SUMMARY

A simple and rapid method for the determination of humic acid and iron in solution is described. Two absorbance measurements are required, one on an untreated sample aliquot, and the other on an aliquot treated to enhance iron absorptivity. The method requires sample volumes of less than 15 ml and is sensitive enough for direct application to most natural waters. Limits of detection for each component vary with concentration of the other, but 0.01 mg l⁻¹ for humic acid and 0.04 μM for iron can be achieved. For six natural waters, determinations based on independent calibration curves for each component gave results 6–40% higher for iron, and 6–29% higher for humic acid, than results obtained by the proposed method. The interference of fulvic acid and the use of different humic acid standards are examined.

Humic substances constitute the bulk of organic matter in natural fresh waters [1]. They affect the surface properties of suspended particulate matter in lakes [2] and estuaries [3], and they form complexes with trace metals [4]. Iron is stabilized in solution by humic acid [5], and acts as a scavenger for trace metals and other components [6, 7]. These properties make humic acid and iron important in the study of geochemical processes. The average total concentration of iron in river water is 360 μM [8], while the dissolved concentration depends on the delineation between dissolved and particulate fractions [9]. Humic acid is found in fresh waters at concentrations up to 100 mg l⁻¹ with an average of 10 mg l⁻¹ [1].

Humic acid has been determined by oxidative [10], chemiluminescent [11], electrochemical [12], and fluorescent [13] procedures, but the majority are spectrophotometric [14–17]. The similarity in u.v.-visible absorption spectra of humic acid, colloidal iron hydroxide, and iron-humic acid solutions [18] (Fig. 1) complicates spectrophotometric procedures. This problem has been resolved by separation of the humic acid by precipitation in acidic solution [14, 15, 19]; or by simultaneous determination of iron and humic acid using measurement of solution absorbance at multiple wavelengths [17]. It was found here that iron coprecipitates with humic acid in acidified solutions, and redissolves over a period of hours (Fig. 2). This lengthens procedures based on separation. Simultaneous determination

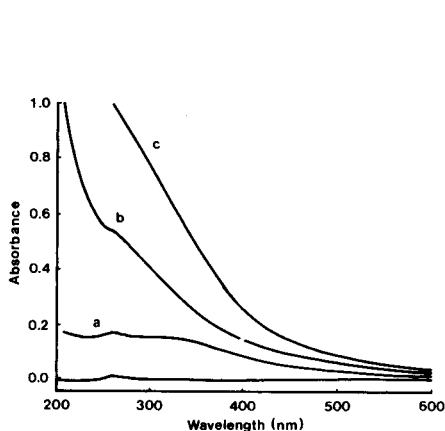


Fig. 1. Absorption spectra (light path 1 cm) of: (a) 140 μM hydrated iron(III) oxide (colloidal) at pH 8.3; (b) 18 mg l^{-1} humic acid at pH 8.1; (c) 18 mg l^{-1} humic acid and 140 μM iron(III) at pH 8.0.

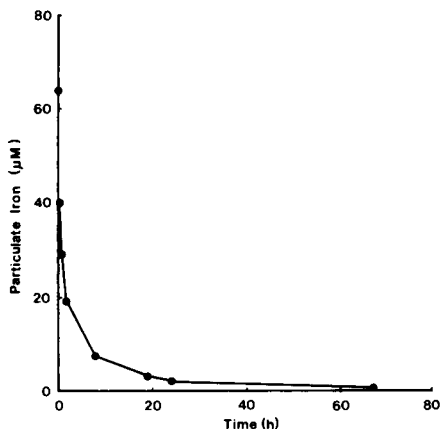


Fig. 2. Rate of redissolution of iron coprecipitated with humic acid at pH 1.0 and stored exposed to light and air at 20°C. Initial solution contained 9.0 mg l^{-1} humic acid and 64 μM iron at pH 8.0.

previously required absorbance measurements at six wavelengths [17] and had a detection limit for iron which was inadequate for most natural waters.

Spectrophotometric procedures are among the most sensitive for the determination of iron. In this work, a procedure for iron determination based on ferrozine [20, 21] was modified to allow for the presence of humic acid, and was incorporated in a method for the simultaneous determination of iron and humic acid. The method requires absorbance measurements on two solutions at one wavelength each, and has sensitivity suitable for most natural waters even when only 15 ml of sample is used.

THEORY

For simultaneous spectrophotometric determination of n components in solution, the absorbance is measured at n different wavelengths, ideally corresponding to the absorption maxima of the components. At each wavelength Beer's law must be obeyed by all absorbing components, and the absorbance must be equal to the sum of the component absorbances [22]. The absorbance of each component may be maximized by altering the pH, or by the addition of complexing, reducing, or oxidizing reagents. These optimum conditions can be employed when separate sample aliquots are taken for each component. The set of equations applying to this situation is

$$A_j = l_j/f_j \sum_{i=1}^n C^i \epsilon_j^i \quad (\text{for } j = 1 \dots n) \quad (1)$$

where, at the j th optimum condition, A_j is the measured absorbance, l_j is the light path length of the cuvette used, f_j is the ratio of final volume to sample aliquot taken (the dilution factor), C^i is the concentration of the i th component in the undiluted sample solution, and ϵ_j^i is its absorptivity.

In the recommended procedure, absorbance of the undiluted sample is measured at 365 nm, where both humic acid and iron absorb. Equation 1 becomes

$$A_{365} = l_{365}(C^{\text{HA}}\epsilon_{365}^{\text{HA}} + C^{\text{Fe}}\epsilon_{365}^{\text{Fe}}) \quad (2)$$

where $\epsilon_{365}^{\text{Fe}}$ is the molar absorptivity of iron stabilized in solution by humic acid, and $\epsilon_{365}^{\text{HA}}$ is the absorptivity of humic acid.

An aliquot of the sample has reagents added to form the iron(II)-ferrozine complex and absorbance is measured at 562 nm where the complex, humic acid and the added reagents absorb. Equation 1 then becomes

$$A_{562} = l_{562}/f_{562}(C^{\text{HA}}\epsilon_{562}^{\text{HA}} + C^{\text{Fe}}\epsilon_{562}^{\text{FeFz}}) \quad (3)$$

where A_{562} is corrected for reagent blank absorbance, and $\epsilon_{562}^{\text{FeFz}}$ is the molar absorptivity of the iron-ferrozine complex. The iron and humic acid concentrations in the sample are derived by solving Eqns. 2 and 3 simultaneously to give

$$C^{\text{Fe}} = [(A_{562}f_{562}/l_{562}) - (RA_{365}/l_{365})]/(\epsilon_{562}^{\text{FeFz}} - R\epsilon_{365}^{\text{Fe}}) \quad (4)$$

where $R = \epsilon_{562}^{\text{HA}}/\epsilon_{365}^{\text{HA}}$, and

$$C^{\text{HA}} = (A_{365} - \epsilon_{365}^{\text{Fe}}C^{\text{Fe}}l_{365})/(\epsilon_{365}^{\text{HA}}l_{365}) \quad (5)$$

EXPERIMENTAL

Apparatus

Absorbances at single wavelengths were measured with a Pye-Unicam SP500 spectrophotometer and 2-cm cuvettes. Time-dependent absorbance measurements and spectra were obtained by using a Varian-Techtron model 635D spectrophotometer. Wavelengths were calibrated by using a didymium filter. Measurements of pH were made with an Orion Research model 701A/digital Ionalyser and a combination pH electrode (91-02-00). For titrations a Metrohm E636 Titroprocessor was used with E635 Dosimat and EA120 combination pH electrode. The Ionalyser and Titroprocessor were calibrated with Merck Titrosol buffer solutions. Microlitre volumes were transferred with Gilson model P200 and P1000 Pipetman variable pipettes. Glassware was soaked for 24 h in 10% (w/v) nitric acid solution, then 10% (w/v) hydrochloric acid solution and rinsed with distilled water. Between uses, glassware was stored in the hydrochloric acid solution. Polycarbonate membrane filters of 0.2- μm pore size (Nuclepore) were washed in 0.5 M hydrochloric acid for 24 h, rinsed, and stored in water.

Chemicals and solutions

Water was distilled, deionized in a mixed bed resin, redistilled in an all-glass still, and stored in polyethylene. Humic acid was extracted from sediment (from the Yarra River, Victoria, Australia) by repeated dissolution in sodium hydroxide and precipitation with hydrochloric acid [23], dialysed (using Visking No. 30 tubing preboiled in water) against 3.5% (w/v) sodium chloride solution for three weeks and then against distilled water until chloride-free, and freeze-dried. Concentrations of humic acid are given on an ash and moisture-free basis. Goethite (α -FeOOH) and haematite (α -Fe₂O₃) were prepared [24, 25], purified [25], and stored as aqueous suspensions. Ascorbic acid was laboratory-reagent grade. All other chemicals were of analytical-reagent grade.

For the humic acid standard solution (90 mg l⁻¹), humic acid (18 mg) was suspended in 70 ml of water, dissolved by titration with 0.01 M sodium hydroxide to pH 8.0 under a stream of nitrogen, and diluted to 200 ml with water. Acidic reductant solution (0.5 M ascorbic acid/2.5 M hydrochloric acid) was prepared immediately before use. Iron colour reagent (2.0 M Tris/0.156% ferrozine) was prepared from 2-amino-2-(hydroxymethyl)propane-1,3-diol (Tris) and 3-(2-pyridyl)-5,6-bis(4-phenylsulfonic acid)-1,2,4-triazine, monosodium, monohydrate (ferrozine; Hach Chemical Co., U.S.A.). The iron standard solution was 10 mg l⁻¹ iron(III) in 0.05 M hydrochloric acid.

Recommended procedure

Filter about 15 ml of the water sample. Measure the absorbance of the solution at 365 nm against distilled water as reference (A_{365}). Transfer an aliquot of the filtered water (≥ 8 ml, containing up to 36 nmol of iron) to a 10-ml volumetric flask, add 400 μ l of acidic reductant solution, mix and leave for 30 min. Add 800 μ l of the ferrozine reagent, mix and dilute to volume with water. After at least 30 min, measure the absorbance at 562 nm against distilled water and correct for reagent blank (A_{562}).

Prepare a series of solutions (≥ 8 ml) containing 4–36 nmol of iron, by dilution of the iron standard solution with water and treat these solutions as described above for the aliquot of filtered water. Calculate the molar absorptivity of the iron–ferrozine complex ($\epsilon_{562}^{\text{Fe}}$) from the slope of the calibration graph. Prepare a second series of solutions containing 1.0–9.0 mg l⁻¹ humic acid by dilution of the humic acid standard solution with water. Measure the absorbance of these solutions at 365 and 562 nm, and calculate the absorptivity of the humic acid at each wavelength ($\epsilon_{365}^{\text{HA}}$, $\epsilon_{562}^{\text{HA}}$) as described above, and hence the ratio (R). Prepare a third series of solutions containing iron in the expected concentration range, and sufficient humic acid to maintain the highest iron concentration in solution (in this work, 8–80 μ M iron with 9.0 mg l⁻¹ humic acid). To prepare these solutions, pre-determine the volume of 1 M sodium hydroxide required to neutralize the acid present in an aliquot of iron standard solution. To a 250-ml volu-

metric flask half-filled with water, add the required aliquot of humic acid standard solution, the aliquot of 1 M sodium hydroxide and the corresponding aliquot of iron standard solution. Check that the pH is between 7 and 8, adjusting if necessary with dilute hydrochloric acid or sodium hydroxide, and dilute to volume with water. Measure the absorbance at 365 nm against distilled water as reference. Plot a calibration graph of absorbance versus iron concentration and calculate the effective molar absorptivity of iron stabilized in solution by humic acid ($\epsilon_{365}^{\text{Fe}}$).

Calculate the concentrations of humic acid and iron by substitution of the absorbance data and calculated absorptivities into Eqns. 4 and 5.

The absorptivities and the ratio (R) are determined, and Beer's law confirmed at each wavelength when the method is first used. For subsequent determinations only a blank, a standard iron—ferrozine solution, and a standard humic acid solution need be prepared.

RESULTS AND DISCUSSION

Iron—ferrozine complex

Iron present in sample solutions was dissolved by addition of hydrochloric acid to pH 1.0 [21, 26], and reduced by a 10 000-fold molar excess of ascorbic acid. These reagents were combined to minimize sample dilution. Reduction of iron(III) by ascorbic acid is almost instantaneous in the pH range 3–6 [27]. At pH 1.0, iron, whether present as a colloidal hydrated oxide or associated with humic acid, was found to be completely dissolved and reduced within 30 min. Humic acid precipitated at this stage but did not interfere. Under the same conditions, less than 4% of iron present in aqueous suspensions of haematite or goethite was dissolved.

The pH of the solution was raised by addition of Tris, which formed a pH 7.6 buffer with the hydrochloric and ascorbic acids. Complex formation was complete in the pH range 2.0–8.6, which is similar to ranges found with other reagents [21, 28]. It was found that humic acid redissolved only partially at the lower pH (3.5–5.5) used previously for complex formation [21, 27, 28], but completely at pH 7.6.

A ferrozine/iron mole ratio of at least 65 was required for complete complex formation when humic acid was present, compared with 20 when humic acid was absent (Fig. 3), indicating the degree to which humic acid hinders formation of the complex. Ferrozine was added as a combined reagent with Tris at a concentration which gave a minimum ferrozine/iron mole ratio of 68. The complex was completely formed within 30 min, and was stable for at least 11 days.

Beer's law was obeyed up to the highest iron concentration prepared (7.2 μM) at the absorption maximum of the complex (562 nm), with a molar absorptivity of $2.72 \times 10^4 \text{ dm}^3 \text{ mol}^{-1} \text{ cm}^{-1}$ (Table 1). The absorptivity is within 5% of values reported previously [21, 28]. The linear range was extended at least twofold when the ferrozine concentration was increased

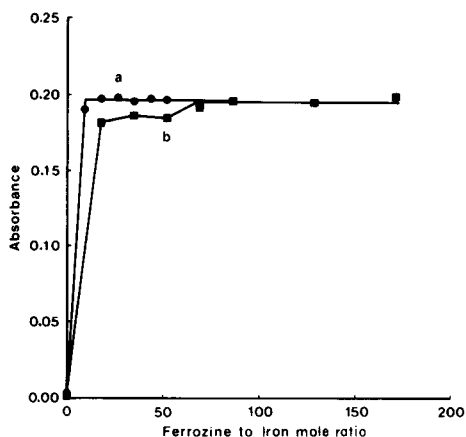


Fig. 3. Effect of humic acid on the ratio of ferrozine to iron required for complete colour development. Solutions contained $3.58 \mu\text{M}$ iron and the recommended concentrations of other reagents. Humic acid (mg l^{-1}): (a) 0.0; (b) 9.0. Absorbances were measured at 562 nm against blanks containing no iron.

fourfold. The presence of up to 9.0 mg l^{-1} humic acid did not significantly change the molar absorptivity of the complex (Fig. 4A).

Measurements of humic acid and iron

The smooth absorption spectrum of humic acid over the u.v.-visible wavelength range (Fig. 1) has resulted in different wavelengths being used for humic acid measurements [14–17]. Humic acid obeyed Beer's law at 562 nm up to the highest concentration prepared (9.0 mg l^{-1}) (Table 1). The presence of up to $3.58 \mu\text{M}$ of iron—ferrozine complex and associated reagents did not significantly change the absorptivity of the humic acid

TABLE 1

Linear least-squares data for the calibration graphs used in the recommended procedure (Light path 2.0 cm)

Species measured	No. of points	Intercept ^a	Slope ^a	<i>r</i>
<i>At 562 nm</i>				
Iron—Fz complex	5	0.010 ± 0.0006	0.0543 ± 0.0003	0.99997
Humic acid	4	0.010 ± 0.0006	0.00546 ± 0.00001	0.99959
<i>At 365 nm</i>				
Iron with humic acid			0.00289 ± 0.00007^b	
Humic acid with iron			0.0250 ± 0.0003^c	

^aWith standard deviation. ^bMean of three lines, each of four points. ^cMean of four lines, each of three points.

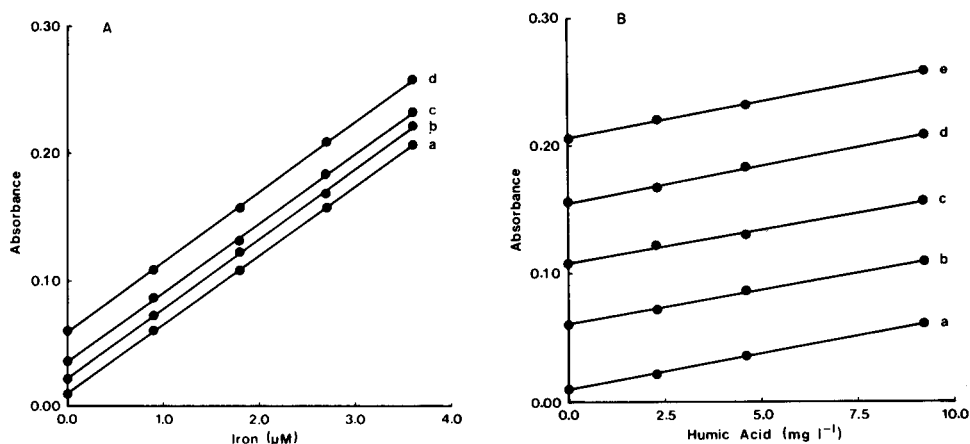


Fig. 4. A, Effect of different amounts of humic acid on the absorptivity of the iron—ferrozine complex at 562 nm; humic acid concentrations (mg l^{-1}) are (a) 0.0, (b) 2.3, (c) 4.6, (d) 9.2. B, Effect of different amounts of iron—ferrozine complex on the absorptivity of humic acid at 562 nm; iron concentrations (μM) are (a) 0.00, (b) 0.90, (c) 1.79, (d) 2.69, (e) 3.58. Absorbances were measured against distilled water.

(Fig. 4B). Humic acid obeyed Beer's law at 365 nm up to the highest concentration prepared (9.0 mg l^{-1}) (Table 1). The presence of up to $20 \mu\text{M}$ iron did not significantly change the absorptivity of the humic acid (Fig. 5A).

Iron stabilized in solution with humic acid obeyed Beer's law at 365 nm up to the highest iron concentration prepared ($20 \mu\text{M}$) (Table 1). The presence of up to 9.0 mg l^{-1} humic acid did not significantly change the molar absorptivity of iron (Fig. 5B). A separate experiment showed that iron obeyed Beer's law up to $82 \mu\text{M}$ in the presence of 9.0 mg l^{-1} humic acid. Precipitation of humic acid and iron occurred at higher iron concentrations.

Variation in pH of a solution containing 9.0 mg l^{-1} humic acid and $70 \mu\text{M}$ iron from 4.7 to 9.7 increased the absorbance at 365 nm by less than 4%. The absorbances at 365 nm of humic acid and iron-humic acid solutions at pH 8.0 were stable for at least 9 days when stored in glass at 20°C and exposed to natural and fluorescent lighting.

Performance of the method

The limits of detection were 0.01 mg l^{-1} for humic acid and $0.04 \mu\text{M}$ for iron, estimated from twice the standard deviation of six replicate analyses of distilled water. Precision was estimated from six replicate analyses of each of two solutions. The relative standard deviations (and concentrations) were respectively: (a) humic acid 7% (0.90 mg l^{-1}), iron 20% ($0.39 \mu\text{M}$); and (b) humic acid 3% (8.1 mg l^{-1}), iron 2% ($3.71 \mu\text{M}$). For solutions of known composition, the recommended procedure gave results that were accurate, while concentrations determined by reference to external calibration graphs were in error by up to 138% (Table 2).

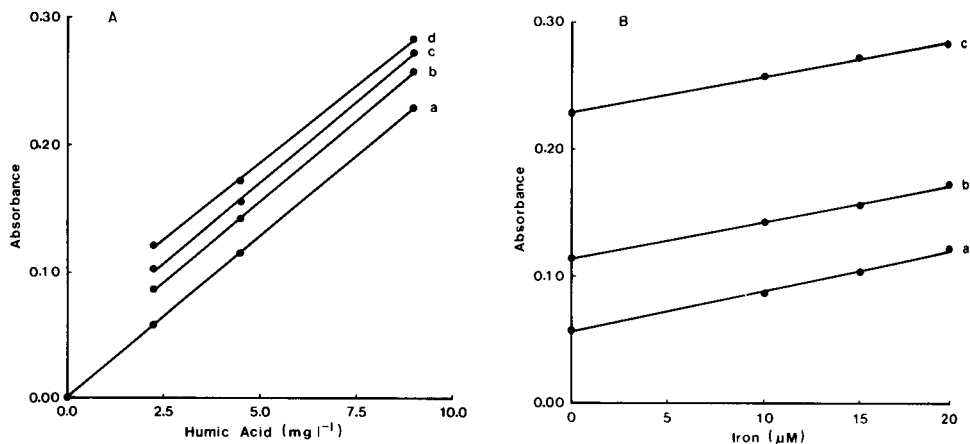


Fig. 5. ^A Effect of different amounts of iron on the absorptivity of humic acid at 365 nm in solutions at pH 8.0 for iron concentrations (μM) of (a) 0, (b) 10, (c) 15, (d) 20. ^B Effect of different amounts of humic acid on the molar absorptivity of iron (in the presence of humic acid) at 365 nm in solutions at pH 8.0 for humic acid concentrations (mg l^{-1}) of (a) 2.3, (b) 4.5, (c) 9.0. Absorbances were measured against distilled water. Details of solution preparation are given in the recommended procedure.

Elements reported to interfere with the determination of iron with ferrozine are cobalt, copper and nickel [21, 29]. Table 3 shows the degree to which Co, Cu, Cd, Ni and As(V) ($200 \mu\text{g l}^{-1}$) interfered in the determination of iron and humic acid in solutions of known composition. These elements will not significantly affect the determination when present at concentrations reported for natural waters [8]. Sample salinity had no significant interference. Tannin and lignin absorb significantly compared to humic acid at wavelengths less than 360 nm but not above [16] and should not interfere. The recommended procedure determines fulvic and humic acids, as both have similar absorption spectra [18] and reactions with iron

TABLE 2

Concentrations of iron and humic acid in known solutions determined by using the recommended procedure, and by using independent calibration curves (Reported concentrations are the mean of three determinations)

Solution	Iron (μM)			Humic acid (mg l^{-1})		
	Added	Found	% Error	Added	Found	% Error
<i>Recommended procedure</i>						
A	7.16	7.18	0	0.90	1.15	+28
B	3.58	3.73	+4	4.60	4.54	-2
C	0.90	1.09	+21	9.20	9.15	-1
<i>From conventional calibration graphs</i>						
A	7.16	7.27	+2	0.90	2.15	+138
B	3.58	4.10	+14	4.60	5.13	+12
C	0.90	1.83	+103	9.20	9.44	+3

TABLE 3

Interference caused by some trace metals ($200 \mu\text{g l}^{-1}$) added to iron and humic acid solutions

Trace metal added	River average ^a ($\mu\text{g l}^{-1}$)	Solution 1		Solution 2	
		Iron (μM)	Humic acid (mg l^{-1})	Iron (μM)	Humic acid (mg l^{-1})
—	—	<i>Added</i>			
		0.00	9.0	3.58	9.0
		<i>Found</i>			
Cu	10	0.36	9.0	3.31	8.7
Co	0.2	0.16	9.2	3.29	8.9
Cd	(<1)	0.14	8.9	2.86	8.9
Ni	2.2	0.19	9.1	1.73	9.5
As	1.7	0.12	8.9	2.80	9.1

^aWorld average dissolved river water concentrations [8].

[1, 30]. This is usual for spectrophotometric methods that do not employ prior separation of these acids [16, 17, 31].

Previous spectrophotometric methods for iron would normally make a correction for background absorbance (i.e., for humic acid), but spectrophotometric methods for humic acid are not corrected for iron interference [16, 31]. The accuracy of humic acid concentrations determined by using the recommended procedure is dependent on the absorptivity of the humic acid used for calibration. Reported absorptivities vary by over 100% [18], but could have been influenced by the presence of iron.

The effect of humic acid on iron concentrations determined by using the recommended procedure depends on the ratio of absorptivities of the

TABLE 4

Comparison of iron and humic acid concentrations obtained for six natural waters by the recommended procedure (RP) with those obtained using separate calibration graphs (CG)

Sample	(1)	(2)	(3)	(4)	(5)	(6)
<i>Iron (μM)</i>						
RP ^a	0.30	0.35	1.95	1.06	1.17	1.87
CG	0.42	0.45	2.07	1.32	1.58	2.04
Difference (%) ^b	+39	+30	+6	+25	+35	+9
<i>Humic acid (mg l^{-1})</i>						
RP ^a	1.19	1.05	1.19	2.72	4.10	1.80
CG	1.35	1.21	1.53	2.96	4.36	2.13
Difference (%) ^b	+13	+15	+29	+9	+6	+19

^aCalculated by using humic acid extracted from the Yarra River sediment as a standard.

^bRelative to the concentrations calculated with the recommended procedure.

humic acid at the two wavelengths used ($R = \epsilon_{562}/\epsilon_{365}$) and not their absolute values (Eqn. 4). The variation in R for humic substances from different sources is not well known. Ratios of absorptivities at two wavelengths (not those used here) show variations of about 50% for soil humic substances [18], and less than 25% for those from Baltic waters [31], but the reports are not specific about the presence of iron. Arbitrary variations in R of up to 50% did not significantly change the computed concentrations of iron.

Application

Waters from six streams in northeast Victoria, Australia, were analysed for iron and humic acid. Independent calibration graphs gave results 6–40% higher for iron and 6–29% higher for humic acid, than the results obtained with the recommended procedure (Table 4).

One of us (P. D. C.) acknowledges financial support given by a University of Melbourne Postgraduate Scholarship.

REFERENCES

- 1 J. H. Reuter and E. M. Perdue, *Geochim. Cosmochim. Acta*, 41 (1977) 325.
- 2 E. Tipping and D. Cooke, *Geochim. Cosmochim. Acta*, 46 (1982) 75.
- 3 K. A. Hunter and P. S. Liss, *Limnol. Oceanogr.*, 27 (1982) 322.
- 4 R. F. C. Mantoura, A. Dickson and J. P. Riley, *Estuarine Coastal Mar. Sci.*, 6 (1978) 387.
- 5 E. M. Perdue, K. C. Beck and J. H. Reuter, *Nature*, 260 (1976) 418.
- 6 E. A. Jenne, *Adv. Chem. Ser.*, 73 (1968) 337.
- 7 J. A. Davis and J. O. Leckie, *J. Colloid Interface Sci.*, 74 (1980) 32.
- 8 J.-M. Martin and M. Meybeck, *Mar. Chem.*, 7 (1979) 173.
- 9 G. Figueres, J.-M. Martin and M. Meybeck, *Neth. J. Sea Res.*, 12 (1978) 329.
- 10 A. L. Wilson, *J. Appl. Chem.*, 9 (1959) 510.
- 11 D. F. Marino and J. D. Ingle Jr., *Anal. Chim. Acta*, 124 (1981) 23.
- 12 A. Cominoli, J. Buffle and W. Haerdi, *J. Electroanal. Chem.*, 110 (1980) 259.
- 13 T. Almgren, B. Josefsson and G. Nyquist, *Anal. Chim. Acta*, 78 (1975) 411.
- 14 D. F. Martin and R. H. Pierce Jr., *Environ. Lett.*, 1 (1971) 49.
- 15 E. R. Sholkovitz, E. A. Boyle and N. B. Price, *Earth Planet. Sci. Lett.*, 40 (1978) 130.
- 16 J. Lawrence, *Water Res.*, 14 (1980) 373.
- 17 E. Tipping, *Geochim. Cosmochim. Acta*, 45 (1981) 191.
- 18 M. Schnitzer and S. U. Khan, *Humic Substances in the Environment*, M. Dekker, New York, NY, 1972.
- 19 L. E. Fox, *Estuarine Coastal Shelf Sci.*, 16 (1983) 431.
- 20 J. D. Smith and A. R. Longmore, *Nature*, 287 (1980) 532.
- 21 L. L. Stookey, *Anal. Chem.*, 42 (1970) 779.
- 22 D. A. Skoog and D. M. West, *Fundamentals of Analytical Chemistry*, 2nd edn., Holt, Rinehart and Winston, London, 1969, p. 678.
- 23 A. M. Posner, *J. Soil Sci.*, 17 (1966) 65.
- 24 R. J. Atkinson, A. M. Posner and J. P. Quirk, *J. Phys. Chem.*, 71 (1967) 550.
- 25 G. A. Parks and P. L. DeBruyn, *J. Phys. Chem.*, 66 (1962) 967.
- 26 M. M. Gibbs, *Water Res.*, 13 (1979) 295.
- 27 B. Jaselskis and S. J. Nelapaty, *Anal. Chem.*, 44 (1972) 379.
- 28 C. R. Gibbs, *Anal. Chem.*, 48 (1976) 1197.
- 29 S. K. Kundra, M. Katyal and R. P. Singh, *Anal. Chem.*, 46 (1974) 1605.
- 30 C. H. Langford and T. R. Khan, *Can. J. Chem.*, 53 (1975) 2979.
- 31 M. Brown, *Estuarine Coastal Mar. Sci.*, 5 (1977) 309.

SPECTROPHOTOMETRIC STUDY OF REACTIONS OF SCANDIUM, YTTRIUM AND LANTHANUM IONS WITH SOME TRIPHENYLMETHANE DYES IN THE PRESENCE OF CATIONIC SURFACTANTS

M. JAROSZ and Z. MARCZENKO*

Department of Analytical Chemistry, Technical University, 00-664 Warsaw (Poland)

(Received 23rd September 1983)

SUMMARY

Optimum conditions for the formation of ternary complexes of scandium, yttrium and lanthanum ions with chrome azurol S, eriochrome cyanine R and pyrocatechol violet in the presence of cetyltrimethylammonium, cetylpyridinium and tetradecyldimethylbenzylammonium (zephiramine) ions are described. The spectrophotometric determination of scandium with chrome azurol S and zephiramine exhibits the greatest sensitivity ($\epsilon = 1.50 \times 10^5 \text{ l mol}^{-1} \text{ cm}^{-1}$ at 610 nm). In the spectrophotometric determination of scandium with eriochrome cyanine R and cetylpyridinium ion ($\epsilon = 9.2 \times 10^4$ at 600 nm), the interference caused by yttrium is the least. In the best method for yttrium (with pyrocatechol violet and zephiramine), the molar absorptivity is 3.3×10^4 at 660 nm. Lanthanum does not form ternary complexes of analytical interest in these systems. Some aspects of the formation of ternary complexes with cationic surfactants are discussed.

Ternary systems containing metals that hydrolyze in weakly acidic or neutral medium, chelating triphenylmethane reagents and cationic surfactants, form the basis of very sensitive spectrophotometric methods [1–3]. Methods involving binary systems (without the surfactant) provide considerably smaller sensitivities. Table 1 shows a comparison of molar absorptivities for the spectrophotometric determinations of scandium, yttrium and lanthanum based on binary complexes with chrome azurol S (CAS), eriochrome cyanine R (ECR) and pyrocatechol violet (PV), as well as those based on ternary complexes with these chromophoric reagents and cetyltrimethylammonium (CTA), cetylpyridinium (CP) or tetradecyldimethylbenzylammonium (zephiramine; zeph) ions, which are cationic surfactants. The data are taken from the literature or were obtained in this work. The work described here was designed to examine the conditions for the formation of ternary complexes of Sc, Y and La with the above-mentioned reagents in order to establish optimum systems for spectrophotometric purposes, and also to try to explain some aspects of the formation mechanism of such ternary complexes. Previous papers have dealt with similar ternary complexes of aluminium [13] and vanadium [14].

TABLE 1

Some data on spectrophotometric methods for Sc, Y and La based on binary and ternary systems

Binary system	ϵ (10^4 l mol ⁻¹ cm ⁻¹)	M:R ^a	Ref.	Ternary system	ϵ (10^4 l mol ⁻¹ cm ⁻¹)	M:R ^a	Ref.
Sc-ECR	5.2	1:2	4	Sc-CAS-CTA	13.2	1:2	8
Sc-PV	1.7	1:1	5	Sc-CAS-zeph	13.7	ND ^b	9
Y-ECR	2.9	1:2	4		15.0	1:2	This work
Y-PV	2.6	ND ^b	6	Sc-CAS-CP	14.2	1:2	10
La-ECR	2.4	1:2	4	Sc-ECR-CTA	15.0	1:2	11
La-PV	0.9	1:1	7	Sc-ECR-CP	9.2	1:2	This work
				Sc-PV-CTA	6.9	1:2	12
				Y-CAS-CTA	3.2	1:2	8
				Y-PV-zeph	3.3	1:2	This work

^aR is the triphenylmethane dye. ^bND means no data.

EXPERIMENTAL

Reagents and apparatus

For the scandium standard solution (1 mg Sc ml⁻¹), 0.1530 g of scandium oxide was dissolved in 10 ml of hot 2 M hydrochloric acid and the solution was diluted with water to exactly 100 ml. For the yttrium standard solution (1 mg Y ml⁻¹), 0.1270 g of yttrium oxide was dissolved in 5 ml of hot hydrochloric acid (1 + 1) and the solution was diluted with water to exactly 100 ml. For the lanthanum standard solution (1 mg La ml⁻¹), 0.1170 g of lanthanum oxide was dissolved in 5 ml of hot hydrochloric acid (1 + 1) and the solution was diluted with water to exactly 100 ml.

The oxides used were first dehydrated and freed from CO₂ by ignition.

Chrome azurol S (BDH), eriochrome cyanine R (Loba) and pyrocatechol violet (POCh) were purified as described earlier [15]. Aqueous solutions (5×10^{-4} M) of the reagents were used.

Cetyltrimethylammonium bromide (International Enzymes), cetylpyridinium chloride (Loba) and zephiramine (ICN) were used as aqueous solutions (5×10^{-3} M).

The absorbances were measured with a VSU2-P spectrophotometer and the absorption spectra were recorded on a Specord UV-VIS spectrophotometer. The pH was measured with an ELPO N-517 pH-meter.

General procedure

A solution containing an appropriate amount of scandium, yttrium or lanthanum was placed in a 25-ml beaker. The solutions of triphenylmethane dye and cationic surfactant were added and the pH was adjusted to the

optimum value for the system examined. The solution was transferred to a 25-ml volumetric flask and diluted with water to volume. After 5 min, the absorbance of the solution was measured at the appropriate wavelength against a reagent blank.

In the examination of the ternary complexes with chelating triphenylmethane reagents and cationic surfactants, the metal ion concentrations were 7.5×10^{-6} M (Sc) and 1.5×10^{-5} M (Y and La).

Recommended procedure for scandium with ECR and CP

A solution containing not more than 10 μ g of scandium is placed in a 25-ml beaker and 5 ml of the ECR solution and 5 ml of the CP solution are added. The pH is adjusted to 5.5 ± 0.1 , and the solution is transferred to a 25-ml volumetric flask and diluted with water to volume. After 5 min, the absorbance of the solution is measured at 600 nm against a reagent blank.

RESULTS

The ternary systems of yttrium with ECR and a cationic surfactant cannot be regarded as a basis for spectrophotometric methods. When CTA or zephiramine is used, the complexes form only to a small extent at about pH 5.5. In the Y-ECR-CP system, no ternary complex is formed in the pH range 4-9.

It was shown that lanthanum does not form ternary complexes with CAS or ECR and a cationic surfactant in the pH range 2-11. Introduction of a cationic surfactant into the La-PV system at about pH 9 causes a shift of the peak maximum of the absorption spectra from 600 to 670 nm, which proves the formation of ternary complexes; but the absorbances measured are so small that none of these ternary systems can be regarded as the basis of a sensitive spectrophotometric method for lanthanum.

Ternary systems of scandium and yttrium with chrome azurol S and a cationic surfactant

The optimum pH ranges for the formation of ternary complexes of scandium and yttrium with CAS and a cationic surfactant do not differ substantially. Scandium complexes form at pH 5.2 ± 0.4 (zeph), 5.5 ± 0.2 (CTA) and 5.5 ± 0.1 (CP); yttrium complexes form at 5.1 ± 0.1 (CTA) and 5.2 ± 0.1 (CP, zeph). The molar excesses of CAS with respect to metal that guarantee the greatest absorbances are relatively narrow: for scandium, the optimal molar excesses are 2-3 (zeph), 4-6 (CP) and 4-8 (CTA); and for yttrium, the optimal molar excesses are 3-4 (CP), 7-8 (CTA) and 9-10 (zeph) (all at a 100-fold molar excess of the surfactant with respect to the metal). Any increase in the excess of chromophoric reagent above the optimum leads to the occurrence of hypsochromic effects and lower absorbances.

Cationic surfactants ensure the greatest absorbances if they are used in excesses above the turbidity ranges [13]. The optimum molar excesses of

cationic surfactants with respect to metal are: for scandium 50–100 (CP), 100–125 (zeph) and 100–150 (CTA), and for yttrium 25–30 (CTA, CP) and 100–120 (zeph). The influence of increasing amounts of CP on the absorption spectra in the ternary scandium–CAS–CP system is shown in Fig. 1.

The absorption maximum of the ternary complexes of scandium and yttrium with CAS and the cationic surfactants examined is situated at 610 nm. The complexes with CTA and zeph are stable with time; the absorbances reach their maximum 5 min after mixing of the reagents and establishing the pH, and then remain unchanged for 30 min. If CP is used, the absorbances reach their maximum in 5 min and then decrease.

The mole ratios CAS:Sc and CAS:Y in the ternary complexes, evaluated by Job's method of isomolar series are 1.5:1 for the Sc–CAS–CTA and Y–CAS–zeph systems, slightly below 2:1 for the systems of both these metals with CP, and 2:1 for the Sc–CAS–zeph and Y–CAS–CTA systems. The mole ratio of scandium to the cationic surfactant was not evaluated because the complexes with maximum absorbance are formed at a large excess of the cationic surfactant and undoubtedly micelles rather than simple ions participate in the reaction.

Curves showing the dependence of absorbance on scandium concentration based on the systems with CAS and a cationic surfactant satisfy Beer's law up to a concentration of $0.4 \mu\text{g Sc ml}^{-1}$. Molar absorptivities (at 610 nm) are: 1.50×10^5 (zeph), 1.42×10^5 (CP) and $1.22 \times 10^5 \text{ l mol}^{-1} \text{ cm}^{-1}$ (CTA). As far as yttrium is concerned, the spectrophotometric methods based on the CAS ternary systems are considerably less sensitive. The linear calibration ranges and molar absorptivities are: $0.5\text{--}1.6 \mu\text{g Y ml}^{-1}$ and $8.3 \times 10^3 \text{ l mol}^{-1} \text{ cm}^{-1}$ at 610 nm (zeph), and $0.5\text{--}1.6 \mu\text{g Y ml}^{-1}$ and $8.0 \times 10^3 \text{ l mol}^{-1} \text{ cm}^{-1}$ at 610 nm (CTA). The standard curve for the Y–CAS–CP system does not satisfy Beer's law.

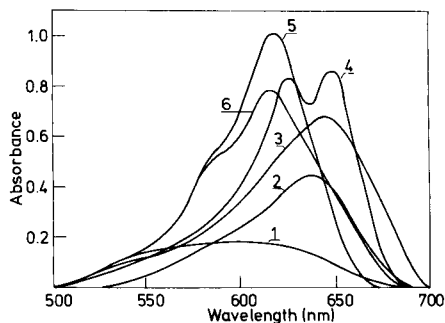


Fig. 1. Effect of the excess of CP with respect to scandium on absorption spectra in the Sc–CAS–CP system. $c_{\text{Sc}} = 7.5 \times 10^{-6} \text{ M}$, $c_{\text{CAS}} = 3.8 \times 10^{-5} \text{ M}$, pH 5.5 ± 0.1 . Molar excess of CP: (1) without CP; (2) 3:1; (3) 10:1; (4) 25:1; (5) 50:1; (6) 150:1. (A turbidity appears between the molar ratios 10:1 and 25:1.)

Ternary systems of scandium with eriochrome cyanine R and a cationic surfactant

The optimum pH ranges for the formation of ternary complexes of scandium with ECR and a surfactant are: 5.5 ± 0.1 (CP), 5.5 ± 0.2 (CTA) and 5.5 ± 0.2 (zeph). Maximum and reproducible absorbances are ensured by making the molar excess of ECR with respect to scandium 8–10 with zephiramine, 10–15 with CTA, and 15–20 with CP. As in the case of the CAS systems, increases in the amounts of the chromophoric reagent lead to the hypsochromic shift of the absorption maximum. Absorbances are maximal for the following excesses of cationic surfactants with respect to scandium: 40–100 (CTA), 50–150 (CP), and 50–200 (zeph). At these concentrations of the surfactant, there is no turbidity. The changes in the absorption spectra of the complexes caused by increasing amounts of CP are shown in Fig. 2. The stability with time of the ternary complexes of scandium with ECR and a surfactant is similar to that found for the CAS complexes.

The mole ratios ECR:Sc in ternary complexes evaluated by Job's method are 2:1 in the presence of CTA and a little over 2:1 when CP or zephiramine is used.

The spectrophotometric methods of measuring scandium based on these ternary systems with ECR exhibit lower sensitivity than those based on CAS. The absorption maximum of the complexes is situated at 600 nm. Molar absorptivities are: 9.8×10^4 (zeph), 9.3×10^4 (CTA) and 9.2×10^4 l mol⁻¹ cm⁻¹ (CP). Standard curves satisfy Beer's law up to the concentration of $0.4 \mu\text{g Sc ml}^{-1}$.

Ternary systems of scandium and yttrium with pyrocatechol violet and a cationic surfactant

The optimum pH ranges for the formation of the ternary complexes of scandium and yttrium with PV and the surfactant lie at higher pH than in

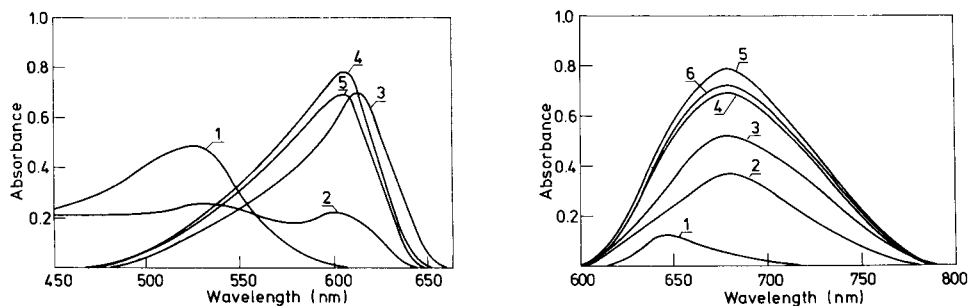


Fig. 2. Effect of the excess of CP with respect to scandium on absorption spectra in the Sc-ECR-CP system. $c_{\text{Sc}} = 7.5 \times 10^{-6}$ M, $c_{\text{ECR}} = 1.2 \times 10^{-4}$ M, pH 5.5 ± 0.1 . Molar excess of CP: (1) without CP; (2) 3:1; (3) 10:1; (4) 50:1; (5) 200:1.

Fig. 3. Effect of the excess of CP with respect to scandium on absorption spectra in the Sc-PV-CP system. $c_{\text{Sc}} = 1.5 \times 10^{-5}$ M, $c_{\text{PV}} = 4.5 \times 10^{-5}$ M, pH 8.5 ± 0.2 . Molar excess of CP: (1) without CP; (2) 5:1; (3) 10:1; (4) 25:1; (5) 100:1; (6) 150:1.

the case of CAS and ECR. The ranges are: for scandium, 8.0 ± 0.3 (zeph), 8.5 ± 0.2 (CP) and 8.5 ± 0.3 (CTA), and for yttrium, 9.0 ± 0.1 (CTA, zeph) and 9.0 ± 0.2 (CP). Maximum absorbances are obtained when the molar excesses of PV with respect to metal are as follows: 3–4 (Sc, CTA or CP), 4–5 (Sc, zeph), 5–10 (Y, CTA) and 8–10 (Y, CP or zeph). As in the ternary complexes with CAS and ECR, increasing amounts of PV cause hypsochromic shifts of the maximum wavelength. Molar excesses of the surfactant must be greater than the turbidity ranges for the formation of these ternary complexes. The optimum excesses are as follows: for scandium, 40–50 (CTA), 40–125 (CP) and 125–175 (zeph), and for yttrium, 50–75 (CTA), 50–100 (CP) and 75–100 (zeph). With only small excesses of the surfactant, the ternary complexes with PV are not formed at all (in contrast to CAS and ECR). Increasing amounts of the surfactant do not lead to hypsochromic shifts (Fig. 3) such as are characteristic of the complexes with CAS and ECR.

The stability with time of these coloured ternary complexes of scandium and yttrium is similar to that found in the CAS systems. Maximum absorbances appear 5 min after the system reaches the optimum pH. The absorbances of the solutions of the complexes with CP decrease after 5 min.

The mole ratios of PV to metal ion evaluated by Job's method are slightly over 2:1 for the ternary complexes of both scandium and yttrium.

The spectrophotometric methods of measuring scandium based on PV and a surfactant exhibit considerably smaller sensitivity than the methods based on CAS and ECR. Standard curves satisfy Beer's law up to a scandium concentration of $0.7 \mu\text{g ml}^{-1}$ (CTA, CP) or in the range $0.2\text{--}0.7 \mu\text{g ml}^{-1}$ (if zephiramine is the third component). Molar absorptivities are as follows: 5.8×10^4 at 670 nm (CTA), 4.7×10^4 at 690 nm (zeph) and $4.5 \times 10^4 \text{ l mol}^{-1} \text{ cm}^{-1}$ at 670 nm (CP).

Pyrocatechol violet in the presence of a cationic surfactant produces yttrium complexes that show stronger absorbances than the analogous ternary complexes of this metal with CAS. These complexes absorb at 660 nm. If zephiramine is used, the standard curve satisfies Beer's law up to an yttrium concentration of $1.2 \mu\text{g ml}^{-1}$. The range of measurement for the methods based on CTA and CP is $0.1\text{--}1.0 \mu\text{g Y ml}^{-1}$. Molar absorptivities are as follows: 3.3×10^4 (zeph), 3.0×10^4 (CP) and 2.4×10^4 (CTA) $\text{l mol}^{-1} \text{ cm}^{-1}$.

Determination of scandium with ECR and CP in the presence of yttrium and lanthanum

As has been said above, yttrium forms ternary complexes with CAS and a cationic surfactant. With ECR and CP, yttrium does not form ternary complexes. Therefore the system with ECR and CP provides the most selective method for determining scandium. The procedure recommended is given under Experimental.

The influence of yttrium and lanthanum on this spectrophotometric determination of scandium was examined. The results are presented in

Table 2. Above certain limits, both metals cause an increase in the results obtained for microgram quantities of scandium. In these cases, a preliminary separation of scandium by extraction or ion-exchange methods becomes necessary [16, 17].

DISCUSSION

The work described above shows that the most sensitive spectrophotometric methods of determination are as follows: for scandium in the system of Sc—CAS—zeph ($\epsilon = 1.50 \times 10^5 \text{ l mol}^{-1} \text{ cm}^{-1}$ at 610 nm, pH 5.2 ± 0.4) and for yttrium in the system of Y—PV—zeph ($\epsilon = 3.3 \times 10^4 \text{ l mol}^{-1} \text{ cm}^{-1}$ at 660 nm, pH 9.0 ± 0.1). The determination of scandium with ECR and CP is of analytical interest, because the influence of yttrium is the least in this system. Lanthanum does not form ternary complexes with CAS, ECR or PV in the pH range 2–11 in the presence of CTA, CP or zephiramine. This is due to the high basicity of this metal; its reactive forms, hydrolyzed ions, appear only at pH > 9.

The sensitivity of these spectrophotometric methods based on the ternary systems with CAS, ECR or PV depends mainly on the triphenylmethane reagent. In a weakly acidic or neutral medium (pH 3–8), ECR makes it possible to achieve very high sensitivities for determinations of easily hydrolyzed metals such as aluminium [13] and vanadium(IV) [14]; this reagent reacts with highly hydrolyzed metal forms, mainly $\text{VO}(\text{OH})_2$ and $\text{Al}(\text{OH})_3$ [18]. Methods based on CAS show the highest molar absorptivities for scandium, a metal of stronger basicity. Weakly hydrolyzed ions $\text{Sc}(\text{OH})^{2+}$ [18] take part in the formation of the ternary complexes of scandium with CAS. Pyrocatechol violet reacts with more hydrolyzed metal ions such as $\text{Y}(\text{OH})_n^{3-n}$ and $\text{VO}(\text{OH})_2$. The highest sensitivities for methods based on ternary systems with PV, in comparison with CAS or ECR, were obtained for yttrium, a comparatively basic metal.

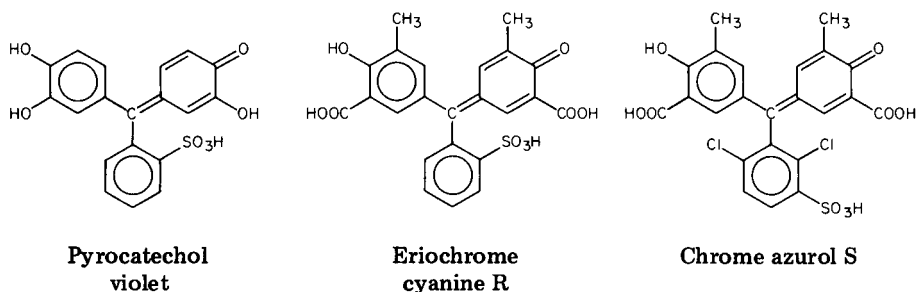
In the optimum pH ranges for the formation of ternary complexes with a

TABLE 2

Spectrophotometric determination of scandium (2.0 μg) with ECR and CP in the presence of yttrium and lanthanum

Y added (μg)	Sc found (μg)	La added (μg)	Sc found (μg)
—	2.0, 1.9, 1.9	20	2.0, 2.0, 2.1
—	2.1, 2.0, 1.9	50	2.6, 2.5, 2.6
5	2.3, 2.1, 2.2	100	3.1, 3.1, 3.2
20	2.4, 2.5, 2.5	20 ^a	2.5, 2.5, 2.5
50	3.1, 3.0, 3.2		

^a5 μg Y also added.



cationic surfactant, CAS and ECR are present in the forms $H_2R^{2-} \rightleftharpoons HR^{3-}$ with the equilibrium tending to the right, whereas PV appears in the forms $H_3R^- \rightleftharpoons H_2R^{2-}$. Higher sensitivities of methods based on PV are obtained at lower pH values, at which the H_3R^- form prevails. The much greater sensitivity of spectrophotometric methods based on these ternary systems with a cationic surfactant, compared with the analogous binary systems, is due to the bigger mole ratio of triphenylmethane dye to metal in the ternary complexes.

The ternary complexes discussed absorb at longer wavelengths than the chromophoric reagents themselves or their binary complexes with metals. In the series of metals V(IV), Y, Sc, Al, the wavelengths of maximum absorption change from 600 nm for vanadium(IV) through 610 nm for Y and Sc) to 630 nm for aluminium for the complexes with CAS and a surfactant. Bathochromic shifts result not only from bonding between the metal ion and the phenolic oxygen atom affecting the conjugated system of the triphenylmethane reagent, but also from interactions of the cationic surfactants with π -electrons of these bonds.

The metal-phenolic oxygen bonding is of a mixed ionic-covalent character [19]. The greater is the participation of the ionic bond, the longer is the maximum wavelength; therefore, the smaller the size of the metal ion and the greater its charge, the longer is the wavelength at which the absorption maximum of the ternary complex is situated. The influence of ionic bonds on the location of the absorption maximum of ternary complexes is also observed when the excess of cationic surfactant with respect to metal is changed. Below the turbidity range, the complexes, which are formed mainly with ionic forms of the surfactant, absorb at much longer wavelengths (Fig. 1) than the complexes formed at greater concentrations of the surfactant, which is usually then present as micelles.

Cationic surfactants cause strong bathochromic shifts because of electrostatic and hydrophobic interactions with the chromophoric reagent ions. The difference in position of the maximum wavelength with different cationic surfactants is usually small (5–10 nm). The ternary complexes of aluminium and scandium with CAS absorb at the longest wavelength when CP is the third component. For complexes of these metals with ECR or PV, zephir-

amine causes the strongest bathochromic shift. When the binary complexes of a metal ion with a triphenylmethane reagent are solubilized with a micellar cationic surfactant, the role played by electrostatic interactions predominates in the case of chrome azurol S, whereas hydrophobic interactions predominate with eriochrome cyanine R or pyrocatechol violet.

REFERENCES

- 1 V. N. Tikhonov, *Zh. Anal. Khim.*, 32 (1977) 1435.
- 2 S. B. Savvin, *Crit. Rev. Anal. Chem.*, 8 (1979) 55.
- 3 Z. Marczenko, *Crit. Rev. Anal. Chem.*, 11 (1981) 195.
- 4 V. N. Tikhonov and S. N. Fedotova, *Zh. Anal. Khim.*, 37 (1982) 1888.
- 5 S. P. Onosova and G. K. Kuncevitch, *Zh. Anal. Khim.*, 20 (1965) 802.
- 6 J. P. Young, I. C. White and R. G. Ball, *Anal. Chem.*, 32 (1960) 1264.
- 7 T. Takano, *Bunseki Kagaku*, 15 (1966) 1087.
- 8 V. N. Tikhonov and S. G. Danilova, *Zh. Anal. Khim.*, 35 (1980) 1264.
- 9 Y. Horiuchi and H. Nishida, *Bunseki Kagaku*, 17 (1968) 756.
- 10 J. Jurkevičtute and M. Malat, *Collect. Czech. Chem. Commun.*, 44 (1979) 3236.
- 11 V. N. Tikhonov and V. T. Samarkina, *Khim. Khim. Tekhnol.*, 21 (1978) 1116.
- 12 V. N. Tikhonov and O. K. Pavlova, *Zh. Anal. Khim.*, 37 (1982) 1809.
- 13 Z. Marczenko and M. Jarosz, *Analyst (London)*, 107 (1982) 1431.
- 14 M. Jarosz and Z. Marczenko, *Analyst (London)*, 109 (1984) 35.
- 15 F. J. Langmyhr and K. S. Klausen, *Anal. Chim. Acta*, 29 (1963) 149.
- 16 Z. Marczenko, *Spectrophotometric Determination of Elements*, Ellis Horwood, Chichester, 1976.
- 17 E. B. Sandell and H. Onishi, *Photometric Determination of Traces of Metals. General Aspects*. Wiley, New York, 1978.
- 18 V. A. Nazarenko, V. P. Antonovich and E. M. Nevskaa, *Metal Ions Hydrolysis in Dilute Solutions (in Russian)*, Atomizdat, Moskva, 1979.
- 19 S. Murakami and T. Yoshino, *Talanta*, 28 (1981) 623.

SIMULTANEOUS SPECTROFLUORIMETRIC DETERMINATION OF IRON AND MANGANESE BY A DIFFERENTIAL KINETIC CATALYTIC METHOD

A. MORENO, M. SILVA and D. PEREZ-BENDITO*

Department of Analytical Chemistry, Faculty of Science, University of Cordoba (Spain)

(Received 10th October 1983)

SUMMARY

A kinetic method is presented for the simultaneous determination of iron(III) and manganese(II) based on the different reaction rates resulting from the catalytic effect of both metal ions on the oxidation of 2-hydroxybenzaldehyde thiosemicarbazone by hydrogen peroxide in an ammoniacal medium. The reaction is monitored spectrofluorimetrically at 440 nm and with excitation at 365 nm. Two sets of reaction conditions are established to maximize the effect of manganese compared to iron, and vice versa, and the data are evaluated from simultaneous equations. Mixtures of these metal ions at ng ml^{-1} levels for iron/manganese ratios from 8:1 to 1:2 can be determined with an accuracy and precision of about 3% and 1%, respectively. The method has been applied successfully to the determination of both metals in aluminium and copper alloys, beer, cheeses and soils.

There are few differential kinetic methods for the determination of inorganic species based on a catalyzed reaction. In all instances, indicator systems involving inorganic reagents are used. Thus, the cerium(IV)—arsenite reaction has been applied in the analysis of mixtures of iodide and osmium [1], based on the masking of iodide by mercury(II) or silver(I), and for the determination of mixtures of osmium and ruthenium [2] because of the different kinetic dependence on the reaction with respect to the concentration of cerium(IV) and arsenite. Another indicator reaction is based on the oxidation of iodide by hydrogen peroxide. Zirconium—hafnium mixtures [3] have been analysed by their catalytic effect on this reaction. The maximum catalytic effect is shown for zirconium at pH 1.1 and for hafnium at pH 2.2. Molybdenum—tungsten mixtures have been determined because in the presence of citric acid the catalytic effect of tungsten is suppressed whilst the effect of molybdenum is slightly increased [4]. Mixtures of niobium and tantalum [5] have been determined by means of the different catalytic activity of the peroxide complexes of the respective metal ions. When iodide is oxidized by bromate [6], this system serves as a basis for the analysis of mixtures of molybdenum and tungsten and of molybdenum and chromium by amperometric recording of the effect of each of these ions on the reaction rate. Finally, Alekseeva and Nemzer [7] proposed the deter-

mination of germanium and phosphorus in mixtures by means of the oxidation of iodide by isopolymolybdic acids based on their different catalytic dependence on pH.

The oxidation of 2-hydroxybenzaldehyde thiosemicarbazone (HBTS) by hydrogen peroxide is catalyzed by iron(III) and manganese(II) with different efficiencies. This system has previously been used for the kinetic determination of nanogram amounts of manganese [8] and iron [9] as well as for the indirect kinetic determination of zinc [10] and silver [11]. This reaction is used in the present paper to determine iron and manganese in the same sample by choosing two sets of conditions which provide the greatest discrimination between the catalytic effects of iron and manganese.

EXPERIMENTAL

Reagents and apparatus

2-Hydroxybenzaldehyde thiosemicarbazone solutions (0.1 and 0.03%, w/v) were prepared in ethanol. The reagent was synthesized according to the procedure of Sah and Daniels [12]. A standard iron solution (1.000 mg ml^{-1}) was prepared by dissolving 1.000 g of pure iron in 50 ml of (1 + 1) nitric acid and diluting to exactly 1 l with distilled water. A standard manganese solution (4.098 mg ml^{-1}) was prepared by dissolving manganese(II) nitrate (Merck) in distilled water. It was standardized by titration with EDTA. These solutions were diluted as required, just before use. All solvents and reagents were of analytical grade.

The Perkin-Elmer MPF-43A spectrofluorimeter used was equipped with a recorder and thermostat for kinetic measurements and with 1.0-cm quartz cells. In all measurements the sensitivity was $\times 0.1$ and the emission and excitation slits were 6 nm. Under these conditions, a $8 \times 10^{-6} \text{ M}$ solution of quinine sulphate showed a fluorescence intensity of 70%. A Radiometer PHM62 pH meter with a combined glass-calomel electrode and Hewlett-Packard HP-85 computer were also used.

Simultaneous determination of iron and manganese

Two kinetic runs are needed for each sample.

Procedure 1. To a solution containing 100–600 ng of iron and 50–220 ng of manganese in a 10-ml volumetric flask, add 0.5 ml of 0.03% HBTS solution, 1 ml of 1% (v/v) hydrogen peroxide solution, 1.5 ml of 3.2 M ammonia solution, 2.5 ml of ethanol and 2.0 ml of 2.5 M potassium chloride, and make up to the mark with distilled water. Start the stopwatch just after the addition of ammonia, and after 1 min transfer a portion of this solution to the spectrofluorimeter cell maintained at $35 \pm 0.1^\circ\text{C}$. Wait for 2 min before starting to record the fluorescence intensity ($\lambda_{\text{em}} = 440 \text{ nm}$, $\lambda_{\text{ex}} = 365 \text{ nm}$) as a function of time. Calculate the slope of the linear plot.

Procedure 2. To a solution containing 0.1–0.7 μg of iron and 50–200 ng of manganese in a 10-ml volumetric flask, add 0.2 ml of 0.1% HBTS solu-

tion, 0.5 ml of 0.3% (v/v) hydrogen peroxide solution, 1 ml of 3.2 M ammonia solution and 2 ml of 2.5 M potassium chloride, and make up to the mark with distilled water. Proceed as in Procedure 1.

Preparation of samples

Aluminium alloy. Place an exactly weighed amount of alloy (100 mg) and 5 ml of 6 M hydrochloric acid in a beaker. Warm the solution and add several drops of hydrogen peroxide to complete the dissolution. Cool, and dilute to 100 ml in a volumetric flask with distilled water. Use 50- μ l aliquots for the above procedures.

Copper alloys. To a sample of alloy (50 mg) in a beaker, add the minimum volume of (1 + 1) nitric acid. Heat until dissolution is complete. Cool, transfer the solution to a 250-ml volumetric flask and dilute with distilled water to the mark. Use 50- μ l aliquots for the above procedures.

Cheese. In a beaker, gently warm an accurately weighed quantity (10 g) of cheese with 10 ml of sulphuric–nitric acid (1 + 1, v/v). In order to destroy the organic matter completely add several drops of hydrogen peroxide. Collect the remaining solution in a 50-ml volumetric flask and dilute to volume with distilled water. Take 0.5-ml aliquots for the simultaneous determination of iron and manganese.

Beer. Evaporate 25 ml of beer in a porcelain crucible to dryness on a sand bath and place in a furnace at 500°C for 2 h. After cooling, extract the residue with 25 ml of (1 + 15) nitric acid and dilute to the mark with water in a 50-ml volumetric flask. Take 0.5-ml aliquots for the above procedures.

Soil. Add a known amount of sample (2 g), 20 ml of distilled water and 20 ml of concentrated hydrochloric acid in a beaker, and evaporate to dryness on a sand bath. Cool and add 10 ml of (1 + 1) hydrochloric acid. Digest for 10 min, dilute with 10 ml of hot water and filter quickly. Wash the precipitate with dilute hydrochloric acid and dilute to the mark with water in a 100-ml volumetric flask. Take 0.5-ml aliquots for the above procedures.

RESULTS AND DISCUSSION

In an ammoniacal medium, HBTS can be oxidized to a product with an intense blue fluorescence ($\lambda_{\text{ex}} = 365 \text{ nm}$, $\lambda_{\text{em}} = 440 \text{ nm}$) by the action of several oxidizing agents. When the oxidant is hydrogen peroxide, this reaction is catalyzed by iron and manganese. Because of their different catalytic efficiencies, both ions can be determined by choosing conditions where the catalytic effect of manganese is most enhanced with respect to that of iron, and vice versa. Two simultaneous equations are solved to give the manganese and iron concentrations.

Effect of reaction variables

The influence of reaction variables was studied separately for each catalyst and their optimum values were selected by choosing the maximum difference

between the initial rate/concentration plots for the iron as well as the manganese catalytic effects. Two sets of reaction conditions must be fulfilled. In the first, iron catalysis is enhanced (Procedure 1) and in the second, the manganese catalysis is increased (Procedure 2).

Effect of the temperature. In both cases, the influence of temperature on the catalyzed reactions was examined in the range 25–50°C. The same temperature, 35°C, was chosen for each procedure, for greater simplicity and rapidity of the proposed determination when the thermostat can be fixed at a single temperature. Figure 1 shows plots of fluorescence intensity vs. time at different temperatures for both catalysts, that correspond to the experimental conditions in which the iron catalysis is enhanced.

Influence of the reagents. In the conditions for Procedure 1, the HBTS effect was studied in the range $0.3\text{--}1.1 \times 10^{-4}$ M; 7×10^{-5} M (0.5 ml of 0.03% reagent solution) was selected for further use (Fig. 2a). Two kinetic dependences with respect to HBTS were found in this range for the iron catalysis. A logarithmic plot showed that the reaction rate is first order with respect to HBTS below 7×10^{-5} M and has an order of -1 at higher values. In the experimental conditions for Procedure 2, greater concentrations of HBTS are necessary in order to test its influence on both catalyzed reactions. Figure 2(b) shows that in the $0.5\text{--}1.1 \times 10^{-4}$ M interval, the order of reaction in HBTS is zero for manganese catalysis and at higher concentrations this order is $-3/2$. For the iron(III)-catalyzed reaction, the initial rate decreased exponentially (order of reaction is -2) as the HBTS concentration

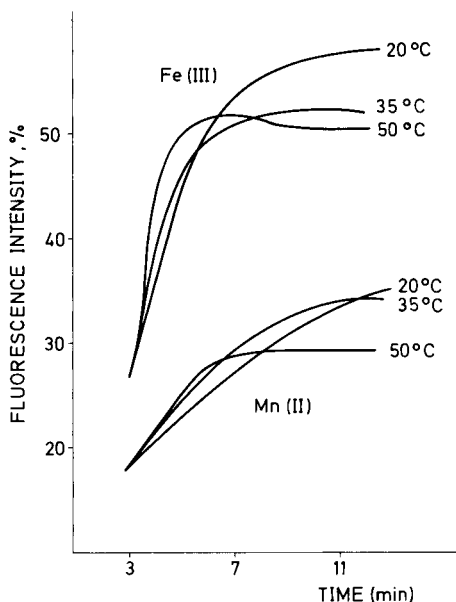


Fig. 1. Recorded fluorescence/time curves at different temperatures for both catalyzed reactions with $40 \text{ ng ml}^{-1} \text{ Fe}^{3+}$ or $5 \text{ ng ml}^{-1} \text{ Mn}^{2+}$. Other conditions are described in Procedure 1.

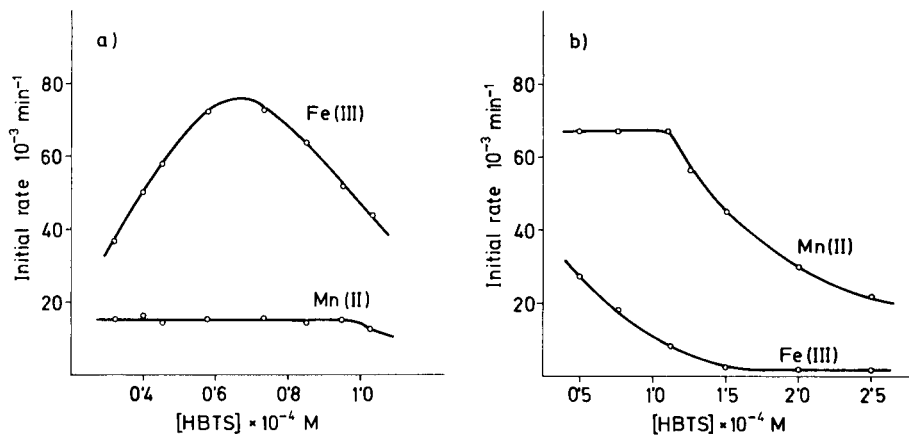


Fig. 2. Dependence of the initial rate of both catalyzed reactions on the HBTS concentration. (a) Procedure 1, $40 \text{ ng ml}^{-1} \text{ Fe}^{3+}$, $5 \text{ ng ml}^{-1} \text{ Mn}^{2+}$, $2.5 \times 10^{-2} \text{ M H}_2\text{O}_2$, 0.5 M NH_3 , pH 11.6, 25% ethanol, 35°C ; (b) Procedure 2, $8 \text{ ng ml}^{-1} \text{ Mn}^{2+}$, $40 \text{ ng ml}^{-1} \text{ Fe}^{3+}$, $4.6 \times 10^{-3} \text{ M H}_2\text{O}_2$, 0.15 M NH_3 , pH 10.77, 35°C .

increased. Because the maximum difference between the rates of the catalyzed reactions occurs at $1.1 \times 10^{-4} \text{ M}$ HBTS (0.2 ml of 0.1% reagent solution), this value is recommended.

The effect of hydrogen peroxide on these catalyzed reactions is shown in Fig. 3. In the experimental conditions for Procedure 1 (see Fig. 3a), concentrations of this variable greater than $3.2 \times 10^{-2} \text{ M}$ (1 ml of 1% hydrogen peroxide solution) do not affect the iron catalysis, and so this concentration was used in subsequent studies. The influence of hydrogen peroxide on the manganese-catalyzed reaction was negligible because under these experimental

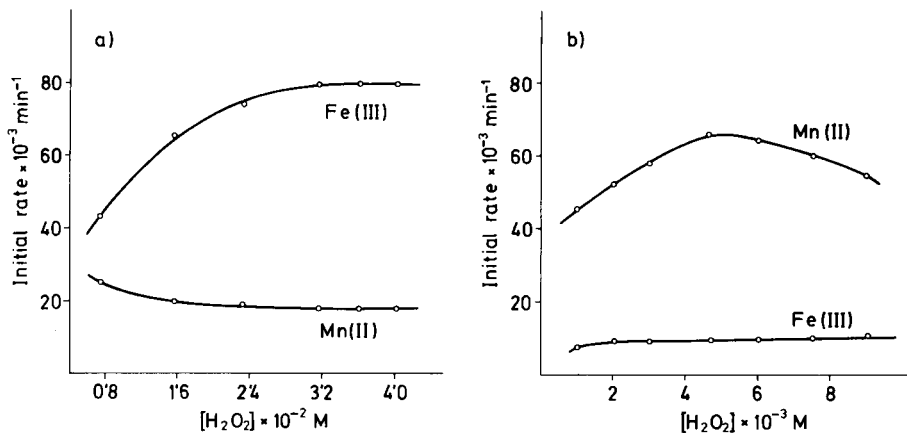


Fig. 3. Influence of hydrogen peroxide on iron and manganese catalysis. (a) Procedure 1, $7 \times 10^{-5} \text{ M HBTS}$; (b) Procedure 2, $1.1 \times 10^{-4} \text{ M HBTS}$. Other experimental conditions as in Fig. 2.

conditions manganese catalysis is greatly suppressed. A suppression of catalysis is shown by iron in Procedure 2 (Fig. 3b). However, the catalytic action of manganese(II) shows a maximum at 4.6×10^{-3} M hydrogen peroxide and therefore this value was selected for further study (0.5 ml of 0.3% hydrogen peroxide solution). In the range $1.0\text{--}4.6 \times 10^{-3}$ M hydrogen peroxide, the partial order is $1/4$ and at higher concentrations, $-1/2$.

The influence of ammonia concentration was also important. In Procedure 1, the initial rate of the iron-catalyzed reaction is proportional to the square root of ammonia concentration up to 0.5 M and, at higher values, the reaction rate remains constant (Fig. 4a); 1.5 ml of 3.2 M ammonia (0.5 M in a final volume of 10 ml of solution) is regarded as optimal. The effect of ammonia on the catalytic action of manganese was negligible. Figure 4(b) shows a lack of effect of ammonia on the iron catalysis, but its effect on manganese catalysis was at a maximum at 0.32 M, as is used in Procedure 2 (1 ml of 3.2 M ammonia solution). From the log-log plot, the partial orders are $1/4$ for ammonia concentrations >0.32 M, and -1 for lower concentrations.

The influence of pH on the fluorescence/time curves was examined at a fixed initial concentration of ammonia by the addition of dilute hydrochloric acid or sodium hydroxide. In the conditions for Procedure 1, the difference between the initial rates of the two catalyzed reactions is constant at $\text{pH} > 11.6$ (Fig. 5a) and therefore this value is recommended. The iron catalysis shows an order of reaction of -1 with respect to the hydrogen ion concentration at $\text{pH} 11.15\text{--}11.60$. In the experimental conditions for Procedure 2, at $\text{pH} < 10.77$, no kinetic dependence was found for either catalyzed reaction (Fig. 5b), thus $\text{pH} 10.77$ is recommended. However, the initial rate decreased for manganese catalysis at higher pH values. In this interval, a partial order of $3/2$ with respect to hydrogen ion concentration was found.

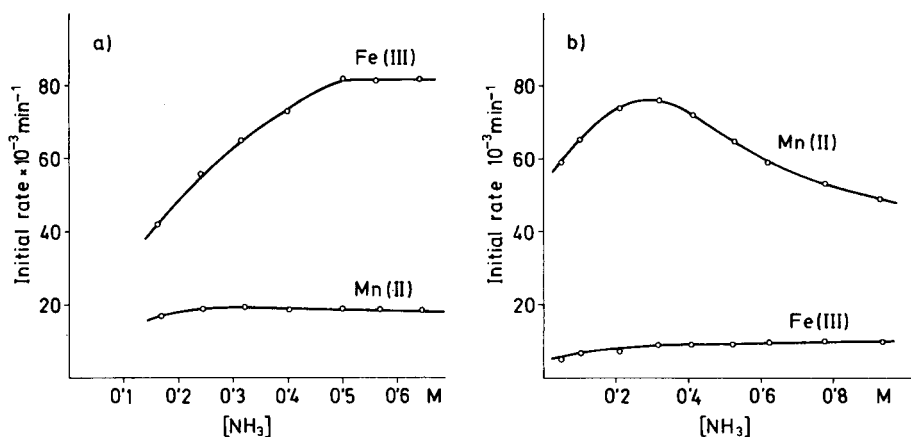


Fig. 4. Effect of ammonia on the two catalyzed reactions. (a) Procedure 1; (b) Procedure 2. Experimental conditions as in Fig. 3.

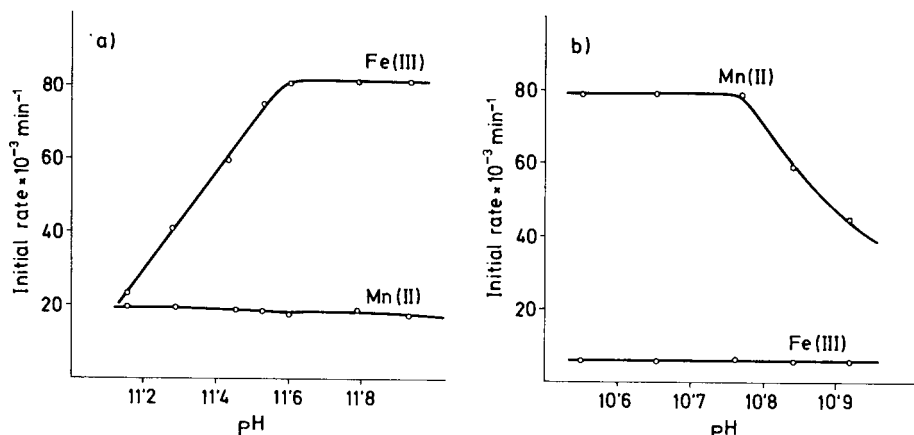


Fig. 5. Dependence of the reaction rate of iron and manganese catalysis on the pH. (a) Procedure 1; (b) Procedure 2. Conditions as in experimental procedures.

The difference in the pH values used in the two experimental procedures gives the best differentiation of iron and manganese.

Variation of ionic strength up to 1 M had no influence on the fluorescence/time curves of either catalyzed reaction in Procedure 1. However, in Procedure 2, there was an effect at ionic strengths >0.4 M. Therefore, in both Procedures, 2 ml of 2.5 M potassium chloride was added to a 10-ml volumetric flask ($\mu = 0.5$ M) in order to control the ionic strength. In the conditions of Procedure 1, the ethanol concentration strongly affected the iron catalysis, but not that of manganese. Because the differences between the initial rates of the two catalyzed reactions remained constant at ethanol concentrations $\geq 25\%$, this value was used in this procedure. The effect of ethanol on the iron catalysis was discussed previously [9]. In Procedure 2, variations in the ethanol concentration of up to 50% did not affect the rate of the manganese-catalyzed reaction. In this case, because the iron catalysis is greatly suppressed, the ethanol concentration does not appreciably affect its reaction rate.

Rate equations

The various kinetic dependences indicated above are summarized in Table 1. The following rate equations are operative for the simultaneous determination of iron and manganese

$$\text{Procedure 1: } d[\text{HBTS}]_{\text{ox}}/dt = k_1[\text{HBTS}][\text{NH}_3]^{1/2}[\text{Fe}^{3+}] + k_2[\text{Mn}^{2+}]$$

$$\text{Procedure 2: } d[\text{HBTS}]_{\text{ox}}/dt = k_3[\text{H}_2\text{O}_2]^{1/4}[\text{NH}_3]^{1/4}[\text{Mn}^{2+}] \\ + k_4[\text{HBTS}]^{-2}[\text{Fe}^{3+}]$$

where $k_1 \dots k_4$ are the conditional rate constants and $[\text{HBTS}]_{\text{ox}}$ is the concentration of the fluorescent product.

TABLE 1

Summary of kinetic data: partial orders of reaction under the recommended conditions

Species	Concentration range	Partial orders		Species	Concentration range	Partial orders	
		Fe catalysis	Mn catalysis			Fe catalysis	Mn catalysis
<i>Procedure 1</i>				<i>Procedure 2</i>			
HBTS	$3-7 \times 10^{-5}$ M	1	0	HBTS	$0.5-1.1 \times 10^{-4}$ M	-2	0
H ₂ O ₂	$>3.2 \times 10^{-2}$ M	0	0	H ₂ O ₂	$1.0-4.6 \times 10^{-3}$ M	0	1/4
NH ₃	0.1-0.5 M	1/2	0	NH ₃	0.05-0.32 M	0	1/4
H ⁺	pH > 11.6	0	0	H ⁺	pH < 10.77	0	0
Fe ³⁺	10-60 ng ml ⁻¹	1		Fe ³⁺	10-170 ng ml ⁻¹	1	
Mn ²⁺	5-22 ng ml ⁻¹		1	Mn ²⁺	5-20 ng ml ⁻¹		1

Simultaneous determination of iron and manganese

Under the optimum conditions used in each Procedure, two linear calibration graphs are obtained for each catalyst separately. Table 2 lists the characteristics of these plots. From this table and taking into account that under the conditions of each Procedure no synergic catalytic effects are observed between iron and manganese, the following equations can be used for the simultaneous determination of iron and manganese

$$V_1 = 3.4 \times 10^{-3} [\text{Fe}^{3+}] - 5.8 \times 10^{-3} + 3.8 \times 10^{-3} [\text{Mn}^{2+}] + 6.5 \times 10^{-3}$$

$$V_2 = 9.7 \times 10^{-3} [\text{Mn}^{2+}] + 2.6 \times 10^{-3} + 3.5 \times 10^{-4} [\text{Fe}^{3+}] + 2.1 \times 10^{-3}$$

where V_1 and V_2 are the initial rates for Procedure 1 and 2, respectively, and the concentrations are in ng ml⁻¹. Thus, for a mixture of iron and manganese, a fluorescence/time curve is recorded under the conditions of each Procedure. From these, the values of V_1 and V_2 are determined and the concentrations of iron and manganese are calculated from the equations. A simple computer program in BASIC was used for the solution of these equations.

The results for various synthetic mixtures containing different amounts of iron(III) and manganese(II) are summarized in Table 3. Mixtures of these ions can be determined with manganese/iron ratios from 1:1 to 1:8 and between 1:1 and 1:2 for the iron/manganese ratio. These limits correspond to a relative error of $\leq 3\%$. These results are satisfactory because the content of iron in real samples is usually higher than that of manganese.

TABLE 2

Characteristics of the calibration graphs for the determination of iron and manganese

Metal ion	Procedure	Range (ng ml ⁻¹)	Slope (min ⁻¹ ng ⁻¹ ml)	Intercept (min ⁻¹)	Regression coefficient ($n = 9$)
Fe ³⁺	1	10-60	3.4×10^{-3}	-5.8×10^{-3}	0.999
	2	10-170	3.5×10^{-4}	2.1×10^{-3}	0.998
Mn ²⁺	1	5-22	3.8×10^{-3}	6.5×10^{-3}	0.998
	2	5-20	9.7×10^{-3}	2.6×10^{-3}	0.999

TABLE 3

Analysis of synthetic mixtures of iron(III) and manganese(II)

Mixtures taken ($\mu\text{g l}^{-1}$)		Found			
Iron	Manganese	Iron ($\mu\text{g l}^{-1}$)	Error (%)	Manganese ($\mu\text{g l}^{-1}$)	Error (%)
10.0	10.0	10.3	3.0	9.9	-1.0
20.0	10.0	19.8	-1.0	9.9	-1.0
40.0	10.0	40.3	0.8	10.0	0.0
60.0	10.0	58.6	-2.3	10.3	3.0
40.0	5.0	38.8	-3.0	4.9	-2.0
10.0	20.0	10.2	2.0	20.3	1.5

The mean values of results from 11 samples each containing 10 ng ml⁻¹ manganese and 20 ng ml⁻¹ iron gave the overall coefficient of variation of the method as $\pm 0.45\%$.

Study of interferences. A study was made to determine the tolerance limits for various ions that are commonly associated with iron and manganese in natural and synthetic mixtures. For a mixture of 20 ng ml⁻¹ iron(III) and 10 ng ml⁻¹ manganese(II), the maximum level of foreign ions studies was 2 $\mu\text{g ml}^{-1}$, except for aluminium(III) (5 $\mu\text{g ml}^{-1}$) because of the high content of this ion in the aluminium alloy examined. As can be observed in Table 4, the method suffers from few interferences. However, when amounts larger than those specified are added, bismuth, lead, molybdenum(VI), nickel, EDTA and cyanide give negative interferences and zinc, cobalt(II) and copper(II) give positive interference.

TABLE 4

Influence of foreign ions on the simultaneous determination of 20 ng ml⁻¹ iron(III) and 10 ng ml⁻¹ manganese(II)

Ion added	Tolerance limit ^a ($\mu\text{g ml}^{-1}$)	Ion added	Tolerance limit ^a ($\mu\text{g ml}^{-1}$)
Cu ²⁺	1	Hg ²⁺	2
Tartrate	2	V(V)	2
Citrate	2	Bi ³⁺	0.2
EDTA	0.02	Pb ²⁺	0.2
Oxalate	2	Zn ²⁺	0.5
F ⁻	2	Mo(VI)	0.1
CN ⁻	0.05	Cd ²⁺	2
SCN ⁻	2	Ni ²⁺	0.2
S ²⁻	2	Co ²⁺	0.5

^aDefined as the concentration of added ion causing an error of $< 3\%$.

TABLE 5

Simultaneous determination of iron and manganese in samples

Sample	Composition of sample		Composition found ^a	
	Fe	Mn	Fe	Mn
<i>Alloys^b</i>				
Aluminium alloy (B.A.S. No. 20b)	0.43 ^c	0.19 ^c	0.43 ± 0.01	0.19 ± 0.01
Copper alloy (B.A.S. No. 10g)	1.56 ^c	1.36 ^c	1.57 ± 0.01	1.37 ± 0.01
<i>Foodstuffs^d</i>				
Beer	0.52	0.35	0.52 ± 0.01	0.36 ± 0.01
Cheese 1	5.9	0.81	5.9 ± 0.1	0.81 ± 0.02
Cheese 2	3.9	0.80	3.9 ± 0.1	0.82 ± 0.02
<i>Soils</i>				
Soil 1	10.8	9.8	10.7 ± 0.5	9.9 ± 0.3
Soil 2	11.5	17.9	11.2 ± 0.5	17.5 ± 0.2
Soil 3	10.0	13.3	10.0 ± 0.4	13.2 ± 0.1

^aMean ± standard deviation of 5 complete determinations. ^bResults given as percentages. ^cCertificate values. ^dResults given in mg kg⁻¹.

Simultaneous determination of iron and manganese in samples

To test the reliability of the method, it was applied to the determination of iron and manganese in several samples of alloys, foodstuffs and soils. Table 5 shows the results obtained which, except for the alloys, were compared with results obtained by atomic absorption spectrometry. These data demonstrate the reliability of the proposed method for the simultaneous determination of iron and manganese in these samples.

This work was supported by the grant given by the C.A.I.C.Y.T. to Project No. 0248.

REFERENCES

- 1 P. A. Rodriguez and H. L. Pardue, *Anal. Chem.*, 41 (1969) 1376.
- 2 J. B. Worthington and H. L. Pardue, *Anal. Chem.*, 42 (1970) 1157.
- 3 K. B. Yatsimirskii and L. P. Raizman, *Zhur. Anal. Khim.*, 18 (1963) 829.
- 4 I. I. Alekseeva, L. P. Khachatryan, L. P. Ruzinov and L. M. Chemysova, *Zhur. Anal. Khim.*, 35 (1980) 60.
- 5 I. I. Alekseeva, L. P. Ruzinov, E. G. Khachatryan and L. M. Chemysova, *Izv. Vyssh. Uchebn. Zaved. Khim. Technol.*, 16 (1973) 1145.
- 6 C. M. Wolff and J. P. Schwing, *Bull. Soc. Chim. Fr.*, 5-6 (1976) 679.
- 7 I. I. Alekseeva and I. I. Nemzer, *Zhur. Anal. Khim.*, 25 (1970) 1118.
- 8 A. Moreno, M. Silva, D. Perez-Bendito and M. Valcarcel, *Talanta*, 30 (1983) 107.
- 9 A. Moreno, M. Silva, D. Perez-Bendito and M. Valcarcel, *Anal. Chim. Acta*, 157 (1984) 333.
- 10 A. Moreno, M. Silva, D. Perez-Bendito and M. Valcarcel, *Analyst*, (London), 108 (1983) 85.
- 11 A. Moreno, M. Silva and D. Perez-Bendito, *Anal. Lett.*, Part A, 16 (1983) 747.
- 12 P. P. T. Sah and T. C. Daniels, *Rec. Trav-Chim.*, 69 (1950) 1545.

DETERMINATION OF RARE-EARTH ELEMENTS, YTTRIUM AND SCANDIUM IN MANGANESE NODULES BY INDUCTIVELY-COUPLED ARGON-PLASMA EMISSION SPECTROMETRY

TERRY FRIES* and PAUL J. LAMOTHE

U.S. Geological Survey, Menlo Park, CA 94025 (U.S.A.)

JOSEPH J. PESEK

Department of Chemistry, San Jose State University, San Jose, CA 95136 (U.S.A.)

(Received 3rd October 1983)

SUMMARY

A sequential-scanning, inductively-coupled argon plasma emission spectrometer is used for the determination of the rare-earth elements, plus yttrium and scandium, in manganese nodules. Wavelength selection is optimized to minimize spectral interferences from manganese nodule components. Samples are decomposed with mixed acids in a sealed polycarbonate vessel, and elements are quantified without further treatment. Results for U.S. Geological Survey manganese nodule standards A-1 and P-1 had average relative standard deviations of 6.8% and 8.1%, respectively, and results were in good agreement with those obtained by other methods.

Inductively-coupled plasma emission spectrometry (i.c.p.e.s.) has become an accepted technique for the routine determination of elements in geological materials. Most reported applications focus on silicate materials [1, 2]. Specific applications to the determination of rare-earth and associated elements in similar geological matrices, usually involving separation by ion-exchange, have also been reported [3, 4].

Reports of rare-earth data in manganese nodules, based on determinations made by neutron activation (n.a.) and spark source mass spectrometry (s.s.m.s.), indicate relatively high concentrations of the rare earth elements [5–8]. The elevated abundances, the low detection limits of i.c.p.e.s. for the elements of interest, and the systematic selection of useful wavelengths and operating conditions should make it possible to make these determinations without separation or concentration prior to the measurement step for most of the elements of interest by this technique.

The complex i.c.p.e.s. spectrum provides a large number of potentially useful spectral lines for the quantitation of the rare-earth elements, yttrium and scandium [9–11]. Selection of wavelengths for the determination of these elements in manganese nodules included consideration of those spectral lines which provide useful limits of detection and require minimum corrections for background and spectral line overlap. The sequential instrument

used in this study allows neither the use of internal standards to correct for short-term variations nor simultaneous measurements of elements of interest and elements responsible for spectral interferences. Therefore, a sequential instrument would not be the instrument of choice for routine quantitation of rare-earth elements in manganese nodules. However, the ability to collect data at the rate of three to four wavelengths per minute was particularly attractive for this study.

Two methods of sample preparation are discussed, and the wavelength-evaluation protocol is outlined. The wavelengths selected, and the methods used for determining and applying correction factors for interferences are given. Finally, quantitative data obtained with this method applied to U.S.G.S. manganese nodule standards A-1 and P-1 are presented.

EXPERIMENTAL

Instrumentation

An ARL 35 000 sequential i.c.p. spectrometer was used. Options allowing saturation of nebulizer argon with water and washing of the nebulizer tip were used to reduce clogging of the nebulizer in processing solutions containing high total dissolved solids. An optional optical cut-off filter was also used to eliminate spectral interferences for wavelengths above 320.00 nm.

Additional instrumentation included a Gilson peristaltic pump for sample delivery and a Tylan mass flow controller for control of the argon flow to the nebulizer.

Sample dissolution techniques

Two methods of sample decomposition were investigated. In both methods, samples were dried at 120°C for 24 h before weighing.

The first method consisted of a mixed-acid ($\text{HNO}_3/\text{HClO}_4/\text{HF}$, 1 + 1 + 1) digestion of 1-g samples in teflon containers. The samples were placed in teflon beakers, and 10 ml of each acid was added in the order: nitric acid, perchloric acid (70%), hydrofluoric acid (40%). Care was taken to make sure that any organic matter had reacted completely with the nitric acid before the perchloric acid was added. The beakers were then covered and allowed to stand overnight on a hot plate at 100°C in a perchloric acid fume hood. The covers were removed, and the temperature was slowly increased to 225°C. When fuming had ceased, the beakers were removed from the hot plate. After cooling to room temperature, 10 ml of nitric acid and 10 ml of perchloric acid were added to each sample. The beakers were then returned to the hot plate and heated again at 225°C until fumes ceased to be evolved. Samples were cooled and 10 ml of 6 M hydrochloric acid was added. After gentle heating, a dark residue remained. Addition of 5 ml of 30% hydrogen peroxide dissolved this residue. Excess of peroxide was removed by gentle boiling; the solution was cooled and was diluted to 100 ml with water.

The second method of dissolution was based on an acid mixture (HCl/HNO₃/HF, 7 + 4 + 3) in sealed polycarbonate containers as described by Farrell et al. [12]. Approximately 0.5 g of each sample was placed in a 250-ml polycarbonate bottle. To each bottle, 5 ml of a mixture of hydrochloric and hydrofluoric acids (7 + 3) and 2 ml of nitric acid was added. The bottles were then sealed and allowed to stand in a boiling water bath for 30 min. After the bottles had been removed from the water bath, they were cooled in running water, the caps were removed, and 100 ml of 1.5% (w/v) boric acid solution was added to each bottle. The bottles were again sealed and returned to the boiling water bath for 30 min. The bottles were then removed from the bath and cooled. All samples were filtered as part of standard i.c.p. operating procedures to avoid clogging of the nebulizer.

Visual inspection of the solutions obtained by both procedures indicated virtually complete decomposition of the nodule samples available. To check the composition of any undecomposed material or material adsorbed during filtering, filter papers were dried and then ashed at 550°C. Approximately 3 mg of residue remained for either decomposition method. Residues were collected from several repetitions of the decomposition methods and d.c. arc spectroscopy was used to check for the elements of interest. The results indicated that even though some elements of interest were detected in the residues (La, Ce, Yb, Y), recoveries of greater than 99% can be expected from either dissolution procedure. Because the method with the polycarbonate pressure vessel involves less time, requires only standard hood space, and avoids the hazards involved in handling perchloric acid, this method was chosen for the remainder of this study.

Standard solutions

Standards were prepared from 1000 $\mu\text{g ml}^{-1}$ solutions obtained from commercial suppliers and had final concentrations of 1.5% H₃BO₃, 1.9% HCl, and 1.4% HNO₃. To avoid errors from impurities in the standards, single-element solutions were used for calibration. Multielement solutions were used for routine normalization of calibration curves.

RESULTS AND DISCUSSION

Operating conditions for the i.c.p. were optimized by first adjusting the observation height of the plasma to give the highest net signal above background for the elements of interest in aqueous solution. Plasma height was optimized with the nebulizer operating in a free uptake mode at the argon flow rates specified by the manufacturer. The peristaltic pump was then used to optimize the sample-uptake rate to provide the highest net signal consistent with reproducible data. Under the operating conditions listed in Table 1, the optimum sample delivery rate was 1.9 ml min⁻¹ (compared to 2.2 ml min⁻¹ for free uptake) with this nebulizer and spray chamber assembly.

TABLE 1

Operating conditions

<i>Plasma</i>		<i>Sample introduction system</i>	
Incident r.f. power	1.25 kW	Nebulizer	Meinhardt Model TR-30-A3
Reflected power	< 5 W	Spray chamber	Conical with impact ball
Coolant Ar flow	12.0 l min ⁻¹	Peristaltic pump	Gilson Minipuls 2
Sample Ar flow	1.0 l min ⁻¹	Pumping rate	1.90 ml min ⁻¹
Auxiliary Ar flow	0.7 l min ⁻¹		
Observation height above load coil	17 mm	<i>Spectrometer</i>	
Height of observation zone	8 mm	Type	1-m Czerny-Turner
		Grating	Ruled, 1200 grooves mm ⁻¹ , blazed for 300 nm
		Reciprocal linear dispersion	0.8 nm mm ⁻¹
		Slits	Entrance 20 μm × 3.5 mm, exit 20 μm
		Filters	Cut-off filter used for > 320.0 nm

Recent studies indicate that the freedom from matrix and ionization effects assumed for the i.c.p. may not be universal [13]. As a check for matrix effects arising from differences between samples and standards, background-corrected intensities for spiked samples were compared to background-corrected intensities for single-element aqueous standards. The solutions were prepared by placing aliquots of standard solutions in volumetric flasks and diluting to volume with a solution that had 1.5% H₃BO₃, 1.9% HCl, and 1.4% HNO₃ for the spiked standard matrix and with a manganese nodule solution for the spiked sample. Blank solutions were prepared in an identical manner by placing a volume of deionized water, equivalent to the volume of standard solution used for the element of interest, in a volumetric flask and diluting with H₃BO₃/HCl/HNO₃ or manganese nodule solution.

Triplicate measurements for each determination were made and net intensity ratios between sample and standards were calculated. Averaged over the 16 elements examined, net intensity ratio data indicated a general signal suppression in the manganese nodule solutions of approximately 4%. It should be noted that lutetium consistently showed 7% lower net intensity for the manganese nodule solution. The cause of this behavior is not known. Although a peristaltic pump was used for sample delivery, the lower intensities observed for the nodule solutions may be due in part to the effect of viscosity on nebulization, resulting in attenuation of signal intensity as observed by Greenfield et al. [14].

The choices of wavelengths to be used were based on: (a) a systematic consideration of detection limits, (b) expected elemental concentration in sample solutions, and (c) spectral interferences. Initial selection was made by first establishing expected concentration ranges of the trace elements of

interest, using previously published data of the elemental composition of typical manganese nodules [5–8]. These ranges of concentration were then compared with published detection limits for various wavelengths [10]. Lines with detection limits which indicated that quantitative results could be obtained in the estimated concentration ranges were chosen for further examination.

An estimated range of major element concentrations for manganese nodules was then established, again based on available data [15, 16]. These concentration ranges were then used to evaluate all wavelengths meeting the detection limit criteria by calculating an estimated spectral interference level based on Boumans' Critical Concentration Ratio (CCR) data [11]. If the estimated interference constituted more than 25% of the estimated analyte concentration for a given wavelength, that wavelength was rejected. On the basis of the above criteria, 70 wavelengths were selected for consideration.

However, none of the currently available references provides a comprehensive means of evaluating interference due to argon line overlap, molecular bands, line broadening, or background shifts caused by instrumental contributions. Therefore, each of the 70 lines was scanned over a ± 0.10 -nm range, once while aspirating water, once while aspirating a manganese nodule solution, and once for an aqueous standard. Final selection of wavelengths was based on a consideration of the spectral interferences and background levels observed in these scans. These optimal wavelengths, detection limits, and lower limits of quantification are listed in Table 2.

The selection process described ensures that the wavelengths chosen will be useful in the expected concentration ranges and that interferences will be

TABLE 2

Wavelengths selected for the determination of rare earths, yttrium and scandium in manganese nodules

Element	Wave-length (nm)	Detection limit ^a ($\mu\text{g ml}^{-1}$)	Lower limit of quantification ($\mu\text{g g}^{-1}$)	Element	Wave-length (nm)	Detection limit ^a ($\mu\text{g ml}^{-1}$)	Lower limit of quantification ^b ($\mu\text{g g}^{-1}$)
La(II)	408.671	0.008	5	Dy(II)	394.469	0.020	10
Ce(II)	456.236	0.063	40	Ho(II)	345.600	0.006	4
Pr(II)	406.282	0.047	30	Er(II)	349.910	0.012	8
Nd(II)	430.357	0.039	25	Tm(II)	346.220	0.008	5
Sm(II)	446.734	0.033	20	Yb(II)	328.937	0.001	1
Eu(II)	381.966	0.002	1	Lu(II)	261.542	0.001	1
Gd(II)	335.048	0.018	10	Sc(II)	361.384	0.001	1
Tb(II)	350.917	0.018	10	Y(II)	371.029	0.002	1

^aConcentration corresponding to three times the standard deviation of the blank. ^bConcentration in the manganese nodule corresponding to 10 times the standard deviation of the blank and a dilution factor of 200.

minimized for manganese nodules. However, the i.c.p. emission spectra of manganese nodules is so complex that interference-free lines for rare-earth elements, yttrium and scandium could not be found. To obtain correction coefficients for the spectral interferences present, 38 solutions each containing 1 mg ml⁻¹ of one of 38 different elements (Al, B, Ba, Ca, Ce, Co, Cr, Cu, Dy, Er, Eu, Fe, Gd, Ho, K, La, Lu, Mg, Mn, Mo, Na, Nd, Ni, P, Pb, Pr, Sc, Si, Sm, Sr, Tb, Ti, Tm, V, Y, Yb, Zn, Zr) were aspirated and the wavelengths selected above were scanned. The correction coefficients obtained by this method were of the same order of magnitude as would have been predicted by Boumans' CCR approach for wavelengths included in that compilation. All correction coefficients were calculated as the apparent analyte concentration ($\mu\text{g ml}^{-1}$) for each interfering element. Corrected concentrations were obtained by subtracting the contribution to apparent analyte concentration from interfering elements, from the apparent analyte concentration using the formula

$$C_{A, \text{corr.}} = C_{A, \text{apparent}} - c_1 C_{I1} - c_2 C_{I2} \dots - c_n C_{In}$$

where C_A is the analyte concentration, C_I is the interferent concentration, and c is the correction coefficient.

TABLE 3

Comparison of concentrations determined by neutron activation, spark-source mass spectrometry and i.c.p. emission spectrometry of U.S.G.S. manganese nodule standards A-1 and P-1

Element	Concentration ($\mu\text{g g}^{-1}$)							
	A-1				P-1			
	N.a. ^a	S.s.m.s. ^b	I.c.p. ^c	RSD ^c (%)	N.a. ^a	S.s.m.s. ^b	I.c.p. ^c	RSD ^c (%)
La	132.5	130	104	1.9	120	82	100	2.0
Ce	668	>300	760	1.7	289	280	310	3.5
Pr	—	23	<30	—	—	27	<30	—
Nd	85.3	94	81	2.5	112.8	110	124	1.6
Sm	20.9	21	18	11	30.4	28	20	15
Eu	4.48	4.8	4.3	2.3	6.57	6.8	7.0	2.9
Gd	26.5	22	29	6.9	29.4	24	21	19
Tb	4.87	3.8	<10	—	5.31	4.2	<10	—
Dy	—	22	20	25	—	25	28	18
Ho	—	5.3	5.8	12	—	5.1	6.5	12
Er	—	15	14.6	6.2	—	13	13.6	4.4
Tm	1.72	—	<5	—	1.77	—	<5	—
Yb	16.3	13.5	13.2	1.5	13.8	13	11.8	2.5
Lu	2.16	—	2.8	14	1.85	—	1.7	18
Y	—(115) ^d	—	97	2.1	—(89) ^d	—	75	2.7
Sc	11.23	—	10.8	1.9	9.47	—	9.3	3.2
	Average RSD(%) 6.8				Average RSD(%) 8.1			

^a See Ref. [8]. ^b See Ref. [7]. ^c This work. ^d Y determined by x.r.f. [8].

To demonstrate the application of the method, two manganese nodule reference samples (A-1 and P-1), prepared by Flanagan and Gottfried, were analyzed in triplicate. The averages and relative standard deviations for results are reported in Table 3 along with data obtained by n.a. and s.s.m.s.

The data in Table 3 indicate that the precision of data for Dy, Sm, Gd, and Lu is poor. This can be attributed to interference corrections which were larger than predicted by Boumans' CCR data and therefore contributed an uncertainty which was large in comparison to the final result. However, the average relative standard deviation of 6–8% is comparable to that estimated for s.s.m.s. (2–5%) or n.a. (1–5%) [17].

These data also show large discrepancies in measured concentrations for Sm, Gd, La, and Ce. For samarium and gadolinium, the large corrections noted above are probably responsible for most of the disagreement observed. However, the corrections on lanthanum and cerium were relatively small and could not have contributed significantly to the observed disagreement. The spread of values for lanthanum in P-1 and the incomplete data for cerium in A-1 make accepted values for these elements uncertain. Further studies of the samples for lanthanum and cerium by i.c.p.e.s. using the method of standard additions produced results in agreement with the i.c.p. data listed in Table 3. With these exceptions noted, the data indicate that results for yttrium, scandium and most of the rare-earth elements by i.c.p.e.s. are in reasonable agreement with results obtained by s.s.m.s. or n.a., without the use of separation or preconcentration procedures.

A complete listing of interelement interferences includes many not given by Boumans [11]. A compilation of interferences and correction coefficients used in this work is available from the author.

REFERENCES

- 1 M. A. Floyd, V. A. Fassel and A. P. D'Silva, *Anal. Chem.*, 52 (1980) 2168.
- 2 S. E. Church, *Geostand. Newsl.*, 5 (1981) 133.
- 3 J. N. Walsh, F. Buckley and J. Barker, *Chem. Geol.*, 33 (1981) 141.
- 4 J. G. Crock and F. E. Lichte, *Anal. Chem.*, 54 (1982) 1329.
- 5 D. Z. Piper, *Geochim. Cosmochim. Acta*, 38 (1974) 1007.
- 6 G. P. Glasby, R. R. Keays and P. C. Rankin, *Geochem. J.*, 12 (1978) 229.
- 7 P. C. Rankin and G. P. Glasby, in J. L. Bischoff and D. Z. Piper (Eds.), *Marine Geology and Oceanography of the Pacific Manganese Nodule Province*, Plenum Press, New York, 1979, pp. 684–685.
- 8 F. J. Flanagan and D. Gottfried, *USGS Professional Paper 1155*, 1980, pp. 1–39.
- 9 S. Nikdel, A. Massoumi and J. D. Winefordner, *Microchem. J.*, 24 (1979) 1.
- 10 R. K. Winge, V. J. Peterson and V. A. Fassel, *Appl. Spectrosc.*, 33 (1979) 206.
- 11 P. W. J. M. Boumans, *Line Coincidence Tables for Inductively Coupled Plasma Atomic Emission Spectrometry*, Pergamon, New York, 1980.
- 12 R. F. Farrell, S. A. Matthes and A. J. Mackie, *Report of Investigations*, Bureau of Mines, 8480, 1980.
- 13 M. W. Blades and G. Horlick, *Spectrochim. Acta, Part B*, 36 (1981) 861, 881.
- 14 S. Greenfield, H. McD. McGreachin and P. B. Smith, *Anal. Chim. Acta*, 84 (1976) 67.
- 15 J. L. Mero, *The Mineral Resources of the Sea*, Elsevier, New York, 1965, pp. 180–223.

- 16 D. S. Cronan, *Underwater Minerals*, Academic Press, New York, 1980, pp. 151–153; 340–350.
- 17 R. D. Reeves and R. R. Brooks, *Trace Element Analysis of Geological Materials*, Wiley, New York, 1978, pp. 291, 332.

Short Communication

STOPPED-FLOW KINETIC DETERMINATION OF GLUCOSE AND LACTATE WITH IMMOBILIZED ENZYMES

R. Q. THOMPSON^a and S. R. CROUCH*

Department of Chemistry, Michigan State University, East Lansing, MI 48824 (U.S.A.)

(Received 4th November 1983)

Summary. Kinetic procedures are described for the measurement of lactate and glucose with enzymes immobilized in the observation cell of a stopped-flow spectrophotometer. Kinetic data are obtained by two-point or multipoint methods with data acquisition over any time range desired. Glucose was quantified in a fixed-time mode with a linear range of 0–10 mM. Lactate was quantified in the range 0–50 μ M by obtaining the slope of the absorbance/time profile between 10 and 20 s after each reaction was initiated. Results for these two substrates in control sera are presented.

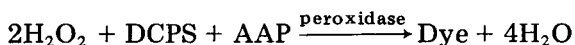
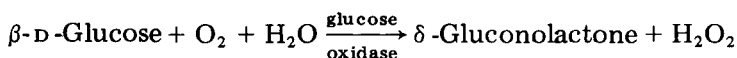
Immobilized enzymes have become popular as reagents for quantifying substrates in recent years because they combine the selectivity and sensitivity of aqueous enzymes with the convenience and low cost of reusable reagents [1]. Substrate determinations have been based on immobilized enzyme electrodes [1–4], open-tubular reactors in continuous flow manifolds [5–7], packed-bed reactors [8, 9], and enzymes immobilized on pipet tips [10] and stirring bars [11]. Most of these determinations are based on single-point, fixed-time kinetic methods [12]. Consequently, instrument response can be affected by any enzyme lag period so that non-zero intercepts and non-linear calibration plots can result. Single-point fixed-time methods are also inherently less accurate than multipoint methods. A stopped-flow instrument which allows continuous monitoring of immobilized enzyme-catalyzed reactions has been described [13]. The enzyme is immobilized on the inside of a nylon tube, which is inserted into the observation cell of a commercial stopped-flow instrument. The nylon insert serves as a combined observation cell and immobilized enzyme reactor and hereafter is referred to as the cell-reactor. After the proper reagents have been mixed and forced into the cell-reactor, the progress of the reaction can be monitored directly by spectrophotometry.

The determination of fixed-time absorbance changes and linear regression slopes of absorbance/time plots over any time range from milliseconds to minutes is possible. The initial time of data acquisition can be nonzero and set to a value subsequent to any lag phase. Reactions occur under static

^aPresent address: Department of Chemistry, Oberlin College, Oberlin, OH 44074, U.S.A.

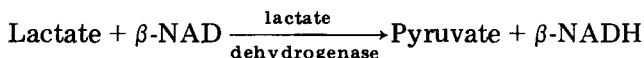
conditions and, therefore, are influenced by substrate diffusion [13]. This is also advantageous, because diffusional limitations often extend the linear range for substrate concentration. This communication describes evaluation of the system for kinetic methods for two clinically important substrates, glucose and lactate. Fixed-time conditions were used for the glucose procedure whereas the lactate results were obtained from rates calculated by linear regression of the absorbance/time data. The instrument allows calculation of the initial reaction rate by two-point methods (fixed-time, variable-time) or multi-point methods [12]. Results for glucose and lactate in control sera are reported.

The Trinder method [14, 15] for glucose with glucose oxidase was adopted. The reactions involved are



where DCPS is 2,4-dichlorophenolsulfonate, and AAP is 4-aminoantipyrine. The absorbance of the dye product at 505 nm was monitored.

Lactate was quantified by measuring at 340 nm the absorbance of β -NADH (β -nicotinamide adenine dinucleotide, reduced form), produced in the reaction



An alkaline solution and hydrazine were used to drive the reaction to completion.

Experimental

Reagents. All solutions were prepared in distilled-deionized water.

The glucose stock solution was prepared by dissolving 2.000 g of anhydrous β -D-glucose and 0.50 g of benzoic acid in about 0.75 l of water and then diluting to exactly 1 l; standard solutions were prepared by appropriate dilution of the stock, which was stable for a month at 4°C.

The method of Barham and Trinder [15] was used to prepare a solution of 2,4-dichlorophenolsulfonate. A portion (2 ml; ca. 0.2 mmol) of this solution, 10 mg (1670 U) of peroxidase (Type II, Sigma), and 10 mg (ca. 0.05 mmol) of 4-aminoantipyrine were dissolved in 75 ml of 0.1 M phosphate buffer, pH 6.4, and the solution was diluted to exactly 1 l with the pH 6.4 buffer; this reagent was prepared daily.

Purified L-lactic acid (0.960 g, Grade L-X, Sigma) and 0.125 ml of concentrated sulfuric acid were added to 500 ml of water and the resulting solution was diluted to exactly 1 l with water. This stock was diluted appropriately to give the desired standard solutions. The stock was stable for two weeks; standards were prepared daily.

For the preparation of β -NAD reagent, 10.0 g of tris(hydroxyamino)-

methane, 13.0 g of hydrazine sulfate, and 2.0 g of ethylenediaminetetraacetic acid were dissolved in water, the pH of the solution was adjusted to 9.6 with sodium hydroxide, and the solution was then diluted to 1.0 l with water; this buffer was stable for one week. In 40 ml of this buffer was dissolved 0.300 g of β -NAD (Grade III, Sigma) and the solution was diluted to exactly 50.0 ml to give a 8.5 mM β -NAD solution; this reagent was prepared daily.

Serum samples. The control sera (Monitrol and Pathotrol, Dade Division, American Hospital Supply) were reconstituted according to manufacturer's instructions. For glucose, protein precipitation was used. To a centrifuge tube, 1.00 ml of the serum, 1.50 ml of a 20 g l⁻¹ solution of barium hydroxide, and 1.40 ml of a 20 g l⁻¹ solution of zinc sulfate were added in that order. The solution was thoroughly mixed and then centrifuged for 3 min. The supernatant liquid was used directly in the measurement step. For lactate, 1.00 ml of the control serum was diluted to exactly 0.1 l with water, and the resulting solution was used in the measurement step.

Enzyme immobilization. The enzymes, glucose oxidase (Type II, Sigma) and beef muscle lactate dehydrogenase (Type X, Sigma), were immobilized on Type 6 nylon tubing (0.1 cm i.d., Portex Ltd.) by a procedure adapted from that described by Morris et al. [16]. The steps are summarized in Table 1. The tubing was washed with water between steps, and the triethyl-oxonium tetrafluoroborate (TOTFB) was rinsed out of the nylon with cold methanol after step 1. A 10 mg ml⁻¹ solution of glucose oxidase was prepared for use in step 4; the lactic dehydrogenase suspension was used directly as purchased. The completed reactor was filled with buffer (pH 6.4 phosphate) and stored at 4°C when not in use. Short (1.75 cm) segments of the tubing were cut for use in the stopped-flow observation cell as required.

Instrumentation. The design and operation of the stopped-flow instrument and filter photometer have been described in detail [13]. For the fixed-time measurements, the photometer output voltage was acquired by a sample-and-hold circuit [17] thirty seconds (V_1) and sixty seconds (V_2) after the reaction had been initiated (flow stopped). The change in absorbance (ΔA) over the 30-s interval was taken as $\Delta A = \log(V_1/V_2)$. This assumes no drift in the 100% T level during the interval. The times were chosen as a compromise between sample throughput and errors arising from mixing effects and enzyme lag periods.

TABLE 1

Summary of steps in the enzyme-immobilization procedure

Step	Reagent	Duration	Temp. (°C)
1	0.1 M TOTFB in CH ₂ Cl ₂	3 min	22
2	0.1 M Diaminobutane in pH 9.4 HCO ₃ ⁻ -buffer	4.5 h	22
3	5% (w/v) Glutaraldehyde in pH 8.0 phosphate-buffer	1.5 h	22
4	Enzyme in pH 6.85 phosphate buffer	18 h	4

The lactate data were acquired at 2 Hz by a microcomputer [13]. The photometer voltage corresponding to 100% T was taken as the first data point acquired. Linear regression of the absorbance/time data between 10 and 20 s gave reliable estimates of the initial slopes. A minicomputer (PDP-8/e, Digital Equipment Corporation) was used to calculate the absorbance values and to perform the regression.

Results and discussion

Glucose. Glucose standards and the DCPS/AAP/oxidase reagent were mixed rapidly and pushed into the cell-reactor by the stopped-flow instrument. The decrease in light intensity reaching the detector was monitored, and the change in absorbance was determined as described above. A blank was tested between each sample because the Trinder reagents and product adsorbed strongly to the nylon, producing some carry-over. Thus, the sample throughput was limited to a maximum of thirty samples per hour.

Figure 1 shows the glucose calibration graph; each data point represents five separate ΔA measurements taken over a four-day period with the same glucose oxidase reactor. The error bars represent the ranges of the five measurements. Linear least-squares statistics for the data are included in the figure legend. When the reactor was stored at room temperature for five days, a decrease in activity of about 8% was observed. The linear range of the method, 0–10 mM, covers the normal levels found in human blood serum (3.8–5.9 mM [18]). The Michaelis constant (K_m) of glucose for aqueous glucose oxidase is about 0.09 M [19], and, thus, the linear range extends beyond 0.1 K_m . The reason for the abnormally large linear region is most likely due to diffusional effects on the overall reaction rate [13].

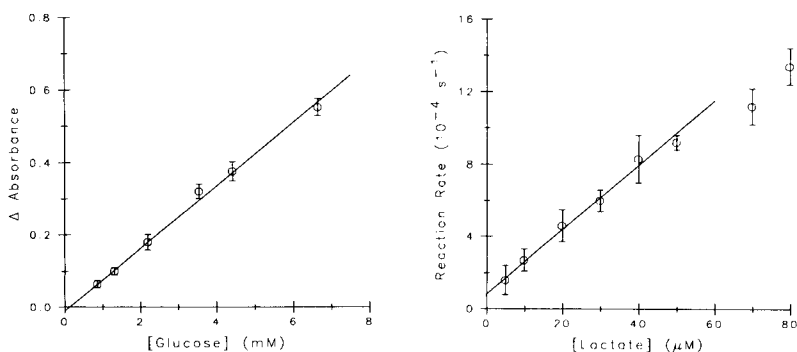


Fig. 1. Glucose calibration plot. Error bars represent range of values obtained at each concentration. Least-squares statistics are $\Delta A = (87 \pm 4) C(M) - 0.01 \pm 0.01$ with $S_{yx} = 1.04 \times 10^{-2}$ and $r = 0.998$.

Figure 2 shows the lactate calibration plot. The graph shows a linear relationship between Lactate concentration (μM) on the x-axis and Reaction Rate ($\cdot 10^{-4} s^{-1}$) on the y-axis. The x-axis ranges from 0 to 80 μM , and the y-axis ranges from 0 to 16. Data points are plotted with error bars, and a straight line is fitted to the data. The two highest data points at approximately 70 and 80 μM are excluded from the linear regression.

[Lactate] (μM)	Reaction Rate ($\cdot 10^{-4} s^{-1}$)
0	0
5	1.5
10	2.5
20	4.5
30	6.0
40	8.0
50	9.5
70	11.5
80	13.5

Fig. 2. Lactate calibration plot. Error bars represent ranges obtained at each concentration. Data at highest two lactate concentrations were excluded in linear regression calculations. Least-squares statistics are $\Delta A/\Delta t (s^{-1}) = (18 \pm 3) C(M) + (8 \pm 6) s^{-1}$ with $S_{yx} = 2.2 \times 10^{-5} s^{-1}$ and $r = 0.996$.

Three control sera were assayed. During the protein precipitation treatment, the samples were diluted 1:3.9; the resulting concentrations were still within the linear range. Table 2 compares the concentrations found by the proposed method with those given on the data sheets accompanying the samples. The largest difference occurred with samples of low glucose content. This error is possibly due to the presence of ascorbic acid, gentisic acid, and other reducing agents, which can interfere with peroxidase-catalyzed reactions [20, 21].

Lactate. Sets of lactate standards were tested with an immobilized lactic dehydrogenase reactor incorporated in the stopped-flow instrument. The β -NAD reagent mixed with water was used as a blank, and tested at the end of each set of standards. Sample carry-over was small with the lactate dehydrogenase system, apparently because little adsorption of reagents or products on the nylon occurred. Thus, the processing of 90 samples per hour was possible.

Five rate measurements were made at each concentration over a four-day period with the same reactor and the rates are plotted versus lactate concentrations in Fig. 2. Good linearity was obtained up to a concentration of 40 μ M; least-squares statistics are included in the figure legend. The intercept may have been caused by a slow nonenzymatic reaction, which was not compensated by the reagent blank.

The errors in the rate data are most likely due to fluctuations in the reactor activity. Sixty percent of the original enzyme activity remained after seven days of heavy use at room temperature. The linear range of the method, 0–50 μ M, extends to about 0.025 K_m (lactate) [13]. The linear range is not as wide as in the glucose determination because diffusional limitations are not as extensive. Lactic dehydrogenase is a less active enzyme than glucose oxidase, and the mass transport may be increased in the lactate study by coulombic attraction between the positively-charged nylon and the lactate anion.

Serum assays were done on 1:100 dilutions of the reconstituted controls

TABLE 2

Results for glucose and lactate in serum control samples

Serum type	No. of detns.	Expected (mM)	Found (mM)
<i>Glucose</i>			
Monitrol I	5	5.67	4 \pm 1
Pathotrol	6	12.8	13.3 \pm 0.3
Monitrol II	9	13.4	13.2 \pm 0.5
<i>Lactate</i>			
Monitrol II	6	1.8	2.1 \pm 0.2
Monitrol I	5	2.2	2.2 \pm 0.4
Monitrol I	6	3.1	3.2 \pm 0.6

with water in order to adjust the sample concentrations to within the linear range. Table 2 shows that the lactate concentrations in all three samples were accurately determined. The very slight positive errors may result from the small amount of soluble lactate dehydrogenase present in the sera.

The ability to follow absorbance versus time directly inside the reactor allows most of the kinetic methods classified previously [12] to be implemented. Potential errors caused by induction periods can be readily avoided. With a greater degree of automation, it should be feasible to improve the throughput of the system and make the method more practical. In addition, the stopped-flow system can be used for fundamental studies [13], such as determinations of Michaelis constants or the effects of inhibitors.

This work was partially supported by National Science Foundation grant no. CHE 79-26490 and by a Union Carbide Summer Fellowship (RQT).

REFERENCES

- 1 P. W. Carr and L. D. Bowers, *Immobilized Enzymes in Analytical and Clinical Chemistry*, Wiley, New York, 1980.
- 2 G. G. Guilbault and M. H. Sadar, *Acc. Chem. Res.*, 12 (1979) 344.
- 3 A. Attiyat and G. D. Christian, *Analyst (London)*, 105 (1980) 154.
- 4 W. J. Blaedel and R. C. Engstrom, *Anal. Chem.*, 52 (1980) 1691.
- 5 L. D. Bowers and P. W. Carr, *Anal. Chem.*, 48 (1976) 544A.
- 6 C. Horvath and H. Pederson, *Advances in Automated Analysis*, Technicon Int. Congress, 1976, Vol. 1, Mediad, Tarrytown, NY, 1977, pp. 86-95.
- 7 J. Růžička and E. H. Hansen, *Anal. Chim. Acta*, 106 (1979) 207.
- 8 C. H. Spink, *CRC Crit. Rev. Anal. Chem.*, 9 (1980) 1.
- 9 B. Danielsson, B. Mattiasson and M. Mosbach, *Pure Appl. Chem.*, 51 (1979) 1443.
- 10 P. V. Sundaram and S. Jarayaman, *Clin. Chim. Acta*, 94 (1979) 309.
- 11 J.-C. W. Kuan, S. S. Kuan and G. C. Guilbault, *Anal. Chim. Acta*, 100 (1978) 229.
- 12 H. L. Pardue, *Clin. Chim.*, 12 (1977) 2189.
- 13 R. Q. Thompson and S. R. Crouch, *Anal. Chim. Acta*, 144 (1982) 155.
- 14 P. Trinder, *Ann. Clin. Biochem.*, 6 (1969) 24.
- 15 D. Barham and P. Trinder, *Analyst (London)*, 97 (1972) 142.
- 16 D. L. Morris, J. Campbell and W. E. Hornby, *Biochem. J.*, 147 (1975) 593.
- 17 H. V. Malmstadt, C. G. Enke and S. R. Crouch, *Electronics and Instrumentation for Scientists*, Benjamin/Cummings, Menlo Park, CA, 1981, pp. 386-389.
- 18 N. W. Tietz, *Fundamentals of Clinical Chemistry*, W. B. Saunders, Philadelphia, PA, 1976, p. 1213.
- 19 V. Linek, P. Benes, J. Sinkule, O. Holecek and V. Maly, *Biotech. Bioeng.*, 22 (1980) 2515.
- 20 R. H. White-Stevens, *Clin. Chem.*, 28 (1982) 578.
- 21 J. A. Lott and K. Turner, *Clin. Chem.*, 21 (1975) 1754.

Short Communication

KINETIC SPECTROPHOTOMETRIC ASSAY OF SULFONAMIDES BY USE OF THE GRIESS REACTION AND A STOPPED-FLOW PROCEDURE

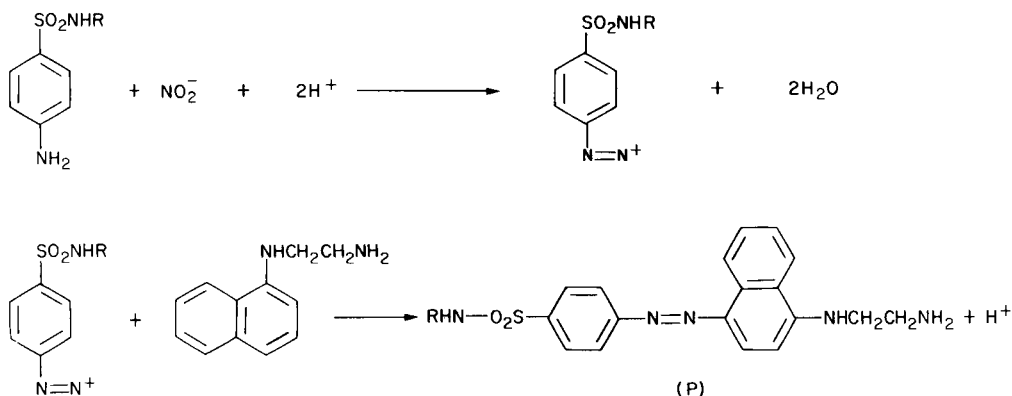
A. G. XENAKIS^a and M. I. KARAYANNIS*

Laboratory of Analytical Chemistry, University of Ioannina, Ioannina (Greece)

(Received 23rd September 1983)

Summary. The time interval between two preset levels of the output signal is used as a measure of the sulfonamide concentration. Nitrite and *N*-(1-naphthyl)ethylenediamine, are used as reagents, and $0.5\text{--}5 \times 10^{-5}$ M of a sulphonamide can be determined. The method is applied to urine.

Many methods for the determination of sulfonamides have been developed, most based on spectrophotometric [1], electrometric [2], bromometric [3], coulometric [4] or chromatographic [5] techniques. However most are complicated, and have limited sensitivities and accuracies. This communication describes the application of the Griess reaction in connection with an automatic kinetic method based on stopped-flow spectrophotometry [6] to determine sulfonamides. It is based on the color which is developed when a sulfonamide, nitrite and *N*-(1-naphthyl)ethylenediamine [7] are mixed in acid



The initial rate of formation of *P* is given by $dP/dt = (\epsilon b)^{-1} dA/dt$ where *A* is the absorbance, ϵ the molar absorptivity of the product *P*, and *b* is the

^aPresent address: Laboratoire de Chimie Physique Organique, ERA CNRS 222, Université de Nancy (France).

optical path length. Keeping the concentration of nitrite and *N*-naphthylethylenediamine constant and high relative to that of the sulfonamide gives a pseudo first-order reaction with respect to the sulfonamide. Under such conditions, the initial rate of formation of *P* is a linear function of the initial concentration of sulfonamide $[SA]_0$ in the sample, and therefore $(dE/dt)_0 = k_{obs}[SA]_0$, where $(dE/dt)_0$ is the initial slope of the reaction curve observed on the oscilloscope, k_{obs} is the observed rate constant, and E is the instrumental signal, which is proportional to absorbance. If Δt is the time taken by the signal to traverse a preset window between two values E_2 and E_1 ($\Delta E = E_2 - E_1$), $[SA]_0 = \Delta E/k_{obs}\Delta t = S/\Delta t$, where $S = E/k_{obs}$, is constant. This relation is the basis for the "reciprocal time method" [8] used also in this investigation.

Experimental

Instrumentation. A Durrum-Gibson stopped-flow spectrophotometer model D-110 equipped with a logarithmic photometric unit and a storage oscilloscope was used. The initial rate was measured by a system which consisted of an operational amplifier, a window comparator and a scaler, to measure the counts coming from a 1-MHz square-wave generator [9]. This system allows the time interval to be measured between two preset levels E_1 and E_2 of the amplified electric signal. The two levels are set so that they lie on the linear part of the reaction curve and if possible at its beginning. The pH of the solutions was measured by a Beckman Research Model pH-meter.

Stock solutions. These were prepared with deionized-distilled water from reagent-grade materials. *N*-(1-naphthyl)ethylenediamine (NEDA; 5×10^{-2} M) solution was prepared by dissolving 0.9413 g in 100 ml of water; it was kept in amber-coloured bottles. Sodium nitrite (1.000 M; Merck) and sulfanilamide (0.01 M) solutions were prepared in water. For the acetate buffer solution, 0.1 M solutions of acetic acid and sodium acetate were mixed to give a pH of 4.0.

The calibration solutions were prepared as follows. Solution A was an 0.100 M solution of sodium nitrite prepared by diluting 10 ml of stock solution to 100 ml. Solution B contained 2.5×10^{-3} M NEDA and various concentrations of sulfanilamide in the buffer solution, and was prepared by mixing the appropriate volumes of solutions B₁ and B₂ (below). For solution B₁, 1.0 ml of stock sulfanilamide and 5.0 ml of stock NEDA solutions were pipetted into a 100-ml volumetric flask and diluted to volume with buffer solution. The resulting concentrations were 1×10^{-4} M sulfanilamide and 2.5×10^{-3} M NEDA. For solution B₂, 5.0 ml of the stock NEDA solution was pipetted into a 100-ml volumetric flask and diluted to volume with buffer solution to give a 2.5×10^{-3} M solution.

Procedure. The settings of the instrument and the details of the measuring procedure are as given elsewhere [10]. All measurements were made at 545 nm and 25°C except where otherwise stated. One each of the two 20-ml

reservoir syringes and the two 2-ml syringes was filled with solution A or B. The ACTUATE button was pushed twice to clean the mixing cell. The reaction curve was displayed on the oscilloscope and, using the sensitivity scale and the zero offset knob, the linear part of the curve was located. On the comparator unit, a window $\Delta E = 50$ mV was set; this window could be moved to any level on the linear part of the reaction curve either by changing E_1 and E_2 or by using the zero offset of the photometric unit. For kinetic studies, the traces could be photographed with a Polaroid camera. By pushing the button ACTUATE, the time Δt appeared on the digital TIMER. Each run took about 10 s, therefore 5–10 repeated measurements could be made in 2 min with the same solutions, to give a reliable mean value of Δt . By plotting $(\Delta t)^{-1}$ against concentration of sulfonamide, a calibration graph was constructed, with slope S .

Standard addition procedure. Into four 50-ml volumetric flasks were pipetted 10 ml of urine, 2.5 ml of NEDA solution and 50, 100, 150 and 200 μl of the stock solution of sulfanilamide. The mixtures were diluted to 50 ml with acetate buffer and measured as above. No change in pH was observed.

Results and discussion

Effect of reagents on the reaction rate. The effects of pH and the concentrations of nitrite and NEDA on the reaction rate were studied. The effect of pH at constant concentrations of nitrite, NEDA and sulfanilamide (0.1 M, 2.5×10^{-3} M and 2×10^{-5} M, respectively) is shown in Fig. 1; the slope of

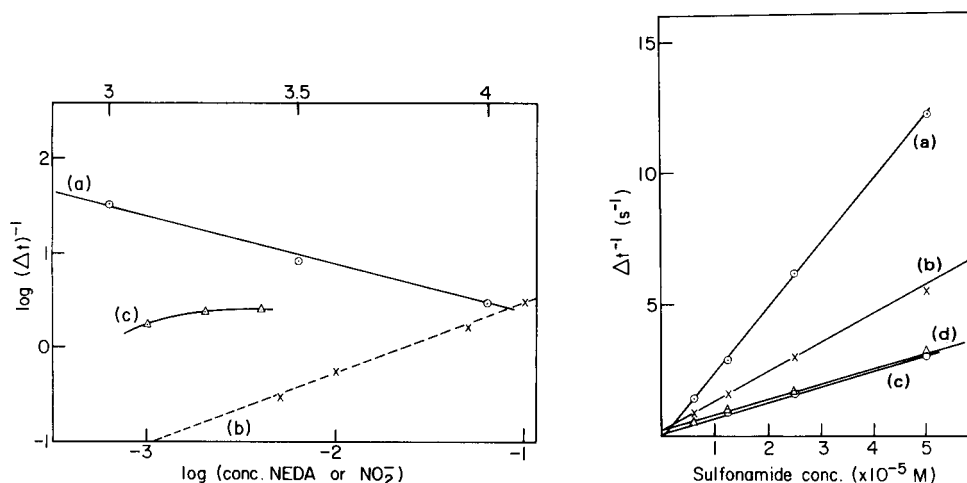


Fig. 1. Effect of the concentrations of different reagents on the reaction rate: (a) pH; (b) nitrite; (c) *N*-(1-naphthyl)ethylenediamine.

Fig. 2. Calibration graphs for the determination of: (a) sulfanilamide; (b) Sulfadimidine (sulfomethazine); (c) Gantrisin; (d) Bactrimel.

the linear graph is almost -1 . Figure 1 also shows the effect of nitrite concentration on the reaction rate, for 2.5×10^{-5} M sulfanilamide and 2.5×10^{-3} M NEDA at pH 4; the slope is 1.0. Finally, Fig. 1 shows the effect of NEDA concentration at 2.5×10^{-5} M sulfanilamide and 0.1 M nitrite at pH 4. Therefore the reaction is first and minus first-order with respect to nitrite and hydrogen ions, respectively. The NEDA dependence is not simple, probably because of parallel reactions with nitrite. For analytical work, the most suitable conditions are pH 4.0, 0.1 M nitrite and 2.5×10^{-3} M NEDA.

Phthalate and acetate buffers were investigated, the latter giving the better sensitivity and reproducibility. Phthalate buffers interfered, probably because of the reaction of phthalate with nitrite.

Calibration and accuracy. The calibration graphs obtained were linear. The linear regression equations [11] were $(\Delta t)^{-1} = -0.136 + 249\,400[\text{SA}]$ ($r = 0.9999$) for the recommended procedure and $(\Delta t)^{-1} = 0.367 + 84\,000[\text{SA}]$ ($r = 0.9999$) for the phthalate-buffered solutions (where SA is sulfanilamide, and the concentration is in mol l^{-1}).

To check the accuracy of the method, solutions of sulfanilamide of known concentrations were processed. The results are shown in Table 1. The mean error is 2.4% in acetate buffer and 1.0% in phthalate buffer.

Determinations of different sulfonamides. Four sulfonamides in tablets or powders were investigated by the proposed method. The samples were water-soluble and according to the specifications of the manufacturers they were at least 90% pure. The four compounds were sulfanilamide, sulfadimidine (or sulfamethazine; 2-sulfanilamide-4,6-dimethylpyrimidine), Gantrisin (3,4-dimethyl-5-sulfanilamide-isoxazole), and Bactrimel (3-sulfanilamide-4-methylisoxazole). Figure 2 shows the linear calibration graphs obtained. Each sulfonamide shows a different reaction rate under the experimental conditions, so that the method can be applied only to samples containing one sulfonamide. Sulfanilamide, the simplest molecule, has the fastest reaction, probably because the other sulfonamides are sterically hindered.

TABLE 1

Determination of sulfanilamide in aqueous solutions

$(\Delta t)^{-1}$ (s^{-1})	Sulfanilamide conc. ($\times 10^{-5}$ M)		Error (%)	$(\Delta t)^{-1}$ (s^{-1})	Sulfanilamide conc. ($\times 10^{-5}$ M)		Error (%)
	Taken	Found ^a			Taken	Found ^a	
<i>Phthalate buffer</i>				<i>Acetate buffer</i>			
0.900	0.625	0.64	-2.6	1.44	0.625	0.64	-2.7
1.427	1.250	1.25	0.2	2.89	1.250	1.21	3.6
2.46	2.500	2.49	0.5	6.20	2.500	2.55	-1.9
4.58	5.000	5.04	-0.8	12.3	5.000	4.92	1.6
			Mean 1.0				Mean 2.4

^aMean of 5 runs.

Assay of a sulfonamide in urine. Attempts to apply the above calibration graphs for the determination of a sulfonamide in urine failed. The method gave low results probably because interfering substances decreased the reaction rate. Better results were obtained by using the standard addition method. The linear graph obtained is described by $(\Delta t)^{-1} = 1.15 + 153\,000[\text{SA}]$. Its slope is less than that of curve (a) in Fig. 2, confirming the decreased reaction rate. The ratio of the slopes is 0.61. This value was found to be constant over many experiments, so that it can be used in conjunction with the calibration graph for aqueous solutions to determine sulfanilamide in urine, measuring only one sample instead of using the standard addition method. The intercept on the standard addition graph indicated the presence of 7.5×10^{-7} M sulfanilamide in the urine sample. This is ten times lower than the concentration in the most dilute calibration solution.

Conclusions

The proposed method has several advantages. The measurement time is very small. It takes less than 30 min to calibrate the apparatus, prepare the sample and measure the standard solutions and the sample. In the conventional spectrophotometric method, just the development of the colour can take over 2 h [1, 12]. The handling of the instrument is quite simple and the measurement can be fully automated. Concentrations as low as 5.0×10^{-6} M can be measured, with satisfactory accuracy and reproducibility. Samples which show colour and matrix interferences, such as biological fluids and pharmaceutical products, can be analysed.

REFERENCES

- 1 H. Haury and E. Naumann, *Arzneim. Forsch.*, 16 (1966) 1090.
- 2 E. J. Nicholas, *Aust. J. Pharm.*, 28 (1947) 868.
- 3 H. Wojahn, *Sueddtsch. Apoth. Ztg.*, 88 (1948) 395.
- 4 K. Sykut, *Ann. Univ. Mariae Curie-Sklodowska, Sect. AA*, 6 (1951) 47.
- 5 P. Heinänen, L. Tuberman and L. Rämö, *Farm. Aikak.*, 3 (1954) 56.
- 6 Q. H. Gibson, *Discuss. Faraday Soc.*, 17 (1954) 137.
- 7 A. C. Bratton and E. K. Marshall, *J. Biol. Chem.*, 128 (1939) 537.
- 8 H. V. Malmstadt, C. J. Deaney and E. A. Cordos, *CRC Crit. Rev. Anal. Chem.*, 2 (1972) 559.
- 9 C. E. Efstathiou and T. P. Hadjiioannou, *Anal. Chim. Acta*, 89 (1977) 55.
- 10 M. I. Karayannis, *Anal. Chim. Acta*, 76 (1975) 121.
- 11 M. I. Karayannis, *Treatment, Evaluation, Presentation of Analytical Data* (in Greek), Athens, 1978, pp. 166, 188.
- 12 K. Kacl and J. Wagner, *Chem. Listy*, 43 (1949) 141.

Short Communication

SEPARATION AND DETERMINATION OF INORGANIC ANIONS BY MEANS OF ION-PAIR CHROMATOGRAPHY

ALESSANDRO MANGIA*

Istituto di Chimica Generale ed Inorganica, Università di Parma, Via M. D'Azeglio 85, 43100 Parma (Italy)

MARIA TERESA LUGARI

Istituto di Chimica Farmaceutica e Tossicologica, Università di Parma, Via M. D'Azeglio 85, 43100 Parma (Italy)

(Received 26th September 1983)

Summary. Bromide, iodide, bromate, iodate, thiocyanate, nitrite and nitrate can be separated by means of ion-pair chromatography on a reversed-phase column (LiChrosorb RP2), using the tricaprylylmethylammonium ion (Aliquat-336) as counter ion in an acetonitrile-water mobile phase. The elution is monitored with an ultraviolet detector at 205 and 226 nm. The detection limits are in the low nanogram range.

Among the wide range of methods available for the determination of inorganic anions, chromatographic procedures based on ion-exchange mechanisms have been widely studied in recent years [1–7]. Ion pairing has also been used, though the difference between the mechanism of ion exchange and that of ion pairing is not always well defined. Ion-pair chromatography was first used for the separation of organic anions, such as sulphonates, carboxylates and phenols [8–11], and was later extended to inorganic anions [12] by using cyano phases [12, 13], RP-18 [14, 15] and Partisil-ODS [16] columns; hexadecyltrimethylammonium, tetrabutylammonium or *N*-octylamine salts were used as counter ion in the mobile phase.

In a program of research on the use of high-performance liquid chromatography (h.p.l.c.) for inorganic and organometallic analysis [17] and in particular on the application of the ion-pair chromatography [18], simple and effective procedures were sought for the determination of inorganic anions such as nitrate, nitrite and halides with particular reference to environmental and food analysis. The goal was to use ordinary commercial h.p.l.c. equipment in a system which would provide good sensitivity and precision without requiring concentrated buffer solutions or long equilibration time.

This paper reports the results obtained in the separation of some inorganic anions with tricaprylylmethylammonium ion as counter ion in the mobile phase and a LiChrosorb RP-2 bonded phase.

Experimental

The liquid chromatograph was a Perkin-Elmer series 3B, equipped with a variable-wavelength spectrophotometric detector LC75 and a Rheodyne 7105 injection valve. The LiChrosorb RP-2 column (Merck) was 25 cm \times 4 mm i.d. with a mean particle size of 10 μ m.

The mobile phases were prepared from solutions of tricaprylylmethylammonium chloride (Aliquat-336) in water-acetonitrile, adjusted with hydrochloric, sulphuric or phosphoric acid to the apparent pH 6. The concentration of the quaternary ammonium salt (Fluka) ranged between 0.05 and 0.8% (w/v). The percentage of acetonitrile was 40–60% (v/v). Twice-distilled water was used and the ammonium salt solutions were filtered on HWAP-047 membranes (Millipore).

Aqueous solutions of the inorganic anions were prepared from the corresponding potassium salts. Acetonitrile (h.p.l.c. grade) and inorganic salts were from Carlo Erba (Milan).

The injected sample volumes ranged between 2 and 10 μ l; the u.v.-detection was set at 205 or 226 nm, and an 8- μ l flow cell was used.

Results and discussion

Various combinations of eluents and columns were tested to establish the best reversed-phase system. From the points of view of the time required for equilibration, efficiency and reproducibility, the best results were obtained with tricaprylylmethylammonium ion as counter ion in a water-acetonitrile mobile phase on a LiChrosorb RP-2 column.

Table 1 shows the chromatographic data (corrected retention volumes, resolution factors, number of theoretical plates) for seven inorganic anions. Figure 1(a) shows the corresponding separation, obtained with a 40/60 (v/v) acetonitrile-water mixture containing 0.5% (w/v) of the quaternary ammonium salt at pH 6. The elution order is different from that obtained on a Partisil ODS-3 column with octylamine and phosphoric acid in the mobile phase [16].

The retention volumes are strongly influenced by the percentage of acetonitrile in the mobile phase. Figure 1(b) shows the effect of changing the mobile phase to a 50/50 (v/v) acetonitrile-water mixture with the same

TABLE 1

Chromatographic data for the separation of inorganic anions on a reversed-phase column^a

	NO ₂ ⁻	IO ₃ ⁻	BrO ₃ ⁻	Br ⁻	NO ₃ ⁻	I ⁻	SCN ⁻
V _R (cm ³)	2.4	6.0	10.8	16.0	25.6	60.8	96.8
k'	0.7	2.1	3.9	5.7	9.1	21.7	34.6
N	1025	1120	1155	2300	3870	4810	5020

^aConditions as given for Fig. 1(a). $V'_R = V_R - V_0$; $k' = (V_R - V_0)/V_0$; $N = 16(V/w)^2$.

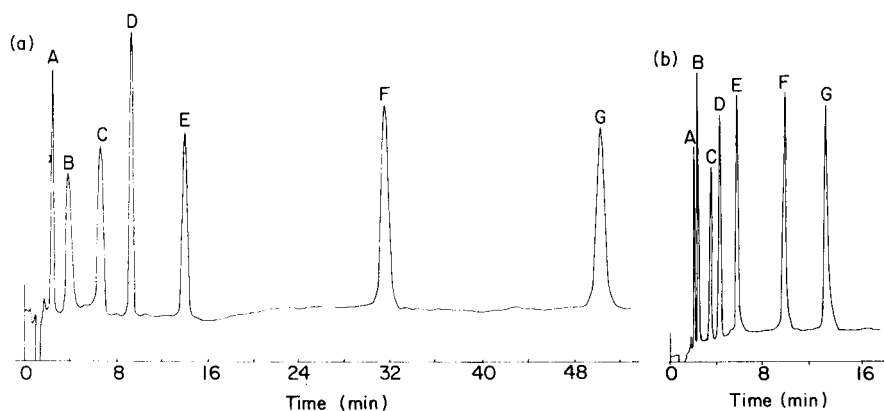


Fig. 1. Separation of some inorganic anions on a reversed-phase column. (a) LiChrosorb RP-2 column; mobile phase, acetonitrile-water (40/60 v/v), containing tricaprylmethylammonium chloride (0.5% w/v); flow rate $2 \text{ cm}^3 \text{ min}^{-1}$, pressure 7.2 MPa; detector at 205 nm. Peaks: (A) NO_2^- ; (B) IO_3^- ; (C) BrO_3^- ; (D) Br^- ; (E) NO_3^- ; (F) I^- ; (G) SCN^- . (b) As for (a) except that the acetonitrile-water ratio was 50/50 (v/v).

content of quaternary ammonium salt. This behaviour suggests that gradient elution, with the content of acetonitrile increasing from 40% to 50%, would provide an efficient separation of all anions within an acceptable period. Variation of the acetonitrile content in this range does not significantly influence the baseline. However, it is always possible to set the conditions to obtain efficient and fast separations of mixtures which are of interest from a practical point of view, e.g., nitrate/nitrite, bromide/iodide/thiocyanate, and bromate/iodate (Fig. 2).

The dependence of the retention volumes on the composition of the mobile phase was tested for some compounds, by varying alternately the percentages of acetonitrile and of the quaternary ammonium salt in the

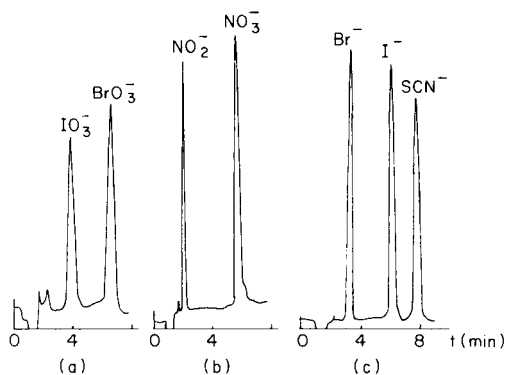


Fig. 2. Separation of some anions by using mobile phases with different acetonitrile-water solution ratios: (a) 40/60; (b) 50/50; (c) 60/40.

mobile phase. The dependence of the corrected retention volumes on the percentage of the quaternary ammonium salt and of acetonitrile are shown in Fig. 3 for nitrate, nitrite and bromide ions.

The effects of different counter ions in the mobile phase were tested by adding phosphate or sulphate to the usual mobile phase in a stoichiometric amount of ca. 2:1 of the added anion with respect to the chloride from Aliquat-336. The ionic strength was always maintained at 0.1 (by adding KCl to the initial mobile phase) and the pH was adjusted to 6 with the corresponding acid. The results of these tests, with a 50/50 water-acetonitrile (Table 2), indicate decreased retention times compared to those obtained with the original mobile phase. This behaviour does not appear to be related to the nature of the added counter ion.

To establish the concentration range in which these anions could be determined by the proposed system, the dependence of the detector response on the amount of compounds injected was checked for nitrate, nitrite, bromide and iodide. The eluents were monitored at 205 nm, except for iodide, for which 226 nm was used. Aqueous solutions of the salts in the concentration range 5–40 mg l⁻¹ were injected; sample volumes were 2–10 μ l so that the

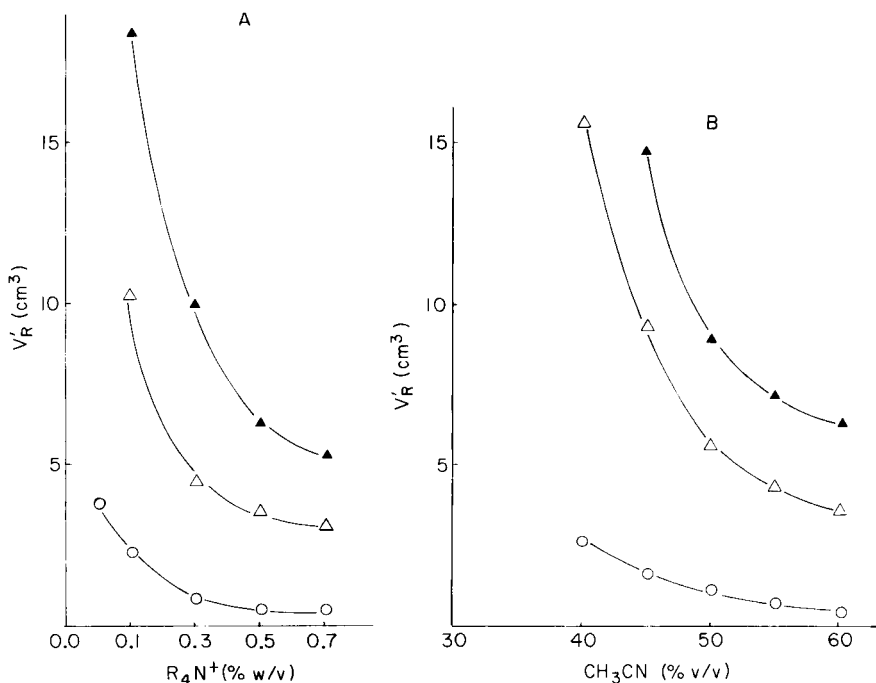


Fig. 3. Dependence of the corrected retention volumes on (A) the percentage of quaternary ammonium salt in a mobile phase containing 60% acetonitrile, and (B) the percentage of acetonitrile in a mobile phase containing 0.5% quaternary ammonium salt. (o) nitrite; (Δ) bromide; (▲) nitrate.

TABLE 2

Corrected retention volumes in presence of different salts in the mobile phase for 50/50 acetonitrile-water with 0.5% (w/v) quaternary ammonium salt at ionic strength 0.1

Salt added	Retention volume (cm ³)						
	NO ₂ ⁻	IO ₃ ⁻	BrO ₃ ⁻	Br ⁻	NO ₃ ⁻	I ⁻	SCN ⁻
—	1.2	1.6	4.0	5.6	8.8	17.2	24.4
KCl	1.0	1.2	1.6	2.8	4.2	9.2	13.0
K ₂ SO ₄	1.0	1.2	1.6	2.4	4.2	10.2	15.2
KH ₂ PO ₄	1.0	1.2	1.8	2.8	4.6	10.4	15.4

amounts of compounds injected ranged between 10 and 200 ng. The injections were repeated five times at each concentration level. The dependence of the response was linear for the examined compounds up to about 100 ng of ion injected (Fig. 4). For higher quantities the data fit parabolic curves.

The detection limits are in the low nanogram range. For nitrate, the detection limit (S/N = 3) is about 2 ng (expressed as NO₃⁻), which is of the same order of magnitude as that obtained using ion chromatography with a conductivity detector [14]. These detection limits, together with the high efficiency of the separation, render ion-pair reversed-phase chromatography a method of practical interest for the determination of some inorganic anions. Although the u.v. detector limits some applications, it reduces the possibility of interference from common anions such as chloride and sulphate.

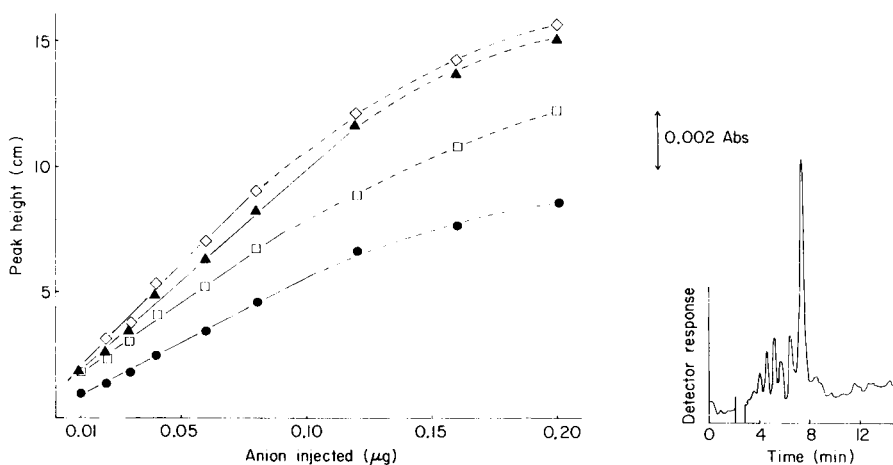


Fig. 4. Dependence of the detector response on the mass of compound injected: (\diamond) I⁻; (\blacktriangle) NO₃⁻; (\square) Br⁻; (\bullet) NO₂⁻. Detection at 226 nm for I⁻ and 205 nm for the other anions. Each point corresponds to the average of 5 values. Recorder sensitivity, 2×10^{-3} absorbance/cm.

Fig. 5. Chromatogram of tap water (2 μ l) containing about 10 mg l⁻¹ nitrate. Mobile phase, 45/55 (v/v) acetonitrile-water solution; other conditions as in Fig. 1(a).

In many cases, samples may be analyzed without preliminary treatment. As an example, Fig. 5 shows a chromatogram obtained by injecting 2 μ l of tap water containing about 10 mg l⁻¹ nitrate. Further research on the application of ion-pair h.p.l.c. in food and environmental analysis is in progress.

This work was financially supported by the Ministero della Pubblica Istruzione (Italy).

REFERENCES

- 1 H. Small, T. S. Stevens and W. C. Bauman, *Anal. Chem.*, 47 (1975) 1801.
- 2 A. W. Wolkoff and R. H. Larose, *Anal. Chem.*, 47 (1975) 1003.
- 3 D. T. Gjerde, J. S. Fritz and G. Schmuckler, *J. Chromatogr.*, 186 (1979) 590.
- 4 T. Kamiura and T. Masanobu, *Anal. Chim. Acta*, 110 (1979) 117.
- 5 D. T. Gjerde, G. Schmuckler and J. S. Fritz, *J. Chromatogr.*, 187 (1980) 35.
- 6 M. J. Van Os, J. Slanina, C. L. De Ligny, W. E. Hammers and J. Agterdenbos, *Anal. Chim. Acta*, 144 (1982) 73.
- 7 R. J. Williams, *Anal. Chem.*, 55 (1983) 851.
- 8 S. Eksborg, P.-O. Lagerstroem, R. Modin and G. Schill, *J. Chromatogr.*, 83 (1973) 99.
- 9 J. C. Kraak and J. F. K. Huber, *J. Chromatogr.*, 10 (1979) 333.
- 10 K.-G. Wahlund, *J. Chromatogr.*, 115 (1975) 411.
- 11 S. P. Sood, L. E. Sartori, D. P. Wittmer and W. G. Haney, *Anal. Chem.*, 48 (1976) 796.
- 12 R. N. Reeve, *J. Chromatogr.*, 177 (1979) 393.
- 13 J. P. de Kleijn, *Analyst (London)*, 107 (1982) 223.
- 14 I. Molnar, H. Knauer and D. Wilk, *J. Chromatogr.*, 201 (1980) 225.
- 15 B. B. Wheals, *J. Chromatogr.*, 262 (1983) 61.
- 16 N. E. Skelly, *Anal. Chem.*, 54 (1982) 712.
- 17 A. Mangia, G. Predieri and E. Sappa, *Anal. Chim. Acta*, 136 (1983) 278 and references therein.
- 18 A. Mangia and M. T. Lugari, *J. Liq. Chromatogr.*, 6 (1983) 1073.

Short Communication

QUANTITATIVE LIQUID CHROMATOGRAPHY OF METAL TETRAALKYLS

HARMON B. ABRAHAMSON* and RICHARD A. VANDERPOOL

Department of Chemistry, University of Oklahoma, Norman, OK 73019 (U.S.A.)

(Received 12th September 1983)

Summary. A method is presented for determining the concentrations of transition metal tetraalkyls in alkane solutions by liquid chromatography. Data for standard solutions of tetranorbornylchromium and tetranorbornyltitanium demonstrate that concentrations are determined with an average error of 2–3%. The method is particularly useful in the determination of disappearance quantum yields for the metal alkyls.

In investigations of the photochemistry of tetraalkyl metal complexes [1, 2] the determination of concentrations of complexes, and thus of disappearance quantum yields, by electronic absorption spectroscopy is difficult in some cases and impossible in others. The primary cause of these problems is the partial or total overlap of absorption spectra of products with those of the starting material. What is desired is a method that separates the photoproducts from the starting material so that the concentration of remaining starting material can be determined. Chromatography on alumina serves to separate photoproducts from unreacted metal tetraalkyls. This observation has allowed the development of a simple liquid chromatographic method for the separation and quantitation of metal alkyl complexes, the details of which are reported here.

Experimental

Materials. The tetranorbornyl complexes of titanium and chromium (norbornyl = [2.2.1]-bicyclohept-1-yl) were prepared by literature methods [3–5]. Reagent-grade hexane was purified by repeated stirring over one tenth its volume of concentrated sulfuric acid, changing the acid daily, until no coloration of the acid was observed. The hexane was then washed twice with distilled water, neutralized with aqueous sodium hydrogencarbonate, and washed once more with distilled water. The washed hexane was dried with anhydrous calcium or magnesium sulfate and stored over molecular sieves. Other materials were reagent grade, used as received.

Liquid chromatography. The system consisted of a Milton-Roy/LDC miniPump, normally run at 60 ml h⁻¹, followed by a damping coil of 15 m of 0.5-mm i.d. teflon tubing. A two-position six-port Rheodyne valve with a

110- μ l sample loop was used for sample injection. The glass column (3-mm i.d., 50-cm long) was packed with Whatman HC Pellumina 40- μ m pellicular alumina. A Chromatronix 220 ultraviolet detector was used, usually at 280 nm and 0.32 absorbance range. Detector output was recorded on a Houston Instruments Omniscrite recorder and peak heights were measured by hand. The eluting solvent was normally hexane containing 0.03% methanol (v/v). Long periods of use resulted in a loss of resolution and some peak broadening. Column performance could be restored by a regime involving flushing the column at normal pumping speed with chloroform for 30 min, followed by methanol for up to 2 h, followed by chloroform again for about 30 min, and finally returning to the normal eluting solvent.

Procedures. Normal class A volumetric glassware was used for all volume measurements except for microliter volumes which were measured with a GK-PDP-75 positive displacement micropipettor with volume adjustable from 1 to 100 μ l (precision $\pm 0.4\%$ at 50 μ l, $\pm 0.3\%$ at 100 μ l). Because of the photosensitivity of the metal alkyls, all operations were done under reduced light. For a calibration run, four samples were prepared by pipetting a volume (usually 5.00 ml) of standard solution (2.4×10^{-3} M anthraquinone and 0.03% (v/v) methanol in hexane) into four tubes containing, respectively, one, two, three, and four aliquots (usually 50.0 μ l) of a hexane solution of the metal tetranorbonyl complex of known concentration. Four aliquots of each sample were injected, and the average of the four peak-height ratios was used in the calculation. Each pair of peaks took 5–10 min to elute, depending on conditions. An identical set of blanks was also run, substituting aliquots of hexane for the metal alkyl solution. Once the standards and blanks had been run, single or double aliquots of metal alkyl solutions of unknown concentration were mixed with the same volume of anthraquinone standard solution as above, and four aliquots of each sample were also injected.

Calculations. The metal tetralkyls were observed to follow Beer's Law; consequently, peak height is a measure of the concentration of metal complex. The inverse of the blank-corrected peak height ratio (complex/standard) was plotted vs. the ratio of standard and sample aliquot volumes for a series of dilutions of a sample of known concentration. The slope and y-intercept obtained from a linear regression [6] of this standardization plot was then used to calculate values for metal complex concentrations for other injections. Standardization should be done daily because peak shape and separation can vary.

Results and discussion

Transition metal tetranorbonyls, $M(\text{NOR})_4$, $M(\text{C}_7\text{H}_{11})_4$ ($M = \text{Ti}, \text{Cr}$) are stable homoleptic alkyls [7] of interest for their spectroscopic and photochemical properties [1, 2]. Because these complexes present a very nonpolar hydrocarbon exterior to the surrounding solvent, they are very soluble in nonpolar solvents such as hexane. This nonpolar character also means

that they have very short retention times on polar absorbents, e.g., an R_f of 0.94 on neutral alumina for $\text{Cr}(\text{NOR})_4$ eluted with hexane (t.l.c.).

In contrast, the photoproducts of these complexes are very reactive and bind nearly irreversibly to alumina (R_f of 0.00 for elution with methanol). The $\text{M}(\text{NOR})_4$ complexes both have substantial absorptions in the ultraviolet [1, 2] so that detection at either 254 or 280 nm can be used.

Because the hexane used to prepare samples sometimes contained some impurity that also eluted close to the solvent front, blank injections were normally run to correct for this contribution. The impurity peak height was typically 1–5% of the sample peak height. Negative blanks were possible when the eluting solvent was less pure than that used for the samples.

Initial experiments were done using pure distilled hexane as the solvent and benzophenone as the standard. When this combination was used, increasing retention times and peak broadening were observed for the standard after a few dozen injections. After some experimentation, the behavior was stabilized with a solvent mixture of 0.03% methanol (by volume) in hexane. This solvent system gives too short a retention time for benzophenone, hence anthraquinone was adopted for use with this solvent.

To test the method, solutions of tetranorbornylchromium in hexane with concentrations of 3.68×10^{-3} M (A), 4.10×10^{-4} M (B), and 2.85×10^{-3} M (C) were prepared. Four different dilutions of each standard solution were made to mimic solutions of unknown concentrations. In addition, a solution of tetranorbornyl titanium in hexane with a nominal concentration of 1.5×10^{-3} M (4.5 mg in 7 ml) (D) was prepared and serially diluted. Because of the errors associated with the dilution process, actual concentrations for the members of this series were determined from absorbance data. These samples were processed as described above by using the most concentrated member of the series as the "known". Figure 1 illustrates the separation and reproducibility achieved. Comparisons of the concentrations calculated from the chromatographic data to those known from the dilution volumes show averages of the absolute values of the relative errors of 1.2, 3.9, and 2.1% for series A, B, and C, respectively.

The absorbance of each solution was also measured and concentrations of $\text{M}(\text{NOR})_4$ were calculated from previously measured [1, 2] molar absorptivities. Comparisons of the concentrations calculated from chromatographic data to those calculated from absorbance data show averages of the absolute values of the relative errors of 1.5, 2.9, 3.5, and 2.4% for series A–D, respectively.

The method is sensitive to the choice of the "known" concentration of metal alkyl in the calculation of the absolute concentration of the sample. However, agreement between prepared (x) and determined (y) concentrations is very good as illustrated by the least-squares equation for series A ($y = 1.01 \pm 0.02 x - 0.01 \pm 0.05$ with $r = 0.9998$ and standard error = 0.038) which is typical of all series with the x value based on dilution (except series D) and absorbance measurements. Because relative changes in

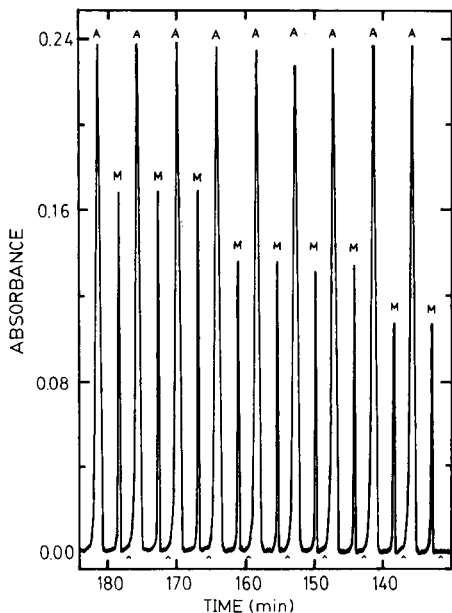


Fig. 1. Portion of a typical chromatogram showing peaks for three different dilutions in series D. Peaks M are for the metal complex, $\text{Ti}(\text{NOR})_4$, and peaks A are for the standard, anthraquinone. Chart speed is 0.25 cm min^{-1} . \wedge indicates injection.

concentration are most important in the intended use of this method it works well for that purpose. Errors inherent in this method are much less than those ($\approx 15\%$) inherent in quantum yield studies. Accordingly, the method is acceptable for its intended use. Quantum yields determined by this method agree well with those determined by absorbance methods in cases where both can be used. For example, for the disappearance of $\text{Cr}(\text{NOR})_4$ under 366-nm irradiation, quantum yields of $0.033\text{--}0.037 \text{ mol/einstein}$ were obtained from absorbance data [1], and values of $0.035\text{--}0.044 \text{ mol einstein}^{-1}$ were obtained from the chromatographic data.

We thank C. L. Blank for advice on liquid chromatography and for the use of the u.v. detector, and B. D. Card for assistance in the search for a suitable standard/solvent combination. Partial funding for this work was provided by grants from the Petroleum Research Fund, administered by the American Chemical Society, and from the University of Oklahoma Research Council.

REFERENCES

- 1 H. B. Abrahamson and E. Dennis, *J. Organomet. Chem.*, 201 (1980) C19.
- 2 H. B. Abrahamson and M. E. Martin, *J. Organomet. Chem.*, 238 (1982) C58.
- 3 B. K. Bower and H. G. Tennent, *J. Am. Chem. Soc.*, 94 (1972) 2512.
- 4 B. K. Bower, U.S. Pat. 3,705,916 (1972).
- 5 G. A. Ward, B. K. Bower, M. Findlay and J. C. Chien, *Inorg. Chem.*, 13 (1974) 614.
- 6 P. R. Bevington, *Data Reduction and Error Analysis for the Physical Sciences*, McGraw-Hill, New York, 1969, Ch. 5.
- 7 P. J. Davidson, M. F. Lappert and R. Pearce, *Chem. Rev.*, 76 (1976) 219.

Short Communication

**HIGHLY-RESOLVED FLUORESCENCE SPECTROMETRY OF PYRENE
ON A THIN-LAYER CHROMATOGRAPHIC PLATE**

J. W. HOFSTRAAT, M. ENGELSMA, W. P. COFINO, G. Ph. HOORNWEG,
C. GOOIJER and N. H. VELTHORST*

*Department of General and Analytical Chemistry, Free University, De Boelelaan 1083,
1081 HV Amsterdam (The Netherlands)*

(Received 16th September 1983)

Summary. Site-selection spectroscopy, by using suitable laser line excitation, gives spectra of molecules on thin-layer chromatographic plates comparable in quality to Shpol'skii spectra. Pyrene is investigated as a model compound.

The selectivity of luminescence methods in analytical chemistry is generally hampered by the low resolution of the spectra. The width of the luminescent band can be hundreds of cm^{-1} because of site inhomogeneity in liquid and solid solutions. There are, however, possibilities to achieve line narrowing in broadened electronic spectra. In the Shpol'skii method, suitable n-alkane matrices are used to obtain quasi-line spectra [1, 2]. Broadening of the bands is strongly diminished by reducing the number of possible sites which the guest molecules may occupy. The Shpol'skii effect has been employed by several groups as an analytical tool, e.g., to determine polynuclear aromatic hydrocarbons in various matrices [3, 4]. The Shpol'skii method provides a selective and relatively simple way of analyzing samples containing various organic compounds. The quasi-lines are already observed at 77 K for most molecules [5] and excitation can be done with ordinary broad-band sources. There are, however, a number of disadvantages to this method. Many compounds of analytical interest have limited solubility in n-alkanes. This problem can be partly overcome by using vapor deposition of a mixture of the compound involved and an n-alkane [6]. Another complication is presented by the matrix-dependence of the spectra, which thwarts quantification of the results [7]. Finally, there are various compounds that do dissolve in a Shpol'skii matrix but do not yield quasi-line spectra.

Another approach makes use of the laser as excitation source to obtain highly resolved spectra in glassy matrices at low temperatures (around 50 K or less) [8, 9]. With this so-called site-selection or fluorescence line-narrowing technique, the inhomogeneous broadening of the luminescent bands can be greatly decreased by selecting a restricted number of sites. In many cases, highly resolved spectra emerge. Apart from quasi-lines, broader bands (usually denoted as zero-phonon lines and phonon wings, respectively) are also observed in the spectra. These broader bands lie to the long wavelength

side of the quasi-lines and are due to creation or annihilation of matrix phonons [9]. Generally, the site-selection effect only occurs when the $s_1 \rightarrow s_0$ transition is probed. The simplest spectra are produced by excitation in the 0-0 absorption area of the fluorescent state. If the wavelengths of the laser line and the 0-0 transition of the molecule involved do not match well, more sites or even relatively broad bands appear in the spectrum. The site-selection technique seems to be more versatile than the Shpol'skii method because a large variety of matrices can be employed, e.g., ethanol [8], glycerol/water [10], diethyl ether/chloroform [11], and even polymer films [12]. Analytical applications of site-selection spectrometry have been reported by, for example, Brown et al. [10] and Bykovskaya et al. [13]. Of course, additional selectivity can be introduced by varying the excitation wavelength of the laser. Furthermore, use can be made of time-resolved detection [14], or advantage can be taken of the polarization properties of the exciting or the emitted light [15] or both.

Site-selection spectrometry has more potential than the Shpol'skii method, but needs more sophisticated apparatus. The potential detection limit, however, is lower in the latter technique, because all the molecules are divided over a few sites, whereas in fluorescence line-narrowing only one of the many sites is probed. Yang et al. [16] and Maple et al. [6] have combined laser excitation and Shpol'skii spectrometry to obtain an extremely sensitive quantitative method.

In this communication, the combination of site-selection spectrometry and thin-layer chromatography (t.l.c.) is introduced. Colmsjö and Stenberg [17] have reported an off-line method, in which vacuum sublimation of polycyclic aromatic hydrocarbons separated by t.l.c. was followed by detection using the Shpol'skii effect. The method provides an opportunity for investigating the compounds directly on t.l.c. plates. Pyrene is chosen as a model compound as it has been the subject of extensive studies with site-selection [10, 18], Shpol'skii [4, 19, 20] and laser-excited Shpol'skii spectrometry [6, 21]. Apart from site-selection spectra of pyrene on a t.l.c. plate, the Shpol'skii and "conventional" site-selection spectra are also recorded and used for comparison. The results obtained indicate that the new technique provides a selective method, which adds an extra dimension to conventional t.l.c.

Experimental

The experimental set-up of the site-selection procedure has been described in detail [12]. For excitation, the 363.8-nm line of the coherent argon ion laser was employed. In the Shpol'skii measurement the sample was excited by the radiation of a 450-W xenon lamp passed through a 0.5-m Bausch and Lomb grating monochromator. The emitted light was separated with a Jobin-Yvon HR 1000 1-m monochromator and detected with an EMI 9558-QA photomultiplier in a photon-counting configuration (Ortec Brookdeal 5-C-1). All measurements were made at about 20 K. The samples were cooled in a Model 20 cryocooler (Cryogenic Technology). This temperature was reached within 30 min.

Pyrene (Goldmarke; EGA-Chemie) was used as received; no fluorescing impurities were detected. A silica gel t.l.c. plate (Merck Kieselgel 60H, without fluorescence indicator) was employed; $20\ \mu\text{l}$ of a solution of pyrene in diethyl ether (10^{-5} – 10^{-6} M) was put on the plate so that spots with a diameter of about 1.5 mm were formed. A diethyl ether/3-methylpentane (4:3, v/v) mixture was used for elution over a distance of 8 cm; pyrene had an R_F value of 0.8. The plate was air-dried before measurement. In one experiment, the thin-layer plate was sprayed with n-heptane after elution and drying (Baker Analyzed). The Shpol'skii spectrum of pyrene was recorded in n-octane (Baker Analyzed; >99.7%). Pyrene was dissolved in 3-methylpentane (Janssen Pharmaceutica; >99%) for the conventional site-selection experiment in a glassy matrix. All solvents were used as received; they showed no fluorescence in the wavelength region of interest.

Results and discussion

The fluorescence spectrum of pyrene in a Shpol'skii matrix (n-octane) is reported in Fig. 1. The spectrum clearly offers a fingerprint of pyrene with prominent characteristic lines at 404, 452, 732, 801, 1065, 1104, 1404 and

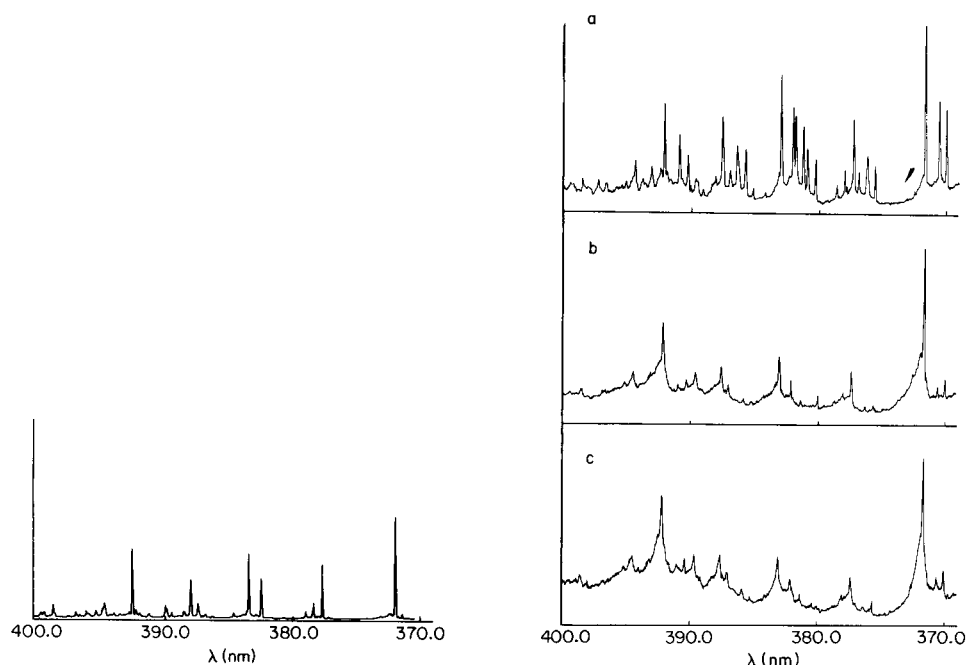


Fig. 1. Fluorescence spectrum of 1.0×10^{-3} M pyrene in n-octane with broad-band excitation ($T = 20$ K, $\lambda_{\text{ex}} \approx 320$ nm).

Fig. 2. Site-selection fluorescence spectra of pyrene ($T = 20$ K, $\lambda(\text{laser}) = 363.8$ nm): (a) in 3-methylpentane (1.0×10^{-3} M); (b) on a dry t.l.c. plate (590 ng of pyrene); (c) on a t.l.c. plate sprayed with n-heptane (59 ng of pyrene).

TABLE 1

Comparison of the site-selection fluorescence spectrum of pyrene on a t.l.c. plate with the Shpol'skii spectrum and the site-selection spectrum in 3-methylpentane

λ (nm)	Shpol'skii		3-Methylpentane ^a			T.l.c. plate		
	$\bar{\nu}$ (cm ⁻¹)	Assignment	λ (nm)	$\bar{\nu}$ (cm ⁻¹)	Assignment	λ (nm)	$\bar{\nu}$ (cm ⁻¹)	Assignment
372.03	26880	0-0	370.04	27024	0-0''	371.75	26900	0-0
			370.64	26980	0-0'			
			371.73	26901	0-0			
377.70	26476	0-404	377.43	26495	0-406	377.47	26492	0-408
378.39	26428	0-452	378.11	26447	0-454	378.14	26445	0-455
382.44	26148	0-732	382.18	26166	0-735	382.22	26163	0-737
383.45	26079	0-801	383.11	26104	0-799	383.24	26093	0-807
387.37	25815	0-1065	387.09	25834	0-1067	287.09	35834	0-1066
387.96	25776	0-1104	387.67	25795	0-1106	387.70	25793	0-1107
392.53	25476	0-1404	392.23	25495	0-1406	392.20	25497	0-1403
394.76	25332	0-1548	394.51	25348	0-1553	394.56	25345	0-1555

^aOnly the vibrational bands corresponding to the 0-0 transition are listed.

1548 cm⁻¹ from the 0-0 transition, which predominantly appears in one site. The spectral data for the most intense lines are collected in Table 1.

Figure 2 shows site-selection spectra of pyrene. In Fig. 2(a) the site-selection spectrum of pyrene in a 3-methylpentane glass is depicted; here three sites of more or less comparable strength appear, because excitation is induced at several hundred cm⁻¹ from the 0-0 region. Unfortunately, a more suitable laser line was not available; the argon ion laser produces only a limited number of lines. The intensity distribution over the three sites is matrix- and temperature-dependent. The site-selection spectrum of pyrene in glycerol/water or glycerol/ethanol at 4.2 K gives one prominent and two very weak sites [10]. The fluorescence line-narrowing spectrum of pyrene on a t.l.c. plate (as shown in Figs. 2b and c) at 20 K also exhibits one strong and two weak sites, with the wavelengths shown in Fig. 2(a).

It is known that generally more than one site appears when excitation is effected in the vibrational band region [9]; vibrational bands belonging to different sites, but having about the same energy can be simultaneously excited. It is also possible that other sites are excited in their phonon wings. The intensity ratio between the zero-phonon line and the phonon wing is strongly temperature-dependent, because it is determined by the Debye-Waller factor [9].

The spectrum shown in Fig. 2(b) was recorded from a dry t.l.c. plate. The detection limit for this method is estimated to lie in the low nanogram region. Spraying the t.l.c. plate with n-heptane before the spectrometric step improves the signal-to-noise ratio by at least a factor of 10 (see Fig. 2c). Presumably, the n-heptane molecules cause the pyrene molecules to accumulate at the surface of the t.l.c. plate. It is possible that in the case of the sprayed plate, a combination of the Shpol'skii and site-selection effects is observed. Further investigations on this matter are in progress.

The spectral data are compared in Table 1. Apart from a slight red shift of the Shpol'skii spectrum with respect to the site-selection spectra and the different multiplet structures discussed above, the general features of the spectra are similar; the same vibrational transitions, in relative intensity as well as in vibrational energy (with respect to the 0—0 transition), are observed. The small red shift of pyrene in n-octane compared to a solution in tetrahydrofuran has also been reported by Kirkbright and de Lima [22]. There can be no doubt about the fingerprint properties of the site-selection technique applied to thin-layer chromatography.

Conclusions

In principle, site-selection spectroscopy used in combination with thin-layer chromatography yields spectra of quality comparable to Shpol'skii spectra and to fluorescence line-narrowed spectra in glasses. Site-selection spectroscopy shows potential as a selective and sensitive detection technique in t.l.c. Sensitivity can apparently be improved by spraying the t.l.c. plate with a suitable solvent. Research on other compounds, as well as various types of t.l.c. plates and spraying agents is in progress.

U.A.Th. Brinkman is gratefully acknowledged for his critical reading of the manuscript.

REFERENCES

- 1 E. V. Shpol'skii, A. A. Il'ina and L. A. Klimova, Dokl. Akad. Nauk SSSR, 87 (1952) 935.
- 2 E. V. Shpol'skii, Soviet Phys. Usp., 5 (1962) 522.
- 3 G. F. Kirkbright and C. G. de Lima, Analyst, (London), 99 (1974) 338.
- 4 A. Colmsjö and U. Stenberg, Anal. Chem., 51 (1979) 145.
- 5 E. P. Lai, E. L. Inman, Jr. and J. D. Winefordner, Talanta, 29 (1982) 601.
- 6 J. R. Maple, E. L. Wehry and G. Mamantov, Anal. Chem., 52 (1980) 920.
- 7 R. J. Lukaszewicz and J. D. Winefordner, Talanta, 19 (1972) 381.
- 8 R. I. Personov, E. I. Al'shits and L. A. Bykovskaya, Opt. Commun., 6 (1972) 169.
- 9 R. I. Personov, in V. M. Agranovich and R. M. Hochstrasser (Eds.), Spectroscopy and Excitation Dynamics of Condensed Molecular Systems, North-Holland, Amsterdam, 1983.
- 10 J. C. Brown, M. C. Edelson and G. J. Small, Anal. Chem., 50 (1978) 1394.
- 11 Yu. V. Romanovskii, L. A. Bykovskaya and R. I. Personov, Biofizika, 26 (1981) 621.
- 12 W. P. Cofino, J. W. Hofstraat, G. Ph. Hoornweg, C. Gooijer, C. MacLean and N. H. Velthorst, Chem. Phys. Lett., 89 (1982) 17.
- 13 L. A. Bykovskaya, R. I. Personov and Yu. V. Romanovskii, Anal. Chim. Acta, 125 (1981) 1.
- 14 R. B. Dickinson, Jr. and E. L. Wehry, Anal. Chem., 51 (1979) 778.
- 15 J. R. Maple and E. L. Wehry, Anal. Chem., 53 (1981) 1244.
- 16 Y. Yang, A. P. D'Silva and V. A. Fassel, Anal. Chem., 53 (1981) 894.
- 17 A. Colmsjö and U. Stenberg, J. Chromatogr., 169 (1979) 205.
- 18 J. C. Brown, J. A. Duncanson, Jr. and G. J. Small, Anal. Chem., 52 (1980) 1711.
- 19 T. Ya. Gaevaya and A. Ya. Khesina, Zh. Anal. Khim., 29 (1974) 2225.
- 20 A. L. Colmsjö and C. E. Oestman, Anal. Chem., 52 (1980) 2093.
- 21 V. I. Vershinin, I. V. Kuzovenko, G. I. Baranov and A. M. Sizikov, Zh. Anal. Khim., 36 (1981) 981.
- 22 G. F. Kirkbright and C. G. de Lima, Chem. Phys. Lett., 37 (1976) 165.

Short Communication

SYNTHESIS OF A NEW TETRAZOLIUM SALT GIVING A WATER-SOLUBLE FORMAZAN AND ITS APPLICATION IN THE DETERMINATION OF LACTATE DEHYDROGENASE ACTIVITY

MASANOBU SHIGA*, MIKIHICO SAITO, KEIYU UENO and KENYU KINA

Dojindo Laboratories, 2861, Kengun-machi, Kumamoto-shi, 862 (Japan)

(Received 1st August 1983)

Summary. A pyridine analog of 3-(4,5-dimethyl-2-thiazolyl)-2,5-diphenyltetrazolium bromide was synthesized. The new reagent, 2-phenyl-3-(4,5-dimethyl-2-thiazolyl)-5-(4-pyridyl)tetrazolium bromide, gave a water-soluble formazan dye on enzymatic reduction and was applied in the spectrophotometric determination of lactate dehydrogenase ($0-84 \text{ mU ml}^{-1}$) in blood serum. The sensitivity ($\epsilon = 1.83 \times 10^4 \text{ l mol cm}^{-1}$ at 539 nm) was about 70% of that obtainable with nitrotetrazolium blue.

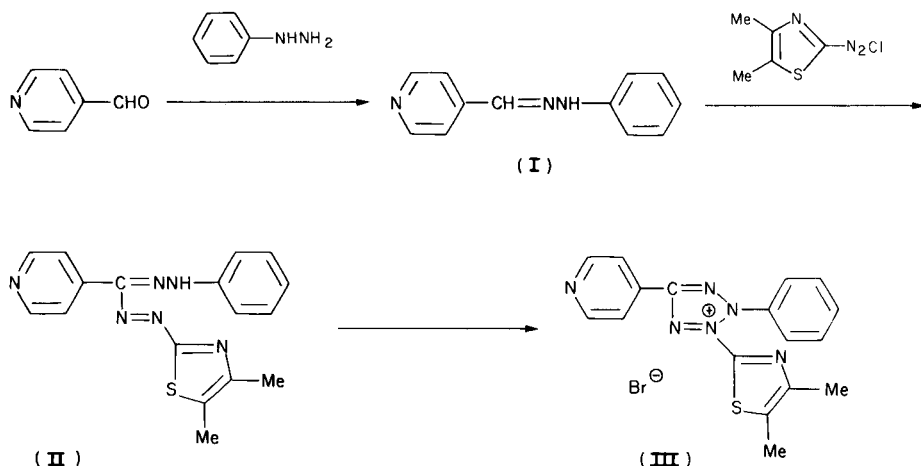
The most widely accepted method for the determination of dehydrogenase activity in human serum is the spectrophotometric method based on the color reaction of tetrazolium salts [1] which are reduced to formazan dyes in the presence of substrate, NAD and phenazine methosulfate (PMS) [2]. However, the formazan dyes resulting from conventional tetrazolium salts are insoluble in water, which leads to problems in manual spectrophotometric measurements as well as in continuous flow instruments. Such problems can be avoided by the use of surfactants, but a fundamental solution of this problem would be to develop new tetrazolium salts yielding water-soluble formazan dyes.

This communication is concerned with the synthesis of 2-phenyl-3-(4,5-dimethyl-2-thiazolyl)-5-(4-pyridyl)tetrazolium bromide (PDTPT) which is a pyridine analog of 3-(4,5-dimethyl-2-thiazolyl)-2,5-diphenyltetrazolium bromide [3, 4]. The formazan dye which results from reduction of PDTPT is water-soluble in acidic solutions because of the presence of pyridine group, and it has an absorption band at 539 nm where bilirubin and related substances do not interfere. As an example of its application in clinical analysis, the determination of lactate dehydrogenase (LDH) activity in human serum is described.

Experimental

Synthesis of the new tetrazolium salt (PDTPT). Compound III was synthesized by the scheme outlined.

4-Pyridylphenylhydrazone (I) was prepared as follows. Add 10.8 g (0.10 mol) of phenylhydrazine to a methanol (50 ml) solution of 10.7 g (0.10 mol)



of 4-pyridinecarboxaldehyde, and stir the mixture for 1 h at room temperature. Filter off the resulting yellow precipitate, wash with cold methanol and dry. [Yield 18.7 g (95%); m.p. 179–180°C. I.r. (cm^{-1}) 1600, 1560, 1278, 1140, 984, 738. Found: 73.3% C, 5.6% H, 21.1% N; calculated for $\text{C}_{12}\text{H}_{11}\text{N}_3$, 73.1% C, 5.6% H, 21.3% N.]

To prepare 2-phenyl-3-(4,5-dimethyl-2-thiazolyl)-5-(4-pyridyl)formazan (II), dissolve 15.0 g (76.1 mmol) of (I) and 75 g of sodium acetate (anhydrous) in 200 ml of mixed solvent (pyridine-methanol, 1:3) and cool the solution at 0°C. Prepare the diazonium salt by dropwise addition of an aqueous solution of 5.28 g (76.5 mmol) of sodium nitrite at 0°C to a solution of 12.6 g (76.5 mmol) of 4,5-dimethyl-2-aminothiazole hydrochloride in 100 ml of 4 M hydrochloric acid. After stirring this solution for another hour, add it dropwise to the pyridine-methanol solution of (I) at 0°C and stir the mixture for 24 h at room temperature. To this, add 50 ml of water and filter off the resulting precipitate. Wash it with water, then with methanol-water (1:1), and dry. [Yield 8.50 g (33.2%); m.p. 138–141°C. I.r. (cm^{-1}) 3330, 1598, 1496, 1270, 1185, 830. Found: 61.0% C, 4.8% H, 24.7% N, calculated for $\text{C}_{17}\text{H}_{10}\text{N}_6\text{S}$, 60.7% C, 4.8% H, 25.0% N.]

To prepare 2-phenyl-3-(4,5-dimethyl-2-thiazolyl)-5-(4-pyridyl)tetrazolium bromide (III, PDTPT), add 4.24 g (23.8 mmol) of *N*-bromosuccinimide in portions to an ethyl acetate (50 ml) solution of 8.0 g (23.8 mmol) of formazan(II), at room temperature, filter off the resulting precipitate and wash it with ethyl acetate. Dissolve the precipitate in 200 ml of methanol, treat the solution with active carbon and finally concentrate the solution by evaporation. Add 50 ml of ethyl acetate to the residue to precipitate the pure crystalline powder; filter it and dry.

Pure (III) is a pale yellow crystalline powder which is readily soluble in water or methanol, but is not soluble in common organic solvents. [Yield 5.83 g (59.0%); m.p. 190–191°C (decomp.). I.r. (cm^{-1}) 1525, 1380, 1158,

780. Found: 49.4% C, 3.7% H, 20.0% N, calculated for $C_{17}H_{15}N_6SBr$, 49.2% C, 3.6% H, 20.2% N.]

Reagents and apparatus. Phosphate buffer solutions (pH 7.0–8.5) were prepared from 0.1 M KH_2PO_4 and 0.1 M Na_2HPO_4 . Lactic acid solution (0.1 M), 0.25 mM 1-methoxyphenazine methosulfate (Dojindo), 5.0 mM nicotinamide adenine dinucleotide (NAD; Wako Pure Chemicals) and 1.0–10 mM PDTPT solutions were protected from light and stored in a refrigerator. All reagents were of analytical grade.

Nescol-X (Nippon Shoji Kaisha, Ltd) was used as the standard serum.

A Shimadzu UV-210A double-beam spectrophotometer was used with 1 cm standard cells.

Standard procedure for the determination of LDH activity. To a test tube containing 1.0 ml of 0.1 M phosphate buffer solution (pH 8.0), add 100 μ l of 0.1 M lactic acid, 100 μ l of 5 mM PDTPT solution, 100 μ l of 0.25 mM 1-methoxyphenazine methosulfate and 100 μ l of 5.0 mM NAD; thermostat the mixture at 37°C. To this, add an exact amount of the standard serum and incubate the mixture at 37°C for 10 min. Then add 3.0 ml of 0.1 M hydrochloric acid to stop the enzymatic reaction and measure the absorbance at 539 nm against a reagent blank without the serum.

The calibration graph was prepared by using various amount of serum corresponding to an LDH activity range of 21–84 mU ml⁻¹. The graph was linear over this range.

Results and discussion

Synthesis of the tetrazolium salt. 4-Pyridine analogs of various tetrazolium salts were synthesized by procedures similar to that shown above. However, the diformazan dyes resulting from the reduction of these tetrazolium salts were not soluble in water even in acidic solutions, so that these analogs were not investigated in detail. The synthesis of 4-*N,N*-dimethylaminophenyl analogs was also examined, but the formazan corresponding to (II) could not be obtained.

The only successful tetrazolium salt was PDTPT. The corresponding formazan dye after reduction with excess of glucose, gave an absorption band at 539 nm with a molar absorptivity of 1.83×10^4 l mol⁻¹ cm⁻¹, which is comparable to that obtained from the parent tetrazolium salt ($\lambda_{\max} = 565$ nm, $\epsilon = 2 \times 10^4$ l mol⁻¹ cm⁻¹). This formazan dye is quite soluble in neutral or acidic aqueous solutions, so that it is not adsorbed on the surfaces of photometric cells or on plastic tubing. This advantage is important for enzymatic determinations in automatic flow systems.

Effect of pH on the color reaction. The reaction was studied at various pH values in the range 7.0–8.5. The absorbance at 539 nm increased slightly with increasing pH (Fig. 1), but was almost constant in the pH range 7.5–8.5, as was the absorbance of the blank. Accordingly, the mixtures were incubated at pH 8.0.

Effect on reagent concentration on the color reaction. The reaction was

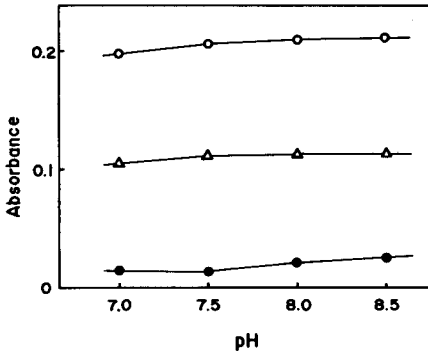


Fig. 1. Effect of pH on color reaction of PDTPT: (●) blank; (○) serum (LDH activity 84 mU ml⁻¹); (Δ) serum diluted 1 + 1 (LDH activity 42 mU ml⁻¹).

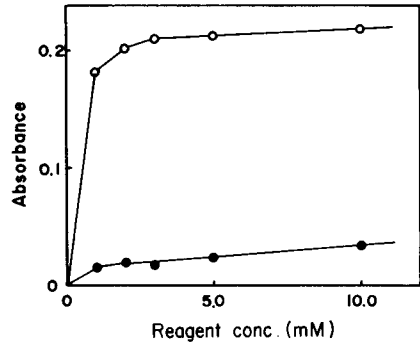


Fig. 2. Effect of PDTPT concentration: (●) blank; (○) serum (LDH activity 84 mU ml⁻¹).

examined at pH 8.0, various amounts of PDTPT (1.0–10 mM) being used. The absorbance increased with increasing concentration of the reagent, but so did the absorbance of the blank solutions (Fig. 2). Therefore, a 5.0 mM reagent solution was added in the standard procedure. The color intensity, once developed, was quite stable; the absorbance was constant over 60 min after termination of the enzymatic reaction.

The sensitivity of the color reaction. The calibration graph was linear over the LDH activity range of 21–84 mU ml⁻¹. A similar enzymatic assay for LDH was done with nitrotetrazolium blue [5]. The sensitivity with the new reagent was only about 70% of that obtained with nitrotetrazolium blue. However, the solubility of the resulting formazan in water gives a definite advantage over the conventional tetrazolium salts which form insoluble pigments on enzymatic reduction.

The authors express their gratitude to Professor Keihei Ueno for helpful discussions.

REFERENCES

- 1 R. D. Lillie, *Conn's Biological Stains*, 9th edn., Williams & Wilkins Co., Baltimore, MD, 1977, p. 225.
- 2 S. Nakamura, K. Arimura, K. Osawa and T. Yagi, *Clin. Chim. Acta*, 101 (1980) 321.
- 3 A. G. E. Pearse, *J. Histochem. Cytochem.*, 5 (1957) 515.
- 4 A. G. E. Pearse, R. Hess, *Experientia*, 17 (1961) 136.
- 5 M. M. Nachlas, K. C. Tsou, E. De Souza, C. S. Cheng and A. M. Seligman, *J. Histochem. Cytochem.*, 5 (1957) 420.

Short Communication

1,4-DIOXANE AS A SOLVENT IN SPECTROSCOPY AND
PHOTOCHEMISTRY

JERZY BŁAŻEJOWSKI* and JERZY SZYCHLIŃSKI

Institute of Chemistry, University of Gdańsk, 80-952 Gdańsk (Poland)

(Received 8th September 1983)

Summary. Commercially available 1,4-dioxane, even of spectroscopic grade, contains various impurities that arise mostly from reaction of the solvent with oxygen. Aspects relevant to the spectroscopy and photochemistry of the dioxane/oxygen system are discussed. Methods of purification and storage of the solvent are presented.

1,4-Dioxane is an apolar (dipole moment = 0, dielectric constant = 2.209 [1]) cyclic ether. In spite of being apolar, it is a good solvent for both polar and apolar compounds such as mineral acids, salts, water, ethers, aliphatic and aromatic hydrocarbons [2–4]. The lone-pair electrons of oxygen atoms and the fairly low ionization potential of dioxane [5] impart electron-donor properties to the molecule [6]. It is also known as a weak proton acceptor [7, 8].

Absorption of electromagnetic radiation by the dioxane molecule occurs over the far ultraviolet region [9–12]. The first long-wavelength absorption band is assigned to the $n_o \rightarrow \sigma_{C-O}^*$ transition. In the gas phase, this band appears with its maximum at 180.2 nm. Its long-wavelength shoulder probably has a vibrational structure and extends to the near-ultraviolet region [10, 12]. In the liquid phase, the long-wavelength band is red-shifted by about 10 nm with simultaneous loss of the vibrational structure [11, 13]. Various authors and solvent manufacturers have reported different transmittances for dioxane above 200 nm, depending on the method of its production and purification (see, e.g. [1, 9, 13–15]). Exceptionally pure dioxane was obtained by Hentz et al. [14] who found the solvent to have no absorption (1 cm pathlength) above 290 nm and only a residual absorption over the range 240–290 nm. The absorption increases sharply on moving from 212 nm to shorter wavelengths. The residual absorption above 212 nm has been postulated as being due to traces of impurities [14, 15]. It cannot be assigned to the forbidden $S \rightarrow T$ transitions, because, as has been pointed out by Watson and Parrish [16], these should occur over the range 320–430 nm.

The above-described properties of dioxane indicate that it is a suitable solvent for spectroscopic and photochemical experiments (see, e.g. [1, 17–19]). Unfortunately, dioxane is not inert in the presence of oxygen which, of

course, easily appears in any solvent during typical measurements. The presence of oxygen makes it unsuitable for two reasons: first, in the presence of oxygen, dioxane starts to absorb radiation strongly over the range 200–300 nm [11, 20, 21]; secondly, peroxides can be formed [11] which may initiate further reactions in the system.

In this work, an effort was made to find an effective method of purification and storage of the solvent, and some investigations were made on the influence of oxygen on the results of spectroscopic and photochemical measurements. Some aspects of the photochemistry of the dioxane/oxygen system were examined; the available information on the latter problem is fragmentary [22].

Experimental

Purification of dioxane. Dioxane contains various impurities which are formed during its production (acetals and benzene) or on storage, and which can have a disastrous effect when it is used as a solvent for spectroscopic and photochemical purposes. Most of them were removed by triple crystallization (m.p. 285 K), followed by refluxing of the solvent with 1.8 M hydrochloric acid in the proportion 10:1 (solvent:acid) by volume for 10 h. During refluxing, a stream of argon was bubbled through the dioxane and small amounts of ammonium iron(II) sulfate were added. After cooling, the solvent was shaken four times with potassium hydroxide (50 g dm^{-3}) and left over the last portion of potassium hydroxide for 24 h. Then it was decanted, refluxed for 10 h over lithium aluminum hydride (20 g dm^{-3}) under argon and doubly-distilled from the lithium aluminum hydride over a 1-m long Vigreux column under argon. The fraction boiling at 374.5 K was collected. For further studies, only those parts of the solvent were used which were gas-chromatographically (g.c.) homogeneous and which had the absorptions shown in Fig. 1.

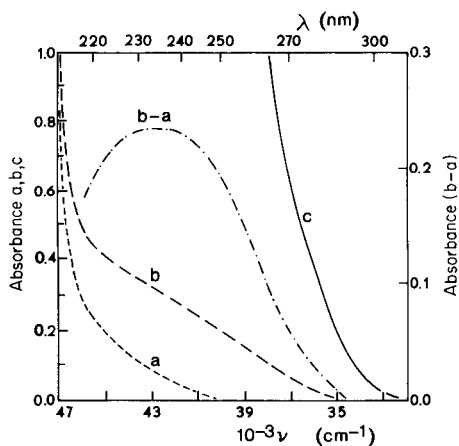


Fig. 1. Absorption spectra: (a) degassed dioxane; (b) dioxane saturated with oxygen at $8.6 \times 10^3 \text{ N m}^{-2}$; (c) dioxane saturated with oxygen at $1.01 \times 10^5 \text{ N m}^{-2}$.

Lithium aluminum hydride should be used with extreme care because it can decompose explosively above 400 K. It can be especially dangerous at the end of distillation and subsequent cooling period [23]. Thus, for safety, the refluxing and collection can be done under reduced pressure. Calcium hydride or sodium can be used instead of lithium aluminum hydride for drying the solvent, but there are numerous difficulties in cleaning the sodium surface if it is stored under oil and calcium hydride is less efficient. All operations during purification of the solvent were done with standard-taper Quickfit equipment.

Reagents other than dioxane were of the purest available grade. Oxygen was removed from argon by passing the gas over copper at 420 K [24].

Spectral measurements. The ultraviolet absorption spectra were recorded on a Specord UV-VIS (Carl Zeiss, Jena) spectrophotometer. The spectra of solutions and pure solvent were recorded in a quartz tube (i.d. 17 mm) which was connected to a system enabling samples to be degassed or saturated with oxygen at the required pressure, if necessary [25]. Doubly-distilled water placed in a similar tube served as the reference.

Photochemical experiments. The photolyses of oxygen-free and oxygen-saturated dioxane were done with standard photochemical equipment [26]; the light source was a medium-pressure mercury lamp (Q-400, Hanovia). The lines at 254, 313 and 366 nm were selected for irradiations, by using appropriate filters.

The photolytes were checked for the presence of oxidative substances (iodimetrically). Other products were examined by gas chromatography and by gas chromatography/mass spectrometry (g.c./m.s.).

Results and discussion

Absorption spectra of degassed dioxane and dioxane saturated with oxygen at two different pressures, recorded at room temperature, are shown in Fig. 1. A difference spectrum (curves b—a) indicates the formation of a new species in the system; this species can be identified as a charge-transfer complex of dioxane with oxygen [20]. The observed charge-transfer absorption corresponds to the transfer of an electron from a nonbonding orbital of the oxygen atom of dioxane to either of the partly filled antibonding π -orbitals of the oxygen molecule [27, 28]. A maximum of the charge-transfer band occurs at approximately 235 nm; this value is in accord with that mentioned earlier by Baxendale et al. [21]. The long-wavelength shoulder of the band extends far above 300 nm and is responsible for residual absorption by the dioxane/O₂ system even at 366 nm. The complex of dioxane with oxygen is fairly labile [29] and can be decomposed by expelling oxygen from the solvent. Because purging with argon is a rather ineffective method of removing oxygen, the residual absorption appears always around the maximum of the charge-transfer band [17]. Total reversion of the process can be achieved, however, by three pump/thaw cycles followed by degassing under high vacuum.

Ultraviolet irradiation of oxygen-saturated dioxane at atmospheric pressure caused formation of oxidative substances, which, by analogy to compounds formed in other ethers in the presence of oxygen [11], might be hydrogen peroxide and dioxane hydroperoxide. Examination by g.c./m.s. indicated the formation of more than ten products. The structures of some of these were evaluated on the basis of the mass spectra and on knowledge of the photochemistry of other ethers in the presence of oxygen [11]. These compounds are: formaldehyde, dioxanol, dioxanone, dioxane hydroperoxide, hydroxyacetaldehyde and 1,2-ethanediol monoformate. It is worth noting that irradiations of oxygen-saturated dioxane at 254, 313 and 366 nm led to the same products. The relative rates of formation of the compounds decreased in the same order, mainly because of differences in the amount of energy absorbed at certain wavelengths.

Prolonged irradiation of degassed dioxane at 254 nm afforded only minor amounts of several products, which were analogous to those observed by other authors [11, 30, 31]. In contrast, radiation above 300 nm did not initiate any photoreactions.

In spite of possessing favorable chemical and physical properties, the use of dioxane as a solvent in spectroscopy and photochemistry is associated with certain difficulties. First, the above results show that dioxane interacts with dissolved oxygen so that its spectral characteristics change. The strong charge-transfer absorption in the region 215–300 nm can introduce a systematic error in the spectroscopic measurements, which is difficult to assess. Obviously, the effect will be especially significant if weak absorption bands are examined. Reliable results can be obtained only in the absence of oxygen, i.e. when samples are degassed or oxygen is carefully removed by purging with argon. The use of the same batch of dioxane as solvent and as reference does not eliminate this oxygen error, because absorption by the solvent may be too strong for accurate spectrophotometric measurements to be possible. Furthermore, the solute may compete with oxygen for the solvent molecules, thereby changing the concentration of the initial charge-transfer complex. Secondly, it was shown that dioxane/O₂ system is photochemically reactive over most of the u.v. region. Compounds thus formed may not only affect the spectral characteristics of the solvent (e.g., carbonyl compounds or peroxides) but may also initiate various radical reactions. Accordingly, the course of photochemical processes may be quite different in the presence and absence of oxygen in the solvent. The last effect may also account for fast "ageing" of dioxane solutions.

It is worth mentioning that the course of both photochemical and thermal processes is quite similar in the dioxane/O₂ system. Consequently, the solvent can be stored undecomposed only in the absence of oxygen in evacuated ampuls. Degassing of the solvent with oxygen-free argon did not protect it from changes on storage; after a few days, new compounds were again detected in it.

The authors thank the Mass Spectrometry Laboratory, University of Gdansk, for the g.c./m.s. data. This work was supported by the Polish Academy of Science through Grant No. MR-I.12.1.1.8.

REFERENCES

- 1 S. L. Murov, *Handbook of Photochemistry*, M. Dekker, New York, 1973.
- 2 W. Stumpf, *Chemie und Anwendungen des 1,4-Dioxans*, Verlag Chemie, Weinheim, 1956.
- 3 T. Weber, in B. Ernst, B. Ernst and H. Heinrich (Eds.), *Ullmans Encykl. Tech. Chem.*, Aufl. 4, Vol. X, Verlag Chemie, Weinheim, 1975, p. 151.
- 4 P. Suppan, *J. Photochem.*, 18 (1982) 289.
- 5 A. S. N. Murthy and A. R. Reddy, *Spectrochim. Acta*, Part A, 38 (1982) 91.
- 6 A. V. Dombrovskii, *Usp. Khim.*, 30 (1961) 1453.
- 7 R. Mateva, F. Frater and M. Pavlova, *Makromol. Chem.*, 169 (1973) 235.
- 8 L. S. Levitt and B. W. Levitt, *Z. Naturforsch., Teil B*, 34 (1979) 614.
- 9 L. W. Pickett, N. J. Hoeflich and T.-C. Liu, *J. Am. Chem. Soc.*, 73 (1951) 4865.
- 10 G. J. Hernandez and A. B. F. Duncan, *J. Chem. Phys.*, 36 (1962) 1504.
- 11 C. von Sonntag and H.-P. Schuchmann, *Adv. Photochem.*, 10 (1977) 59.
- 12 H.-P. Schuchmann, H. Bandmann and C. von Sonntag, *Z. Naturforsch., Teil B*, 34 (1979) 327.
- 13 P. Hirayama, C. W. Lawson and S. Lipsky, *J. Phys. Chem.*, 74 (1970) 2411.
- 14 R. R. Hentz, P. W. Mellows and W. V. Sherman, *J. Phys. Chem.*, 71 (1967) 3365.
- 15 R. R. Hentz and W. V. Sherman, *J. Phys. Chem.*, 72 (1968) 2635.
- 16 E. Watson and C. F. Parrish, *J. Chem. Phys.*, 54 (1971) 1427.
- 17 D. D. Tunnicliff, *Talanta*, 2 (1959) 341.
- 18 R. M. Silverstein and G. C. Bassler, *Spectrometric Identification of Organic Compounds*, Wiley, New York, 1967.
- 19 W. G. Herkstroeper, Vol. I, Part A, p. 12 and W. M. Hardham, Vol. X, Part B, p. 626, in A. A. Lamola (Ed.), *Creation and Detection of the Excited States*, M. Dekker, New York, 1971.
- 20 H. Tsubomura and R. S. Mulliken, *J. Am. Chem. Soc.*, 82 (1960) 5966.
- 21 J. H. Baxendale, D. Beaumont and M. A. J. Rodgers, *Chem. Phys. Lett.*, 4 (1969) 3.
- 22 J. H. B. Chenier, M. Finkelman and J. A. Howard, *Am. Chem. Soc. Div. Pet. Chem., Prepr.*, 14 (1969) A107.
- 23 L. Bretherick, *Handbook of Reactive Chemical Hazards*, 2nd edn., Butterworths, London, 1979, pp. 222-225.
- 24 D. S. Gibbs, H. J. Svec and R. E. Harrington, *Ind. Eng. Chem.*, 48 (1956) 289.
- 25 D. F. Shriver, *The Manipulation of Air-Sensitive Compounds*, McGraw-Hill, New York, 1969, p. 96.
- 26 J. G. Calvert and J. N. Pitts, *Photochemistry*, Wiley, New York, 1966, ch. 7.
- 27 A. Yu. Karmilov, N. A. Sysoeva and A. L. Buchachenko, *Zh. Strukt. Khim.*, 18 (1977) 817.
- 28 A. N. Dharamsi and J. Tulip, *Chem. Phys. Lett.*, 71 (1980) 224.
- 29 N. Brueckl and J. I. Kim, *Z. Phys. Chem. (N.F.)*, 126 (1981) 133.
- 30 J. J. Houser and B. A. Sibbio, *J. Org. Chem.*, 42 (1977) 2145.
- 31 J. Kiwi, *J. Photochem.*, 7 (1977) 237.

Short Communication

DETERMINATION OF CHROMIUM IN GALLIUM ARSENIDE BY ELECTROTHERMAL ATOMIC ABSORPTION SPECTROMETRY

M. TADDIA*

Istituto Chimico "G. Ciamician", Università di Bologna, 40126 Bologna (Italy)

P. LANZA

Istituto di Tecnologie Chimiche Speciali, Università di Bologna, 40136 Bologna (Italy)

(Received 15th November 1983)

Summary. The sample is decomposed with 50% (v/v) aqua regia and the diluted solution is injected into the graphite furnace. The temperature program developed minimizes non-specific background signals, so that correction is not required. For a 100-mg sample, the 3σ detection limit is 70 ng Cr g⁻¹. The relative standard deviation of the overall procedure is 5–7%.

Semi-insulating gallium arsenide is used to make many electronic devices such as field effect transistors, laser diodes and high-speed digital integrated circuits. The term "semi-insulating" describes a material with a resistivity in the range 10^4 – 10^{12} ohm cm⁻¹. Semi-insulating gallium arsenide is currently prepared by extensive purification or by adding chromium during crystal growth to compensate for residual n-type impurities such as sulphur, silicon or tellurium. Control of the doping level and uniform distribution of chromium is necessary in order to achieve a substrate having the required properties [1]. Various techniques have been applied for chromium determinations in gallium arsenide. They include secondary ion mass spectrometry (s.i.m.s.) [2], neutron activation analysis [3], i.r. spectrometry [4] and atomic absorption spectrometry (a.a.s.) [5]. Very recently, a method based on differential pulse polarography was described [6]. The performance of three of these techniques (s.i.m.s., i.r. and a.a.s.), used in more general studies of gallium arsenide impurities, has recently been critically reviewed [7].

The use of graphite-furnace a.a.s. for the determination of chromium in gallium arsenide is very attractive with regard to cost, speed and ease of sample preparation. However, it has properly been noted [7] that the temperature program is critical in determining the selectivity and sensitivity of the method. For example, the matrix is not easily removed after charring, giving rise to non-selective absorption. Nevertheless, some authors [5] found that background correction was unnecessary, except when solid gallium arsenide samples were processed. However, the factors which influence the non-selective absorption have not been investigated systematically. The aim

of the present study was to assess the value of the furnace a.a.s. method for the determination of traces of chromium in gallium arsenide, and especially to establish conditions for background minimization. This is particularly important because accurate background subtraction at the 357.9-nm chromium line cannot be achieved with a deuterium lamp. However, Zeeman a.a.s., which has been used for the direct measurement of impurities in solid gallium arsenide [8], and eliminates background absorbance is not available in most analytical laboratories.

Experimental

Apparatus. The Perkin-Elmer 372 atomic absorption spectrometer used was equipped with a HGA-500 graphite furnace and a Leeds-Northrup 681A chart recorder. A Juniper chromium hollow-cathode lamp was employed as a light source (10 mA, 357.9 nm). Sample aliquots (10 μ l) were injected manually with Brand micropipettes. Argon was used as the inert atmosphere. The operating parameters used are given in Table 1. Background measurements were done at 352.0 nm (Ne I).

Reagents. Stock standard solutions (1000 mg Cr l⁻¹) were prepared from potassium chromate (Merck) and chromium trichloride (Titrisol, Merck). More dilute working standards in 0.2% (w/v) nitric acid were prepared daily. Dilute (1 + 1) aqua regia was prepared just before use by mixing three volumes of 37% hydrochloric acid and one volume of 65% nitric acid (both RSE, Erba), with four volumes of water. The chromium contamination in undiluted aqua regia was found to be 5.5 ± 1.5 ng ml⁻¹.

Procedure. Accurately weigh 25–100 mg of finely powdered gallium arsenide in a 12-ml test tube and add 2 ml of (1 + 1) aqua regia. Warm gently on a water bath until moderate effervescence occurs. Complete the dissolution at room temperature, and add water to bring to a known volume of 8–9 ml. Determine chromium by using a standard addition technique. Atomize at least three replicate 10- μ l portions of the sample solution,

TABLE 1

Operating parameters for the graphite furnace^a

	Analysis of standards				Analysis of GaAs samples			
	Temp. (°C)	Ramp (s)	Hold (s)	Ar (ml min ⁻¹)	Temp. (°C)	Ramp (s)	Hold (s)	Ar (ml min ⁻¹)
Dry	120	5	20	300	120	5	20	300
Ash	1000	5	10	300	900	60	60	300
Atomize	2700 ^b	1	10	50 ^c	2700 ^b	4	6	70

^aSample size: 20 μ l (aqueous standards) or 10 μ l (GaAs solutions). ^bUnless otherwise specified, atomization at 2600°C was chosen for experiments with pyrolytically coated tubes. ^cOperation with interrupted gas flow is preferred for blank evaluation.

and repeat after adding 20, 40 and 60 μl of 10 $\mu\text{g Cr(VI) ml}^{-1}$ solution. Do a blank determination under identical conditions.

Results and discussion

When gallium arsenide is dissolved in aqua regia, the major product is gallium arsenate [6], with the excess of hydrochloric and nitric acids remaining. It seemed advisable to investigate the effect of these acids on the signal obtained from chromium(III) and chromium(VI). In the first experiments, the ashing temperature was optimized, and then the effects of increasing concentrations (0.1–2.0 M) of acid on the analyte absorbance were measured. It was found that chromium in either oxidation state at the 30 ng ml^{-1} level, was not significantly lost until 1100–1200°C and that no interference was caused by hydrochloric acid over the whole concentration range examined. These results confirm and extend those previously reported for chromate [9]. Probably hydrochloric acid is efficiently removed in the drying and ashing steps, whereas this is more difficult for other less volatile chlorides. The interference from nitric acid was also investigated. A slight suppressive effect (–6%) was produced by 0.4 M nitric acid on the signal given by chromium(III). The combined effect of the two acids was examined by using diluted aqua regia. A calibration graph for chromium(III) in 16% (v/v) aqua regia, was linear in the range 10–80 ng ml^{-1} . The ratio between the slope of this graph and that in 0.2% nitric acid was 0.84. The results refer to uncoated tubes, for which the characteristic amount of chromium (giving 1% absorption) was 14 μg , in the absence of interferents. It is interesting to note that the simultaneous presence of hydrochloric and nitric acid, produces an absorbance decrease greater than expected from the addition of the two separate effects.

Minimization of non-specific absorbance. Preliminary attempts to process gallium arsenide solutions (2% w/v), by using tubes coated with pyrolytic graphite and a temperature program similar to that employed for the standards, gave indications of a non-specific signal. This was confirmed by absorbance measurements at 352 nm. Guenais et al. [5] measured the background absorption at 357.6 nm (Nb I). It should be noted that the selection of an appropriate spectral bandwidth is critical in order to obtain reliable results when this line is used. In addition, the emission intensity of the lamp at 352 nm was found to be 12 times greater than at 357.6 nm. For these reasons, the neon line was preferred for background correction in the present investigation. When the sample was atomized, the signal profile, the poor repeatability and the evidence of fumes released from the furnace just at the beginning of the atomization step, suggested the background to be a typical case of light scattering. Molecular absorption from species such as GaCl and GaO was excluded because these bands occur in the region 225–275 nm [10]. By measuring the non-specific absorbance at 352 nm as a function of the final ashing temperature, the background signal was eliminated at about 1600°C (Fig. 1). This was not of practical importance as

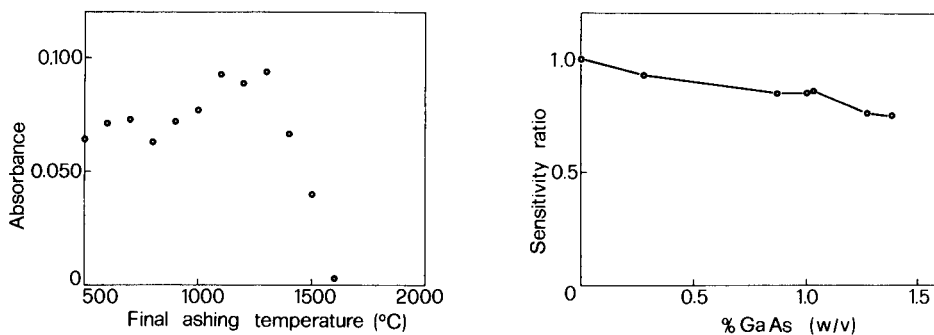


Fig. 1. Effect of ashing temperature on non-specific background absorbance for 2% (w/v) GaAs in 10% (v/v) aqua regia. (352.0 nm, without background correction, 20- μ l sample, pyrolytically-coated graphite tube, atomization at 2700°C for 10 s, ramp 1 s and argon internal flow 50 ml min⁻¹; 40 s ashing time at the indicated temperature (Table 1), ramp time 5 s.)

Fig. 2. Ratio between slope of standard addition calibration graph for additions to the sample and to the reagents blank, as a function of matrix concentration. (Conditions as in Table 1.)

chromium was also completely lost at that temperature. Thus it was not possible selectively to remove the matrix during the ashing step. It was decided, therefore, to control the ramp time for the atomization temperature, the argon internal flow and the amount of sample injected to minimize the background. The ramp time was gradually increased to 10 s, the argon flow was increased to 80 ml min⁻¹ and the amount of sample was decreased to 10 μ l. Such modifications influenced also the chromium peak-height sensitivity. A compromise between these effects was achieved by using the program given in Table 1. It makes the use of a background corrector unnecessary, the background signal at 352 nm being of the same order of the furnace blank. It should be stressed that attempts to increase the sensitivity by interrupting the gas flow may considerably increase the non-specific absorbance.

Calibration and detection limit. Calibration graphs were obtained by adding known amounts of standards to gallium arsenide solutions (1.2% w/v), prepared from a sample having a low chromium concentration (<1 μ g g⁻¹). Both uncoated and pyrolytically-coated graphite tubes were tested to compare their performances. When uncoated tubes were used, the linear calibration range extended up to 0.3 μ g Cr ml⁻¹; the least-squares correlation coefficient for a 13-point graph was 0.999. The characteristic amount of chromium was 22 pg. The sensitivity obtained by using pyrolytically-coated tubes was 2.3 times greater. A similar difference in response was observed in the absence of gallium arsenide. The decreased sensitivity in uncoated tubes may be ascribed to the retention of chromium by the graphite, which was less evident on a pyrolytically-coated surface [11]. In spite of the lower

TABLE 2

Comparison between furnace a.a.s. and differential pulse polarography for the determination of chromium in GaAs

Sample	Cr found ($\mu\text{g g}^{-1}$) ^a			
	A.a.s.	No. of results	Polarography	No. of results
GaAs TEC	3.5 \pm 0.4	3	4.0 \pm 0.3	7
GaAs 32A	3.9 \pm 0.2	3	4.0 \pm 0.3	7
GaAs 32B	2.1 \pm 0.1	4	2.0 \pm 0.04	4
GaAs TS	2.4 \pm 0.2	3	2.3 \pm 0.2	7

^aMean and standard deviation.

sensitivity, uncoated tubes were used for subsequent analytical work, as they were adequate for the problem under investigation.

A moderate depressive effect on the chromium signal from the gallium arsenide matrix was observed (Fig. 2). Although the slope of the calibration graph in the presence of a fixed amount of dissolved gallium arsenide was constant (r.s.d. = 2.6%, $n = 7$), some dependence of the sensitivity on the "age" of the tube led to the standard addition method being preferred for more accurate chromium determinations. The 3σ detection limit for uncoated tubes was 70 ng Cr g^{-1} in gallium arsenide.

Validation of the method. Because of the lack of suitable reference samples, analyses of spiked samples and by an independent method were used to assess the accuracy of the proposed procedure. Two series of replicate determinations were made on 100-mg gallium arsenide samples spiked with 0.100 and 0.400 μg of chromium. The recoveries were 0.098 ± 0.020 (3 results) and $0.409 \pm 0.025 \mu\text{g}$ (4 results), respectively. The concentrations of chromium in unknown samples (C.N.R. MASPEC, Parma, Italy) were also determined by differential pulse polarography [6]. The results obtained by the two methods are shown in Table 2. It can be seen that the agreement is good. The coefficient of variation for the overall furnace a.a.s. procedure is 5–7%, depending on the chromium concentration. Thus graphite-furnace a.a.s. is useful for chromium determination in chromium-doped gallium arsenide.

This work was supported by the National Research Council (C.N.R.), under a contract related to the "Progetto Finalizzato per la Chimica Fine e Secondaria".

REFERENCES

- 1 R. D. Fairman and J. R. Oliver, in G. J. Rees (Ed.), *Semi-insulating III–V Materials*, Shiva, Nottingham, 1980, p. 83.
- 2 J. B. Clegg, *SIA Surf. Interface Anal.*, 2 (1980) 91.

- 3 M. R. Brozel, B. Tuck, D. Rumsby and R. M. Ware, *J. Cryst. Growth*, 60 (1982) 113.
- 4 G. M. Martin, G. Jacob and G. Poibland, *Acta Electron.*, 23 (1980) 37.
- 5 B. Guenais, A. Poudoulec and M. Minier, *Analisis*, 10 (1982) 78.
- 6 P. Lanza and M. Taddia, *Anal. Chim. Acta*, 157 (1984) 37.
- 7 J. B. Clegg, in S. Makram-Ebeid and E. B. Tuck (Eds.), *Semi-Insulating III—V Materials*, Shiva, Evian 1982, p. 80.
- 8 T. Hadeishi and H. Kimura, *J. Electrochem. Soc.*, 126 (1979) 1988.
- 9 K. Matsusaki, T. Yoshino and Y. Yamamoto, *Anal. Chim. Acta*, 113 (1980) 247.
- 10 K. Dittrich, W. Mothes and P. Weber, *Spectrochim. Acta, Part B*, 33 (1978) 325.
- 11 C. Veillon, B. E. Guthrie and W. R. Wolf, *Anal. Chem.*, 52 (1980) 457.

Short Communication

THE DETERMINATION OF CADMIUM IN MICROGRAM AMOUNTS OF PANCREATIC TISSUE BY ELECTROTHERMAL ATOMIC ABSORPTION SPECTROMETRY

THOMAS NILSSON and PER-OLOF BERGGREN*

Department of Medical Cell Biology, Biomedicum, Box 571, S-751 23 Uppsala (Sweden)

(Received 25th July 1983)

Summary. Cadmium was determined either by direct insertion of freeze-dried biological samples (1–13 μg) or by injection of 2- μl samples of perfusion medium into the graphite furnace. At 228.8 nm, >10 fmol of cadmium could be measured. The endogenous cadmium contents in the endocrine and exocrine parts of the pancreas were 8.5 ± 2.0 and 15.1 ± 1.4 μmol (dry wt.), respectively. A less sensitive wavelength (326.1 nm) was employed for measuring the larger amounts obtained after specimens had been incubated in the presence of cadmium.

Atomic absorption spectrometry (a.a.s.) in conjunction with an electrothermal atomizer is a valuable tool in the analysis of biological tissues for their metal content [1–8]. Especially high sensitivity is required when only minute amounts of material (e.g., samples of the endocrine part of the pancreas, the islets of Langerhans) are available. Although these islets represent no more than μg amounts of tissue, electrothermal a.a.s. has been used successfully for metal determinations [6–8].

The calcium ion participates in important physiological processes including regulation of insulin secretion from the β -cells in the pancreatic islets [9, 10]. Calcium analogues and antagonists are often used in the exploration of calcium-regulated mechanisms. Previous studies have both shown that the cadmium ion mimics the role of the calcium ion in mediating catecholamine release from the adrenal medulla [11] and can replace calcium in calcium-binding proteins [12, 13]. Furthermore, it has been shown that both ions are accumulated by a transport mechanism in kidney mitochondria [14]. It has been reported that microsomes accumulate more cadmium than other subcellular fractions when the pH of the medium is raised from 7.4 to 8.3, which suggested that microsomal structures remove cadmium ions from the cytoplasm to limit adrenal catecholamine release [15]. The above data indicate that cadmium might be useful in discriminating between various subcellular organelles that regulate the cytoplasmic calcium ion concentration.

The present communication describes the use of a carbon rod atomizer for direct determination by a.a.s. of cadmium in μg -amounts of freeze-dried pancreatic tissue and in 2- μl samples of perfusion medium. The choice of two wavelengths makes it possible to determine widely differing amounts of the element.

Experimental

Apparatus. A Varian-Techtron AA-6 atomic absorption spectrometer was provided with background correction and fitted with a carbon rod atomizer (CRA-90). The heating rate was controlled independently of the final temperature by the device described by Lundgren [16]. The optimized three-step temperature program is shown in Table 1. The graphite furnace was flushed with argon at 5 l min^{-1} [17]. The signal damping of the AA-6 readout module was modified to obtain a faster response time, the value of the "DAMP A" time constant being reduced from the original 260 ms to 47 ms [18]. A peak reader module was connected to the recorder output of the spectrometer [19], providing simultaneous recording of peak height and area. Peak shapes were checked with a fast-response (250 ms) stripchart recorder (Philips 8202). Background correction was used for measuring cadmium at both 228.8 nm and 326.1 nm.

Reagents and biological material. All chemicals were of analytical grade and the water used was purified in a Millipore Milli-Q water treatment system. The calibration solutions were prepared from cadmium nitrate (BDH Chemicals) and water. Chelex-100 (Bio-Rad) was used. Pancreatic tissue was taken from adult non-inbred obese hyperglycaemic mice (*ob/ob*) [20]. Islets of Langerhans were isolated by a collagenase technique [21], whereas the pieces of exocrine pancreas were obtained by microdissection [22].

Procedures. Calibration solutions and perfusion media ($2 \mu\text{l}$) were transferred to the graphite tube by a microsampler (Unimetrics) with a disposable teflon tip. The islets and pieces of exocrine pancreas were either taken directly after isolation or incubated for 60 min at 37°C in physiological media augmented with 0.25 mM cadmium solution. The specimens were freeze-dried overnight and weighed on a quartz-fibre balance [23]. The freeze-dried samples ($1\text{--}13 \mu\text{g}$) were placed directly into the graphite furnace for the cadmium determinations.

Possible interference from other metals was evaluated by measuring the recovery of known amounts of cadmium added to both pancreatic islets and perfusion media, and by analysis of NBS Bovine Liver.

TABLE 1

Operating conditions for the determination of cadmium^a

Wavelength	228.8 nm	326.1 nm
Lamp current (mA)	4.0	2.5
Dry (22.6 s) ^b	85°C for 45 s	85°C for 45 s
Ash (3.3 s) ^b	300°C for 30 s	300°C for 30 s
Atomize (1.2 s) ^b	1190°C for 3 s	1190°C for 3 s

^aBackground correction was used when cadmium was determined at either wavelength.

^bTime required to reach set temperature is given within brackets; total times include this period.

Results and discussion

Its high sensitivity and reproducibility make electrothermal a.a.s. a convenient technique for measuring trace amounts of metals in biological tissues. Here, the technique was used for determining the cadmium content of freeze-dried pancreatic tissue and perfusion media under a variety of experimental conditions. The endogenous values in the μg -amounts of pancreatic specimens and in the amounts of the perfusion media ($2\ \mu\text{l}$) were in the range of 10–180 fmol. After incubation with 0.25 mM cadmium solution, the endocrine and exocrine parts of the pancreas contained 18–120 pmol of the metal. Although slightly non-linear, the calibration graphs within these intervals were reproducible and presented no problems (Fig. 1). The coefficient of variation in measuring 5 samples containing 107 pmol of cadmium was 6.6% and the corresponding coefficient for 6 samples containing 107 fmol was 16.3%. When cadmium was dissolved in a perfusion medium, the coefficient of variation for 5 samples containing 107 fmol was 9.9%.

Despite attempts to remove endogenous traces of cadmium in the perfusion media with Chelex-100, the basal level of the metal was higher (approximately 20 times) than in the calibration solutions. It has been reported that Chelex-100 can decrease the cadmium concentration in sucrose and glucose solutions to about $10^{-8}\ \text{M}$ [24]. Even though the exact dissociation constant for cadmium bound to Chelex-100 in various types of media is not known, the present study indicates that it is not possible to decrease the cadmium concentration below $10^{-8}\ \text{M}$. The existence of cadmium in the perfusion media might be due, at least partly, to impurities of the sodium chloride because even a Suprapur salt contains a maximum of $10^{-6}\%$ cadmium. It is unlikely that the high concentration of sodium chloride used in this study (125 mM) increases the absorbance signal for cadmium. According

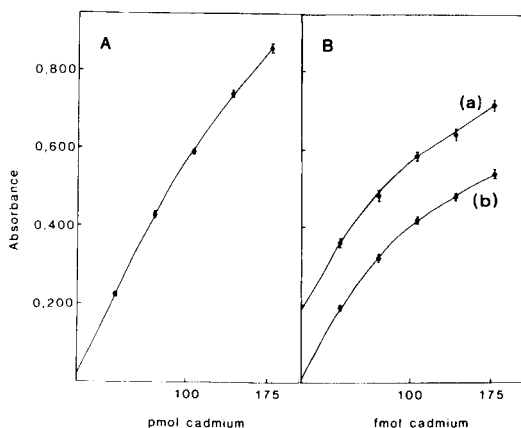


Fig. 1. Calibration graphs for cadmium: (A) aqueous solutions, 326.1 nm; (B) perfusion medium (a) and aqueous solution (b), both at 228.8 nm. Data are mean peak absorbance \pm standard error of the mean for 5–9 measurements.

TABLE 2

Recovery of cadmium^a

Wavelength (nm)	Cadmium recovery (%) ^b	
	Islets	Perifusion medium
228.8	126.9 ± 12.0 (16)	94.9 ± 1.8 (5)
326.1	101.9 ± 3.0 (8)	—

^aCadmium was added to the islets and perifusion medium in amounts corresponding to 71.2 fmol (228.8 nm) and 71.2 pmol (326.1 nm). ^bMean values ± standard error of the mean for indicated number of observations.

to previous studies, about 9 mM of the salt suppresses the signal for cadmium [25]. Further evidence supporting the notion that physiological concentrations of sodium chloride do not increase the absorption signal for cadmium is given in Table 2. It can be seen that there is no interference with the recoveries of cadmium added to either pancreatic tissue, represented by the islets of Langerhans, or perifusion media. Also, the cadmium content in 15 samples of NBS bovine liver measured according to the present technique corresponded to $2.3 \pm 0.3 \mu\text{mol kg}^{-1}$ (dry wt.), which does not significantly differ from that reported by the National Bureau of Standards.

Table 3 shows the amounts of cadmium determined in the endocrine and exocrine part of the pancreas when the tissue specimens were taken directly or incubated in the presence of cadmium. The biological significance of the differences in amounts of cadmium between the two components of the pancreas is unknown and merits further investigations. An important piece of information is that cadmium is accumulated in sufficient amounts to be detected when the less sensitive wavelength is used. This means that pancreatic tissue exposed to cadmium (0.25 mM) can be analyzed for cadmium without influence from endogenous stores of the element. To clarify the

TABLE 3

Cadmium content of tissue^a

Cd ²⁺ concentration in medium (mM)	Cadmium content in tissue (mmol kg ⁻¹ dry wt.) ^b	
	Endocrine tissue	Exocrine tissue
0	$8.5 \pm 2.0 (\times 10^{-3})$ (5)	$15.1 \pm 1.4 (\times 10^{-3})$ (5) ^c
0.25	7.6 ± 0.6 (9)	18.5 ± 1.2 (6) ^d

^aThe tissue specimens were either taken directly after isolation in a Cd²⁺-free medium (0 mM) or incubated for 60 min in the presence of 0.25 mM Cd²⁺. In the latter case, the tissue specimens were washed for 30 min in a Cd²⁺-free medium supplemented with 0.5 mM EGTA before samples were taken. ^bMean values ± standard error of the mean for indicated number of experiments; statistical significances evaluated by Student's *t*-test. ^c $P < 0.05$; ^d $P < 0.001$.

pattern of cadmium fluxes in the endocrine and exocrine part of the pancreas, it would be advantageous to record continuously the cadmium appearing in the medium during perfusion of specimens preloaded with the metal. By making measurements at 228.8 nm it will be possible to detect minor variations in the kinetics of such fluxes. In order to clarify further the handling of cadmium, this latter wavelength might be useful for measuring variations in the endogenous pools of the metal in pancreatic specimens incubated in the presence of various physiological stimuli or pharmacological drugs or both.

This work was supported by the Swedish Diabetes Association, Sättra Brunns forskningsstipendium, Swedish Royal Academy of Sciences and the Swedish Medical Research Council (12x-562).

REFERENCES

- 1 J. P. Matousek and B. J. Stevens, *Clin. Chem.*, 17 (1971) 363.
- 2 R. T. Ross and J. C. Gonzales, *Bull. Environ. Contam. Toxicol.*, 12 (1974) 470.
- 3 D. J. D'Amico and H. L. Klawans, *Anal. Chem.*, 48 (1976) 1469.
- 4 D. J. Paynter, *Anal. Chem.*, 51 (1979) 2086.
- 5 D. I. Halls and G. S. Fell, *Anal. Chim. Acta*, 129 (1981) 205.
- 6 P.-O. Berggren, O. Berglund and B. Hellman, *Anal. Biochem.*, 84 (1978) 393.
- 7 P.-O. Berggren, *Anal. Chim. Acta*, 119 (1980) 161.
- 8 P. Rorsman and P.-O. Berggren, *Anal. Chim. Acta*, 140 (1982) 325.
- 9 R. P. Rubin, *Calcium and the Secretory Process*, Plenum Press, New York, 1974, p. 1.
- 10 B. Hellman, T. Andersson, P.-O. Berggren, P. Flatt, E. Gylfe and K. D. Kohnert, *Hormones and Cell Regulation*, Vol. 3, Elsevier/North-Holland Biomedical Press, Amsterdam, 1979, p. 69.
- 11 I. O. Shanbaky, J. L. Borowitz and W. V. Kessler, *Toxicol. Appl. Pharmacol.*, 44 (1978) 99.
- 12 T. Drakenberg, B. Lindman, A. Cavé and J. Parello, *FEBS Lett.*, 92 (1978) 346.
- 13 S. Forsén, E. Thulin and H. Lilja, *FEBS Lett.*, 104 (1979) 123.
- 14 N. E. Saris and J. Järvisala, in S. S. Brown (Ed.), *Clinical Chemistry and Chemical Toxicology of Metals*, Elsevier/North-Holland Biomedical Press, Amsterdam, 1977, p. 109.
- 15 N. M. Shanbaky, A. Emran and J. Borowitz, *Toxicol. Appl. Pharmacol.*, 62 (1982) 167.
- 16 G. Lundgren, *Doctoral Dissertation*, University of Umeå, Sweden, 1975.
- 17 E. Lundberg and K. Lundmark, *Biomed. Environ. Instrum.*, 9 (1979) 91.
- 18 E. Lundberg, *Chem. Instrum.*, 8 (1978) 197.
- 19 E. Lundberg, *Appl. Spectrosc.*, 32 (1978) 276.
- 20 B. Hellman, *Ann. N.Y. Acad. Sci.*, 131 (1965) 541.
- 21 K.-D. Kohnert, H.-J. Hahn, E. Gylfe, H. Borg and B. Hellman, *Mol. Cell. Endocrinol.*, 16 (1979) 205.
- 22 C. Hellerström, *Acta Endocrinol. (Copenhagen)*, 45 (1964) 122.
- 23 B. Hellman, *Diabetologia*, 6 (1970) 110.
- 24 M. I. Harris and J. E. Coleman, *J. Biol. Chem.*, 243 (1968) 5063.
- 25 C. M. Lau, A. M. Ure and T. S. West, *Anal. Chim. Acta*, 146 (1983) 171.

Short Communication

THE PREPARATION OF IRON-FREE SOLUTIONS FROM GEOLOGICAL MATERIALS FOR THE DETERMINATION OF BORON (AND OTHER ELEMENTS) BY INDUCTIVELY-COUPLED PLASMA EMISSION SPECTROMETRY

VICTOR K. DIN

Department of Mineralogy, British Museum (Natural History), Cromwell Road, London SW7 5BD (Great Britain)

(Received 15th November 1983)

Summary. A procedure based on successive fusions with potassium dihydrogenphosphate and potassium hydroxide is described which yields an iron-free solution for the determination of boron in a wide variety of geological matrices. Data obtained for boron and other trace elements in geological reference materials are presented.

The procedure described was developed primarily for the determination of boron in rock and mineral samples from the Mendip Hills, Somerset, England, as part of an investigation of the geochemistry of areas of mineralogical interest in the region. The samples submitted were composed mainly of silicates, carbonates, sulphates and oxides, frequently with two or more of these mixed in various proportions. Boron is known to be present as an essential constituent of some minerals from the area [1, 2] and is disseminated through at least one of the iron oxides which occur there [3].

Iron interferes with the determination of boron by inductively-coupled plasma emission spectrometry (i.c.p.e.s.) [4, 5] because of the proximity of the iron and boron emission lines at 249.65 and 249.68 nm, respectively [6]. The lack of sensitivity of the 208.9-nm boron line generally precludes its use for trace analysis. Because the iron:boron concentration ratio for a given sample may exceed 10 000:1, correction factors can be unacceptably large. It is therefore necessary to measure the boron content in sample solutions from which the iron has been removed in order to exclude a significant source of error.

A standard carbonate fusion procedure such as that described by Owens et al. [7] was ineffective for several of the Mendip samples because complete removal of iron as carbonate was not achieved (cf. Doležal et al. [8]). Furthermore, separation of sulphate from the alkaline earth metals was incomplete, with the result that sulphates precipitated on acidification of the aqueous leach of alkali metal carbonate or hydroxide fusions; the extract must be acidified to avoid corrosion of glass or quartz components of the equipment contacted by the analyte solution.

The procedure described here avoids these problems by using two fusions. During a preliminary phosphate fusion, sulphates are decomposed with the

evolution of sulphur trioxide, and a subsequent fusion with potassium hydroxide is used to decompose other constituents. The aqueous leach of the fusion mixture provides an iron-free solution which is acidified for the determination of boron. A second solution, prepared from the residue of the aqueous leach, can be used for measurements of other elements.

Experimental

Reagents and apparatus. Analytical-grade reagents and deionised water were used in the preparation of samples. Calibration solutions were prepared from commercially available standard concentrates and high-purity compounds, with the sample preparation reagents added as necessary.

Initial experimental i.c.p.e.s. measurements were made with a Jarrell-Ash Mark III AtomComp spectrometer, but for later work, including the data recorded here, a Philips PV8210 ICP spectrometer was used. Both spectrometers were operated at the optimum instrumental settings for simultaneous multi-element measurements. The concentration data were calculated from background-corrected intensity measurements for samples and standards by a linear regression program.

Sample preparation. Prepare a reagent blank with each batch of samples. Accurately weigh 100–150 mg of powdered sample into a clean 15-ml vitreous carbon crucible. Add 500 ± 1 mg of potassium dihydrogenphosphate and mix with the sample using a PTFE rod. Place the crucible in a cold muffle furnace, and raise the temperature to 800°C over 1 h; to minimise oxidation of the crucible, purge the furnace with oxygen-free nitrogen whilst the temperature is above 450°C . Maintain the furnace at $800\text{--}820^{\circ}\text{C}$ for 1 h, remove the crucible and allow it to cool. Add 1.00 ± 0.02 g of potassium hydroxide and return the crucible to the cooled (ambient temperature) furnace. Increase the temperature to 450°C and maintain it for 1 h. Remove the crucible, allow it to cool, then stand it in a 100-ml plastic beaker and add ca. 8 ml of deionised water.

Determination of boron (preparation of solution X). Place the covered beaker on a boiling water bath for at least 30 min to dissolve and disintegrate the fused cake. Occasionally stir the contents with a PTFE rod, to assist dissolution. When the cake has disintegrated, and if the sample is known to contain more than a trace of manganese, or if the solution is green or purple from manganate or permanganate, respectively, add hydrogen peroxide (30 vol.) dropwise until manganese dioxide is completely precipitated. Leave the beaker on the water bath for a further 30 min, remove it, allow the contents to cool, and transfer the solution and precipitate to a 15-ml plastic centrifuge tube with 2–3 ml of deionised water. Centrifuge, pour the supernatant liquid into a 50-ml plastic beaker, and wash the first beaker and crucible therein with 2 ml of 0.2 M potassium hydroxide. Pour the washings into the tube, centrifuge and retain the clear liquid as before. Repeat the washing and centrifuging procedure twice more, collect the washings in the 50-ml beaker and, if further treatment of the residue is required, retain

the precipitate together with the 100-ml beaker and carbon crucible (see below).

Cover the 50-ml beaker containing the alkaline leach solution, carefully add 4 ml of 7 M nitric acid, and swirl to mix thoroughly. When the solution has cooled, transfer it to a 25-ml volumetric flask. Wash the beaker with deionised water, collect the washings in the flask and make up to volume. Store the prepared solution in a clean plastic bottle (solution X).

Dissolution of the residue (preparation of solution Y). Pour 4 ml of 7 M nitric acid into the crucible in the 100-ml beaker, cover the beaker and place it on a boiling water bath for 10 min. Empty the crucible into the beaker, rinsing with water into the beaker. Wash the precipitate contained in the centrifuge tube into the beaker with ca. 5 ml of water. Cover the beaker again and return it to the water bath to accelerate dissolution of the precipitate. If manganese dioxide is present, add hydrogen peroxide (30 vol.) dropwise to dissolve it. Remove the beaker from the bath after the precipitate has dissolved and the excess of hydrogen peroxide has been destroyed, and allow the solution to cool. If the solution is clear, transfer it to a 25-ml volumetric flask, but if it contains particles of carbon as a result of crucible degradation, centrifuge it first. Wash and centrifuge the carbon residue and pour the washings into the volumetric flask. Dilute the solution to volume with water (solution Y).

Calibrate the i.c.p. equipment, using a range of standards prepared in the appropriate strength of reagent blank solution for the spectrometry of solution X. Similarly, use standards prepared in nitric acid solution to calibrate the system for the spectrometry of solution Y.

Results and discussion

The results obtained for replicate determinations of boron in each of several geological reference materials are given in Table 1 together with an uncertainty equal to one standard deviation. The general accuracy of the method is shown by the good agreement between the concentrations found and recommended, the mean ratio of found/recommended values being 0.97 with a standard deviation of 0.16. The mean ratio and standard deviation are improved to 1.01 and 0.10, respectively, if the data for JB-1 are omitted from the calculation. Unfortunately, the accuracy of the determination for samples with very high iron contents cannot be assessed because of the lack of reference data for BCS 302 iron ore, though the precision is satisfactory (relative mean deviation 2.7%). The solution detection limit for boron, calculated as that concentration which generated a signal equal to 3 times the standard deviation of the blank signal (10 readings), was found to be $5 \mu\text{g l}^{-1}$ when instrumental parameters were optimised for multi-element work. This figure corresponds to $1.3\text{--}0.8 \text{ mg kg}^{-1}$ in the specimen for a sample weight of 100–150 mg. Unfortunately, the presence of boron in the flux reagents resulted in a real detection limit of approximately 5 mg kg^{-1} in the original sample (cf. Owens et al. [7]).

TABLE 1

Boron determined in some geochemical reference materials

Sample	Boron content (mg kg ⁻¹ , dry basis)			Ref.
	Mean ± s.d.	No. of measurements	Published values	
MAG-1	138 ± 1.5	2	130? 141 ± 15 ^a	9 10
QLO-1	35 ± 0.6	2	37? 38 ± 4 ^a	9 10
W-1	16 ± 0.3	2	13 ± 4 ^a 15?	11 12
GSD	49 ± 3.5	4	50 ^a	13
GSE	468	1	500 ^a	13
BCS302	42 ± 1.5	5	—	
BCS319	182 ± 6.0	16	b	
BCS389	94 ± 2.5	4	96	14
BR	8.9 ± 0.4	2	10?	12
GA	23 ± 1.5	5	20	12
JB-1	6.3 ± 0.7	5	12?	12

^aRecalculated to dry basis using data from the reference quoted; only the figure for MAG-1 ("wet" basis 138 ± 15) is significantly affected. ^bOne uncertified value of 0.14% B₂O₃ (435 mg kg⁻¹ B) is listed [15].

TABLE 2

Some element concentrations in three geochemical reference materials, found from spectrometer of solutions X and Y

Element	Sample	Element concentration (mg kg ⁻¹ , dry basis)			Recommended values [12]
		This work			
		Solution X	Solution Y	Total found	
Ti ^a	BR	nf ^b	15630	15630	15650 ^c
	GA	nf	2224	2224	2280 ^c
	JB-1	nf	8043	8043	8030 ^c
Mn	BR	9	1501	1510	1550 ^c
	GA	14	694	708	700 ^c
	JB-1	15	1211	1226	1160 ^c
Li	BR	nf	14	14	13
	GA	68	20	88	90
	JB-1	1	10	11	11
V	BR	196	29	225	240
	GA	35	5	40	38
	JB-1	192	19	211	210

^aBa, Co, Cr, Cu, Ni, Sc, Sr and Zn behaved similarly. ^bnf = none found (background-corrected sample signal < 3 × standard deviation of the background). ^cCalculated from the oxide concentrations listed.

Although most of the elements determined were precipitated quantitatively during the aqueous leach and therefore appeared only in solution Y, some were distributed variably between solutions X and Y. Consequently, it was necessary to process both solutions to determine the concentration of those elements in all samples. Table 2 presents the results obtained for some elements other than boron and shows whether or not they were found exclusively in one of the solutions.

During the development of the method, fusions were made with different combinations of some phosphates with sodium or potassium hydroxide. The disadvantage of using compounds of sodium and potassium together is that the determination of both elements is precluded. When only sodium compounds were used, the aqueous leach of some fusion melts yielded gels, presumably of complex phosphates, which were difficult to wash effectively within a final solution volume of < 25 ml without introducing an evaporation step.

The author thanks the staff of the U.S. Geological Survey, particularly Dr F. E. Lichte and his colleagues at the Branch of Analytical Laboratories, Arvada, Colorado, for the provision of technical facilities. Thanks are similarly due to Dr J. N. Walsh, Department of Geology, King's College, University of London.

REFERENCES

- 1 R. F. Symes and P. G. Embrey, *Mineral. Rec.*, 8 (1977) 298.
- 2 R. F. Symes, *Mineral. Mag.*, 41 (1977) 410.
- 3 V. K. Din and P. Henderson, in P. H. Fowler and V. M. Clapham (Eds.), *Solid State Nuclear Track Detectors*, Pergamon Press, Oxford, 1982, p. 597.
- 4 N. R. McQuaker, P. D. Kluckner and G. N. Chang, *Anal. Chem.*, 51 (1979) 888.
- 5 A. Strasheim, M. E. Thain, N. M. Walters, C. Claase, H. G. C. Human and N. P. Ferreira, *Spectrochim. Acta, Part B*, 38 (1983) 921.
- 6 P. W. J. M. Boumans, *Line Coincidence Tables for Inductively Coupled Plasma Atomic Emission Spectrometry*, Pergamon Press, Amsterdam, 1980.
- 7 J. W. Owens, E. S. Gladney and D. Knab, *Anal. Chim. Acta*, 135 (1982) 169.
- 8 J. Doležal, P. Povondra and Z. Šulček, *Decomposition Techniques in Inorganic Analysis*, Iliffe, London, 1968, p. 100.
- 9 S. Abbey, *Geostandards Newsl.*, 6 (1982) 47.
- 10 E. S. Gladney and W. E. Goode, *Geostandards Newsl.*, 5 (1981) 31.
- 11 E. S. Gladney, C. E. Burns and I. Roelandts, *Geostandards Newsl.*, 7 (1983) 3.
- 12 S. Abbey, *Geostandards Newsl.*, 4 (1980) 163.
- 13 A. T. Myers, R. G. Havens, J. J. Connor, N. M. Conklin and H. J. Rose Jr., *Glass Reference Standards for the Trace-Element Analysis of Geological Materials, Compilation of Interlaboratory Data*, U.S. Geological Survey Professional Paper 1013, 1976.
- 14 Bureau of Analysed Samples Ltd., *Certificate of Analysis, prelim. edn.*, B.C.S. No. 389, 1973.
- 15 Bureau of Analysed Samples Ltd., *Certificate of Analysis, main edn.*, B.C.S. No. 319, 1968.

Short Communication

CONSTRUCTION AND ANALYTICAL APPLICATIONS OF AN IMPROVED LIQUID-MEMBRANE ELECTRODE FOR SALICYLATE

A. MITSANA-PAPAZOGLU, E. P. DIAMANDIS and T. P. HADJIOANNOU*

Laboratory of Analytical Chemistry, University of Athens, 104 Solonos Street, Athens 144 (Greece)

(Received 17th October 1983)

Summary. The construction and analytical applications of an improved liquid-membrane electrode for salicylate are described. Tests of various combinations of symmetrical tetraalkylammonium salicylates and solvents showed that the best liquid ion-exchanger was tetraoctylammonium salicylate in *p*-nitrocumene. Electrode response is Nernstian down to 2×10^{-5} M. Major interferences are perchlorate and periodate; the working pH range is 6–9. The electrode is useful for direct potentiometric determinations of salicylate in pharmaceutical preparations.

The construction and analytical applications of electrodes sensitive to salicylate ion have already been reported [1–5]. Although there is a need for salicylate electrodes with good response characteristics for application in pharmaceutical analysis, most of the reported electrodes are not very sensitive or selective.

In this communication, the performance characteristics of a new liquid-membrane salicylate-sensitive electrode are described. The best liquid ion-exchanger for the electrode was found to be tetraoctylammonium salicylate dissolved in *p*-nitrocumene; other compounds tested were tetraheptylammonium, tetraoctylammonium, tetradecylammonium, tetradodecylammonium or tetraoctadecylammonium salicylate dissolved in 4-nitro-*m*-xylene, 2-nitro-*m*-xylene, *p*-nitrocumene, 3-nitrotoluene or 2-nitrotoluene. The electrode response is Nernstian down to 2.00×10^{-5} M and the selectivity in presence of various common anions is satisfactory.

Experimental

Instrumentation. The reference electrode was an Orion 90-01-00 Ag/AgCl single-junction electrode, filled with Orion 90-00-01 solution. The e.m.f. values were measured with a Corning Model 12 Research pH/mV meter, at ambient temperature with constant magnetic stirring.

Reagents. All solutions were prepared with deionized-distilled water from reagent-grade materials, unless otherwise stated. Pharmaceutical preparations were obtained from local drugstores. Standard 0.1000 M sodium salicylate solution was prepared by dissolving 1.381 g of salicylic acid in 45 ml of

0.2 M sodium hydroxide, adjusting the pH to 7.0 with 0.1 M sodium hydroxide and diluting to 100.0 ml. The purity of the salicylic acid used was checked by potentiometric titration with standard sodium hydroxide solution. Salicylate solutions were stored in amber bottles. All other salicylate solutions were prepared by dilution with water.

Preparation of the liquid ion-exchangers. An appropriate amount of tetraoctylammonium bromide (or tetraheptylammonium, tetradecylammonium, tetradodecylammonium or tetraoctadecylammonium bromide) was dissolved in 5.0 ml of *p*-nitrocumene (or 2-nitrotoluene, 3-nitrotoluene, 4-nitro-*m*-xylene or 2-nitro-*m*-xylene) to give a 0.01 M solution (or 5×10^{-3} M for the last two bromide salts). After extraction with three 10-ml portions of aqueous 0.10 M sodium salicylate (to exchange bromide with salicylate), the organic phase was dried thoroughly with anhydrous sodium sulfate and used for preparation of the electrode.

Construction of the electrodes. An Orion liquid-membrane electrode body (model 92) was used with Orion perchlorate membranes and the above ion-exchange solution. The internal reference solution was 0.01 M sodium salicylate/0.1 M sodium chloride. The electrodes were conditioned for 24 h before use in 0.01 M sodium salicylate and stored in this solution when not in use.

Calibration graphs. Phosphate buffer (30 ml, 0.50 M, pH 7.0) was pipetted into a 100-ml beaker, the electrodes were immersed, constant stirring was started, and 0.001 ml of 0.1 M sodium salicylate standard solution was added. The reading was recorded after stabilization to ± 0.1 mV. Further increments of 0.1 M standard solution were added to cover the 3.3×10^{-6} – 1.2×10^{-2} M range and the calibration graphs were plotted in the usual way.

Determination of salicylate in pharmaceutical preparations. Locacorten Tar ointment (10 g), Locasalen ointment (5 g), Olamyc tincture (10 ml), Volog tincture (10 ml) or Pyralvex solution (4 ml) was dissolved in chloroform (120 ml). The chloroform solution was centrifuged at 4000 rpm for 5 min, transferred to a separatory funnel and extracted with four 40-ml portions of 0.1 M sodium hydroxide. The aqueous solution was neutralized with 1 M hydrochloric acid and transferred to a 250-ml volumetric flask. Phosphate buffer (50 ml, 0.50 M, pH 7.0) was added and the solution was diluted to the mark; 30.00 ml of this solution was pipetted into the measuring cell for e.m.f. recording. The salicylate concentration was found from the above calibration graph. Collodion BAG (2 ml), a Greek product, was dissolved in 100 ml of water, the solution was mixed with buffer and the e.m.f. was measured, as described before.

Results and discussion

Characteristics of the electrodes. Twenty-one electrodes were constructed with the salicylates of various symmetric tetraalkylammonium cations dissolved in different organic solvents. The slopes of the calibration graphs and the lower limits of linear response for these electrodes are summarized in

TABLE 1

Slope and lower limit of linear response for various salicylate electrodes at 25°C

Quaternary ammonium ion	Slope and lower limit ^a in different solvents				
	2-Nitro- <i>m</i> -xylene	4-Nitro- <i>m</i> -xylene	2-Nitro-toluene	3-Nitro-toluene	<i>p</i> -Nitro-cumene
Tetraheptyl	—	—	59(3.7)	—	—
Tetraoctyl	58(4.3) ^a	54(4.4)	53(4.2)	58(4.5)	59(4.7)
Tetradecyl	52(4.3)	53(4.4)	53(4.4)	51(4.7)	53(4.7)
Tetradodecyl	54(4.4)	60(4.4)	54(4.2)	57(4.7)	56(4.7)
Tetraoctadecyl	52(4.2)	23(4.4)	53(4.6)	53(4.7)	47(4.7)

^aThe first number indicates the slope of the linear response plot in mV, with the p[salicylate] corresponding to the lower limit of linear response in parenthesis.

Table 1. The results show that the limit of linear response is affected markedly when tetraheptylammonium is replaced by tetraoctylammonium in the liquid ion-exchanger but remains practically unchanged when tetraoctylammonium is replaced by bulkier quaternary compounds up to tetraoctadecylammonium. In terms of sensitivity, slightly better results were obtained when 3-nitrotoluene or *p*-nitrocumene was used as solvent. The combination of tetraoctylammonium salicylate in *p*-nitrocumene was chosen for further studies. A typical calibration graph for this electrode is shown in Fig. 1.

The pH dependence of the electrode response was checked at three salicylate concentrations (Fig. 2). At pH 6–9, the potentials are practically stable,

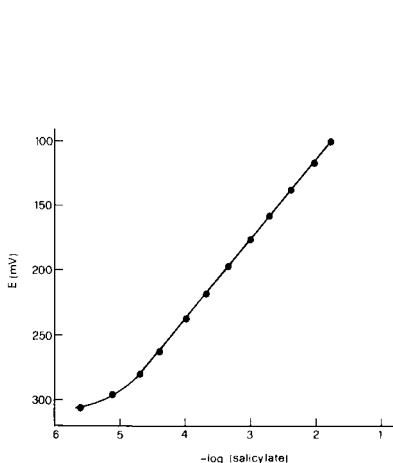


Fig. 1. Calibration graph for the electrode based on tetraoctylammonium salicylate in *p*-nitrocumene.

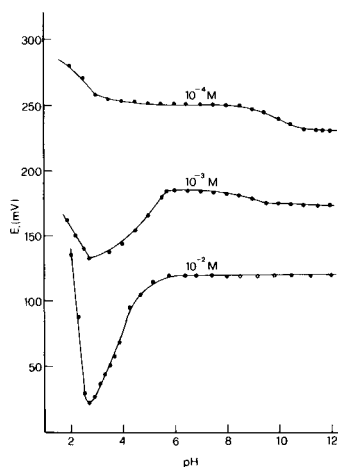


Fig. 2. The pH dependence of the response to 10^{-2} – 10^{-4} M salicylate.

but change slightly up to pH 12; at pH < 6, the potential changes markedly with pH especially at high concentrations, in an unpredictable way. For direct potentiometric measurements, a pH of 7 (phosphate buffer) was selected as the optimum.

Potentiometric selectivity coefficients for the salicylate electrode were measured by the mixed solution method and calculated as described previously [6]. The results are presented in Table 2.

Analytical applications. The salicylate electrode was applied in the direct potentiometric determination of salicylic acid in some pharmaceutical preparations. The salicylic acid was isolated by extractions and measured directly in the aqueous extract after pH adjustment. The results (with the nominal values in parentheses) were: Locacorten Tar ointment, 1.20 g/100 g (1.0); locazalen ointment, 2.9 g/100 g (3.0); Olamyc tincture, 22.3 mg ml⁻¹ (20.0); Volog tincture, 22.1 mg ml⁻¹ (20.0); Pyralvex solution, 12.9 mg ml⁻¹ (10.0); BAG, 8.4 g/100 g (8.4). Thus the electrode seems suitable for application in pharmaceutical analysis.

TABLE 2

Potentiometric selectivity coefficients for the salicylate electrode^a

Ion _j	α'_{sal} ($\times 10^{-4}$ M)	$K_{\text{sal},j}^{\text{pot}}$	Ion _j	α'_{sal} ($\times 10^{-4}$ M)	$K_{\text{sal},j}^{\text{pot}}$
NO ₃ ⁻	7.5	3.8×10^{-2}	SO ₄ ²⁻ ^b	6.6	<10 ⁻⁴
Cl ⁻	7.5	<10 ⁻⁴	CO ₃ ²⁻ ^b	6.6	<10 ⁻⁴
Br ⁻	7.5	4.4×10^{-3}	C ₆ H ₅ COO ⁻	7.5	4.5×10^{-3}
I ⁻	7.5	5.6×10^{-1}	ClO ₄ ⁻	7.5	20
CH ₃ COO ⁻	7.5	<10 ⁻⁴	IO ₄ ⁻	7.5	28

^aExcept where mentioned, the activity of ion j (present as the sodium salt) was 7.5×10^{-2} M. The activity of salicylate in pure solutions was 10^{-3} M in all cases, α'_{sal} is the activity of salicylate in mixed salicylate/interferent solutions. ^bAt an activity of 1.9×10^{-2} M.

REFERENCES

- 1 M. W. Haynes and J. A. Wagenkuecht, *Anal. Lett.*, 4 (1971) 491.
- 2 T. Shigematsu, A. Ota and M. Matsui, *Bull. Inst. Chem. Res. Kyoto Univ.*, 51 (1973) 268.
- 3 E. A. Materova, S. A. Orchinnicova and S. A. Smekalova, *Elektrokhimiya*, 14 (1978) 71.
- 4 H. Freiser, H. J. James, G. Carmack, R. W. Cattrall, and B. M. Kneebone, U.S. Patent 4115209, Sept. 19, 1978, Appl. 219119, Jan. 19, 1972, *Chem. Abst.*, 90 (1979) 15804X.
- 5 K. K. Choi and K. W. Fung, *Anal. Chim. Acta*, 138 (1982) 385.
- 6 E. P. Diamandis and T. P. Hadjiioannou, *Anal. Lett.*, 13 (B15) (1980) 1317.

Short Communication

EFFECT OF CELL GEOMETRY ON CONDUCTANCE MEASUREMENTS IN FLOW CELLS

DOUGLAS TAYLOR and TIMOTHY A. NIEMAN*

School of Chemical Sciences, University of Illinois, Urbana, IL 61801 (U.S.A.)

(Received 12th October 1983)

Summary. Solution resistance is monitored as the spacer thickness in the flow cell is increased. Different trends are observed for electrode pairs in series on the same side of the cell, directly opposing each other in opposite sides of the cell, and diagonally opposing each other in opposite sides of the cell. For the diagonal and series arrangements, anomalously high resistances are measured for narrow spacers.

Conductimetric monitoring of flowing streams is becoming widespread. It has found use in ion-chromatography [1], in a flow-injection system [2], in ion-selective electrode monitoring [3] and in critical micelle concentration studies [4]. In many flow-cell designs, the principal goal has been to minimize the cell volume without degrading performance. Recent work in this laboratory on bipolar-pulse conductimetric monitoring of ion-selective electrodes in flowing streams has shown unusual effects on individual measurements and shapes of working curves depending on the relative location of the electrodes [5]. This phenomenon seemed to deserve further study in order to learn general principles relevant to flow-cell design for conductimetric measurements. This communication presents results obtained when the distance between electrodes was varied for three different relative placements, and two different sizes of electrodes.

Experimental

Instrumentation. A computer-controlled conductance instrument based on the bipolar-pulse method (BICON) was used. The theory of BICON and description of the instrument can be found elsewhere [3, 6, 7]. The instrument allows very fast measurement (30 μ s) and signal-averaging for precise readings (0.1% relative standard deviation). Solutions to be monitored were fed into the cell by a Sage Model 355 syringe pump. The flow rate was nominally 1 ml min⁻¹. A flowing stream was used only to minimize any possible heating. Resistance measurements in static solutions gave identical results.

The flow cells were similar to those used previously [5]. The basic design of the cell is presented in Fig. 1. The cell design was originally developed

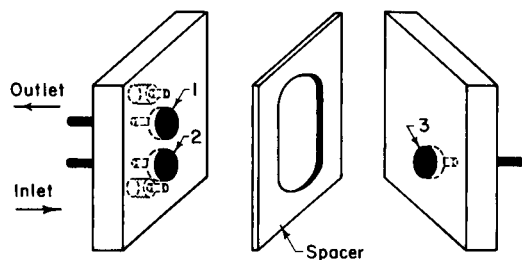


Fig. 1. Schematic of the conductance flow cell. For detail, see text.

to allow a variety of counter-electrode geometries for use with commercially available (and therefore relatively large) ion-selective electrodes. Although the resulting cell volume is larger than would be desirable for simple conductimetric monitoring in flowing streams, this cell was very useful for the present study because it offered the flexibility of studying several electrode geometries and spacings. In one cell, the electrodes were stainless steel, approximately 8 mm in diameter. A second cell had small platinum rods which were about 1 mm in diameter, but all other cell dimensions were the same. Electrodes 1 and 2 are 1.0 cm center to center. The cells were made from plexiglas and teflon. Teflon was used for the spacers which ranged in thickness from 1.6 to 25 mm. The cell cavity cut in the spacers was approximately 1-cm wide and 2-cm long with rounded ends. The nominal cell volume then varied from 0.3 to 4.8 ml for the 1.6 to 25 mm spacers. The same spacers were used for both the steel and platinum electrodes. Because the platinum electrodes were smaller than the steel electrodes, it would have been possible to have reduced cell volumes to 50 to 800 μl for the same spacer thicknesses. To distinguish between the three possible combinations, the following labels are used: electrodes 1 and 2 were the series, 2 and 3 were the opposing, and 1 and 3 were the diagonal configurations.

Procedure. Potassium chloride solution (0.010 M) was fed into the cell and measurements were taken with the instrument; the pulse height was 5.0 V and the pulse width 10 μs . An individual data point was the average of 128 readings. Ten of these individual points were then averaged to get the final resistance value for a given spacer. This was done for all possible electrode arrangements before a new spacer was inserted.

Potassium chloride (analytical grade; Mallinckrodt) was dissolved in water (from a Continental/Millipore Milli-Q reagent grade water system) to make the 0.010 M solution.

Results and discussion

Figure 2 shows the trends of the solution resistance vs. spacer width for the three configurations with the stainless steel electrodes and the platinum electrodes. The resistances with platinum were higher because of the smaller area. There was no systematic variation in precision with spacer thickness.

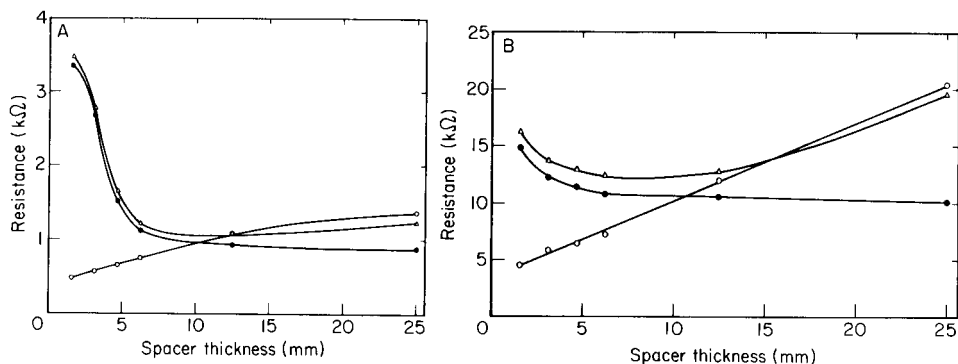


Fig. 2. Variation of measured resistance with spacer thickness for different electrodes: (A) stainless-steel electrodes of ca. 8 mm diameter; (B) platinum electrodes of ca. 1 mm diameter. Electrode geometry; (●) series, (○) opposing, (Δ) diagonal.

The relative standard deviation for all measurements was 0.5% or better. The shapes of the curves and the magnitudes of the measured resistances were independent of the solution flow rate and the flow characteristics of the cell. The same values were obtained in measurements with flowing and static solutions.

Theory predicts the measured resistance to be proportional to $d A^{-1}$, where d is the distance between electrodes and A is the electrode area. The opposing configuration gave the expected results. As the electrodes were moved further apart, the resistance increased monotonically. The observed increase is more nearly linear for the small platinum electrodes than for the large steel electrodes. The other two arrangements behaved differently than originally expected. It was believed that because electrode spacing and area for the series configuration never changed, the resistance measured should be constant. However, as Fig. 2 shows, this is not the case until the opposite wall is relatively far away. The large electrodes show a much larger deviation at close distance than the small electrodes.

The diagonal electrodes show behavior similar to each of the other two configurations. The diagonal electrodes behave like series electrodes at small spacings, then they act more like the opposing electrodes at large spacing. This behavior is reasonable considering the inter-electrode distances. For a 1.59-mm spacer, the distances for the series, opposing, and diagonal pairs are 10.0 mm, 1.59 mm and 10.13 mm; the series and diagonal pairs are nearly the same distance apart, and show nearly the same resistance. For a 25.4-mm spacer, the distances for the series, opposing, and diagonal pairs are 10.0 mm, 25.4 mm, and 27.3 mm; then it is the opposing and diagonal pairs that are nearly the same distance apart and show nearly the same resistances. The effective electrode area (the projected geometric area) decreases for the diagonal pair as the spacer thickness decreases. One can calculate the projected electrode area as a function of spacer thickness and calculate the product, $d A^{-1}$. Such a calculation correctly predicts that for

the cell geometry used, the resistance for the diagonal pair should pass through a minimum at around 10–15 mm.

For the series electrodes, and perhaps somewhat for the diagonal position, the effect of the opposite wall on the electric fields would explain the data. When the walls are close, the field tends to run into the wall, but at larger spacings, the electric field can follow its natural path. This "wall effect" was also noticed with a solution in a beaker. If the positions of the rods used for the electrodes were changed relative to the wall (but not to each other), the measured resistance changed.

Calibration plots of log resistance vs. log concentration were prepared for 10^{-6} – 10^{-2} M potassium chloride using all three electrode configurations (stainless-steel electrodes) in cells with 1.6- and 12.7-mm spacers. For these conditions, the absolute magnitudes of the resistances were very different, as given in Fig. 2A, but the shapes of the log–log plots were the same. From 10^{-5} to 10^{-2} M, the plots were linear and parallel, but flattened out below 10^{-5} M.

Electrode placement within a cell and electric field effects can make a substantial difference to the signal from a cell. For the small spacing, the opposing configuration gives the largest signals (current measured is inversely proportional to resistance). Because larger signals need less amplification, and this usually means less noise, the opposing configuration is the best. Considerable reduction of cell volume can be made if the cell is designed with only opposing electrodes of small area. Such a cell can be made with a total volume of 10 μ l or less, and is thus very attractive for detection in flowing streams.

REFERENCES

- 1 T. Stevens, J. Davies and H. Small, *Anal. Chem.*, 53 (1982) 1488.
- 2 Yokogawai Electrical Works, Japanese Patent, 83 55, 857 (1983).
- 3 C. R. Powley, R. F. Geiger and T. A. Nieman, *Anal. Chem.*, 52 (1980) 705.
- 4 D. Taylor and T. A. Nieman, *Anal. Chem.*, 56 (1984) 593.
- 5 C. R. Powley and T. A. Nieman, *Anal. Chim. Acta*, 152 (1983) 173.
- 6 K. J. Caserta, F. J. Holler, S. R. Crouch and C. G. Enke, *Anal. Chem.*, 50 (1978) 1534.
- 7 R. F. Geiger, Ph.D. Thesis, University of Illinois, 1983.

ANALYTICA CHIMICA ACTA, VOL. 159 (1984)

AUTHOR INDEX

- Abrahamson, H. B.
— and Vanderpool, R. A.
Quantitative liquid chromatography of metal tetraalkyls 355
- Baer, von, D., see Momberg V., A. 119
- Barthová, J., see Pacáková, V. 71
- Berggren, P.-O., see Nilsson, T. 381
- Bhattacharyya, S. N., see Das, N. R. 255
- Błazejowski, J.
— and Szychliński, J.
1,4-Dioxane as a solvent in spectroscopy and photochemistry 369
- Bottalico, A., see Visconti, A. 111
- Brabcová, D., see Pacáková, V. 71
- Bruhn F., C., see Momberg V., A. 119
- Bursey, M. M.
—, Nystrom, J. A. and Hass, J. R.
survey of reaction types in low-energy collisional activation of protonated methyl alkyl ketones, 265
- Bursey, M. M.
—, Nystrom, J. A. and Hass, J. R.
survey of reactions of protonated acetate esters induced on low-energy collisions with helium and nitrogen, 275
- Carpenter, P. D.
— and Smith, J. D.
Simultaneous spectrophotometric determination of humic acid and iron in water 299
- Carr, P. W., see Shih, Y. T. 211
- Carre, B.
— and Devynck, J.
The acidity of superacidic media derived from fluorosulfuric acid and trifluoromethanesulfonic acid 149
- Carrera B., M. E., see Momberg V., A. 119
- Cofino, W. P., see Hofstraat, J. W. 359
- Covington, A. K., see Sibbald, A. 47
- Crouch, S. R., see Thompson, R. Q. 337
- Das, N. R.
—, Nandi, B. and Bhattacharyya, S. N.
Separation of molybdenum from tungsten with di(2-ethylhexyl)-phosphoric acid as extractant 255
- Devynck, J., see Carre, B. 149
- Diamandis, E. P., see Mitsana-Papazoglou, A. 393
- Din, V. K.
The preparation of iron-free solutions from geological materials for the determination of boron (and other elements) by inductively-coupled plasma emission spectrometry 387
- Doerffel, K., see Sorkau, E. 173
- Doornbos, D. A., see van der Voet, H. 159
- Engelsma, M., see Hofstraat, J. W. 359
- Fardy, J. J.
—, McOrist, G. D. and Florence, T. M.
Rapid radiochemical separation in neutron activation analysis. Part 1. The use of C₁₈-bonded silica gel and selective complexation for determinations of manganese, copper and zinc in biological materials 199
- Florence, T. M., see Fardy, J. J. 199
- Frenzel, W., see Schulze, G. 95
- Fries, T.
—, Lamothé, P. J. and Pesek, J. J.
Determination of rare-earth elements, yttrium and scandium in manganese nodules by inductively-coupled argon-plasma emission spectrometry 329
- Gooijer, C., see Hofstraat, J. W. 359
- Gunasingham, H.
Large-volume wall-jet cells as electrochemical detectors for high-performance liquid chromatography 139
- Haar, van de, G., see van der Voet, H. 159
- Hadjioannou, T. P., see Mitsana-Papazoglou, A. 393
- Hass, J. R., see Bursey, M. M. 265, 275
- Hayashi, M., see Kihara, K. 81
- Hirose, S., see Kihara, K. 81
- Hofstraat, J. W.
—, Engelsma, M., Cofino, W. P., Hoornweg, G. Ph., Gooijer, C. and Velthorst, N. H.
Highly-resolved fluorescence spectrom-

- etry of pyrene on a thin-layer chromatographic plate 359
- Hoornweg, G. Ph., see Hofstraat, J. W. 359
- Janse, T. A. H. M.
— and Kateman, G.
Enhancement of the performance of analytical laboratories by a digital simulation approach 181
- Jarosz, M.
— and Marczenko, Z.
Spectrophotometric study of reactions of scandium, yttrium and lanthanum ions with some triphenylmethane dyes in the presence of cationic surfactants 309
- Karayannis, M. I., see Xenakis, A. G. 343
- Kateman, G., see Janse, T. A. H. M. 181
- Kihara, K.
—, Yasukawa, E., Hayashi, M. and Hirose, S.
Determination of glutamate-pyruvate transaminase activity in blood serum with a pyruvate oxidase/poly(vinyl chloride) membrane sensor 81
- Kina, K., see Shiga, M. 365
- Kopanica, M., see Stará, V. 105
- Koryta, J.
Theory and applications of ion-selective electrodes. Part 5 1
- Kowalski, Z.
— and Kubiak, W.
Linear-sweep voltammetry at a dropping mercury electrode in continuous flow systems 129
- Kubiak, W., see Kowalski, Z. 129
- Lamothe, P. J., see Fries, T. 329
- Lanza, P., see Taddia, M. 375
- Lugari, M. T., see Mangia, A. 349
- Mangia, A.
— and Lugari, M. T.
Separation and determination of inorganic anions by means of ion-pair chromatography 349
- Marczenko, Z., see Jarosz, M. 309
- Matsunaga, T.
— and Namba, Y.
Selective determination of microbial cells by graphite electrode modified with adsorbed 4,4'-bipyridine 87
- McOrist, G. D., see Fardy, J. J. 199
- Meems, M., see van der Voet, H. 159
- Meier, P. C., see Sorkau, E. 173
- Midgley, D.
Lead-selective electrodes based on lead(IV) oxide 63
- Mitsana-Papazoglou, A.
—, Diamandis, E. P. and Hadjiioannou, T. P.
Construction and analytical applications of an improved liquid-membrane electrode for salicylate 393
- Momberg V., A.
—, Carrera, B., M. E., von Baer, D., Bruhn F., C. and Smyth, M. R.
The oxidative voltammetric behaviour of some sulphonamides at the glassy carbon electrode 119
- Moreno, A.
—, Silva, M. and Perez-Bendito, D.
Simultaneous spectrofluorimetric determination of iron and manganese by a differential kinetic catalytic method 319
- Nakagawa, G., see Wada, H. 289
- Namba, Y., see Matsunaga, T. 87
- Nandi, B., see Das, N. R. 255
- Nieman, T. A., see Taylor, D. 397
- Nilsson, T.
— and Berggren, P.-O.
The determination of cadmium in microgram amounts of pancreatic tissue by electrothermal atomic absorption spectrometry 381
- Nystrom, J. A., see Bursey, M. M. 265, 275
- Ohki, A.
—, Takagi, M. and Ueno, K.
Liquid-liquid extraction of Group IB metal ions by thioethers 245
- Ohshita, K., see Wada, H. 289
- Pacáková, V.
—, Štulík, K. Brabcová, D. and Barthová, J.
Use of the Clark oxygen sensor with immobilized enzymes for determinations in flow systems 71
- Palmisano, F., see Visconti, A. 111
- Perez-Bendito, D., see Moreno, A. 319
- Pesek, J. J., see Fries, T. 329
- Petrukhin, O. M., see Timerbaev, A. R. 229
- Reiher, T., see Sorkau, E. 173
- Saito, M., see Shiga, M. 365

- Schulze, G.
— and Frenzel, W.
Potentiometric stripping analysis and anodic stripping voltammetry with carbon fiber electrodes 95
- Shiga, M.
—, Saito, M., Ueno, K. and Kina, K.
Synthesis of a new tetrazolium salt giving a water-soluble formazan and its application in the determination of lactate dehydrogenase activity 365
- Shih, Y. T.
— and Carr, P. W.
A post-column photochemical detector for use in the determination of trace metals with *n*-butyl-2-naphthylemethyl-dithiocarbamate by high-performance liquid chromatography 211
- Sibbald, A.
—, Whalley, P. D. and Covington, A. K.
A miniature flow-through cell with a four-function ChemFET integrated circuit for simultaneous measurements of potassium, hydrogen, calcium and sodium ions 47
- Silva, M., see Moreno, A. 319
- Smith, J. D., see Carpenter, P. D. 299
- Smyth, M. R., see Momberg V., A. 119
- Sorkau, E.
—, Doerffel, K., Reiher, T. and Meier, P. C.
Bewertung von glättungsexperimenten 173
- Stará, V.
— and Kapanica, M.
Adsorptive stripping voltammetric determination of thiourea and thiourea derivatives 105
- Štulík, K., see Pacáková, V. 71
- Suzuki, N., see Watarai, H. 283
- Szychliński, J., see Błazejowski, J. 369
- Taddia, M.
— and Lanza, P.
Determination of chromium in gallium arsenide by electrothermal atomic absorption spectrometry 375
- Takagi, M., see Ohki, A. 245
- Taylor, D.
— and Nieman, T. A.
Effect of cell geometry on conductance measurements in flow cells 397
- Thompson, R. Q.
— and Crouch, S. R.
Stopped-flow kinetic determination of glucose and lactate with immobilized enzymes 337
- Timerbaev, A. R.
— and Petrukhin, O. M.
Liquid adsorption chromatography of chelates. The effect of structure on the thin-layer chromatographic behaviour of chelates 229
- Ueno, K., see Ohki, A. 245
- Ueno, K., see Shiga, M. 365
- van de Haar, G., see van der Voet, H. 159
- Vanderpool, R. A., see Abrahamson, H. B. 355
- van der Voet, H.
—, Doornbos, D. A., Meems, M. and van de Haar, G.
The use of pattern recognition techniques in chemical differentiation between Bordeaux and Bourgogne wines 159
- Velthorst, N. H., see Hofstraat, J. W. 359
- Visconti, A.
—, Bottalico, A., Palmisano, F. and Zambonin, P. G.
Differential-pulse polarography of trichothecene mycotoxins. Determination of deoxynivalenol, nivalenol and fusarenone-x in maize 111
- Voet, van der, H., see van der Voet, H. 159
- von Baer, D., see Momberg V., A. 119
- Wada, H.
—, Nakagawa, G. and Ohshita, K.
Synthesis of *o,o'*-dihydroxyazo compounds and their application to the determination of magnesium and calcium by flow injection analysis 289
- Watarai, H.
— and Suzuki, N.
Flow fluorimetry of trace amounts of uranium(VI) after preconcentration on a tri-*n*-octylphosphine oxide/polyethylene column and elution with hydrogen-phosphate solution 283
- Whalley, P. D., see Sibbald, A. 47
- Xenakis, A. G.
— and Karayannis, M. I.
Kinetic spectrophotometric assay of sulfonamides by use of the Griess reaction and a stopped-flow procedure 343
- Yasukawa, E., see Kihara, K. 81
- Zambonin, P. G., see Visconti, A. 111

ACA announcements

GABOR SZASZ PRIZE

GABOR SZASZ PRIZE FOR CLINICAL ENZYMOLOGY 1985

The Deutsche Gesellschaft für Klinische Chemie will award the third Gabor Szasz Prize in 1985. This prize of DM 10,000.—, in honour of the late Gabor Szasz, is donated by the Deutsche Gesellschaft für Klinische Chemie. It is awarded for outstanding advances in the field of clinical enzymology.

Applicants for the Gabor Szasz Prize 1985 may submit scientific papers on suitable topics which either have been published or have been accepted for publication after January 1, 1982. Applicants are requested to send 3 copies of each paper to the Secretary of the Prize Committee before November 1, 1984. In cases where there is more than one author, please indicate name(s).

Secretary: Professor Dr. G. Gundlach, Biochemisches Institut der Justus-Liebig-Universität, Friedrichstrasse 24, 6300 Giessen, F.R.G.

ANNOUNCEMENTS OF MEETINGS

1985 EUROPEAN WINTER CONFERENCE ON PLASMA SPECTROCHEMISTRY, LEYSIN, SWITZERLAND, JANUARY 7-11, 1985

The 1985 European Winter Conference on Plasma Spectrochemistry will feature developments in plasma spectrochemical analysis by inductively-coupled plasma, direct-current plasma and microwave plasma sources. The meeting will be held in Leysin, Switzerland on Monday, January 7 through Friday 11 at the "Hotel Reine Fabiola". Leysin is located east of the lake of Geneva and is one of the most important Swiss mountain resorts.

Original papers will be published following the meeting after a peer review in *Spectrochimica Acta*, part B. An exhibition on plasma instrumentation will be a feature.

Further information: Professor J.M. Mermet, Plasma Conference, Service Central d'Analyse, CNRS, BP 22, F-69390 Vernaison, France.

FLOW ANALYSIS III - AN INTERNATIONAL CONFERENCE ON FLOW ANALYSIS, BIRMINGHAM, U.K., SEPTEMBER 5-8, 1985

The 3rd International Conference on Flow Analysis will be organized by the Midlands Region of the Analytical Division of the Royal Society of Chemistry. The scope of the Conference will be similar to that of the Flow Analysis Conferences held in Amsterdam, 1979, and Lund, 1982, and will cover research on all aspects of continuous flow analysis. The scientific programme will consist of plenary and invited lectures, submitted research papers and posters, and working demonstrations. An exhibition of commercial equipment will be organized. As with the earlier conferences, proceedings will be published in a special issue of *Analytica Chimica Acta*.

The Conference will be held in the Department of Chemistry, University of Birmingham; accommodation will be available in the University Halls of Residence.

For further information, contact: Flow Analysis III, Dr. A.M.G. Macdonald, Department of Chemistry, The University, P.O. Box 363, Birmingham B15 2TT, U.K.

CALENDAR OF FORTHCOMING MEETINGS

- June 12-14, 1984
Gaithersburg, MD,
U.S.A.
37th Annual Summer Symposium on Analytical Chemistry - Trends and Accomplishments in Electroanalytical Chemistry
Contact: Harry Hertz, A309 Chemistry Building, NBS, Washington, DC 20234, U.S.A. Tel.: (301) 921-2851.
- June 12-14, 1984
Széged, Hungary
2nd Symposium on the Analysis of Steroids
Contact: Professor S. Görög, Chairman of the Organizing Committee of the 2nd Symposium on the Analysis of Steroids, c/o Hungarian Chemical Society, H-1061 Budapest, Anker köz 1, Hungary.
- June 18-20, 1984
Milan, Italy
2nd International Conference on Chromatography and Mass Spectrometry in Biomedical Sciences
Contact: Dr. Alberto Frigerio, Italian Group for Mass Spectrometry in Biochemistry and Medicine, Via Eustachi 36, I-20219 Milan, Italy; or, Dr. Hubert Milon, P.O. Box 88, CH-1814 La Tour-de-Peilz, Switzerland. Tel: (24) 42 11 91; Telex: 457302 lino ch. (Further details published in Vol. 155.)
- June 18-21, 1984
Ronneby, Sweden
International Symposium on Liquid Chromatography in the Biomedical Sciences
Contact: Swedish Academy of Pharmaceutical Sciences, P.O. Box 1136, S-111 81 Stockholm, Sweden. (Further details published in Vol. 152.)
- June 24-28, 1984
Jerusalem, Israel
9th International CODATA (Committee on Data for Science and Technology) Conference
Contact: Kopel Tours Ltd. - Conventions, P.O. Box 4413, 61 044 Tel Aviv, Israel. Tel.: (03) 653616; Telex: 35562 ktor il; Cable: Kopel Tel Aviv.
- July 10-13, 1984
Leeds, U.K.
2nd Biennial National Atomic Spectroscopy Symposium
Contact: Mr. F. Buckley, Department of Earth Sciences, University of Leeds, Leeds, W. Yorks. LS2 9JT, U.K. Tel. 0532-431751, ext. 6464 or 6465. (Further details published in Vol. 155.)
- Aug. 21-24, 1984
Colombo, Sri Lanka
Analytical Chemistry in Development
Contact: Centre for Analytical Research and Development, Department of Chemistry, University of Colombo, Colombo, Sri Lanka; or, Trace Analysis Research Centre, Chemistry Department, Dalhousie University, Halifax, N.S. B3H 4J1, Canada. (Further details published in Vol. 151, No 1.)
- Aug. 26-31, 1984
Philadelphia, PA, U.S.A.
188th National Meeting of the American Chemical Society
Contact: A.T. Winstead, American Chemical Society, 1155 16th Street, NW, Washington, DC 20036, U.S.A.
- Aug. 26-Sept. 1, 1984
Cracow, Poland
EUROANALYSIS V - 5th European Conference on Analytical Chemistry
Contact: Professor Zygmunt Kowalski, Secretary-General, Euroanalysis V, Academy of Mining and Metallurgy, Mickiewiczza 30, 30-059 Kraków, Poland. (Further details published in Vol. 148.)
- Aug. 27-31, 1984
Göttingen, F.R.G.
Electrophoresis 84. 4th International Meeting of the Electrophoresis Society
Contact: Dr. V. Neuhoff, Max-Planck-Institut für experimentelle Medizin, Hermann-Rein-Strasse 3, D-3400 Göttingen, F.R.G. Tel.: 0551-303248.

- Sept. 2-6, 1984
Hradec Králové,
Czechoslovakia
- Sept. 3-6, 1984
Ghent, Belgium
- Sept. 16-21, 1984
Philadelphia, PA, U.S.A.
- Oct. 1-5, 1984
Nürnberg, F.R.G.
- Oct. 8-10, 1984
Tarrytown, NY, U.S.A.
- Oct. 13-18, 1984
Mátrafüred, Hungary
- Oct. 24-26, 1984
Montreux,
Switzerland
- Nov. 13-16, 1984
New York, NY, U.S.A.
- Nov. 19-24, 1984
Barcelona, Spain
- Nov. 22-24, 1984
Barcelona, Spain
- Nov. 22-24, 1984
Barcelona, Spain
- 4th International Symposium on Isotachophoresis - ITP 84**
Contact: ITP 84, Dr. Z. Prusik, C.Sc., Institute of Organic Chemistry and Biochemistry, Czechoslovak Academy of Sciences, Flemingovo nám. 2, CS-166 10 Praha 6, Czechoslovakia. (Further details published in Vol. 146.)
- International Symposium on Quantitative Luminescence Spectrometry in Biomedical Sciences**
Contact: Dr. W. Baeyens, Symposium Chairman, Laboratoria voor Farmaceutische Chemie en voor Ontleding van Geneesmiddelen, Rijksuniversiteit Gent, Harelbekestraat 72, B-9000 Ghent, Belgium. (Further details published in Vol. 157, No. 1.)
- 11th Annual FACSS Meeting**
Contact: FACSS IX Program Chairman, Dr. P.B. Roush, Perkin-Elmer Corporation, M/S 903, 901 Ethan Allen Highway, Ridgefield, CT 06877, U.S.A. Tel.: (203) 797-9481
- 15th International Symposium on Chromatography**
Contact: Gesellschaft Deutscher Chemiker, Abteilung Fachgruppen, Postfach 90 04 40, Varrentrappstrasse 40-42, D-6000 Frankfurt (Main) 90, F.R.G.
- 3rd International Symposium on Capillary Chromatography**
Contact: Dr. A. Zlatkis, Chemistry Department, University of Houston, Houston, TX 77004, U.S.A.
- 4th Scientific Session on Ion-Selective Electrodes**
Contact: Organizing Committee, 4th Scientific Session on Ion-Selective Electrodes, Institute for General and Analytical Chemistry, Technical University, 1502 Budapest, Gellért tér 4, Hungary. (Further details published in Vol. 155.)
- Third Workshop on LC-MS and MS-MS**
Contact: Professor Dr. R.W. Frei, Department of Analytical Chemistry, Free University, De Boelelaan 1083, 1081 HV Amsterdam, The Netherlands. (Further details published in Vol. 151, No. 1.)
- 23rd Annual Eastern Analytical Symposium**
Contact: Dr. S. David Klein, EAS Publicity, Merck & Co., Inc., P.O. Box 2000/R80L-106, Rahway, NJ 07065, U.S.A. Tel.: (201) 846-1582. (Further details published in Vol. 157, No. 1.)
- EXPOQUIMIA 84 - Salón Internacional de la Química**
Contact: EXPOQUIMIA, Feria de Barcelona, Barcelona 4, Spain.
- 14th Annual Symposium on Analytical Chemistry of Pollutants**
Contact: 3rd International Congress on Analytical Techniques in Environmental Chemistry/EXPOQUIMIA, Av. Reina Ma. Christina, Palacio No. 1, Barcelona 4, Spain. Tel.: 223.31.01; telex: 50458 FOIMB-E.
- 3rd International Congress on Analytical Techniques in Environmental Chemistry**
Contact: 3rd International Congress on Analytical Techniques in Environmental Chemistry/EXPOQUIMIA, Av. Reina Ma. Christina, Palacio No. 1, Barcelona 4, Spain. Tel.: 223.31.01; telex: 50458 FOIMB-E. (Further details published in Vol. 157, No. 1.)

- Dec. 10–12, 1984
Baltimore, MD, U.S.A.
- 4th International Symposium on HPLC of Proteins, Peptides, and Polynucleotides**
Contact: Shirley E. Schlessinger, Symposium Manager, Fourth International Symposium on HPLC of Proteins, Peptides, and Polynucleotides, 400 East Randolph, Chicago, IL 60601, U.S.A. Tel.: (312) 527-2011.
- Jan. 7–11, 1985
Leysin, Switzerland
- 1985 European Winter Conference on Plasma Spectrochemistry**
Contact: Prof. J.M. Mermet, Plasma Conference, Service Central d'Analyse, CNRS, B.P. 22, F-69390 Vernaison, France
- Feb. 25–March 1, 1985
New Orleans, LA, U.S.A.
- 36th Pittsburgh Conference and Exposition on Analytical Chemistry and Applied Spectroscopy**
Contact: Linda Biggs, Pittsburgh Conference, 437 Donald Road, Dept. J-005, Pittsburgh, PA 15235, U.S.A.
- April 28–May 3, 1985
Miami Beach, FL, U.S.A.
- 189th National Meeting of the American Chemical Society**
Contact: Meetings Department, American Chemical Society, 1155 Sixteenth Street, NW, Washington, DC 20036, U.S.A.
- May 15–19, 1985
Pretoria, South Africa
- IUPAC Symposium on Analytical Chemistry in the Exploration, Mining and Processing of Materials**
Contact: The Symposium Secretariat, S. 328, CSIR, P.O. Box 395, Pretoria 0001, South Africa. Tel.: (012) 86-9211.4412 or (012) 86-9211.2077. Telex: 3630 SA.
- July 1–5, 1985
Edinburgh, Scotland, U.K.
- 9th International Symposium on Column Liquid Chromatography**
Contact: J.H. Knox, Department of Chemistry, University of Edinburgh, Edinburgh EH9 3JJ, Scotland, U.K.
- Sept. 5–8, 1985
Birmingham, U.K.
- Flow Analysis III – An International Conference on Flow Analysis**
Contact: Flow Analysis III, Dr. A.M.G. Macdonald, Department of Chemistry, The University, P.O. Box 363, Birmingham B15 2TT, U.K.
- Sept. 8–13, 1985
Chicago, IL, U.S.A.
- 190th National Meeting of the American Chemical Society**
Contact: Meetings Department, American Chemical Society, 1155 Sixteenth Street, NW, Washington, DC 20036, U.S.A.
- Sept. 9–13, 1985
Manchester, U.K.
- 30th International Congress of Pure and Applied Chemistry**
Contact: The Royal Society of Chemistry, Burlington House, London W1V 0BN, U.K. (Further details published in Vol. 155.)
- Sept. 15–21, 1985
Garmisch-Partenkirchen, F.R.G.
- Colloquium Spectroscopicum Internationale XXIV**
Contact: CSI XXIV, Organisationsbüro, Institut für Spektrochemie und angewandte Spektroskopie, Postfach 778, D 4600 Dortmund 1, F.R.G.
- Nov. 11–16, 1985
Yalta, U.S.S.R.
- 5th Danube Symposium on Chromatography**
Contact: Dr. L.N. Kolomiets, The Scientific Council of Chromatography, Academy of Sciences of the U.S.S.R., Institute of Physical Chemistry, Lenin-Prospect 31, Moscow 117312, U.S.S.R.
- July 20–26, 1986
Bristol, U.K.
- SAC 86 – International Conference and Exhibition on Analytical Chemistry**
Contact: Miss P.E. Hutchinson, Royal Society of Chemistry, Analytical Division, Burlington House, London W1V 0BN, U.K. Tel.: (01) 735-9971.

NEW!

THEORY, PRACTICE AND APPLICATIONS...

Microcolumn High-Performance Liquid Chromatography

P. KUCERA, *Pharmaceutical Research Products Section,
Hoffmann La Roche Inc., Nutley, NJ, USA (editor)*

(Journal of Chromatography Library 28)

Written by experts in this dynamic, rapidly moving field of chromatography, this is the only book currently available that treats the large and diverse subject of microcolumn chromatographic techniques in such a way as to satisfy both the practical and the theoretical needs of analytical chemists and chromatographers.

The distinguished research workers and university professors who have contributed to this important work have adopted a textbook-type approach to the discussion of the theoretical aspects of new microcolumn techniques. The practical coverage includes instrumentation, design, columns, detectors, injectors, connecting tubing, gradient elution and special analytical techniques, LC-MS, derivatization, etc., and applications are described using various compounds (e.g. drugs, substances of biological origin, proteins, nucleotides, industrial extracts).

The book represents a vast amount of information collected over a period of many years of intensive work and is an essential acquisition for all those who need to keep up-to-date with the latest developments in microcolumn techniques.

Contents: Chapter 1. Narrow-Bore and Micro-Bore Columns in Liquid Chromatography (*G. Guiochon, H. Colin*). 2. Design of a Microbore Column Liquid Chromatograph (*P. Kucera*). 3. Theory and Practice of High-Speed Microbore HPLC (*R.A. Hartwick, D.D. Dezaro*). 4. Special Analytical Techniques (*P. Kucera, G. Manius*). 5. Chemical Derivatization Techniques Using Microcolumns (*P. Kucera, H. Umagat*). 6. Applications of Microbore HPLC (*P. Kucera, R.A. Hartwick*). 7. Liquid Chromatography in Columns of Capillary Dimensions (*M. Novotny*). 8. Micro LC/MS Coupling (*H. Henion*). Subject Index.

1984 xvi + 302 pages
US \$ 63.50/Dfl. 165.00
ISBN 0-444-42290-0

ELSEVIER



P.O. Box 211
1000 AE Amsterdam
The Netherlands

P.O. Box 1663
Grand Central Station
New York, NY 10163, USA

ELSEVIER LAUNCHES SCIENTIFIC SOFTWARE

ELSEVIER SCIENTIFIC SOFTWARE

software with unique features. . .

- all programs extensively refereed and operationally tested
- extensive program manuals usually including source code listings
- free updates for a year, at cost thereafter
- comprehensive information available before ordering

Elsevier, publisher of many journals in the field of analytical chemistry, including the Journal of Chromatography and Analytica Chimica Acta, now has a number of software programs available for use on mini- and microcomputers:

REFVALUE: calculates reference intervals from total hospital-patients laboratory data. (Baadenhuysen and Smit) **for PDP and HP 85.**

Price: Mini computer
Dfl. 3025,00/US\$ 1080,00/£ 756,00/
Yen 252,000.

Micro computer
Dfl. 1400,00/US\$ 500,00/£ 350,00/
Yen 116,700.

BALANCE: a program to statistically compare two series of measurements (Massart) **for IBM-PC and APPLE.**

Price:
Dfl. 420,00/US\$ 150,00/£ 105,00/Yen 35,000.

CLEOPATRA: Chemometrics Library: an Extendable set Of Programs as an Aid in Teaching, Research and Application. (Kateman) **for IBM-PC and HP 9845 B.**

Price:
Dfl. 1680,00/US\$ 600,00/£ 420,00/
Yen 140,000.

INSTRUMENTUNE-UP: helps the user to improve the performance of common scientific laboratory instruments (Deming and Morgan) **for IBM-PC and APPLE.**

Price:
Dfl. 420,00/US\$ 150,00/£ 105,00/Yen 35,000.

and in preparation:

CHEOPS: CHEMometrical OPTimization by Simplex. The program offers an intelligent, sequential experimental plan, based on the modified or super-modified simplex method. It optimizes the response of a system by varying up to ten instrumental parameters.

Please send me further information on:

- REFVALUE BALANCE CHEOPS
 CLEOPATRA INSTRUMENTUNE-UP

ESS
ELSEVIER SCIENTIFIC SOFTWARE

Name _____
Address _____
City _____ Country _____

send this coupon to:

Keith Foley, Elsevier Scientific Software,
P.O. Box 330, 1000 AH Amsterdam,
The Netherlands. (Tel.: 020 - 5803 447)

or:
John Tagler, Elsevier Scientific Software (NASD),
52 Vanderbilt Ave, New York, NY 10017.
(Tel.: (212) 867 9040)

NP

INTERNATIONAL JOURNAL OF BIO-MEDICAL COMPUTING

Editors-in-Chief

J. ROSE, Blackburn, U.K., **J.H. MITCHELL**, Paisley, U.K. and
(manuscript receiving centre for the Americas)
J.G. LLURADO, Loma Linda, CA, U.S.A.

The International Journal of Bio-Medical Computing

provides an international forum for the presentation of original work, interpretative reviews and discussion of fundamental research and new developments in the application of various types of computers (digital, analogue and hybrid) to medicine and the biosciences.

In addition to original research papers and reviews, a Commentary section provides short digests on recent developments in clinical applications of computing.

Aims and Scope

The scope of the journal covers all aspects of computer applications to medicine and the biosciences, including: biochemistry, pharmacokinetics, dietetics, nuclear medicine, imaging techniques, X-ray dosage, hospital administration, pathological data analysis, epidemiology, instrumentation, simulation, cybernetics, medical engineering and medical informatics.

The criteria for acceptance of a paper are: originality of thought, quality of work and clarity of style; mere catalogues of references will not be published. The International Journal of Bio-

Medical Computing is of vital importance for everyone engaged in basic biomedical research, medical information handling and clinical computer applications.

Editorial Board

N.M. Amosov, Kiev
J. Anderson, London
A.N. Barrett, Mill Hill
R. Bellmann, Los Angeles, CA
L.L. Cavalli-Sforza, Stanford, CA
Y. Cherruault, Paris
C. Delisi, Bethesda, MD
R. Fortet, Paris
D.M. Gedeveni, Tbilisi
B.K. Gilbert, Rochester, MN
P. Hall, Stockholm
T.C. Helvey, Nashville, TN
J. Horgan, Milwaukee, WI
G. Karreman, Philadelphia
R.P. Knill-Jones, Glasgow
M.C. MacKey, Montreal, Que.
H.M. Martinez, San Francisco, CA
R.D.H. Maxwell, Wakefield
I. Mirsky, Boston, MA
C.A. Muses, Nice
J. Nagumo, Tokyo
E. Nicolau, Bucharest

K.H. Norwich, Toronto, Ont.
J. Panasewicz, Warsaw
B.H. Rudall, Bangor
J.P. Schadé, Utrecht
T.D. Sterling, Burnaby
H.R.A. Townsend, Edinburgh
R. Vallé, Paris

1984 - Vol. 15 (1 volume in
6 issues)
Subscription price: US\$ 227.00
including postage and handling.
ISSN 0020-7101

Journals are automatically sent by air to the
USA, Canada and India at no extra cost.
Subscribers in Japan, Australasia and
Taiwan, please apply for postal charges.

ELSEVIER

Send your orders to:
Elsevier Scientific Publishers Ireland Ltd., P.O. Box 85, Limerick, Ireland

Requests for free sample copies should be sent to:

In the U.S.A. and Canada:
JOURNAL INFORMATION CENTER
Elsevier Science Publishing Co., Inc.
52 Vanderbilt Avenue, New York, NY 10017, U.S.A.

In all other countries:
ELSEVIER SCIENTIFIC PUBLISHERS IRELAND LTD.,
P.O. Box 85,
Limerick, Ireland

(Continued from inside back cover)

The preparation of iron-free solutions from geological materials for the determination of boron (and other elements) by inductively-coupled plasma emission spectrometry V. K. Din (London, Great Britain)	387
Construction and analytical applications of an improved liquid-membrane electrode for salicylate A. Mitsana-Papazoglou, E. P. Diamandis and T. P. Hadjiioannou (Athens, Greece)	393
Effect of cell geometry on conductance measurements in flow cells D. Taylor and T. A. Nieman (Urbana, IL, U.S.A.)	397
<i>Author Index</i>	401

All rights reserved. No part of this publication may be reproduced, stored in a retrieval system or transmitted in any form or by any means, electronic, mechanical, photocopying, recording or otherwise, without the prior written permission of the publisher, Elsevier Science Publishers B.V., P.O. Box 330, 1000 AH Amsterdam, The Netherlands. Upon acceptance of an article by the journal, the author(s) will be asked to transfer copyright of the article to the publisher. The transfer will ensure the widest possible dissemination of information.

Submission of an article for publication entails the author(s) irrevocable and exclusive authorization of the publisher to collect any sums or considerations for copying or reproduction payable by third parties (as mentioned in article 17 paragraph 2 of the Dutch Copyright Act of 1912 and in the Royal Decree of June 20, 1974 (S. 351) pursuant to article 16b of the Dutch Copyright Act of 1912) and/or to act in or out of Court in connection therewith.

Special regulations for readers in the U.S.A. — This journal has been registered with the Copyright Clearance Center, Inc. Consent is given for copying of articles for personal or internal use, or for the personal use of specific clients. This consent is given on the condition that the copier pays through the Center the per-copy fee for copying beyond that permitted by Sections 107 or 108 of the U.S. Copyright Law. The per-copy fee is stated in the code-line at the bottom of the first page of each article. The appropriate fee, together with a copy of the first page of the article, should be forwarded to the Copyright Clearance Center, Inc., 21 Congress Street, Salem, MA 01970, U.S.A. If no code-line appears, broad consent to copy has not been given and permission to copy must be obtained directly from the author(s). All articles published prior to 1980 may be copied for a per-copy fee of US \$ 2.25, also payable through the Center. This consent does not extend to other kinds of copying, such as for general distribution, resale, advertising and promotion purposes, or for creating new collective works. Special written permission must be obtained from the publisher for such copying.

(Continued from outside back cover)

Liquid adsorption chromatography of chelates. The effect of structure on the thin-layer chromatographic behaviour of chelates A. R. Timerbaev and O. M. Petrukhin (Moscow, U.S.S.R.)	229
Liquid-liquid extraction of Group IB metal ions by thioethers A. Ohki, M. Takagi (Fukuoka, Japan) and K. Ueno (Kumanoto, Japan)	245
Separation of molybdenum from tungsten with di(2-ethylhexyl)-phosphoric acid as extractant N. R. Das, B. Nandi and S. N. Bhattacharyya (Calcutta, India)	255
Optical Methods	
Survey of reaction types in low-energy collisional activation of protonated methyl alkyl ketones M. M. Burse, J. A. Nystrom (Chapel Hill, NC, U.S.A.) and J. R. Hass (Triangle Park, NC, U.S.A.)	265
Survey of reactions of protonated acetate esters induced on low-energy collisions with helium and nitrogen M. M. Burse, J. A. Nystrom (Chapel Hill, NC, U.S.A.) and J. R. Hass (Triangle Park, NC, U.S.A.)	275
Flow fluorimetry of trace amounts of uranium(VI) after preconcentration on a tri-n-octylphosphine oxide/polyethylene column and elution with hydrogenphosphate solution H. Watarai and N. Suzuki (Sendai, Japan)	283
Synthesis of <i>o,o'</i> -dihydroxyazo compounds and their application to the determination of magnesium and calcium by flow injection analysis H. Wada, G. Nakagawa and K. Ohshita (Nagoya, Japan)	289
Simultaneous spectrophotometric determination of humic acid and iron in water P. D. Carpenter and J. D. Smith (Melbourne, Parkville, Australia)	299
Spectrophotometric study of reactions of scandium, yttrium and lanthanum ions with some triphenylmethane dyes in the presence of cationic surfactants M. Jarosz and Z. Marczenko (Warsaw, Poland)	309
Simultaneous spectrofluorometric determination of iron and manganese by a differential kinetic catalytic method A. Moreno, M. Silva and D. Perez-Bendito (Cordoba, Spain)	319
Determination of rare-earth elements, yttrium and scandium in manganese nodules by inductively-coupled argon-plasma emission spectrometry T. Fries, P. J. Lamothe (Menlo Park, CA, U.S.A.) and J. J. Pesek (San Jose, CA, U.S.A.)	329
Short Communications	
Stopped-flow kinetic determination of glucose and lactate with immobilized enzymes R. Q. Thompson and S. R. Crouch (East Lansing, MI, U.S.A.)	337
Kinetic spectrophotometric assay of sulfonamides by use of the Griess reaction and a stopped-flow procedure A. G. Xenakis and M. I. Karayannis (Ioannina, Greece)	343
Separation and determination of inorganic anions by means of ion-pair chromatography A. Mangia and M. T. Lugari (Parma, Italy)	349
Quantitative liquid chromatography of metal tetraalkyls H. B. Abrahamson and R. A. Vanderpool (Norman, OK, U.S.A.)	355
Highly-resolved fluorescence spectrometry of pyrene on a thin-layer chromatographic plate J. W. Hofstraat, M. Engelsma, W. P. Cofino, G. Ph. Hoornweg, C. Gooijer and N. H. Velthorst (Amsterdam, The Netherlands)	359
Synthesis of a new tetrazolium salt giving a water-soluble formazan and its application in the determination of lactate dehydrogenase activity M. Shiga, M. Saito, K. Ueno and K. Kina (Kumamoto-shi, Japan)	365
1,4-Dioxane as a solvent in spectroscopy and photochemistry J. Błażejowski and J. Szychliński (Gdansk, Poland)	369
Determination of chromium in gallium arsenide by electrothermal atomic absorption spectrometry M. Taddia and P. Lanza (Bologna, Italy)	375
The determination of cadmium in microgram amounts of pancreatic tissue by electrothermal atomic absorption spectrometry T. Nilsson and P.-O. Berggren (Uppsala, Sweden)	381

(Continued on facing page)

CONTENTS

(Abstracted, Indexed in: Anal. Abstr.; Biol. Abstr.; Chem. Abstr.; Curr. Contents Phys. Chem. Earth Sci.; Life Sci.; Index Med.; Mass Spectrom. Bull.; Sci. Citation Index; Excerpta Med.)

Electrometric Methods

Theory and applications of ion-selective electrodes. Part 5 J. Koryta (Prague, Czechoslovakia)	1
A miniature flow-through cell with a four-function ChemFET integrated circuit for simultaneous measurements of potassium, hydrogen, calcium and sodium ions A. Sibbald, P. D. Whalley and A. K. Covington (Newcastle-upon-Tyne, Great Britain)	4
Lead-selective electrodes based on lead(IV) oxide D. Midgley (Leatherhead, Great Britain)	63
Use of the Clark oxygen sensor with immobilized enzymes for determinations in flow systems V. Pacáková, K. Štulík, D. Brabcová and J. Barthová (Prague, Czechoslovakia)	71
Determination of glutamate-pyruvate transaminase activity in blood serum with a pyruvate oxidase/poly(vinyl chloride) membrane sensor K. Kihara, E. Yasukawa, M. Hayashi and S. Hirose (Ibaraki, Japan)	81
Selective determination of microbial cells by graphite electrode modified with adsorbed 4,4'-bipyridine T. Matsunaga and Y. Namba (Koganei, Tokyo, Japan)	87
Potentiometric stripping analysis and anodic stripping voltammetry with carbon fiber electrodes G. Schulze and W. Frenzel (Berlin, Germany)	95
Adsorptive stripping voltammetric determination of thiourea and thiourea derivatives V. Stará and M. Kopanica (Prague, Czechoslovakia)	105
Differential-pulse polarography of trichothecene mycotoxins. Determination of deoxynivalenol, nivalenol and fusarenone-x in maize A. Visconti, A. Bottalico, F. Palmisano and P. G. Zamboni (Bari, Italy)	111
The oxidative voltammetric behaviour of some sulphonamides at the glassy carbon electrode A. Momberg V., M. E. Carrera B., D. von Baer, C. Bruhn F. (Concepción, Chile) and M. R. Smyth (Dublin, Ireland)	119
Linear-sweep voltammetry at a dropping mercury electrode in continuous flow systems Z. Kowalski and W. Kubiak (Kraków, Poland)	129
Large-volume wall-jet cells as electrochemical detectors for high-performance liquid chromatography H. Gunasingham (Kent Ridge, Singapore)	139
The acidity of superacidic media derived from fluorosulfuric acid and trifluoromethanesulfonic acid B. Carre (Tours, France) and J. Devynck (Paris, France)	149

Computer Methods and Applications

The use of pattern recognition techniques in chemical differentiation between Bordeaux and Bourgogne wines H. van der Voet, D. A. Doornbos, M. Meems and G. van de Haar (Groningen, The Netherlands)	159
Bewertung von glättungsexperimenten E. Sorkau, K. Doerffel, T. Reiher (Merseburg, D.D.R.) and P. C. Meier (Zürich, Schweiz)	170
Enhancement of the performance of analytical laboratories by a digital simulation approach T. A. H. M. Janse and G. Kateman (Nijmegen, The Netherlands)	181

Separations

Rapid radiochemical separation in neutron activation analysis. Part 1. The use of C ₁₈ -bonded silica gel and selective complexation for determinations of manganese, copper and zinc in biological materials J. J. Fardy, G. D. McOrist and T. M. Florence (Sutherland, N.S.W., Australia)	199
A post-column photochemical detector for use in the determination of trace metals with n-butyl-2-naphthylmethylthiocarbamate by high-performance liquid chromatography Y. T. Shih and P. W. Carr (Minneapolis, MN, U.S.A.)	211

(Continued on inside back cover)